EXPLORING RELIABLE MARKERS AND PREDICTION INDEXES FOR THE PROGRESSION FROM SUBJECTIVE COGNITIVE DECLINE TO COGNITIVE IMPAIRMENT

EDITED BY: Ying Han, Frank Jessen and Jiehui Jiang

PUBLISHED IN: Frontiers in Aging Neuroscience

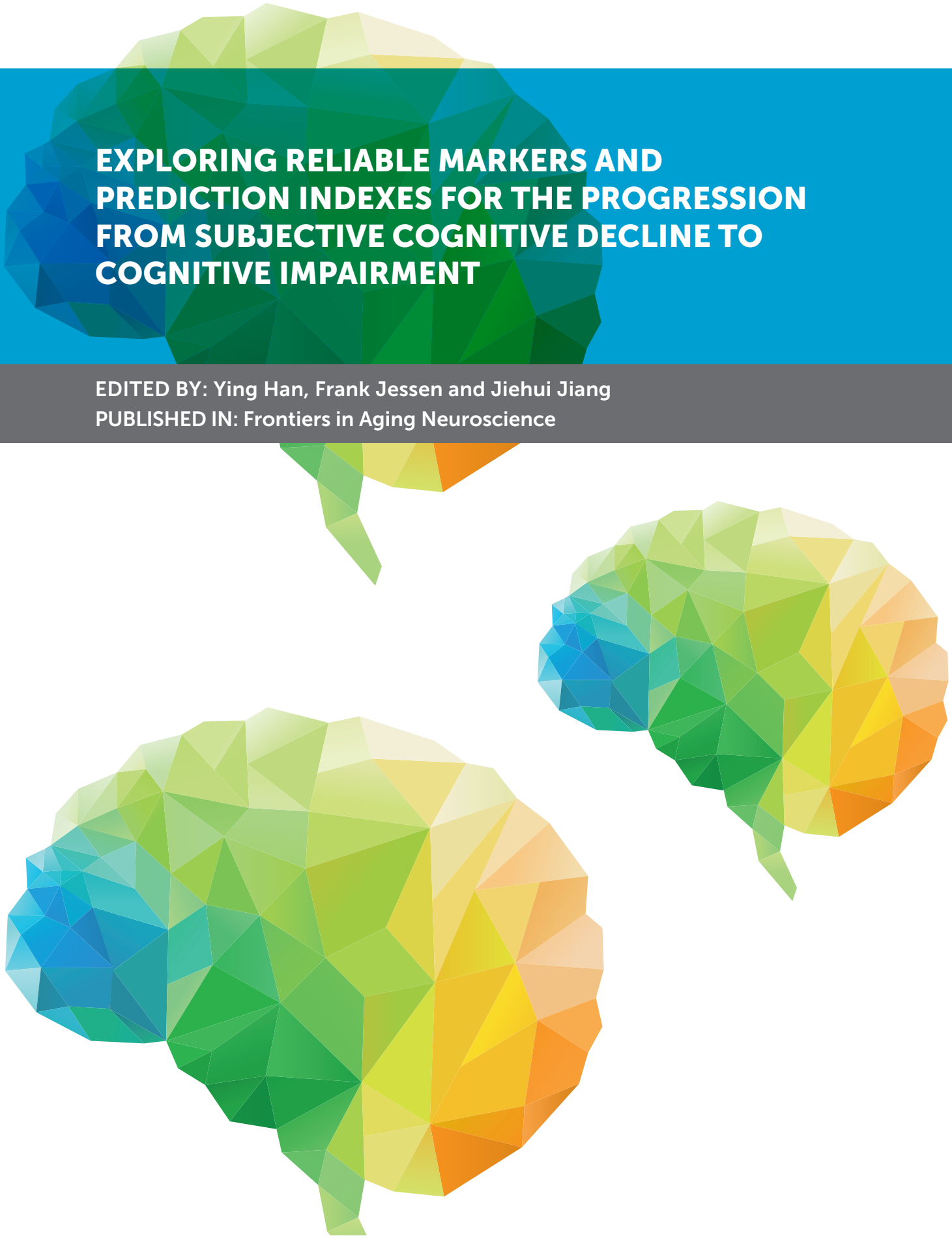

frontiers Research Topics

ISSN 1664-8714
ISBN 978-2-88971-599-2
DOI 10.3389/978-2-88971-599-2

About Frontiers

Frontiers is more than just an open-access publisher of scholarly articles: it is a pioneering approach to the world of academia, radically improving the way scholarly research is managed. The grand vision of Frontiers is a world where all people have an equal opportunity to seek, share and generate knowledge. Frontiers provides immediate and permanent online open access to all its publications, but this alone is not enough to realize our grand goals.

Frontiers Journal Series

The Frontiers Journal Series is a multi-tier and interdisciplinary set of open-access, online journals, promising a paradigm shift from the current review, selection and dissemination processes in academic publishing. All Frontiers journals are driven by researchers for researchers; therefore, they constitute a service to the scholarly community. At the same time, the Frontiers Journal Series operates on a revolutionary invention, the tiered publishing system, initially addressing specific communities of scholars, and gradually climbing up to broader public understanding, thus serving the interests of the lay society, too.

Dedication to Quality

Each Frontiers article is a landmark of the highest quality, thanks to genuinely collaborative interactions between authors and review editors, who include some of the world's best academicians. Research must be certified by peers before entering a stream of knowledge that may eventually reach the public - and shape society; therefore, Frontiers only applies the most rigorous and unbiased reviews.
Frontiers revolutionizes research publishing by freely delivering the most outstanding research, evaluated with no bias from both the academic and social point of view. By applying the most advanced information technologies, Frontiers is catapulting scholarly publishing into a new generation.

What are Frontiers Research Topics?

Frontiers Research Topics are very popular trademarks of the Frontiers Journals Series: they are collections of at least ten articles, all centered on a particular subject. With their unique mix of varied contributions from Original Research to Review Articles, Frontiers Research Topics unify the most influential researchers, the latest key findings and historical advances in a hot research area! Find out more on how to host your own Frontiers Research Topic or contribute to one as an author by contacting the Frontiers Editorial Office: frontiersin.org/about/contact

EXPLORING RELIABLE MARKERS AND PREDICTION INDEXES FOR THE PROGRESSION FROM SUBJECTIVE COGNITIVE DECLINE TO COGNITIVE IMPAIRMENT

Topic Editors:
Ying Han, Capital Medical University, China
Frank Jessen, University of Cologne, Germany
Jiehui Jiang, Shanghai University, China

Citation: Han, Y., Jessen, F., Jiang, J., eds. (2021). Exploring Reliable Markers and Prediction Indexes for the Progression From Subjective Cognitive Decline to Cognitive Impairment. Lausanne: Frontiers Media SA.
doi: 10.3389/978-2-88971-599-2

Table of Contents

frontiers in Aging Neuroscience

EDITORIAL
published: 20 September 2021
doi: 10.3389/fnagi.2021.760920

Editorial: Exploring Reliable Markers and Prediction Indexes for the Progression From Subjective Cognitive Decline to Cognitive Impairment

Jiehui Jiang[1]*, *Ying Han*[2] and *Frank Jessen*[3]

[1] Institute of Biomedical Engineering, School of Information and Communication Engineering, Shanghai University, Shanghai, China, [2] Department of Neurology, Xuanwu Hospital of Capital Medical University, Beijing, China, [3] Department of Psychiatry, University of Cologne, Cologne, Germany

Keywords: preclinical Alzheimer's disease, subjective cognitive decline, marker, neuroimaging, prediction indexes

Editorial on the Research Topic

Exploring Reliable Markers and Prediction Indexes for the Progression From Subjective Cognitive Decline to Cognitive Impairment

Alzheimer's disease (AD) is a neurodegenerative disorder and the most common cause of dementia. There is currently no effective treatment, which makes preclinical prediction for AD particularly important (Huang et al., 2020). Subjective cognitive decline (SCD) has been proposed as important preclinical stages in the development of AD (Sperling et al., 2011). A growing body of evidence shows that SCD may be one of the earliest noticeable symptoms of AD and related dementias. Therefore, it is required to explore reliable biomarkers and prediction indexes for patients with high progression risks from SCD to cognitive impairment.

Taking this into consideration, the Research Topic "Exploring Reliable Markers and Prediction Indexes for the Progression from Subjective Cognitive Decline to Cognitive Impairment" by Frontiers in Aging Neuroscience makes a contribution with updates and different perspectives on this important theme, developed over 19 papers. These updates focus on exploring reliable markers and prediction indexes for the progression of SCD from multidisciplinary perspectives including neuroimaging techniques, genetic or inflammation mechanisms, as well as Artificial Intelligence (AI) applications.

The author Wang X. et al., focus on subjects with low and high plasma Aβ levels among individual with SCD. They investigate the microstructural changes in white matter (WM) based on diffusion tensor imaging from dataset of Sino Longitudinal Study on Cognitive Decline (SILCODE). Result shows a correlation between WM integrity (e.g., fractional anisotropy and mean diffusivity) and plasma β-amyloid (Aβ) 40 levels rather than Aβ42 in individuals with SCD. This indicates plasma Aβ40 levels may represent a useful biomarker to predict different trajectories of aging in individuals with SCD.

Another case-control study by Qiao et al., analyses the associations between WM disruptions and cognitive declines at the early stage of subcortical vascular cognitive impairment (SVCI). This study concludes the damage of long WM in right hemisphere in the pre-SVCI patients and correlated with declines in executive functions and spatial processing.

The study by Huang et al., uses multi-kernel support vector machine (SVM) to examine whether WM structural networks can be used for screening SCD and aMCI. Their findings promote the development of potential brain imaging markers for the early detection of AD.

Edited and reviewed by:
Thomas Wisniewski, NYU Grossman School of Medicine, United States

***Correspondence:**
Jiehui Jiang
jiangjiehui@shu.edu.cn

Received: *19 August 2021*
Accepted: *25 August 2021*
Published: *20 September 2021*

Citation:
Jiang J, Han Y and Jessen F (2021) Editorial: Exploring Reliable Markers and Prediction Indexes for the Progression From Subjective Cognitive Decline to Cognitive Impairment. Front. Aging Neurosci. 13:760920. doi: 10.3389/fnagi.2021.760920

Based on diffusional kurtosis imaging (DKI) and three-dimensional (3D) arterial spin labeling (ASL), Yang et al., explore microstructural and cerebral blood flow (CBF) abnormalities in individuals with SCD plus and aMCI. They point out the mean kurtosis of DKI may be used as an early potential neuroimaging biomarker and may be more sensitive than CBF at the very early stage of AD.

The paper by Wu Z. et al., examines group differences in gray matter surface morphometry, including cortical thickness, the gyrification index (GI), and the sulcus depth. The authors aim to track the progression of the disease in different stages of AD, including health controls, early MCIs, late MCIs, and ADs. Based on region-of-interest (ROI) analysis, their study shows that cortical thickness and sulcus depth indices are predominant during AD progression while GI is insensitive. The findings highlight the relevance between gray matter surface morphometry and the stages of AD, laying the foundation for *in vivo* tracking of AD progression.

The study by Fu et al., extracts gray matter volumes to predict the regional densities in the whole brain in normal control (NC), SCD, Amnestic mild cognitive impairment (aMCI) and AD. In this study, decreased structural covariance and weakened connectivity strength are observed in SCD compared with NC. In addition, increased structural covariance in aMCI and decreased structural covariance in AD are also found. These results provide evidence to the structural disconnection hypothesis in individuals with SCD.

The study by Li et al., points out the impairment in spatial navigation (SN) in patients with MCI. They demonstrate that structural connectivity network abnormalities, especially in the frontal and parietal gyri, are associated with a lower SN accuracy, independently of white matter hyper intensities, which providing a new insight into the brain mechanisms associated with SN impairment in MCI.

The study by Cui et al., points out different functional activity of the SCD patients with aMCI patients, which suggest SCD may be a separate stage of cognitive decline before aMCI and is helpful to the study of preclinical cognitive decline.

Based on the topological characteristics of the WM network, Tao et al., further identify individuals with SCD or aMCI from healthy control (HC) and to describe the relationship of pathological changes in these two stages. They conclude that the neural degeneration from SCD to aMCI follows a gradual process, from abnormalities at the nodal level to those at both nodal and network levels.

The study by Chen Q. et al., identifies distinct functional states and explore the reconfiguration functional connectivity (FC) in individuals with SCD. Results indicate that the alterations of dynamic FC may underlie the early cognitive decline in SCD patients and could be served as sensitive neuroimaging biomarkers.

Taking the important role of self-reference processing into account, Wei et al., discover four interactions among self-reference network (SRN), dorsal attention network (DAN), and salience network (SN) using resting-state fMRI. These results point out that the influence of the SRN in the ultra-early stages of AD is non-negligible.

The study by Xu et al., explores the specific characteristic based on the multimodal brain networks, including individual morphological, structural and functional brain networks. Results highlight the role of cortical-subcortical circuit in individuals with SCD, providing potential biomarkers for the diagnosis and prediction of the preclinical stage of AD.

The study by Wu L. et al., investigates the cognitive impairment in individuals with chronic pontine stroke based on voxel-mirrored homotopic connectivity. Results indicate the important role of lingual gyrus and precuneus as ROIs in the early diagnosis of cognitive impairment individuals with chronic pontine stroke.

The study by Wang Y. et al., demonstrates that the carotid calcifications are associated with post-stroke cognitive impairment (PSCI). They conclude that the significant role of large vessel atherosclerosis in PSCI should be concerned in future study.

The study by Chen Y. et al., concludes that the methylation of peripheral NCAPH2 could be used as a useful peripheral biomarker in the early stage of AD screening. Low levels of NCAPH2 methylation are observed in SCD, and which is independent of the APOE ε4 status. In addition, there is a positive correlation between NCAPH2 methylation levels and the hippocampal volumes in SCD APOE ε4 non-carriers.

The study by Dakterzada et al., compares the results of Innotest enzyme-linked immunoassay (ELISA) with two automated methods (Lumipulse and Elecsys). Both Lumipulse and Elecsys methods are highly concordant with clinical diagnoses, and the combination of Lumipulse Ab42 and P-tau has the highest discriminating power. They recommend both automated methods for the measurement of CSF biomarkers.

The study by Shi et al., explores whether adenosine receptor 1 (A1 R) is involved in electroacupuncture (EA) pretreatment induced cognitive impairment after focal cerebral ischemia in rats. The results showed that EA pretreatment revered cognitive impairment, improved neurological outcome, and inhibited apoptosis at 24 h after reperfusion. Pretreatment with CCPA (a selective A1 receptor agonist) could imitate the beneficial effects.

The study by Lin et al., examines the relationship between spinal cord injury (SCI) and olfactory dysfunction. They point out that the SCI initiates pathological processes, including inflammatory response and impaired neurogenesis. These results provide a basis for pathological mechanisms of early neurodegenerative diseases involving the olfactory bulb and enable early clinical drug intervention.

Essential tremor (ET) is occasionally associated with a high risk for MCI and dementia. The retrospective study by Wu P. et al., proposes the sustained clinical efficacy of unilateral magnetic resonance-guided focused ultrasound (MRgFUS) thalamotomy in Chinese patients with ET.

AUTHOR CONTRIBUTIONS

JJ, YH, and FJ have written this editorial for the Research Topic they have edited. All authors contributed to the article and approved the submitted version.

REFERENCES

Huang, L. K., Chao, S. P., and Hu, C. J. (2020). Clinical trials of new drugs for Alzheimer disease. *J. Biomed. Sci.* 27, 1–13. doi: 10.1186/s12929-019-0609-7

Sperling, R. A., Aisen, P. S., Beckett, L. A., Bennett, D. A., Craft, S., Fagan, A. M., et al. (2011). Toward defining the preclinical stages of Alzheimer's disease: recommendations from the National Institute on Aging-Alzheimer's Association workgroups on diagnostic guidelines for Alzheimer's disease. *Alzheimer's Dement.* 7, 280–292. doi: 10.1016/j.jalz.2011.03.003

Conflict of Interest: The authors declare that the research was conducted in the absence of any commercial or financial relationships that could be construed as a potential conflict of interest.

Publisher's Note: All claims expressed in this article are solely those of the authors and do not necessarily represent those of their affiliated organizations, or those of the publisher, the editors and the reviewers. Any product that may be evaluated in this article, or claim that may be made by its manufacturer, is not guaranteed or endorsed by the publisher.

frontiers in Aging Neuroscience

ORIGINAL RESEARCH
published: 12 January 2021
doi: 10.3389/fnagi.2020.592024

Plasma β-Amyloid Levels Associated With Structural Integrity Based on Diffusion Tensor Imaging in Subjective Cognitive Decline: The SILCODE Study

Xiaoni Wang[1], *Mingyan Zhao*[1], *Li Lin*[1] *and Ying Han*[1,2,3]*

[1] *Department of Neurology, Xuanwu Hospital of Capital Medical University, Beijing, China,* [2] *National Clinical Research Center for Geriatric Disorders, Beijing, China,* [3] *Center of Alzheimer's Disease, Beijing Institute for Brain Disorders, Beijing, China*

Background: Accumulating evidence has demonstrated that plasma β-amyloid (Aβ) levels are useful biomarkers to reflect brain amyloidosis and gray matter structure, but little is known about their correlation with subclinical white matter (WM) integrity in individuals at risk of Alzheimer's disease (AD). Here, we investigated the microstructural changes in WM between subjects with low and high plasma Aβ levels among individuals with subjective cognitive decline (SCD).

Methods: This study included 142 cognitively normal individuals with SCD who underwent a battery of neuropsychological tests, plasma Aβ measurements, and diffusion tensor imaging (DTI) based on the Sino Longitudinal Study on Cognitive Decline (SILCODE). Using tract-based spatial statistics (TBSS), we compared fractional anisotropy (FA), and mean diffusivity (MD) in WM between subjects with low ($N = 71$) and high ($N = 71$) plasma Aβ levels (cut-off: 761.45 pg/ml for Aβ40 and 10.74 pg/ml for Aβ42).

Results: We observed significantly decreased FA and increased MD in the high Aβ40 group compared to the low Aβ40 group in various regions, including the body, the genu, and the splenium of the corpus callosum; the superior longitudinal fasciculus; the corona radiata; the thalamic radiation; the external and internal capsules; the inferior fronto-occipital fasciculus; and the sagittal stratum [$p < 0.05$, familywise error (FWE) corrected]. Average FA values were associated with poor performance on executive and memory assessments. No significant differences were found in either MD or FA between the low and high Aβ42 groups.

Conclusion: Our results suggest that a correlation exists between WM integrity and plasma Aβ40 levels in individuals with SCD.

Keywords: plasma β-amyloid, diffusion tensor imaging, subjective cognitive decline, white matter, blood-based biomarker

OPEN ACCESS

Edited by:
Stephen D. Ginsberg, Nathan Kline Institute for Psychiatric Research, United States

Reviewed by:
SangYun Kim, Seoul National University Bundang Hospital, South Korea
Jean-Sébastien Vidal, Hôpital Broca, France

***Correspondence:**
Ying Han
hanying@xwh.ccmu.edu.cn

Received: *06 August 2020*
Accepted: *11 December 2020*
Published: *12 January 2021*

Citation:
Wang X, Zhao M, Lin L and Han Y (2021) Plasma β-Amyloid Levels Associated With Structural Integrity Based on Diffusion Tensor Imaging in Subjective Cognitive Decline: The SILCODE Study. Front. Aging Neurosci. 12:592024. doi: 10.3389/fnagi.2020.592024

INTRODUCTION

Extracellular β-amyloid (Aβ) accumulation and intracellular tau deposition are the core features of Alzheimer's disease (AD; Jack et al., 2018). Amyloid pathology is defined as the initiating step of AD, which leads to subsequent tau deposition and neurodegeneration (Long and Holtzman, 2019); however, the well-established and validated biomarkers for brain amyloidosis detection, including cerebrospinal fluid (CSF) analysis and amyloid PET, are expensive, invasive, and difficult to implement on a large scale in clinical practice (Sperling et al., 2011, 2014; Dubois et al., 2014; Honig et al., 2018). Therefore, minimally invasive and affordable techniques to support early screening are urgently needed.

Blood-based biomarkers represent a logical alternative. Circulating Aβ peptides are the most studied AD biomarkers in plasma. Growing evidence has demonstrated that plasma Aβ concentrations are highly correlated with brain amyloidosis (Nakamura et al., 2018; Risacher et al., 2019; Schindler et al., 2019; Vergallo et al., 2019; Doecke et al., 2020), and the plasma Aβ42/Aβ40 ratio has an accuracy of over 90% in identifying brain amyloid positivity (Schindler et al., 2019; Doecke et al., 2020). Several studies have also reported an association between plasma Aβ levels and gray matter changes, including gray matter volume and cerebral cortex thickness, in both cognitively normal subjects and subjects with mild cognitive impairment (MCI) and AD-related dementia (Kaffashian et al., 2015; Llado-Saz et al., 2015; Cantero et al., 2016; Hanon et al., 2018; Hilal et al., 2018; Youn et al., 2019), suggesting that plasma Aβ levels may reflect downstream neurodegeneration.

White matter (WM) neurodegeneration of associative fiber tracts in AD may result from gray matter atrophy and Wallerian degeneration (Hardy and Higgins, 1992). Accumulating evidence has demonstrated disrupted WM integrity in patients with AD, MCI, and preclinical AD, which is related to cognitive decline (Mayo et al., 2017; Brueggen et al., 2019; Power et al., 2019). Though studies have shown an association of plasma Aβ levels with WM macrostructures such as lesions, hyperintensities, and atrophy (Janelidze et al., 2016; Hilal et al., 2017; Lippa et al., 2019; Youn et al., 2019), the relationship between plasma Aβ levels and WM microstructure has not been clarified.

Subjective cognitive decline (SCD) refers to those who experience subjective cognitive deficits without measurable cognitive impairment (Jessen et al., 2014, 2020). It is suggested as one of the earliest manifestations of the AD continuum, and accumulating evidence has demonstrated that individuals with SCD may exhibit an increased risk of progression to cognitive impairment and of developing AD (Mitchell et al., 2014; Slot et al., 2019) and may present increased AD pathology (Amariglio et al., 2015). Regardless of the absence of objective cognitive impairment (OCI), SCD might become important for clinical practice as an early trigger for seeking medical help because of an increase in the number of individuals with SCD in the healthcare system (Jessen et al., 2020). Thus, taking individuals with SCD as an interesting target population to study may enhance our understanding of early AD diagnosis and preventive treatment. Recently, several studies have identified the correlation between plasma Aβ and gray matter volume by performing structural magnetic resonance imaging (sMRI) in individuals with SCD (Cantero et al., 2016; Youn et al., 2019). Our previous study showed widespread WM microstructure impairment in SCD (Li et al., 2016); however, studies on its correlation with plasma Aβ in this stage remain lacking.

Diffusion tensor imaging (DTI) can be employed for *in vivo* detection of WM microstructural properties. Fractional anisotropy (FA) and mean diffusivity (MD) are the most commonly used types of indices in AD research, and they reflect microstructural neuronal dysfunctions that precede macroscopic atrophy (Soares et al., 2013; Qin et al., 2020). In this study, we aimed to assess whether plasma Aβ levels are related to subclinical microstructural WM integrity as measured by DTI, and first, we hypothesized that higher plasma Aβ40 and lower Aβ42 levels are associated with WM integrity. Second, we hypothesized that plasma Aβ-related WM impairment is associated with cognitive decline.

MATERIALS AND METHODS

Participants

The baseline dataset of the Sino Longitudinal Study on Cognitive Decline (SILCODE; Li et al., 2019) from March 20, 2017 to September 17, 2018, was included in the study. Excluding all cases that failed to meet the inclusion criteria, a total of 142 cognitively normal elderly Han Chinese subjects with SCD (mean age: 66.07 ± 3.88 years) were included. In addition, 26 patients with MCI and AD-related dementia categorized as patients with OCI in the present study were included for complementary analyses. All participants underwent clinical assessment, a battery of neuropsychological tests, blood sample collections, and MRI scans.

All participants were between 60 and 80 years old. SCD is defined as follows (Jessen et al., 2014): (1) the onset of self-experienced persistent decline (>6 months) within the last 5 years; (2) the onset of subjective decline in memory rather than other domains (language, attention, planning, and any other cognitive decline); (3) participants within the normal range upon cognitive testing (adjusted for age, sex, and education) and failure to meet the criteria for MCI or dementia. MCI was diagnosed if they met any one of the following three criteria (Bondi et al., 2008; Jak et al., 2009): (1) impaired scores (defined as >1 SD below the age-corrected normative means) on both measures in at least one cognitive domain (memory, language, or speed/executive function); (2) impaired scores in each of the three cognitive domains (memory, language, or speed/executive function); and (3) the Functional Activities Questionnaire (FAQ) ≥9. AD-related dementia was diagnosed based on the Diagnostic and Statistical Manual of Mental Disorders, Fourth Edition (DSM-IV) and the National Institute on Aging and the Alzheimer's Association (NIA-AA) workgroup guidelines for dementia due to AD. To eliminate the impact of cerebral vascular disease, we excluded subjects with a history of stroke, large-vessel disease (cortical and/or subcortical infarcts and watershed infarcts), moderate WM changes, and multiple lacunar infarcts (>1) on brain imaging. The SILCODE exclusion

criteria ensured that no subjects with current major psychiatric diagnosis; neurological disease; systematic disease that causes cognitive decline, head trauma, or unstable medical conditions were included. All subjects gave their written informed consent prior to participation. The study protocol was approved by the Medical Research Ethics Committee and Institutional Review Board of Xuanwu Hospital. The SILCODE is listed in the ClinicalTrail.gov registry (NCT02225964).

Neuropsychological Assessments

We performed a battery of neuropsychological tests covering memory, language, and executive function. Auditory Verbal Learning Test - Huashan version (AVLT)-long delayed recall and -recognition (Xu et al., 2020) was used to evaluate memory; Semantic Verbal Fluency Test (VFT; Guo et al., 2007) and Boston Naming Test (BNT; Guo et al., 2006) were administered to evaluate language; and time consumed in Shape Trail Test A (STT-A) and B (STT-B; Zhao et al., 2013) were used to evaluate executive function. The thresholds for memory, language, and executive function tests are summarized in **Supplementary Table 1**. The SCD questionnaire including nine reliable SCD items (SCD-Q9) was used for the quantitative assessment of the severity of SCD (Gifford et al., 2015). Mini-Mental State Examination (MMSE) and Montreal Cognitive Assessment Basic Version (MoCA-B) were used to evaluate general cognitive ability. Besides, all subjects were assessed with Hamilton Anxiety Scale (HAMA), Hamilton Depression Scale (HAMD), Geriatric Depression Scale (GDS), and the FAQ.

Plasma Aβ Measurements

Blood samples were collected in the morning after an overnight fast. After centrifugation, the samples were aliquoted, stored at −80°C, and thawed immediately on ice before assaying. Meso Scale Discovery (MSD) kits (Rockville, Maryland, USA) were used to quantify the concentrations of plasma Aβ. All the samples were measured in duplicate using the same aliquot following the manufacturer's instructions. The detection limits were 20–6,000 pg/ml for Aβ40 and 2.5–1,271 pg/ml for Aβ42. The mean inter-assay and intra-assay coefficients of variation were <10 and 6%, respectively, for both Aβ40 and Aβ42. The 142 subjects with SCD were then divided into low and high Aβ groups ($N = 71$ case/group) with the cut-off defined by the mean value (Aβ40: 761.45 pg/ml; Aβ42: 10.74 pg/ml).

Image Acquisition and Analysis

All MRI data were acquired on an integrated simultaneous 3.0 T TOF PET/MR (Signa PET/MR, GE Healthcare, Milwaukee, WI, USA) at Xuanwu Hospital of Capital Medical University. DTI scans were collected axially with a single-shot spin-echo diffusion-weighted echo planar imaging (EPI) sequence. The parameters were as follows: 30 gradient directions and 5 b0 images (b = 1,000 s/mm^2), field of view (FOV) = 256 × 256 × 256, matrix = 112 × 112, repetition time = 16,500 ms, echo time = 95.6 ms, slice number = 70, slice thickness = 2 mm, and voxel size = 2 × 2 × 2 mm^3. Three-dimensional T1 weighted images were acquired with a Spoiled Gradient Recalled Echo (SPGR) sequence. Additionally, T2 weighted and resting-state functional MR images were collected. The parameter details have been described in previous studies (Li et al., 2019; Sun et al., 2019; Dong et al., 2020).

The DTI data of each subject were processed with a pipeline tool for analyzing brain diffusion images (PANDA; Cui et al., 2013), which integrates the FMRIB Software Library (FSL; Smith et al., 2004), the Pipeline System for Octave and Matlab (PSOM; Bellec et al., 2012), the Diffusion Toolkit, and the MRIcron. The main steps of data preprocessing were as follows: (1) converting DICOM files into NIFIT format; (2) estimating the brain mask: The *bet* command of FSL was used to remove the skull from b0 image; (3) cropping the raw image: The *fslroi* command of FSL was used to remove non-brain tissue; (4) correcting for the eddy-current effect: Head motion and eddy current distortions were corrected by registration of the diffusion-weighted images to the b0 images using the *eddy_correct* command of FSL; and (5) calculating diffusion tensor parameters: The *dtifit* command of FSL was applied to calculate FA and MD maps. Tract-based spatial statistics (TBSS) were performed for the voxel-wise analysis of FA and MD (Smith et al., 2006). All individual images were registered to the 1 × 1 × 1 mm Montreal Neurological Institute (MNI) standard space with the FMRIB58_FA template as the target image (http://www.fmrib.ox.ac.uk/fsl/data/FMRIB58_FA). Then, a mean FA average was obtained by averaging the FA images from each subject in the standard space and thinning to create a custom mean FA skeleton. The mean FA skeleton was thresholded at 0.2 to include only voxels indicative of WM. Then, the individual FA maps were projected onto the FA skeleton to obtain the FA skeletons of each participant and the deformation matrixes. This projection information was also applied to MD. The skeletonized FA and MD maps were used in further statistical analysis.

Statistical Analysis

Differences between the low and high Aβ groups in demographic data and vascular comorbidity distribution were compared using the two-sample *t*-test for continuous variables and the chi-square test for categorical variables. To compare cognitive functions, the general linear model (GLM) controlling for age, sex, and years of education was conducted with neuropsychological tests as independent variables and Aβ groups as dependent variables.

Voxel-wise cross-subject comparisons were performed using the randomize tool in FSL, which is used for non-parametric permutation-based testing. FA and MD were compared through a GLM with Aβ groups as dependent variables. The design matrix included age, sex, and years of education as nuisance covariates. Significant differences were estimated with 5,000 random permutations using threshold-free cluster enhancements (TFCE) and FWE correction for multiple comparisons. The significance threshold was $p < 0.05$ and voxels > 100 (TFCE and FWE corrected). Then, the significant results were thickened with the tbss_fill tool in FSL for better visualization. Finally, the John Hopkins University (JHU) White-Matter Tractography Atlas and JHU-ICBM-DTI-81 White-Matter Labels Atlas were used to identify regions of statistical significance (Mori et al., 2008). Complementary analyses were conducted using the plasma Aβ levels as continuous variables and by assessing subclinical WM

TABLE 1 | Demographic and neuropsychological results.

	Aβ40		*p*	Aβ42		*p*
	Low	**High**		**Low**	**High**	
Age	65.68 ± 3.64	66.45 ± 4.10	0.241	66.67 ± 3.92	66.47 ± 3.83	0.215
Sex (M/F)	23/48	22/49	0.857	22/49	23/48	0.857
Education	12.51 ± 2.94	11.96 ± 3.01	0.279	12.25 ± 2.76	12.22 ± 3.18	0.944
ApoE ε4 carrier, n%	21 (29.6)	14 (19.7)	0.173	14 (19.7)	21 (29.6)	0.173
Hypertension, n%	26(36.7)	30 (42.3)	0.492	32 (45.1)	24 (33.8)	0.170
Diabetes, n%	11 (15.5)	9 (12.7)	0.629	13 (18.3)	7 (9.6)	0.148
Hyperlipidemia, n%	27 (38.0)	26 (36.6)	0.862	27 (38.0)	26 (36.6)	0.862
Smoking, n%	15 (21.1)	14 (19.7)	0.835	16 (22.5)	13 (18.3)	0.532
SCD-9	4.80 ± 1.70	4.68 ± 1.91	0.607	4.52 ± 1.63	5.03 ± 1.94	0.057
AVLT-DR	7.56 ± 1.93	6.73 ± 2.20	0.033	6.89 ± 1.87	7.41 ± 2.30	0.088
AVLT-R	22.72 ± 1.40	21.096 ± 1.74	0.008	22.27 ± 1.68	22.27 ± 1.68	0.697
STT-A	57.73 ± 15.29	64.20 ± 16.43	0.041	61.40 ± 16.68	60.52 ± 15.71	0.636
STT-B	134.18 ± 34.16	139.89 ± 31.52	0.564	141.24 ± 33.68	132.83 ± 31.73	0.060
VFT	19.79 ± 4.45	17.89 ± 4.29	0.023	19.14 ± 4.55	18.54 ± 4.38	0.470
BNT	25.30 ± 2.74	24.63 ± 2.96	0.223	24.83 ± 3.02	25.10 ± 2.71	0.628
MMSE	28.93 ± 1.18	28.59 ± 1.72	0.285	28.68 ± 1.32	28.85 ± 1.63	0.395
MoCA-B	25.97 ± 2.47	25.37 ± 2.15	0.218	25.41 ± 2.20	24.93 ± 2.44	0.117
GDS	2.41 ± 2.00	2.94 ± 2.61	0.174	2.54 ± 2.21	2.83 ± 2.46	0.358
HAMA	4.37 ± 3.17	4.56 ± 3.93	0.856	4.30 ± 3.56	4.63 ± 3.58	0.580
HAMD	3.97 ± 3.95	4.37 ± 8.39	0.438	4.21 ± 4.34	4.13 ± 3.46	0.957
FAQ	0.18 ± 0.49	0.28 ± 0.83	0.46	0.20 ± 0.50	0.27 ± 0.83	0.587

Values of p for neuropsychological tests were obtained with the general linear model adjusted for age, sex, and years of education. ApoE, apolipoprotein E; AVLT-DR, Auditory Verbal Learning Test-long delayed recall; AVLT-R, Auditory Verbal Learning Test-recognition; STT-A Shape Trail Test A; STT-B, Shape Trail Test B; VFT, Verbal Fluency Test; BNT, Boston Naming Test; MMSE, Mini-Mental State Examination; MoCA-B, Montreal Cognitive Assessment Basic Version; GDS, Geriatric Depression Scale; HAMA, Hamilton Anxiety Scale; HAMD, Hamilton Depression Scale; FAQ, Functional Activities Questionnaire.

integrity correlations. The correlations were run separately in the SCD and OCI groups.

To determine the relationships between the WM parameters and cognitive function, partial correlation analysis controlling for age, sex, and year of education was performed between the impaired cognitive scores and average FA (MD) values of regions showing significant group differences. The significance threshold was $p < 0.05$.

RESULTS

Behavioral Results

Table 1 summarizes the demographic and neuropsychological results according to plasma Aβ levels in SCD. Age, sex, years of education, ApoE genotype distribution, and vascular comorbidities were statistically homogeneous. The high Aβ40 group exhibited poorer performance on memory, executive, and language tests (AVLT-DR: F = 4.652, $p = 0.033$; AVLT-R: F = 7.219, $p = 0.008$; STT-A: F = 4.271, $p = 0.0341$; VFT: F = 5.260, $p = 0.023$). The low and high Aβ42 groups showed no significant difference in cognitive tests in the three domains. No significant differences in SCD-Q9 scores between the low and high Aβ groups were detected (neither Aβ40 nor Aβ42). The demographic and neuropsychological results in the total SCD sample and the OCI sample are summarized in **Supplementary Table 2**.

Comparisons of Whole Brain WM Between the Low and High Aβ Groups

Compared with the low Aβ40 group, the high Aβ40 group exhibited decreased FA and increased MD in widespread WM tracts (TFCE and FWE corrected, $p < 0.05$), mainly located in the body, the genu, and the splenium of corpus callosum; the superior longitudinal fasciculus; the anterior, superior, and posterior corona radiata; the thalamic radiation; the external and internal capsules; the inferior fronto-occipital fasciculus; the sagittal stratum; the cerebral peduncle; and the fornix (see **Figure 1** and **Supplementary Table 3**). After FWE correction, no significant differences were noted for FA and MD between the low and high Aβ42 groups.

Relationship Between WM and Neuropsychological Tests

In the extracted cluster, the relationship between average MD and FA values and impaired cognitive tests (AVLT-DR, AVLT-R, STT-A, and VFT) observed in the high Aβ40 group was investigated. Age, sex, and years of education were included as covariates. Average FA values were negatively correlated with STT-A ($r = -0.174$, $p = 0.041$) and positively correlated with AVLT-R ($r = 0.192$, $p = 0.023$; see **Figure 2**). No significant correlation between MD values and cognitive scores was noted (see **Supplementary Table 4**).

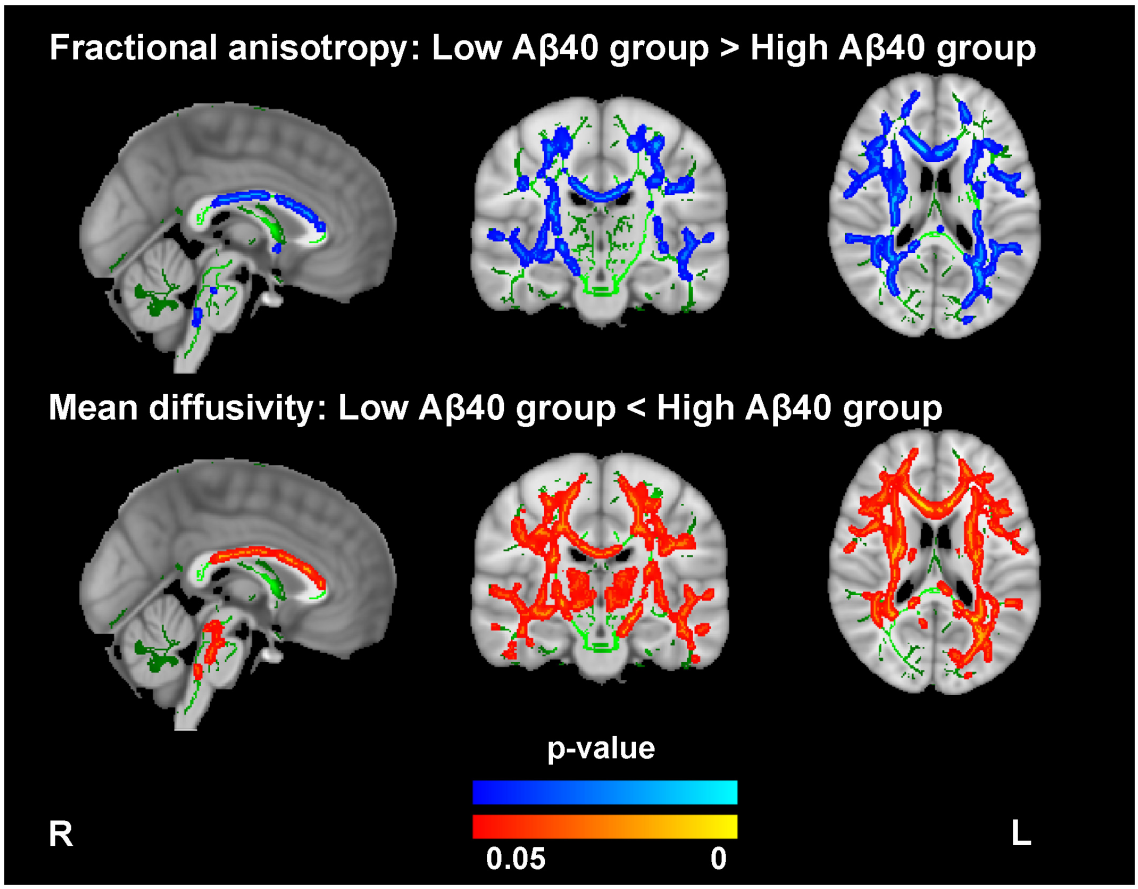

FIGURE 1 | Comparison of the fractional anisotropy (FA) and mean diffusivity (MD) findings between the high and low Aβ40 groups. The averaged skeleton (green color) was overlaid with significantly lower FA (blue-light color) and higher MD (red-yellow color) in the high Aβ40 group compared with the low Aβ40 group (TFCE and FWE corrected $p < 0.05$, voxels > 100). The analysis controlled for age, sex, and years of education.

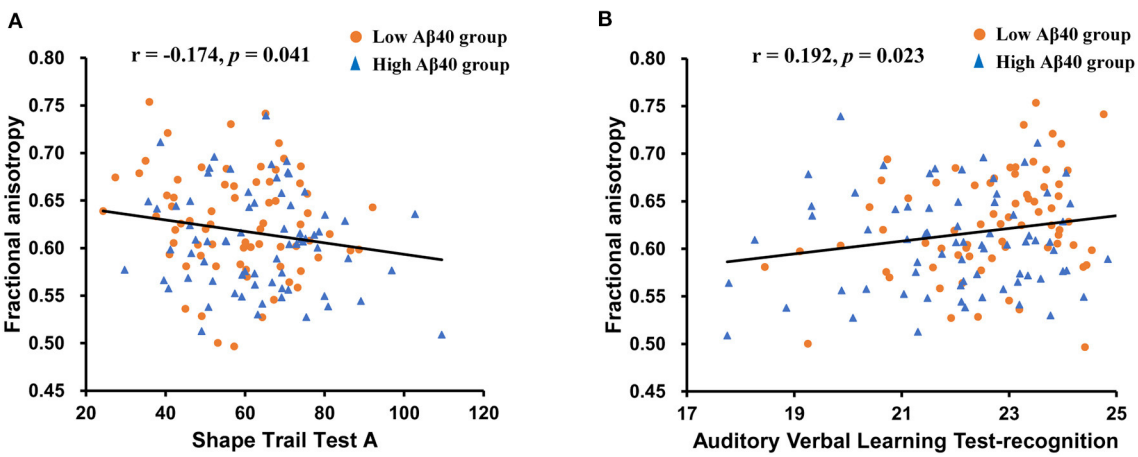

FIGURE 2 | Scatter plots illustrating the relationships between average white matter (WM) parameters and neuropsychological tests controlling for age, sex, and years of education. **(A)** A significant negative correlation was found between the FA values and the Shape Trail Test-A (STT-A) scores. **(B)** A significant positive correlation was found between FA values and Auditory Verbal Learning Test (AVLT)-recognition scores.

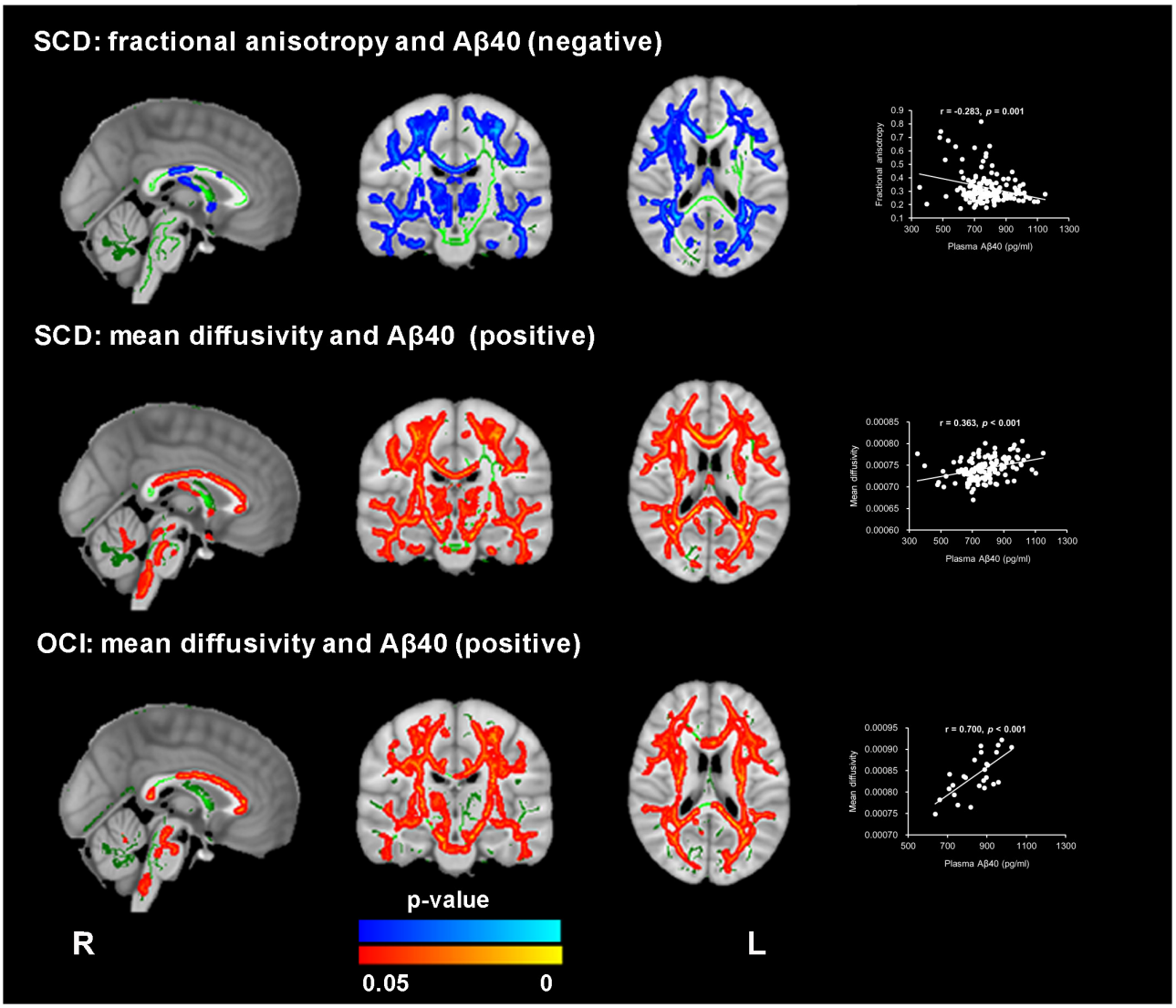

FIGURE 3 | Significant association between WM microstructure parameters and plasma Aβ40 in subjective cognitive decline (SCD) and patients with objective cognitive impairment (OCI). FA revealed a negative correlation with plasma Aβ40 in SCD (blue-light color), and MD exhibited a positive correlation with plasma Aβ40 in both the SCD and OCI groups (red-yellow color) (TFCE and FWE corrected $p < 0.05$, voxels > 100). The regions with statistical significance were projected on the averaged skeleton (green color). The scatter plots show the average values (y-axis) from the significant regions for each subject against plasma Aβ40 (x-axis) for each participant. The analysis controlled for age, sex, and years of education.

Complementary Analysis

In the SCD group, the voxel-wise analysis using the plasma Aβ levels as continuous variables revealed a significant association of higher plasma Aβ40 levels with decreased FA and increased MD values (TFCE and FWE corrected, $p < 0.05$), which were located in similar regions as noted in the group comparison (see **Figure 3** and **Supplementary Table 5**). In the OCI group, a positive correlation between MD and plasma Aβ40 levels was identified in the bilateral forceps minor, the superior longitudinal fasciculus, the inferior longitudinal fasciculus, the anterior thalamic radiation, the inferior fronto-occipital fasciculus, the cingulum, and the corticospinal tract (see **Figure 3** and **Supplementary Table 5**). Both correlations between Aβ42 and FA and MD were not significant within the SCD and OCI groups.

DISCUSSION

In the present study, we investigated the association between plasma Aβ levels and WM microstructure. Both decreased FA and increased MD values were found in the high Aβ40 group and were mainly located in the corpus callosum, the superior longitudinal fasciculus, the corona radiata, the thalamic

radiation, the external and internal capsules, the inferior fronto-occipital fasciculus, the sagittal stratum, the cerebral peduncle, and the fornix. Moreover, the decreased FA was associated with poor performance on STT-A and AVLT-R; however, no significant differences were found in the DTI parameters between the low and high Aβ42 groups.

This study identified an association between higher plasma Aβ40 levels and WM microstructure abnormalities in individuals with SCD and OCI. Though some studies have investigated the association between plasma Aβ40 levels and WM hyperintensities, lesions and WM volume (Janelidze et al., 2016; Hilal et al., 2017; Youn et al., 2019), we found that the correlation between the plasma Aβ40 levels and WM integrity remained significant after excluding those with cerebral vascular disease. Our results were consistent with previous studies that showed the association between plasma Aβ40 levels and neurodegeneration biomarkers, such as hippocampal atrophy and thinner cerebral cortex thickness, in both cognitively normal elderly subjects and patients with AD (Kaffashian et al., 2015; Llado-Saz et al., 2015; Hanon et al., 2018). The association between plasma Aβ40 and WM integrity may result from the role of Aβ40 in cerebrovascular abnormalities in AD. Aβ40 was found to reproduce the cerebrovascular alterations in transgenic mice overexpressing the amyloid precursor protein (APP; Niwa et al., 2000), and circulating Aβ40 could enhance the cerebrovascular dysfunction induced by brain Aβ40, which may contribute to WM impairment (Park et al., 2013). Though the age was matched between the low and high Aβ40 groups and included as a covariate for statistical analysis, we cannot exclude the possibility that the association of age with both plasma Aβ40 levels and DTI parameters contributed to the correlation found in our study (Kleinschmidt et al., 2016; Lovheim et al., 2017; Jiang et al., 2019; Zavaliangos-Petropulu et al., 2019).

The correlations with Aβ40 seemed to be more widespread and pronounced in MD compared with FA in both the SCD and OCI groups. The biological bases of MD and FA may differ and are not fully understood. FA corresponds to the degree of directionality and anisotropic diffusion, which is assumed to reflect WM impairment caused by microstructural damage such as axonal degradation (Soares et al., 2013; Brueggen et al., 2019). In contrast, MD is calculated based on the mean of three eigenvalues and corresponds to the diffusion rate, which is assumed to reflect WM impairment caused by membrane integrity damage. FA analysis can be influenced by crossing fibers more than MD, which may limit its power to detect WM degeneration (Soares et al., 2013; Brueggen et al., 2019).

Contrary to our hypothesis, we did not identify significant differences in FA and MD between the low and high Aβ42 groups, where the identification is consistent with a previous study in patients with a history of traumatic brain injury (Lippa et al., 2019). Peripheral Aβ42 is highly correlated with brain amyloid pathology (Nakamura et al., 2018; Schindler et al., 2019; Doecke et al., 2020); whereas, several studies have indicated that the loss of WM integrity reflects early tau accumulation other than amyloid pathology (Strain et al., 2018). Kantarci et al. (2017) reported higher MD and lower FA in higher Braak neurofibrillary tangle staging than in those with high Aβ neuritic plaques, which may result in the lack of association between WM parameters and plasma Aβ42 in our study. Our results indicated that plasma Aβ42 levels may not reflect subclinical WM impairment.

We observed significant differences between the low and high Aβ40 groups in memory, executive, and language domains. Subjects with increased Aβ40 performed poorly on cognitive tests, though the performance of the participants in the present study on cognitive tests was within the normal range. Consistent with our findings, large population-based studies have reported the association of increased Aβ40 with the risk of dementia as well as with declining cognitive measurements (Hilal et al., 2018; Verberk et al., 2018); however, some studies also found an association between plasma Aβ42 and impaired cognition (Llado-Saz et al., 2015). Differences in patient age, clinical status, and analysis techniques may affect plasma Aβ quantification and result in inconsistencies between studies (Toledo et al., 2013; Palmqvist et al., 2018; Wang et al., 2018). We further found an association between the STT-A and AVLT-R scores, and the average FA values within the regions exhibit significant group differences, indicating that plasma Aβ40-related WM structural changes may reflect cognitive function in individuals with SCD.

Our study has several limitations. First, this study employed a cross-sectional design. We found that higher Aβ40 levels were associated with disrupted diffusion in WM; however, whether the plasma Aβ40 level correlated with the cause of WM abnormalities in subjects with SCD was not clarified. The lack of repeated measurements of blood Aβ concentrations limits the evaluation of the trajectory of plasma levels in relation to WM impairment. Thus, longitudinal studies are needed to identify the dynamic correlation between plasma Aβ levels and WM integrity. Second, we did not analyze brain amyloid or tau pathology; therefore, further studies are needed to determine whether central amyloid or tau induces the association between plasma Aβ levels and WM integrity. Finally, additional studies should be conducted in subjects with different cognitive statuses to determine whether the correlations are dependent on disease progression.

CONCLUSION

In summary, the current study demonstrated different WM microstructures between subjects with low and high Aβ40 levels among individuals with SCD. The findings suggest that plasma Aβ40 levels could reflect central neurodegeneration and may represent a useful biomarker to predict different trajectories of aging in individuals with SCD.

DATA AVAILABILITY STATEMENT

The raw data supporting the conclusions of this article will be made available by the authors, without undue reservation.

ETHICS STATEMENT

The studies involving human participants were reviewed and approved by Medical Research Ethics Committee and Institutional Review Board of Xuanwu Hospital. The

patients/participants provided their written informed consent to participate in this study.

AUTHOR CONTRIBUTIONS

XW and YH did manuscript preparation and drafting. XW, MZ, LL, and YH did the clinical assessments and data acquisition. MZ and YH did the clinical diagnosis. XW, MZ, LL, and YH did the data analysis and interpretation. YH is responsible for the study conception and design. All authors contributed to the article and approved the submitted version.

FUNDING

This work was supported by the National Key Research and Development Program of China (2016YFC1306300) and the National Natural Science Foundation of China (61633018 and 82020108013).

SUPPLEMENTARY MATERIAL

The Supplementary Material for this article can be found online at: https://www.frontiersin.org/articles/10.3389/fnagi.2020.592024/full#supplementary-material

REFERENCES

Amariglio, R. E., Mormino, E. C., Pietras, A. C., Marshall, G. A., Vannini, P., Johnson, K. A., et al. (2015). Subjective cognitive concerns, amyloid-β, and neurodegeneration in clinically normal elderly. *Neurology* 85, 56–62. doi: 10.1212/WNL.0000000000001712

Bellec, P., Lavoie-Courchesne, S., Dickinson, P., Lerch, J. P., Zijdenbos, A. P., and Evans, A. C. (2012). The pipeline system for Octave and Matlab (PSOM): a lightweight scripting framework and execution engine for scientific workflows. *Front. Neuroinform.* 6:7. doi: 10.3389/fninf.2012.00007

Bondi, M. W., Jak, A. J., Delano-Wood, L., Jacobson, M. W., Delis, D. C., and Salmon, D. P. (2008). Neuropsychological contributions to the early identification of Alzheimer's disease. *Neuropsychol. Rev.* 18, 73–90. doi: 10.1007/s11065-008-9054-1

Brueggen, K., Dyrba, M., Cardenas-Blanco, A., Schneider, A., Fliessbach, K., Buerger, K., et al. (2019). Structural integrity in subjective cognitive decline, mild cognitive impairment and Alzheimer's disease based on multicenter diffusion tensor imaging. *J. Neurol.* 266, 2465–2474. doi: 10.1007/s00415-019-09429-3

Cantero, J. L., Iglesias, J. E., Van Leemput, K., and Atienza, M. (2016). Regional hippocampal atrophy and higher levels of plasma amyloid-beta are associated with subjective memory complaints in nondemented elderly subjects. *J. Gerontol. A Biol. Sci. Med. Sci.* 71, 1210–1215. doi: 10.1093/gerona/glw022

Cui, Z., Zhong, S., Xu, P., He, Y., and Gong, G. (2013). PANDA: a pipeline toolbox for analyzing brain diffusion images. *Front. Hum. Neurosci.* 7:42. doi: 10.3389/fnhum.2013.00042

Doecke, J. D., Perez-Grijalba, V., Fandos, N., Fowler, C., Villemagne, V. L., Masters, C. L., et al. (2020). Total Aβ42/Aβ40 ratio in plasma predicts amyloid-PET status, independent of clinical AD diagnosis. *Neurology* 94, e1580–e1591. doi: 10.1212/WNL.0000000000009240

Dong, G., Yang, L., Li, C. R., Wang, X., Zhang, Y., Du, W., et al. (2020). Dynamic network connectivity predicts subjective cognitive decline: the Sino-Longitudinal Cognitive impairment and dementia study. *Brain Imaging Behav.* 14, 2692–2707. doi: 10.1007/s11682-019-00220-6

Dubois, B., Feldman, H. H., Jacova, C., Hampel, H., Molinuevo, J. L., Blennow, K., et al. (2014). Advancing research diagnostic criteria for Alzheimer's disease: the IWG-2 criteria. *Lancet Neurol.* 13, 614–629. doi: 10.1016/S1474-4422(14)70090-0

Gifford, K. A., Liu, D., Romano, R. III., Jones, R. N., and Jefferson, A. L. (2015). Development of a subjective cognitive decline questionnaire using item response theory: a pilot study. *Alzheimers Dement.* 1, 429–439. doi: 10.1016/j.dadm.2015.09.004

Guo, Q. H., Hong, Z., Shi, W. X., Sun, Y. M., and Lv, C. Z. (2006). Boston naming test in Chinese elderly, patient with mild cognitive impairment and Alzheimer's dementia. *Chinese Ment. Health J.* 20, 81–84. doi: 10.3321/j.issn:1000-6729.2006.02.003

Guo, Q. M., Jin, L. L., and Hong, Z. (2007). A specific phenomenon of animal fluency test in Chinese Elderly *Chinese Ment. Health J.* 12, 622–625. doi: 10.1016/j.conbuildmat.2005.08.001

Hanon, O., Vidal, J. S., Lehmann, S., Bombois, S., Allinquant, B., Treluyer, J. M., et al. (2018). Plasma amyloid levels within the Alzheimer's process and correlations with central biomarkers. *Alzheimers Dement.* 14, 858–868. doi: 10.1016/j.jalz.2018.01.004

Hardy, J. A., and Higgins, G. A. (1992). Alzheimer's disease: the amyloid cascade hypothesis. *Science* 256, 184–185. doi: 10.1126/science.1566067

Hilal, S., Akoudad, S., van Duijn, C. M., Niessen, W. J., Verbeek, M. M., Vanderstichele, H., et al. (2017). Plasma amyloid-β levels, cerebral small vessel disease, and cognition: the Rotterdam study. *J. Alzheimers Dis.* 60, 977–987. doi: 10.3233/JAD-170458

Hilal, S., Wolters, F. J., Verbeek, M. M., Vanderstichele, H., Ikram, M. K., Stoops, E., et al. (2018). Plasma amyloid-β levels, cerebral atrophy and risk of dementia: a population-based study. *Alzheimers Res. Ther* 10:63. doi: 10.1186/s13195-018-0395-6

Honig, L. S., Vellas, B., Woodward, M., Boada, M., Bullock, R., Borrie, M., et al. (2018). Trial of solanezumab for mild dementia due to Alzheimer's disease. *N. Engl. J. Med.* 378, 321–330. doi: 10.1056/NEJMoa1705971

Jack, C. R. Jr., Bennett, D. A., Blennow, K., Carrillo, M. C., Dunn, B., Haeberlein, S. B., et al. (2018). NIA-AA research framework: toward a biological definition of Alzheimer's disease. *Alzheimers Dement.* 14, 535–562. doi: 10.1016/j.jalz.2018.02.018

Jak, A. J., Bondi, M. W., Delano-Wood, L., Wierenga, C., Corey-Bloom, J., Salmon, D. P., et al. (2009). Quantification of five neuropsychological approaches to defining mild cognitive impairment. *Am. J. Geriatr. Psychiatry* 17, 368–375. doi: 10.1097/JGP.0b013e31819431d5

Janelidze, S., Stomrud, E., Palmqvist, S., Zetterberg, H., van Westen, D., Jeromin, A., et al. (2016). Plasma β-amyloid in Alzheimer's disease and vascular disease. *Sci. Rep.* 6:26801. doi: 10.1038/srep26801

Jessen, F., Amariglio, R. E., Buckley, R. F., van der Flier, W. M., Han, Y., Molinuevo, J. L., et al. (2020). The characterisation of subjective cognitive decline. *Lancet Neurol.* 19, 271–278. doi: 10.1016/S1474-4422(19)30368-0

Jessen, F., Amariglio, R. E., van Boxtel, M., Breteler, M., Ceccaldi, M., Chetelat, G., et al. (2014). A conceptual framework for research on subjective cognitive decline in preclinical Alzheimer's disease. *Alzheimers Dement.* 10, 844–852. doi: 10.1016/j.jalz.2014.01.001

Jiang, Y., Tian, Y., and Wang, Z. (2019). Age-related structural alterations in human amygdala networks: reflections on correlations between white matter structure and effective connectivity. *Front. Hum. Neurosci.* 13:214. doi: 10.3389/fnhum.2019.00214

Kaffashian, S., Tzourio, C., Soumare, A., Dufouil, C., Mazoyer, B., Schraen-Maschke, S., et al. (2015). Association of plasma β-amyloid with MRI markers of structural brain aging the 3-City Dijon study. *Neurobiol. Aging* 36, 2663–2670. doi: 10.1016/j.neurobiolaging.2015.03.016

Kantarci, K., Murray, M. E., Schwarz, C. G., Reid, R. I., Przybelski, S. A., Lesnick, T., et al. (2017). White-matter integrity on DTI and the pathologic staging of Alzheimer's disease. *Neurobiol. Aging* 56, 172–179. doi: 10.1016/j.neurobiolaging.2017.04.024

Kleinschmidt, M., Schoenfeld, R., Gottlich, C., Bittner, D., Metzner, J. E., Leplow, B., et al. (2016). Characterizing aging, mild cognitive impairment, and dementia

with blood-based biomarkers and neuropsychology. *J. Alzheimers Dis.* 50, 111–126. doi: 10.3233/JAD-143189

Li, X., Wang, X., Su, L., Hu, X., and Han, Y. (2019). Sino Longitudinal Study on Cognitive Decline (SILCODE): protocol for a Chinese longitudinal observational study to develop risk prediction models of conversion to mild cognitive impairment in individuals with subjective cognitive decline. *BMJ Open* 9:e028188. doi: 10.1136/bmjopen-2018-028188

Li, X. Y., Tang, Z. C., Sun, Y., Tian, J., Liu, Z. Y., and Han, Y. (2016). White matter degeneration in subjective cognitive decline: a diffusion tensor imaging study. *Oncotarget* 7, 54405–54414. doi: 10.18632/oncotarget.10091

Lippa, S. M., Yeh, P. H., Gill, J., French, L. M., Brickell, T. A., and Lange, R. T. (2019). Plasma tau and amyloid are not reliably related to injury characteristics, neuropsychological performance, or white matter integrity in service members with a history of traumatic brain injury. *J. Neurotrauma* 36, 2190–2199. doi: 10.1089/neu.2018.6269

Llado-Saz, S., Atienza, M., and Cantero, J. L. (2015). Increased levels of plasma amyloid-β are related to cortical thinning and cognitive decline in cognitively normal elderly subjects. *Neurobiol. Aging* 36, 2791–2797. doi: 10.1016/j.neurobiolaging.2015.06.023

Long, J. M., and Holtzman, D. M. (2019). Alzheimer disease: an update on pathobiology and treatment strategies. *Cell* 179, 312–339. doi: 10.1016/j.cell.2019.09.001

Lovheim, H., Elgh, F., Johansson, A., Zetterberg, H., Blennow, K., Hallmans, G., et al. (2017). Plasma concentrations of free amyloid β cannot predict the development of Alzheimer's disease. *Alzheimers Dement.* 13, 778–782. doi: 10.1016/j.jalz.2016.12.004

Mayo, C. D., Mazerolle, E. L., Ritchie, L., Fisk, J. D., Gawryluk, J. R., and Alzheimer's Disease Neuroimaging Initiative (2017). Longitudinal changes in microstructural white matter metrics in Alzheimer's disease. *Neuroimage Clin.* 13, 330–338. doi: 10.1016/j.nicl.2016.12.012

Mitchell, A. J., Beaumont, H., Ferguson, D., Yadegarfar, M., and Stubbs, B. (2014). Risk of dementia and mild cognitive impairment in older people with subjective memory complaints: meta-analysis. *Acta Psychiatr. Scand.* 130, 439–451. doi: 10.1111/acps.12336

Mori, S., Oishi, K., Jiang, H., Jiang, L., Li, X., Akhter, K., et al. (2008). Stereotaxic white matter atlas based on diffusion tensor imaging in an ICBM template. *Neuroimage* 40, 570–582. doi: 10.1016/j.neuroimage.2007.12.035

Nakamura, A., Kaneko, N., Villemagne, V. L., Kato, T., Doecke, J., Dore, V., et al. (2018). High performance plasma amyloid-β biomarkers for Alzheimer's disease. *Nature* 554, 249–254. doi: 10.1038/nature25456

Niwa, K., Carlson, G. A., and Iadecola, C. (2000). Exogenous A β1-40 reproduces cerebrovascular alterations resulting from amyloid precursor protein overexpression in mice. *J. Cereb. Blood Flow Metab.* 20, 1659–1668. doi: 10.1097/00004647-200012000-00005

Palmqvist, S., Insel, P. S., Zetterberg, H., Blennow, K., Brix, B., Stomrud, E., et al. (2018). Accurate risk estimation of β-amyloid positivity to identify prodromal Alzheimer's disease: cross-validation study of practical algorithms. *Alzheimers Dement.* 15, 194–204. doi: 10.1016/j.jalz.2018.08.014

Park, L., Zhou, P., Koizumi, K., El Jamal, S., Previti, M. L., Van Nostrand, W. E., et al. (2013). Brain and circulating levels of Aβ 1-40 differentially contribute to vasomotor dysfunction in the mouse brain. *Stroke* 44, 198–204. doi: 10.1161/strokeaha.112.670976

Power, M. C., Su, D., Wu, A., Reid, R. I., Jack, C. R., Knopman, D. S., et al. (2019). Association of white matter microstructural integrity with cognition and dementia. *Neurobiol. Aging* 83, 63–72. doi: 10.1016/j.neurobiolaging.2019.08.021

Qin, L., Guo, Z., McClure, M. A., and Mu, Q. (2020). White matter changes from mild cognitive impairment to Alzheimer's disease: a meta-analysis. *Acta Neurol. Belg.* doi: 10.1007/s13760-020-01322-5. [Epub ahead of print].

Risacher, S. L., Fandos, N., Romero, J., Sherriff, I., Pesini, P., Saykin, A. J., et al. (2019). Plasma amyloid β levels are associated with cerebral amyloid and tau deposition. *Alzheimers Dement.* 11, 510–519. doi: 10.1016/j.dadm.2019.05.007

Schindler, S. E., Bollinger, J. G., Ovod, V., Mawuenyega, K. G., Li, Y., Gordon, B. A., et al. (2019). High-precision plasma β-amyloid 42/40 predicts current and future brain amyloidosis. *Neurology* 93, e1647–e1659. doi: 10.1212/WNL.0000000000008081

Slot, R. E. R., Sikkes, S. A. M., Berkhof, J., Brodaty, H., Buckley, R., Cavedo, E., et al. (2019). Subjective cognitive decline and rates of incident Alzheimer's disease and non-Alzheimer's disease dementia. *Alzheimers Dement.* 15, 465–476. doi: 10.1016/j.jalz.2018.10.003

Smith, S. M., Jenkinson, M., Johansen-Berg, H., Rueckert, D., Nichols, T. E., Mackay, C. E., et al. (2006). Tract-based spatial statistics: voxelwise analysis of multi-subject diffusion data. *Neuroimage* 31, 1487–1505. doi: 10.1016/j.neuroimage.2006.02.024

Smith, S. M., Jenkinson, M., Woolrich, M. W., Beckmann, C. F., Behrens, T. E., Johansen-Berg, H., et al. (2004). Advances in functional and structural MR image analysis and implementation as FSL. *Neuroimage* 23(Suppl. 1), S208–S219. doi: 10.1016/j.neuroimage.2004.07.051

Soares, J. M., Marques, P., Alves, V., and Sousa, N. (2013). A hitchhiker's guide to diffusion tensor imaging. *Front. Neurosci.* 7:31. doi: 10.3389/fnins.2013.00031

Sperling, R. A., Aisen, P. S., Beckett, L. A., Bennett, D. A., Craft, S., Fagan, A. M., et al. (2011). Toward defining the preclinical stages of Alzheimer's disease: recommendations from the National Institute on Aging-Alzheimer's Association workgroups on diagnostic guidelines for Alzheimer's disease. *Alzheimers Dement.* 7, 280–292. doi: 10.1016/j.jalz.2011.03.003

Sperling, R. A., Rentz, D. M., Johnson, K. A., Karlawish, J., Donohue, M., Salmon, D. P., et al. (2014). The A4 study: stopping AD before symptoms begin? *Sci. Transl. Med.* 6:228fs213. doi: 10.1126/scitranslmed.3007941

Strain, J. F., Smith, R. X., Beaumont, H., Roe, C. M., Gordon, B. A., Mishra, S., et al. (2018). Loss of white matter integrity reflects tau accumulation in Alzheimer disease defined regions. *Neurology* 91, e313–e318. doi: 10.1212/WNL.0000000000005864

Sun, Y., Wang, X. N., Wang, Y. S., Dong, H. M., Lu, J., Scheininger, T., et al. (2019). Anxiety correlates with cortical surface area in subjective cognitive decline: APOE epsilon 4 carriers versus APOE epsilon 4 non-carriers. *Alzheimers Res. Ther.* 11:10. doi: 10.1186/s13195-019-0505-0

Toledo, J. B., Shaw, L. M., and Trojanowski, J. Q. (2013). Plasma amyloid beta measurements - a desired but elusive Alzheimer's disease biomarker. *Alzheimers Res. Ther.* 5:8. doi: 10.1186/alzrt162

Verberk, I. M. W., Slot, R. E., Verfaillie, S. C. J., Heijst, H., Prins, N. D., van Berckel, B. N. M., et al. (2018). Plasma amyloid as prescreener for the earliest Alzheimer pathological changes. *Ann. Neurol.* 84, 648–658. doi: 10.1002/ana.25334

Vergallo, A., Megret, L., Lista, S., Cavedo, E., Zetterberg, H., Blennow, K., et al. (2019). Plasma amyloid β 40/42 ratio predicts cerebral amyloidosis in cognitively normal individuals at risk for Alzheimer's disease. *Alzheimers Dement.* 15, 764–775. doi: 10.1016/j.jalz.2019.03.009

Wang, J., Qiao, F., Shang, S., Li, P., Chen, C., Dang, L., et al. (2018). Elevation of plasma amyloid-β level is more significant in early stage of cognitive impairment: a population-based cross-sectional study. *J. Alzheimers Dis.* 64, 61–69. doi: 10.3233/JAD-180140

Xu, Y., Chen, K., Zhao, Q., Li, F., and Guo, Q. (2020). Short-term delayed recall of auditory verbal learning test provides equivalent value to long-term delayed recall in predicting MCI clinical outcomes: a longitudinal follow-up study. *Appl. Neuropsychol. Adult* 27, 73–81. doi: 10.1080/23279095.2018.1481067

Youn, Y. C., Kang, S., Suh, J., Park, Y. H., Kang, M. J., Pyun, J. M., et al. (2019). Blood amyloid-β oligomerization associated with neurodegeneration of Alzheimer's disease. *Alzheimers. Res. Ther.* 11:40. doi: 10.1186/s13195-019-0499-7

Zavaliangos-Petropulu, A., Nir, T. M., Thomopoulos, S. I., Reid, R. I., Bernstein, M. A., Borowski, B., et al. (2019). Diffusion MRI indices and their relation to cognitive impairment in brain aging: the updated multi-protocol approach in ADNI3. *Front. Neuroinform.* 13:2. doi: 10.3389/fninf.2019.00002

Zhao, Q., Guo, Q., Li, F., Zhou, Y., Wang, B., and Hong, Z. (2013). The Shape Trail Test: application of a new variant of the Trail making test. *PLoS ONE* 8:e57333. doi: 10.1371/journal.pone.0057333

Conflict of Interest: The authors declare that the research was conducted in the absence of any commercial or financial relationships that could be construed as a potential conflict of interest.

frontiers in Aging Neuroscience

ORIGINAL RESEARCH
published: 01 February 2021
doi: 10.3389/fnagi.2021.625843

Microstructural and Cerebral Blood Flow Abnormalities in Subjective Cognitive Decline Plus: Diffusional Kurtosis Imaging and Three-Dimensional Arterial Spin Labeling Study

*Zhongxian Yang[1,2], Yu Rong[2,3], Zhen Cao[2], Yi Wu[4], Xinzhu Zhao[1], Qiuxia Xie[1], Min Luo[1] and Yubao Liu[1]**

[1] Medical Imaging Center, Shenzhen Hospital, Southern Medical University, Shenzhen, China, [2] Medical Imaging Center, The Second Affiliated Hospital, Medical College of Shantou University, Shantou, China, [3] Department of Neurology, The People's Hospital of Gaozhou City, Maoming, China, [4] Department of Neurology, Shantou Central Hospital and Affiliated Shantou Hospital of Sun Yat-sen University, Shantou, China

Objective: To explore microstructural and cerebral blood flow (CBF) abnormalities in individuals with subjective cognitive decline plus (SCD plus) using diffusional kurtosis imaging (DKI) and three-dimensional (3D) arterial spin labeling (ASL).

Methods: Twenty-seven patients with SCD plus, 31 patients with amnestic mild cognitive impairment (aMCI), and 33 elderly controls (ECs) were recruited and underwent DKI and 3D ASL using a GE 3.0-T MRI. Mean kurtosis (MK), fractional anisotropy (FA), mean diffusivity (MD), and CBF values were acquired from 24 regions of interest (ROIs) in the brain, including the bilateral hippocampal (Hip) subregions (head, body, and tail), posterior cingulate cortex (PCC), precuneus, dorsal thalamus subregions (anterior nucleus, ventrolateral nucleus, and medial nucleus), lenticular nucleus, caput nuclei caudati, white matter (WM) of the frontal lobe, and WM of the occipital lobe. Pearson's correlation analysis was performed to assess the relationships among the DKI-derived parameters, CBF values, and key neuropsychological tests for SCD plus.

Results: Compared with ECs, participants with SCD plus showed a significant decline in MK and CBF values, mainly in the Hip head and PCC, and participants with aMCI exhibited more significant abnormalities in the MK and CBF values than individuals with ECs and SCD plus in multiple regions. Combined MK values showed better discrimination between patients with SCD plus and ECs than that obtained using CBF levels, with areas under the receiver operating characteristic (ROC) curve (AUC) of 0.874 and 0.837, respectively. Similarly, the AUC in discriminating SCD plus from aMCI patients obtained using combined MK values was 0.823, which was also higher than the combined AUC of 0.779 obtained using CBF values. Moreover, MK levels in the left Hip (h) and left PCC positively correlated with the auditory verbal learning test-delayed recall (AVLT-DR) score in participants with SCD plus. By contrast, only the CBF value in the left Hip head positively correlated with the AVLT-DR score.

OPEN ACCESS

Edited by:
Ying Han,
Xuanwu Hospital, Capital Medical University, China

Reviewed by:
Li Su,
University of Cambridge, United Kingdom
Mingrui Xia,
Beijing Normal University, China

***Correspondence:**
Yubao Liu
ybliu28@163.com

Received: *04 November 2020*
Accepted: *04 January 2021*
Published: *01 February 2021*

Citation:
Yang Z, Rong Y, Cao Z, Wu Y, Zhao X, Xie Q, Luo M and Liu Y (2021) Microstructural and Cerebral Blood Flow Abnormalities in Subjective Cognitive Decline Plus: Diffusional Kurtosis Imaging and Three-Dimensional Arterial Spin Labeling Study. Front. Aging Neurosci. 13:625843. doi: 10.3389/fnagi.2021.625843

Conclusions: Our results provide new evidence of microstructural and CBF changes in patients with SCD plus. MK may be used as an early potential neuroimaging biomarker and may be a more sensitive DKI parameter than CBF at the very early stage of Alzheimer's disease (AD).

Keywords: diffusional kurtosis imaging, arterial spin labeling, subjective cognitive decline plus, mild cognitive impairment, Alzheimer's disease

INTRODUCTION

Subjective cognitive decline (SCD), the first clinical manifestation in the Alzheimer's disease (AD) continuum, refers to a self-experienced cognitive capacity decline and has been shown to be associated with a high risk of conversion to AD (Tandetnik et al., 2015). As the cognitive function in patients with SCD is within normal limits, most neuropsychological evaluations find it difficult to capture the subtle cognitive decline, especially memory loss. Patients with SCD are twice as likely to develop mild cognitive impairment (MCI) than those without SCD (Mitchell et al., 2014). Previous studies have also shown that SCD patients present with atrophy in the hippocampus (Hip), the paraHip, the medial temporal, and the frontoparietal gray matter (GM) (van der Flier et al., 2004; Saykin et al., 2006; Wen et al., 2019); alterations in the white matter (WM) (Song et al., 2016); decline of brain metabolism (Jeong et al., 2017); accumulation of high β-amyloid (Aβ) (Snitz et al., 2013); and disruption of functional activity (Sun et al., 2016). These results showed that SCD, MCI, and AD are regarded as a spectrum of clinical disorders (Kiuchi et al., 2014; Yan et al., 2018; Reisberg et al., 2020). However, SCD may also be caused by many other factors in addition to the pathophysiology underlying AD, such as psychological factors, drug use, and other medical or neurological conditions (Perrotin et al., 2017). SCD plus, which leads to a higher risk of AD than SCD, may be a very early stage of AD that precedes amnestic MCI (aMCI). The features of SCD plus include (Jessen et al., 2014) subjective decline limited only to memory rather than other cognitive domains, complaints of SCD within the last 5 years, an age at onset of SCD $\geq$ 60 years, concerns (memory loss) associated with SCD, complaints of feeling worse than others in the same age group, confirmation of cognitive decline by an informant, and the presence of the apolipoprotein E-ε4 (APOE-ε4) genotype and other biomarker evidence for AD. Thus, identifying neuroimaging biomarkers for SCD plus is essential for early detection, early intervention, and reduction of the burden of dementia in the population.

Diffusion kurtosis imaging (DKI), developed based on diffusion tensor imaging (DTI), can provide additional metrics related to the non-Gaussianity of water diffusion, such as mean kurtosis (MK), axial kurtosis, and radial kurtosis (Jensen et al., 2005). Diffusion parameters, such as fractional anisotropy (FA) and mean diffusivity (MD), can also be obtained from DKI. As one of the main parameters of DKI, MK has been used to describe the microstructural complexity or heterogeneity of the tissue. It can assess the microstructure of both WM and GM, particularly GM (Jensen et al., 2005). FA is mostly used for assessing WM fiber tract integrity, and MD can assess microstructural alterations of GM and WM. DKI has shown great potential in diagnosing several disorders of the nervous system, such as neurodegenerative disease, brain infarction, gliomas, and mental illness (Guo et al., 2016; Zhao et al., 2016; Guan et al., 2019; Haopeng et al., 2020; Huang et al., 2020; McKenna et al., 2020). Previous studies have also reported that, in patients with MCI and AD, DKI can detect microstructural alterations in GM (Falangola et al., 2013; Gong et al., 2013; Struyfs et al., 2015; Chen et al., 2017), as well as in WM (Yuan et al., 2016; Gong et al., 2017; Song et al., 2019). Regarding GM and the subcortical nucleus, one study found that subjects with aMCI showed significant MK abnormalities in many regions, including the bilateral Hip, the thalamus, the putamen, and the globus pallidus. MD revealed the second most significant changes of the DKI parameters (Gong et al., 2017). Another study showed that MK and FA could detect microstructural complexities, such as the globus pallidus, the substantia nigra, and the red nucleus, in healthy participants (Gong et al., 2014). Thus, estimating microstructural changes related to GM and the subcortical nucleus is very important to improve the early diagnosis of AD. However, no report has investigated SCD plus-related DKI regarding microstructural alterations. Arterial spin labeling (ASL) is a valuable non-invasive imaging tool that is used to magnetically label arterial blood water as an endogenous contrast medium tracer to quantify cerebral blood flow (CBF; Alsop et al., 2000). Compared with PET imaging, the major advantages of ASL are its lower costs, its non-invasiveness, and its reduced scan time (Henriksen et al., 2012), particularly at 3.0 Tesla (T) (Yoshiura et al., 2009). As the technology underlying MRI hardware and software continues to improve, ASL-measured CBF is becoming an increasingly widely available method for distinguishing MCI/AD from elderly controls (ECs) with comparable accuracy to PET (Haller et al., 2016; Fällmar et al., 2017; Riederer et al., 2018). The most consistent findings in ASL studies from patients with MCI and AD have revealed brain hypoperfusion mainly in the posterior cingulate cortex (PCC) and the precuneus (Pr), as well as in the bilateral parietal and temporal areas. Many previous studies have described the association of changes and vulnerable regions with MCI/AD [including Hip, PCC, Pr, dorsal thalamus (DT), nuclei basales, WM of the frontal lobe (FLWM) and WM of the occipital lobe (OLWM), particularly Hip, PCC, and Pr] by structural MRI, DTI, magnetic resonance spectroscopy, and functional MRI (Pennanen et al., 2004; De Jong et al., 2008; Van Straaten et al., 2008; Jahng et al., 2011; Yang Z. X. et al., 2012). These findings suggest that MCI and/or AD are caused by damage not to a single brain area but to multiple areas of the brain. With advanced

MRI techniques, DKI and ASL may supply microstructural and hemodynamic information at the early stage of AD. Additionally, the underlying mechanism regarding which imaging metrics (MK, FA, MD, and CBF) changed first in subjects with SCD plus must be precisely elaborated. Furthermore, changes in CBF in subjects with SCD plus are rarely reported, particularly when combined with substructural measures. To our best knowledge, the diagnostic performance of DKI and ASL in assessing brain microstructural and CBF alterations in subjects with SCD plus has not been investigated.

To enhance our knowledge of the underlying dementia processes, facilitate an early diagnosis, guide clinical trials, and understand the characteristics of the pathophysiological basis of the SCD plus stage, in the current study, we aimed to evaluate brain microstructural and CBF changes in patients with SCD plus using DKI and three-dimensional (3D) ASL imaging measured in multiple brain regions to determine how these regions are altered in this stage. Additionally, we also assessed the relationships between DKI-derived parameters, CBF values, and key neuropsychological test scores among patients with SCD plus.

MATERIALS AND METHODS

Human Subjects and Neuropsychological Testing

Ninety-one participants were recruited for this study from September 2017 to July 2019, including 27 patients with SCD plus, 31 patients with aMCI, and 33 age- and sex-matched ECs. The SCD plus and aMCI groups were recruited from the outpatient clinic, and ECs were recruited through a medical examination center. Before enrollment, written informed consent was obtained from all participants or their legal guardians. The study was approved by the Ethical Committee of Second Affiliated Hospital of Shantou University Medical College (Registration No. 2017-10), and all procedures were performed in accordance with the Declaration of Helsinki. All participants provided their demographic and clinical data (including age, sex, education, and living conditions) and had undergone cognitive evaluations by two expert neurologists. All participants had also undergone a series of standardized neuropsychological evaluations, including tests that measured cognitive functioning in the domains of memory, executive functioning, attention, and language. The basic set of psychological tests included the Mini-Mental State Examination (MMSE; Folstein et al., 1975), the Montreal Cognitive Assessment (MoCA, Beijing version; Lu et al., 2011), the Clinical Dementia Rating (CDR) Scale (Morris, 1993), the Global Deterioration Scale (GDS; Reisberg et al., 1982), Chinese Huashan version of auditory verbal learning test [AVLT, including AVLT-immediate recall, AVLT-delayed recall (AVLT-DR), and AVLT-recognition; Xu et al., 2020], activities of daily living assessment (Barberger-Gateau et al., 1992), the Hachinski Ischemic Scale (HIS; Larson et al., 1989), and the Hamilton Depression Rating Scale (HAM-D; Worboys, 2013).

Patients with SCD plus met the following criteria proposed by the SCD Initiative (SCD-I; Jessen et al., 2014): (a) self-reported persistent cognitive complaints of memory decline $\leq$ 5 years; (b) confirmation of cognitive decline by an informant; (c) onset age $\geq$ 60 years; (d) feeling worse than peers of the same age and concerns associated with SCD; (e) performance within normal limits for age and educational attainment on the MMSE, MoCA, and ADL after sex, age, and education adjustment; (f) a GDS score of 2; (g) a CDR score of 0; and (h) a HIS score < 4. Patients with aMCI met the criteria defined by Petersen et al. (2001) as follows: (a) memory decline according to clinical judgment or confirmed by an informant; (b) objective decline of episodic memory, determined by the neurologists' judgment based on a neuropsychological evaluation; (c) normal general cognitive function determined by a CDR score of 0.5, a GDS score of 3, a HIS score < 4, and an MMSE $\geq$ 24; and (d) ineligibility for AD according to the criteria of the National Institute of Neurological and Communicative Diseases and Stroke-Alzheimer's Disease and Related Disorders Association. ECs were defined as those without subjective cognitive complaints, without physical, psychiatric, or neurological disorders, without abnormal findings on conventional brain MRI, and with normal performance on neuropsychological tests. The exclusion criteria for all participants included the following: (a) a HIS score > 4; (b) a HAM-D score > 24; (c) specific causes of WM lesions, such as multiple sclerosis, epilepsy, encephalitis, tumors, cranial arteritis, and trauma; (d) AD, Lewy body dementia, frontotemporal dementia, or Parkinson's disease; (e) intracranial hemorrhage, Moyamoya disease, aphasia, hepatic encephalopathy, systemic diseases, and signs of normal pressure hydrocephalus or carbon monoxide poisoning; and (f) alcohol dependence and other psychoactive substance abuse history, serious medical disease, or mental illness.

Conventional MRI, DKI, and ASL Data Acquisition

Conventional MRI scans were acquired using a standard quadrature eight-channel head coil with a 3.0T MRI scanner (Signa HDx Twin speed; GE Medical Systems, Milwaukee, Wisconsin, USA). Next, we changed the host scanning method from the clinical mode to the research mode. Using the research mode, DKI scanning parameters were obtained using an echo-planar imaging (EPI) sequence as follows: repetition time (TR)/echo time (TE) = 6,000 ms/109 ms; diffusion gradient pulse duration = 32.2 ms; diffusion gradient separation = 38.8 ms; slice thickness = 4 mm; slice gap = 0 mm; field of view (FOV) = 240 × 240 mm; matrix = 256 × 256; number of excitations (NEX) = 1; b-values = 0, 1,000, 2,000 s/mm^2; diffusion-encoding directions = 15; number of slices = 24; and scanning time = 250 s. 3D pseudocontinuous ASL images were acquired using the following scanning parameters: TR/TE = 4,580/9.8 ms; FOV = 240 × 240 mm; slice thickness = 4 mm; slice gap = 0 mm; postlabeling delay time = 1,500 ms; and scanning time = 266 s. We used the oblique sagittal position as the scanning standard. The bottom of the slab was positioned at the bottom of the cerebellum, and the top of the slab was positioned at the top of the semioval center, with coverage of mostly the cerebrum. Cushions and cotton balls were used to reduce subject movement and scanner noise.

Image Post-processing and Data Analysis

All raw DKI images were transferred to a GE Advantage Workstation version 4.6 (GE Medical System, Rue de la Minière, France) and post-processed in the FuncTool software package 9.0 environment. Before DKI parametric maps were generated, all raw data were automatically performed with the affine and rigid body registrations to the B0 image for reducing EPI distortion, eddy-current distortion, and head motion. Next, the DKI parameters, including MK, FA, and MD, were automatically generated by the DKI software, which was developed using the Applied Science Laboratory of GE (http://www.nitrc.org/projects/dke/). Quantitative MK, FA, and MD maps were generated from the DKI model with b-values = 0, 1,000, and 2,000 s/mm^2 by the following equation:

$$\ln[S_{(n,b)}/S_0] = -b\sum_{i=1}^{3}\sum_{j=1}^{3} n_i n_j D_{ij} + \frac{1}{6}b^2 D^{-2}\sum_{i=1}^{3}\sum_{j=1}^{3}\sum_{k=1}^{3}\sum_{l=1}^{3} n_i n_j n_k n_l W_{ijkl}$$

$S_{(n,b)}$ represents the diffusion encoding direction n and diffusion signal intensity for diffusion weighting b, and S_0 represents the signal intensity for minimally diffusion-weighted imaging (b_0). D_{ij} and W_{ijkl} represent the components of the diffusion and kurtosis tensors, respectively. A description of the DKI analysis method can be found in our previous studies (Guo et al., 2016; Zheng et al., 2017).

The raw ASL data were also transferred to the GE Advantage Workstation 4.6 and post-processed by the ReadyView software (version 10.3.67) in the FuncTool environment. The CBF values were reacquired before the quality control step as follows. First, a high level of background suppression was used to suppress the surrounding static tissue around the pseudocontinuous labeling pulse. Second, motion correction, temporal and spatial filtering, and partial volume effect correction were performed. Subsequently, the CBF values were calculated by intensity normalization. A quantitative CBF map was generated based on the following equation:

$$\mathrm{CBF} = \frac{\lambda\left(1-e^{\frac{-t_{sat}}{T_{1g}}}\right)}{2\alpha T_{1b}\left(1-e^{\frac{\tau}{T_{1b}}}\right)}\frac{\Delta S}{S_0}e^{\frac{\omega}{T_{1b}}}$$

where T_{1b} represents the T1 relaxation time of the blood, T_{1g} represents the T1 relaxation time of the GM, t_{sat} represents the duration time of the saturation pulse performed before imaging, α represents the labeling efficiency, λ represents the brain/blood partition coefficient, τ represents the labeling duration, and ω represents the post-labeling delay time. In addition, CBF analysis has been described in previous studies (Wu et al., 2014; Zhao et al., 2016).

Regions of interest (ROIs) were carefully delineated and analyzed by two independently experienced neuroradiologists who were blinded to the status of the subjects with B0 images as references. Each ROI was selected on the maximum level of the structures that were best demonstrated according to each corresponding parametric map. When the ROIs were placed, we also tried to avoid major vascular structures, cerebrospinal fluids, and interhemispheric regions. To ensure that the same locations were extracted from each subject, the ROIs (the ROI areas ranged from 18 to 22 mm^2) in the brain were mainly obtained from 24 regions using mirror symmetry tools (after drawing an ROI in the left hemisphere, it is copied and then left-to-right flipped across the brain midline to obtain the same shape and size of ROI) derived from FuncTool software, as shown in **Figures 1A–P** for the DKI maps and **Supplementary Figures 1A–D** for the ASL maps. These regions included the bilateral Hip subregions [head; Hip (h), body; Hip (b) and tail; Hip (t)], PCC, Pr, and DT subregions [anterior nucleus: DT (a), ventrolateral nucleus: DT (vl), and medial nucleus (m)], lenticular nucleus (LN), caput nuclei caudati (CNC), FLWM, and OLWM. The values of MK, FA, MD, and CBF were calculated and averaged across three replicates by two senior radiologists to correct and reduce offset errors. After that, an intraclass correlation coefficient (ICC) analysis was performed to further assess the consistency of MK, FA, MD, and CBF obtained from the measurements taken by two neuroradiologists (Landis and Koch, 1977). Usually, ICC values >0.75 are regarded as a good correlation.

Statistical Analysis

Statistical analyses were performed using Statistical Package for Social Science version 25.0 (SPSS Inc., Chicago, III, USA) and GraphPad Prism software 8.3.0 (https://www.graphpad.com/scientific-software/prism). Sex distributions were analyzed using the chi-squared test among the three groups. One-way ANOVA was used to assess age, education, imaging metrics, and neuropsychological test results among patients with SCD plus, patients with aMCI, and ECs. ANOVA with false discovery rate (FDR) correction as described by the Benjamini–Hochberg method was used to compare the DKI parameters and CBF values using the R soft package (R for Windows v. 4.0.3, https://cran.r-project.org) among three groups to compare the symmetrical ROIs in the left and right cerebral hemisphere, respectively. The non-parametric Kruskal–Wallis test was used if the data were not normally distributed. Pearson's correlation analysis was used to evaluate the relationship between the measured parameters and the key neuropsychological scores for SCD plus controlled for age, sex, and the education level as nuisance covariates. The measured neuroimaging parameters were determined by receiver operating characteristic (ROC) curve analysis to evaluate the diagnostic accuracy. To determine the predictive accuracy of the parameters in discriminating patients with SCD plus from patients with aMCI or ECs, the area under the ROC curve (AUC) was calculated to assess the diagnostic ability of the imaging metrics, both alone and in combination. Combined AUC values were obtained by binary logistic regression. All data were expressed as means ± SD, and the values of $p < 0.05$ were considered statistically significant.

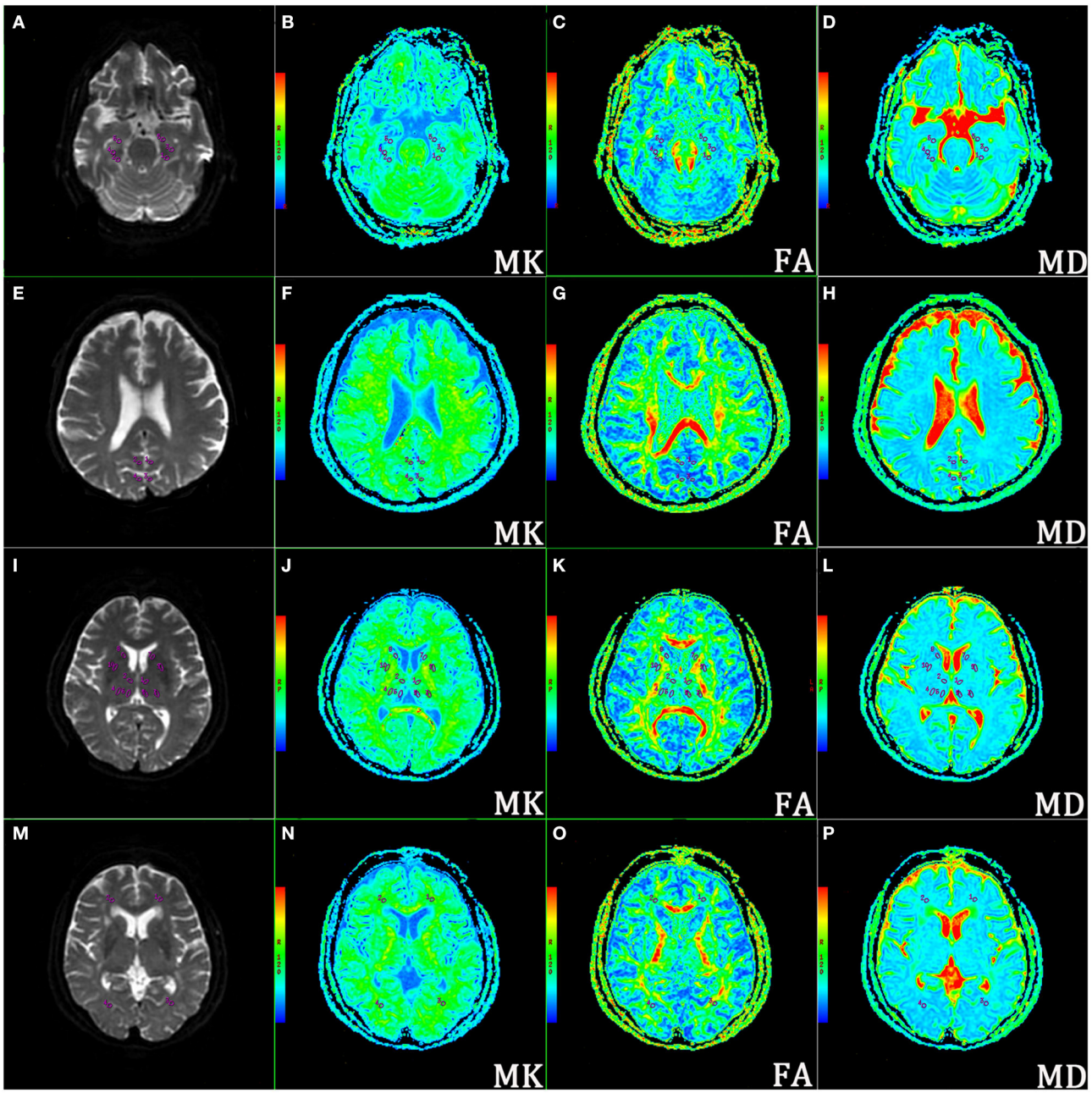

FIGURE 1 | Representative locations of the regions of interest (ROIs) on corresponding axial b0 images and mean kurtosis (MK), fractional anisotropy (FA), and mean diffusivity (MD) maps. **(A–D)** ROIs of the bilateral hippocampal (Hip) subregions (head, body, and tail); **(E–H)** ROIs of bilateral posterior cingulate cortex (PCC) and precuneus (Pr); **(I–L)** ROIs of bilateral dorsal thalamus (DT) subregions (anterior nucleus, ventrolateral nucleus, and medial nucleus), lenticular nucleus (LN), and caput nuclei caudati (CNC); **(M–P)** ROIs of bilateral white matter of the occipital lobe (OLWM) and white matter of the frontal lobe (FLWM).

RESULTS

Demographic and Key Neuropsychological Assessment Scores in Participants With SCD Plus, aMCI, and ECs

The baseline demographic characteristics and key neuropsychological scores of the studied participants are presented in **Table 1**. No significant differences were found with respect to age, sex, and education among participants with SCD plus, aMCI, and ECs. The AVLT, MMSE, and MoCA scores decreased gradually among the three groups. Only the MMSE scores and MoCA scores were lower in participants with aMCI than in ECs. Only the AVLT-DR scores between patients with SCD plus and ECs were significantly different. The SCD plus

TABLE 1 | Demographic information and key neuropsychological tests for participants with SCD plus, participants with aMCI, and ECs.

Characteristics	Groups			χ^2/F/t	*P*-value	Multiple comparison *p*-values		
	ECs (n = 33)	*SCD plus (n = 27)*	*aMCI (n = 31)*			*SCD plus vs. ECs*	*SCD plus vs. aMCI*	*aMCI vs. ECs*
Age (years)	67.061 ± 6.067	68.074 ± 7.014	68.645 ± 6.879	0.227	0.826	0.929	0.986	0.642
Sex (M/F)	13/20	12/15	12/19	0.615	0.735	0.803	0.599	0.439
Education (years)	10.061 ± 1.619	9.852 ± 1.747	9.907 ± 1.578	0.632	0.557	0.951	0.248	0.055
AVLT-immediate recall (score)	8.727 ± 1.292	8.111 ± 1.281	7.335 ± 1.119	5.035	<0.01	0.069	0.053	<0.01
AVLT-delayed recall (score)	8.970 ± 1.185	7.556 ± 0.934	5.387 ± 1.066	11.396	<0.001	<0.05	<0.01	<0.001
AVLT-recognition (score)	10.061 ± 1.166	9.370 ± 1.214	8.419 ± 1.317	6.653	<0.01	0.081	<0.01	<0.05
MMSE (score)	27.879 ± 1.783	26.856 ± 2.135	25.386 ± 1.317	3.722	<0.05	0.168	0.056	<0.05
MoCA (score)	26.324 ± 2.205	25.763 ± 2.573	22.365 ± 3.216	5.808	<0.01	0.159	0.052	<0.01

group had significantly lower AVLT-DR and AVLT-recognition scores than the aMCI group. Additionally, all subgroups of the AVLT scores, including AVLT-immediate recall scores, AVLT-DR scores, and AVLT-recognition scores, were significantly lower in patients with aMCI than in ECs.

Changes in the DKI Parameters and CBF in Participants With SCD Plus, aMCI, and ECs

Mean kurtosis, FA, MD, and CBF values were acquired in the bilateral Hip (h), Hip (b), Hip (t), PCC, Pr, DT (a), DT (vl), DT (m), LN, CNC, FLWM, and OLWM among the three groups (**Supplementary Raw Data**). **Supplementary Table 1** showed the ICC analysis of DKI and 3D-ASL parameters in the left and right ROIs in individuals with SCD plus, aMCI, and ECs. The ICC values showed that all measurements were > 0.75 and were regarded as relatively reliable among the three groups. Therefore, the levels of MK, FA, MD, and CBF were used for subsequent statistical analysis. **Figures 2A,B**, **3A,B** showed the differences in all the measured MK and CBF values from the left and right ROIs among the three groups, respectively. **Supplementary Figures 2A,B, 3A,B** showed the differences in the FA and MD values from the left and right ROIs among the three groups, respectively. **Supplementary Tables 2–4** showed the differences in the MK, FA, MD, and CBF values from all the ROIs among the three groups.

Compared with the ECs, participants with SCD plus had significantly lower MK values in the bilateral Hip (h), left PCC, left DT (a), and left OLWM. Decreased CBF values were also found in the left Hip (h) and bilateral PCC. However, the MK and CBF values were increased in the left Pr. The FA value was decreased only in the left OLWM. No significant MD changes were found in any ROI between the two groups.

Compared with ECs, participants with aMCI had a lower level of MK in the bilateral Hip (h), left Hip (b), bilateral PCC, bilateral DT (a), left DT (vl), bilateral OLWM, and left CNC. Similarly, the level of CBF was decreased in the bilateral Hip (h), bilateral PCC, bilateral DT (a), left OLWM, left CNC, and left FLWM. The FA levels were also decreased in the bilateral PCC, left Pr, bilateral OLWM, and bilateral FLWM. Additionally, the MD values were elevated in the left Hip (h), left PCC, left DT (a), and left OLWM. No significant differences in the MD values were found in any right ROIs between the two groups.

Compared with participants with SCD plus, patients with aMCI had lower MK levels in the bilateral PCC and left Pr. Decreased FA values in the right OLWM along with the CBF levels in the left Pr and the left DT (a) were also observed. No significant differences were found in the MD values in any ROIs, the FA values in the left ROIs, or the CBF levels in the right ROIs between the two groups.

Diagnostic Performance of the MK and CBF Values and Their Correlations With Key Neuropsychological Scores From Patients With SCD Plus

The above results showed that the changes in the DKI and the ASL parameters in patients with SCD plus and patients with aMCI are multiregional, particularly the MK and CBF values. Thus, combined AUC values with multiple subregions, rather than a single AUC, might better distinguish among the groups, provide a better cumulative accuracy, and supply more useful clinical information. Therefore, we mainly evaluated the changes in MK or CBF, which could serve as a good imaging biomarker for a more accurate discrimination of patients with SCD plus from ECs or patients with aMCI using the ROC curve analysis. When we used a single AUC, we found that the MK values in the left Hip (h) had the best group discriminability, with an AUC of 0.768 (95% CI: 0.648–0.887) for the "SCD plus vs. ECs" comparison, while the CBF value in the left Pr had the best group discriminability, with an AUC of 0.751 (95% CI: 0.629–0.874) for the "SCD plus vs. aMCI" comparison. However, based on the combined AUC analysis method, the combined AUC (**Figure 4A**) in discriminating patients with SCD plus from ECs obtained using the MK levels of the bilateral Hip (h), left PCC, left Pr, left DT (a), and left OLWM increased to 0.874 (95% CI: 0.783–0.966), while the combined AUC (**Figure 4B**) in discriminating the two groups obtained using the CBF values in the left Hip (h), left PCC, left Pr, and right PCC increased to 0.837 (95% CI: 0.737–0.937). Similarly, the combined AUC (**Figure 4C**) in distinguishing patients with SCD plus from patients with aMCI obtained using the MK

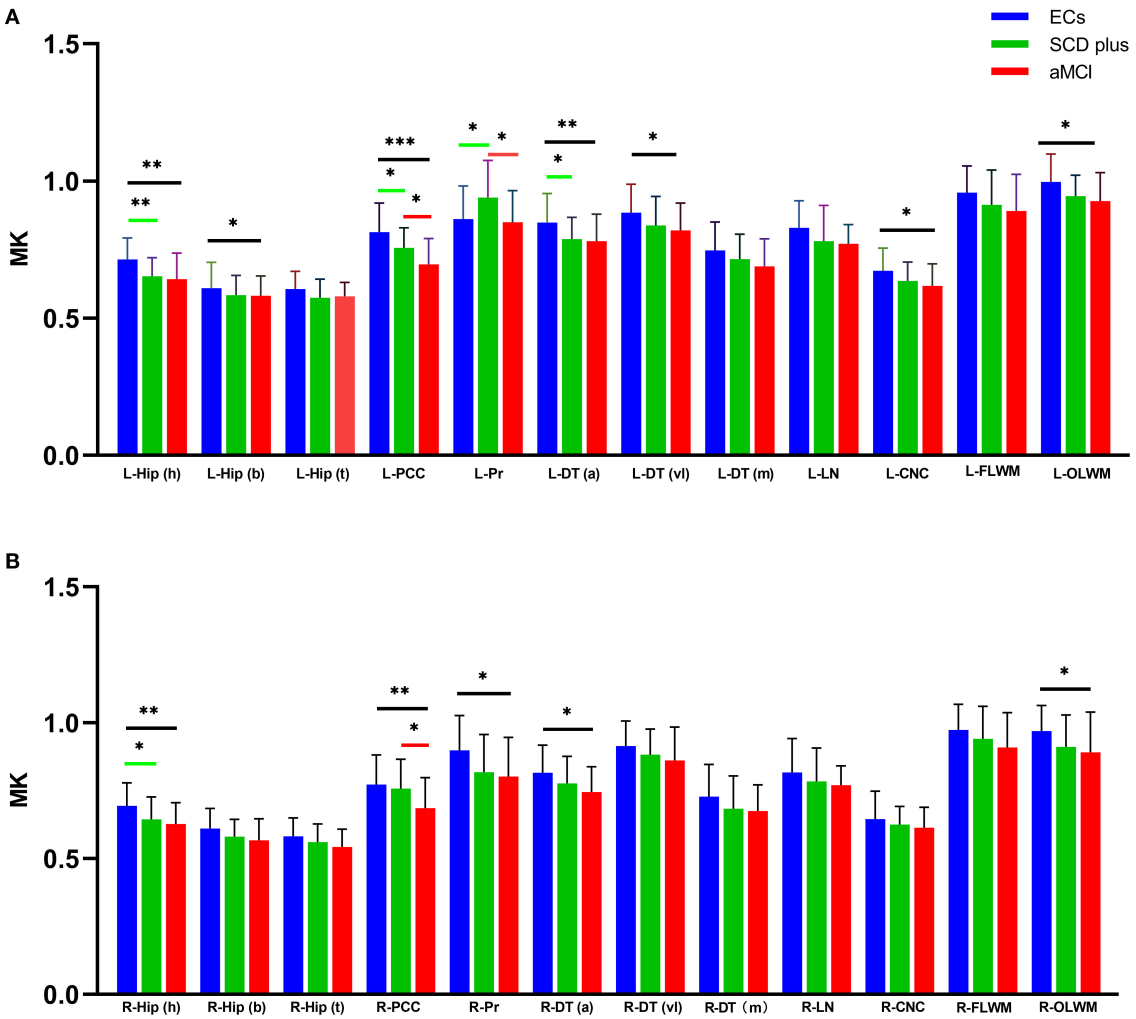

FIGURE 2 | Groups differences in all measured MK values from the left **(A)** and right **(B)** ROIs. *$p < 0.05$, **$p < 0.01$, and ***$p < 0.001$. [false discovery rate (FDR)-corrected].

values in the left PCC, left Pr, and right PCC increased to 0.823 (95% CI: 0.718–0.928). The combined AUC (**Figure 4D**) in distinguishing patients with SCD plus from patients with aMCI obtained using the CBF values in the left Pr and left DT (a) increased to 0.779 (95% CI: 0.660–0.898). Furthermore, correlation analyses between key cognitive scores and MK/CBF values were performed for patients with SCD plus after adjusting for age, sex, and education levels. Positive correlations were found between the AVLT-DR score and the MK values in the left Hip (h) ($r = 0.423$; $p = 0.028$) and in the left PCC ($r = 0.393$; $p = 0.042$) (**Figures 5A,B**, respectively). However, the CBF level was positively correlated with the AVLT-DR score ($r = 0.386$; $p = 0.046$) only in the left Hip (h) (**Figure 5C**). No significant correlations were found between the remaining DKI or ASL parameters in these regions and key cognitive scores in patients with SCD plus.

DISCUSSION

Subjective cognitive decline is known to be pervasive in elderly individuals older than 65 years (∼25–56%), and approximately half of them remain cognitively stable (Jonker et al., 2000). Although SCD is associated with a risk of dementia, the rate of development to MCI/AD is relatively low due to its heterogeneity (Perrotin et al., 2017). To the best of our knowledge, this is the first study to investigate brain tissue microstructural and perfusion changes, including those in bilateral Hip and DT subfields, in patients with SCD plus. In this study, we used the DKI and 3D-ASL techniques, which combine features from different regional distributions of imaging metrics, combine output data from multiple voxels, and generate a wealth of information. Thus, we could detect the CBF and microstructural abnormality distribution in different brain regions and obtain

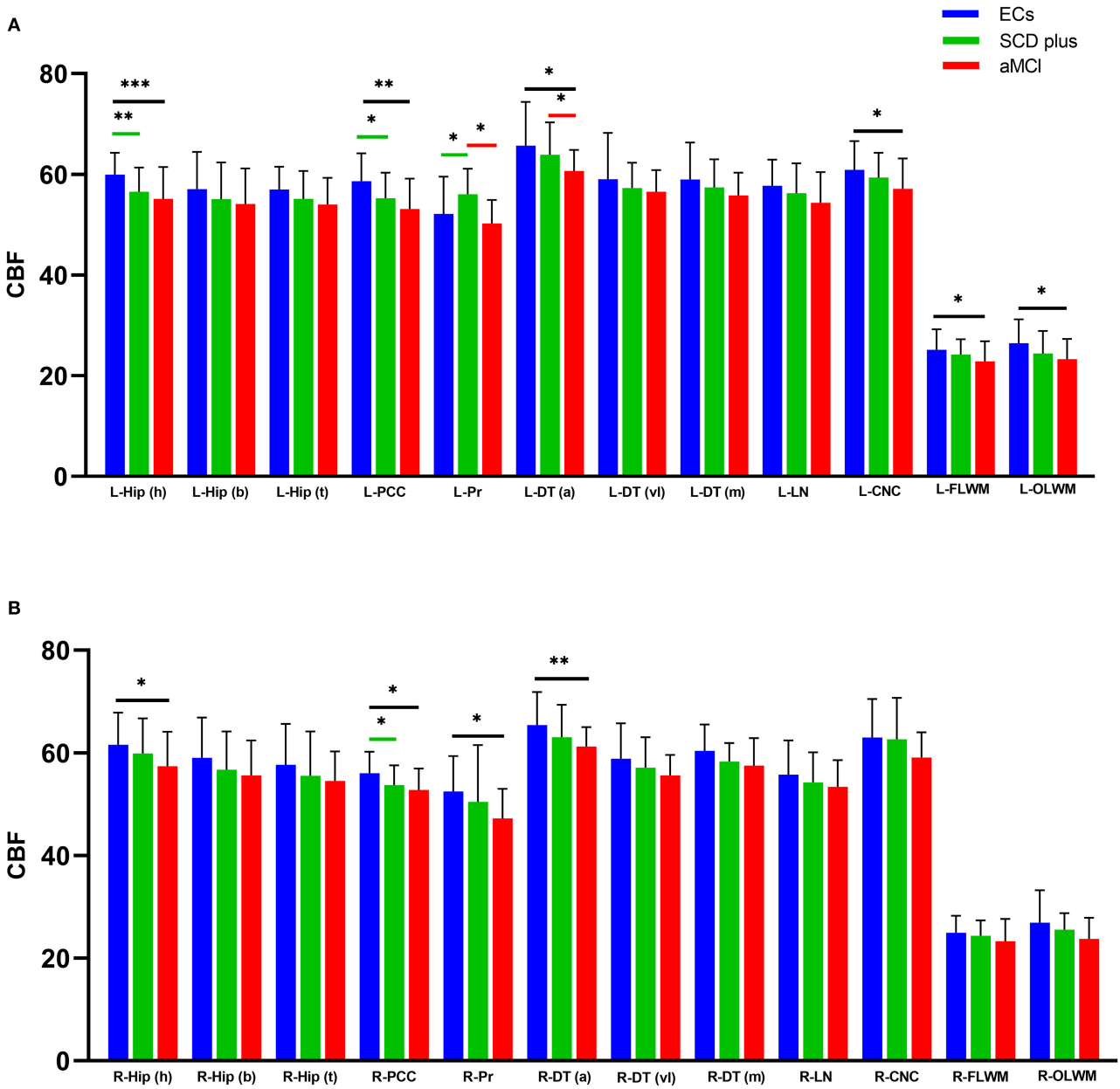

FIGURE 3 | Groups differences in all the measured cerebral blood flow (CBF unit: ml/100g/min) values from the left **(A)** and right **(B)** ROIs. *$p < 0.05$, **$p < 0.01$, and ***$p < 0.001$. (FDR-corrected).

highly accurate diagnostic information using these practical techniques. First, our main findings showed that SCD plus group exhibits microstructural and perfusion alterations in multiple encephalic regions, particularly in the Hip (h) and PCC. The aMCI group exhibited more significant abnormalities in MK and CBF values than ECs and patients with SCD plus in multiple regions. These results indicated that patients with SCD plus might share a similar trend of microstructural and perfusion changes with individuals with aMCI (Sánchez-Benavides et al., 2018; Hao et al., 2020). Second, MK seems to contribute more significantly than CBF to the diagnostic performance in patients with SCD plus when combined AUC values are used. Moreover, the changes in MK values in the left Hip (h) and left PCC of the SCD plus group were positively correlated with AVLT-DR scores, whereas the CBF value in only the left Hip (h) was positively correlated with the AVLT-DR scores.

In a previous series of studies, patients with aMCI and patients with AD demonstrated aberrant microstructures according to DKI (Struyfs et al., 2015; Chen et al., 2017; Cheng et al., 2018; Song et al., 2019) or CBF changes according to ASL (Yoshiura

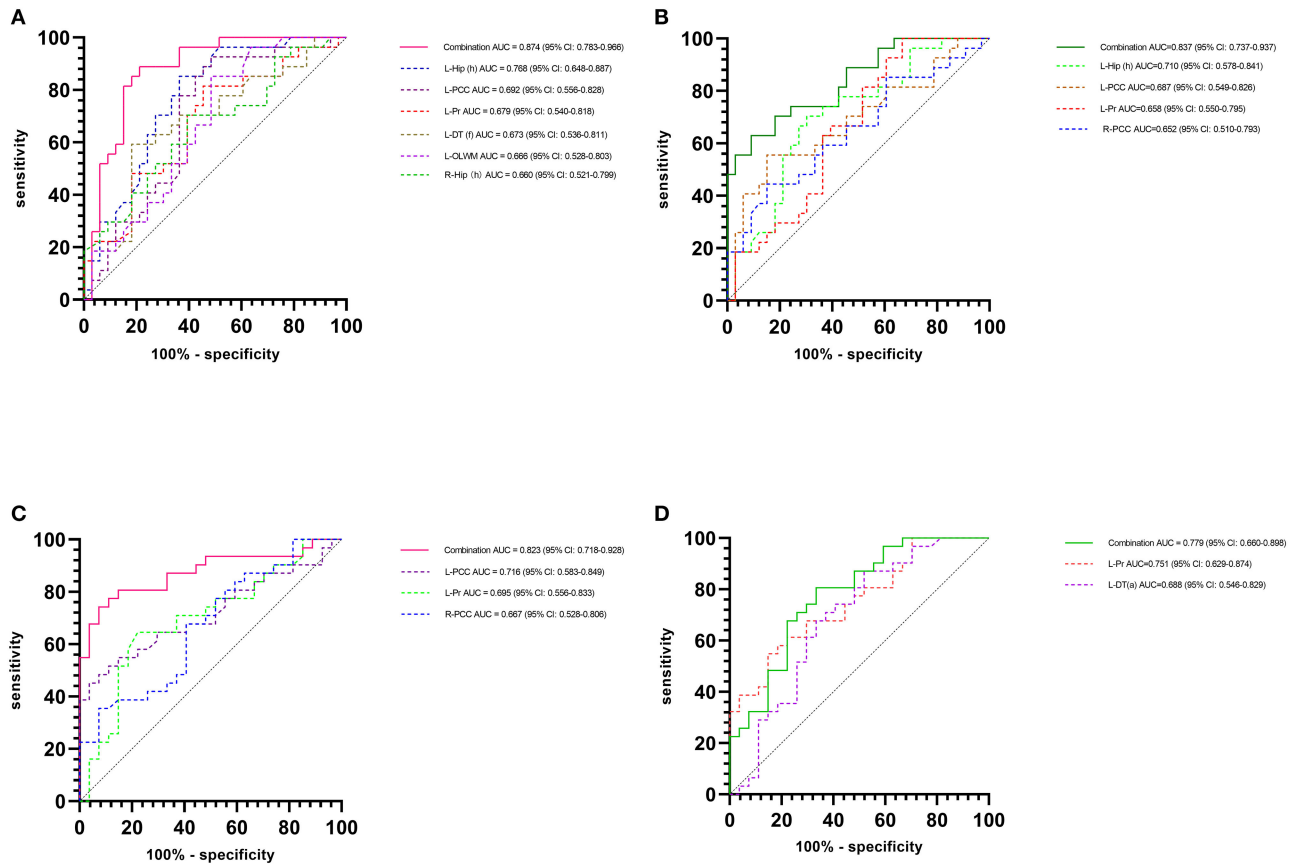

FIGURE 4 | Receiver operating characteristic (ROC) curves of the discriminatory power between subjective cognitive decline (SCD) plus and elderly controls (ECs)/amnestic mild cognitive impairment (aMCI) individuals. The combined area under the ROC curve (AUC) in discriminating SCD plus from ECs obtained with MK **(A)** and CBF values **(B)**. Combined AUC in discriminating participants with SCD plus from participants with aMCI obtained with MK values **(C)** and CBF values **(D)**.

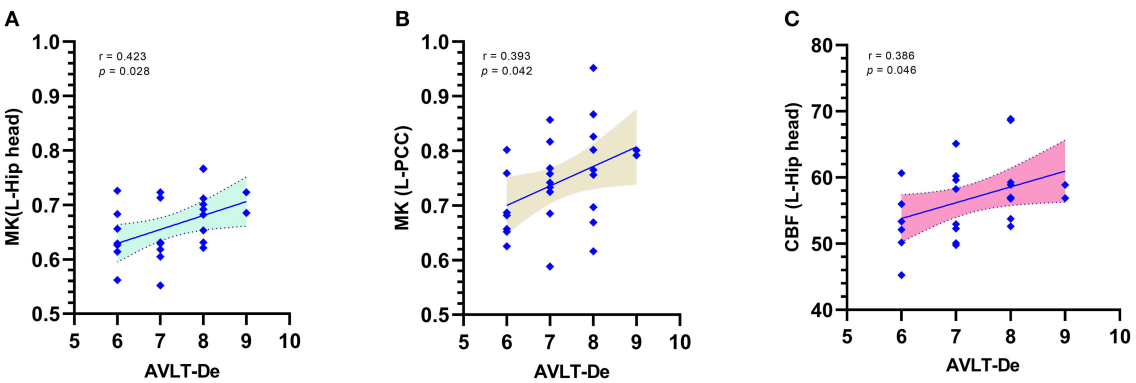

FIGURE 5 | Correlations between the MK/CBF values and Auditory Verbal Learning Test-delayed recall (AVLT-DR) scores for SCD plus after adjusting for the effects of age, sex, and the education level. Positive correlations between the AVLT-DR scores and MK levels in the L-Hip head **(A)** and L-PCC **(B).** Positive correlations between the AVLT-DR scores and CBF in the L-Hip head **(C)**. AVLT-DR, Auditory Verbal Learning Test-delayed recall.

et al., 2009; Haller et al., 2016; Fällmar et al., 2017; Riederer et al., 2018) in many brain regions. In this study, we also observed CBF and microstructural abnormalities in the Hip, PCC, Pr, OLWM, DT, FLWM, and CNC regions in patients with aMCI, a finding that agrees with findings from the previous study describing the association of changes in these regions with the likelihood of AD. Two studies investigated SCD-related ASL findings, and the results were inconsistent. One study showed

that, compared with ECs, patients with SCD had decreased CBF in the medial orbitofrontal cortex and increased CBF in the right putamen (Hays et al., 2018), while the other study found no discrepancy in the total CBF between patients with SCD and ECs (de Eulate et al., 2017). Our study showed decreased CBF values in the left Hip (h), bilateral PCC, and increased CBF in the left Pr. The inconsistent results were compared with our results due to the inclusion criteria being different (our study population is SCD plus, while the others mainly chose patients with SCD). Another possible reason was the different scanning protocols and parameters used, or different post-processing analysis method performed, which might also make the results different. Additionally, different sample sizes can also lead to different results. However, our main purpose was to explore brain microstructural changes and CBF alterations in patients with SCD plus, as well as their relationships with key neurocognitive scores. Additionally, we compared the advantages of MK and CBF in distinguishing patients with SCD plus from ECs or patients with aMCI.

Alzheimer's disease is a diffuse neurodegenerative disease involving many brain regions, including GM and WM (Cappa et al., 2001). As a relatively new MRI technique, DKI is sufficiently sensitive for detecting brain microstructural changes in GM and WM simultaneously, similar to ASL. In this study, MK and CBF values showed more robust and significant changes than FA or MD values among the three groups. MK, the most commonly used DKI parameter, is related to the complexity of the microstructure and is considered a complex micro index. Theoretically, non-Gaussian water molecule diffusion in the brain tissue microarchitecture is restricted by many factors, such as the cell membrane, axons, and myelin (Hansen, 2019). Degeneration and atrophy of nerve cells lead to a decline in the complexity of the brain microstructure during the course of AD, leading to a decrease in the values of MK in turn. The decline in CBF values may reflect neuronal dysfunction and synaptic failure (Hays et al., 2016). A controversy remains regarding whether the CBF values measured by ASL show hypoperfusion or hyperperfusion patterns in SCD or MCI, and the hypoperfusion/hyperperfusion areas may involve different brain regions simultaneously (Alexopoulos et al., 2012; Bron et al., 2014; Leeuwis et al., 2017; Chau et al., 2020; Kim et al., 2020). Compared with those of ECs, we found decreased MK values in the bilateral Hip (h), left PCC, left DT (a), and left OLWM and increased MK values in the left Pr in participants with SCD plus. Significantly, lower CBF values in the left Hip (h) and bilateral PCC and higher CBF values in the left Pr were also observed in participants with SCD plus. Both evaluations revealed changes in most regions in the left cerebral hemisphere, particularly in vulnerable areas such as the Hip, PCC, and Pr. The affected brain regions (left cerebral hemisphere) more often tend to involve functional asymmetry and cerebral laterality (Agarwal et al., 2016). The pronounced asymmetry between the left and right brain hemispheres is a hallmark of humans because the left cerebral hemisphere is more involved in language skills, memory function, and logic problems (Keller et al., 2018; Corballis, 2019). Furthermore, the AUC in discriminating patients with SCD plus from ECs obtained using the combined MK values was 0.874, which was higher than the combined AUC of 0.837 obtained using the CBF values. The combined AUC in discriminating patients with SCD plus from patients with aMCI obtained using the MK levels was 0.823, which was also higher than the combined AUC of 0.779 obtained with the CBF levels. These results showed that the combined AUC obtained with MK values made more significant contributions to the classification between participants with SCD plus and ECs/participants with aMCI than those calculated using the CBF values. Several possible reasons may explain this observation. The pathological changes in AD are accompanied by significantly reduced numbers of neurons as nerve cells undergo degeneration and atrophy (Morris and Price, 2001). The course of AD is associated with disruptions to mitochondrial function, decreased apoptosis, and decreased neuronal shrinkage (Leuner et al., 2007). Previous articles have suggested that mitochondrial dysfunction plays a key role in the early stage of AD (Cadonic et al., 2016). Several reports have indicated that the mitochondrial function is disrupted in patients with MCI and patients with AD (Delbarba et al., 2016; Mastroeni et al., 2017; Terada et al., 2020). Mitochondrial dysfunction, in turn, accelerates the production of reactive oxygen species, further contributing to oxidative stress and damage to cell membrane lipids, intracellular proteins, and DNA (Butterfield and Boyd-Kimball, 2020). The accumulation of β-amyloid (Aβ) peptides decreases ATP production, impairs the mitochondrial membrane potential, and exacerbates oxidative stress (Swomley and Butterfield, 2015). Moreover, reactive oxygen species generated from mitochondrial dysfunction can drive amyloidogenesis and tau phosphorylation, thus generating a cycle that decreases energy utilization for normal cellular function and drives the pathology and progression of nerve cell death in AD (Lejri et al., 2019). Due to neuron cell body death and loss and neuronal atrophy and apoptosis, the complexity of the brain tissue decreases, resulting in lowered MK as part of this process. MK is also a good probe for the presence of cell microstructural impairment and is sensitive in detecting the underlying Aβ-induced pathology (De Santis et al., 2011). Therefore, the slight modification in MK values found in this study could be an early reflection of mitochondrial energy metabolism dysfunction in conditions with a fairly high risk of the very early stage of AD. The decrease in the CBF value can also be attributed to the inhibited activity or dysfunction of neurons or neural synaptic loss, as well as the changes in neural activity due to the progression of AD pathology (Hays et al., 2016). As described above, the mitochondria, which convert oxygen and a metabolic product of glucose into ATP to generate energy, are the powerhouses of cells, including neurons; mitochondrial dysfunction in nerve cells will cause them to function improperly. As the activity of the neuron changes, the demand for oxygen decreases (mainly in the mitochondria), and the demand for energy (ATP production) decreases further, moderating the CBF (Ogoh and Ainslie, 2009). Therefore, mitochondrial dysfunction may precede changes in CBF. Our results also suggested that changes in MK are observed slightly before those in CBF. Measurement of the changes in MK seems to be a promising method for evaluating participants at risk for dementia because they may reflect early and impaired

energetic metabolism in the brain, a factor involved in the pathogenesis of AD. Of course, although we excluded vascular factors (high blood pressure, diabetes, and WM hyperintensity lesion burden), diagnosis biases, heterogeneity factors, and/or individual variability of disease expression with SCD plus should still be considered (Jessen et al., 2014). Additionally, limitations related to the ASL techniques, including their sensitivity to transit time effects and relatively low spatial and space resolution, must also be considered.

Our results are consistent with the findings of a study reporting that GM hypometabolism and microstructural abnormalities are the core characteristics of aMCI/AD (Gong et al., 2017). The focal areas in patients with SCD plus and patients with aMCI are mainly in the limbic system, including the Hip, PCC, and Pr, which are predominantly related to neuropsychological activities such as learning, memory, the generation of emotional responses, and behavior (Zhang et al., 2014). Moreover, the ROI analysis revealed significantly altered values of MK/CBF in the DT and basal ganglia of participants with SCD plus that also play an important role in attention and working memory (Cho et al., 2014; de Bourbon-Teles et al., 2014). Compared with the ECs, the individuals in the SCD plus group showed the most obvious abnormalities in MK/CBF values in the Hip (h). Previous studies have shown that the Hip (h) plays a key role in memory performance and is the most sensitive and vulnerable region to memory impairment among the Hip subregions (Ouchi et al., 1998; Yakushev et al., 2010). It may also be the earliest region susceptible to pathological changes in patients with aMCI/AD (Gordon et al., 2013; Luo et al., 2014). The detection of reduced MK/CBF in the left Hip is also consistent with the previous results of DKI/ASL perfusion studies (Dai et al., 2009; Binnewijzend et al., 2013; Gong et al., 2017; Cheng et al., 2018; Song et al., 2019). As a limbic cortical region, the PCC is affected relatively early in the pathological progression to AD. The decreased MK/CBF levels may be tightly associated with the derangement of neurometabolism and neuronal/axonal loss (Thomas et al., 2019). The exploration of other ROIs, such as in the left DT (a) and left OLWM, could also aid in improving predictions. However, decreased or increased MK/CBF can coexist in the early stages of the neurodegenerative process. Our results showed that compared with ECs, patients with SCD plus had higher values of MK/CBF only in the left Pr. The hyperperfusion patterns are thought to reflect compensatory mechanisms for the neuronal damage that occurs early in the disease process to counterbalance cognitive decline (Sierra-Marcos, 2017). We speculate that the beneficial effects of elevated MK/CBF values on cognition may be destroyed in patients with SCD plus because decreased MK/CBF values in most brain regions and only higher levels of MK/CBF in the left Pr cannot support normal cognitive function within regions associated with normal aging and AD risk. Alternatively, the results may reflect changes in the brain microvasculature due to increased neurocerebrovascular reactivity without any significant gains in the cognitive performance (Miki et al., 2009; Sam et al., 2016). Therefore, the present observations combining MK and CBF measures clearly support this view.

Consistent with most previous DTI studies, we observed decreased FA and increased MD values between the EC and aMCI groups. However, decreased FA values were found only in the left OLWM in the EC and SCD plus groups. Additionally, abnormalities in FA values were found only in the right OLWM between participants with SCD plus and participants with aMCI. FA represents directional variation in water molecule diffusion, whereas MD reflects the average diffusivity. The observed decline in FA and increase in MD values parallel the axonal loss and myelin damage that restrict the random motion of water molecules along the nerve fiber tracts. Consistent with a previous study, our results demonstrate that FA is preferable to MD for evaluating WM (OLWM and FLWM) (Medina et al., 2006; Chen et al., 2009). Additionally, FA is more advantageous than MD in detecting early-stage AD (Yang D. W. et al., 2012). In general, among the three DKI parameters, MK is the most sensitive metric for capturing GM and WM microstructural abnormalities in patients with SCD plus and aMCI (Struyfs et al., 2015).

Furthermore, significant correlations between AVLT-DR scores and MK values in the left Hip (h) and PCC were observed in patients with SCD plus. A correlation only between the AVLT-DR scores and CBF values was observed in the left Hip. We assumed that the decreased MK/CBF in the left Hip (h) may be crucial for progressive memory impairment. Our correlation results also support the possibility that changes in MK are the strongest predictor of cognitive impairment scores, particularly in the very early stage of AD.

CONCLUSION

Several limitations of this study should be noted. First, as a cross-sectional study, few SCD plus patients were included. The sample size should be increased, and a longitudinal study of this study population is needed to identify early neuroimaging biomarkers for the prediction of AD. Second, patients with AD were not included in our study; therefore, the continuous spectrum of AD could not be fully explored. Further research should be designed with more participants to assess the distinction among SCD plus converters, SCD plus non-converters, and probable AD. Third, the inclusion criteria for SCD plus were based on the number of SCD plus features met; typically, patients are expected to meet more than three (Jessen et al., 2014). Although the MK level is emerging as a very useful imaging marker in AD because it may strongly relate to the presence of an underlying amyloid pathology and neurodegeneration, we did not test the statuses of APOE-ε4, tau protein, or Aβ, reflecting a limitation and lack of completeness in our study. Incorporating examinations of these objective biomarkers associated with AD pathology may be more important for detecting patients with SCD plus. Finally, multimodal imaging techniques and more advanced post-processed methods (Zhang et al., 2016; Jiskoot et al., 2019) would yield a more comprehensive understanding for elucidating the pathophysiologic mechanisms underlying SCD plus (Parker et al., 2020; Wang et al., 2020).

In summary, our results suggest that DKI and ASL can provide effective information to detect the characteristics of

CBF and microstructure abnormalities in patients with SCD plus. MK may provide valuable information and function as one of the earliest potential neuroimaging biomarkers associated with AD. Changes in the MK value in the Hip (h) and PCC appear to represent an optimal, effective, and potentially useful non-invasive disease biomarker of the preclinical phase of AD.

DATA AVAILABILITY STATEMENT

The original contributions presented in the study are included in the article/**Supplementary Material**, further inquiries can be directed to the corresponding author/s.

ETHICS STATEMENT

The studies involving human participants were reviewed and approved by the Ethical Committee of Second Affiliated Hospital of Shantou University Medical College (Registration No. 2017-10). The patients/participants provided their written informed consent to participate in this study.

AUTHOR CONTRIBUTIONS

ZY, YR, and ZC: designed the study and collected the data. YR, YW, and ZC: collected the data. XZ, QX, and ML: performed the statistical analysis. ZY and YL: conceived and designed the experiments and prepared the manuscript. All authors contributed to the article and approved the submitted version.

FUNDING

This study was supported by the National Natural Science Foundation of China (Grant No: 81671660), the Natural Science Foundation of Guangdong Province (Grant No: 2018A030310154), the Medical Science Research Foundation of Guangdong Province (Grant No: A2017532), Science and Technology Project of Shenzhen (Grant No: JCYJ20170307144338570), Clinical Research Startup Program of Southern Medical University by High-level University Construction Funding of Guangdong Provincial Department of Education (Grant No: LC2016PY061), and Shenzhen Hospital of Southern Medical University, Research Promotion Funds for the Key Discipline Construction Program (Grant No: ZDXKKYTS011).

ACKNOWLEDGMENTS

We thank Dr. Long Qian from GE Healthcare for help in solving some MR technical problems and related consultation.

SUPPLEMENTARY MATERIAL

The Supplementary Material for this article can be found online at: https://www.frontiersin.org/articles/10.3389/fnagi.2021.625843/full#supplementary-material

REFERENCES

Agarwal, S., Stamatakis, E. A., Geva, S., and Warburton, E. A. (2016). Dominant hemisphere functional networks compensate for structural connectivity loss to preserve phonological retrieval with aging. *Brain Behav.* 6:e00495. doi: 10.1002/brb3.495

Alexopoulos, P., Sorg, C., Förschler, A., Grimmer, T., Skokou, M., Wohlschläger, A., et al. (2012). Perfusion abnormalities in mild cognitive impairment and mild dementia in Alzheimer's disease measured by pulsed arterial spin labeling MRI. *Eur. Arch. Psychiatry Clin. Neurosci.* 262, 69–77. doi: 10.1007/s00406-011-0226-2

Alsop, D. C., Detre, J. A., and Grossman, M. (2000). Assessment of cerebral blood flow in Alzheimer's disease by spin-labeled magnetic resonance imaging. *Ann. Neurol.* 47, 93-100. doi: 10.1002/1531-8249(200001)47:1<93::AID-ANA15>3.0.CO;2-8

Barberger-Gateau, P., Commenges, D., Gagnon, M., Letenneur, L., Sauvel, C., and Dartigues, J. F. (1992). Instrumental activities of daily living as a screening tool for cognitive impairment and dementia in elderly community dwellers. *J. Am. Geriatr. Soc.* 40, 1129–1134. doi: 10.1111/j.1532-5415.1992.tb01802.x

Binnewijzend, M. A., Kuijer, J. P., Benedictus, M. R., van der Flier, W. M., Wink, A. M., Wattjes, M. P., et al. (2013). Cerebral blood flow measured with 3D pseudocontinuous arterial spin-labeling MR imaging in Alzheimer disease and mild cognitive impairment: a marker for disease severity. *Radiology* 267, 221–230. doi: 10.1148/radiol.12120928

Bron, E. E., Steketee, R. M., Houston, G. C., Oliver, R. A., Achterberg, H. C., Loog, M., et al. (2014). Diagnostic classification of arterial spin labeling and structural MRI in presenile early stage dementia. *Hum. Brain Mapp.* 35, 4916–4931. doi: 10.1002/hbm.22522

Butterfield, D. A., and Boyd-Kimball, D. (2020). Mitochondrial oxidative and nitrosative stress and alzheimer disease. *Antioxidants* 9, 1–22. doi: 10.3390/antiox9090818

Cadonic, C., Sabbir, M. G., and Albensi, B. C. (2016). Mechanisms of mitochondrial dysfunction in Alzheimer's disease. *Mol. Neurobiol.* 53, 6078–6090. doi: 10.1007/s12035-015-9515-5

Cappa, A., Calcagni, M. L., Villa, G., Giordano, A., Marra, C., De Rossi, G., et al. (2001). Brain perfusion abnormalities in Alzheimer's disease: comparison between patients with focal temporal lobe dysfunction and patients with diffuse cognitive impairment. *J. Neurol. Neurosurg. Psychiatry* 70, 22–27. doi: 10.1136/jnnp.70.1.22

Chau, A. C. M., Cheung, E. Y. W., Chan, K. H., Chow, W. S., Shea, Y. F., Chiu, P. K. C., et al. (2020). Impaired cerebral blood flow in type 2 diabetes mellitus - a comparative study with subjective cognitive decline, vascular dementia and Alzheimer's disease subjects. *Neuroimage Clin.* 27:102302. doi: 10.1016/j.nicl.2020.102302

Chen, T. F., Chen, Y. F., Cheng, T. W., Hua, M. S., Liu, H. M., and Chiu, M. J. (2009). Executive dysfunction and periventricular diffusion tensor changes in amnesic mild cognitive impairment and early Alzheimer's disease. *Hum. Brain Mapp.* 30, 3826–3836. doi: 10.1002/hbm.20810

Chen, Y., Sha, M., Zhao, X., Ma, J., Ni, H., Gao, W., et al. (2017). Automated detection of pathologic white matter alterations in Alzheimer's disease using combined diffusivity and kurtosis method. *Psychiatry Res. Neuroimaging* 264, 35–45. doi: 10.1016/j.pscychresns.2017.04.004

Cheng, J. X., Zhang, H. Y., Peng, Z. K., Xu, Y., Tang, H., Wu, J. T., et al. (2018). Divergent topological networks in Alzheimer's disease: A diffusion kurtosis imaging analysis. *Transl. Neurodegener.* 7:10. doi: 10.1186/s40035-018-0115-y

Cho, H., Kim, J. H., Kim, C., Ye, B. S., Kim, H. J., Yoon, C. W., et al. (2014). Shape changes of the basal ganglia and thalamus in Alzheimer's disease: a three-year longitudinal study. *J. Alzheimers Dis.* 40, 285–295. doi: 10.3233/JAD-132072

Corballis, M. C. (2019). Evolution of cerebral asymmetry. *Prog. Brain Res.* 250, 153–178. doi: 10.1016/bs.pbr.2019.04.041

Dai, W., Lopez, O. L., Carmichael, O. T., Becker, J. T., Kuller, L. H., and Gach, H. M. (2009). Mild cognitive impairment and alzheimer disease: patterns of altered cerebral blood flow at MR imaging. *Radiology* 250, 856–866. doi: 10.1148/radiol.2503080751

de Bourbon-Teles, J., Bentley, P., Koshino, S., Shah, K., Dutta, A., Malhotra, P., et al. (2014). Thalamic control of human attention driven by memory and learning. *Curr. Biol.* 24, 993–999. doi: 10.1016/j.cub.2014.03.024

de Eulate, R. G., Goñi, I., Galiano, A., Vidorreta, M., Recio, M., Riverol, M., et al. (2017). Reduced cerebral blood flow in mild cognitive impairment assessed using phase-contrast MRI. *J. Alzheimers Dis.* 58, 585–595. doi: 10.3233/JAD-161222

De Jong, L. W., Van Der Hiele, K., Veer, I. M., Houwing, J. J., Westendorp, R. G. J., Bollen, E. L. E. M., et al. (2008). Strongly reduced volumes of putamen and thalamus in Alzheimer's disease: an MRI study. *Brain* 131, 3277–3285. doi: 10.1093/brain/awn278

De Santis, S., Gabrielli, A., Palombo, M., Maraviglia, B., and Capuani, S. (2011). Non-Gaussian diffusion imaging: a brief practical review. *Magn. Reson. Imaging* 29, 1410–1416. doi: 10.1016/j.mri.2011.04.006

Delbarba, A., Abate, G., Prandelli, C., Marziano, M., Buizza, L., Arce Varas, N., et al. (2016). Mitochondrial alterations in peripheral mononuclear blood cells from Alzheimer's disease and mild cognitive impairment patients. *Oxid. Med. Cell. Longev.* 2016:5923938. doi: 10.1155/2016/5923938

Falangola, M. F., Jensen, J. H., Tabesh, A., Hu, C., Deardorff, R. L., Babb, J. S., et al. (2013). Non-Gaussian diffusion MRI assessment of brain microstructure in mild cognitive impairment and Alzheimer's disease. *Magn. Reson. Imaging* 31, 840–846. doi: 10.1016/j.mri.2013.02.008

Fällmar, D., Haller, S., Lilja, J., Danfors, T., Kilander, L., Tolboom, N., et al. (2017). Arterial spin labeling-based Z-maps have high specificity and positive predictive value for neurodegenerative dementia compared to FDG-PET. *Eur. Radiol.* 27, 4237–4246. doi: 10.1007/s00330-017-4784-1

Folstein, M. F., Folstein, S. E., and McHugh, P. R. (1975). "Mini-mental state". A practical method for grading the cognitive state of patients for the clinician. *J. Psychiatr. Res.* 12, 189–198. doi: 10.1016/0022-3956(75)90026-6

Gong, N. J., Chan, C. C., Leung, L. M., Wong, C. S., Dibb, R., and Liu, C. (2017). Differential microstructural and morphological abnormalities in mild cognitive impairment and Alzheimer's disease: evidence from cortical and deep gray matter. *Hum. Brain Mapp.* 38, 2495–2508. doi: 10.1002/hbm.23535

Gong, N. J., Wong, C. S., Chan, C. C., Leung, L. M., and Chu, Y. C. (2013). Correlations between microstructural alterations and severity of cognitive deficiency in Alzheimer's disease and mild cognitive impairment: a diffusional kurtosis imaging study. *Magn. Reson. Imaging* 31, 688–694. doi: 10.1016/j.mri.2012.10.027

Gong, N. J., Wong, C. S., Chan, C. C., Leung, L. M., and Chu, Y. C. (2014). Aging in deep gray matter and white matter revealed by diffusional kurtosis imaging. *Neurobiol. Aging* 35, 2203–2216. doi: 10.1016/j.neurobiolaging.2014.03.011

Gordon, B. A., Blazey, T., Benzinger, T. L., and Head, D. (2013). Effects of aging and Alzheimer's disease along the longitudinal axis of the hippocampus. *J. Alzheimers Dis.* 37, 41–50. doi: 10.3233/JAD-130011

Guan, J., Ma, X., Geng, Y., Qi, D., Shen, Y., Shen, Z., et al. (2019). Diffusion kurtosis imaging for detection of early brain changes in Parkinson's disease. *Front. Neurol.* 10:1285. doi: 10.3389/fneur.2019.01285

Guo, Y. L., Zhang, Z. P., Zhang, G. S., Kong, L. M., Rao, H. B., Chen, W., et al. (2016). Evaluation of mean diffusion and kurtosis MRI mismatch in subacute ischemic stroke: comparison with NIHSS score. *Brain Res.* 1644, 231–239. doi: 10.1016/j.brainres.2016.05.020

Haller, S., Zaharchuk, G., Thomas, D. L., Lovblad, K. O., Barkhof, F., and Golay, X. (2016). Arterial spin labeling perfusion of the brain: emerging clinical applications. *Radiology* 281, 337–356. doi: 10.1148/radiol.2016150789

Hansen, B. (2019). An introduction to kurtosis fractional anisotropy. *AJNR Am. J. Neuroradiol.* 40, 1638–1641. doi: 10.3174/ajnr.A6235

Hao, L., Sun, Y., Li, Y., Wang, J., Wang, Z., Zhang, Z., et al. (2020). Demographic characteristics and neuropsychological assessments of subjective cognitive decline (SCD) (plus). *Ann. Clin. Transl. Neurol.* 7, 1002–1012. doi: 10.1002/acn3.51068

Haopeng, P., Xuefei, D., Yan, R., Zhenwei, Y., Wei, H., Ziyin, W., et al. (2020). Diffusion kurtosis imaging differs between primary central nervous system lymphoma and high-grade glioma and is correlated with the diverse nuclear-to-cytoplasmic ratio: a histopathologic, biopsy-based study. *Eur. Radiol.* 30, 2125–2137. doi: 10.1007/s00330-019-06544-7

Hays, C. C., Zlatar, Z. Z., Campbell, L., Meloy, M. J., and Wierenga, C. E. (2018). Subjective cognitive decline modifies the relationship between cerebral blood flow and memory function in cognitively normal older adults. *J. Int. Neuropsychol. Soc.* 24, 213–223. doi: 10.1017/S135561771700087X

Hays, C. C., Zlatar, Z. Z., and Wierenga, C. E. (2016). The utility of cerebral blood flow as a biomarker of preclinical Alzheimer's disease. *Cell. Mol. Neurobiol.* 36, 167–179. doi: 10.1007/s10571-015-0261-z

Henriksen, O. M., Larsson, H. B., Hansen, A. E., Grüner, J. M., Law, I., and Rostrup, E. (2012). Estimation of intersubject variability of cerebral blood flow measurements using MRI and positron emission tomography. *J. Magn. Reson. Imaging* 35, 1290–1299. doi: 10.1002/jmri.23579

Huang, N. X., Zou, Z. Y., Xue, Y. J., and Chen, H. J. (2020). Abnormal cerebral microstructures revealed by diffusion kurtosis imaging in amyotrophic lateral sclerosis. *J. Magn. Reson. Imaging* 51, 554–562. doi: 10.1002/jmri.26843

Jahng, G. H., Xu, S., Weiner, M. W., Meyerhoff, D. J., Park, S., and Schuff, N. (2011). DTI studies in patients with Alzheimer's disease, mild cognitive impairment, or normal cognition with evaluation of the intrinsic background gradients. *Neuroradiology* 53. doi: 10.1007/s00234-011-0845-3

Jensen, J. H., Helpern, J. A., Ramani, A., Lu, H., and Kaczynski, K. (2005). Diffusional kurtosis imaging: the quantification of non-gaussian water diffusion by means of magnetic resonance imaging. *Magn. Reson. Med.* 53, 1432–1440. doi: 10.1002/mrm.20508

Jeong, H. S., Park, J. S., Song, I. U., Chung, Y. A., and Rhie, S. J. (2017). Changes in cognitive function and brain glucose metabolism in elderly women with subjective memory impairment: a 24-month prospective pilot study. *Acta Neurol. Scand.* 135, 108–114. doi: 10.1111/ane.12569

Jessen, F., Amariglio, R. E., van Boxtel, M., Breteler, M., Ceccaldi, M., Chételat, G., et al. (2014). A conceptual framework for research on subjective cognitive decline in preclinical Alzheimer's disease. *Alzheimers Dement.* 10, 844–852. doi: 10.1016/j.jalz.2014.01.001

Jiskoot, L. C., Panman, J. L., Meeter, L. H., Dopper, E. G. P., Donker Kaat, L., Franzen, S., et al. (2019). Longitudinal multimodal MRI as prognostic and diagnostic biomarker in presymptomatic familial frontotemporal dementia. *Brain* 142. doi: 10.1093/brain/awy288

Jonker, C., Geerlings, M. I., and Schmand, B. (2000). Are memory complaints predictive for dementia? A review of clinical and population-based studies. *Int. J. Geriatr. Psychiatry* 15, 983–991. doi: 10.1002/1099-1166(200011)15:11<983::AID-GPS238>3.0.CO;2-5

Keller, S. S., Roberts, N., Baker, G., Sluming, V., Cezayirli, E., Mayes, A., et al. (2018). A voxel-based asymmetry study of the relationship between hemispheric asymmetry and language dominance in Wada tested patients. *Hum. Brain Mapp.* 39, 3032–3045. doi: 10.1002/hbm.24058

Kim, C. M., Alvarado, R. L., Stephens, K., Wey, H. Y., Wang, D. J. J., Leritz, E. C., et al. (2020). Associations between cerebral blood flow and structural and functional brain imaging measures in individuals with neuropsychologically defined mild cognitive impairment. *Neurobiol. Aging* 86, 64–74. doi: 10.1016/j.neurobiolaging.2019.10.023

Kiuchi, K., Kitamura, S., Taoka, T., Yasuno, F., Tanimura, M., Matsuoka, K., et al. (2014). Gray and white matter changes in subjective cognitive impairment, amnestic mild cognitive impairment and Alzheimer's disease: a voxel-based analysis study. *PLoS ONE* 9:e104007. doi: 10.1371/journal.pone.0104007

Landis, J. R., and Koch, G. G. (1977). The measurement of observer agreement for categorical data. *Biometrics* 33:159. doi: 10.2307/2529310

Larson, D. B., Lyons, J. S., Bareta, J. C., Burns, B. J., Blazer, D. G., and Goldstrom, I. D. (1989). The construct validity of the ischemic score of Hachinski for the detection of dementias. *J. Neuropsychiatry Clin. Neurosci.* 1, 181–187. doi: 10.1176/jnp.1.2.181

Leeuwis, A. E., Benedictus, M. R., Kuijer, J. P. A., Binnewijzend, M. A. A., Hooghiemstra, A. M., Verfaillie, S. C. J., et al. (2017). Lower cerebral blood flow is associated with impairment in multiple cognitive domains in Alzheimer's disease. *Alzheimers Dement.* 13, 531–540. doi: 10.1016/j.jalz.2016.08.013

Lejri, I., Agapouda, A., Grimm, A., and Eckert, A. (2019). Mitochondria- and oxidative stress-targeting substances in cognitive decline-related disorders:

from molecular mechanisms to clinical evidence. *Oxidative Med. Cell. Longev.* 2019:9695412. doi: 10.1155/2019/9695412

Leuner, K., Pantel, J., Frey, C., Schindowski, K., Schulz, K., Wegat, T., et al. (2007). "Enhanced apoptosis, oxidative stress and mitochondrial dysfunction in lymphocytes as potential biomarkers for Alzheimer's disease", in *Neuropsychiatric Disorders An Integrative Approach. Journal of Neural Transmission*, Vol 72, eds M. Gerlach, J. Deckert, K. Double, and E. Koutsilieri (Vienna: Springer), 207–215. doi: 10.1007/978-3-211-73574-9_27

Lu, J., Li, D., Li, F., Zhou, A., Wang, F., Zuo, X., et al. (2011). Montreal cognitive assessment in detecting cognitive impairment in Chinese elderly individuals: a population-based study. *J. Geriatr. Psychiatry Neurol.* 24, 184–190. doi: 10.1177/0891988711422528

Luo, Z. R., Zhuang, X. J., Zhang, R. Z., Wang, J. Q., Yue, C., and Huang, X. (2014). Automated 3D segmentation of hippocampus based on active appearance model of brain MR images for the early diagnosis of Alzheimer's disease. *Minerva Med.* 105, 157–165.

Mastroeni, D., Khdour, O. M., Delvaux, E., Nolz, J., Olsen, G., Berchtold, N., et al. (2017). Nuclear but not mitochondrial-encoded oxidative phosphorylation genes are altered in aging, mild cognitive impairment, and Alzheimer's disease. *Alzheimers Dement.* 13, 510–519. doi: 10.1016/j.jalz.2016.09.003

McKenna, F., Babb, J., Miles, L., Goff, D., and Lazar, M. (2020). Reduced microstructural lateralization in males with chronic schizophrenia: a diffusional kurtosis imaging study. *Cereb. Cortex* 30, 2281–2294. doi: 10.1093/cercor/bhz239

Medina, D., DeToledo-Morrell, L., Urresta, F., Gabrieli, J. D., Moseley, M., Fleischman, D., et al. (2006). White matter changes in mild cognitive impairment and AD: a diffusion tensor imaging study. *Neurobiol. Aging* 27, 663–672. doi: 10.1016/j.neurobiolaging.2005.03.026

Miki, K., Ishibashi, S., Sun, L., Xu, H., Ohashi, W., Kuroiwa, T., et al. (2009). Intensity of chronic cerebral hypoperfusion determines white/gray matter injury and cognitive/motor dysfunction in mice. *J. Neurosci. Res.* 87, 1270–1281. doi: 10.1002/jnr.21925

Mitchell, A. J., Beaumont, H., Ferguson, D., Yadegarfar, M., and Stubbs, B. (2014). Risk of dementia and mild cognitive impairment in older people with subjective memory complaints: meta-analysis. *Acta Psychiatr. Scand.* 130, 439–451. doi: 10.1111/acps.12336

Morris, J. C. (1993). The Clinical Dementia Rating (CDR): current version and scoring rules. *Neurology* 43, 2412–2414. doi: 10.1212/WNL.43.11.2412-a

Morris, J. C., and Price, J. L. (2001). Pathologic correlates of nondemented aging, mild cognitive impairment, and early-stage Alzheimer's disease. *J. Mol. Neurosci.* 17, 101–118. doi: 10.1385/JMN:17:2:101

Ogoh, S., and Ainslie, P. N. (2009). Cerebral blood flow during exercise: mechanisms of regulation. *J. Appl. Physiol.* 107, 1370–1380. doi: 10.1152/japplphysiol.00573.2009

Ouchi, Y., Nobezawa, S., Okada, H., Yoshikawa, E., Futatsubashi, M., and Kaneko, M. (1998). Altered glucose metabolism in the hippocampal head in memory impairment. *Neurology* 51, 136–142. doi: 10.1212/WNL.51.1.136

Parker, A. F., Smart, C. M., Scarapicchia, V., and Gawryluk, J. R. (2020). Identification of earlier biomarkers for alzheimer's disease: a multimodal neuroimaging study of individuals with subjective cognitive decline. *J. Alzheimers Dis.* 77, 1067–1076. doi: 10.3233/JAD-200299

Pennanen, C., Kivipelto, M., Tuomainen, S., Hartikainen, P., Hänninen, T., Laakso, M. P., et al. (2004). Hippocampus and entorhinal cortex in mild cognitive impairment and early AD. *Neurobiol. Aging* 25, 303–310. doi: 10.1016/S0197-4580(03)00084-8

Perrotin, A., La Joie, R., de La Sayette, V., Barr,é, L., Mézenge, F., Mutlu, J., et al. (2017). Subjective cognitive decline in cognitively normal elders from the community or from a memory clinic: differential affective and imaging correlates. *Alzheimers Dement.* 13, 550–560. doi: 10.1016/j.jalz.2016.08.011

Petersen, R. C., Doody, R., Kurz, A., Mohs, R. C., Morris, J. C., Rabins, P. V., et al. (2001). Current concepts in mild cognitive impairment. *Arch. Neurol.* 58, 1985–1992. doi: 10.1001/archneur.58.12.1985

Reisberg, B., Ferris, S. H., de Leon, M. J., and Crook, T. (1982). The global deterioration scale for assessment of primary degenerative dementia. *Am. J. Psychiatry* 139, 1136–1139. doi: 10.1176/ajp.139.9.1136

Reisberg, B., Shao, Y., Moosavi, M., Kenowsky, S., Vedvyas, A., Marsh, K., et al. (2020). Psychometric cognitive decline precedes the advent of subjective cognitive decline in the evolution of Alzheimer's disease. *Dement. Geriatr. Cogn. Disord.* 49, 16–21. doi: 10.1159/000507286

Riederer, I., Bohn, K. P., Preibisch, C., Wiedemann, E., Zimmer, C., Alexopoulos, P., et al. (2018). Alzheimer disease and mild cognitive impairment: integrated pulsed arterial spin-labeling MRI and (18)F-FDG PET. *Radiology* 288, 198–206. doi: 10.1148/radiol.2018170575

Sam, K., Crawley, A. P., Conklin, J., Poublanc, J., Sobczyk, O., Mandell, D. M., et al. (2016). Development of white matter hyperintensity is preceded by reduced cerebrovascular reactivity. *Ann. Neurol.* 80, 277–285. doi: 10.1002/ana.24712

Sánchez-Benavides, G., Grau-Rivera, O., Suárez-Calvet, M., Minguillon, C., Cacciaglia, R., Gramunt, N., et al. (2018). Brain and cognitive correlates of subjective cognitive decline-plus features in a population-based cohort. *Alzheimers Res. Ther.* 10:123. doi: 10.1186/s13195-018-0449-9

Saykin, A. J., Wishart, H. A., Rabin, L. A., Santulli, R. B., Flashman, L. A., West, J. D., et al. (2006). Older adults with cognitive complaints show brain atrophy similar to that of amnestic MCI. *Neurology* 67, 834–842. doi: 10.1212/01.wnl.0000234032.77541.a2

Sierra-Marcos, A. (2017). Regional cerebral blood flow in mild cognitive impairment and Alzheimer's disease measured with arterial spin labeling magnetic resonance imaging. *Int. J. Alzheimers Dis.* 2017:5479597. doi: 10.1155/2017/5479597

Snitz, B. E., Weissfeld, L. A., Lopez, O. L., Kuller, L. H., Saxton, J., Singhabahu, D. M., et al. (2013). Cognitive trajectories associated with β-amyloid deposition in the oldest-old without dementia. *Neurology* 80, 1378–1384. doi: 10.1212/WNL.0b013e31828c2fc8

Song, G. P., Yao, T. T., Wang, D., and Li, Y. H. (2019). Differentiating between Alzheimer's disease, amnestic mild cognitive impairment, and normal aging via diffusion kurtosis imaging. *Neural Regen. Res.* 14, 2141–2146. doi: 10.4103/1673-5374.262594

Song, I. U., Choi, E. K., Oh, J. K., Chung, Y. A., and Chung, S. W. (2016). Alteration patterns of brain glucose metabolism: comparisons of healthy controls, subjective memory impairment and mild cognitive impairment. *Acta Radiol.* 57, 90–97. doi: 10.1177/0284185114566088

Struyfs, H., Van Hecke, W., Veraart, J., Sijbers, J., Slaets, S., De Belder, M., et al. (2015). Diffusion kurtosis imaging: a possible MRI biomarker for AD diagnosis? *J. Alzheimers Dis.* 48, 937–948. doi: 10.3233/JAD-150253

Sun, Y., Dai, Z., Li, Y., Sheng, C., Li, H., Wang, X., et al. (2016). Subjective cognitive decline: mapping functional and structural brain changes-a combined resting-state functional and structural MR imaging study. *Radiology* 281, 185–192. doi: 10.1148/radiol.2016151771

Swomley, A. M., and Butterfield, D. A. (2015). Oxidative stress in Alzheimer disease and mild cognitive impairment: evidence from human data provided by redox proteomics. *Arch. Toxicol.* 89, 1669–1680. doi: 10.1007/s00204-015-1556-z

Tandetnik, C., Farrell, M. T., Cary, M. S., Cines, S., Emrani, S., Karlawish, J., et al. (2015). Ascertaining subjective cognitive decline: a comparison of approaches and evidence for using an age-anchored reference group. *J. Alzheimers Dis.* 48, S43–S55. doi: 10.3233/JAD-150251

Terada, T., Obi, T., Bunai, T., Matsudaira, T., Yoshikawa, E., Ando, I., et al. (2020). In vivo mitochondrial and glycolytic impairments in patients with Alzheimer disease. *Neurology* 94, e1592–e1604. doi: 10.1212/WNL.0000000000009249

Thomas, B., Sheelakumari, R., Kannath, S., Sarma, S., and Menon, R. N. (2019). Regional cerebral blood flow in the posterior cingulate and precuneus and the entorhinal cortical atrophy score differentiate mild cognitive impairment and dementia due to Alzheimer disease. *AJNR Am. J. Neuroradiol.* 40, 1658–1664. doi: 10.3174/ajnr.P0057

van der Flier, W. M., van Buchem, M. A., Weverling-Rijnsburger, A. W., Mutsaers, E. R., Bollen, E. L., Admiraal-Behloul, F., et al. (2004). Memory complaints in patients with normal cognition are associated with smaller hippocampal volumes. *J. Neurol.* 251, 671–675. doi: 10.1007/s00415-004-0390-7

Van Straaten, E. C. W., Harvey, D., Scheltens, P., Barkhof, F., Petersen, R. C., Thal, L. J., et al. (2008). Periventricular white matter hyperintensities increase the likelihood of progression from amnestic mild cognitive impairment to dementia. *J. Neurol.* 255, 1302–1308. doi: 10.1007/s00415-008-0874-y

Wang, X., Huang, W., Su, L., Xing, Y., Jessen, F., Sun, Y., et al. (2020). Neuroimaging advances regarding subjective cognitive decline in preclinical Alzheimer's disease. *Mol. Neurodegener.* 15:55. doi: 10.1186/s13024-020-00395-3

Wen, Q., Mustafi, S. M., Li, J., Risacher, S. L., Tallman, E., Brown, S. A., et al. (2019). White matter alterations in early-stage Alzheimer's disease: a tract-specific study. *Alzheimers Dement.* 11, 576–587. doi: 10.1016/j.dadm.2019.06.003

Worboys, M. (2013). The hamilton rating scale for depression: the making of a "gold standard" and the unmaking of a chronic illness, 1960-1980. *Chronic Illn.* 9, 202–219. doi: 10.1177/1742395312467658

Wu, B., Lou, X., Wu, X., and Ma, L. (2014). Intra- and interscanner reliability and reproducibility of 3D whole-brain pseudo-continuous arterial spin-labeling MR perfusion at 3T. *J. Magn. Reson. Imaging* 39, 402–409. doi: 10.1002/jmri.24175

Xu, Y., Chen, K., Zhao, Q., Li, F., and Guo, Q. (2020). Short-term delayed recall of auditory verbal learning test provides equivalent value to long-term delayed recall in predicting MCI clinical outcomes: a longitudinal follow-up study. *Appl. Neuropsychol. Adult* 27, 73–81. doi: 10.1080/23279095.2018.1481067

Yakushev, I., Müller, M. J., Lorscheider, M., Schermuly, I., Weibrich, C., Dellani, P. R., et al. (2010). Increased hippocampal head diffusivity predicts impaired episodic memory performance in early Alzheimer's disease. *Neuropsychologia* 48, 1447–1453. doi: 10.1016/j.neuropsychologia.2010.01.014

Yan, T., Wang, W., Yang, L., Chen, K., Chen, R., and Han, Y. (2018). Rich club disturbances of the human connectome from subjective cognitive decline to Alzheimer's disease. *Theranostics* 8, 3237–3255. doi: 10.7150/thno.23772

Yang, D. W., Hong, Y. J., Yoon, B., Han, I. W., Lim, S. C., Shim, Y. S., et al. (2012). IC-P-062: diffusion tensor imaging as a diagnostic tool for Alzheimer's disease. *Alzheimer's Dement.* 8:P37. doi: 10.1016/j.jalz.2012.05.095

Yang, Z. X., Huo, S. S., Cheng, X. F., Xu, Z. F., Cao, Z., Zeng, J. X., et al. (2012). Quantitative multivoxel proton MR spectroscopy study of brain metabolites in patients with amnestic mild cognitive impairment: a pilot study. *Neuroradiology* 54, 451–458. doi: 10.1007/s00234-011-0900-0

Yoshiura, T., Hiwatashi, A., Noguchi, T., Yamashita, K., Ohyagi, Y., Monji, A., et al. (2009). Arterial spin labelling at 3-T MR imaging for detection of individuals with Alzheimer's disease. *Eur. Radiol.* 19, 2819–2825. doi: 10.1007/s00330-009-1511-6

Yuan, L., Sun, M., Chen, Y., Long, M., Zhao, X., Yin, J., et al. (2016). Non-Gaussian diffusion alterations on diffusion kurtosis imaging in patients with early Alzheimer's disease. *Neurosci. Lett.* 616, 11–18. doi: 10.1016/j.neulet.2016.01.021

Zhang, Z., Liu, Y., Zhou, B., Zheng, J., Yao, H., An, N., et al. (2014). Altered functional connectivity of the marginal division in Alzheimer's disease. *Curr. Alzheimer Res.* 11, 145–155. doi: 10.2174/1567205011666140110112608

Zhang, Z., Wang, Y., Shen, Z., Yang, Z., Li, L., Chen, D., et al. (2016). The neurochemical and microstructural changes in the brain of systemic lupus erythematosus patients: a multimodal MRI study. *Sci. Rep.* 6:19026. doi: 10.1038/srep19026

Zhao, L., Wang, Y., Jia, Y., Zhong, S., Sun, Y., Zhou, Z., et al. (2016). Cerebellar microstructural abnormalities in bipolar depression and unipolar depression: a diffusion kurtosis and perfusion imaging study. *J. Affect. Disord.* 195, 21–31. doi: 10.1016/j.jad.2016.01.042

Zheng, W., Wu, C., Huang, L., and Wu, R. (2017). Diffusion kurtosis imaging of microstructural alterations in the brains of paediatric patients with congenital sensorineural hearing loss. *Sci. Rep.* 7:1543. doi: 10.1038/s41598-017-01263-9

Conflict of Interest: The authors declare that the research was conducted in the absence of any commercial or financial relationships that could be construed as a potential conflict of interest.

frontiers in Aging Neuroscience

ORIGINAL RESEARCH
published: 02 February 2021
doi: 10.3389/fnagi.2021.632382

Blood *NCAPH2* Methylation Is Associated With Hippocampal Volume in Subjective Cognitive Decline With Apolipoprotein E ε4 Non-carriers

Ying Chen[1,2†], *Tao-Ran Li*[1†], *Shu-Wen Hao*[3], *Xiao-Ni Wang*[1*], *Yan-Ning Cai*[3*] and *Ying Han*[1,4,5*]

[1] Department of Neurology, Xuanwu Hospital of Capital Medical University, Beijing, China, [2] Department of Neurology, Zhejiang Taizhou Municipal Hospital, Taizhou, Zhejiang, China, [3] Department of Neurobiology, Xuanwu Hospital of Capital Medical University, Beijing, China, [4] Center of Alzheimer's Disease, Beijing Institute for Brain Disorders, Beijing, China, [5] National Clinical Research Center for Geriatric Disorders, Beijing, China

OPEN ACCESS

Edited by:
Boon-Seng Wong, Singapore Institute of Technology, Singapore

Reviewed by:
Nobuyuki Kobayashi, Jikei University School of Medicine, Japan
Bing Zhang, Nanjing Drum Tower Hospital, China

***Correspondence:**
Xiao-Ni Wang
wxnanna@163.com
Yan-Ning Cai
caiyanning@xwh.ccmu.edu.cn
Ying Han
hanying@xwh.ccmu.edu.cn

[†] These authors have contributed equally to this work and share first authorship

Received: 23 November 2020
Accepted: 06 January 2021
Published: 02 February 2021

Citation:
Chen Y, Li T-R, Hao S-W, Wang X-N, Cai Y-N and Han Y (2021) Blood NCAPH2 Methylation Is Associated With Hippocampal Volume in Subjective Cognitive Decline With Apolipoprotein E ε4 Non-carriers. Front. Aging Neurosci. 13:632382. doi: 10.3389/fnagi.2021.632382

Objective: This study assessed the methylation of peripheral *NCAPH2* in individuals with subjective cognitive decline (SCD), identified its correlation with the hippocampal volume, and explored whether the correlation is influenced by apolipoprotein E ε4 (APOE ε4) status.

Methods: Cognitively normal controls (NCs, $n = 56$), individuals with SCD ($n = 81$), and patients with objective cognitive impairment (OCI, $n = 51$) were included from the Sino Longitudinal Study on Cognitive Decline (NCT03370744). All participants completed neuropsychological assessments, blood tests, and structural MRI. *NCAPH2* methylation was compared according to the diagnostic and APOE ε4 status. Partial correlation analysis was conducted to assess the correlations between the hippocampal volume, cognitive tests, and the *NCAPH2* methylation levels.

Results: Individuals with SCD and patients with OCI showed significantly lower levels of *NCAPH2* methylation than NCs, which were independent of the APOE ε4 status. The *NCAPH2* methylation levels and the hippocampal volumes were positively correlated in the SCD *APOE* ε4 non-carriers but not in the OCI group. No association was found between the *NCAPH2* methylation levels and the cognitive function.

Conclusion: Abnormal changes in blood *NCAPH2* methylation were found to occur in SCD, indicating its potential to be used as a useful peripheral biomarker in the early stage of Alzheimer's disease screening.

Keywords: Alzheimer's disease, *NCAPH2*, methylation, subjective cognitive decline, SCD

INTRODUCTION

Alzheimer's disease (AD) is a progressive and highly debilitating neurodegenerative disorder, accounting for about two-thirds of 50 million people with dementia worldwide (Lane et al., 2018). There is still no therapy to treat the underlying cause of the disease or slow down its progression. The pathogenesis of AD is complex and may involve genetic and environmental factors. A growing

body of evidence points to the epigenetic contribution of AD, and both global and gene-specific changes in DNA methylation have been observed in the affected postmortem brain regions (Bakulski et al., 2012; De Jager et al., 2014; Cronin et al., 2017). The search for peripheral blood epigenetic biomarkers of AD is of particular interest because of the unavailability of brain DNA samples until postmortem and the inability to collect longitudinal brain samples to track disease diagnosis (Bakulski et al., 2016).

Recently, two large-scale epigenome-wide association studies (EWAS) have reported the first replicable and robust association of brain methylation and AD pathology in independent cohorts (De Jager et al., 2014; Lunnon et al., 2014). Given the stable changes in DNA methylation levels in older asymptomatic individuals with amyloid pathology, the altered DNA methylation in the brain has been identified as an early feature of preclinical AD. *NCAPH2* is a subunit of the condensin-2 complex involved in chromosome condensation during mitosis and meiosis (Martin et al., 2016). Peripheral blood DNA methylation levels in the *NCAPH2/LMF2* promoter region were significantly decreased in patients with AD and those with amnestic mild cognitive impairment (aMCI) (Kobayashi et al., 2016); therefore, these are considered to be a potentially useful biomarker for the diagnosis of AD. However, while the hypomethylation of *NCAPH2* has been reported in the Japanese population, its presence in the Chinese population remains unclear. Furthermore, whether *NCAPH2* methylation changes across the AD spectrum is still unknown. To date, there have been relatively few studies devoted to the determination of *NCAPH2* methylation patterns in peripheral blood in the early stages of AD.

Subjective cognitive decline (SCD) is characterized by subjective self-perception of worsening cognitive capacity but without any impairment observed in objective evaluations (Jessen et al., 2014; Molinuevo et al., 2017). It has been suggested that SCD precedes MCI and is the preclinical stage of AD (Rabin et al., 2017). Several studies have shown that SCD may be associated with risk factors for dementia, such as the apolipoprotein E (APOE) ε4 allele and the neuropathology of AD (Perrotin et al., 2015; Risacher et al., 2017; Vogel et al., 2017). Thus, recognizing the early characterization of DNA methylation patterns in SCD may help to better understand the role of methylation in the early stages of AD.

Recent research has demonstrated a robust decrease in global DNA methylation in the hippocampus of patients with AD, and this was significantly correlated with amyloid plaque load (Chouliaras et al., 2013). Moreover, a large multisite EWAS revealed DNA methylation in the superior temporal gyrus-mediated associations between blood DNA methylation and the hippocampal volume (Jia et al., 2019). These findings suggest that DNA methylation and the relationship with the hippocampal volume are involved in the pathophysiology of AD. However, whether DNA methylation changes in the blood are correlated with the hippocampal volume in the early stage of AD remain unknown.

Thus, the objectives of this study were (1) to identify cross-sectional differences in peripheral blood *NCAPH2* methylation among patients with SCD and objective cognitive impairment (OCI) relative to normal control (NC) participants and (2) to identify the correlation between the hippocampal volume, the cognitive function, and the *NCAPH2* methylation levels and their interaction with the APOE ε4 status.

METHODS

Participants

Altogether, 56 NCs, 81 participants with SCD, and 51 participants with OCI (34 MCI and 17 AD) from the Sino Longitudinal Study on Cognitive Decline (SILCODE) project were included in the present research. The SILCODE project is a large, multicenter-based longitudinal observational study in China (ClinicalTrials.gov, NCT 03370744) that is based in Xuanwu Hospital, Capital Medical University, China, and aims to construct a high-precision multimodal model for the ultra-early diagnosis of AD. The study was approved by the institutional review board at Xuanwu Hospital in Capital Medical University, and written informed consent was obtained from all participants.

All 188 individuals fulfilled the inclusion criteria of the SILCODE project (Li et al., 2019). Briefly, SCD is defined using the following criteria (Jessen et al., 2014): (1) self-experienced persistent decline in memory rather than other domains of cognition within the last 5 years; (2) concerns related to SCD and a feeling of worsened performance when compared to others of the same age group; and (3) performance on standardized cognitive tests within age-, gender-, and education-adjusted norms and failure to meet the criteria for MCI or dementia. MCI was diagnosed using the Jak–Bondi approach (Bondi et al., 2014). Impairment in a cognitive domain was defined as having at least two tests >1.0 SD below the age-adjusted normative means or having impaired scores in each of the three sampled cognitive domains (memory, language, and speed/executive functioning). The diagnosis of AD was determined by the published diagnostic criteria (McKhann et al., 1984; Dubois et al., 2007). Individuals with no cognitive complaints and normal performance on the standardized neuropsychological tests were included as controls. The exclusion criteria contained brain trauma or disorder, including clinical stroke, severe psychiatric, and/or severe somatic disease, that may account for symptoms, intellectual disability or other developmental disorders, and other systemic diseases. All participants were assessed using a standardized clinical evaluation protocol comprised of the Mini-Mental State Examination (MMSE), Montreal Cognitive Assessment Basic Version (MoCA-B), Hamilton Depression Scale (HAMD), and Hamilton Anxiety Scale (HAMA).

Peripheral *NCAPH2* Methylation Measurements

Venous blood samples were collected early in the morning from 6:00 a.m. to 8:00 a.m. Genomic DNA was prepared from leukocytes using the QIAamp DNA Mini Kit (Qiagen, Hilden, Germany), with sodium bisulfite treatment performed as described previously (Ghodsi et al., 2020). Briefly, for the bisulfite reaction (in which cytosine is converted to uracil and 5-methylcytosine remains non-reactive), genomic DNA was initially denatured with 0.3 M NaOH. Sodium metabisulfite

solution (pH 5.0) and hydroquinone were then added at final concentrations of 3.0 M and 0.5 mM, respectively. Reaction mixtures were incubated under mineral oil in the dark at 50°C for 16 h. Denatured DNA was purified with Wizard DNA Purification Resin (Promega, Fitchburg, WI, USA), and the reaction terminated by treatment with 0.3 M NaOH at 37°C for 15 min, followed by ethanol precipitation. For bisulfite pyrosequencing analysis, 50 ng of bisulfite-treated genomic DNA was amplified in a DNA Engine Opticon 2 system (MJ Research, Waltham, MA, USA) using a Taq DNA Polymerase kit, hot-start (Takara Bio, Otsu Shiga, Japan). The sequences of the PCR amplification primers, as well as the sequencing primer for *NCAPH2*, were as follows: forward: 5′-GTATTTTTTTGGGAGGGAATAGTAAAATG-3′, reverse: 5′-CCACCTCCCAATTCTTAATAAAA-3′, sequencing: 5′-AGTAAAATGGAGTTAGAATTAGTG-3′, with an amplicon of 187 bp. The reverse primer contained biotin at the 5′ position. The amplification conditions for *NCAPH2* were as follows: 1 cycle of 94°C for 2 min; 50 cycles of 94°C for 20 s, 61°C for 20 s, and 72°C for 20 s; and 1 cycle of 72°C for 5 min. For the pyrosequencing reaction, single-stranded DNA templates were immobilized on Streptavidin Sepharose High Performance beads (GE Healthcare, Uppsala, Sweden) using the PSQ Vacuum Prep Tool and Vacuum Prep Worktable (Qiagen, Hilden, Germany) according to the manufacturer's instructions. Reactions were incubated at 80°C for 2 min and allowed to anneal with the sequencing primers (0.4 mM) at room temperature. Pyrosequencing was performed using PyroMark Gold Reagents (Qiagen) on a PyroMark Vaccum Workstation (Qiagen), according to the manufacturer's instructions.

APOE Genotyping

Apolipoprotein E was amplified with the following primers: 5′-ACGCGGGCACGGCTGTCCAAGG-3′ (forward) and 5′-GGCGCTCGCGGATGGCGCTGA-3′ (reverse), using the following conditions: 1 cycle of 98°C for 10 s, 35 cycles of 72°C for 5 s, and 1 cycle of 72°C for 5 min. PCR was performed in a final volume of 30 μl, containing 10 pmol of forward and reverse primers and 50 ng of genomic DNA template, using PrimeSTAR HS DNA Polymerase with GC Buffer (Takara Bio), according to the manufacturer's instructions. Then, APOE was genotyped using the standard Sanger sequencing method (Sangon, Shanghai, China).

MRI Acquisition

All individuals were scanned on an integrated simultaneous 3.0 T TOF PET/MR (Signa PET/MR, GE Healthcare, WI, USA) at Xuanwu Hospital, Capital Medical University, China. The 3D BRAVO T1-weighted sequence was obtained with the following parameters: repetition time (TR)/echo time (TE) = 6.9 ms/2.98 ms, flip angle (FA) = 12°, inversion time (TI) = 450 ms, field of view = 256 × 256 mm^2, matrix = 256 × 256, slices = 192, slice thickness = 1 mm, no interslice gap, and voxel size = 1 × 1 × 1 mm^3.

MRI Processing

Briefly, the entire workflow was as follows: (1) spatially adaptive non-local means denoising, (2) rough inhomogeneity correction, (3) an aligned image into the Montreal Neurological Institute-Hospital (MNI) space, (4) inhomogeneity correction, (5) intensity normalization, (6) non-local intracranial cavity extraction, and (7) subcortical nucleus segmentation. Steps from 1 to 7 were implemented in the volBrain pipeline (http://volbrain.upv.es). The left and right hippocampal volumes were presented as relative values (%), which were measured in relation to the total intracranial volume (Manjon and Coupe, 2016).

Statistical Analysis

Demographic data and neuropsychological tests were compared by the ANOVA and the chi-squared test for continuous and categorical variables. To compare the *NCAPH2* methylation levels and the hippocampal volumes, a one-way analysis of covariance (ANCOVA) was conducted with age, gender, and years of education as covariates. Bonferroni's multiple comparison tests were conducted for *post-hoc* comparison. We also performed group comparisons among the NC, SCD, MCI, and AD groups. A two-way ANCOVA was used to assess the interactions between the diagnostic status and the APOE ε4 allele on *NCAPH2* methylation controlling for age, gender, and years of education. Then, several partial correlation analyses were conducted with age, gender, and years of education as covariates. First, we assessed the correlations between the hippocampal volumes (left and right side) and the *NCAPH2* methylation levels in the SCD group and further in the SCD APOE ε4 non-carriers and carriers separately to examine whether the correlation differed according to the APOE ε4 status. We also assessed the correlation between the *NCAPH2* methylation levels and the hippocampal volumes in NC and OCI groups. Second, we evaluated the correlation between the *NCAPH2* methylation levels and the cognitive scores (MMSE and MoCA-B) in all individuals and subgroups (APOE ε4 non-carriers and carriers groups). All *p*-values were calculated using two-sided tests, and $p < 0.05$ was considered statistically significant. All analyses were performed using SPSS Statistics (version 24.0, IBM).

RESULTS

Demographic Characteristics and Cognitive Function

Table 1 summarizes the demographic and neuropsychological scores for each group. All groups were statistically comparable in terms of sex distribution. The one-way ANOVA showed group differences in age ($F = 15.79$, $p < 0.001$) and years of education ($F = 8.88$, $p < 0.001$). The OCI group was significantly older and less educated than the control and SCD groups. There were significant differences in the APOE ε4 prevalence among groups ($\chi^2 = 9.88$, $p = 0.007$); patients with SCD and OCI had higher proportions of APOE ε4 carriers (32.1 and 41.2%, respectively) when compared to the controls (14.3%). Patients with OCI showed lower MMSE and MoCA-B scores than controls and individuals with SCD (MMSE: $F = 53.85$, $p < 0.001$; MoCA-B: $F = 92.62$, $p < 0.001$). The SCD and OCI groups scored significantly higher on the HAMD than the controls ($F = 6.62$, $p = 0.002$). Similarly, the HAMA score was higher among the patients with OCI than among the controls ($F = 4.06$, $p = 0.019$), but there was no difference between the SCD and control

TABLE 1 | Demographics and clinical characteristics of the subjects.

	NC ($n = 56$)	SCD ($n = 81$)	OCI ($n = 51$)
Age (y)	66.7 ± 5.0	66.4 ± 4.5	71.6 ± 7.3$^{**\#\#}$
Male, n (%)	23 (41.1%)	26 (32.1%)	24 (47.1%)
Education (y)	12.4 ± 3.4	12.0 ± 2.9	9.9 ± 3.9$^{**\#\#}$
APOE ε4, n (%)	8 (14.3%)	26 (32.1%)**	21 (41.2%)**
MMSE	28.7 ± 1.3	28.7 ± 1.2	22.5 ± 6.5$^{**\#\#}$
MOCA-B	26.1 ± 2.0	25.6 ± 2.3	17.6 ± 5.9$^{**\#\#}$
HAMD	3.0 ± 3.1	5.0 ± 3.7*	5.9 ± 5.5**
HAMA	3.3 ± 3.3	4.4 ± 3.6	5.5 ± 4.4*

*Results are expressed as mean ± standard deviation. n = number of subjects; NC, normal control; SCD, subjective cognitive decline; OCI, objective cognitive impairment; MMSE, Mini-Mental Status Examination; MoCA-B, Montreal Cognitive Assessment-Basic Version; HAMD, Hamilton Depression Rating Scale; HAMA, Hamilton Anxiety Rating Scale. *$p < 0.05$, **$p < 0.01$, compared with NC; $^{\#\#}p < 0.01$, compared with SCD.*

groups. No significant differences were found in the HAMD or HAMA scores between patients with SCD and patients with OCI (all $p > 0.1$).

Group Differences in the *NCAPH2* Methylation Levels

One-way ANCOVA revealed that the *NCAPH2* methylation levels were significantly different among the three groups ($F = 6.43$, $p = 0.002$) after controlling for age, gender, and years of education. **Figure 1** shows that patients with SCD and patients with OCI had significantly lower *NCAPH2* methylation levels than the controls (both $p < 0.001$; Bonferroni corrected), but there was no difference between patients with SCD and patients with OCI ($p > 0.1$; Bonferroni corrected). Further comparison among the four groups showed that the *NCAPH2* methylation levels were lower in patients with MCI and patients with AD than the controls, but there was no difference among patients with SCD, patients with MCI, and patients with AD (**Supplementary Figure 1**).

The *NCAPH2* methylation levels were significantly low in the APOE ε4 carriers than in the APOE ε4 non-carriers (**Supplementary Table 1** and **Supplementary Figure 2**). Furthermore, no significant additive interactions were observed in *NCAPH2* methylation between the diagnostic groups and the APOE ε4 allele ($F = 0.41$, $p = 0.665$).

Group Differences in the Hippocampal Volume

Figure 2 shows the significant differences in the volume proportion of the bilateral hippocampus among the three groups (right hippocampus: $F = 27.95$, $p < 0.001$; left hippocampus: $F = 25.61$, $p < 0.001$). Compared with the controls and SCD groups, patients with OCI exhibited significant volume loss in the right and left hippocampus (all $p < 0.001$; Bonferroni corrected). However, there were no significant differences between the SCD and control groups ($p > 0.05$; Bonferroni corrected).

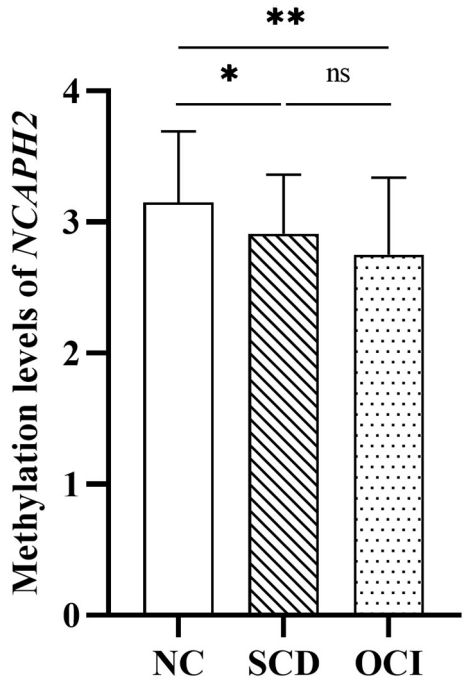

FIGURE 1 | Group differences in the *NCAPH2* methylation levels among the three groups. The analysis was adjusted with age, gender, and years of education. Asterisks indicate *post-hoc* comparisons with respect to controls (Bonferroni corrected). The error bars indicated SDs. *$p < 0.05$, **$p < 0.01$; ns, not significant. NC, normal control; SCD, subjective cognitive decline; OCI, objective cognitive impairment.

Relationship Between the *NCAPH2* Methylation Levels and the Hippocampal Volume

In the SCD group, there was a significant positive correlation between the *NCAPH2* methylation levels and the volume proportion of the left hippocampus (r = 0.245, $p = 0.027$); however, the positive correlation in the right hippocampus was not significant (r = 0197, $p = 0.078$). Moreover, the positive correlation between the *NCAPH2* methylation levels and the volume proportion of the hippocampus was significant in the APOE ε4 non-carriers in the SCD group (left/right: r = 0.347/0.279, $p = 0.009/0.039$). Nevertheless, there were no significant associations in the APOE ε4 carriers in the SCD group (left/right: r = −0.017/−0.026, $p = 0.935/0.900$) (**Figure 3**).

The correlations between the *NCAPH2* methylation levels and the volume proportion of the hippocampus in NC and OCI groups were not significant (all $p > 0.1$, **Supplementary Table 2**).

Relationship Between the *NCAPH2* Methylation Levels and the Cognitive Scores

There was no correlation between the *NCAPH2* methylation levels and the cognitive scores in all individuals (MMSE: r = 0.077, $p = 0.304$; MoCA-B: r = 0.126, $p = 0.095$, **Supplementary Figures 3, 4**). Further, subgroup analysis showed

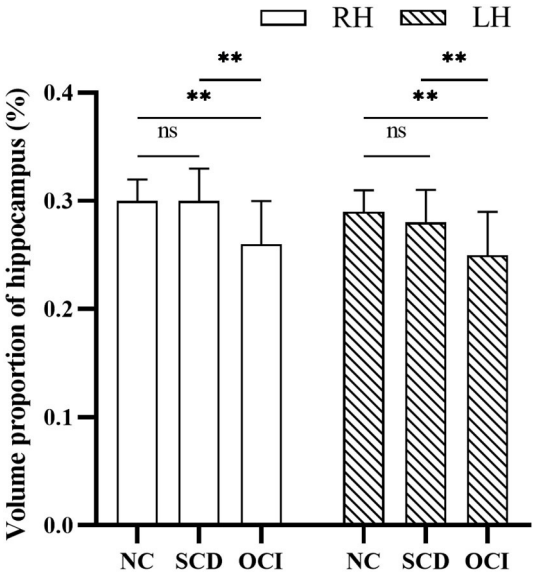

FIGURE 2 | Group differences in the volume proportion of the right and left hippocampus. Results were corrected for multiple comparisons (Bonferroni corrected). $^{**}p < 0.01$; ns, not significant. NC, normal control; SCD, subjective cognitive decline; OCI, objective cognitive impairment; LH, left hippocampus; RH, right hippocampus.

no significant correlation in both APOE ε4 carriers and non-carriers groups (all $p > 0.1$, **Supplementary Table 3**).

DISCUSSION

In the present study, we found that *NCAPH2* methylation was decreased in the peripheral blood of patients with SCD and patients with OCI compared to the controls. Notably, *NCAPH2* hypomethylation was significantly positively associated with the hippocampal volume in patients with SCD, especially in the APOE ε4 non-carriers. No association was found between the *NCAPH2* methylation levels and the cognitive function.

It has been reported that DNA methylation modifications of several genes are fundamental to the development of AD, which has been considered relevant to AD progression. However, empirical evidence is hard to come by, and the results thus far have been conflicting and controversial. One study has confirmed that higher peripheral methylation levels of brain-derived neurotrophic factor, a member of the neurotrophin family, are associated with a significant AD conversion propensity for patients with MCI (Xie et al., 2017). Other β-amyloid precursor protein (APP)-related genes, such as BACE1, were hypomethylated in the peripheral blood of patients with AD (Marques et al., 2012). Nevertheless, one large case-control study found that there was no difference in the blood DNA methylation levels of *PSEN1* or *BACE1*, both codes for proteins directly involved in the APP cleavage, between patients with AD and the controls, leading to the formation of the β-amyloid (Aβ) (Tannorella et al., 2015). The different methods of methylation analysis and small samples of the varying population may account for divergent findings (Fransquet et al., 2018). The decreased *NCAPH2* methylation in patients with OCI found in our study was consistent with the hypomethylation of the *NCAPH2/LMF2* promoter region reported in a previous Japanese study (Kobayashi et al., 2016). Moreover, the altered methylation pattern was also been found in individuals with SCD, and no difference among patients with SCD, patients with MCI, and patients with AD was observed. Our results indicated that the *NCAPH2* methylation levels decreased during the SCD stage of the disease and reached a plateau at the cognitive impairment stage, suggesting that altered blood *NCAPH2* methylation might be an early feature of AD pathology.

The hippocampus, a brain area critical for learning and memory, is vulnerable to damage at the early stages of AD. In addition, altered neurogenesis in the hippocampus has been suggested as an early critical event in AD due to its relevance for neural plasticity and network maintenance (Mu and Gage, 2011). DNA methylation during neurogenesis has been shown to be responsive to many extrinsic signals, both under normal conditions and during the development of the disease. Our study found that there was a relationship between the *NCAPH2* methylation levels and the hippocampal volume in SCD individuals, but not in patients with MCI and patients with AD. This is not consistent with observations from the previous research, showing a correlation between *NCAPH2/LMF2* methylation and hippocampal atrophy in AD (Shinagawa et al., 2016). A possible explanation for this difference in outcome could be that *NCAPH2* methylation has reached a plateau phase in the early stage of AD, leading to little meaningful variance in methylation levels between patients with cognitive impairment. Thus, a dissociation between *NCAPH2* hypomethylation and the markers of neurodegeneration, including hippocampal atrophy and cognitive impairment, was observed in the late stage of AD. Besides, we observed a significant positive association between the *NCAPH2* methylation levels and the left hippocampal volume rather than the right hippocampus in the SCD group. A previous study of community-dwelling Chinese people showed asymmetry patterns in the hippocampus in SCD, and the correlation between the volume of the right hippocampus and the cognitive function was shown (Yue et al., 2018). Another study reported that SCD with a smaller left hippocampal volume was associated with greater depressive symptomatology (Buckley et al., 2016). Further work is needed to provide a better understanding of the different correlations with hippocampal asymmetry, for instance, in the context of brain function and compensation. Previous studies have shown that epigenetic regulation may be involved in defective T-cell function in *NCAPH2* mutant mice (Gosling et al., 2008). Recent work has identified numerous extravascular CD8+ T-cells in the perivascular space of blood vessels with cerebral amyloid angiopathy in the hippocampi of patients with AD. Furthermore, there was a negative correlation in aMCI and AD between T-cells and cognition (Gate et al., 2020). We hypothesize that dysregulation of *NCAPH2* methylation may lead to an abnormal immune response and finally to hippocampal atrophy. Therefore, a large sample and longitudinal analyses are required to investigate the role of *NCAPH2* methylation, and the

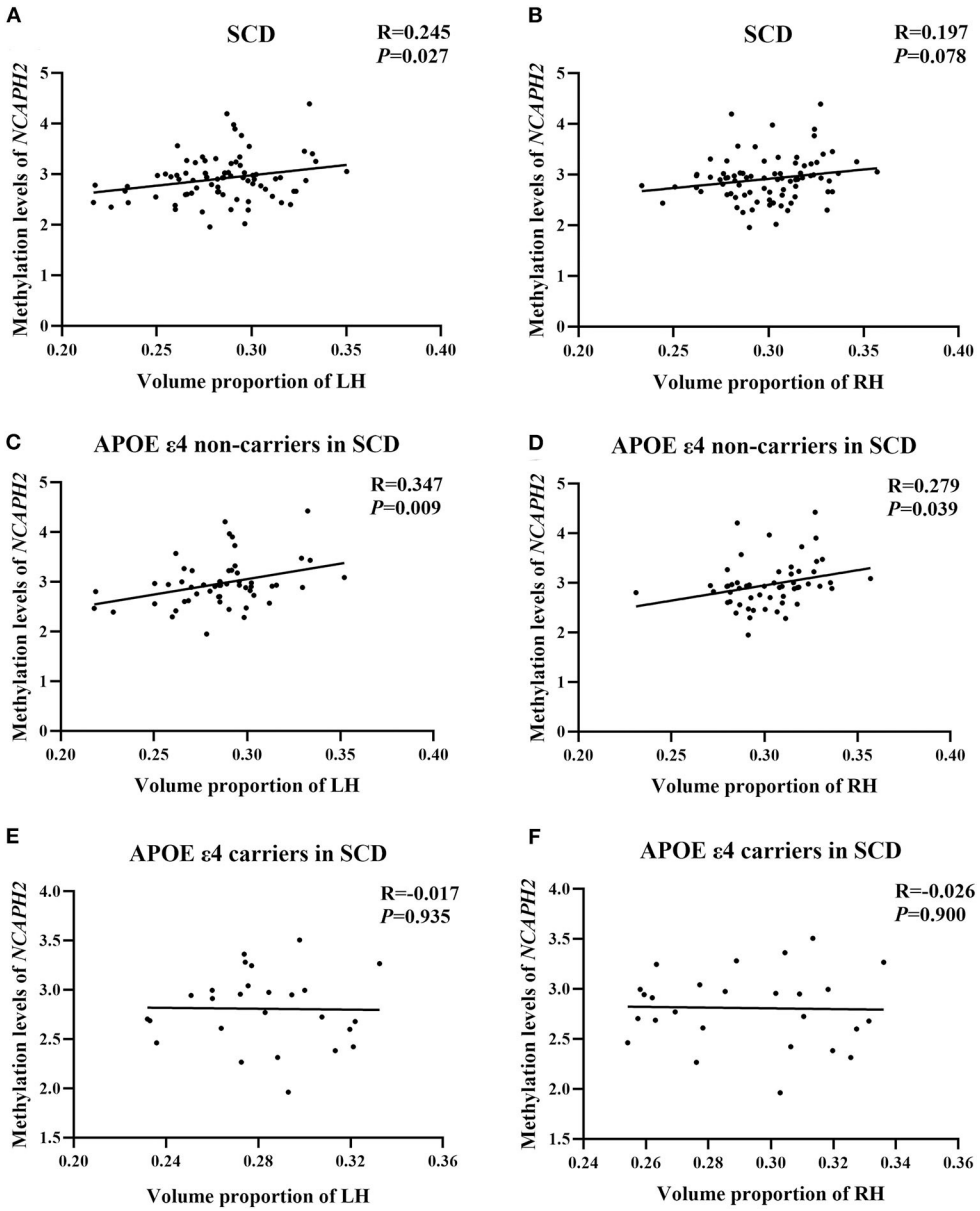

FIGURE 3 | The relationship between the *NCAPH2* methylation levels and the volume proportion of hippocampus in participants with SCD. **(A)** The *NCAPH2* methylation levels were significantly associated with the volume proportion of the LH in participants with SCD; **(B)** The positive correlation was not significant in the RH; Furthermore, the *NCAPH2* methylation levels were significantly associated with the volume proportion of both the LH **(C)** and the RH **(D)** in the APOE ε4 non-carriers. There were no significant associations in the APOE ε4 carriers in the LH **(E)** or the RH **(F)**. SCD, subjective cognitive decline; LH, left hippocampus; RH, right hippocampus.

correlation with the hippocampus contributes to the pathologic process of AD.

Among the several genes that are considered as risk factors for late-onset AD, the APOE ε4 confers the strongest risk. APOE ε4 isoforms have been shown to affect the disease pathogenesis by regulating Aβ aggregation (Ramanan et al., 2013, 2015) and impairing Aβ clearance in the brain (Castellano et al., 2011). However, it is neither necessary nor sufficient for incident AD; thus, it is of great interest to identify AD risk factors for the APOE ε4-non-carriers population. In this study, we found a positive correlation between *NCAPH2* hypomethylation and smaller hippocampal volume in the APOE ε4 non-carriers of the SCD group but not in the APOE ε4 carriers. Previous studies found that the APOE ε4 carriers have greater hippocampal atrophy than the non-carriers in patients with AD, cognitively normal elderly, and healthy young adults (O'Dwyer et al., 2012; Chang et al., 2019; Dong et al., 2019). This finding further strengthens the idea that AD

pathology has multiple factors and suggests that hippocampal atrophy is partly due to DNA methylation in the early stage of the disease. It seems that *NCAPH2* methylation is a useful peripheral biomarker to be used in combination with the analysis of genetic risk alleles to identify the disease pathogenesis, especially in the SCD APOE ε4-non-carriers risk population (Di Francesco et al., 2015).

This study has several limitations. First, the sample size in our study was relatively small. The lack of amyloid biomarkers for the underlying pathology of patients with SCD, patients with MCI, and patients with AD is another limitation of the current study. Further research, especially a follow-up large sample study with biomarkers of AD-type pathology in the preclinical disease stage, is needed to confirm this issue.

Taken together, our results indicated the *NCAPH2* methylation patterns in peripheral blood of individuals with SCD. Moreover, our data revealed the relationship between the *NCAPH2* methylation levels and the hippocampal volume in the APOE ε4-non-carriers of SCD. This information would suggest that changes in blood methylation may be an early indicator of individuals at risk for dementia as well as potential targets for intervention in the early stage of the disease.

DATA AVAILABILITY STATEMENT

The raw data supporting the conclusions of this article will be made available by the authors, without undue reservation.

ETHICS STATEMENT

Written informed consent was obtained from the individual(s) for the publication of any potentially identifiable images or data included in this article.

AUTHOR CONTRIBUTIONS

YH, Y-NC, and X-NW provided data and designed the study. YC and T-RL assembled and analyzed the data, consulted literature, and drafted the manuscript. S-WH reviewed the manuscript. YH and Y-NC critically revised the manuscript for important intellectual content. All authors read and approved the final manuscript.

FUNDING

This work was supported by grants from the National Key Research and Development Program of China (2016YFC1306300) and the National Natural Science Foundation of China (61633018 and 82020108013).

ACKNOWLEDGMENTS

Data collection and sharing for this study was funded by the Sino Longitudinal Study on Cognitive Decline (SILCODE) project (ClinicalTrials.gov, NCT 03370744). Colleagues of Xuanwu Hospital, Capital Medical University who have made contributions to build the SILCODE cohort are Weina Zhao, Ziqi Wang, Yuxia Li, Bin Mu, Xing Zhao, Jun Wang, Mingyan Zhao, Liu Yang, Xuanyu Li, Yu Sun, Guanqun Chen, Qin Yang, Can Sheng, Jiachen Li, Wenying Du, Xiaoqi Wang, Li Lin, Yang Zhan, Yi Liu, Lianghui Ni, and Xuan Jia.

SUPPLEMENTARY MATERIAL

The Supplementary Material for this article can be found online at: https://www.frontiersin.org/articles/10.3389/fnagi.2021.632382/full#supplementary-material

REFERENCES

Bakulski, K. M., Dolinoy, D. C., Sartor, M. A., Paulson, H. L., Konen, J. R., Lieberman, A. P., et al. (2012). Genome-wide DNA methylation differences between late-onset Alzheimer's disease and cognitively normal controls in human frontal cortex. *J. Alzheimer's Dis.* 29, 571–588. doi: 10.3233/jad-2012-111223

Bakulski, K. M., Halladay, A., Hu, V. W., Mill, J., and Fallin, M. D. (2016). Epigenetic research in neuropsychiatric disorders: the "tissue issue". *Curr. Behav. Neurosci. Rep.* 3, 264–274. doi: 10.1007/s40473-016-0083-4

Bondi, M. W., Edmonds, E. C., Jak, A. J., Clark, L. R., Delano-Wood, L., McDonald, C. R., et al. (2014). Neuropsychological criteria for mild cognitive impairment improves diagnostic precision, biomarker associations, and progression rates. *J. Alzheimers Dis.* 42, 275–289. doi: 10.3233/JAD-140276

Buckley, R. F., Maruff, P., Ames, D., Bourgeat, P., Martins, R. N., Masters, C. L., et al. (2016). Subjective memory decline predicts greater rates of clinical progression in preclinical Alzheimer's disease. *Alzheimers Dement* 12, 796–804. doi: 10.1016/j.jalz.2015.12.013

Castellano, J. M., Kim, J., Stewart, F. R., Jiang, H., DeMattos, R. B., Patterson, B. W., et al. (2011). Human apoE isoforms differentially regulate brain amyloid-beta peptide clearance. *Sci. Transl. Med.* 3:89ra57. doi: 10.1126/scitranslmed.3002156

Chang, Y. T., Kazui, H., Ikeda, M., Huang, C. W., Huang, S. H., Hsu, S. W., et al. (2019). Genetic interaction of APOE and FGF1 is associated with memory impairment and hippocampal atrophy in Alzheimer's disease. *Aging Dis.* 10, 510–519. doi: 10.14336/AD.2018.0606

Chouliaras, L., Mastroeni, D., Delvaux, E., Grover, A., Kenis, G., Hof, P. R., et al. (2013). Consistent decrease in global DNA methylation and hydroxymethylation in the hippocampus of Alzheimer's disease patients. *Neurobiol. Aging* 34, 2091–2099. doi: 10.1016/j.neurobiolaging.2013.02.021

Cronin, P., McCarthy, M. J., Lim, A. S. P., Salmon, D. P., Galasko, D., Masliah, E., et al. (2017). Circadian alterations during early stages of Alzheimer's disease are associated with aberrant cycles of DNA methylation in BMAL1. *Alzheimers Dement* 13, 689–700. doi: 10.1016/j.jalz.2016.10.003

De Jager, P. L., Srivastava, G., Lunnon, K., Burgess, J., Schalkwyk, L. C., Yu, L., et al. (2014). Alzheimer's disease: early alterations in brain DNA methylation at ANK1, BIN1, RHBDF2 and other loci. *Nat. Neurosci.* 17, 1156–1163. doi: 10.1038/nn.3786

Di Francesco, A., Arosio, B., Falconi, A., Micioni Di Bonaventura, M. V., Karimi, M., Mari, D., et al. (2015). Global changes in DNA methylation in Alzheimer's disease peripheral blood mononuclear cells. *Brain Behav. Immunity* 45, 139–144. doi: 10.1016/j.bbi.2014.11.002

Dong, Q., Zhang, W., Wu, J., Li, B., Schron, E. H., McMahon, T., et al. (2019). Applying surface-based hippocampal morphometry to study APOE-E4 allele dose effects in cognitively unimpaired subjects. *Neuroimage Clin.* 22:101744. doi: 10.1016/j.nicl.2019.101744

Dubois, B., Feldman, H. H., Jacova, C., Dekosky, S. T., Barberger-Gateau, P., Cummings, J., et al. (2007). Research criteria for the diagnosis of Alzheimer's

disease: revising the NINCDS-ADRDA criteria. *Lancet Neurol.* 6, 734–746. doi: 10.1016/S1474-4422(07)70178-3

Fransquet, P. D., Lacaze, P., Saffery, R., McNeil, J., Woods, R., and Ryan, J. (2018). Blood DNA methylation as a potential biomarker of dementia: a systematic review. *Alzheimer's Dement.* 14, 81–103. doi: 10.1016/j.jalz.2017.10.002

Gate, D., Saligrama, N., Leventhal, O., Yang, A. C., Unger, M. S., Middeldorp, J., et al. (2020). Clonally expanded CD8 T cells patrol the cerebrospinal fluid in Alzheimer's disease. *Nature* 577, 399–404. doi: 10.1038/s41586-019-1895-7

Ghodsi, M., Shahmohammadi, M., Modarressi, M. H., and Karami, F. (2020). Investigation of promoter methylation of MCPH1 gene in circulating cell-free DNA of brain tumor patients. *Exp. Brain Res.* 238, 1903–1909. doi: 10.1007/s00221-020-05848-1

Gosling, K. M., Goodnow, C. C., Verma, N. K., and Fahrer, A. M. (2008). Defective T-cell function leading to reduced antibody production in akleisin-βmutant mouse. *Immunology* 125, 208–217. doi: 10.1111/j.1365-2567.2008.02831.x

Jessen, F., Amariglio, R. E., van Boxtel, M., Breteler, M., Ceccaldi, M., Chetelat, G., et al. (2014). A conceptual framework for research on subjective cognitive decline in preclinical Alzheimer's disease. *Alzheimers Dement* 10, 844–852. doi: 10.1016/j.jalz.2014.01.001

Jia, T., Chu, C., Liu, Y., van Dongen, J., Papastergios, E., Armstrong, N. J., et al. (2019). Epigenome-wide meta-analysis of blood DNA methylation and its association with subcortical volumes: findings from the ENIGMA Epigenetics Working Group. *Mol. Psychiatry*. doi: 10.1038/s41380-019-0605-z. [Epub ahead of print].

Kobayashi, N., Shinagawa, S., Nagata, T., Shimada, K., Shibata, N., Ohnuma, T., et al. (2016). Development of biomarkers based on DNA methylation in the *NCAPH2*/LMF2 promoter region for diagnosis of Alzheimer's disease and amnesic mild cognitive impairment. *PLoS ONE* 11:e0146449. doi: 10.1371/journal.pone.0146449

Lane, C. A., Hardy, J., and Schott, J. M. (2018). Alzheimer's disease. *Europ. J. Neurol.* 25, 59–70. doi: 10.1111/ene.13439

Li, X., Wang, X., Su, L., Hu, X., and Han, Y. (2019). Sino Longitudinal Study on Cognitive Decline (SILCODE): protocol for a Chinese longitudinal observational study to develop risk prediction models of conversion to mild cognitive impairment in individuals with subjective cognitive decline. *BMJ Open* 9:e028188. doi: 10.1136/bmjopen-2018-028188

Lunnon, K., Smith, R., Hannon, E., De Jager, P. L., Srivastava, G., Volta, M., et al. (2014). Methylomic profiling implicates cortical deregulation of ANK1 in Alzheimer's disease. *Nat. Neurosci.* 17, 1164–1170. doi: 10.1038/nn.3782

Manjon, J. V., and Coupe, P. (2016). volBrain: an online MRI brain volumetry system. *Front. Neuroinform* 10:30. doi: 10.3389/fninf.2016.00030

Marques, S. C. F., Lemos, R., Ferreiro, E., Martins, M., de Mendonça, A., Santana, I., et al. (2012). Epigenetic regulation of BACE1 in Alzheimer's disease patients and in transgenic mice. *Neuroscience* 220, 256–266. doi: 10.1016/j.neuroscience.2012.06.029

Martin, C.-A., Murray, J. E., Carroll, P., Leitch, A., Mackenzie, K. J., Halachev, M., et al. (2016). Mutations in genes encoding condensin complex proteins cause microcephaly through decatenation failure at mitosis. *Genes Dev.* 30, 2158–2172. doi: 10.1101/gad.286351.116

McKhann, G., Drachman, D., Folstein, M., Katzman, R., Price, D., and Stadlan, E. M. (1984). Clinical diagnosis of Alzheimer's disease: report of the NINCDS-ADRDA work group under the auspices of department of health and human services task force on Alzheimer's disease. *Neurology* 34, 939–944. doi: 10.1212/wnl.34.7.939

Molinuevo, J. L., Rabin, L. A., Amariglio, R., Buckley, R., Dubois, B., Ellis, K. A., et al. (2017). Implementation of subjective cognitive decline criteria in research studies. *Alzheimer's Dement.* 13, 296–311. doi: 10.1016/j.jalz.2016.09.012

Mu, Y., and Gage, F. H. (2011). Adult hippocampal neurogenesis and its role in Alzheimer's disease. *Mol. Neurod.* 6:85. doi: 10.1186/1750-1326-6-85

O'Dwyer, L., Lamberton, F., Matura, S., Tanner, C., Scheibe, M., Miller, J., et al. (2012). Reduced hippocampal volume in healthy young ApoE4 carriers: an MRI study. *PLoS ONE* 7:e48895. doi: 10.1371/journal.pone.0048895

Perrotin, A., de Flores, R., Lamberton, F., Poisnel, G., La Joie, R., de la Sayette, V., et al. (2015). Hippocampal subfield volumetry and 3d surface mapping in subjective cognitive decline. *J. Alzheimer's Dis.* 48, S141–S150. doi: 10.3233/jad-150087

Rabin, L. A., Smart, C. M., and Amariglio, R. E. (2017). Subjective cognitive decline in preclinical Alzheimer's disease. *Annu. Rev. Clin. Psychol.* 13, 369–396. doi: 10.1146/annurev-clinpsy-032816-045136

Ramanan, V. K., Risacher, S. L., Nho, K., Kim, S., Shen, L., McDonald, B. C., et al. (2015). GWAS of longitudinal amyloid accumulation on 18F-florbetapir PET in Alzheimer's disease implicates microglial activation gene IL1RAP. *Brain* 138(Pt 10), 3076–3088. doi: 10.1093/brain/awv231

Ramanan, V. K., Risacher, S. L., Nho, K., Kim, S., Swaminathan, S., Shen, L., et al. (2013). APOE and BCHE as modulators of cerebral amyloid deposition: a florbetapir PET genome-wide association study. *Mol. Psychiatry* 19, 351–357. doi: 10.1038/mp.2013.19

Risacher, S. L., Tallman, E. F., West, J. D., Yoder, K. K., Hutchins, G. D., Fletcher, J. W., et al. (2017). Olfactory identification in subjective cognitive decline and mild cognitive impairment: association with tau but not amyloid positron emission tomography. *Alzheimers Dement (Amst)* 9, 57–66. doi: 10.1016/j.dadm.2017.09.001

Shinagawa, S., Kobayashi, N., Nagata, T., Kusaka, A., Yamada, H., Kondo, K., et al. (2016). DNA methylation in the *NCAPH2*/LMF2 promoter region is associated with hippocampal atrophy in Alzheimer's disease and amnesic mild cognitive impairment patients. *Neurosci. Lett.* 629, 33–37. doi: 10.1016/j.neulet.2016.06.055

Tannorella, P., Stoccoro, A., Tognoni, G., Petrozzi, L., Salluzzo, M. G., Ragalmuto, A., et al. (2015). Methylation analysis of multiple genes in blood DNA of Alzheimer's disease and healthy individuals. *Neurosci. Lett.* 600, 143–147. doi: 10.1016/j.neulet.2015.06.009

Vogel, J. W., Varga Dolezalova, M., La Joie, R., Marks, S. M., Schwimmer, H. D., Landau, S. M., et al. (2017). Subjective cognitive decline and beta-amyloid burden predict cognitive change in healthy elderly. *Neurology* 89, 2002–2009. doi: 10.1212/WNL.0000000000004627

Xie, B., Xu, Y., Liu, Z., Liu, W., Jiang, L., Zhang, R., et al. (2017). Elevation of Peripheral BDNF promoter methylation predicts conversion from amnestic mild cognitive impairment to Alzheimer's disease: a 5-year longitudinal study. *J. Alzheimer's Dis.* 56, 391–401. doi: 10.3233/jad-160954

Yue, L., Wang, T., Wang, J., Li, G., Wang, J., Li, X., et al. (2018). Asymmetry of hippocampus and amygdala defect in subjective cognitive decline among the community dwelling chinese. *Front. Psychiatry* 9:226. doi: 10.3389/fpsyt.2018.00226

Conflict of Interest: The authors declare that the research was conducted in the absence of any commercial or financial relationships that could be construed as a potential conflict of interest.

frontiers in Aging Neuroscience

ORIGINAL RESEARCH
published: 03 February 2021
doi: 10.3389/fnagi.2021.593898

Gray Matter Deterioration Pattern During Alzheimer's Disease Progression: A Regions-of-Interest Based Surface Morphometry Study

Zhanxiong Wu[1,2], *Yun Peng*[2], *Ming Hong*[1] *and Yingchun Zhang*[2]*

[1] School of Electronic Information, Hangzhou Dianzi University, Hangzhou, China, [2] Department of Biomedical Engineering, University of Houston, Houston, TX, United States

Accurate detection of the regions of Alzheimer's disease (AD) lesions is critical for early intervention to effectively slow down the progression of the disease. Although gray matter volumetric abnormalities are commonly detected in patients with mild cognition impairment (MCI) and patients with AD, the gray matter surface-based deterioration pattern associated with the progression of the disease from MCI to AD stages is largely unknown. To identify group differences in gray matter surface morphometry, including cortical thickness, the gyrification index (GI), and the sulcus depth, 80 subjects from the Alzheimer's Disease Neuroimaging Initiative (ADNI) database were split into healthy controls (HCs; $N = 20$), early MCIs (EMCI; $N = 20$), late MCIs (LMCI; $N = 20$), and ADs ($N = 20$). Regions-of-interest (ROI)-based surface morphometry was subsequently studied and compared across the four stage groups to characterize the gray matter deterioration during AD progression. Co-alteration patterns (Spearman's correlation coefficient) across the whole brain were also examined. Results showed that patients with MCI and AD exhibited a significant reduction in cortical thickness ($p < 0.001$) mainly in the cingulate region (four subregions) and in the temporal (thirteen subregions), parietal (five subregions), and frontal (six subregions) lobes compared to HCs. The sulcus depth of the eight temporal, four frontal, four occipital, and eight parietal subregions were also significantly affected ($p < 0.001$) by the progression of AD. The GI was shown to be insensitive to AD progression (only three subregions were detected with a significant difference, $p < 0.001$). Moreover, Spearman's correlation analysis confirmed that the co-alteration pattern of the cortical thickness and sulcus depth indices is predominant during AD progression. The findings highlight the relevance between gray matter surface morphometry and the stages of AD, laying the foundation for *in vivo* tracking of AD progression. The co-alteration pattern of surface-based morphometry would improve the researchers' knowledge of the underlying pathologic mechanisms in AD.

Keywords: gray matter, surface morphometry, Alzheimer's disease, cognition impairment, magnetic resonance imaging

OPEN ACCESS

Edited by:
Jiehui Jiang,
Shanghai University, China

Reviewed by:
Roberta Lizio,
Institute of Research and Medical Care (IRCCS) SDN, Italy
Zhen Yuan,
University of Macau, China

***Correspondence:**
Yingchun Zhang
yzhang94@uh.edu

Received: *11 August 2020*
Accepted: *13 January 2021*
Published: *03 February 2021*

Citation:
Wu Z, Peng Y, Hong M and Zhang Y (2021) Gray Matter Deterioration Pattern During Alzheimer's Disease Progression: A Regions-of-Interest Based Surface Morphometry Study. Front. Aging Neurosci. 13:593898. doi: 10.3389/fnagi.2021.593898

INTRODUCTION

Alzheimer's disease (AD) is a neurodegenerative disorder and the most common cause of dementia, which presumably starts with the aggregation of amyloid beta (Dicks et al., 2019). Gray matter volume reductions, a prominent AD feature because of neuronal loss, are considered as a close biological substrate of decline in cognitive functions. The decreases in gray matter volume can be measured by MRI. Studies have indicated gray matter abnormalities in patients with AD (Karas et al., 2004). Compared with healthy controls (HCs), patients with AD showed significantly lower global gray matter volume, lower whole brain volume, and greater ventricles (Guo et al., 2010). As the disease advances, gray matter abnormalities start to spread from the bilateral hippocampus, the amygdala, the entorhinal cortex, the posterior cingulate gyrus, and the medial thalamus to the parietal and frontal lobes (Moller et al., 2013). The symptomatic pre-dementia stage of AD, most commonly referred to as mild cognitive impairment (MCI), is critical to the development of predictive methods for early detection of AD and for further intervention programs (Li et al., 2018; Li K. et al., 2019; Ottoy et al., 2019; Wee et al., 2019). Different machine learning methods have been proposed to discriminate MCIs from HCs and ADs, based on the features extracted from structural MRI (Dimitriadis et al., 2017; Gomez-Sancho et al., 2018; Hojjati et al., 2018; Liu et al., 2020). Furthermore, recent evidence (Dicks et al., 2018; Tijms et al., 2018; Li R. et al., 2019; Wang et al., 2020) suggest that neuronal alterations in brain disorders tend to form patterns that resemble those of cerebral connectivity (co-alteration patterns). Therefore, to monitor disease progression, powerful non-invasive biomarkers, such as gray matter diffusivity (Jacobs et al., 2013) and gray matter volume (Lee et al., 2016; Qian et al., 2019), as well as their co-alteration patterns across the whole brain, are necessary to identify AD at early MCI stage and to advance the diagnosis, treatment, and prevention of these disorders.

Voxel-based morphometry (VBM) has been frequently used to examine gray matter differences across the whole brain. Using VBM, gray and white matter volume reductions were simultaneously detected between HCs and ADs (Baxter et al., 2006; Guo et al., 2010; Ha et al., 2012; Beejesh et al., 2019). An AD progression model was proposed to provide anatomically specific predictions of disease spread over time with VBM (Phillips et al., 2018). Dicks et al. (2019) modeled the gray matter atrophy in AD as a function of time and aging using Mini-Mental State Examination (MMSE) and found that the association of atrophy with MMSE was weaker than those with time or age. Based on VBM, local gray matter volumes were compared between patients with late- and early-onset AD and older and younger control subjects (Moller et al., 2013, Wu et al., 2020), and interactions of age and diagnosis on the volumes of the hippocampus and the precuneus were assessed, suggesting that the patterns of atrophy might vary in the spectrum of AD (Moller et al., 2013). Besides gray matter volume, revealing cross effects between AD-related incipient lesions helps to understand the progression to AD from MCI. Machine learning models were trained on VBM and connectome estimates to detect accurately AD-related neurodegeneration across the whole brain in a data-driven manner (Wang et al., 2019). Association between regional gray matter volume and two subtypes of psychotic symptoms in patients with mild AD was investigated, showing a distinct neural correlation between the paranoid and the non-psychosis groups (Lee et al., 2016). With the VBM technique, Cauda et al. (2018) found that structural alterations in the gray matter tended to follow the network-like patterns, indicating that structural co-alterations were influenced by connectivity constraints rather than being randomly distributed. Manuello et al. (2017) have investigated gray matter co-alterations of AD and found a series of co-altered areas that include the left hippocampus, left and right amygdalae, right parahippocampal gyrus, and right temporal inferior gyrus. Based on VBM, these studies consistently showed a widespread gray matter co-atrophy pattern due to AD. The co-alteration pattern may accelerate the development of neuronal abnormalities.

Unlike VBM, the surface-based morphometry methods can measure the cortical thickness and folding patterns, as well as the shape or curvature measures derived from brain surface meshes (Gutman et al., 2009; Lui et al., 2010). Previous studies demonstrated an increased accuracy of brain registration using brain surface meshes for spatial registration, compared to volume-based registration (Desai et al., 2005). Brain surface meshes permit new forms of analyses, such as the GI and the sulcus index, which measure surface complexity in 3D (Yotter et al., 2011) or cortical thickness (Righart et al., 2017). In addition, inflation or spherical mapping of the cortical surface mesh raises the buried sulci to the surface so that the mapped functional activity in these regions can be made visible. However, few studies have attempted to monitor gray matter alterations associated with MCIs and ADs using regions-of-interest (ROI)-based surface morphometry based on brain surface meshing. In this study, we investigated ROI-based surface morphometry of gray matter in different stages of AD, including HC, EMCI, LMCI, and AD, aiming to identify characteristic gray matter alteration patterns in terms of cortical thickness, GI, and the sulcus depth during AD progression.

METHODS AND MATERIALS

Subjects

Data used in this study were obtained from the Alzheimer's Disease Neuroimaging Initiative (ADNI) database (http://adni.loni.usc.edu). The ADNI was initially launched in 2004. The primary goal of ADNI is to identify MRI, PET, biomarkers, and genetic characteristics that would support the early detection and tracking of AD and improve the clinical trial design (Risacher et al., 2009; Jack et al., 2010a; Petersen et al., 2010). Scans were acquired with a 3.0-T head-only Siemens Medical Solutions MRI scanner (Erlangen, Germany). T1-weighted imaging parameters were: repetition time = 2,250 ms, echo time = 2.6 ms, flip angle = 9, field of view = 256 × 256 mm, acquisition matrix = 256 × 256, voxel size = 1 mm isotropic, and number of slices = 192. The demographic data of the subjects are summarized in **Table 1**. The flowchart of the ROI-based surface morphometry analysis is shown in **Figure 1**.

TABLE 1 | Demographics of healthy controls (HCs), mild cognition impairments (MCIs), and Alzheimer's disease (ADs).

	HC	Early MCIs (EMCI)	Late MCIs (LMCI)	AD
Number of subjects	20	20	20	20
Gender	12F:8M	8F:12M	9F:11M	11F:9M
Mean age (Std)	73.75 (4.78)	75.95 (7.12)	74.35 (5.72)	74.85 (8.27)
CDR	0	0.5	0.5	0.5–1
MMSE	24–30	24–30	24–30	20–26

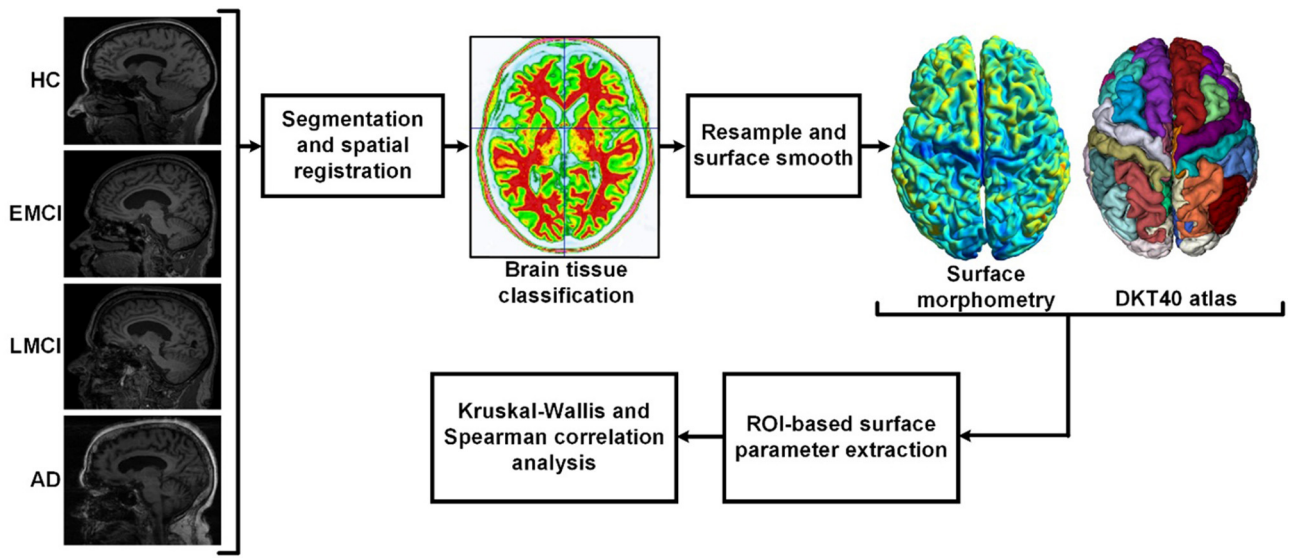

FIGURE 1 | Flowchart of the regions-of-interest (ROI)-based surface morphometry analysis. After brain extraction and segmentation (white matter, gray matter, and cerebrospinal fluid), spatial normalization was performed to correct the orientation and the size of the brain. Then, the surface of gray matter was resampled and smoothed. The ROI-based surface parameters were extracted according to the DKT40 parcellation atlas. Cortical thickness, gyrification index (GI), and sulcus depth were used to characterize the deterioration patterns of gray matter during Alzheimer's disease (AD) progression.

Regions-of-Interest-Based Surface Morphometry

T1-weighted MR image preprocessing was performed using automated procedures included in the Computational Anatomical Toolbox (CAT12), an extension to the Statistical Parametric Mapping (SPM12) package (http://www.neuro.uni-jena.de/cat/). First, T1-weighted images were preprocessed with intensity normalization and skull stripping, followed by the normalization of the head position along the commissural axis and the labeling of the cortical and subcortical regions. Second, the images were segmented into gray matter, white matter, and cerebrospinal fluid with the parameter of Markov random fields set to 2, and co-registered to a probabilistic brain atlas with non-linear morphing. According to the probability that a given location is of a particular tissue class (gray matter, white matter, and cerebrospinal fluid), the intensity of the image at the location, and the local spatial configuration of the location related to the labels, each MRI voxel was assigned to one specific tissue class (Dahnke et al., 2013). In this process, all T1-weighted images were spatially normalized using combinations of affine linear transformation and non-linear registration to the standard Montreal Neurological Institute (MNI) template and segmented into gray matter, white matter, and cerebrospinal fluid. Third, a DKT40 labeling atlas was warped from standard space to subject space using the subject-specific inversed normalization parameters. All results were estimated in the native space before spatial normalization. Last, an individual brain atlas that consisted of 68 different gray matter areas was created for each participant according to the DKT40 parcellation atlas, as shown in **Figure 2**. The names and the corresponding indices of the parcellated regions are reported in **Table 2**. The pipeline used topology correction and spherical mapping to handle the partial volume effect, sulcal blurring, and asymmetry (Righart et al., 2017).

In this study, three ROI-based surface morphometry parameters were used to characterize the deterioration pattern of gray matter, including cortical thickness, the GI, and the sulcus depth:

Cortical Thickness

It is defined as the distance between the inner and the outer surface estimated from brain surface meshes, was related to

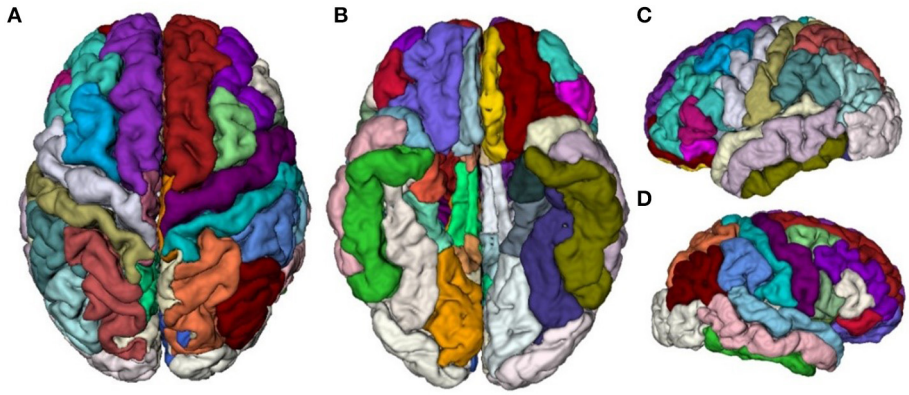

FIGURE 2 | Visualization of the DKT40 cortical parcellation atlas, comprising 68 local regions. **(A)** Top view, **(B)** Bottom view, **(C)** Right view, and **(D)** Left view.

TABLE 2 | Names and indices of the DKT40 parcellated cortical regions.

Region	Region	Region	Region
1 bankssts_left	2 bankssts_right	3 caudalanteriorcingulate_left	4 caudalanteriorcingulate_right
5 caudalmiddlefrontal_left	6 caudalmiddlefrontal_right	7 cuneus_left	8 cuneus_right
9 entorhinal_left	10 entorhinal_right	11 fusiform_left	12 fusiform_right
13 inferiorparietal_left	14 inferiorparietal_right	15 inferiortemporal_left	16 inferiortemporal_right
17 isthmuscingulate_left	18 isthmuscingulate_right	19 lateraloccipital_left	20 lateraloccipital_right
21 lateralorbitofrontal_left	22 lateralorbitofrontal_right	23 lingual_left	24 lingual_right
25 medialorbitofrontal_left	26 medialorbitofrontal_right	27 middletemporal_left	28 middletemporal_right
29 parahippocampal_left	30 parahippocampal_right	31 paracentral_left	32 paracentral_right
33 parsopercularis_left	34 parsopercularis_right	35 parsorbitalis_left	36 parsorbitalis_right
37 parstriangularis_left	38 parstriangularis_right	39 pericalcarine_left	40 pericalcarine_right
41 postcentral_left	42 postcentral_right	43 posteriorcingulate_left	44 posteriorcingulate_right
45 precentral_left	46 precentral_right	47 precuneus_left	48 precuneus_*right*
49 rostralanteriorcingulate_left	50 rostralanteriorcingulate_right	51 rostralmiddlefrontal_left	52 rostralmiddlefrontal_right
53 superiorfrontal_left	54 superiorfrontal_right	55 superiorparietal_left	56 superiorparietal_right
57 superiortemporal_left	58 superiortemporal_right	59 supramarginal_left	60 supramarginal_right
61 frontalpole_left	62 frontalpole_right	63 temporalpole_left	64 temporalpole_right
65 transversetemporal_left	66 transversetemporal_right	67 insula_left	68 insula_right

cortical development (Dahnke et al., 2013), and identified as an important biomarker for normal development and aging (Sowell et al., 2004, 2007; Fjell et al., 2006) and pathological changes such as AD (Kuperberg et al., 2003; Sailer et al., 2003; Thompson et al., 2004; Rosas et al., 2008). Here, brain tissue segmentation was used to estimate the white matter distance and to project the local maxima (which is equal to the cortical thickness) onto other gray matter voxels using a neighboring relationship described by the white matter distance. This projection-based thickness allowed the handling of partial volume information, sulcal blurring, and sulcal asymmetries without explicit sulcus reconstruction (Dahnke et al., 2013).

Gyrification Index

It is defined as the ratio of the inner surface size to the outer surface size of an outer (usually convex) hull and was computed by averaging the absolute curvature values from each vertex of the spherical surface mesh (Luders et al., 2006).

Sulcus Depth

It is extracted based on the Euclidean distance between the central surface and its convex hull. Transformation with square root is used to render the data more normally distributed.

These surface parameters were estimated using the CAT toolbox (designed by Structural Brain Mapping Group, Departments of Psychiatry and Neurology, Jena University Hospital, Germany), which uses an internal interpolation to provide more reliable results even with low-resolution images and anisotropic spatial resolutions. Although interpolation cannot add more details to the images, the computations would benefit from the higher number of voxels, and the strip artifacts in preprocessed images are greatly reduced. While cortical thickness was estimated from the surface smoothed to 15 mm of full width at half maximum Gaussian kernel, GI and sulcus

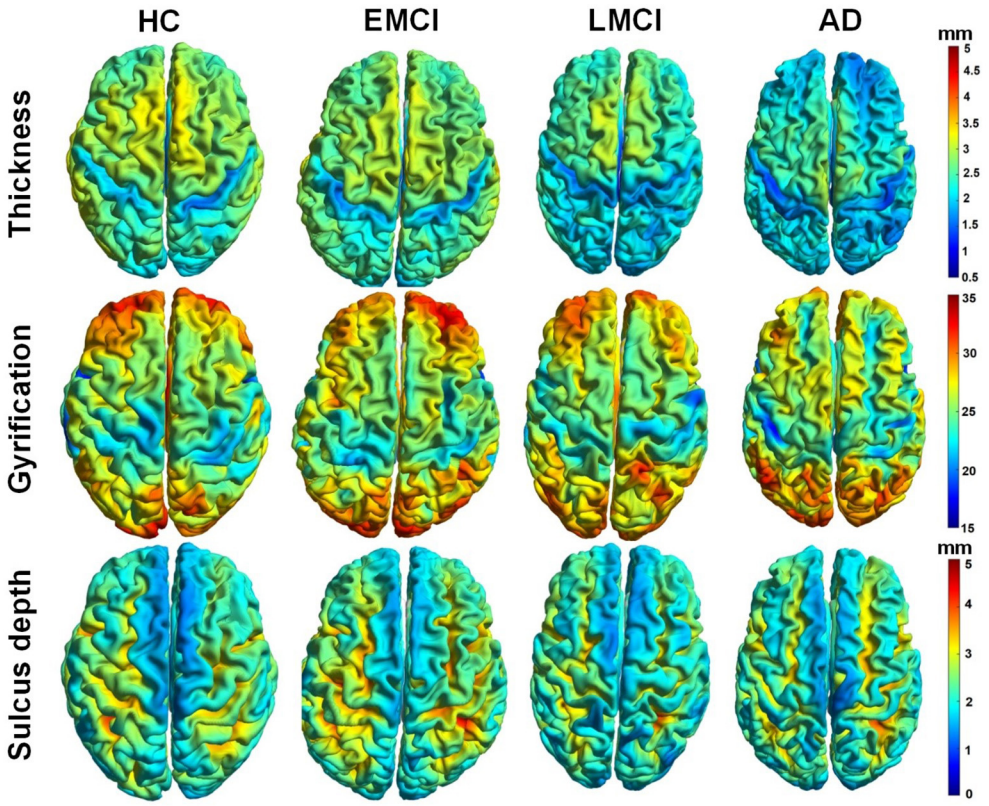

FIGURE 3 | Whole-brain mapping of surface thickness, gyrification index (GI), and sulcus depth maps estimated using CAT12 toolbox. From left to right, each column represents a subject in control, early mild cognitive impairment (EMCI), late MCI (LMCI), and AD groups, respectively.

depth were computed from the surface smoothed with 20 mm full width at half maximum (Dahnke et al., 2013).

Statistical Analysis

For each region (total 68 regions in DKT40 atlas), the gender covariate was first regressed out. Group-wise differences in cortical thickness, the GI, and the sulcus depth were assessed using the Kruskal–Wallis test. To additionally characterize the structural co-alterations in the evolution of AD, the Spearman's correlation analysis was used to investigate whether the alteration of a brain area was associated with the alteration of other brain areas. Statistical analyses were performed in MATLAB. For all analyses, significance was set at the value of $p < 0.001$ (uncorrected). Effect sizes for the Kruskal–Wallis tests can be defined as the chi-squared statistic divided by $(N - 1)$.

$$\eta^2 = \frac{\chi^2}{N-1} \tag{1}$$

where χ^2 is chi-squared statistic and N is sample size.

RESULTS

Figure 3 demonstrated whole-brain mapping of cortical thickness, the GI, and the sulcus depth, where, from left to right, each column represents a subject in HC, EMCI, LMCI, and AD groups. Overall, across the four groups, the distributions of these parameters exhibited similarities. The greatest local cortical thickness appeared to be located in the left and right parietal lobes. The highest local gyrification was located in the frontal lobe, as well as in the occipital lobe, while the lowest GI in the left and right hemispheres appears surrounding the superior parietal gyrus and expanding into the inferior temporal gyrus. The least sulcus depth was detected in the elongated regions along the longitudinal fissure between the left and right hemispheres. As demonstrated in **Figure 3**, there were some differences in these surface complexity parameters across these groups, especially in cortical thickness (first row in **Figure 3**). Subsequently, the Kruskal–Wallis and Spearman's correlation tests were used to assess regional differences in these surface morphometry parameters across the groups.

Figures 4–6 show the nodal distribution (mean ± SD) of cortical thickness, GI, and sulcus depth for each group. After the ROI-based surface complexity was estimated according to the DKT40 atlas, the Kruskal–Wallis test was repeated for 68 regions and the regions that could be significantly identified across four groups were provided in **Table 3**. As reported in this table, statistically significant differences ($p < 0.001$, uncorrected) in the regions, namely temporal lobe: 1, 9, 10, 11, 15, 16, 27, 28, 57, 58, 63, 64, and 67; frontal lobe: 22, 26, 33, 34, 51, and 52;

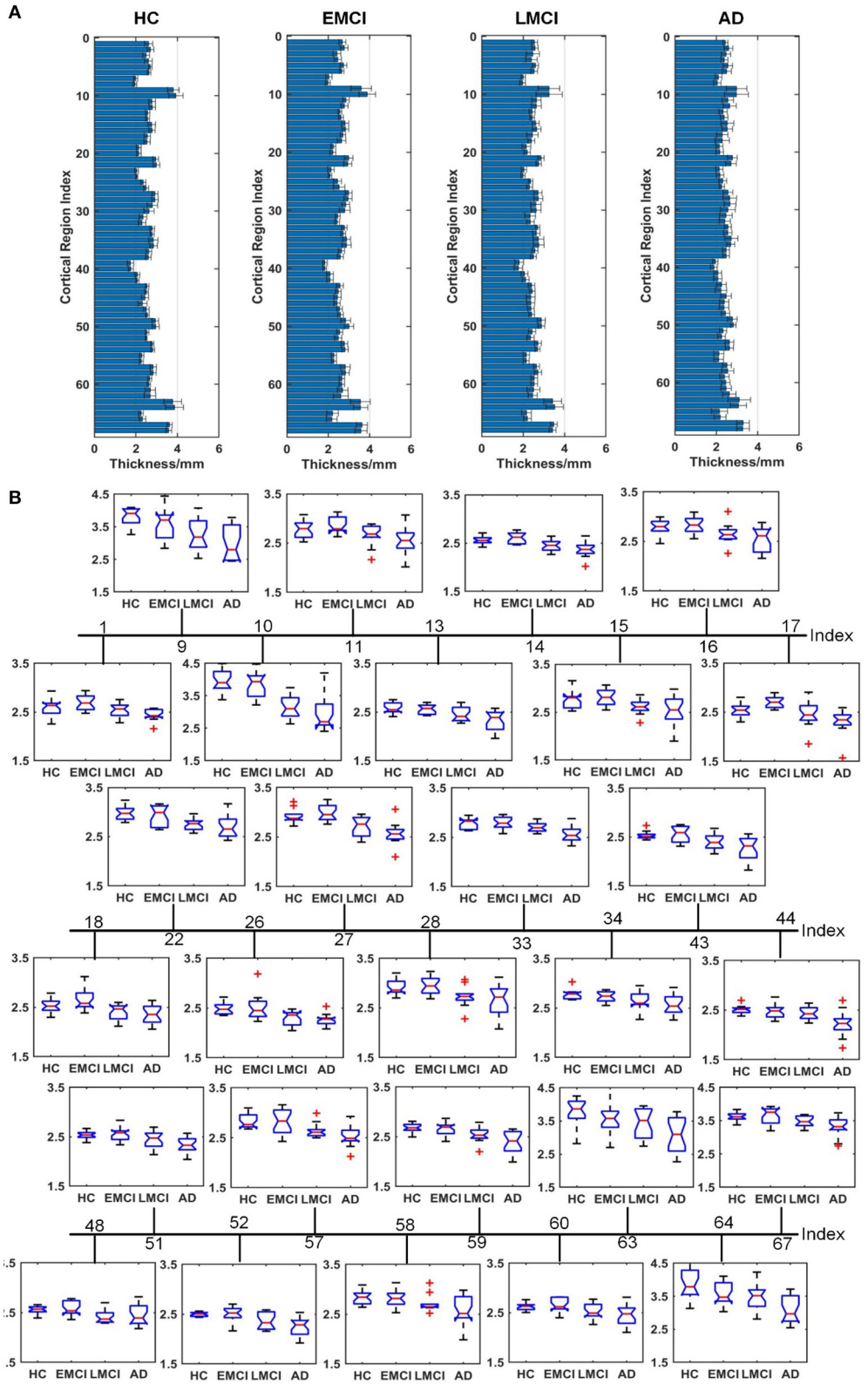

FIGURE 4 | Comparison of cortical thickness across HC, EMCI, LMCI, and AD groups. **(A)** The nodal distribution (mean ± SD) of cortical thickness for each group. **(B)** The Kruskal–Wallis test was performed, and ROIs that exhibit significant difference across four groups were listed. The value of *p* of the Kruskal–Wallis test is reported in **Table 3**. Region indexes refer to **Table 2**. Red crosses denote outliers.

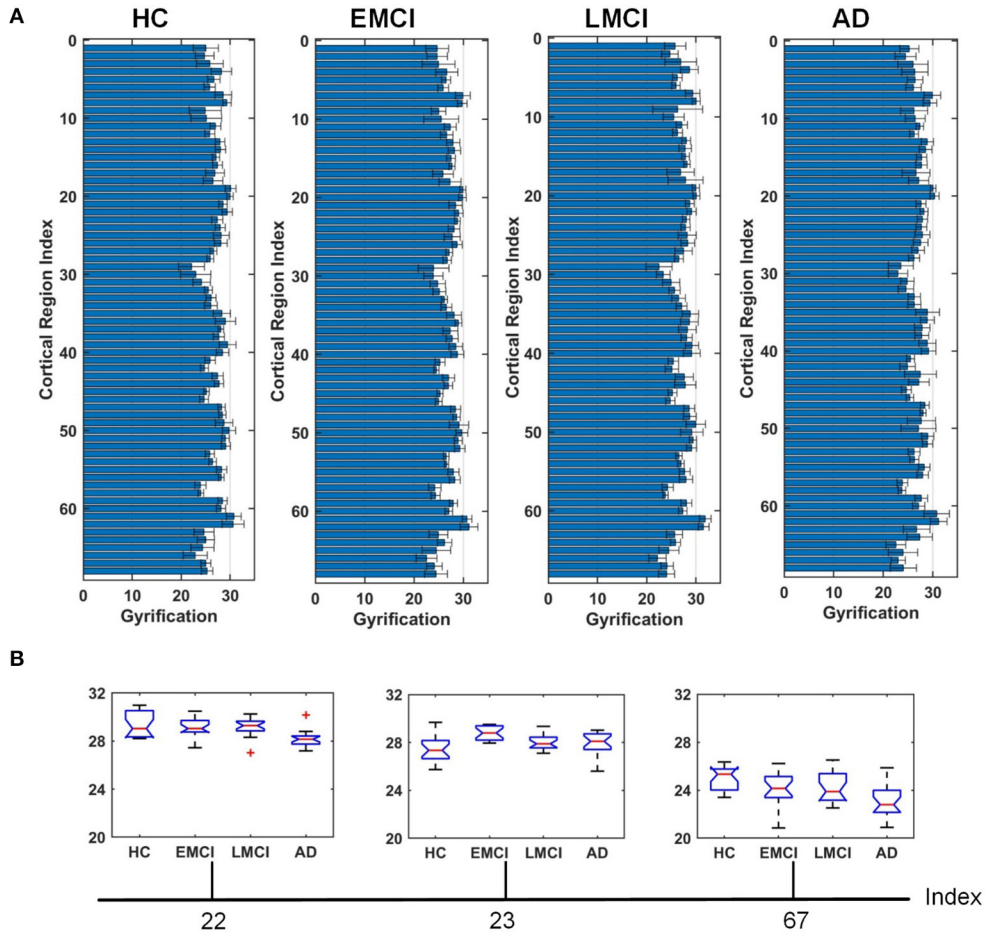

FIGURE 5 | Comparison of the GI across HC, EMCI, LMCI, and AD groups. **(A)** The nodal distribution (mean ± SD) of the GI for each group. **(B)** The Kruskal–Wallis test was performed, and ROIs that exhibit significant difference across four groups were listed. The value of p of the Kruskal–Wallis test is reported in **Table 3**. Region indexes refer to **Table 2**. Red crosses denote outliers.

parietal lobe: 13, 14, 48, 59, and 60; and cingulate: 17, 18, 43, 44, were found in cortical thickness. A significant difference in the GI ($p < 0.001$, uncorrected) was found only in three regions, namely 22, 23, and 67. Significant sulcus depth reductions ($p < 0.001$, uncorrected) over AD progression were revealed, which mainly occurred in the local regions, namely temporal lobe: 2, 12, 16, 58, 65, 66, 67, and 68; frontal lobe: 5, 6, 26, and 33; parietal lobe: 13, 14, 41, 45, 46, 55, 56, and 59; occipital lobe: 8, 19, 20, and 24; and cingulate: 18 and 30.

To reveal gray matter changes occurring simultaneously in different gray matter subregions, we characterized co-alteration patterns of ROI-based surface morphometry during the evolution of AD with the Spearman's correlation analysis. Given the nodes previously designed according to the DKT40 atlas, the co-alteration matrices were constructed for cortical thickness, GI, and sulcus depth. **Figure 7A** shows the Spearman's correlation matrices between 68 local regions in terms of cortical thickness, GI, and sulcus depth. The matrices were binarized, and the value of +1 indicates a perfect positive correlation, i.e., the related subregions share the same decreased trend in the surface morphometric metrics. The corresponding binary networks were also illustrated in **Figure 7B**. Interestingly, the three co-alteration networks are different. The node degree is the number of connections that the node has with the other nodes, and it was computed to evaluate co-alteration patterns of the surface morphometric metrics over AD progression (**Figure 7C**). In the co-alteration network of cortical thickness, we can find that the degrees of 26 nodes (see **Figure 7C**) are 25. In the sulcus depth network, the degrees of 23 nodes (see **Figure 7C**) are >20. However, for the gyrification network, the node degrees are much smaller (see **Figure 7C**). In accordance with the Kruskal–Wallis test, the metrics of cortical thickness and the sulcus depth are more sensitive and specific in distinguishing MCIs and ADs from HCs.

DISCUSSION

Alzheimer's disease is a progressive neurodegenerative disease characterized by a decline in memory processing and cognitive

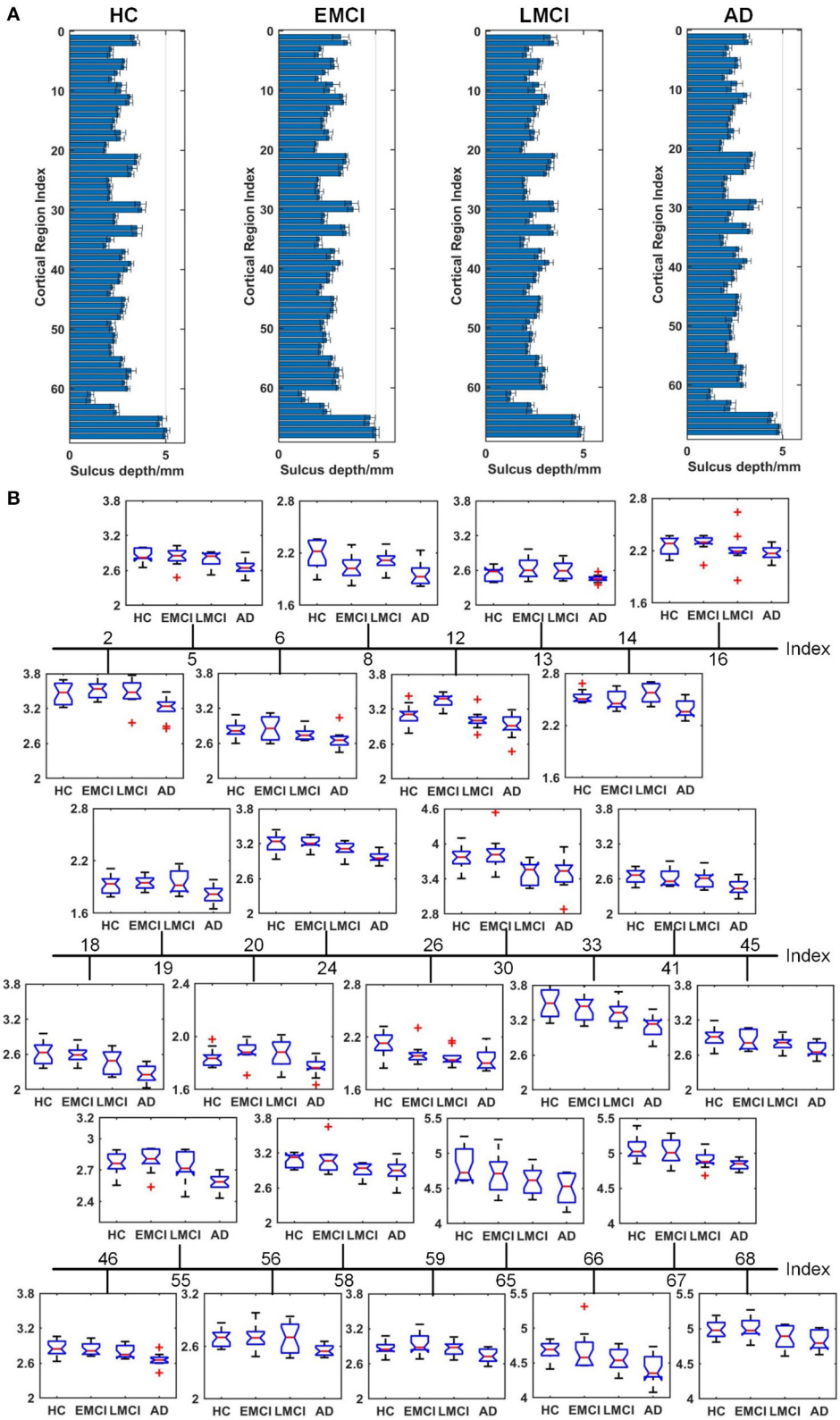

FIGURE 6 | Comparison of the sulcus depth across HC, EMCI, LMCI, and AD groups. **(A)** The nodal distribution (mean ± SD) of the sulcus depth for each group. **(B)** The Kruskal–Wallis test was performed, and ROIs that exhibit significant difference across four groups were listed. The value of p of the Kruskal–Wallis test is reported in **Table 3**. Region indexes refer to **Table 2**. Red crosses denote outliers.

function. Gray matter atrophy is considered as a close biological substrate of decline in cognitive functioning (Jack et al., 2010b). In this study, with ROI-based surface morphometry analyses based on brain surface meshes, gray matter alterations over AD progression were investigated. Besides cortical thickness, surface complexity (GI and sulcus depth) was estimated at a local scale, revealing a global reduction in the sulcus depth of the MCI and AD groups. The main findings of this study provide a novel perspective for understanding the pathophysiological mechanisms underlying AD and could potentially enhance the accuracy in the early detection and intervention of AD.

A clear deterioration pattern of gray matter over AD progression was shown with the Kruskal–Wallis test. Cortical thickness and sulcus depth were more pronounced during AD progression (**Figures 4**, **6**), and the GI was found to be significantly different only in three local regions (22, 23, 67) (**Figure 5**). This finding is broadly consistent with the findings in previous studies. Patients with AD mainly exhibited significant gray matter volume reductions in the hippocampus, the temporal lobes, the precuneus, the cingulate gyrus, the insula, and the inferior frontal cortex (Guo et al., 2010; Moller et al., 2013; Lee et al., 2016; Dicks et al., 2019). Our findings also confirmed that the brain regions exhibiting high topological centrality, considered as brain hubs, are more likely to be affected by AD processes, as they are located at the center of important functional networks (Cauda et al., 2018). As reported in **Table 3**, areas showing significant statistical decreases include insulae (67 and 68); cingulate cortices (17, 18, 43, and 44); inferior, superior, and middle temporal gyri (15, 16, 27, 28, 57, and 58); middle and inferior frontal (22, 26, 33, 34, 51, and 52); pre- and postcentral gyri (13, 14, 41, 45, 46, 55, and 56). Disruption in these hub regions could impede communication between distinct gray matter regions, resulting in impaired cognitive functioning and the rapid development of AD abnormalities from MCI.

Evidence suggests that pathological alteration occurs long before the onset of clinical AD symptoms due to the toxic effects of amyloid-beta plaques (Chetelat et al., 2010; Johnson et al., 2014; Juan et al., 2015). In previous studies, cortical thickness changes were found to be circumscribed to the left hemisphere in patients with MCI and patients with AD using either VBM (Chetelat et al., 2002; Karas et al., 2003; Thompson et al., 2003) or the surface-based cortical thickness analysis (Lerch et al., 2005; Vivek et al., 2006). Specifically, longitudinal studies showed that the left gray matter loss of medial temporoparietal regions was strongly correlated with worse cognitive performance and that faster leftward reduction of gray matter loss was uncovered in patients with AD (Thompson et al., 2003). Our results indicated that eight regions in the left temporal lobe (1, 9, 11, 15, 27, 57, 63, and 67) and five regions in the right temporal lobe (10, 16, 28, 58, and 64) displayed a significant reduction in cortical thickness, supporting the hypothesis that AD-related cortical thickness reduction predominantly occurs in the left hemisphere. However, this spatial deterioration distribution was not observed in the parietal lobe (left: 13 and 59; right: 14, 48, and 60), the frontal lobe (left: 33 and 51; right: 22, 26, 34, and 52), and the cingulate region (left: 17 and 43; right: 18 and 44). Additionally, in the statistical analysis of sulcus depth, we found that five regions in the left parietal lobe (13, 41, 45, 55, and 59) and three regions (14, 46, and 56) in the right parietal lobe exhibited significant reduction. As the spatial deterioration patterns of MCI and AD may be individually different, a larger sample is needed for testing in the next step.

TABLE 3 | The Kruskal–Wallis test on cortical thickness, GI, and sulcus depth across healthy controls (HC), early mild cognitive impairment (EMCI), late MCI (LMCI), and AD groups.

	Region index
Cortical thickness	1, 9, 10, 11, 13, 14, 15, 16, 17, 18, 22, 26, 27, 28, 33, 34, 43, 44, 48, 51, 52, 57, 58, 59, 60, 63, 64, 67
Gyrification	22, 23, 67
Sulcus depth	2, 5, 6, 8, 12, 13, 14, 16, 18, 19, 20, 24, 26, 30, 33, 41, 45, 46, 55, 56, 58, 59, 65, 66, 67, 68

The regions associated with $p < 0.001$ (uncorrected) were provided.

The pathological brains of patients with MCI and patients with AD are also characterized by structural co-alterations in the gray matter, which tend to follow identifiable network-like patterns (Cauda et al., 2018). The co-alteration patterns of surface morphometry parameters indicated the synchronization of gray matter deterioration between distinct gray matter parcels. Studies have revealed that gray matter co-alteration patterns of patients with MCI and patients with AD have a less optimal topological organization characterized by increased segregation and decreased integration (Yong et al., 2008; Tijms et al., 2013; Romerogarcia et al., 2016). By considering the cortical co-alteration pattern as a graph and by studying its edge strength (Spearman's correlation) features at the network level, the cross effects between AD-related incipient lesions may be disclosed. In this study, correlated changes in cortical thickness, GI, and sulcus depth were used to assess the correlation strength across the whole brain and to investigate temporal differences in cross-cortical correlations between groups. Our results provide evidence that alterations of gray matter thickness and sulcus depth are network-like distributed (**Figure 7B**). This co-alteration exhibits a topological structure and includes some pathological regions that have been thought to be important functional hubs of the brain. As shown in **Figure 7C**, the degree of these local regions (**Table 3**) estimated from the cortical thickness correlation matrix was between 18 and 25, except region 48 (precuneus_right), and the degree extracted from the sulcus depth correlation coefficient was between 8 and 22, except 8 (cuneus_right), 14 (inferiorparietal_right), and 19 (lateraloccipital_left). The finding confirms that the primary deterioration in some atrophic regions might lead to a secondary deterioration in other connected areas. The co-alteration patterns of brain atrophy caused by AD appeared to considerably resemble the patterns of brain structural connections (Cauda et al., 2018). However, from the gray matter co-alteration analyses, we still cannot identify the causal relationship between the altered gray matter parcels. It may be a chance to reveal neuropathological co-alterations patterns in patients with MCI

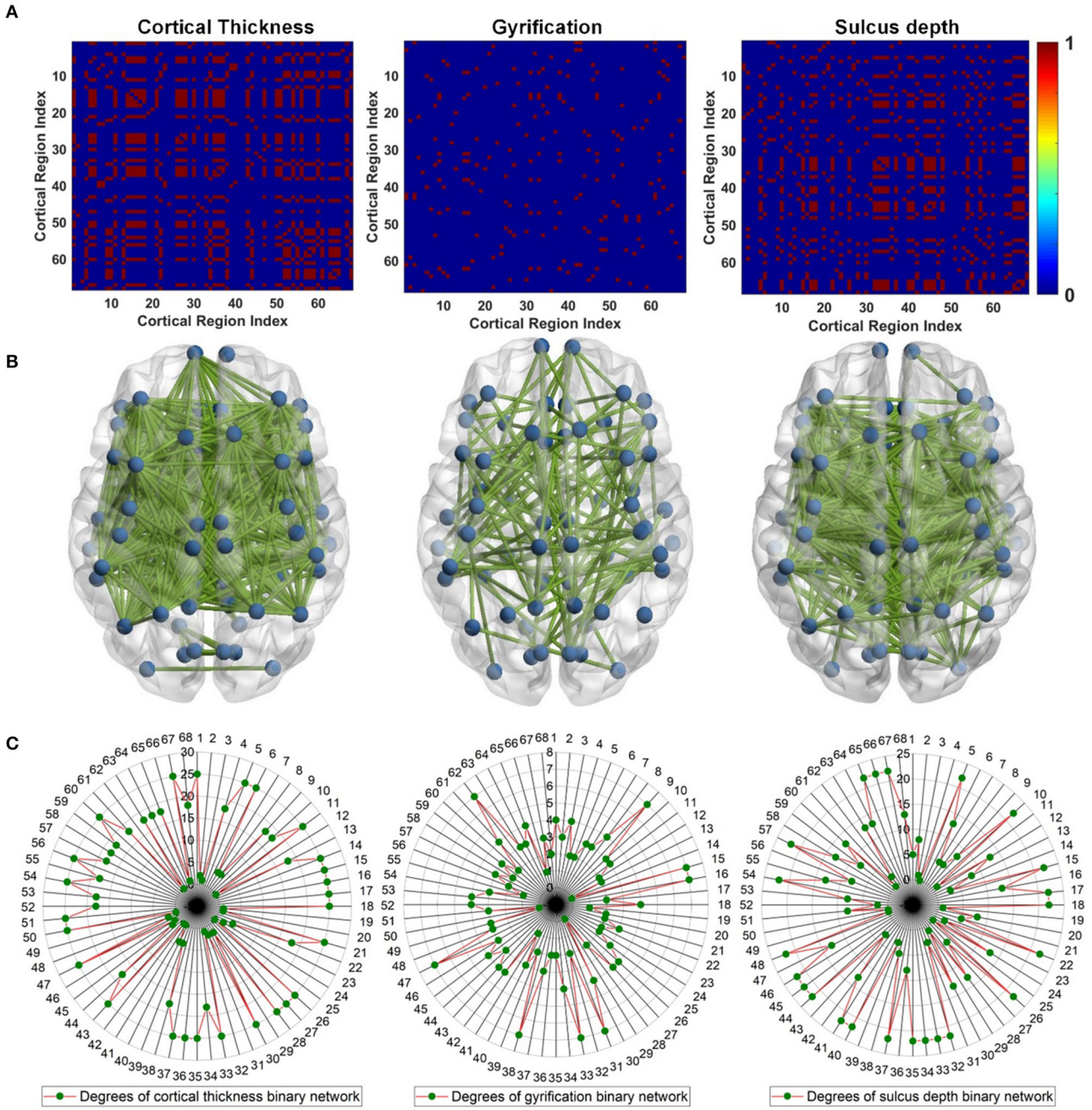

FIGURE 7 | Surface morphometric co-alteration patterns among different cortical subregions. For cortical subregion indices, please refer to **Table 2**. **(A)** Binarized Spearman's correlation matrices estimated from the ROI-based surface morphometric metrics, including cortical thickness, GI, and sulcus depth. The correlation matrices were thresholded at the value of 1. The value of 1 indicates that the related subregions share the same decreased trend in surface morphometry **(B)** Binary networks correspond to the Spearman's correlation matrices in **(A)**. **(C)** Degree of each cortical subregion estimated from **(A)**.

and patients with AD, with a combination of functional and anatomic connectivity estimation.

A novel aspect of this study is the assessment of the ROI-based surface morphometric alteration across HC, EMCI, LMCI, and AD groups. The findings are basically in line with the literature showing the associations of gray matter volume morphometry with MCIs and ADs. This might suggest a greater sensitivity of surface estimates in detecting MCI- and AD-related neurodegeneration compared with gray matter voxel-based morphometry. However, the results in this study have several limitations to be interpreted with caution. First, this study was limited by a relatively small sample size. Although we were able to detect effects with this sample size, a larger sample would be optimal for surface morphometry

analysis. Second, there is an increased risk for false-positive results because we used uncorrected ($p < 0.001$) thresholds for surface morphometry analysis due to our sample size. Third, brain parcellation may influence the characterization of surface morphometry during AD progression (Messe, 2019; Wu et al., 2019), which deserves further study. Last, the education information of participants and neuropsychological markers are not available in the ADNI database, so they have not been taken into account in the statistical analysis in this study. Despite these limitations, to our knowledge, this is the first report to show the association of brain regional gray matter surface complexity with AD progression. Further, multimodal neuroimaging studies are needed to investigate associations between regional structural brain atrophy and cognition declines in patients with AD. More rigorous methods to combine multimodal MRI brain imaging (structural MRI, diffusion MRI, and functional MRI) may be required. Combining structural brain imaging and connectivity for *in vivo* tracking of AD-related lesions in the asymptomatic stages may be a promising method, facilitating an understanding of how the co-alteration patterns found in this study were constrained by structural or functional connectivity.

CONCLUSION

This study reported the ROI-based surface morphometry of gray matter across HC, EMCI, LMCI, and AD groups and identified characteristic alteration patterns in surface morphometry during AD progression. Patients with MCI and patients with AD showed considerable reduction in cortical thickness and surface complexity indices. These parameters could potentially serve as biomarkers for the prediction of AD progression. Future longitudinal studies should determine whether these markers are able to detect gray matter changes with therapies aimed at slowing the disease progression. The possibility of combining structural brain imaging and anatomical or functional connectivity for *in vivo* tracking of AD-linked lesions in the asymptomatic stages is worth further exploration.

DATA AVAILABILITY STATEMENT

Publicly available datasets were analyzed in this study. This data can be found at: http://adni.loni.usc.edu/.

ETHICS STATEMENT

Ethical review and approval was not required for the study on human participants in accordance with the local legislation and institutional requirements. Written informed consent for participation was not required for this study in accordance with the national legislation and the institutional requirements.

AUTHOR CONTRIBUTIONS

ZW: data analysis, result interpretation, manuscript drafting and revision. YP: result interpretation, manuscript drafting, and revision. MH: data analysis and manuscript drafting. YZ: data analysis, result interpretation, and manuscript revision. All authors contributed to the article and approved the submitted version.

FUNDING

The research is supported in part by the Natural Science Foundation of Zhejiang Province (LY20E070005 and LY17E070007), National Natural Science Foundation of China (51207038), China Scholarship Council, and the University of Houston. Data collection and sharing for this project was funded by the Alzheimer's Disease Neuroimaging Initiative (ADNI) (National Institutes of Health Grant No. U01AG024904) and DOD ADNI (Department of Defense award number W81XWH-12-2-0012). ADNI is funded by the National Institute on Aging, the National Institute of Biomedical Imaging and Bioengineering, and through generous contributions from the following: AbbVie, Alzheimer's Association; Alzheimer's Drug Discovery Foundation; Araclon Biotech; BioClinica, Inc.; Biogen; Bristol-Myers Squibb Company; CereSpir, Inc.; Cogstate; Eisai Inc.; Elan Pharmaceuticals, Inc.; Eli Lilly and Company; EuroImmun; F. Hoffmann-La Roche Ltd and its affiliated company Genentech, Inc.; Fujirebio; GE Healthcare; IXICO Ltd.; Janssen Alzheimer Immunotherapy Research & Development, LLC.; Johnson & Johnson Pharmaceutical Research & Development LLC.; Lumosity; Lundbeck; Merck & Co., Inc.; Meso Scale Diagnostics, LLC.; NeuroRx Research; Neurotrack Technologies; Novartis Pharmaceuticals Corporation; Pfizer Inc.; Piramal Imaging; Servier; Takeda Pharmaceutical Company; and Transition Therapeutics. The Canadian Institutes of Health Research is providing funds to support ADNI clinical sites in Canada. Private sector contributions are facilitated by the Foundation for the National Institutes of Health (www.fnih.org). The grantee organization is the Northern California Institute for Research and Education.

ACKNOWLEDGMENTS

The study is coordinated by the Alzheimer's Therapeutic Research Institute at the University of Southern California. ADNI data are disseminated by the Laboratory for Neuro Imaging at the University of Southern California.

REFERENCES

Baxter, L. C., Sparks, D. L., Johnson, S. C., Lenoski, B., Lopez, J. E., Connor, D. J., et al. (2006). Relationship of cognitive measures and gray and white matter in Alzheimer's disease. *J. Alzheimer Dis.* 9, 253–260. doi: 10.3233/JAD-2006-9304

Beejesh, A. G., Gopi, V. P., and Hemanth, J. (2019). Brain MR kurtosis imaging study: contrasting gray and white matter. *Cogn. Syst. Res.* 55, 135–145. doi: 10.1016/j.cogsys.2019.01.005

Cauda, F., Nani, A., Manuello, J., Premi, E., Palermo, S., Tatu, K., et al. (2018). Brain structural alterations are distributed following functional,

anatomic and genetic connectivity. *Brain* 141, 3211–3232. doi: 10.1093/brain/awy252

Chetelat, G., Desgranges, B., De La Sayette, V., Viader, F., Eustache, F., and Baron, J. C. (2002). Mapping gray matter loss with voxel-based morphometry in mild cognitive impairment. *Neuroreport* 13, 1939–1943. doi: 10.1097/00001756-200210280-00022

Chetelat, G., Villemagne, V. L., Pike, K. E., Baron, J. C., Bourgeat, P., Jones, G., et al. (2010). Larger temporal volume in elderly with high versus low beta-amyloid deposition. *Brain* 133, 3349–3358. doi: 10.1093/brain/awq187

Dahnke, R., Yotter, R. A., and Gaser, C. (2013). Cortical thickness and central surface estimation. *Neuroimage* 65, 336–348. doi: 10.1016/j.neuroimage.2012.09.050

Desai, R., Liebenthal, E., Possing, E. T., Waldron, E., and Binder, J. R. (2005). Volumetric vs. surface-based alignment for localization of auditory cortex activation. *Neuroimage* 26, 1019–1029. doi: 10.1016/j.neuroimage.2005.03.024

Dicks, E., Tijms, B. M., Kate, M., Gouw, A. A., Benedictus, M. R., Teunissen, C. E., et al. (2018). Gray matter network measures are associated with cognitive decline in mild cognitive impairment. *Neurobiol. Aging* 61, 198–206. doi: 10.1016/j.neurobiolaging.2017.09.029

Dicks, E., Vermunt, L., van der Flier, W. M., Visser, P. J., Barkhof, F., Scheltens, P., et al. (2019). Modeling grey matter atrophy as a function of time, aging or cognitive decline show different anatomical patterns in Alzheimer's disease. *Neuroimage Clin.* 22:101786. doi: 10.1016/j.nicl.2019.101786

Dimitriadis, S. I., Liparas, D., and Tsolaki, M. N. (2017). Random forest feature selection, fusion and ensemble strategy: combining multiple morphological MRI measures to discriminate among healhy elderly, MCI, cMCI and alzheimer's disease patients: from the alzheimer's disease neuroimaging initiative (ADNI) database. *J. Neurosci. Methods* 302, 14–23. doi: 10.1016/j.jneumeth.2017.12.010

Fjell, A. M., Walhovd, K. B., Reinvang, I., Lundervold, A., Salat, D., Quinn, B. T., et al. (2006). Selective increase of cortical thickness in high-performing elderly-structural indices of optimal cognitive aging. *Neuroimage* 29, 984–994. doi: 10.1016/j.neuroimage.2005.08.007

Gomez-Sancho, M., Tohka, J., and Gomez-Verdejo, V. (2018). Comparison of feature representations in MRI-based MCI-to-AD conversion prediction. *Magn. Reson. Imaging* 50, 84–95. doi: 10.1016/j.mri.2018.03.003

Guo, X., Wang, Z., Li, K., Li, Z., Qi, Z., Jin, Z., et al. (2010). Voxel-based assessment of gray and white matter volumes in Alzheimer's disease. *Neurosci. Lett.* 468, 146–150. doi: 10.1016/j.neulet.2009.10.086

Gutman, B., Wang, Y., Morra, J., Toga, A. W., and Thompson, P. M. (2009). Disease classification with hippocampal shape invariants. *Hippocampus* 19, 572–578. doi: 10.1002/hipo.20627

Ha, S. Y., Youn, Y. C., Kim, S. Y., Hsiung, G. Y. R., Ahn, S. W., Shin, H. W., et al. (2012). A voxel-based morphometric study of cortical gray matter volume changes in Alzheimer's disease with white matter hyperintensities. *J. Clin. Neurosci.* 19, 1506–1510. doi: 10.1016/j.jocn.2011.11.041

Hojjati, S. H., Ebrahimzadeh, A., Khazaee, A., and Babajani-Feremi, A. (2018). Predicting conversion from MCI to AD by integrating rs-fMRI and structural MRI. *Comput. Biol. Med.* 102, 30–39. doi: 10.1016/j.compbiomed.2018.09.004

Jack, C. R., Bernstein, M. A., Fox, N. C., Paul, T., Danielle, H., Bret, B., et al. (2010a). The Alzheimer's disease neuroimaging initiative (ADNI): MRI methods. *J. Magn. Reson. Imaging* 27, 685–691. doi: 10.1002/jmri.21049

Jack, C. R., Knopman, D. S., Jagust, W. J., Shaw, L. M., Aisen, P. S., Weiner, M. W., et al. (2010b). Hypothetical model of dynamic biomarkers of the Alzheimer's pathological cascade. *Lancet Neurol.* 9, 119–128. doi: 10.1016/S1474-4422(09)70299-6

Jacobs, H. I., Van Boxtel, M. P., Gronenschild, E., Uylings, H. B., Jolles, J., and Verhey, F. R. (2013). Decreased gray matter diffusivity: a potential early Alzheimer's disease biomarker?. *Alzheimers Dement.* 9, 93–97. doi: 10.1016/j.jalz.2011.11.004

Johnson, S. C., Christian, B. T., Okonkwo, O. C., Oh, J. M., Harding, S., Xu, G., et al. (2014). Amyloid burden and neural function in people at risk for Alzheimer's disease. *Neurobiol. Aging* 35, 576–584. doi: 10.1016/j.neurobiolaging.2013.09.028

Juan, F., Eduard, V., Daniel, A., María, C. I., María-Belén, S. S., Isabel, S., et al. (2015). Cerebrospinal fluid β-amyloid and phospho-tau biomarker interactions affecting brain structure in preclinical Alzheimer disease. *Ann. Neurol.* 76, 223–230. doi: 10.1002/ana.24186

Karas, G. B., Burton, E. J., Rombouts, S. A. R. B., Schijndel, R. A. V., O'Brien, J. T., Scheltens, P. H., et al. (2003). A comprehensive study of gray matter loss in patients with Alzheimer's disease using optimized voxel-based morphometry. *Neuroimage* 18, 895–907. doi: 10.1016/S1053-8119(03)00041-7

Karas, G. B., Scheltens, P., Rombouts, S. A. R. B., Visser, P. J., van Schijndel, R. A., Fox, N. C., et al. (2004). Global and local gray matter loss in mild cognitive impairment and Alzheimer's disease. *Neuroimage* 23, 708–716. doi: 10.1016/j.neuroimage.2004.07.006

Kuperberg, G. R., Broome, M. R., McGuire, P. K., David, A. S., Eddy, M., Ozawa, F., et al. (2003). Regionally localized thinning of the cerebral cortex in schizophrenia. *Arch. Gen. Psychiatry* 60, 878–888. doi: 10.1001/archpsyc.60.9.878

Lee, Y. M., Chung, Y. I., Park, J. M., Lee, B. D., Moon, E., Jeong, H. J., et al. (2016). Decreased gray matter volume is associated with the subtypes of psychotic symptoms in patients with antipsychotic-naïve mild or moderate Alzheimer's disease: a voxel-based morphometry study. *Psychiatry Res. Neuroimaging* 249, 45–51. doi: 10.1016/j.pscychresns.2015.12.002

Lerch, J. P., Pruessner, J. C., Alex, Z., Harald, H., Teipel, S. J., and Evans, A. C. (2005). Focal decline of cortical thickness in Alzheimer's disease identified by computational neuroanatomy. *Cereb. Cortex* 15, 995–1001. doi: 10.1093/cercor/bhh200

Li, K., Luo, X., Zeng, Q., Huang, P., Shen, Z., Xu, X., et al. (2019). Gray matter structural covariance networks changes along the Alzheimer's disease continuum. *NeuroImage Clin.* 23:101828. doi: 10.1016/j.nicl.2019.101828

Li, R., Rui, G., Chen, W., Li, S., Schulz, P. E., and Zhang, Y. (2018). Early detection of Alzheimer's disease using noninvasive near-infrared spectroscopy. *Front. Aging Neurosci.* 10:366. doi: 10.3389/fnagi.2018.00366

Li, R., Rui, G., Zhao, C., Wang, C., Fang, F., and Zhang, Y. (2019). Functional network alterations in patients with amnestic mild cognitive impairment characterized using functional near-infrared spectroscopy. *IEEE Trans. Neur. Syst. Rehabil. Eng.* 28, 123–132. doi: 10.1109/TNSRE.2019.2956464

Liu, J., Wu, F., and Wang, J. (2020). Enhancing the feature representation of multi-modal MRI data by combining multi-view information for MCI classification. *Neurocomputing* 400, 322–332. doi: 10.1016/j.neucom.2020.03.006

Luders, E., Thompson, P. M., Narr, K. L., Toga, A. W., Jancke, L., and Gaser, C. (2006). A curvature-based approach to estimate local gyrification on the cortical surface. *Neuroimage* 29, 1224–1230. doi: 10.1016/j.neuroimage.2005.08.049

Lui, L. M., Wong, T. W., Zeng, W., Gu, X. F., Thompson, P. M., Chan, T. F., et al. (2010). Detection of shape deformities using yamabe flow and Beltrami coefficients. *Inverse Probl. Imag.* 4, 311–333. doi: 10.3934/ipi.2010.4.311

Manuello, J., Nani, A., Premi, E., Borroni, B., Costa, T., Tatu, K., et al. (2017). The pathoconnectivity profile of Alzheimer's disease: a morphometric coalteration network analysis. *Front. Neurol.* 8:739. doi: 10.3389/fneur.2017.00739

Messe, A. (2019). Parcellation influence on the connectivity-based structure–function relationship in the human brain. *Hum. Brain Mapp.* 41, 1167–1180. doi: 10.1002/hbm.24866

Moller, C., Vrenken, H., Jiskoot, L., Versteeg, A., Barkhof, F., Scheltens, P., et al. (2013). Different patterns of gray matter atrophy in early- and late-onset Alzheimer's disease. *Neurobiol. Aging* 34, 2014–2022. doi: 10.1016/j.neurobiolaging.2013.02.013

Ottoy, J., Niemantsverdriet, E., Verhaeghe, J., Roeck, E. D., Struyfs, H., Somers, C., et al. (2019). Association of short-term cognitive decline and MCI-to-AD dementia conversion with CSF, MRI, amyloid- and ^{18}F-FDG-PET imaging. *NeuroImage Clin.* 22:101771. doi: 10.1016/j.nicl.2019.101771

Petersen, R. C., Aisen, P. S., Beckett, L. A., Donohue, M. C., Gamst, A. C., Harvey, D. J., et al. (2010). Alzheimer's disease neuroimaging initiative (ADNI): clinical characterization. *Neurology* 74, 201–209. doi: 10.1212/WNL.0b013e3181cb3e25

Phillips, J. S., Da Re, F., Dratch, L., Xie, S. X., Irwin, D. J., McMillan, C. T., et al. (2018). Neocortical origin and progression of gray matter atrophy in nonamnestic Alzheimer's disease. *Neurobiol. Aging* 63, 75–87. doi: 10.1016/j.neurobiolaging.2017.11.008

Qian, W., Schweizer, T. A., Churchill, N. W., Millikin, C. P., Ismail, Z., Smith, E. E., et al. (2019). Gray matter changes associated with the development of delusions in Alzheimer disease. *Am. J. Geriatr. Psychiatry* 27, 490–498. doi: 10.1016/j.jagp.2018.09.016

Righart, R., Schmidt, P., Dahnke, R., Biberacher, V., Beer, A., Buck, D., et al. (2017). Volume versus surface-based cortical thickness measurements: a

comparative study with healthy controls and multiple sclerosis patients. *PLoS ONE* 12:e0179590. doi: 10.1371/journal.pone.0179590

Risacher, S. L., Saykin, A. J., West, J. D., Shen, L., Firpi, H. A., and McDonald, B. C. (2009). Baseline MRI predictors of conversion from MCI to probable AD in the ADNI cohort. *Curr. Alzheimer Res.* 6, 347–361. doi: 10.2174/156720509788929273

Romerogarcia, R., Atienza, M., and Cantero, J. L. (2016). Different scales of cortical organization are selectively targeted in the progression to Alzheimer's disease. *Int. J. Neural Syst.* 26:1650003. doi: 10.1142/S0129065716500039

Rosas, H. D., Salat, D. H., Lee, S. Y., Zaleta, A. K., Pappu, V., Fischl, B., et al. (2008). Cerebral cortex and the clinical expression of Huntington's disease: complexity and heterogeneity. *Brain* 131, 1057–1068. doi: 10.1093/brain/awn025

Sailer, M., Fischl, B., Salat, D., Tempelmann, C., Schonfeld, M. A., Busa, E., et al. (2003). Focal thinning of the cerebral cortex in multiple sclerosis. *Brain* 126, 1734–1744. doi: 10.1093/brain/awg175

Sowell, E. R., Peterson, B. S., Kan, E., Woods, R. P., Yoshii, J., Bansal, R., et al. (2007). Sex differences in cortical thickness mapped in 176 healthy individuals between 7 and 87 years of age. *Cerebral Cortex* 17, 1550–1560. doi: 10.1093/cercor/bhl066

Sowell, E. R., Thompson, P. M., Leonard, C. M., Welcome, S. E., Kan, E., and Toga, A. W. (2004). Longitudinal mapping of cortical thickness and brain growth in normal children. *J. Neurosci.* 24, 8223–8231. doi: 10.1523/JNEUROSCI.1798-04.2004

Thompson, P. M., Hayashi, K. M., Greig, D. Z., Janke, A. L., Rose, S. E., James, S., et al. (2003). Dynamics of gray matter loss in Alzheimer's disease. *J. Neurosci.* 23, 994–1005. doi: 10.1523/JNEUROSCI.23-03-00994.2003

Thompson, P. M., Hayashi, K. M., Sowell, E. R., Gogtay, N., Giedd, J. N., Rapoport, J. L., et al. (2004). Mapping cortical change in Alzheimer's disease, brain development, and schizophrenia. *Neuroimage* 23, 2–18. doi: 10.1016/j.neuroimage.2004.07.071

Tijms, B. M., Kate, M., Gouw, A. A., Borta, A., Verfaillie, S., Teunissen, C. E., et al. (2018). Gray matter networks and clinical progression in subjects with predementia Alzheimer's disease. *Neurobiol. Aging* 61, 75–81. doi: 10.1016/j.neurobiolaging.2017.09.011

Tijms, B. M., Möller, C., Vrenken, H., Wink, A. M., De, H. W., Wm, V. D. F., et al. (2013). Single-subject grey matter graphs in Alzheimer's disease. *PLoS ONE* 8:e58921. doi: 10.1371/annotation/6a2e6405-ce1d-49e0-a88c-0017c680d597

Vivek, S., Howard, C., Lerch, J. P., Evans, A. C., Dorr, A. E., and Noor Jehan, K. (2006). Spatial patterns of cortical thinning in mild cognitive impairment and Alzheimer's disease. *Brain* 129, 2885–2893. doi: 10.1093/brain/awl256

Wang, L., Zou, L., Chen, Q., Su, L., Xu, J., Zhao, R., et al. (2020). Gray matter structural network disruptions in survivors of acute lymphoblastic leukemia with chemotherapy treatment. *Acad. Radiol.* 27, 27–34. doi: 10.1016/j.acra.2019.04.010

Wang, Y., Xu, C., Park, J. H., Lee, S., Stern, Y., Yoo, S., et al. (2019). Diagnosis and prognosis of Alzheimer's disease using brain morphometry and white matter connectomes. *Neuroimage Clin.* 23:101859. doi: 10.1016/j.nicl.2019.101859

Wee, C. Y., Liu, C., Lee, A., Poh, J. S., and Ji, H. (2019). Cortical graph neural network for AD and MCI diagnosis and transfer learning across populations. *NeuroImage Clin.* 23, 101929. doi: 10.1016/j.nicl.2019.101929

Wu, Z., Peng, Y., Selvaraj, S., Schulz, P. E., and Zhang, Y. (2020). Development of brain structural networks over age 8: a preliminary study based on diffusion weighted imaging. *Front. Aging Neurosci.* 12:61. doi: 10.3389/fnagi.2020.00061

Wu, Z., Xu, D., Potter, T., and Zhang, Y. (2019). Effects of brain parcellation on the characterization of topological deterioration in Alzheimer's disease. *Front. Aging Neurosci.* 11:113. doi: 10.3389/fnagi.2019.00113

Yong, H., Zhang, C., and Alan, E. (2008). Structural insights into aberrant topological patterns of large-scale cortical networks in Alzheimer's disease. *J. Neurosci.* 28, 4756–4766. doi: 10.1523/JNEUROSCI.0141-08.2008

Yotter, R. A., Nenadic, I., Ziegler, G., Thompson, P. M., and Gaser, C. (2011). Local cortical surface complexity maps from spherical harmonic reconstructions. *Neuroimage* 56, 961–973. doi: 10.1016/j.neuroimage.2011.02.007

Conflict of Interest: The authors declare that the research was conducted in the absence of any commercial or financial relationships that could be construed as a potential conflict of interest.

frontiers in Aging Neuroscience

ORIGINAL RESEARCH
published: 03 February 2021
doi: 10.3389/fnagi.2021.646017

Alterations in Dynamic Functional Connectivity in Individuals With Subjective Cognitive Decline

Qian Chen[1†], Jiaming Lu[2†], Xin Zhang[1,2†], Yi Sun[2], Wenqian Chen[2], Xin Li[1], Wen Zhang[2], Zhao Qing[2,3] and Bing Zhang[1,2,3]*

[1] Department of Radiology, Drum Tower Hospital, Clinical College of Nanjing Medical University, Nanjing, China, [2] Department of Radiology, Drum Tower Hospital, Medical School of Nanjing University, Nanjing, China, [3] Institute of Brain Science, Nanjing University, Nanjing, China

Purpose: To investigate the dynamic functional connectivity (DFC) and static parameters of graph theory in individuals with subjective cognitive decline (SCD) and the associations of DFC and topological properties with cognitive performance.

Methods: Thirty-three control subjects and 32 SCD individuals were enrolled in this study, and neuropsychological evaluations and resting-state functional magnetic resonance imaging scanning were performed. Thirty-three components were selected by group independent component analysis to construct 7 functional networks. Based on the sliding window approach and k-means clustering, distinct DFC states were identified. We calculated the temporal properties of fractional windows in each state, the mean dwell time in each state, and the number of transitions between each pair of DFC states. The global and local static parameters were assessed by graph theory analysis. The differences in DFC and topological metrics, and the associations of the altered neuroimaging measures with cognitive performance were assessed.

Results: The whole cohort demonstrated 4 distinct connectivity states. Compared to the control group, the SCD group showed increased fractional windows and an increased mean dwell time in state 4, characterized by hypoconnectivity both within and between networks. The SCD group also showed decreased fractional windows and a decreased mean dwell time in state 2, dominated by hyperconnectivity within and between the auditory, visual and somatomotor networks. The number of transitions between state 1 and state 2, between state 2 and state 3, and between state 2 and state 4 was significantly reduced in the SCD group compared to the control group. No significant differences in global or local topological metrics were observed. The altered DFC properties showed significant correlations with cognitive performance.

Conclusion: Our findings indicated DFC network reconfiguration in the SCD stage, which may underlie the early cognitive decline in SCD subjects and serve as sensitive neuroimaging biomarkers for the preclinical detection of individuals with incipient Alzheimer's disease.

Keywords: subjective cognitive decline, dynamic functional connectivity, independent component analysis, graph theory, fractional windows

OPEN ACCESS

Edited by:
Ying Han,
Capital Medical University, China

Reviewed by:
Yu Sun,
China-Japan Friendship Hospital, China
Changhao Yin,
Hongqi Hospital of Mudanjiang Medical University, China

***Correspondence:**
Bing Zhang
zhangbing_nanjing@nju.edu.cn

[†] These authors share first authorship

Received: *24 December 2020*
Accepted: *06 January 2021*
Published: *03 February 2021*

Citation:
Chen Q, Lu J, Zhang X, Sun Y, Chen W, Li X, Zhang W, Qing Z and Zhang B (2021) Alterations in Dynamic Functional Connectivity in Individuals With Subjective Cognitive Decline. Front. Aging Neurosci. 13:646017. doi: 10.3389/fnagi.2021.646017

INTRODUCTION

Individuals with subjective cognitive decline (SCD), a self-perceived worsening of cognitive function without objectively detected deficits, have been considered at higher risk of developing Alzheimer's disease (AD) dementia in the future compared to those without cognitive complaints (Reisberg et al., 2010; Jessen et al., 2014). AD is a progressive neurodegenerative disorder that has three stages: the preclinical stage, mild cognitive impairment (MCI), and dementia (Sperling et al., 2011). SCD corresponds to the preclinical stage of the AD spectrum and has the potential to be an effective symptomatic indicator for future cognitive impairment (Dubois et al., 2016; López-Sanz et al., 2017). Due to the lack of effective therapeutic methods targeting late-stage AD patients, it is critical to investigate brain alterations in the SCD stage to pave the way for early diagnosis and intervention (Rabin et al., 2017; Jessen et al., 2020).

Resting-state functional magnetic resonance imaging (rs-fMRI), which reflects intrinsic brain activity, has been proven to be an effective and non-invasive approach for exploring the neural mechanisms underlying neurological disorders (Biswal et al., 1995; Lau et al., 2016). More specifically, functional connectivity (FC), which is defined as the temporal correlation of blood oxygenation level-dependent (BOLD) signals between voxels or brain regions, indicates information processing and transference across functionally coordinated brain networks (Fox et al., 2005). Cognitive impairment could be partly attributable to altered functional coupling in brain-wide networks, and previous studies have reported aberrant FC and disrupted brain networks in AD dementia and MCI patients (Delli Pizzi et al., 2019; Franzmeier et al., 2019). Studies conducted in the SCD cohort have also revealed decreased average FC in the posterior memory system and between the retrosplenial cortex and precuneus (Viviano et al., 2019), reduced FC in cortical midline structures (Yasuno et al., 2015), increased FC between the retrosplenial cortex and frontal cortex (Dillen et al., 2016), and increased occipital and parietal FC associated with the severity of memory complaints compared to normal controls (NCs) (Kawagoe et al., 2019). Therefore, altered FC could be the neural basis underlying early cognitive decline and serve as an objective imaging marker to identify preclinically at-risk AD patients.

To date, most aforementioned rs-fMRI studies have focused on static FC (SFC); however, researchers have suggested that the brain is intrinsically a dynamic system with discrete FC patterns switching rapidly during acquisition (Allen et al., 2014; Vidaurre et al., 2017). Thus, the dynamic characteristics of FC provide a novel perspective on the temporal aspects of information processing across brain networks compared to SFC analysis (Peraza et al., 2015; Schumacher et al., 2019). Currently, dynamic FC (DFC) analysis has been proven to be a promising approach for exploring neural substrates for a variety of neuropsychological disorders, including Parkinson's disease (Díez-Cirarda et al., 2018; Fiorenzato et al., 2019), schizophrenia (Damaraju et al., 2014), and AD (Jones et al., 2012; Córdova-Palomera et al., 2017; Demirtaş et al., 2017; Brenner et al., 2018). More specifically, AD dementia patients were suggested to spend less time in brain functional states with strong posterior default mode network (DMN) region contribution and more time in states with greater anterior DMN region contribution compared to NCs (Jones et al., 2012), and show alterations in local DFC within the temporal, frontal-superior and default-mode networks, as well as decreased global metastability between functional states compared to patients with mild or subjective cognitive impairment and NCs (Córdova-Palomera et al., 2017; Demirtaş et al., 2017). In addition, studies have shown that amnestic MCI patients were more likely to reveal a single dominant state and spent greater time in a costly state relative to the most common state, which may be attributable to reduced flexibility in resource allocation (Brenner et al., 2018). Furthermore, studies have revealed higher accuracy using DFC features to distinguish AD dementia or MCI patients from NCs than SFC features (De Vos et al., 2018; Jie et al., 2018). Alterations in functional network dynamics have been suggested to be related to variations in the subclinical range of memory performance, increased iron accumulation, and the genetic risk of AD (Quevenco et al., 2017). However, few studies have investigated DFC characteristics in SCD individuals. A recent DFC study has shown changes in centrality frequency (the proportion of time a hub with a high degree centrality appeared across the entire time window) in the DMN in SCD individuals, the abnormality of which was related to cognitive performance (Xie et al., 2019). Another recent work has observed higher classification accuracies in distinguishing SCD individuals from NCs using temporal flexibility and spatiotemporal diversity, two measures of DFC, than static parameters of graph theory and structural metrics of voxel-based morphometry analysis (Dong et al., 2020). However, studies employing the DFC temporal properties of fractional windows, mean dwell time, and the number of transitions to SCD subjects are still lacking; these features have been commonly described and proven to be associated with cognition, behavior, and clinical variables in other neuropsychological diseases (Kim et al., 2017; Li et al., 2017; Liu et al., 2017; Díez-Cirarda et al., 2018; Fiorenzato et al., 2019).

Graph theory has been widely used in the investigation of topological features of brain functional networks (Watts and Strogatz, 1998). AD is described as a disconnection syndrome, and previous studies have demonstrated disrupted communication in peripheral regions and preserved organization in rich-club regions in SCD participants (Yan et al., 2018). A recent study based on the Alzheimer's Disease Neuroimaging Initiative (ADNI) has observed higher nodal topological properties (nodal strength, nodal global efficiency, and nodal local efficiency) in SCD individuals than in NCs, and the altered graphic parameters were significantly correlated with amyloid-β and memory function, indicating the compensatory mechanism of the functional connectome underlying SCD (Chen et al., 2020). These findings have suggested the vulnerability of network topology in the SCD stage.

In the present study, we aimed to investigate neuroimaging biomarkers in SCD subjects from both dynamic and static rs-fMRI perspectives and to explore whether temporal properties of DFC were more sensitive than static parameters of graph theory in the SCD stage. We also endeavored to determine the relationships between rs-fMRI measures and cognitive performance. Accordingly, we hypothesized that altered DFC

temporal properties of fractional windows, mean dwell time, and state transitions would be observed in SCD subjects, which may improve the present understanding of the neural basis underlying early cognitive decline and provide more promising neuroimaging biomarkers for the detection of incipient AD patients than global and local graphic parameters of SFC.

METHODS

Subjects

The present study included 32 SCD individuals matched for age, gender, and years of education with 33 NCs. All participants were recruited from the Drum Tower district of Nanjing by advertisement. Individuals could participate in this study if they were 55–75 years old, right-handed, and had at least 9 years of education; in contrast, individuals with a history of stroke, other neuropsychiatric disorders (Parkinson's disease, epilepsy, brain tumor, etc.), severe anxiety or depression, and MRI contraindications were excluded. Individuals showing objective impairment in the following cognitive evaluations were also excluded from the present study (Li et al., 2019). Specifically, three cognitive domains each containing two subtests were assessed: auditory verbal learning test (AVLT) long-delayed memory and AVLT recognition for episodic memory; trail making test part A (TMT-A) and part B (TMT-B) for executive function; and Boston naming test (BNT) and animal fluency test (AFT) for language ability. Participants were considered MCI patients if they had scores >1 standard deviation (SD) below the normative means in both subtests within one cognitive domain or >1 SD below the normative means in three single tests in three different domains. Subjects with memory complaints within the last 5 years and expressed worries associated with memory decline were assigned to the SCD group; those without memory complaints and cognitive impairments were recruited as NCs. The study was conducted according to the Declaration of Helsinki and approved by the institutional review boards of the Nanjing Drum Tower Hospital. Written informed consent was acquired from each participant after a detailed introduction of the study procedure involved.

Neuropsychological Assessment

The standardized cognitive evaluation was performed by an experienced psychologist. The mini-mental state examination (MMSE) was used to assess global cognition. Another five cognitive domains were evaluated: (1) episodic memory measured with the AVLT, including immediate memory, short-delayed memory, long-delayed memory, cued recall, and recognition; (2) executive function tested with the TMT-A and TMT-B; (3) language function evaluated with the BNT and AFT; (4) processing speed tested with the symbol digit modalities test (SDMT); (5) visuospatial ability assessed with the clock drawing test (CDT).

Image Acquisition

Imaging data were acquired on a 3T Philips Achieva TX MRI scanner using an 8-channel head coil in the Nanjing Drum Tower Hospital. The parameters of rs-fMRI were set as follows: field of view (FOV) = 192 × 192 mm^2; slice thickness = 4 mm; matrix size = 64 × 64; repetition time (TR) = 2000 ms; echo time (TE) = 30 ms; flip angle = 90°; number of slices = 35; voxel size = 3 × 3 × 4 mm with no gap. In total, 230 volumes were acquired. Participants were instructed to lie quietly with their eyes closed and stay awake during rs-fMRI scanning. The T_1-weighted images were obtained with the following parameters: TR = 7,600 ms; TE = 3,400 ms; flip angle = 8°; FOV = 256 × 256 × 192 mm^3 and slice thickness = 1 mm.

Image Pre-processing

Pre-processing for rs-fMRI data was performed using the Data Processing Assistant for rs-fMRI advanced edition (DPARSFA, vision 4.3, http://www.restfmri.net) (Chao-Gan and Yu-Feng, 2010). Slice timing, realignment, nuisance regression (white matter and cerebrospinal fluid (CSF) signals and Friston 24 head motion parameters), and spatial normalization to standard Montreal Neurological Institute (MNI) space were carried out. Then all images were smoothed with a 6 mm full-width at half-maximum (FWMH) Gaussian kernel. Realignment parameters were checked, and none showed displacement above 3.0 mm or angular rotation higher than 3.0° among included participants. Two-sample *t*-tests indicated no significant differences in the mean framewise displacement (Jenkinson) (Jenkinson et al., 2002) between the NC and SCD groups (0.11 ± 0.06 mm vs. 0.11 ± 0.07 mm, $p = 0.916$).

Group Independent Component Analysis

After data pre-processing, spatial group independent component analysis (ICA) was conducted to decompose the data into seven functional networks using the Group ICA of fMRI Toolbox (GIFT) (Calhoun et al., 2001a). Two data reduction steps were performed in the principal component analysis (Allen et al., 2014). First, subject-specific data were reduced to 120 principal components and were concatenated across time. Then, the group-level data were decomposed into 100 components with the expectation-maximization algorithm (Roweis, 1998). We repeated the Infomax ICA algorithm in ICASSO 20 times to ensure stability and reliability (Himberg et al., 2004). Subject-specific spatial maps and time courses were extracted by the back-construction approach (GICA) implemented in GIFT software (Calhoun et al., 2001b).

Among the resulting 100 components, we identified 33 of them to construct seven functional networks following a previously described procedure (Allen et al., 2014). First, we manually checked whether the peak activation coordinates were mainly located in gray matter, showing low spatial overlap with vascular, ventricular, or edge regions corresponding to artifacts. Then, only components showing time courses dominated by low-frequency fluctuations were selected (Cordes et al., 2000). Based on the spatial correlation values between the components and the network template (Shirer et al., 2012), we sorted and rearranged the retained 33 independent components into seven functional networks (**Figure 1**): 2 to the basal ganglia network (BG), 2 to the auditory network (AUD), 7 to the visual network (VIS), 4 to the sensorimotor network (SMN), 6 to the cognitive

executive network (CEN), 8 to the DMN, and 4 to the cerebellar network (CB).

Postprocessing steps of the time courses of 33 components were performed according to Allen et al. (2014), including detrending, despiking with AFNI's 3dDespike algorithm, and filtering using a fifth-order Butterworth filter with a 0.15 Hz high frequencies cut-off.

Dynamic Functional Connectivity Analysis

Sliding Window Approach

The DFC analysis was performed with the sliding window approach using the DFC network toolbox in GIFT. Consistent with previous studies, the rs-fMRI data were divided into windows of 22 TR in size with a Gaussian of $\sigma = 3$ TRs, in steps of 1 TR (Allen et al., 2014). The regularized inverse covariance matrix was used to reduce the impact of insufficient information on short time series (Varoquaux et al., 2010). We applied an L1 penalty on the precision matrix to promote sparsity in the graphic LASSO framework with 100 repetitions (Friedman et al., 2008). The FC matrices were z-transformed to stabilize the variance.

Clustering Analysis and Calculation of Temporal Properties

All windowed FC matrices across all subjects were used to estimate the DFC states. The k-means clustering analysis was repeated 100 times, and the Euclidean distance was used to measure the similarity between FC matrices and regroup them into distinct clusters (Díez-Cirarda et al., 2018). Four was determined as the optimal number of clusters following the elbow criteria (Damaraju et al., 2014).

We investigated the temporal properties of DFC states by calculating the fractional windows (the number of total windows belonging to a given state), mean dwell time (the number of consecutive windows belonging to a given state), and the number of transitions (the number of transitions between each pair of states) (Fiorenzato et al., 2019). The differences in dynamic properties were computed by two-sample

TABLE 1 | Demographic and clinical data.

	NC ($n = 33$)	SCD ($n = 32$)	Statistics	p
Age	64.55 ± 5.33	65.22±5.02	$t_{(63)} = 0.524$	0.602
Gender (M/F)	8/25	5/27	$\chi^2_{(1)} = 0.754$	0.385
Education years	12.97 ± 3.34	12.25 ± 2.62	$t_{(63)} = -0.965$	0.338
MMSE	28.97 ± 1.31	28.66 ± 1.31	$t_{(63)} = -0.964$	0.339
AVLT immediate	17.55 ± 4.57	16.94 ± 4.77	$t_{(63)} = -0.525$	0.601
AVLT short delayed	5.27 ± 2.79	4.78 ± 2.32	$t_{(63)} = -0.771$	0.444
AVLT long delayed	5.00 ± 2.86	4.56 ± 2.38	$t_{(63)} = -0.669$	0.506
AVLT cued recall	4.70 ± 2.32	4.53 ± 2.05	$t_{(63)} = -0.305$	0.762
AVLT recognition	21.91 ± 1.44	21.50 ± 1.34	$t_{(63)} = -1.181$	0.242
AFT	19.18 ± 4.00	18.38 ± 4.80	$t_{(63)} = -0.737$	0.464
BNT	27.39 ± 2.45	27.03 ± 2.63	$t_{(63)} = -0.575$	0.567
TMT_A	58.24 ± 21.32	60.44 ± 16.66	$t_{(63)} = 0.462$	0.646
TMT_B	131.42 ± 29.66	164.06 ± 64.81	$t_{(63)} = 2.624$	0.011*
SDMT	41.94 ± 9.22	36.84 ± 10.55	$t_{(63)} = -2.075$	0.042*
CDT	27.91 ± 1.99	26.75 ± 3.04	$t_{(63)} = -1.825$	0.073
APOE (ε3ε3/ε3ε4)	17/5	23/5	$\chi^2_{(1)} = 0.183$	0.669[a]

*Values are the mean ± standard deviation. MMSE, mini-mental state examination; AVLT, auditory verbal learning test; AFT, animal fluency test; BNT, Boston naming test; TMT-A, trail making test part A; TMT-B, trail making test part B; SDMT, symbol digit modalities test; CDT, clock drawing test; APOE, apolipoprotein E. *$p < 0.05$, [a]APOE ε4 status not determined for the whole cohort.*

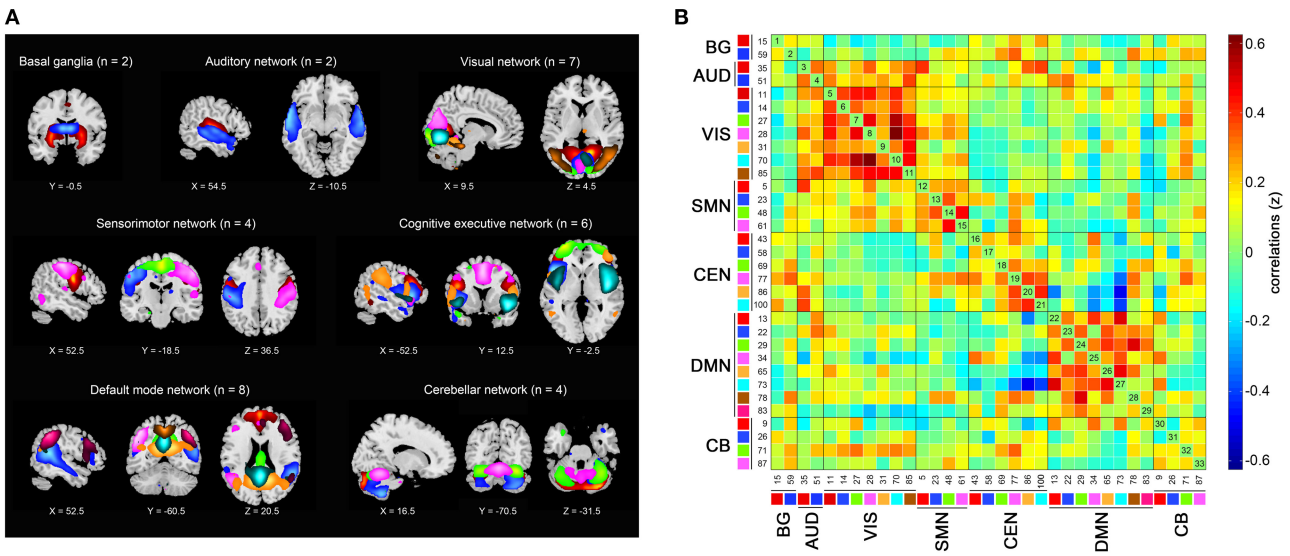

FIGURE 1 | Independent components ($n = 33$) identified by group independent component analysis. **(A)** Independent component spatial maps divided into seven functional networks. **(B)** Group averaged static functional connectivity matrix between pairs of independent components. BG, basal ganglia; AUD, auditory; VIS, visual; SMN, sensorimotor; CEN, cognitive executive; DMN, default mode; CB, cerebellar.

t-tests, except for the state distribution compared by the chi-square test.

Graph Theory Analysis

Graph theory parameters were analyzed using GRETNA software (http://www.nitrc.org/projects/gretna) based on the 33 independent components obtained in the ICA (Wang et al., 2015). The sparsity value of 0.34 was selected to maximize global and local efficiency (Achard and Bullmore, 2007). The global network metrics measured were global efficiency (the efficiency of parallel information transfer in a network) and the clustering coefficient (the mean of clustering coefficients of each node in a network) (Wang et al., 2011). The nodal network metrics measured were clustering coefficients (the likelihood

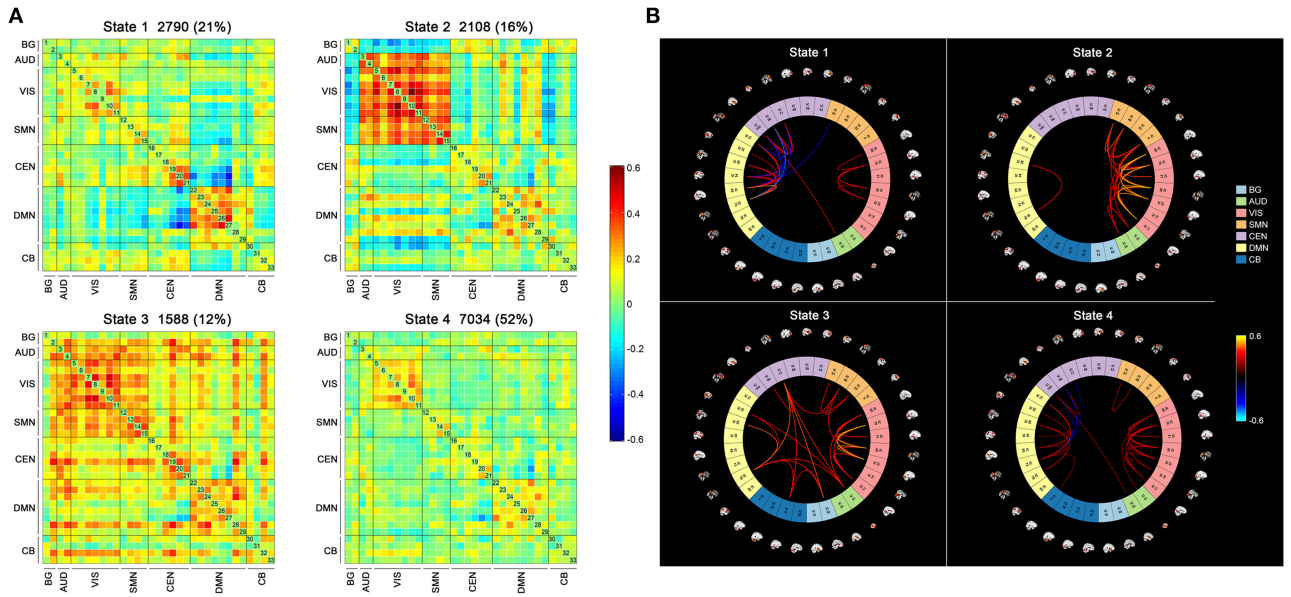

FIGURE 2 | The four states identified by k-means clustering analysis and the corresponding cluster centroids. The total number and percentage of the reoccurrence times of each state are listed above each cluster **(A)**, and the 5% strongest connections of each state are shown **(B)**. BG, basal ganglia; AUD, auditory; VIS, visual; SMN, sensorimotor; CEN, cognitive executive; DMN, default mode; CB, cerebellar.

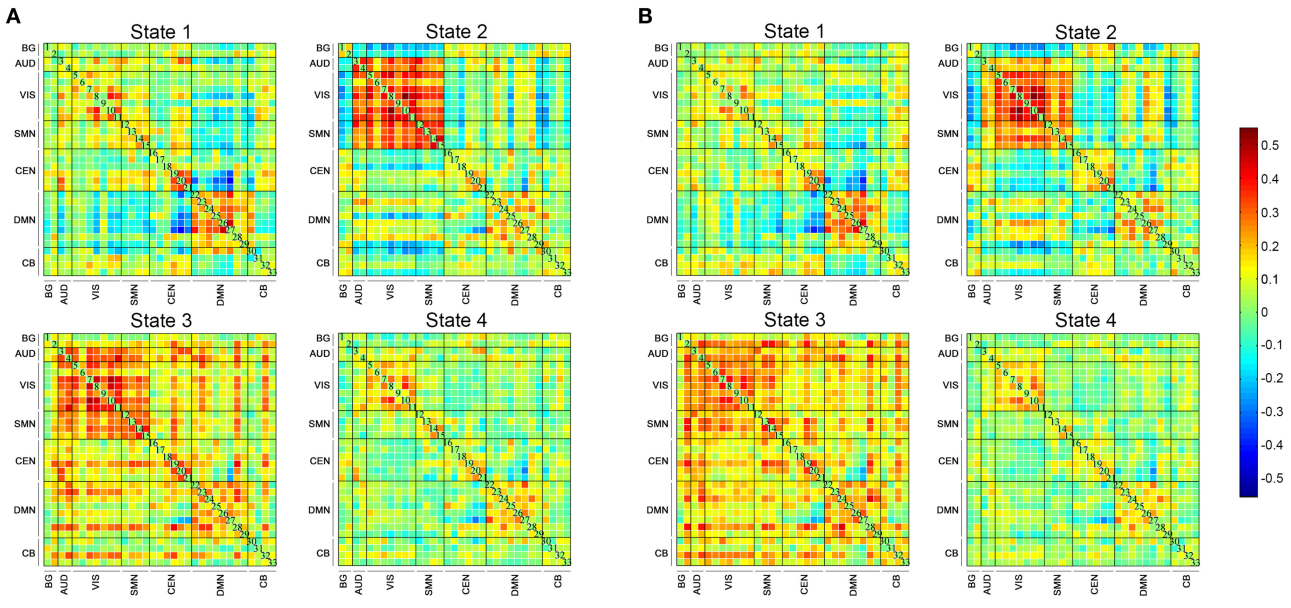

FIGURE 3 | The four dynamic functional connectivity patterns of the two groups. **(A)** The centroid matrices for the normal controls. **(B)** The centroid matrices for the subjective cognitive decline participants.

that the neighborhoods of a given node are connected), shortest path (the mean distance between a given node and all the other nodes in the network), local efficiency (how efficient the communication is among the first neighbors of a given node when it is removed), and degree centrality (the information communication ability of a given node in the functional network) (Wang et al., 2011). The group differences in graph theory parameters were compared with two-sample *t*-tests with false discovery rate (FDR) correction.

Apolipoprotein E Genotyping

DNA extraction from 300 μL of whole blood per subject was performed using an SK2884 DNA extraction kit (Sangon Biotech, Shanghai, China). Apolipoprotein E (APOE) single nucleotide polymorphism (SNP) genotyping was performed for rs429358 and rs7412 using polymerase chain reaction (PCR) technology. We determined the APOE ε4 status for 50 of the 65 participants (22/33 of the NC group and 28/32 of the SCD group).

Statistical Analysis

Age, years of education, and cognitive scores were compared using two-sample *t*-tests, while gender and APOE ε4 status were calculated by chi-square tests. We further calculated the Pearson's correlations between the altered DFC temporal properties, graph theory parameters, and cognitive measures, adjusting for age, gender, and years of education. Statistical analyses were performed with SPSS version 21.0, and $p < 0.05$ was set as the threshold for statistical significance.

RESULTS

Demographic and Cognitive Characteristics

No significant differences in terms of age, gender, or years of education were found between the SCD and NC groups. The SCD participants showed abilities comparable to the controls in the global cognition, episodic memory, language, and visuospatial domains. The SCD group performed worse on the TMT-B [$t_{(63)}$

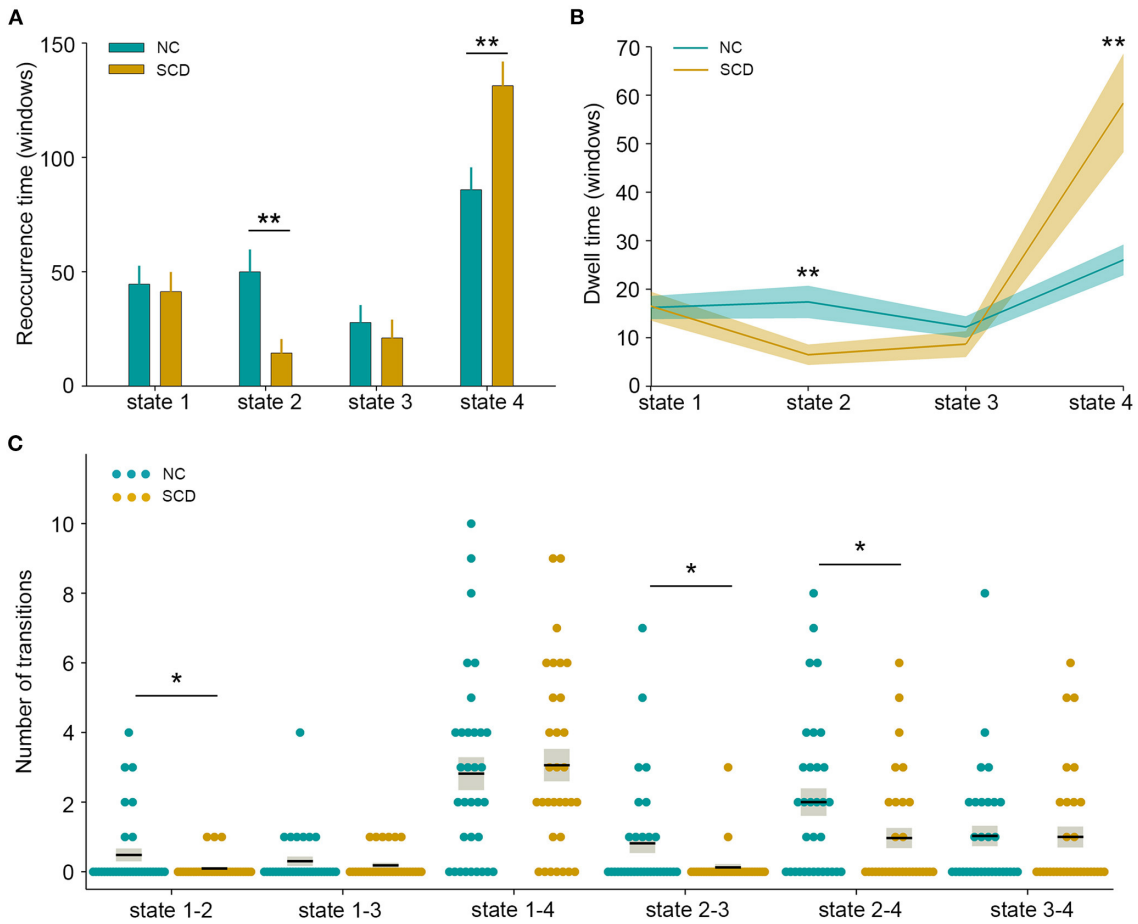

FIGURE 4 | Temporal properties of dynamic functional connectivity states between the two groups. **(A)** Fractional windows in each state. **(B)** Mean dwell time in each state. **(C)** The number of transitions between pairs of states. The parameters of each individual in the normal control (NC) and subjective cognitive decline (SCD) groups are presented in blue and khaki dots respectively. The black lines indicate the mean values, and the light gray rectangles cover the data within one standard error above and below the mean. *$p < 0.05$; **$p < 0.01$.

$= 2.624$, $p = 0.011$] and SDMT [$t_{(63)} = -2.075$, $p = 0.042$]. Detailed demographic and clinical information is shown in **Table 1**.

Dynamic Functional Connectivity Differences

Four DFC states of the whole cohort were identified (**Figure 2**) as follows: (1) state 1, 21% of the windows, characterized by partly strongly connected components within the VIS, CEN and DMN, and anti-related correlations between the DMN and the other networks; (2) state 2, 16% of the windows, distinguished by the predominance of strong positive intra-network and inter-network FC in the AUD, VIS, and SMN, while negative correlations between the AUD-VIS-SMN regions and other networks; (3) state 3, 12% of the windows, a highly connected state demonstrating positive couplings of intra-network and inter-network connections involving components of nearly the whole brain; and (4) state 4, 52% of the windows, a hypo-connected state showing sparsely connected patterns located mostly within each network and between each pair of networks, except for moderate FC within the VIS and DMN.

The state- and group-specific centroids of clusters for the NC and SCD groups are shown in **Figures 3A,B**, respectively. The proportion of the state differed significantly between the two groups [$\chi^2_{(3)} = 973.444$, $p < 0.001$]. More specifically, in the SCD group, state 1 occurred slightly less frequently than it did in the NC group (19.85 vs. 21.40%) as did state 3 (10.10 vs. 13.35%). Also, state 2 occurred less frequently (6.94 vs. 23.98%), whereas state 4 occurred more often (63.12 vs. 41.27%) in the SCD group compared to the NC group. Regarding the temporal properties (**Figure 4A**), the SCD group was observed to have significantly reduced fractional windows in state 2 [$t_{(63)} = -3.053$, $p = 0.003$], and increased fractional windows in state 4 [$t_{(63)} = 3.153$, $p = 0.002$]. The SCD group also showed a significantly reduced mean dwell time in state 2 [$t_{(63)} = -2.736$, $p = 0.008$] and an increased mean dwell time in state 4 [$t_{(63)} = 3.079$, $p = 0.003$] (**Figure 4B**). Additionally, significant reductions in the transitions between state 1 and state 2 [$t_{(63)} = -2.005$, $p = 0.049$], between state 2 and state 3 [$t_{(63)} = -2.307$, $p = 0.024$], and between state 2 and state 4 were observed in the SCD group compared to the NC group [$t_{(63)} = -2.099$, $p = 0.040$] (**Table 2** and **Figure 4C**).

Graph Topological Parameters

After FDR correction, we observed no significant differences either in the global or in the nodal network metrics between the NC and SCD groups.

Relationships Between Altered Neuroimaging Measures and Cognitive Function

Significant associations between altered neuroimaging measures and cognitive variables are summarized in **Supplementary Table 1**. In the whole cohort, the number of fractional windows and mean dwell time of state 4 both showed significant positive correlations with the time spent on the TMT-A ($r = 0.343$, $p = 0.006$; $r = 0.255$, $p = 0.045$, respectively). The transitions between state 1 and state 2 showed positive correlations with AVLT immediate memory scores ($r = 0.265$, $p = 0.037$), and the transitions between state 2 and state

TABLE 2 | Dynamic functional connectivity temporal properties.

		NC ($n = 33$)	SCD ($n = 32$)	Statistics	p	Cohen's d
Fractional windows	State 1	44.52 ± 46.40	41.28 ± 48.41	$t_{(63)} = -0.275$	0.784	0.068
	State 2	49.88 ± 56.26	14.44 ± 34.37	$t_{(63)} = -3.053$	0.003*	0.760
	State 3	27.76 ± 43.88	21.00 ± 45.64	$t_{(63)} = -0.609$	0.545	0.151
	State 4	85.85 ± 56.06	131.28 ± 60.10	$t_{(63)} = 3.153$	0.002*	0.782
Fractional windows (%)	State 1	1469 (21.40)	1321 (19.85)			
	State 2	1646 (23.98)	462 (6.94)			
	State 3	916 (13.35)	672 (10.10)	$\chi^2_{(3)} = 973.444$	<0.001*	
	State 4	2833 (41.27)	4201 (63.12)			
Dwell time (windows)	State 1	16.22 ± 13.72	16.52 ± 16.93	$t_{(63)} = 0.078$	0.938	0.019
	State 2	17.38 ± 19.17	6.49 ± 11.97	$t_{(63)} = -2.736$	0.008*	0.681
	State 3	12.21 ± 12.77	8.68 ± 15.14	$t_{(63)} = -1.015$	0.314	0.252
	State 4	26.04 ± 18.19	58.41 ± 57.52	$t_{(63)} = 3.079$	0.003*	0.759
Number of transitions	State 1-2	0.48 ± 1.06	0.09 ± 0.30	$t_{(63)} = -2.005$	0.049*	0.501
	State 1-3	0.30 ± 0.77	0.19 ± 0.40	$t_{(63)} = -0.757$	0.452	0.179
	State 1-4	2.82 ± 2.71	3.06 ± 2.63	$t_{(63)} = 0.369$	0.713	0.090
	State 2-3	0.82 ± 1.61	0.13 ± 0.55	$t_{(63)} = -2.307$	0.024*	0.574
	State 2-4	2.00 ± 2.26	0.97 ± 1.64	$t_{(63)} = -2.099$	0.040*	0.522
	State 3-4	1.03 ± 1.69	1.00 ± 1.70	$t_{(63)} = -0.072$	0.943	0.018

*Values are the mean ± standard deviation. *p < 0.05.*

3 were positively correlated with AVLT recognition scores ($r = 0.257$, $p = 0.044$).

In the NC group, both more fractional windows of state 4 and longer time dwelt in state 4 correlated with lower MMSE scores ($r = -0.499$, $p = 0.005$; $r = -0.420$, $p = 0.021$). The transitions between state 1 and state 2 showed positive correlations with AVLT immediate memory scores ($r = 0.410$, $p = 0.025$) and BNT scores ($r = 0.364$, $p = 0.048$).

In the SCD group, more fractional windows in state 4 were associated with longer time spent on the TMT-A ($r = 0.370$, $p = 0.048$), whereas longer time dwelt in state 2 predicted higher AVLT recognition scores ($r = 0.392$, $p = 0.036$). The transitions between state 1 and state 3, and between state 2 and state 4 were positively correlated with the AVLT recognition scores ($r = 0.409$, $p = 0.028$; $r = 0.376$, $p = 0.045$).

DISCUSSION

In the present study, we combined the ICA, DFC, and graph theory approaches to investigate the dynamic characteristics and global/local network topology of intrinsic connectivity networks in SCD individuals. The results revealed altered DFC temporal properties of fractional windows, mean dwell time, and the number of transitions in SCD subjects, which showed significant associations with cognitive performance. No significant differences in static parameters of graph theory were observed. These findings shed light on the role of DFC in the early detection of subjects with potential AD, and the alterations in DFC may suggest the neural basis underlying early cognitive decline.

As noted above, four distinct connectivity configurations were identified across the entire cohort. Consistent with previous findings (Allen et al., 2014; Kim et al., 2017; Viviano et al., 2017; Schumacher et al., 2019; Gu et al., 2020), the hypo-connected state occurred most frequently, that is, state 4 in the present study, characterized by a sparse connectivity pattern with relatively weak connections and the absence of strong correlations. This state profile was considered the baseline connectivity pattern, while other states with strong positive or negative connections may reflect neuropsychological processes (Viviano et al., 2017). The high occurrence of state 4 may indicate that, on the whole, the human brain prefers to be in a state with less information transfer but a more energy reservation pattern (Gu et al., 2020). In comparison with the NC group, state 2, showing hyperconnectivity within and between the AUD, VIS, and SMN, occurred 17.04% less frequently in the SCD group. In contrast, state 4 occurred 21.85% more often in SCD participants than in the NCs. The differences in state distribution suggested that the SCD group was more inclined to be in a state with reduced intra-network and inter-network interaction rather than that dominated by high AUD-VIS-SMN communication.

Variability in temporal properties of brain states during the time of the experimentally unconstrained scanning session was detected. The SCD group showed significantly fewer fractional windows and shorter mean dwell time in state 2 than the NC group, suggesting decreased within-network connectivity and reduced AUD-VIS-SMN network integration in the SCD stage. Increasing evidence has suggested that auditory, visual, and sensorimotor dysfunctions are commonly involved during AD progression and may precede the onset of cognitive impairments and dementia (Albers et al., 2015; Deng et al., 2016). Our results of weak connectivity in sensory domains may provide an explanation for these deficits in the earliest stages of AD. In addition, the reduced interaction among AUD-VIS-SMN networks was consistent with the concept that cognitive decline in AD is a disconnection syndrome closely associated with the functional segregation of coordinated brain networks (Delbeuck et al., 2003). A recent DFC study has shown significantly lower temporal variability involving the regions of the SMN and VIS in AD dementia patients, which could be related to reduced flexibility in sensory, motor, and visual functions (Gu et al., 2020). Another study has observed a significant reduction in the frequency and mean dwell time in the state characterized by strong positive correlations within and between the visual and motor networks in AD dementia patients (Schumacher et al., 2019). The present study extends previous findings by showing that brain network reorganization in SCD individuals presents a similar pattern to that of AD dementia patients.

The SCD group also showed significantly increased fractional windows and a significant increase in mean dwell time in state 4 compared to the NC group. A previous study has observed that AD dementia patients spent more time than NCs in sparse connectivity configurations, indicating their inability to switch out of states with low inter-network connectivity into more highly and specifically connected network configurations; this deficiency might be related to cognitive deterioration (Schumacher et al., 2019). Our results of more time spent in the sparsely connected state in the SCD group supported the concept that SCD was a preclinical stage of the AD spectrum from the perspective of DFC state patterns. Notably, the SCD group showed fractional windows and a mean dwell time in state 3 similar to those of NCs, which was dominated by strong connections within and between distinct functional networks. The SCD group also showed similar fractional windows and a similar mean dwell time in state 1, which was characterized by anti-correlations between the DMN and other networks; these anti-correlations have been shown to be crucial for cognitive processes (Fox et al., 2005; Baggio et al., 2015). The absence of this antithetic association has been reported in MCI and AD dementia patients (Esposito et al., 2018; Schumacher et al., 2019). We speculated that contrary to the symptomatic AD stage, the strong connections in the whole brain networks and the antagonism between the DMN and task-positive networks may remain stable in the SCD stage to support objectively unimpaired cognition, and this speculation remains to be further validated.

Regarding the number of transitions between distinct states, the SCD group demonstrated significantly reduced transitions between state 1 and state 2, between state 2 and state 3, and between state 2 and state 4 in the present study. State transitions are believed to reflect neural metastability, which enables multiple brain regions to engage and disengage flexibly in coordination without being locked into fixed interaction patterns (Li et al., 2017). Frequent transitions between

discrete connectivity patterns also facilitate flexible information integration and intensive information exchange across multiple specialized subnetworks (Li et al., 2017). The configurations of multiple brain regions interacting in complex and flexible communication patterns may be disrupted in SCD individuals. These results elucidated the vulnerability of rs-fMRI networks in the SCD stage and emphasized the importance of investigating the dynamic characteristics of the brain.

We observed significant associations between DFC properties and cognitive performance. The more time participants spent in state 4, the worse executive and general cognitive function they had. State 4 represents the most hypo-connected networks among all 4 states, including weak intra-network connectivity in the CEN and weak inter-network connectivity between the CEN and other brain modules, which may contribute to ineffective information transfer and processing, thus resulting in worse executive and general cognitive ability. The more frequent transitions between states predicted better performance on immediate and recognition memory tests, which may imply potential relationships between neural flexibility and memory function. A previous study has revealed a reduction in brain metastability related to cognitive impairments in cognitive flexibility, speed of information processing, and associative memory (Hellyer et al., 2015). The inflexibility of functional networks may result in the loss of memory encoding and retrieval efficiency in SCD individuals. We also observed a significant association between longer time dwelt in state 2 and better recognition memory performance in the SCD group, indicating that functional integration of the AUD-VIS-SMN may help strengthen memory function. In addition, increased switches between distinct dynamic FC states may also contribute to better language ability. These findings provide evidence that altered dynamic functional brain organization is linked to cognitive function, which may further serve as the neural substrates underlying cognitive decline in the SCD stage. Notably, the relationships between DFC temporal properties and the cognitive variables reported above did not survive multiple comparison corrections and further research is needed to confirm these exploratory results.

In contrast to the remarkable dynamic FC alterations, we did not find differences in either global or local topological parameters by graph theory approaches. Previous studies have shown topological alterations in SCD subjects (Chen et al., 2020; Xu et al., 2020), and we speculated that the discrepancies may be attributable to the different diagnostic criteria for SCD, the variations in demographics of the cohorts, and methodological aspects (Wang et al., 2020). These studies also revealed no group differences in the static analysis of global and local efficiency between AD dementia patients and NCs (Peraza et al., 2015; Schumacher et al., 2019). Our findings provide further evidence that DFC, which captures the temporal variations of FC, may be a more informative representation of functional brain networks than SFC for the preclinical detection of incipient AD patients.

Several limitations in the present work should be considered. First, this is a cross-sectional study conducted in a small cohort, while AD is a progressive neurodegenerative disorder; therefore, longitudinal studies with large cohorts are needed to elucidate the role of DFC in the whole AD spectrum. Second, the acquisition time of rs-fMRI data was 8 min 7 s, though researchers have suggested that DFC analysis should be performed with rs-fMRI acquisition times > 10 min. Third, no pathological evidence from amyloid or tau positron emission tomography (PET) and CSF was available. The impact of AD pathology on the interaction and modulation of brain functional networks needs to be further investigated. Notably, the p values in the correlational analysis may not remain significant if multiple comparison corrections were applied, and the large number of zero values may have an impact on the results; thus, the associations between altered DFC parameters and cognitive variables were exploratory results and warrant further validation. Furthermore, the APOE ε4 genotype may have an impact on the fMRI measures, thus in our future study with a larger sample size of APOE ε4 carriers, we will investigate differences in DFC properties between APOE ε4 carriers and non-carriers in SCD subjects.

CONCLUSION

In the present study, we investigated alternations in DFC temporal properties in SCD individuals, with a focus on the fractional windows, mean dwell time, and state transitions. We observed increased fractional windows and mean dwell time in a hypo-connected state and a reduced number of state transitions in the SCD group compared to the NC group. Furthermore, the altered DFC measures were significantly correlated with cognitive variables. Our findings suggested that DFC analysis may provide novel insights into the organization principles of brain networks underlying early cognitive decline in the SCD stage and benefit the preclinical detection of incipient AD patients.

DATA AVAILABILITY STATEMENT

The raw data supporting the conclusions of this article will be made available by the authors, without undue reservation.

ETHICS STATEMENT

The studies involving human participants were reviewed and approved by Human Participants Ethics Committee of the Nanjing Drum Tower Hospital. The patients/participants provided their written informed consent to participate in this study.

AUTHOR CONTRIBUTIONS

QC was responsible for the conception and design of the present study, execution of the experimental work, and wrote the first draft of the manuscript. JL and XZ organized the research project and reviewed and critiqued the manuscript. YS, WC, and XL executed the experimental work. WZ and ZQ reviewed and critiqued the statistical analysis. BZ guided the design of the study protocol, and reviewed and critiqued the manuscript. All authors contributed to the article and approved the submitted version.

FUNDING

This work was supported by the National Natural Science Foundation of China (81720108022 BZ, 81971596, XZ, 82071904, ZQ); the Fundamental Research Funds for the Central Universities, Nanjing University (2020-021414380462); the key project of Jiangsu Commission of Health (K2019025); key medical talents of the Jiangsu province, the 13th Five-Year health promotion project of the Jiangsu province (ZDRCA2016064); Jiangsu Provincial Key Medical Discipline (Laboratory) (ZDXKA2016020); and the project of the sixth peak of talented people (WSN−138). The funders had no role in the study design, data collection and analysis, decision to publish, or preparation of the manuscript.

SUPPLEMENTARY MATERIAL

The Supplementary Material for this article can be found online at: https://www.frontiersin.org/articles/10.3389/fnagi.2021.646017/full#supplementary-material

REFERENCES

Achard, S., and Bullmore, E. (2007). Efficiency and cost of economical brain functional networks. *PLoS Comput. Biol.* 3:e17. doi: 10.1371/journal.pcbi.0030017

Albers, M. W., Gilmore, G. C., Kaye, J., Murphy, C., Wingfield, A., Bennett, D. A., et al. (2015). At the interface of sensory and motor dysfunctions and Alzheimer's disease. *Alzheimers Dement.* 11, 70–98. doi: 10.1016/j.jalz.2014.04.514

Allen, E. A., Damaraju, E., Plis, S. M., Erhardt, E. B., Eichele, T., and Calhoun, V. D. (2014). Tracking whole-brain connectivity dynamics in the resting state. *Cereb. Cortex* 24, 663–676. doi: 10.1093/cercor/bhs352

Baggio, H. C., Segura, B., Sala-Llonch, R., Marti, M. J., Valldeoriola, F., Compta, Y., et al. (2015). Cognitive impairment and resting-state network connectivity in parkinson's disease. *Hum. Brain Mapp.* 36, 199–212. doi: 10.1002/hbm.22622

Biswal, B., Yetkin, F. Z., Haughton, V. M., and Hyde, J. S. (1995). Functional connectivity in the motor cortex of resting human brain using echo-planar MRI. *Magn. Reson. Med.* 34, 537–541. doi: 10.1002/mrm.1910340409

Brenner, E. K., Hampstead, B. M., Grossner, E. C., Bernier, R. A., Gilbert, N., Sathian, K., et al. (2018). Diminished neural network dynamics in amnestic mild cognitive impairment. *Int. J. Psychophysiol.* 130, 63–72. doi: 10.1016/j.ijpsycho.2018.05.001

Calhoun, V. D., Adali, T., Pearlson, G. D., and Pekar, J. J. (2001a). A method for making group inferences from functional MRI data using independent component analysis. *Hum. Brain Mapp.* 14, 140–151. doi: 10.1002/hbm.1048

Calhoun, V. D., Adali, T., Pearlson, G. D., and Pekar, J. J. (2001b). Spatial and temporal independent component analysis of functional MRI data containing a pair of task-related waveforms. *Hum. Brain Mapp.* 13, 43–53. doi: 10.1002/hbm.1024

Chao-Gan, Y., and Yu-Feng, Z. (2010). DPARSF: a MATLAB toolbox for "pipeline" data analysis of resting-state fMRI. *Front. Syst. Neurosci.* 4:13. doi: 10.3389/fnsys.2010.00013

Chen, H., Sheng, X., Luo, C., Qin, R., Ye, Q., Zhao, H., et al. (2020). The compensatory phenomenon of the functional connectome related to pathological biomarkers in individuals with subjective cognitive decline. *Transl. Neurodegener.* 9:21. doi: 10.1186/s40035-020-00201-6

Cordes, D., Haughton, V. M., Arfanakis, K., Wendt, G. J., Turski, P. A., Moritz, C. H., et al. (2000). Mapping functionally related regions of brain with functional connectivity MR imaging. *AJNR Am. J. Neuroradiol.* 21, 1636–1644. Available online at: http://www.ajnr.org/

Córdova-Palomera, A., Kaufmann, T., Persson, K., Alnæs, D., Doan, N. T., Moberget, T., et al. (2017). Disrupted global metastability and static and dynamic brain connectivity across individuals in the Alzheimer's disease continuum. *Sci. Rep.* 7:40268. doi: 10.1038/srep40268

Damaraju, E., Allen, E. A., Belger, A., Ford, J. M., Mcewen, S., Mathalon, D. H., et al. (2014). Dynamic functional connectivity analysis reveals transient states of dysconnectivity in schizophrenia. *Neuroimage Clin.* 5, 298–308. doi: 10.1016/j.nicl.2014.07.003

De Vos, F., Koini, M., Schouten, T. M., Seiler, S., Van Der Grond, J., Lechner, A., et al. (2018). A comprehensive analysis of resting state fMRI measures to classify individual patients with Alzheimer's disease. *Neuroimage* 167, 62–72. doi: 10.1016/j.neuroimage.2017.11.025

Delbeuck, X., Van Der Linden, M., and Collette, F. (2003). Alzheimer's disease as a disconnection syndrome? *Neuropsychol. Rev.* 13, 79–92. doi: 10.1023/a:1023832305702

Delli Pizzi, S., Punzi, M., and Sensi, S. L. (2019). Functional signature of conversion of patients with mild cognitive impairment. *Neurobiol. Aging* 74, 21–37. doi: 10.1016/j.neurobiolaging.2018.10.004

Demirtaş, M., Falcon, C., Tucholka, A., Gispert, J. D., Molinuevo, J. L., and Deco, G. (2017). A whole-brain computational modeling approach to explain the alterations in resting-state functional connectivity during progression of Alzheimer's disease. *Neuroimage Clin.* 16, 343–354. doi: 10.1016/j.nicl.2017.08.006

Deng, Y., Shi, L., Lei, Y., and Wang, D. (2016). Altered topological organization of high-level visual networks in Alzheimer's disease and mild cognitive impairment patients. *Neurosci. Lett.* 630, 147–153. doi: 10.1016/j.neulet.2016.07.043

Díez-Cirarda, M., Strafella, A. P., Kim, J., Peña, J., Ojeda, N., Cabrera-Zubizarreta, A., et al. (2018). Dynamic functional connectivity in Parkinson's disease patients with mild cognitive impairment and normal cognition. *Neuroimage Clin.* 17, 847–855. doi: 10.1016/j.nicl.2017.12.013

Dillen, K. N. H., Jacobs, H. I. L., Kukolja, J., Von Reutern, B., Richter, N., Onur, A., et al. (2016). Aberrant functional connectivity differentiates retrosplenial cortex from posterior cingulate cortex in prodromal Alzheimer's disease. *Neurobiol. Aging* 44, 114–126. doi: 10.1016/j.neurobiolaging.2016.04.010

Dong, G., Yang, L., Li, C. R., Wang, X., Zhang, Y., Du, W., et al. (2020). Dynamic network connectivity predicts subjective cognitive decline: the Sino-Longitudinal Cognitive impairment and dementia study. *Brain Imaging Behav.* 14, 2692–2707. doi: 10.1007/s11682-019-00220-6

Dubois, B., Hampel, H., Feldman, H. H., Scheltens, P., Aisen, P., Andrieu, S., et al. (2016). Preclinical Alzheimer's disease: definition, natural history, and diagnostic criteria. *Alzheimers Dement.* 12, 292–323. doi: 10.1016/j.jalz.2016.02.002

Esposito, R., Cieri, F., Chiacchiaretta, P., Cera, N., Lauriola, M., Di Giannantonio, M., et al. (2018). Modifications in resting state functional anticorrelation between default mode network and dorsal attention network: comparison among young adults, healthy elders and mild cognitive impairment patients. *Brain Imaging Behav.* 12, 127–141. doi: 10.1007/s11682-017-9686-y

Fiorenzato, E., Strafella, A. P., Kim, J., Schifano, R., Weis, L., Antonini, A., et al. (2019). Dynamic functional connectivity changes associated with dementia in Parkinson's disease. *Brain* 142, 2860–2872. doi: 10.1093/brain/awz192

Fox, M. D., Snyder, A. Z., Vincent, J. L., Corbetta, M., Van Essen, D. C., and Raichle, M. E. (2005). The human brain is intrinsically organized into dynamic, anticorrelated functional networks. *Proc. Natl. Acad. Sci. U.S.A.* 102, 9673–9678. doi: 10.1073/pnas.0504136102

Franzmeier, N., Rubinski, A., Neitzel, J., Kim, Y., Damm, A., Na, D. L., et al. (2019). Functional connectivity associated with tau levels in ageing, Alzheimer's, and small vessel disease. *Brain* 142, 1093–1107. doi: 10.1093/brain/awz026

Friedman, J., Hastie, T., and Tibshirani, R. (2008). Sparse inverse covariance estimation with the graphical lasso. *Biostatistics* 9, 432–441. doi: 10.1093/biostatistics/kxm045

Gu, Y., Lin, Y., Huang, L. L., Ma, J. J., Zhang, J. B., Xiao, Y., et al. (2020). Abnormal dynamic functional connectivity in Alzheimer's disease. *CNS Neurosci. Ther.* 26, 962–971. doi: 10.1111/cns.13387

Hellyer, P. J., Scott, G., Shanahan, M., Sharp, D. J., and Leech, R. (2015). Cognitive flexibility through metastable neural dynamics is disrupted by damage to the structural connectome. *J. Neurosci*. 35, 9050–9063. doi: 10.1523/JNEUROSCI.4648-14.2015

Himberg, J., Hyvärinen, A., and Esposito, F. (2004). Validating the independent components of neuroimaging time series via clustering and visualization. *Neuroimage* 22, 1214–1222. doi: 10.1016/j.neuroimage.2004.03.027

Jenkinson, M., Bannister, P., Brady, M., and Smith, S. (2002). Improved optimization for the robust and accurate linear registration and motion correction of brain images. *Neuroimage* 17, 825–841. doi: 10.1006/nimg.2002.1132

Jessen, F., Amariglio, R. E., Buckley, R. F., Van Der Flier, W. M., Han, Y., Molinuevo, J. L., et al. (2020). The characterisation of subjective cognitive decline. *Lancet Neurol.* 19, 271–278. doi: 10.1016/S1474-4422(19)30368-0

Jessen, F., Amariglio, R. E., Van Boxtel, M., Breteler, M., Ceccaldi, M., Chételat, G., et al. (2014). A conceptual framework for research on subjective cognitive decline in preclinical Alzheimer's disease. *Alzheimers Dement*. 10, 844–852. doi: 10.1016/j.jalz.2014.01.001

Jie, B., Liu, M., and Shen, D. (2018). Integration of temporal and spatial properties of dynamic connectivity networks for automatic diagnosis of brain disease. *Med. Image Anal.* 47, 81–94. doi: 10.1016/j.media.2018.03.013

Jones, D. T., Vemuri, P., Murphy, M. C., Gunter, J. L., Senjem, M. L., Machulda, M. M., et al. (2012). Non-stationarity in the "resting brain's" modular architecture. *PLoS ONE* 7:e39731. doi: 10.1371/journal.pone.0039731

Kawagoe, T., Onoda, K., and Yamaguchi, S. (2019). Subjective memory complaints are associated with altered resting-state functional connectivity but not structural atrophy. *Neuroimage Clin*. 21:101675. doi: 10.1016/j.nicl.2019.101675

Kim, J., Criaud, M., Cho, S. S., Díez-Cirarda, M., Mihaescu, A., Coakeley, S., et al. (2017). Abnormal intrinsic brain functional network dynamics in Parkinson's disease. *Brain* 140, 2955–2967. doi: 10.1093/brain/awx233

Lau, W. K., Leung, M. K., Lee, T. M., and Law, A. C. (2016). Resting-state abnormalities in amnestic mild cognitive impairment: a meta-analysis. *Transl. Psychiatry* 6:e790. doi: 10.1038/tp.2016.55

Li, J., Zhang, D., Liang, A., Liang, B., Wang, Z., Cai, Y., et al. (2017). High transition frequencies of dynamic functional connectivity states in the creative brain. *Sci. Rep*. 7: 46072. doi: 10.1038/srep46072

Li, X., Wang, X., Su, L., Hu, X., and Han, Y. (2019). Sino Longitudinal Study on Cognitive Decline (SILCODE): protocol for a Chinese longitudinal observational study to develop risk prediction models of conversion to mild cognitive impairment in individuals with subjective cognitive decline. *BMJ Open* 9:28188. doi: 10.1136/bmjopen-2018-028188

Liu, F., Wang, Y., Li, M., Wang, W., Li, R., Zhang, Z., et al. (2017). Dynamic functional network connectivity in idiopathic generalized epilepsy with generalized tonic-clonic seizure. *Hum. Brain Mapp*. 38, 957–973. doi: 10.1002/hbm.23430

López-Sanz, D., Bruña, R., Garcés, P., Martín-Buro, M. C., Walter, S., Delgado, M. L., et al. (2017). Functional connectivity disruption in subjective cognitive decline and mild cognitive impairment: a common pattern of alterations. *Front Aging Neurosci*. 9:109. doi: 10.3389/fnagi.2017.00109

Peraza, L. R., Taylor, J. P., and Kaiser, M. (2015). Divergent brain functional network alterations in dementia with Lewy bodies and Alzheimer's disease. *Neurobiol. Aging* 36, 2458–2467. doi: 10.1016/j.neurobiolaging.2015.05.015

Quevenco, F. C., Preti, M. G., Van Bergen, J. M., Hua, J., Wyss, M., Li, X., et al. (2017). Memory performance-related dynamic brain connectivity indicates pathological burden and genetic risk for Alzheimer's disease. *Alzheimers Res. Ther*. 9:24. doi: 10.1186/s13195-017-0249-7

Rabin, L. A., Smart, C. M., and Amariglio, R. E. (2017). Subjective cognitive decline in preclinical alzheimer's disease. *Annu. Rev. Clin. Psychol*. 13, 369–396. doi: 10.1146/annurev-clinpsy-032816-045136

Reisberg, B., Shulman, M. B., Torossian, C., Leng, L., and Zhu, W. (2010). Outcome over seven years of healthy adults with and without subjective cognitive impairment. *Alzheimers Dement* 6, 11–24. doi: 10.1016/j.jalz.2009.10.002

Roweis, S. T. (1998). "EM algorithms for PCA and SPCA," in *Advances in Neural Information Processing Systems*, eds M. J. Kearns, S. A. Solla, and D. A. Cohn (Cambridge, FL: MIT Press), 626–632.

Schumacher, J., Peraza, L. R., Firbank, M., Thomas, A. J., Kaiser, M., Gallagher, P., et al. (2019). Dynamic functional connectivity changes in dementia with Lewy bodies and Alzheimer's disease. *Neuroimage Clin*. 22:101812. doi: 10.1016/j.nicl.2019.101812

Shirer, W. R., Ryali, S., Rykhlevskaia, E., Menon, V., and Greicius, M. D. (2012). Decoding subject-driven cognitive states with whole-brain connectivity patterns. *Cereb. Cortex* 22, 158–165. doi: 10.1093/cercor/bhr099

Sperling, R. A., Aisen, P. S., Beckett, L. A., Bennett, D. A., Craft, S., Fagan, A. M., et al. (2011). Toward defining the preclinical stages of Alzheimer's disease: recommendations from the National Institute on Aging-Alzheimer's Association workgroups on diagnostic guidelines for Alzheimer's disease. *Alzheimers Dement* 7, 280–292. doi: 10.1016/j.jalz.2011.03.003

Varoquaux, G., Gramfort, A., Poline, J.-B., and Thirion, B. (2010). "Brain covariance selection: better individual functional connectivity models using population prior," in *Advances in Neural Information Processing Systems*, eds J. D. Lafferty and C. K. I. Williams (Red Hook, FL: Curran Associates Inc.), 2334–2342.

Vidaurre, D., Smith, S. M., and Woolrich, M. W. (2017). Brain network dynamics are hierarchically organized in time. *Proc. Natl. Acad. Sci. U.S.A.* 114, 12827–12832. doi: 10.1073/pnas.1705120114

Viviano, R. P., Hayes, J. M., Pruitt, P. J., Fernandez, Z. J., Van Rooden, S., Van Der Grond, J., et al. (2019). Aberrant memory system connectivity and working memory performance in subjective cognitive decline. *Neuroimage* 185, 556–564. doi: 10.1016/j.neuroimage.2018.10.015

Viviano, R. P., Raz, N., Yuan, P., and Damoiseaux, J. S. (2017). Associations between dynamic functional connectivity and age, metabolic risk, and cognitive performance. *Neurobiol Aging* 59, 135–143. doi: 10.1016/j.neurobiolaging.2017.08.003

Wang, J., Wang, X., Xia, M., Liao, X., Evans, A., and He, Y. (2015). GRETNA: a graph theoretical network analysis toolbox for imaging connectomics. *Front Hum. Neurosci*. 9:386. doi: 10.3389/fnhum.2015.00458

Wang, J. H., Zuo, X. N., Gohel, S., Milham, M. P., Biswal, B. B., and He, Y. (2011). Graph theoretical analysis of functional brain networks: test-retest evaluation on short- and long-term resting-state functional MRI data. *PLoS ONE* 6:e21976. doi: 10.1371/journal.pone.0021976

Wang, X., Huang, W., Su, L., Xing, Y., Jessen, F., Sun, Y., et al. (2020). Neuroimaging advances regarding subjective cognitive decline in preclinical Alzheimer's disease. *Mol. Neurodegener* 15:55. doi: 10.1186/s13024-020-00395-3

Watts, D. J., and Strogatz, S. H. (1998). Collective dynamics of 'small-world' networks. *Nature* 393, 440–442. doi: 10.1038/30918

Xie, Y., Liu, T., Ai, J., Chen, D., Zhuo, Y., Zhao, G., et al. (2019). Changes in centrality frequency of the default mode network in individuals with subjective cognitive decline. *Front Aging Neurosci*. 11:118. doi: 10.3389/fnagi.2019.00118

Xu, X., Li, W., Tao, M., Xie, Z., Gao, X., Yue, L., et al. (2020). Effective and accurate diagnosis of subjective cognitive decline based on functional connection and graph theory view. *Front. Neurosci*. 14:577887. doi: 10.3389/fnins.2020.577887

Yan, T., Wang, W., Yang, L., Chen, K., Chen, R., and Han, Y. (2018). Rich club disturbances of the human connectome from subjective cognitive decline to Alzheimer's disease. *Theranostics* 8, 3237–3255. doi: 10.7150/thno.23772

Yasuno, F., Kazui, H., Yamamoto, A., Morita, N., Kajimoto, K., Ihara, M., et al. (2015). Resting-state synchrony between the retrosplenial cortex and anterior medial cortical structures relates to memory complaints in subjective cognitive impairment. *Neurobiol. Aging* 36, 2145–2152. doi: 10.1016/j.neurobiolaging.2015.03.006

Conflict of Interest: The authors declare that the research was conducted in the absence of any commercial or financial relationships that could be construed as a potential conflict of interest.

frontiers in Aging Neuroscience

ORIGINAL RESEARCH
published: 18 February 2021
doi: 10.3389/fnagi.2021.621767

Voxel-Mirrored Homotopic Connectivity Associated With Change of Cognitive Function in Chronic Pontine Stroke

Luobing Wu[1†], Caihong Wang[1†], Jingchun Liu[2], Jun Guo[3], Ying Wei[1], Kaiyu Wang[4], Peifang Miao[1], Yingying Wang[1] and Jingliang Cheng[1*]*

[1] Henan Key Laboratory of Magnetic Resonance Function and Molecular Imaging, Department of MRI, The First Affiliated Hospital of Zhengzhou University, Zhengzhou, China, [2] Tianjin Key Laboratory of Functional Imaging, Department of Radiology, Tianjin Medical University General Hospital, Tianjin, China, [3] Department of Radiology, Tianjin Huanhu Hospital, Tianjin, China, [4] GE Healthcare MR Research, Beijing, China

OPEN ACCESS

Edited by:
Ying Han,
Capital Medical University, China

Reviewed by:
Peiyu Huang,
Zhejiang University, China
Julien Rossignol,
Central Michigan University, United States
Zhengjia Dai,
Sun Yat-sen University, China

****Correspondence:***
Caihong Wang
fccwangch@zzu.edu.cn
Jingliang Cheng
fccchengjl@zzu.edu.cn

† These authors have contributed equally to this work

Received: *27 October 2020*
Accepted: *18 January 2021*
Published: *18 February 2021*

Citation:
Wu L, Wang C, Liu J, Guo J, Wei Y, Wang K, Miao P, Wang Y and Cheng J (2021) Voxel-Mirrored Homotopic Connectivity Associated With Change of Cognitive Function in Chronic Pontine Stroke. Front. Aging Neurosci. 13:621767. doi: 10.3389/fnagi.2021.621767

Recent neuroimaging studies have shown the possibility of cognitive impairment after pontine stroke. In this study, we aimed to use voxel-mirrored homotopic connectivity (VMHC) to investigate changes in the cognitive function in chronic pontine stroke. Functional MRI (fMRI) and behavioral assessments of cognitive function were obtained from 56 patients with chronic pontine ischemic stroke [28 patients with left-sided pontine stroke (LP) and 28 patients with right-sided pontine stroke (RP)] and 35 matched healthy controls (HC). The one-way ANOVA test was performed for the three groups after the VMHC analysis. Results showed that there were significant decreases in the bilateral lingual gyrus (Lingual_L and Lingual_R) and the left precuneus (Precuneus_L) in patients with chronic pontine ischemic stroke compared to HCs. However, in a *post-hoc* multiple comparison test, this difference remained only between the HC and RP groups. Moreover, we explored the relationship between the decreased *z*-values in VMHC and the behavior-task scores using a Pearson's correlation test and found that both scores of short-term memory and long-term memory in the Rey Auditory Verbal Learning Test were positively correlated with *z*-values of the left lingual gyrus (Lingual_L), the right lingual gyrus (Lingual_R), and the left precuneus (Precuneus_L) in VMHC. Besides that, the *z*-values of Precuneus_L in VMHC were also negatively correlated with the reaction time for correct responses in the Flanker task and the spatial memory task. In conclusion, first, the lingual gyrus played an important role in verbal memory. Second, the precuneus influenced the working memory, both auditory-verbal memory and visual memory. Third, the right-sided stroke played a greater role in the results of this study. This study provides a basis for further elucidation of the characteristics and mechanisms of cognitive impairment after pontine stroke.

Keywords: VMHC, fMRI, cognitive function, pontine stroke, right hemisphere

INTRODUCTION

Cognitive impairment is common and persistent among long-term stroke survivors (Nys et al., 2007; Delavaran et al., 2017; Groeneveld et al., 2019). This important clinical manifestation is not only present in patients with cortical stroke but also in the subcortical brain regions of patients with pontine stroke (Maeshima et al., 2012). Moreover, most patients with pontine stroke still leave varying degrees of cognitive impairment during follow-up (Wei et al., 2020). In fact, cognitive impairment could exert a further negative influence on the daily lives of patients, including deficits in memory and recall, the response capacity to handle complex activities, and the ability to handle the challenges of life (Shimada et al., 2016; Braga et al., 2018; Gajewski et al., 2018), and they deserve more attention.

Characteristics of neural mechanisms are known to be linked with clinical outcomes in patients with stroke, neuroimaging studies like resting-state functional connectivity have provided new insights into functional impairment and improvement. Previous studies have shown that disturbed functional connectivity associated with cognitive function could occur immediately after stroke, and this alteration may persist for a long time (Golestani et al., 2013; Liu et al., 2016). Chen et al. (2019) reported that patients with pontine stroke might exhibit more severe cognitive damage, especially memory processing, compared to patients with subcortical stroke as evidenced by different patterns of functional connectivity alterations in the chronic phase. Multimodal MRI studies have also found that pontine stroke poses a potential risk of memory impairment using dynamic functional network connectivity (Wang et al., 2020) or structural covariance networks (Wei et al., 2020). However, the neurological mechanisms of stroke-induced cognitive impairment in patients with pontine stroke remain to be elucidated, and not only the memory function.

Homotopic cortical areas in both hemispheres play a crucial role in neuroplasticity and in the reorganization of the brain. Impaired interhemispheric functional coordination in the brain regions that are involved in the clinical characteristics and impairment of cognitive performance has been reported in neuroimaging studies (Yang et al., 2017; Fan et al., 2018). As one such approach that reflects interhemispheric homotopic coordination by integrating brain functions underlying coherent cognition, emotion, and behavior control (Zuo and Xing, 2014; Fan et al., 2018), voxel-mirrored homotopic connectivity (VMHC) has been considered a reliable approach that may help us explore and recognize the potential role of behavior-associated alterations of interhemispheric functional connectivity. A considerable number of studies have focused on how damage in VMHC influences stroke (Tang et al., 2016; Shan et al., 2018; Chen et al., 2021). In view of a previous study which demonstrated that connectivity between homotopic FC was significantly associated with clinical performance of the motor control (Urbin et al., 2014), previous VMHC reports (Shan et al., 2018) have only focused on the potential mechanisms of motor function in chronic pontine stroke, but little is known about the relatively hidden mechanism of cognitive impairment. However, cross-hemispheric functional connectivity of ROI to ROI has also revealed that interhemispheric connections involving homotopic areas have the highest degree of efficiency in spatial cognitive impairments after stroke (Ptak et al., 2020). Hence, we speculated whether such patterns of memory processing and spatial cognitive impairments are seen in patients with chronic pontine stroke with the use of VMHC.

To address the aforementioned problems, driven by the interest in cognitive changes of patients with pontine stroke, we used VMHC to explore the difference between pontine stroke patients and healthy controls (HCs). More focus should be given to the following two points of this study. First, we chose to predict the resting-state brain activity in the chronic stage of stroke because couplings between resting-state functional connectivity and individual's task performance or behavior change dynamically with stroke progression of an individual and the strength of couplings increases as the recovery from stroke progresses (Hu et al., 2017). The other reason for choosing the chronic stage was to minimize the impact of motor function on cognitive function, considering that the recovery of motor function reached a stable state after stroke (Kwakkel and Kollen, 2013). Second, different lesion locations would characterize individual contribution to functional outcomes depending on the side of the hemispheres (Cheng et al., 2014). In addition, differences between left and right lesions have been revealed in previous studies (Jiang et al., 2017; Wang et al., 2019c), so patients were subdivided into two groups: a left stroke group and a right stroke group.

Therefore, in this study we aimed to: (1) verify the changes in brain function as measured by VMHC after chronic pontine stroke; (2) identify the lesion-side effect of the alterations of VMHC in patients with pontine stroke; and (3) assess the correlation between the significantly different brain regions and assessments of cognition.

MATERIALS AND METHODS

Participants

Patients with chronic pontine stroke and healthy subjects were recruited from The First Affiliated Hospital of Zhengzhou University, Tianjin Medical University General Hospital, and Tianjin Huanhu Hospital. The experimental protocol was approved by the local medical research ethics committee, and written informed consent was obtained from all participants. In order to ensure the quality of the data, the three cooperative hospitals jointly drafted a strict protocol that formulated and unified the enrollment standards and scanning specifications, organized personnel training, and coordinated the scanning parameters with General Electric (GE) engineers. At the same time, as much as possible, the cognitive test adopted machine evaluation assessment without subjective color. The inclusion criteria for patients with stroke were as follows: (a) the first-onset of stroke with a single lesion that occurred in the pontine area and left and right lesions could be clearly distinguished; (b) the observation time after stroke onset was $>$ 6 months to ensure that the patients were at a stable chronic stage; and (c) right-handed patients aged 40–80 years. The exclusion criteria

were as follows: (a) a previous history of stroke; (b) bilateral or multiple lesions; (c) excessive white matter demyelination, with a modified Fazekas scale for white matter hyperintensities > 1 (Fazekas et al., 1987); (d) a history of mental illness; (e) craniocerebral trauma or other physical organic lesions; and (f) any contraindications to MRI examination. Then, the enrolled patients who met the criteria were subdivided into a left-sided pontine stroke (LP) group and a right-sided pontine stroke (RP) group according to the location of the lesion. The recruitment requirements of the normal HC group were as follows: (a) gender, age, and education level matched with those of the patient group; (b) no cognitive or physical dysfunction; and (c) the exclusion criteria listed above as for patients with pontine stroke. A total of 91 right-handed participants (35 female; mean age, 57.1 ± 7.3 years; 28 LP, 28 RP), and 35 HCs (13 female; mean age, 55.7 ± 7.0 years) were included.

Behavioral Assessment

The patients were assessed and the Fugl–Meyer Assessment (whole extremity, total 100 scores) scores were recorded. All patients and normal volunteers who met the above criteria underwent behavioral assessments before and after the collection of MRI images, including: (a) the Rey Auditory Verbal Learning Test (RAVLT) for evaluating verbal short-term memory (VSTM) and verbal long-term memory (VLTM). The total number of correctly recalled words was recorded as the two terms of RAVLT scores; (b) the Flanker task and the spatial memory task. The selective attention tasks were employed to assess the ability of visual attention, interference suppression, and motor responses of an individual. The details have been previously reported (Shimada et al., 2016; Gajewski et al., 2018). The accuracy rate (ACC, equal to the ratio of the number of correct responses and the total number of possible correct responses) and the average reaction time (RT) for correct responses (time between presentation and manual response) were taken as the dependent variables for the above two spatial tasks.

The evaluation work was supervised by two clinicians with rich clinical experience, who jointly determined the reliability of the results after unifying the standards.

MRI Data Acquisition

All MRI data were obtained using a GE Discovery MR750 3.0T MRI scanner (GE Medical Systems, Waukesha, WI). The imaging parameters for the three hospitals were consistent. These were: (1) resting-state functional MRI (fMRI) with an echo-planar (EPI) sequence: repetition time/echo time (TR/TE) = 2,000/30, fractional anisotropy (FA) = 90°, field-of-view (FOV) = 240 × 240 mm, matrix = 220 × 220, slice thickness = 4 mm, gap = 0.5 mm, interleaved transversal slices = 32, time-point = 180 and (2) high-resolution 3D-T1-weighted structural images with magnetization prepared rapid gradient echo (MPRAGE) sequence: TR/TE = 8.2/3.2, FA = 12°, FOV = 256 × 256 mm, matrix = 256 × 256, slice thickness = 1 mm. During the process of image acquisition, participants were instructed to lie flat on the examination bed, put noise-attenuating earplugs into both ears to reduce the noise during the scan, and place their head firmly between sponge pads on the left and right sides of the head to keep the head in place and to further reduce noise exposure. At the same time, participants were told to stay awake, breathe smoothly, try not to make any movements, or think intentionally.

We manually outlined the lesion profiles on high-resolution 3D-T1-weighted MRI images slice by slice on MRIcron (http://www.mccauslandcenter.sc.edu/mricro/mricron). The generated lesion masks along with the original 3D-T1 images were normalized to the Montreal Neurological Institute (MNI) space for each patient. Next, all normalized patient lesion masks were overlapping by calculation. Finally, the individual lesion masks were averaged and overlaid with a template to create the lesion overlap map, as shown in **Figure 1**.

MRI Data Processing

The preprocessing of the resting-state fMRI data were performed on the software Data Processing Assistant for Resting-State fMRI (DPARSF, http://resting-fmri.sourceforge.net) with Statistical Parametric Mapping (SPM8, http://www.fil.ion.ucl.ac.uk/spm). Procedures were as follows: (1) the first 10 time points were discarded considering the magnetization balance and the subject's adaptation to the environment; (2) time correction for acquisition delay of slices; (3) realignment for head motion correction, in which no participant was excluded due to excessive head movement (rotation, translation, or head movement > 2° or 2 mm). Moreover, mean framewise displacement (FD) was calculated by averaging the FD of each participant across the time points, and three patients were excluded owing to a mean FD > 0.5, one from HC and two from RP. We also found no significant differences in mean FD among the groups ($P = 0.800$); (4) coregistration of each T1 image to the individual functional image after motion correction, and then segmentation into gray matter, white matter, and cerebrospinal fluid; (5) normalization of the functional images to the MNI space and then re-sampling into a voxel size of 3 × 3 × 3 mm; (6) removal of nuisance covariates (cerebrospinal fluid, white matter, 6-head motion parameters, 6-head motion parameters at one time point earlier, and the 12 corresponding squared items (Friston 24-parameter model) as covariates) from the data by linear regression; (7) spatial smoothing with a 6-mm full-width-at-half-maximum (FWHM) Gaussian kernel; and (8) temporal bandpass filtering (0.01–0.08 Hz) and linear detrending.

After preprocessing, the individual VMHC maps were calculated. Specifically, we calculated the Pearson's correlation coefficient between the residual time series of each voxel and that of its symmetrical interhemispheric counterpart. Correlation values were then Fisher *Z*-transformed, and *z*-maps were obtained last to increase the distribution normality. The resultant values (*z*-values) were referred to as the VMHC and were used for subsequent group-level analyses (Zuo et al., 2010).

Statistical Analysis

A two-sample *t*-test was used to compare demographic and clinical characteristics between the LP and the RP groups except for the categorical data, including the duration time after stroke, the lesion volume, and the Fugl–Meyer Assessment (FMA) score. The one-way ANOVA was used to compare age, education level, and assessments of cognitive variables among

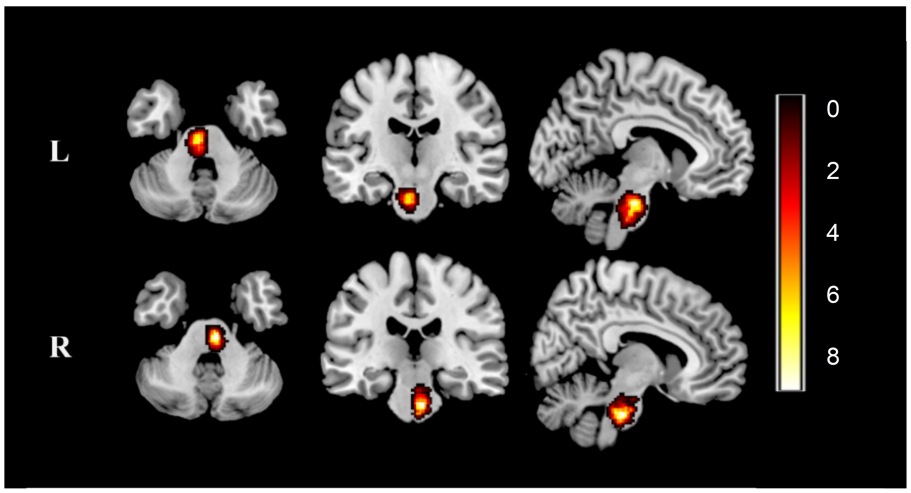

FIGURE 1 | Lesion overlap map across stroke patients. Lesion maps were normalized to an MNI reference brain. Color bar indicates the number of patients with stroke having lesions in each voxel. L, left-sided pontine stroke ($n = 28$); R, left-sided pontine stroke ($n = 26$); MNI, Montreal Neurological Institute.

the HC, LP, and RP groups. Gender was analyzed using a case-weighted chi-square test as categorical data. With individual age, gender, education level, mean FD, and lesion volumes as covariates, one-way ANOVA analysis was also performed to identify the differences of VMHC maps among different groups based on the Gaussian Random Field theory with a cluster-level family-wise error (FWE) correction ($P < 0.05$), accompanied by pairwise comparisons of *post-hoc* multiple corrections (Scheffe). The VMHC values of the brain regions showing abnormal interhemispheric connectivity were then normalized, extracted, and calculated for correlation with the scores of the clinical tasks using the Pearson's correlation coefficient. Statistical Product and Service Solutions (SPSS) version 23.0 statistical software (IBM Corporation, Armonk, NY, USA) was used to compare clinical measurements and correlation analyses.

RESULTS

Sample Characteristics

The final population included 54 patients and 34 HCs. Among the 54 patients, there was a mean duration after stroke of 12.5 ± 7.5 months, a mean lesion volume of 0.39 ± 0.43 cc^3, and a mean FMA score of 94.9 ± 11.5. No significant differences were found for demographic and clinical characteristics between the LP and RP groups. There were no significant differences in gender ($\chi^2 = 1.895$, $P = 0.169$), age ($P = 0.386$), and education level ($P = 0.899$) between the two stroke groups. There were no significant differences in gender ($\chi^2 = 2.350$, $P = 0.125$), age ($P = 0.225$), and education level ($P = 0.359$) among the groups. As for the clinical assessment scores, no significant differences were found, except for the ACC of the spatial memory task ($P = 0.039$). More information is displayed in **Table 1**.

Difference in VMHC Among Groups

Three decreased VMHC values were found in the comparisons among the HC, LP, and RP groups. These were the left lingual gyrus (Lingual_L), the right lingual gyrus (Lingual_R), and the left precuneus (Precuneus_L). The same significant differences were found between the HC and RP groups on the *post-hoc* multiple comparison test. There were no significant differences in VMHC intensity in the comparison between the LP and the RP groups or the HC and the LP groups. These details are shown in **Table 2**, **Figures 2**, **3**.

Correlational Analysis

The correlation analysis showed that the duration since stroke was negatively correlated with the *z*-values of the Lingual_L, Lingual_R, and Precuneus_L in VMHC ($r = -0.31$, $r = -0.31$, and $r = -0.28$, respectively) (**Figure 4**). As for cognitive assessments, both the VSTM and VLTM scores were positively correlated with the *z*-values of the Lingual_L, Lingual_R, and Precuneus_L in VMHC ($r = 0.44$, $r = 0.40$, and $r = 0.42$, respectively; $r = 0.35$, $r = 0.31$, and $r = 0.32$, respectively) (**Figures 5**, **6**). The correlation between the VSTM scores and the decreased *z*-values in VMHC was the strongest. In addition, there was a negative correlation between the *z*-values of the Precuneus_L in VMHC and the RTs for correct responses in the Flanker task ($r = -0.31$, $P < 0.01$) and in the spatial memory task ($r = -0.24$, $P < 0.03$) (**Figure 7**).

DISCUSSION

In this study, we have explored the change of VMHC with patients with chronic pontine stroke and the potential relationship between the change of VMHC and the behavior-task scores. Our main novel findings were as follows: (1) compared with HCs, the VMHC of the bilateral lingual gyrus and the Precuneus_L were significantly decreased in patients with stroke, and these alterations would get more obvious with prolonged duration since chronic stroke; (2) compared with the LP group, the RP group showed greater abnormalities of VMHC in the results; and (3) the decreased *z*-values of the bilateral lingual

TABLE 1 | Demographic and clinical characteristics.

	Left-sided stroke ($n = 28$)	Right-sided stroke ($n = 26$)	*P*-value/t (LP vs. RP)	Healthy Controls ($n = 34$)	*P*-value/F (ANOVA)
Gender(male/female)	18/10	14/12	0.169(χ^2)	21/13	0.125(χ^2)
Age(year)	58.7 ± 6.6 (49–78)	56.9 ± 8.3 (42–72)	0.386	55.4 ± 7.0 (44–75)	0.225
Education(year)	10.2 ± 3.8 (0–16)	10.3 ± 3.8 (22)	0.899	11.4 ± 3.0 (6–16)	0.359
Mean *FD*	0.14 ± 0.10 (0.05–0.43)	0.14 ± 0.08 (0.03–0.32)	0.603	0.14 ± 0.07 (0.04–0.38)	0.800
Duration(month)	11.9 ± 6.6 (6–28)	13.1 ± 8.5 (6–35)	0.574	…	…
Lesion volume(cc^3)	0.46 ± 0.53 (0.04–2.48)	0.31 ± 0.28 (0.01–1.16)	0.182	…	…
FMA	95.5 ± 13.4 (30–100)	94.3 ± 9.1 (65–100)	0.700	…	…
RAVLT					
VSTM	42.1 ± 10.4 (22–65)	45.0 ± 13.5 (26–73)	0.391	48.8 ± 9.0 (30–71)	0.054
VLTM	10.4 ± 2.7 (4–15)	9.3 ± 3.3 (2–15)	0.238	10.9 ± 3.2 (0–15)	0.163
Flanker task					
ACC	0.94 ± 0.10	0.97 ± 0.04	0.225	0.97 ± 0.05	0.211
RT(msec)	696.20 ± 215.55	693.43 ± 230.20	0.968	697.04 ± 232.54	0.998
Spatial memory task					
ACC	0.85 ± 0.16	0.90 ± 0.06	0.107	0.92 ± 0.08	0.039*
RT(msec)	937.23 ± 265.61	946.96 ± 229.66	0.890	904.97 ± 206.89	0.773

*Data represent as mean ± SD (minimum-maximum); *P < 0.05.*
mean FD, mean frame-wise displacement (FD); FMA, the Fugl–Meyer Assessment (whole extremity, total 100 scores); RAVLT, the Rey Auditory Verbal Learning Test; VSTM, verbal short-term memory; VLTM, verbal long-term memory; ACC, accuracy rate; RT, response time for correct response.

TABLE 2 | Results of VMHC among groups and the *post-hoc* multiple comparison test.

Item	Peak Region(*AAL*)	Peak coordinates *MNI*			Cluster size (voxels)	Peak Intensity
		x	y	z		
F	Lingual_L	−33	−69	−18	352	15.80
	Lingual_R	24	−81	21	312	15.11
	Precuneus_L	−21	−78	21	83	17.49
HC vs. RP	Lingual_L	−33	−69	−18	424	4.60
	Lingual_R	24	−81	21	376	4.79
	Precuneus_L	−21	−78	21	162	5.11

VMHC, voxel-mirrored homotopic connectivity; HC, healthy controls; RP, right-sided stroke; F, one-way ANOVA analysis among groups; HC vs. RP, the post-hoc multiple comparison test between the HC and RP groups; AAL, Anatomical Automatic Labeling; MNI, Montreal Neurological Institute; Lingual_L, left lingual gyrus; Lingual_R, right lingual gyrus; Precuneus_L, left precuneus.

gyrus in VMHC predicted poor RAVLT scores, the decreased *z*-values of the Precuneus_L in VMHC predicted not only the poor RAVLT scores but also the prolonged RTs for correct responses in the spatial tasks. Collectively, these findings indicated that the VMHC could provide neurological information to forecast cognitive performance.

The VMHC of the patients was significantly reduced in the occipital cortex away from the pontine. The current result might suggest that pontine stroke has a greater effect on global function than on the local function of the brain, which is consistent with the previous finding that brainstem stroke significantly attenuates long-range functional connectivity (Salvador et al., 2005). Some studies infer that the mechanisms underlying the deficits in VMHC could be related to widespread white matter-integrity abnormalities, dysfunctions in local gray matter structure, and the reorganized pattern of pathways (Yuan et al., 2012; Ding et al., 2015). Therefore, the underlying reason for the change of VMHC is most likely because of the special anatomical structure of the pontine, which involves a large number of ascending and descending fibers staggered throughout the pontine (Querol-Pascual, 2010), and the pontine nucleus works as a relay station for transmitting information from the cerebral cortex. Since structural damages of patients with pontine stroke exist (Jiang et al., 2017; Guo et al., 2019), it can lead to long-range cortical functional damage.

A significant finding of this study was that the RP group exhibited a more extensive VMHC decrease than the LP group in a *post-hoc* multiple comparison test, although these two groups of patients did not differ in terms of any demographic or clinical characteristics. As shown in **Figure 8**, the distribution of decreased *z*-values in VMHC showed an adjacent gradient declining trend among the groups. The lesion-side effect on

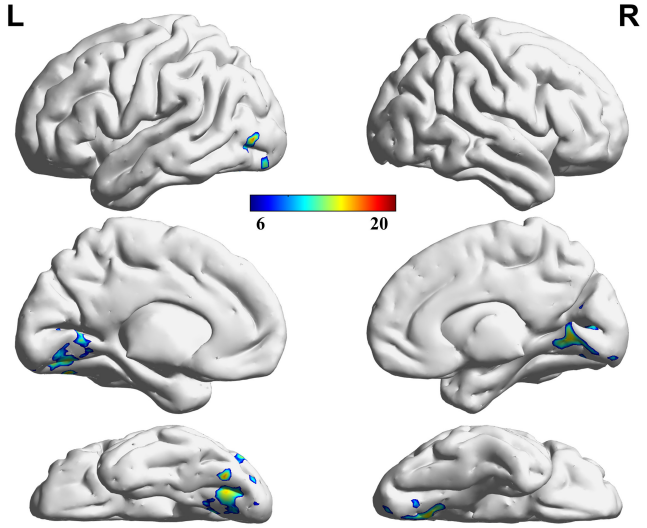

FIGURE 2 | Regions showing significant differences in VMHC among groups. The blue to red color bar indicates the F-value from the one-way ANOVA analysis among groups. Comparisons were corrected by using the Gaussian Random Field theory with a cluster-level family-wise error (FWE) correction ($p < 0.05$).

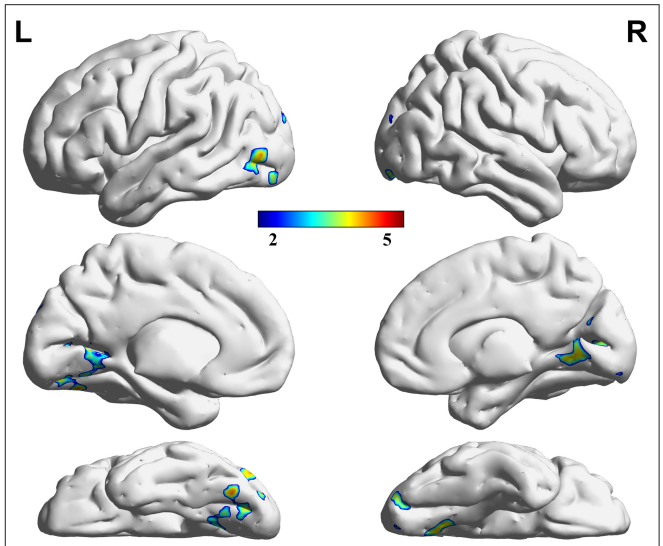

FIGURE 3 | Regions showing significant differences in VMHC between the HC and RP groups. The blue to red color bar indicates the *t*-value from the *post-hoc* multiple correction test (Scheffe) between the HC and RP groups ($p < 0.05$).

VMHC following chronic pontine stroke was clearly observed, and the neural mechanisms related to this effect should be further discussed. The change in structures of fiber tracts, the gray matter volume, and the cortical pathways tends to be more obvious in the right hemisphere than the left hemisphere (Chiang et al., 2015; Liu et al., 2015, 2018; Diao et al., 2017). Generally, the more severe the structural damage, the more extensive the brain reorganization. As we discussed above, the change of VMHC is closely related to structural damage. Thus, this is possibly a neural mechanism underlying that the RP group shows a greater contribution to the VMHC than the LP group. In addition, all patients were right-handed, and previous studies have inferred that an increase in physical activity in daily life can result in increased activation of functional areas to compensate for the damaged ipsilesional area (Verstynen et al., 2005; Diao et al., 2017), specifically in right-handed patients with the left-dominant hemisphere stroke (Wang et al., 2019a). This phenomenon may suggest that the LP group will present with less damage in functional connectivity as a result of the compensation mechanisms compared to the RP group. Of course, further studies are needed to clarify the neural mechanisms underlying the lesion-side effect after chronic pontine stroke.

In the current study, the decreased bilateral lingual gyrus may predict declined performance of verbal working memory. As we know, the lingual gyrus is located in the ventral occipitotemporal cortex, the region that is responsible for word recognition and information integration to and from the language network (Lerma-Usabiaga et al., 2018; Ludersdorfer et al., 2019). Additionally, a previous study reported that memory deficits are closely related to the inferior occipital gyrus and the lingual gyrus (Kraft et al., 2014). Taken together, our results are in line with studies showing that the lingual gyrus in both hemispheres plays an important role in semantic processing, object priming, and output memory (Heath et al., 2012; Ding et al., 2015). Notably, a previous study on acute lacunar stroke reported increased VMHC in the lingual gyrus (Yang et al., 2017), which seems to contradict the current finding. The underlying mechanisms of such discrepancies remain unknown. One possible explanation is that the patient groups in different studies might reside in different disease stages. Furthermore, this is not contradictory to the decreasing trend of the lingual gyrus.

In contrast to both the left and right lingual gyrus, the precuneus was decreased only in the left hemisphere of the brain compared with HCs. However, in the *post-hoc* multiple comparison test, we found that this decreased result was most prominent in patients with RP. The disruption of homotopic FC is considered to be associated with structural impairment. Specifically, previous studies have demonstrated that patients with damage on the right side of the brain have significantly decreased FA values in the right pathway (Grieve et al., 2007; Liu et al., 2018). The unilateral reduced white matter integrity led to a decreased contralateral homotopic connectivity, and this might be a reasonable explanation for the change of VMHC in the Precuneus_L. Additionally, the alternation of the precuneus was consistent with the previously reported VMHC results and was supported by a longitudinal study (Shan et al., 2018). In our study, decreased Precuneus_L suggested a decline in the processing of working memory, including both the verbal working memory (VSTM and VLTM) and the visual working memory (Flanker task and spatial memory task). The default-mode network (DMN) is a collection of brain regions that are typically deactivated in goal-directed tasks and activated during rest periods. The more the default-mode activity of a

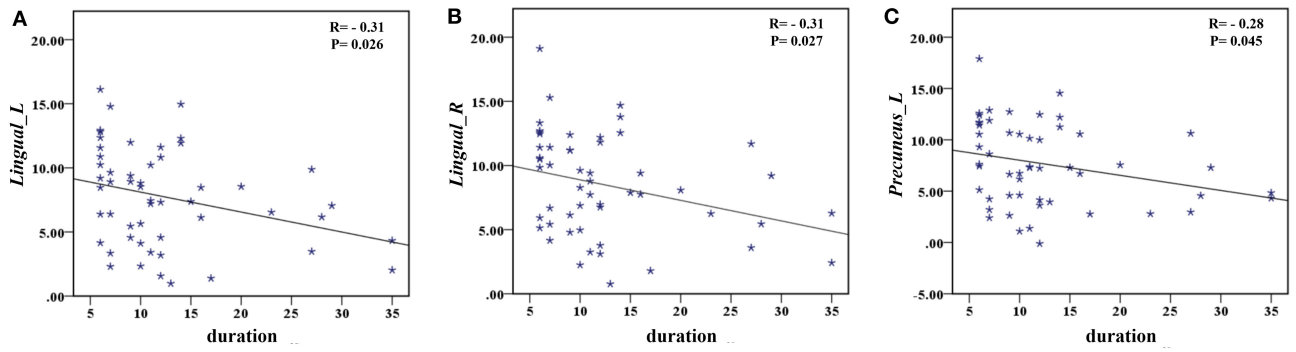

FIGURE 4 | (A) Correlation between *z*-values of Lingual_L in VMHC and the duration since stroke. **(B)** Correlation between *z*-values of Lingual_R in VMHC and the duration since stroke. **(C)** Correlation between *z*-values of Precuneus_L in VMHC and the duration since stroke.

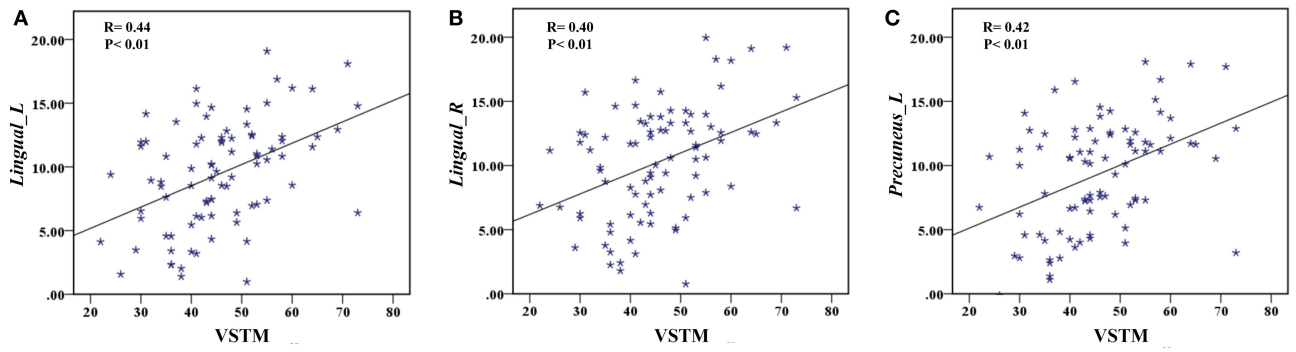

FIGURE 5 | (A) Correlation between *z*-values of Lingual_L in VMHC and the VSTM scores. **(B)** Correlation between *z*-values of Lingual_R in VMHC and the VSTM scores. **(C)** Correlation between *z*-values of Precuneus_L in VMHC and the VSTM scores.

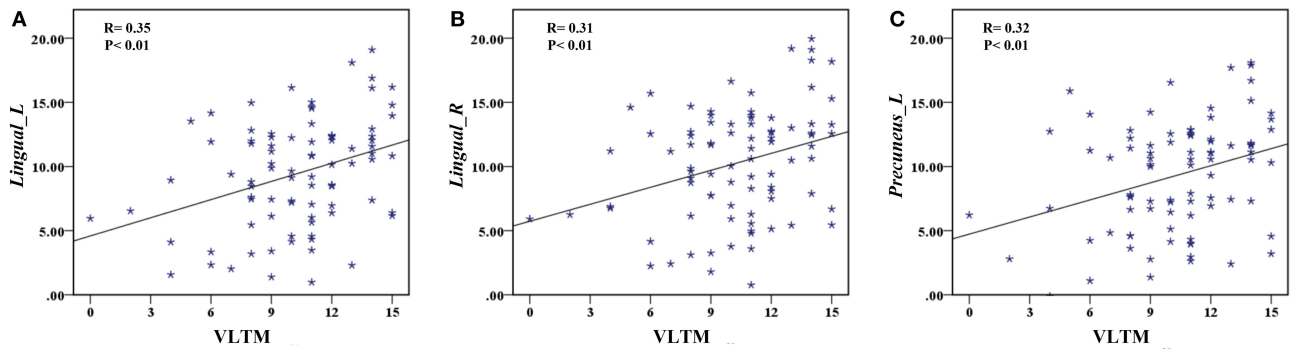

FIGURE 6 | (A) Correlation between *z*-values of Lingual_L in VMHC and the VLTM scores. **(B)** Correlation between *z*-values of Lingual_R in VMHC and the VLTM scores. **(C)** Correlation between *z*-values of Precuneus_L in VMHC and the VLTM scores.

subject correlated with the rest of the periods, the greater the activation of that subject to the visual and auditory stimuli (Greicius and Menon, 2004). As the main node in the DMN, the precuneus plays a central role in cognitive function and neural correlates of a functional connection between these regions, which may be associated with self-referential processing, attentional control, and working memory (Broyd et al., 2009; Liu et al., 2017). The damage to network hubs determines the potential for cognitive recovery after stroke (Aben et al., 2019; Wang et al., 2019b), so the Precuneus_L in the right hemisphere seems to be a great neurological biomarker for stroke-induced cognitive impairment.

In this study, the ACC of the spatial memory task showed the difference among the groups, and we have learned that the RP

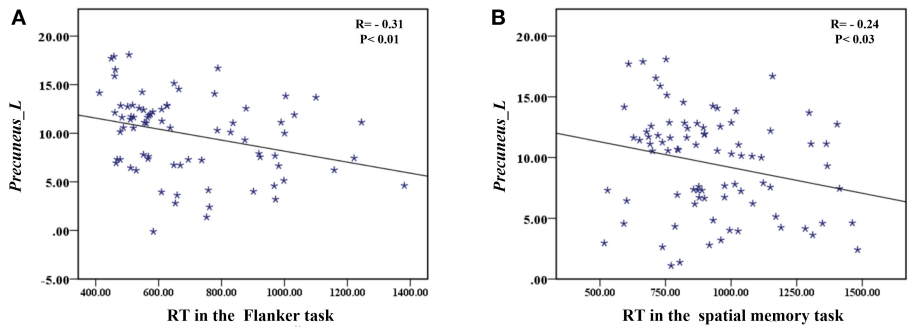

FIGURE 7 | (A) Correlation between *z*-values of Precuneus_L in VMHC and the RT for correct responses in the Flanker task. **(B)** Correlation between *z*-values of Precuneus_L in VMHC and the RT for correct responses in the spatial memory task.

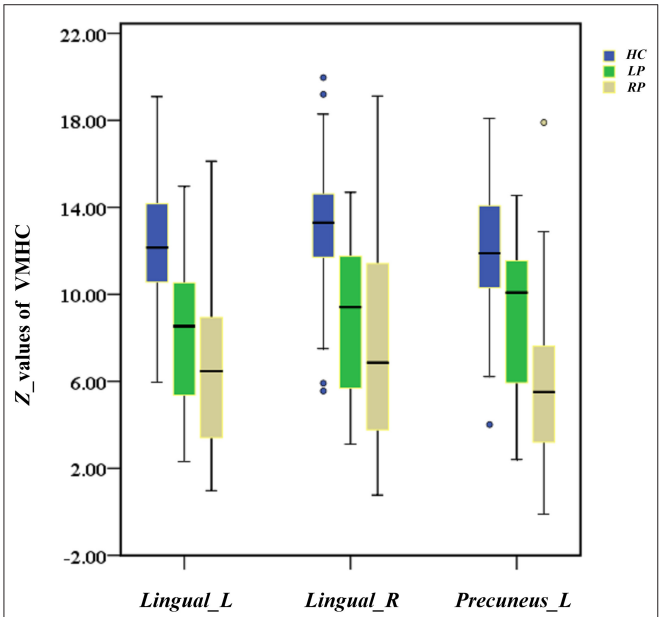

FIGURE 8 | The box diagram shows the distribution of *z*-values of Lingual_L, Lingual_R, and Precuneus_L in VMHC among the groups (HC, LP, RP). Blue for HC, healthy controls; green for the LP, left-sided stroke; yellow for the RP, right-sided stroke.

group played a critical role in our results, so we infer that the right-side stroke may be the main cause of more severe cognitive impairment and poor performance in spatial memory tasks with patients with chronic pontine stroke. To our knowledge, this study is not the first time to indicate that the right hemisphere plays a superior role in spatial tasks (Corbetta and Shulman, 2011; Liu et al., 2018; Shimonaga et al., 2020). In general, attention is considered to be the foundation of cognitive functions for the processing speed, the working memory, and the visuospatial processing we measured in the spatial memory task (Gajewski et al., 2018). The directed attention is thought to be related to spatial neglect, and the sustained attention is thought to be associated with cognitive processing speed, as evaluated by RT (Shimonaga et al., 2020, Lundqvist et al., 1997). The right hemisphere is proved to be responsible for maintaining a balance of attention between the two hemispheres (Fisk et al., 2002; Corbetta and Shulman, 2011). When there is damage to the right hemisphere, which is dominant in arousal, orientation, and duration, the result is a lack of precision to detect targets, leading to an increased RT (Lundqvist et al., 1997; Yuan et al., 2012; Ptak et al., 2020; Shimonaga et al., 2020). Moreover, mapping of the underlying neural mechanisms of the visuospatial working memory has been shown to consistently elicit activity in the right hemisphere of the dominant frontoparietal networks (Cheng et al., 2014; Lamp et al., 2016). Anyhow, our findings are congruent with the fact that the right hemisphere is more important to the change of cognitive function after stroke.

Nevertheless, the current results have facilitated a further understanding of cognitive function after pontine stroke. We encourage testing the modulation of these homotopic connectivities as potential targets for therapeutic intervention in the early phase of the stroke. By stimulating and enhancing such a target region of homotopic connectivity, we hope that this contributes to the effects of cognitive intervention trials, such as transcranial direct-current stimulation (Yun et al., 2015), which is crucial for the overall success of post-stroke rehabilitation.

CONCLUSIONS

In this study, we explored the VMHC changes after chronic pontine stroke among the HC, LP, and RP groups, and compared each of the two groups using the *post-hoc* multiple comparison test. In addition, we demonstrated the relationships of decreased homotopic connectivity with cognitive impairment. Findings highlight the critical role of the lingual gyrus in the language network and the verbal working memory and of the value of the precuneus in working memory, attention control, and executive ability. Importantly, there was a lesion-side effect in decreased VMHC after chronic pontine stroke between the LP and RP groups. The RP group had a greater influence on the VMHC change, which is associated with cognitive function impairment in the cognitive task in this study; therefore, the right hemisphere is regarded as more vulnerable in cognitive impairment. Finally,

we hope our findings may contribute to the improvement of cognitive performance after pontine stroke in the future.

LIMITATIONS

Although interesting results and speculations have been discussed above, there are still several limitations in this study. First, as discussed above, the contribution of the left and right lesions varies between recruited patients, and more standardized larger samples need to be studied. Additionally, although we have learned that cognitive impairment exists in chronic stroke, there is little information about subcortical stroke and how this may impair the development along with the progression of stroke following onset. Therefore, a cross-sectional experimental design, or a longitudinal study design, should be applied in future studies. Finally, since a lesion-side effect on cognitive impairment after chronic pontine stroke was identified, multimodal MRI studies are required to clarify the underlying neural mechanisms. We hope that our results provide a basis for the development of a comprehensive and systematic understanding of post-stroke cognitive changes.

DATA AVAILABILITY STATEMENT

The original contributions presented in the study are included in the article/supplementary material, further inquiries can be directed to the corresponding author/s.

ETHICS STATEMENT

The studies involving human participants were reviewed and approved by The First Affiliated Hospital of Zhengzhou University, Tianjin Medical University General Hospital and Tianjin Huanhu Hospital. The patients/participants provided their written informed consent to participate in this study.

AUTHOR CONTRIBUTIONS

All authors have made significant scientific contributions to this manuscript. LW, CW, YWe, PM, YWa, and JC conceived and designed the experiments. LW, CW, JL, JG, YWe, PM, and YWa performed the experiments. LW, YWe, and CW analyzed the data. LW, YWe, CW, and KW participated in the completion of the manuscript. All authors reviewed the manuscript.

FUNDING

This study was supported by the Natural Science Foundation of China (Nos. 81601467, 81871327, and 81601472) and the Young Talent Lifting Project of Henan Province (No. 2021HYTP012).

ACKNOWLEDGMENTS

We are grateful to our patients and their families for their continued support for our study.

REFERENCES

Aben, H. P., Biessels, G. J., Weaver, N. A., Spikman, J. M., Visser-Meily, J., de Kort, P., et al. (2019). Extent to which network hubs are affected by ischemic stroke predicts cognitive recovery. *Stroke* 50, 2768–2774. doi: 10.1161/STROKEAHA.119.025637

Braga, M. M., Nickel, R., Lange, M., and Piovesan, É. J. (2018). Driving and visual deficits in stroke patients. *Arq. Neuropsiquiatr.* 76, 85–88. doi: 10.1590/0004-282x20170184

Broyd, S. J., Demanuele, C., Debener, S., Helps, S. K., James, C. J., and Sonuga-Barke, E. J. (2009). Default-mode brain dysfunction in mental disorders: a systematic review. *Neurosci. Biobehav. Rev.* 33, 279–296. doi: 10.1016/j.neubiorev.2008.09.002

Chen, H., Shi, M., Zhang, H., Zhang, Y. D., Geng, W., Jiang, L., et al. (2019). Different patterns of functional connectivity alterations within the default-mode network and sensorimotor network in basal ganglia and pontine stroke. *Med. Sci. Monit.* 25, 9585–9593. doi: 10.12659/MSM.918185

Chen, J., Sun, D., Shi, Y., Jin, W., Wang, Y., Xi, Q., et al. (2021). Altered static and dynamic voxel-mirrored homotopic connectivity in subacute stroke patients: a resting-state fMRI study. *Brain Imag. Behav.* 15, 389–400. doi: 10.1007/s11682-020-00266-x

Cheng, B., Forkert, N. D., Zavaglia, M., Hilgetag, C. C., Golsari, A., Siemonsen, S., et al. (2014). Influence of stroke infarct location on functional outcome measured by the modified rankin scale. *Stroke* 45, 1695–1702. doi: 10.1161/STROKEAHA.114.005152

Chiang, H. L., Chen, Y. J., Lo, Y. C., Tseng, W. Y., and Gau, S. S. (2015). Altered white matter tract property related to impaired focused attention, sustained attention, cognitive impulsivity and vigilance in attention-deficit/hyperactivity disorder. *J. Psychiatry Neurosci.* 40, 325–335. doi: 10.1503/jpn.140106

Corbetta, M., and Shulman, G. L. (2011). Spatial neglect and attention networks. *Annu. Rev. Neurosci.* 34, 569–599. doi: 10.1146/annurev-neuro-061010-113731

Delavaran, H., Jönsson, A. C., Lövkvist, H., Iwarsson, S., Elmståhl, S., Norrving, B., et al. (2017). Cognitive function in stroke survivors: a 10-year follow-up study. *Acta Neurol. Scand.* 136, 187–194. doi: 10.1111/ane.12709

Diao, Q., Liu, J., Wang, C., Cao, C., Guo, J., Han, T., et al. (2017). Gray matter volume changes in chronic subcortical stroke: A cross-sectional study. *Neuroimage Clin.* 14, 679–684. doi: 10.1016/j.nicl.2017.01.031

Ding, W., Cao, W., Wang, Y., Sun, Y., Chen, X., Zhou, Y., et al. (2015). Altered functional connectivity in patients with subcortical vascular cognitive impairment–a resting-state functional magnetic resonance imaging study. *PLoS ONE* 10:e0138180. doi: 10.1371/journal.pone.0138180

Fan, H., Yang, X., Zhang, J., Chen, Y., Li, T., and Ma, X. (2018). Analysis of voxel-mirrored homotopic connectivity in medication-free, current major depressive disorder. *J. Affect. Disord.* 240, 171–176. doi: 10.1016/j.jad.2018.07.037

Fazekas, F., Chawluk, J. B., Alavi, A., Hurtig, H. I., and Zimmerman, R. A. (1987). MR signal abnormalities at 1.5 T in Alzheimer's dementia and normal aging. *Am. J. Roentgenol.* 149, 351–356. doi: 10.2214/ajr.149.2.351

Fisk, G. D., Owsley, C., and Mennemeier, M. (2002). Vision, attention, and self-reported driving behaviors in community-dwelling stroke survivors. *Arch. Phys. Med. Rehabil.* 83, 469–477. doi: 10.1053/apmr.2002.31179

Gajewski, P. D., Hanisch, E., Falkenstein, M., Thönes, S., and Wascher, E. (2018). What does the n-back task measure as we get older? relations between working-memory measures and other cognitive functions across the lifespan. *Front. Psychol.* 9:2208. doi: 10.3389/fpsyg.2018.02208

Golestani, A. M., Tymchuk, S., Demchuk, A., Goodyear, B. G., and VISION-2 Study Group. (2013). Longitudinal evaluation of resting-state FMRI after

acute stroke with hemiparesis. *Neurorehabil. Neural Repair* 27, 153–163. doi: 10.1177/1545968312457827

Greicius, M. D., and Menon, V. (2004). Default-mode activity during a passive sensory task: uncoupled from deactivation but impacting activation. *J. Cogn. Neurosci.* 16, 1484–1492. doi: 10.1162/0898929042568532

Grieve, S. M., Williams, L. M., Paul, R. H., Clark, C. R., and Gordon, E. (2007). Cognitive aging, executive function, and fractional anisotropy: a diffusion tensor MR imaging study. *Am. J. Neuroradiol.* 28, 226–235.

Groeneveld, I. F., Goossens, P. H., van Meijeren-Pont, W., Arwert, H. J., Meesters, J., Rambaran Mishre, A. D., et al. (2019). Value-based stroke rehabilitation: feasibility and results of patient-reported outcome measures in the first year after stroke. *J. Stroke Cerebrovasc. Dis.* 28, 499–512. doi: 10.1016/j.jstrokecerebrovasdis.2018.10.033

Guo, J., Liu, J., Wang, C., Cao, C., Fu, L., Han, T., et al. (2019). Differential involvement of rubral branches in chronic capsular and pontine stroke. *Neuroimage Clin.* 24:102090. doi: 10.1016/j.nicl.2019.102090

Heath, S., McMahon, K. L., Nickels, L., Angwin, A., Macdonald, A. D., van Hees, S., et al. (2012). Neural mechanisms underlying the facilitation of naming in aphasia using a semantic task: an fMRI study. *BMC Neurosci.* 13:98. doi: 10.1186/1471-2202-13-98

Hu, J., Du, J., Xu, Q., Yang, F., Zeng, F., Dai, X. J., et al. (2017). Altered coupling between motion-related activation and resting-state brain activity in the ipsilesional sensorimotor cortex after cerebral stroke. *Front. Neurol.* 8:339. doi: 10.3389/fneur.2017.00339

Jiang, L., Liu, J., Wang, C., Guo, J., Cheng, J., Han, T., et al. (2017). Structural alterations in chronic capsular versus pontine stroke. *Radiology* 285, 214–222. doi: 10.1148/radiol.2017161055

Kraft, A., Grimsen, C., Kehrer, S., Bahnemann, M., Spang, K., Prass, M., et al. (2014). Neurological and neuropsychological characteristics of occipital, occipito-temporal and occipito-parietal infarction. *Cortex* 56, 38–50. doi: 10.1016/j.cortex.2012.10.004

Kwakkel, G., and Kollen, B. J. (2013). Predicting activities after stroke: what is clinically relevant? *Int. J. Stroke* 8, 25–32. doi: 10.1111/j.1747-4949.2012.00967.x

Lamp, G., Alexander, B., Laycock, R., Crewther, D. P., and Crewther, S. G. (2016). Mapping of the underlying neural mechanisms of maintenance and manipulation in visuo-spatial working memory using an n-back mental rotation task: a functional magnetic resonance imaging study. *Front. Behav. Neurosci.* 10:87. doi: 10.3389/fnbeh.2016.00087

Lerma-Usabiaga, G., Carreiras, M., and Paz-Alonso, P. M. (2018). Converging evidence for functional and structural segregation within the left ventral occipitotemporal cortex in reading. *Proc. Natl. Acad. Sci. U.S.Am.* 115, E9981–E9990. doi: 10.1073/pnas.1803003115

Liu, C. H., Ma, X., Yuan, Z., Song, L. P., Jing, B., Lu, H. Y., et al. (2017). Decreased resting-state activity in the precuneus is associated with depressive episodes in recurrent depression. *J. Clin. Psychiatry* 78, e372–e382. doi: 10.4088/JCP.15m10022

Liu, H., Tian, T., Qin, W., Li, K., and Yu, C. (2016). Contrasting evolutionary patterns of functional connectivity in sensorimotor and cognitive regions after stroke. *Front. Behav. Neurosci.* 10:72. doi: 10.3389/fnbeh.2016.00072

Liu, J., Qin, W., Zhang, J., Zhang, X., and Yu, C. (2015). Enhanced interhemispheric functional connectivity compensates for anatomical connection damages in subcortical stroke. *Stroke* 46, 1045–1051. doi: 10.1161/STROKEAHA.114.007044

Liu, J., Wang, C., Diao, Q., Qin, W., Cheng, J., and Yu, C. (2018). Connection disruption underlying attention deficit in subcortical stroke. *Radiology* 288, 186–194. doi: 10.1148/radiol.2018171730

Ludersdorfer, P., Price, C. J., Kawabata Duncan, K. J., DeDuck, K., Neufeld, N. H., and Seghier, M. L. (2019). Dissociating the functions of superior and inferior parts of the left ventral occipito-temporal cortex during visual word and object processing. *NeuroImage* 199, 325–335. doi: 10.1016/j.neuroimage.2019.06.003

Lundqvist, A., Alinder, J., Alm, H., Gerdle, B., Levander, S., and Rönnberg, J. (1997). Neuropsychological aspects of driving after brain lesion: simulator study and on-road driving. *Appl. Neuropsychol.* 4, 220–230. doi: 10.1207/s15324826an0404_3

Maeshima, S., Osawa, A., Miyazaki, Y., Takeda, H., and Tanahashi, N. (2012). Functional outcome in patients with pontine infarction after acute rehabilitation. *Neurol. Sci.* 33, 759–764. doi: 10.1007/s10072-011-0812-0

Nys, G. M., van Zandvoort, M. J., de Kort, P. L., Jansen, B. P., de Haan, E. H., and Kappelle, L. J. (2007). Cognitive disorders in acute stroke: prevalence and clinical determinants. *Cerebrovasc. Dis.* 23, 408–416. doi: 10.1159/000101464

Ptak, R., Bourgeois, A., Cavelti, S., Doganci, N., Schnider, A., and Iannotti, G. R. (2020). Discrete patterns of cross-hemispheric functional connectivity underlie impairments of spatial cognition after stroke. *J. Neurosci.* 40, 6638–6648. doi: 10.1523/JNEUROSCI.0625-20.2020

Querol-Pascual, M. R. (2010). Clinical approach to brainstem lesions. *Semin. Ultrasound CT MR* 31, 220–229. doi: 10.1053/j.sult.2010.03.004

Salvador, R., Suckling, J., Coleman, M. R., Pickard, J. D., Menon, D., and Bullmore, E. (2005). Neurophysiological architecture of functional magnetic resonance images of human brain. *Cereb. Cortex* 15, 1332–1342. doi: 10.1093/cercor/bhi016

Shan, Y., Wang, Y. S., Zhang, M., Rong, D. D., Zhao, Z. L., Cao, Y. X., et al. (2018). Homotopic connectivity in early pontine infarction predicts late motor recovery. *Front. Neurol.* 9:907. doi: 10.3389/fneur.2018.00907

Shimada, H., Uemura, K., Makizako, H., Doi, T., Lee, S., and Suzuki, T. (2016). Performance on the flanker task predicts driving cessation in older adults. *Int. J. Geriatr. Psychiatry* 31, 169–175. doi: 10.1002/gps.4308

Shimonaga, K., Hama, S., Tsuji, T., Yoshimura, K., Nishino, S., Yanagawa, A., et al. (2020). The right hemisphere is important for driving-related cognitive function after stroke. *Neurosurg. Rev.* doi: 10.1007/s10143-020-01272-9

Tang, C., Zhao, Z., Chen, C., Zheng, X., Sun, F., Zhang, X., et al. (2016). Decreased functional connectivity of homotopic brain regions in chronic stroke patients: a resting state fMRI Study. *PLoS ONE* 11:e0152875. doi: 10.1371/journal.pone.0152875

Urbin, M. A., Hong, X., Lang, C. E., and Carter, A. R. (2014). Resting-state functional connectivity and its association with multiple domains of upper-extremity function in chronic stroke. *Neurorehabil. Neural Repair* 28, 761–769. doi: 10.1177/1545968314522349

Verstynen, T., Diedrichsen, J., Albert, N., Aparicio, P., and Ivry, R. B. (2005). Ipsilateral motor cortex activity during unimanual hand movements relates to task complexity. *J. Neurophysiol.* 93, 1209–1222. doi: 10.1152/jn.00720.2004

Wang, C., Miao, P., Liu, J., Wei, S., Guo, Y., Li, Z., et al. (2019a). Cerebral blood flow features in chronic subcortical stroke: lesion location-dependent study. *Brain Res.* 1706, 177–183. doi: 10.1016/j.brainres.2018.11.009

Wang, C., Zhao, L., Luo, Y., Liu, J., Miao, P., Wei, S., et al. (2019c). Structural covariance in subcortical stroke patients measured by automated MRI-based volumetry. *Neuroimage Clin.* 22, 101682. doi: 10.1016/j.nicl.2019.101682

Wang, D., Yao, Q., Yu, M., Xiao, C., Fan, L., Lin, X., et al. (2019b). Topological disruption of structural brain networks in patients with cognitive impairment following cerebellar infarction. *Front. Neurol.* 10:759. doi: 10.3389/fneur.2019.00759

Wang, Y., Wang, C., et al. (2020). An imbalance between functional segregation and integration in patients with pontine stroke: a dynamic functional network connectivity study. *Neuroimage Clin.* 28:102507. doi: 10.1016/j.nicl.2020.102507

Wei, Y., Wang, C., Liu, J., Miao, P., Wu, L., Wang, Y., et al. (2020). Progressive gray matter atrophy and abnormal structural covariance network in ischemic pontine stroke. *Neuroscience* 448, 255–265. doi: 10.1016/j.neuroscience.2020.08.033

Yang, H., Bai, L., Zhou, Y., Kang, S., Liang, P., Wang, L., et al. (2017). Increased inter-hemispheric resting-state functional connectivity in acute lacunar stroke patients with aphasia. *Exp. Brain Res.* 235, 941–948. doi: 10.1007/s00221-016-4851-x

Yuan, K., Qin, W., Liu, P., Zhao, L., Yu, D., Zhao, L., et al. (2012). Reduced fractional anisotropy of corpus callosum modulates inter-hemispheric resting state functional connectivity in migraine patients without aura. *PLoS ONE* 7:e45476. doi: 10.1371/journal.pone.0045476

Yun, G. J., Chun, M. H., and Kim, B. R. (2015). The effects of transcranial direct-current stimulation on cognition in stroke patients. *J. Stroke* 17, 354–358. doi: 10.5853/jos.2015.17.3.354

Zuo, X. N., Kelly, C., Di Martino, A., Mennes, M., Margulies, D. S., Bangaru, S., et al. (2010). Growing together and growing apart: regional and sex differences in the lifespan developmental trajectories of functional homotopy. *J. Neurosci.* 30, 15034–15043. doi: 10.1523/JNEUROSCI.2612-10.2010

Zuo, X. N., and Xing, X. X. (2014). Test-retest reliabilities of resting-state FMRI measurements in human brain functional connectomics: a systems neuroscience perspective. *Neurosci. Biobehav. Rev.* 45, 100–118. doi: 10.1016/j.neubiorev.2014.05.009

Conflict of Interest: KW is an employee of GE Healthcare.

The remaining authors declare that the research was conducted in the absence of any commercial or financial relationships that could be construed as a potential conflict of interest.

frontiers in Aging Neuroscience

ORIGINAL RESEARCH
published: 04 March 2021
doi: 10.3389/fnagi.2021.604119

Assessment of the Concordance and Diagnostic Accuracy Between Elecsys and Lumipulse Fully Automated Platforms and Innotest

*Farida Dakterzada†, Ricard López-Ortega†, Alfonso Arias†, Iolanda Riba-Llena†, Maria Ruiz-Julián†, Raquel Huerto†, Nuria Tahan† and Gerard Piñol-Ripoll**

Cognitive Disorders Unit, Clinical Neuroscience Research Group, Santa Maria University Hospital, IRBLleida, Lleida, Spain

Manual ELISA assays are the most commonly used methods for quantification of biomarkers; however, they often show inter- and intra-laboratory variability that limits their wide use. Here, we compared the Innotest ELISA method with two fully automated platforms (Lumipulse and Elecsys) to determine whether these new methods can provide effective substitutes for ELISA assays. We included 149 patients with AD (n = 34), MCI (n = 94) and non-AD dementias (n = 21). Aβ42, T-tau, and P-tau were quantified using the ELISA method (Innotest, Fujirebio Europe), CLEIA method on a Lumipulse G600II (Fujirebio Diagnostics), and ECLIA method on a Cobas e 601 (Roche Diagnostics) instrument. We found a high correlation between the three methods, although there were systematic differences between biomarker values measured by each method. Both Lumipulse and Elecsys methods were highly concordant with clinical diagnoses, and the combination of Lumipulse Aβ42 and P-tau had the highest discriminating power (AUC 0.915, 95% CI 0.822–1.000). We also assessed the agreement of AT(N) classification for each method with AD diagnosis. Although differences were not significant, the use of Aβ42/Aβ40 ratio instead of Aβ42 alone in AT(N) classification enhanced the diagnostic accuracy (AUC 0.798, 95% CI 0.649–0.947 vs. AUC 0.778, 95% CI 0.617–0.939). We determined the cut-offs for the Lumipulse and Elecsys assays based on the Aβ42/Aβ40 ratio ± status as a marker of amyloid pathology, and these cut-offs were consistent with those recommended by manufacturers, which had been determined based on visual amyloid PET imaging or diagnostic accuracy. Finally, the biomarker ratios (P-tau/Aβ42 and T-tau/Aβ42) were more consistent with the Aβ42/Aβ40 ratio for both Lumipulse and Elecsys methods, and Elecsys P-tau/Aβ42 had the highest consistency with amyloid pathology (AUC 0.994, 95% CI 0.986–1.000 and OPA 96.4%) at the ≥0.024 cut-off. The Lumipulse and Elecsys cerebrospinal fluid (CSF) AD assays showed high analytical and clinical performances. As both automated platforms were standardized for reference samples, their use is recommended for the measurement of CSF AD biomarkers compared with unstandardized manual methods, such as Innotest ELISA, that have demonstrated a high inter and intra-laboratory variability.

Keywords: Alzheimer's disease, assay automation, biomarker, cerebrospinal fluid, cut-off

OPEN ACCESS

Edited by:
Ying Han,
Capital Medical University, China

Reviewed by:
Parnetti Lucilla,
University of Perugia, Italy
Tong Li,
Johns Hopkins University, United States

****Correspondence:***
Gerard Piñol-Ripoll
gerard_437302@hotmail.com

† These authors have contributed equally to this work and share first authorship

Received: *08 September 2020*
Accepted: *10 February 2021*
Published: *04 March 2021*

Citation:
Dakterzada F, López-Ortega R, Arias A, Riba-Llena I, Ruiz-Julián M, Huerto R, Tahan N and Piñol-Ripoll G (2021) Assessment of the Concordance and Diagnostic Accuracy Between Elecsys and Lumipulse Fully Automated Platforms and Innotest. Front. Aging Neurosci. 13:604119. doi: 10.3389/fnagi.2021.604119

INTRODUCTION

Alzheimer's disease (AD) is the most prevalent age-related neurodegenerative disease, accounting for 60–80% of cases of dementia. The extracellular amyloid plaques arising from the accumulation of amyloid β42 protein (Aβ42) and intracellular neurofibrillary tangles formed by aggregations of hyperphosphorylated tau protein (P-tau) are the two main pathological hallmarks of AD (Serrano-Pozo et al., 2011). Both of these pathological characteristics are specific to AD, while neurodegeneration, characterized by an increase in total-tau protein (T-tau), is a non-specific biomarker that can be caused by several neurodegenerative diseases (Jack et al., 2018). Aβ42, P-tau, and T-tau are considered core AD biomarkers that can be measured in cerebrospinal fluid (CSF). Their use increases the accuracy of the diagnosis and prediction of the progression from mild cognitive impairment (MCI) to AD and can differentiate between AD and other causes of dementia or neuropsychiatric problems (Albert et al., 2011; McKhann et al., 2011; Sperling et al., 2011). In addition, the inclusion of these biomarkers in diagnosis benefits populations included in clinical trials (Jack et al., 2018).

Currently, enzyme-linked immunoassay (ELISA) is the most widely used approach for the detection of AD core biomarkers in CSF. However, these ELISA methods often show considerable inter and intra-lab variability that prevents the use of standard cut-off values and precludes the wide use of CSF biomarkers in clinical practice. To circumvent this problem, Fujirebio Diagnostics and Roche Diagnostics have recently developed fully automated platforms for the analysis of CSF biomarkers. Fujirebio has implemented four CSF analytes (Aβ42, Aβ40, T-tau, and P-tau) on the fully automated Lumipulse G System. The measurement method is based on a two-step sandwich chemiluminescent enzyme-immunoassay (CLEIA). The Lumipulse Aβ42 assay is standardized according to certified reference material (CRM) developed by the International Federation of Clinical Chemistry and Laboratory Medicine (IFCC) and the Joint Research Centre (JRC). These platforms consist of three CRMs based on human CSF, with low, middle and high concentrations of Aβ42. However, fully automated Elecsys assays for CSF Aβ42, T-tau and P-tau are run on Elecsys and *Cobas e* immunoassay analyzers (Roche Diagnostics GmbH, Penzberg, Germany). The measurement is performed based on the electrochemiluminescence immunoassay (ECLIA) in a two-step sandwich assay. The Elecsys Aβ42 assay has been standardized by a Joint Committee for Traceability in Laboratory Medicine (JCTLM) with an approved reference measurement procedure (RMP). Therefore, all assay lots are standardized to a sample set with target values derived from liquid chromatography–tandem mass spectrometry (LC-MS/MS) (Leinenbach et al., 2014).

Previous studies have evaluated the consistency between each of these automated methods with manual ELISA methods or Amyloid PET imaging (Janelidze et al., 2017; Hansson et al., 2018; Kollhoff et al., 2018; Schindler et al., 2018; Willemse et al., 2018; Alcolea et al., 2019; Bayart et al., 2019; Zecca et al., 2019; Kaplow et al., 2020). However, there are no studies that have compared the efficacy of Innotest, Lumipulse and Elecsys methods in a single cohort of patients.

The aims of this study were (a) to assess the concordance between core AD biomarkers measured in CSF using Innotest, Lumipulse and Elecsys methods; (b) to evaluate the diagnostic accuracy of biomarkers and their ratios measured by each method; (c) to assess the discriminating power of AT(N) groups that were generated by the results of the different biomarkers for each of these three technologies and (d) to define the CSF cut-off points for both Lumipulse and Elecsys assays based on the Lumipulse Aβ42/40 status.

MATERIALS AND METHODS

Study Population

A total of 149 patients [AD (n = 34), MCI (n = 94) and non-AD dementias (n = 21)] were included in this study. The study population was recruited consecutively between July 2018 and July 2019 from patients attending the Cognitive Disorders Unit at the Hospital Universitari Santa Maria (Lleida, Spain). Inclusion criteria comprised presentation with suspected cognitive dysfunction at the memory clinic, for which the neurologist requested CSF analysis. The diagnosis of probable AD and MCI was performed based on NIAA criteria (Albert et al., 2011; McKhann et al., 2011). Each non-AD patient fulfilled the criteria for the specific diagnostic criteria of the disorder considered (e.g., Fronto-temporal dementia, Lewy body dementia, etc.) (Gorno-Tempini et al., 2011; Rascovsky et al., 2011; McKeith et al., 2017). The included patients signed an internal regulatory document stating that residual samples used for diagnostic procedures could be used for research studies without any additional informed consent.

CSF Collection and Storage

Cerebrospinal fluid samples were collected between 8 a.m. and 10 a.m. after an overnight fast into 10-mL polypropylene tubes (Sarstedt, 62.610.201). The tubes were inverted several times, and the CSF was processed based on the recommendations provided by each manufacturer. For the Lumipulse assay, the samples were centrifuged at 2,000 × g for 10 min at room temperature and aliquoted into two 2-mL polypropylene tubes (Sarstedt, 72.694.007), with each tube containing 1 mL of CSF. For the Elecsys method, the samples were aliquoted into two 0.5-mL polypropylene tubes (Sarstedt 72.730.005) after centrifugation. For the Innotest assay, the CSF was aliquoted into two 2-mL polypropylene tubes (Sarstedt, 72.694.007) after centrifugation. The samples were stored at −80°C until analyses.

CSF Analysis

Measurements of Aβ42 and Aβ40 (only for lumipulse), T-tau, and P-tau were performed at the clinical laboratory of Hospital Universitari Arnau de Vilanova, Lleida. On the day of the analysis, samples were thawed at room temperature, and the tubes were vortexed briefly. The biomarkers were measured directly from the storage tube and in five separate batches for all three methods. For each method, the same batch of reagents

was used for each biomarker throughout the study, and for each sample, all analytes were quantified in the same run and from the same aliquot. For the ELISA method, Innotest Aβ42, Innotest htau-Ag, and Innotest P-tau (181P) assays (Fujirebio, Europe) were used. Innotest calibrator concentrations ranged from 63 to 4000 pg/mL for Aβ42, 40 to 2300 pg/mL for T-tau, and 16 to 1000 pg/mL for P-tau. According to previous analyses in clinical practice, cut-offs at our center were determined to be <600 pg/mL for Aβ42, >425 pg/mL for T-tau, and >65 pg/mL for P-tau. For the ECLIA method, the tubes analyzed using the Elecsys Aβ42 CSF, Elecsys T-tau CSF, and Elecsys P-tau (181P) CSF assays (Roche Diagnostics GmbH) were run on the cobas e 601 analyzer (Roche Diagnostics) per the manufacturer's instructions. Elecsys measuring ranges were as follows: 200 to 1700 pg/mL for Aβ42, 80 to 1300 pg/mL for T-tau, and 8 to 120 pg/mL for P-tau. For data analysis, we used the cut-offs recommended by the manufacturer, which were as follows: ≤1000 pg/mL for Aβ42, >300 pg/mL for T-tau, and >27 pg/mL for P-tau. Seventeen samples had Aβ42 levels above the upper limit of the measuring range (1700 pg/mL) and were eliminated from the analysis. The results of the Elecsys Aβ42 assay were standardized to the JCTLM-approved RMP for quantitation of Aβ42 in human CSF, based on LC-MS/MS (Leinenbach et al., 2014). For the CLEIA technology, the CSF biomarkers were quantified using the Lumipulse Aβ42, Aβ40, T-tau, and P-tau (181P) assays on the LUMIPULSE G600II automated platform (Fujirebio) per the manufacturer's instructions. Lumipulse measuring ranges were 9–2,335 pg/mL for Aβ42, 150–2,000 pg/mL for T-tau, and 1.1–400 pg/mL for p-Tau. The following cut-offs that had been determined by Fujirebio were used for data analysis: Aβ42 < 600 pg/mL, Aβ42/40 < 0.069, T-tau > 400 pg/mL, and P-tau > 56.5 pg/mL. The results of the Lumipulse Aβ42 presented in this work have been standardized with CRMs developed by the IFCC and JRC (Kuhlmann et al., 2017). The personnel involved in the CSF analyses were blind to the clinical diagnosis.

Statistical Analyses

All statistical analyses were performed using IBM SPSS version 25 (Armonk, NY, United States). One-way ANOVA and Chi-square tests were used for analysis of quantitative and qualitative variables, respectively. The quantitative variables were presented as means (±standard deviation, SD), and the qualitative variables were presented as percentages. To evaluate the correlation between methods, we used Pearson's correlation coefficient (r), paired *t*-tests for paired samples, and the Bland-Altman plot. The diagnostic accuracy of the biomarkers/AT(N) classification was analyzed using a binary logistic regression model. In this model, the sensitivity was defined as the percentage of correct classification of AD diagnosis and the specificity as the percentage of correct classification of non-AD dementias diagnosis. Furthermore, we used this statistical model to evaluate the predictive value of the biomarkers with respect to AD prognosis. The receiver operating characteristic (ROC) analysis for evaluating diagnostic accuracy was further analyzed using the Hanley and McNeil method (Hanley and McNeil, 1982) to compare the Area Under the Curve (AUC). Values of $|z| \geq 1.96$ were considered evidence that the true ROC areas were different. We also performed ROC analysis to determine the cut-offs for the core AD biomarkers and the ratios that best distinguished Lumipulse Aβ42/40+ individuals. In addition, the cut-offs were also determined based on the Innotest Aβ42 status. We determined the positive percent agreement (PPA) and negative percent agreement (NPA), and the single analyte value (or ratio) with the highest Youden index (PPA + NPA − 1) was identified as the cut-off value. Overall percent agreement (OPA) was defined as the sum of the Aβ42/40 + individuals who were positive for a CSF biomarker measure and the Aβ42/40 − individuals who were negative for a CSF biomarker measure divided by the cohort size, thereby providing an estimate of accuracy.

RESULTS

Patient Characteristics

The demographic characteristics and biomarker results are summarized in **Table 1**. The average age of participants was 74 years, and 55% were female. Syndrome diagnoses in the cohort were the following: 34 (22.8%) with AD, 94 (63.1%) with MCI, and 21 (14.1%) with non-AD dementia. There were no significant differences between diagnostic groups for demographic and clinical variables except for MMSE score and hypertension ($P < 0.0001$ and $P < 0.05$, respectively). The mean MMSE score was lower [19.6 (4.2 SD)] for AD patients compared with the two other groups, followed by non-AD dementia patients [21.9 (4.6 SD)] and MCI subjects [25.2 (3.1 SD)]. For all three assays, all CSF biomarker concentrations were significantly different between the three diagnostic groups, except Lumipulse Aβ40 ($P > 0.05$). For Elecsys, samples that had Aβ42 values above the upper limit of detection (1700 pg/mL) were omitted from analysis ($n = 17$ samples, MCI 11, AD 4, and 2 non-AD patients).

Concordance Between Innotest and Lumipulse Assays

Pearson's correlations indicated a high correlation between biomarkers of both methods. **Figure 1** shows the correlation and Bland-Altman plots for biomarkers quantified by Innotest and Lumipulse. The correlation coefficient between the two methods was 0.87 for Aβ42 ($P < 0.0001$), 0.95 for T-tau ($P < 0.0001$) and 0.95 for P-tau ($P < 0.0001$). The concordance between the values of the biomarkers between the two methods was assessed using paired sample *t*-tests. Our results indicated that there was high consistency in the Aβ42 (observed slope 0.98, *t*-test $p = 0.319$) and T-tau (observed slope 0.96, *t*-test $P = 0.785$) values between the two methods (**Figure 1**). Lumipulse Aβ42 values were slightly higher than those for Innotest, while Lumipulse T-tau values were slightly lower than those for Innotest; however, these differences were not statistically significant (**Figure 1**). As shown in the Bland-Altman plot, the bias (mean of the differences) for Aβ42

TABLE 1 | The demographic characteristics and biomarker results for AD, MCI, and non-AD patients.

	All participants	AD	MCI	Non-AD dementia	*P*-value
n (%)	149 (100%)	34 (22.8%)	94 (63.1%)	21 (14.1%)	
Age (years)	73.82 (6.85)	74.00 (8.78)	73.86 (6.05)	73.33 (7.07)	0.937
Sex (% female)	55.7%	67.6%	54.3%	42.9%	0.178
MMSE score	23.41 (4.29)	19.62 (4.24)	25.16 (3.07)	21.90 (4.57)	<0.0001
Family history of cognitive impairment	28.9%	23.5%	29.8%	33.3%	0.7
Hypertension	57.7%	67.6%	55.3%	52.4%	0.003
Diabetes Mellitus	20.1%	26.5%	19.1%	14.3%	0.509
Dyslipidemia	44.3%	47.1%	44.7%	38.1%	0.803
Depression	35.6%	29.4%	36.2%	42.9%	0.587
Innotest					
Aβ42 pg/mL	581.37 (247.46)	405.65 (115.36)	614.11 (252.18)	722.48 (239.53)	<0.0001
T-tau pg/mL	507.85 (354.32)	684.47 (393.01)	450.71 (277.00)	477.67 (498.05)	0.003
P-tau pg/mL	67.55 (28.62)	83.81 (34.75)	64.68 (25.10)	53.91 (21.14)	<0.0001
T-tau/Aβ42	1.130 (1.092)	1.908 (1.623)	0.935 (0.743)	0.727 (0.687)	<0.0001
P-tau/Aβ42	0.148 (0.116)	0.234 (0.167)	0.130 (0.083)	0.088 (0.056)	<0.0001
Elecsys					
Aβ42 pg/mL	770.69 (363.12)	572.50 (179.97)	807.75 (369.95)	970.04 (433.81)	<0.0001
T-tau pg/mL	287.80 (155.38)	379.65 (188.44)	261.39 (118.65)	251.37 (189.67)	<0.0001
P-tau pg/mL	27.38 (17.17)	38.92 (23.19)	24.73 (13.22)	19.56 (11.71)	<0.0001
T-tau/Aβ42	0.463 (0.338)	0.719 (0.470)	0.390 (0.225)	0.318 (0.242)	<0.0001
P-tau/Aβ42	0.045 (0.040)	0.075 (0.060)	0.038 (0.024)	0.027 (0.022)	<0.0001
Lumipulse					
Aβ42 pg/mL	571.43 (276.75)	415.28 (119.15)	599.55 (289.63)	698.41 (301.96)	<0.0001
Aβ40 pg/mL	10317.68 (3339.78)	10597.44 (3605.39)	10363.14 (3111.28)	9661.24 (3935.09)	0.59
Aβ42/40	0.056 (0.022)	0.041 (0.010)	0.058 (0.022)	0.073 (0.022)	<0.0001
T-tau pg/mL	510.37 (356.34)	731.85 (404.16)	438.84 (256.48)	471.95 (505.21)	<0.0001
P-tau pg/mL	81.50 (56.72)	122.96 (73.80)	72.76 (44.18)	53.49 (40.49)	<0.0001
T-tau/Aβ42	1.144 (1.037)	1.933 (1.504)	0.940 (0.700)	0.779 (0.740)	<0.0001
P-tau/Aβ42	0.190 (0.190)	0.330 (0.291)	0.159 (0.123)	0.101 (0.101)	<0.0001

Unless otherwise specified, results are presented as mean (standard deviation). MMSE, Mini-mental state examination; AD, Alzheimer's disease; MCI, mild cognitive impairment; non-AD dementia, non-Alzheimer's disease dementia. P-values were calculated by comparing AD, MCI, and non-AD dementia participants using one way ANOVA for continuous variables and Pearson Chi2 for categorical variables.

was 11.320 units (pg/mL) (continuous line) between the two methods. The regression line for the differences indicated that there was a non-significant negative trend in the differences as the magnitude of the measured variable increased. For T-tau, there was a bias of −2.157 units between the two methods. However, the results of Lumipulse and Innotest were not consistent with respect to P-tau values (observed slope 1.884, *t*-test $P < 0.0001$). For P-tau, there was a bias of −14.328 units (continuous line). The regression line for the differences indicated that there was a systematic proportional bias between the values of the two methods with a negative trend in the differences as the magnitude of P-tau values increased, especially for values greater than 50 pg/mL. Among all assays evaluated, approximately 95% of the measured values were within ±1.96 SD of the bias (**Figure 1**).

Concordance Between Innotest and Elecsys Assays

Pearson's correlations indicated a high correlation between biomarkers of both methods. The correlation coefficient between the two methods was 0.88 for Aβ42 ($P < 0.0001$), 0.96 for T-tau ($P < 0.0001$) and 0.97 for P-tau ($P < 0.0001$). The paired samples *t*-test demonstrated that there was weak concordance between the two methods for all of the biomarkers. For all three biomarkers, the adjustment line (continuous line) (observed slope of 0.52 for Aβ42, *t*-test $P < 0.0001$; observed slope of 2.05 for T-tau, *t*-test $P < 0.0001$; and observed slope of 1.62 for P-tau, *t*-test $P < 0.0001$) was significantly separated from the perfect agreement line (dashed line) (**Figure 2**). The Bland-Altman plot indicated that there was a bias of −222.13 units (continuous line) between the two methods for Aβ42 (i.e., the Elecsys method quantified on average 222.13 pg/mL more Aβ42 than the Innotest assay). The regression line demonstrated a proportional systematic bias with a negative trend of differences as the magnitude of Aβ42 increased. For T-tau and P-tau, the biases (mean of differences) were 210.70 and 40.16 units, respectively. The regression line of the differences indicated a proportional systematic bias for both biomarkers with a positive trend of differences as the magnitude of these biomarkers increased. For all assays

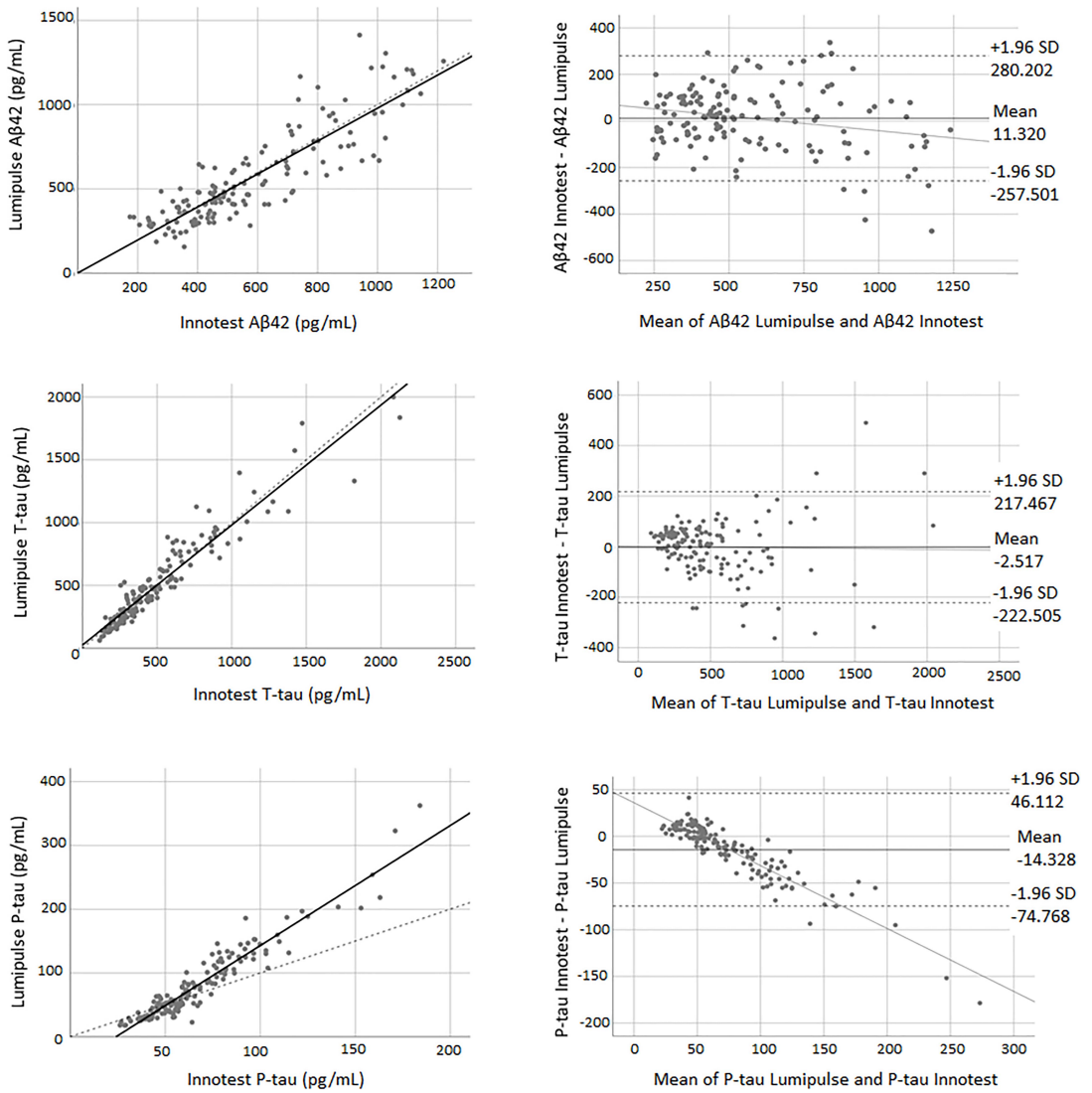

FIGURE 1 | The correlation and Bland-Altman plots for Aβ42, T-tau, and P-tau measurements obtained by Lumipulse and Innotest ELISA methods (n = 149). Each point is defined as the measurements of Lumipulse and ELISA assays on the same biological sample. In correlation plots, the solid lines represent the estimated regression line, and the dotted line represents the identity line ($x = y$). In the Bland-Altman plots, solid lines represent the slope observed.

evaluated, approximately 95% of measured values were within ±1.96 SD of the bias (**Figure 2**).

Concordance Between Elecsys and Lumipulse Assays

There was a high correlation between all three biomarkers for both methods. The correlation coefficient between the two methods was 0.94 for Aβ42 ($P < 0.0001$), 0.95 for T-tau ($P < 0.0001$), and 0.96 for P-tau ($P < 0.0001$). **Figure 3** shows the correlation and Bland-Altman plots for biomarkers quantified by Elecsys and Lumipulse. The t-test results indicated that there was weak concordance between all pairs of biomarkers ($P < 0.0001$). For all three biomarkers, the adjustment line (continuous line) (observed slope of 0.59 for Aβ42, t-test $P < 0.0001$; observed slope of 2.07 for T-tau, t-test $P < 0.0001$; and observed slope 3.21 for P-tau, t-test $P < 0.0001$) was significantly separated from the perfect agreement line (dashed line) (**Figure 3**). The Bland-Altman plot indicated that there was a bias of 243.28 (continuous line) for Aβ42, meaning that Lumipulse quantified 243.28 pg/mL less Aβ42 on average than Elecsys. The regression line demonstrated a proportional systemic bias with a positive trend of differences as the magnitude of Aβ42 increased. For T-tau and P-tau, the biases between the two assays were −210.754 and −54.128 units, respectively. The regression line of the differences indicated a proportional systematic bias for both biomarkers with a negative trend of differences as the magnitude of these biomarkers increased. For all assays evaluated, approximately 95% of measured values were within ± 1.96 SD of the bias (**Figure 3**).

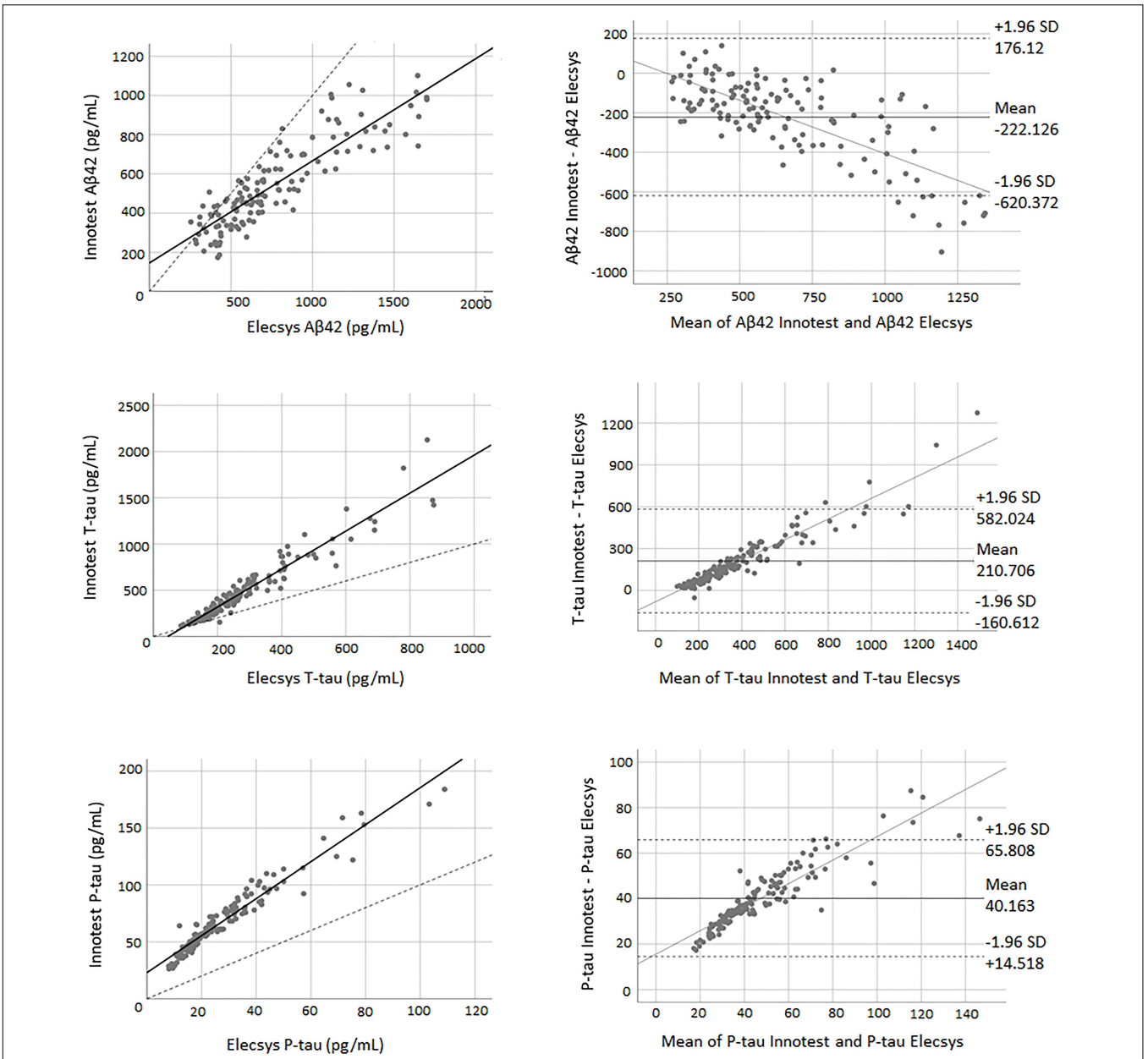

FIGURE 2 | The correlation and Bland-Altman plots for Aβ42, T-tau, and P-tau measurements obtained by Elecsys and Innotest methods (for P-tau and T-tau $n = 145$; for Aβ42 $n = 135$). Each point is defined as the measurement of Elecsys and Innotest assays on the same biological sample. In correlation plots, the solid lines represent the estimated regression line, and the dotted line represents the identity line ($x = y$). In the Bland-Altman plots, solid lines represent the slope observed.

AD Diagnostic Accuracy of the Biomarkers Quantified by Each Method

Using binary logistic regression, we evaluated the diagnostic accuracy of biomarkers quantified by each assay (clinical diagnosis is generally considered the gold standard). To discriminate AD from non-AD patients, the combined use of Aβ42 and P-tau was the best approach for all three assays. The Aβ42/40 ratio of Lumipulse also had high discriminating power, comparable with the combined use of Aβ42 and P-tau, to differentiate between the two diagnostic groups (AUC 0.882, 95% CI 0.785–0.980). Among all three methods, Lumipulse Aβ42 and P-tau had higher discriminating power with an AUC of 0.915 (95% CI 0.822–1.000). This combination of biomarkers had 91.2% sensitivity and 76.2% specificity for a correct classification of diagnostic groups, and their predictive accuracy was estimated to be 85.5%. However, the AUCs were not significantly different between the three methods, as they were assessed using the Hanley and McNeil method ($|z| < 1.96$). However, the sensitivity, specificity and predictive accuracy slightly differed between methods (**Table 2**).

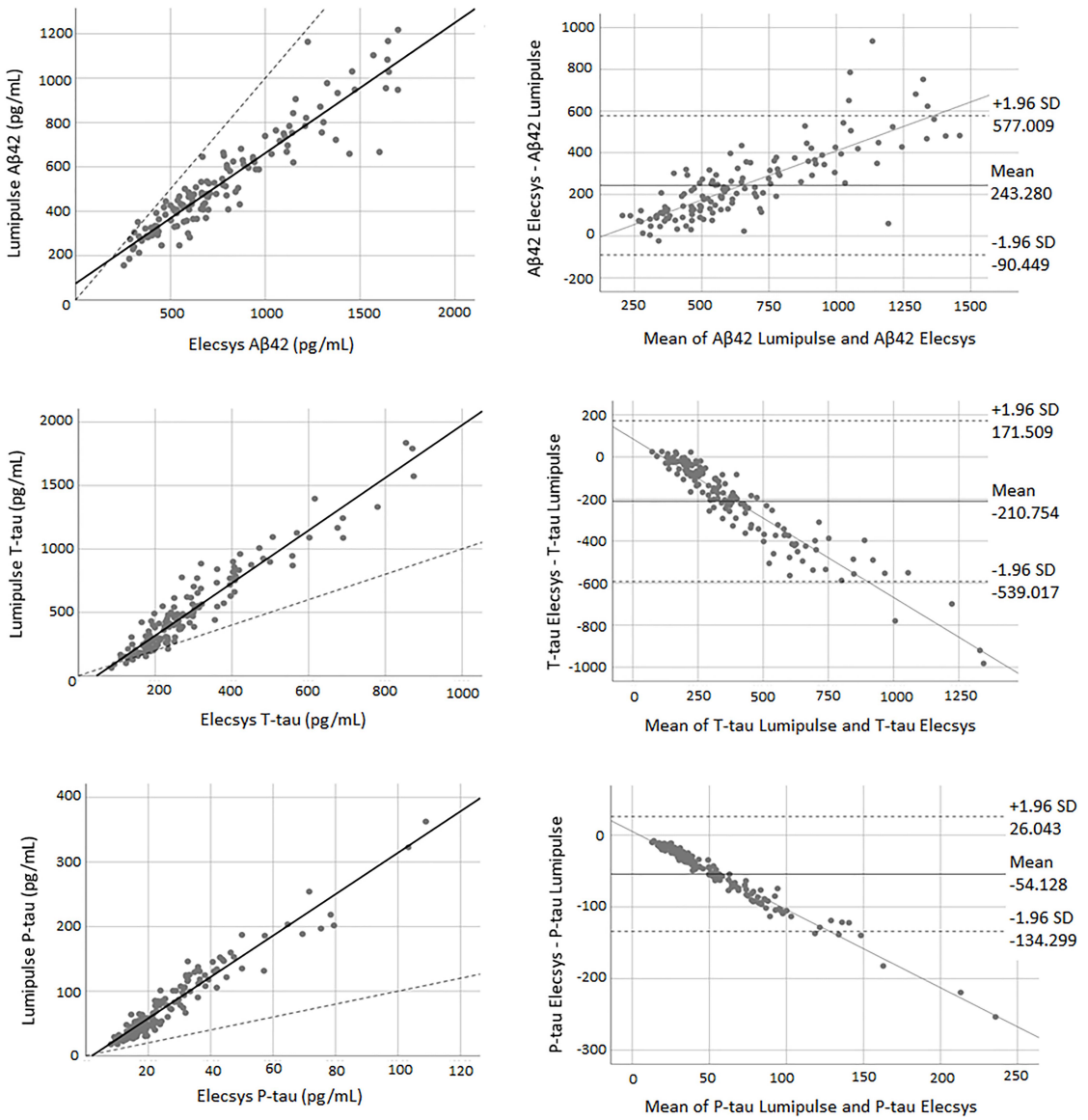

FIGURE 3 | The correlation and Bland-Altman plots for Aβ42, T-tau, and P-tau measurements obtained by Lumipulse and Elecsys methods (for P-tau and T-tau $n = 145$; for Aβ42 $n = 137$). Each point is defined as the measurement of Lumipulse and Elecsys assays on the same biological sample. In correlation plots, the solid lines represent the estimated regression line, and the dotted line represents the identity line ($x = y$). In the Bland-Altman plots, solid lines represent the slope observed.

TABLE 2 | Biomarkers with the best discriminating power between AD and non-AD dementia patients.

	Biomarker	AUC (95% CI)	Sensitivity	Specificity	Total% of predictive accuracy*	*z*-value**
Lumipulse	Aβ42 + P-tau	0.915 (0.822–1.000)	91.2%	76.2%	85.5%	$z = 0.997$ vs. Lumipulse Aβ42/40; $z = 0.639$ vs. Innotest; $z = 1.673$ vs. Elecsys
	Aβ42/40	0.882 (0.785–0.980)	94.1%	71.4%	85.5%	$z = -0.394$ vs. Innotest; $z = 0.033$ vs. Elecsys
Innotest	Aβ42 + P-tau	0.895 (0.801–0.989)	94.1%	76.2%	87.3%	$z = 0.544$ vs. Elecsys
Elecsys	Aβ42 + P-tau	0.881 (0.774–0.988)	91.1%	72.2%	84.6%	

AUC, Area under the curve.
**The percentage of correct classification of AD + correct classification of non-AD/all cases.*
***Values of $|z| < 1.96$ were taken as evidence that the true ROC areas were not different.*

Diagnostic Accuracy of the AT(N) Classification for Each Method

The same statistical model was used to evaluate the discriminating power of the AT(N) classification for each method. We classified our study population into 6 AT(N) (0, 1, 2, 3, 4, and 5) groups based on the results of the three core AD biomarkers (Jack et al., 2018). Biomarkers were grouped into those for β amyloid deposition, pathologic tau, and neurodegeneration [AT(N)]. Here, A referred to levels of Aβ42 (Aβ42/40) in CSF, T referred to levels of P-tau in CSF, and (N) referred to levels of T-tau in CSF. We provided two AT(N) classifications for Lumipulse, one based on the results of Aβ42, T-tau and P-tau and the other one based on the Aβ42/40, T-tau and P-tau values (**Table 3**). Patients who were grouped as AT(N) 0 were negative for all three biomarkers. Patients in the AT(N) 1 group were only positive for Aβ42 or the Aβ42/40 ratio. AT(N) 2 patients were positive for Aβ42 or the Aβ42/40 ratio and P-tau. AT(N) 3 patients had positive results for all three biomarkers. AT(N) 4 patients were positive for Aβ42 or the Aβ42/40 ratio and T-tau. Finally, AT(N) 5 patients were negative for Aβ42 or the Aβ42/40 ratio but positive for P-tau or T-tau or both biomarkers. For Lumipulse and Elecsys assays, classification was made based on the cut-offs provided by the manufacturers. The cut-offs for the Innotest assay were determined in an independent cohort of patients and controls in our lab. Our results indicated that although AT(N) classification based on the Aβ42/40 had the best discriminating power to correctly separate AD patients from non-AD patients with dementia (AUC 0.798; 95% CI 0.649–0.947), there were no significant differences between the four AT(N) classifications [i.e., Innotest, 2 lumipulse and Elecsys biomarkers based on the AT(N) classifications] with respect to diagnostic accuracy after comparing AUCs with the Hanley and McNeil method ($|z| < 1.96$). However, the sensitivity, specificity, and total percentage of predictive accuracy were different between methods, especially between Lumipulse and Innotest or Elecsys (**Table 3**). Among the three methods, Lumipulse AT(N)s had the best sensitivity (91.2%) and total predictive accuracy, while Elecsys AT(N) had the best specificity (77.8%) for discriminating AD from non-AD dementia patients.

CSF Biomarker Cut-Offs Based on Aβ42/40 Ratio Status

As the Aβ42/40 ratio and AT(N) had the best diagnostic accuracy, we selected these variables to serve as references for determining the cut-offs of biomarkers and ratios for Lumipulse and Elecsys. The cut-offs for each biomarker or ratio were established to be values that optimized the concordance with Aβ42/40 status as positive/negative. The determined cut-offs in this study and the established cut-offs by Fujirebio and Roche Diagnostics are presented in **Table 4**. As displayed in **Table 4**, the cut-offs

TABLE 3 | Diagnostic accuracy of the AT(N) classification for each method.

	AT(N)	AUC (95% CI)	Sensitivity	Specificity	Total% of predictive accuracy*	*z*-value**
Lumipulse	Aβ42/40, P-tau, (T-tau)	0.798 (0.649–0.947)	91.2%	71.4%	83.6%	$z = 0.432$ vs. Lumipulse Aβ42, P-tau, (T-tau); 0.288 vs. Innotest; $z = 0.307$ vs. Elecsys
	Aβ42, P-tau, (T-tau)	0.778 (0.617–0.939)	91.2%	71.4%	83.6%	$z = -0.076$ vs. Innotest; $z = -0.034$ vs. Elecsys
Innotest	Aβ42, P-tau, (T-tau)	0.783 (0.627–0.938)	79.4%	76.2%	78.2%	$z = -0.052$ vs. Elecsys
Elecsys	Aβ42, P-tau, (T-tau)	0.780 (0.624–0.937)	67.6%	77.8%	67.3%	

AUC, Area under the curve.
**The percentage of correct classification of AD + correct classification of non-AD/all cases.*
***Values of $|z| < 1.96$ were taken as evidence that the true ROC areas were not different.*

TABLE 4 | Cut-offs of CSF biomarkers that yielded maximum Youden index versus Aβ42/Aβ40 ratio status in the receiver operating characteristics analysis.

		AUC (95% CI)	PPA	NPA	Max Youden index	Cut-off	OPA	Manufacturer cutoffs
Lumipulse	T-tau	0.860 (0.791–0.930)	72.5%	89.4%	61.9%	≥399	77.9%	>400
	P-tau	0.925 (0.884–0.967)	86.3%	85.1%	71.4%	≥51	85.9%	>56.5
	Aβ42	0.923 (0.878–0.967)	82.4%	89.4%	71.7%	≤563	84.6%	<600
	Aβ42/40	1.000 (1.000–1.000)	100%	100%	100%	≤0.070	100%	<0.069
	P-tau/Aβ42	0.992 (0.984–1.000)	95.1%	97.9%	93.0%	≥0.082	95.9%	–
	T-tau/Aβ42	0.956 (0.906–1.000)	96.1%	93.6%	89.7%	≥0.517	95.3%	–
Elecsys	T-tau	0.812 (0.739–0.885)	58.0%	95.6%	53.6%	≥268.15	69.7%	>300
	P-tau	0.867 (0.811–0.923)	70.0%	95.6%	65.6%	≥22.175	78.0%	>27
	Aβ42	0.904 (0.840–0.967)	93.0%	78.4%	71.4%	≤939.150	89.1%	≤1000
	P-tau/Aβ42	0.994 (0.986–1.000)	96.0%	97.3%	93.3%	≥0.023	96.4%	>0.024
	T-tau/Aβ42	0.974 (0.932–1.000)	96.0%	94.6%	90.6%	≥0.26	95.6%	>0.28

AUC, Area under the curve; PPA, Positive percent agreement with Aβ42/40 status; NPA, Negative percent agreement with Aβ42/40 status; Max Youden index, (PPA + NPA – 1); OPA, Overall percent agreement.

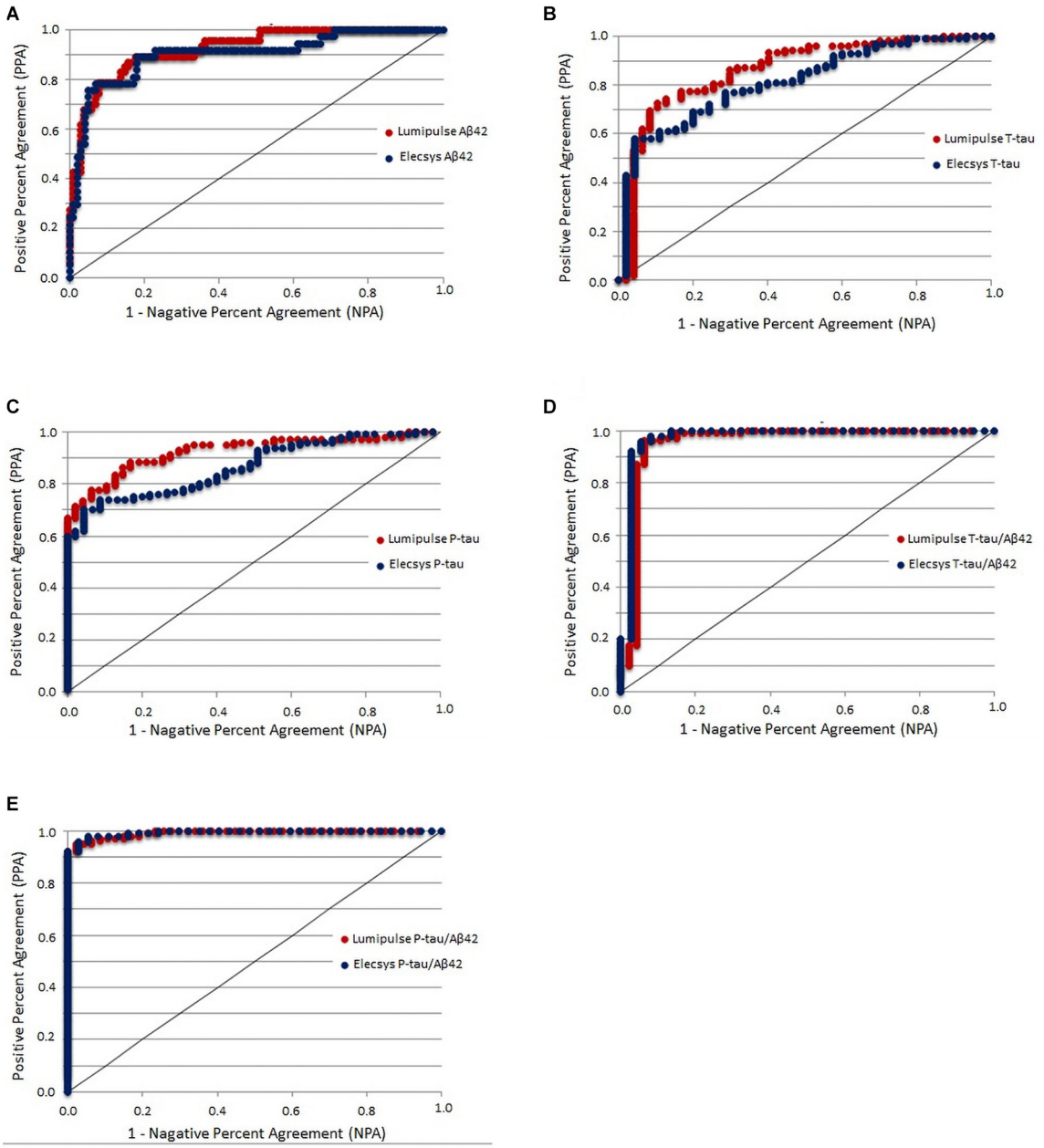

FIGURE 4 | CSF biomarkers that yielded the maximum Youden index versus Aβ42/Aβ40 ratio status in the receiver operating characteristics analysis.

determined according to concordance with the Aβ42/40 ratio were comparable with the manufacturer cut-offs. For Lumipulse and Elecsys biomarkers and ratios, the AUC for discriminating Aβ42/40 status was greater than 0.8. To discriminate between Aβ42/40 positivity/negativity status among Lumipulse assays, the Aβ42/40 AUC was 100, as it was used for calculating the cut-offs. However, the P-tau/Aβ42 and T-tau/Aβ42 ratios had a high discriminating accuracy (AUC 0.922, OPA 95.9% and AUC 0.956, OPA 95.3%, respectively) at the cut-off values of ≥0.082 and ≥0.517, respectively. Among Elecsys markers, the P-tau/Aβ42 and T-tau/Aβ42 ratios had superior discriminating power (AUC 0.994, OPA 96.4% and AUC 0.974, OPA 95.6%, respectively) at the cut-off values of ≥0.023 and ≥0.26, respectively. In fact, the Elecsys P-tau/Aβ42 was the best in discriminating patients based on Aβ42/40 status (**Table 4** and **Figure 4**).

In addition, we determined the cut-offs for biomarkers and ratios of Lumipulse and Elecsys based on the Aβ42 status of Innotest (**Supplementary Table 1**). Among Lumipulse assays, Aβ42 had the highest AUC (0.955, 95% CI 0.924–0.986) followed by P-tau/Aβ42 (AUC 0.933, 95% CI 0.891–0.976) and Aβ42/40 (AUC 0.931, 95% CI 0.892–0.970). For the Elecsys assay, Aβ42 had the highest AUC (0.974, 95% CI 0.954–0.995), followed by

P-tau/Aβ42 (AUC 0.936, 95% CI 0.894–0.978) and T-tau/Aβ42 (AUC 0.920, 95% CI 0.868–0.971).

Furthermore, all statistical analysis was performed for the study cohort separated by sex (**Supplementary Figures 1–8** and **Supplementary Tables 2–7**). We found a high correlation between the three methods for both male and female subjects, although there were systematic differences between biomarker values measured by each method (**Supplementary Figures 1–6**). Interestingly, the cut-offs of CSF biomarkers for male subjects was lower than those of manufacturer, while in the case of female subjects these cut-offs were comparable with corresponding manufacturer's cut-offs (**Supplementary Tables 6, 7**).

DISCUSSION

In this study, we evaluated the concordance between three different methods for measurement of AD CSF biomarkers—Innotest ELISA, Elecsys and Lumipulse platforms—in a cohort of patients with AD, MCI, and non-AD dementias. We also evaluated the diagnostic accuracy of biomarkers and their ratios measured by each method. Furthermore, we determined cut-offs for CSF biomarkers of AD (Aβ42, T-tau, and P-tau) and their ratios measured on the fully automated Lumipulse and Elecsys to optimize their concordance with Aβ42/40 status.

Although there was a high correlation between all three assays, our results showed that there was a lack of consistency between the three methods, except for Aβ42 and T-tau of Lumipulse and Innotest. Because the antibodies used for the Lumipulse assays were produced by the same manufacturer as Innotest ELISA (Fujirebio), the similar specificity of the antibodies between the two methods may partly explain the concordance we observed between Aβ42 and T-tau values between these two methods. Our results were consistent with previous studies that had found a systematic bias between the measurements of biomarkers by Lumipulse and Innotest (Bayart et al., 2019) and by Elecsys and Innotest (Willemse et al., 2018). The lack of concordance between Elecsys, Lumipulse, and Innotest assays may be attributed to the differences that exist between these methods. First, they have different recommended pre-analytical procedures that can affect the measured concentration of CSF biomarkers. Among these three biomarkers, Aβ42 is known to be more sensitive to pre-analytical conditions. Second, these methods use different measurement technologies (ECLIA, CLEIA, and ELISA, respectively), which may affect the detectable concentration. Third, the antibodies that were produced and applied in the AD CSF assays by Roche Diagnostics and Fujirebio Diagnostics may have different specificities. Finally, although both Elecsys and Lumipulse have been standardized for Aβ42, the material used for standardization differed between methods (Bittner et al., 2016; Kuhlmann et al., 2017).

We examined the ability of Aβ42, T-tau, P-tau and their ratios to discriminate AD patients from patients with non-AD dementias. Aβ42 and P-tau combined were both the best biomarkers for discriminating between the two diagnostic groups. Both biomarkers were specific to AD; therefore, it was not surprising that their combination had a high discriminating power for diagnosing AD patients. However, abnormal concentrations of T-tau in CSF, which underlies neurodegeneration, is not specific to AD and occurs in non-AD dementias or in non-AD elderly persons with comorbidities (Kovacs et al., 2013). Evaluation of differences in AUC revealed that there were no significant differences in the discriminating power of Aβ42 + P-tau measured by each method. However, the Innotest Aβ42 + P-tau had a better sensitivity (94%), specificity (76%), and predictive accuracy (87%). The Aβ42/40 ratio also had a high discriminating power for differentiating between patients with AD and non-AD dementias. Consistent with our results, Shoji et al. (1998) and Lewczuk et al. (2004) previously suggested that the Aβ42/40 ratio is superior to the concentration of Aβ42 alone for discriminating AD patients.

We also assessed the discriminating power of AT(N) groups that were generated by the results of CSF Aβ42 (Aβ42/40), P-tau and T-tau for each method. The AT(N) classification was proposed by the NIAA research framework (Jack et al., 2018) and gives a biological rather than a clinical definition of AD. We found that the use of Aβ42/40 instead of Aβ42 in AT(N) improved the classification accuracy (AUC 0.798, 95% CI 0.649–0.947 vs. AUC 0.778, 95% CI 0.617–0.939), However, the sensitivity, specificity and predictive accuracy was the same for both AT(N)s. Among all four AT(N) classifications, Elecsys AT(N) had the highest specificity. In fact, Elecsys AT(N) had better specificity than sensitivity in discriminating the two diagnostic groups. The preference for higher sensitivity or specificity depends on the purpose of different investigation scenarios. For example, for screening purposes, higher sensitivity is always preferable; however, high specificity might be preferable for the selection of patients for clinical trials. These results should be interpreted with caution because of the small population size of both of the diagnostic groups in our study.

Finally, we defined the CSF cut-offs for both Lumipulse and Elecsys assays based on the Lumipulse Aβ42/40 status because of its high diagnostic accuracy in our study, its high stability with respect to pre-analytical variations (Lewczuk et al., 2006; Willemse et al., 2018) and the fact that the ratio probably accounts for inter-individual variability in overall Aβ production and CSF turnover (Janelidze et al., 2017). Given that Innotest assays are among some of the most commonly used methods for the detection of AD CSF biomarkers, we also provided the cut-offs for both Lumipulse and Elecsys assays based on the Innotest Aβ42 status.

In previous studies, amyloid PET visual read (Schindler et al., 2018; Alcolea et al., 2019) or diagnostic accuracy (Bayart et al., 2019) have been used for the determination of AD CSF biomarkers cut-offs for fully automated methods and their ratios. Our results indicated that the cut-offs based on the Aβ42/40 ratio had a close similarity to the cut-offs established by each manufacturer; therefore, the Aβ42/40 ratio is a robust variable that can differentiate AD from non-AD individuals. Based on our results for both the Lumipulse and the Elecsys methods, P-tau/Aβ42 and T-tau/Aβ42 performed better together than each biomarker alone in discriminating Aβ42/Aβ40 ± status. This result is consistent with the results of previous studies where P-tau/Aβ42 (Alcolea et al., 2019) or T-tau/Aβ42

(Bayart et al., 2019) demonstrated superior performance in discriminating the diagnostic groups or amyloid PET status compared with individual biomarkers (Schindler et al., 2018).

Some limitations of this study require consideration. First, our study population lacked health control individuals. The majority of the population consisted of MCI subjects (n = 94) with a short follow-up time; for this reason, we decided to eliminate patients in some analyses and retain a small number of AD (n = 34) and non-AD demented patients (n = 21) when evaluating the diagnostic accuracy of biomarkers. Second, instead of using an independent method, we used the Aβ42/Aβ40 ratio status or Aβ42 status to determine the biomarker cut-offs, and this may have led to the overfitting of the results. Third, Aβ40 cannot be measured by Elecsys or ELISA, so, the comparison was incomplete. Other limitation is that 17 patients were excluded of the analyses because they had Aβ42 values above the upper limit of detection (1700 pg/ml) for Elecsys.

The main strength of our study is that we compared, for the first time, the clinical and analytical performance of fully automated Elecsys and Lumipulse platforms together in the same cohort of patients. In addition, our study population consisted of a real population of patients who attended a memory clinic and, therefore, provided a more realistic application of biomarkers in daily clinical practice.

CONCLUSION

In conclusion, both Lumipulse and Elecsys methods had a high correlation with each other and with Innotest ELISA. The presence of systematic bias between biomarkers measured by each method was expected as there were various pre-analytical and analytical differences between methods. For both Lumipulse and Elecsys methods, ratios had a better analytical performance compared with individual biomarkers, and the Aβ42/Aβ40 ratio had a high concordance with the diagnostic accuracy of AD. Because the calibrators were adjusted with reference samples in both automated platforms, it was expected that these platforms would reduce intra- and inter-laboratory variations and enhance reproducibility.

AUTHOR'S NOTE

Considering the importance of study of cerebrospinal fluid biomarkers in mild cognitive impairment and Alzheimer's disease, we aimed to investigate the concordance between core AD biomarkers measured in CSF using Innotest, Lumipulse and Elecsys methods. We observed that both, Lumipulse and Elecsys methods had a high correlation with each other and with Innotest ELISA. The presence of systematic bias between biomarkers measured by each method was expected as there are various pre-analytical and analytical differences between methods. For both Lumipulse and Elecsys methods, ratios had a better analytical performance compared with individual biomarkers. The Lumipulse and Elecsys CSF AD assays showed high analytical and clinical performances so their use is recommended for the measurement of CSF AD biomarkers compared with unstandardized manual methods.

DATA AVAILABILITY STATEMENT

The raw data supporting the conclusions of this article will be made available by the authors, without undue reservation.

ETHICS STATEMENT

The studies involving human participants were reviewed and approved by the Comite Etica Hospital Arnau Vilanova Lleida. The patients/participants provided their written informed consent to participate in this study.

AUTHOR CONTRIBUTIONS

FD, RL-O, and GP-R designed the study, analyzed the data, interpreted the data, and wrote the manuscript. IR-L, AA, RH, NT, and MR-J collected the data. All authors revised the manuscript and approved it for submission.

FUNDING

This study was supported by the Generalitat of Catalonia, Department of Health (PERIS 2019 SLT008/18/00050 to GP-R). IRBLleida is a CERCA Program/Generalitat of Catalonia. FD was supported by Agency for Management of University and Research Grants and European Social Fund (FI_B100153).

SUPPLEMENTARY MATERIAL

The Supplementary Material for this article can be found online at: https://www.frontiersin.org/articles/10.3389/fnagi.2021.604119/full#supplementary-material

REFERENCES

Albert, M. S., DeKosky, S. T., Dickson, D., Dubois, B., Feldman, H. H., Fox, N. C., et al. (2011). The diagnosis of mild cognitive impairment due to Alzheimer's disease: recommendations from the National Institute on Aging-Alzheimer's Association workgroups on diagnostic guidelines for Alzheimer's disease. *Alzheimers Dement.* 7, 270–279.

Alcolea, D., Pegueroles, J., Muñoz, L., Camacho, V., López-Mora, D., Fernández-León, A., et al. (2019). Agreement of amyloid PET and CSF biomarkers for Alzheimer's disease on lumipulse. *Ann. Clin. Transl. Neurol.* 6, 1815–1824. doi: 10.1002/acn3.50873

Bayart, J. L., Hanseeuw, B., Ivanoiu, A., and van Pesch, V. (2019). Analytical and clinical performances of the automated Lumipulse cerebrospinal fluid Aβ42 and T-Tau assays for Alzheimer's disease

diagnosis. *J. Neurol.* 266, 2304–2311. doi: 10.1007/s00415-019-09418-6

Bittner, T., Zetterberg, H., Teunissen, C. E., Ostlund, R. E. Jr., Militello, M., Andreasson, U., et al. (2016). Technical performance of a novel, fully automated electrochemiluminescence immunoassay for the quantitation of β-amyloid (1-42) in human cerebrospinal fluid. *Alzheimers Dement.* 12, 517–526. doi: 10.1016/j.jalz.2015.09.009

Gorno-Tempini, M. L., Hillis, A. E., Weintraub, S., Kertesz, A., Mendez, M., Cappa, S. F., et al. (2011). Classification of primary progressive aphasia and its variants. *Neurology* 76, 1006–1014.

Hanley, J., and McNeil, B. (1982). The meaning and use of the area under a Receiver Operatin Characteristic (ROC) curve. *Radiology* 143, 29–36. doi: 10.1148/radiology.143.1.7063747

Hansson, O., Seibylc, J., Stomrud, E., Zetterberg, H., Trojanowskih, J., Bittneri, T., et al. (2018). CSF biomarkers of Alzheimer's disease concord with amyloid-β PET and predict clinical progression: a study of fully automated immunoassays in BioFINDER and ADNI cohorts. *Alzheimers Dement.* 14, 1470–1481. doi: 10.1016/j.jalz.2018.01.010

Jack, C. Jr., Bennett, D., Blennow, K., Carrillo, M., Dunn, B., Haebeerlein, S., et al. (2018). NIA-AA research framework: toward a biological definition of Alzheimer's disease. *Alzheimers Dement.* 14, 535–562. doi: 10.1016/j.jalz.2018.02.018

Janelidze, S., Pannee, J., Mikulskis, A., Chiao, P., Zetterberg, H., Blennow, K., et al. (2017). Concordance between different amyloid immunoassays and visual amyloid positron emission tomographic assessment. *JAMA Neurol.* 74, 1492–1501. doi: 10.1001/jamaneurol.2017.2814

Kaplow, J., Vandijck, M., Gray, J., Kanekiyo, M., Huyck, E., Traynham, C. J., et al. (2020). Concordance of Lumipulse cerebrospinal fluid t-tau/Aβ42 ratio with amyloid PET status. *Alzheimers Dement.* 16, 144–152. doi: 10.1002/alz.12000

Kollhoff, A. L., Howell, J. C., and Hu, W. T. (2018). Automation vs. experience: measuring Alzheimer's beta-amyloid 1-42 peptide in the CSF. *Front. Aging Neurosci.* 10:253. doi: 10.3389/fnagi.2018.00253

Kovacs, G. G., Milenkovic, I., Wohrer, A., Hoftberger, R., Gelpi, E., Haberler, C., et al. (2013). Non-Alzheimer neurodegenerative pathologies and their combinations are more frequent than commonly believed in the elderly brain: a community-based autopsy series. *Acta Neuropathol.* 126, 365–384. doi: 10.1007/s00401-013-1157-y

Kuhlmann, J., Andreasson, U., Pannee, J., Bjerke, M., Portelius, E., Leinenbach, A., et al. (2017). CSF Ab 1–42 –an excellent but complicated Alzheimer's biomarker – a route to standardisation. *Clin. Chim. Acta* 467, 27–33. doi: 10.1016/j.cca.2016.05.014

Leinenbach, A., Pannee, J., Dulffer, T., Huber, A., Bittner, T., Andreasson, U., et al. (2014). Mass spectrometry-based candidate reference measurement procedure for quantification of amyloid-beta in cerebrospinal fluid. *Clin. Chem.* 60, 987–994. doi: 10.1373/clinchem.2013.220392

Lewczuk, P., Beck, G., Esselmann, H., Bruckmoser, R., Zimmermann, R., Fiszer, M., et al. (2006). Effect of sample collection tubes on cerebrospinal fluid concentrations of tau proteins and amyloid beta peptides. *Clin. Chem.* 52, 332–334. doi: 10.1373/clinchem.2005.058776

Lewczuk, P., Esselmann, H., Otto, M., Maler, J. M., Henkel, A. W., Henkel, M. K., et al. (2004). Neurochemical diagnosis of Alzheimer's dementia by CSF Abeta42, Abeta42/Abeta40 ratio and total tau. *Neurobiol. Aging* 25, 273–281.

McKeith, I. G., Boeve, B. F., Dickson, D. W., Halliday, G., Taylor, J. P., Weintraub, D., et al. (2017). Diagnosis and management of dementia with Lewy bodies: fourth consensus report of the DLB consortium. *Neurology* 89, 88–100.

McKhann, G. M., Knopman, D. S., Chertkow, H., Hyman, B. T., Jack, C. R. Jr., Kawas, C. H., et al. (2011). The diagnosis of dementia due to Alzheimer's disease: recommendations from the National Institute on Aging Alzheimer's Association workgroups on diagnostic guidelines for Alzheimer's disease. *Alzheimers Dement.* 7, 263–269.

Rascovsky, K., Hodges, J. R., Knopman, D., Mendez, M., Kramer, J. H., van Swieten, J., et al. (2011). Sensitivity of revised diagnostic criteria for the behavioural variant of frontotemporal dementia. *Brain* 134, 2456–2477.

Schindler, S., Graya, J., Gordona, B., Xionga, C., Batrla-Utermannf, R., Quan, M., et al. (2018). Cerebrospinal fluid biomarkers measured by Elecsys§assays compared to amyloid imaging. *Alzheimers Dement.* 14, 1460–1469. doi: 10.1016/j.jalz.2018.01.013

Serrano-Pozo, A., Frosch, M. P., Masliah, E., and Hyman, B. T. (2011). Neuropathological alterations in Alzheimer disease. *Cold Spring Harb. Perspect. Med.* 1:a006189. doi: 10.1101/cshperspect.a006189

Shoji, M., Matsubara, E., Kanai, M., Watanabe, M., Nakamura, T., Tomidokoro, Y., et al. (1998). Combination assay of CSF tau, A beta 1-40 and A beta 1-42(43) as a biochemical marker of Alzheimer's disease. *J. Neurol. Sci.* 158, 134–140. doi: 10.1159/000078534

Sperling, R. A., Aisen, P. S., Beckett, L. A., Bennett, D. A., Craft, S., Fagan, A. M., et al. (2011). Toward defining the preclinical stages of Alzheimer's disease: recommendations from the National Institute on Aging Alzheimer's Association workgroups on diagnostic guidelines for Alzheimer's disease. *Alzheimers Dement.* 7, 280–292.

Willemse, E., van Maurikb, I., Tijmsb, B., Bouwmanb, F., Franked, A., Hubeeke, I., et al. (2018). Diagnostic performance of Elecsys immunoassays for cerebrospinal fluid Alzheimer's disease biomarkers in a nonacademic, multicenter memory clinic cohort: the ABIDE project. *Alzheimers Dement.* 10, 563–572. doi: 10.1016/j.dadm.2018.08.006

Zecca, C., Brescia, V., Piccininni, M., Capozzo, R., Barone, R., Barulli, M. R., et al. (2019). Comparative evaluation of two immunoassays for cerebrospinal fluid β-Amyloid1–42 measurement. *Clin. Chim. Acta* 493, 107–111. doi: 10.1016/j.cca.2019.02.033

Conflict of Interest: The authors declare that the research was conducted in the absence of any commercial or financial relationships that could be construed as a potential conflict of interest.

frontiers in Aging Neuroscience

ORIGINAL RESEARCH
published: 24 March 2021
doi: 10.3389/fnagi.2021.666437

Self-reference Network-Related Interactions During the Process of Cognitive Impairment in the Early Stages of Alzheimer's Disease

Ping-Hsuan Wei[1], Haifeng Chen[1,2,3], Qing Ye[1,2,3], Hui Zhao[1,2,3], Yun Xu[1,2,3] and Feng Bai[1,2,3] on behalf of Alzheimer's Disease Neuroimaging Initiative[†]*

[1]*Department of Neurology, Affiliated Drum Tower Hospital of Medical School and The State Key Laboratory of Pharmaceutical Biotechnology, Institute of Brain Science, Nanjing University, Nanjing, China,* [2]*Jiangsu Province Stroke Center for Diagnosis and Therapy, Nanjing, China,* [3]*Nanjing Neuropsychiatry Clinic Medical Center, Nanjing, China*

Background: Normal establishment of cognition occurs after forming a sensation to stimuli from internal or external cues, in which self-reference processing may be partially involved. However, self-reference processing has been less studied in the Alzheimer's disease (AD) field within the self-reference network (SRN) and has instead been investigated within the default-mode network (DMN). Differences between these networks have been proven in the last decade, while ultra-early diagnoses have increased. Therefore, investigation of the altered pattern of SRN is significantly important, especially in the early stages of AD.

Methods: A total of 65 individuals, including 43 with mild cognitive impairment (MCI) and 22 cognitively normal individuals, participated in this study. The SRN, dorsal attention network (DAN), and salience network (SN) were constructed with resting-state functional magnetic resonance imaging (fMRI), and voxel-based analysis of variance (ANOVA) was used to explore significant regions of network interactions. Finally, the correlation between the network interactions and clinical characteristics was analyzed.

Results: We discovered four interactions among the three networks, with the SRN showing different distributions in the left and right hemispheres from the DAN and SN and modulated interactions between them. Group differences in the interactions that were impaired in MCI patients indicated that the degree of damage was most severe in the SRN, least severe in the SN, and intermediate in the DAN. The two SRN-related interactions showed positive effects on the executive and memory performances of MCI patients with no overlap with the clinical assessments performed in this study.

Conclusion: This study is the first and primary evidence of SRN interactions related to MCI patients' functional performance. The influence of the SRN in the ultra-early stages of AD is nonnegligible. There are still many unknowns regarding the contribution of the SRN in AD progression, and we strongly recommend future research in this area.

Keywords: self-reference network, mild cognitive impairment, interaction, modulation, dorsal attention network, salience network

OPEN ACCESS

Edited by:
Ying Han,
Capital Medical University, China

Reviewed by:
Xi-Nian Zuo,
Beijing Normal University, China
Yu Sun,
China-Japan Friendship Hospital, China

****Correspondence:***
Feng Bai
baifeng515@126.com

[†]Data used in preparation of this article were obtained from the Alzheimer's Disease Neuroimaging Initiative (ADNI) database (adni.loni.usc.edu). As such, the investigators within the ADNI contributed to the design and implementation of the ADNI and/or provided data but did not participate in the analysis or writing of this report. A complete listing of ADNI investigators can be found at http://adni.loni.usc.edu/wp-content/uploads/how_toapply/ADNI AcknowledgementList.pdf.

Received: *10 February 2021*
Accepted: *08 March 2021*
Published: *24 March 2021*

Citation:
Wei P-H, Chen H, Ye Q, Zhao H, Xu Y and Bai F (2021) Self-reference Network-Related Interactions During the Process of Cognitive Impairment in the Early Stages of Alzheimer's Disease. Front. Aging Neurosci. 13:666437. doi: 10.3389/fnagi.2021.666437

INTRODUCTION

Alzheimer's disease (AD) is a neurodegenerative disease accompanied by an irreversible decline in memory, and there is currently no effective treatment (Rafii and Aisen, 2020). Two early stages have been defined that play key roles in AD curative treatment, namely, mild cognitive impairment (MCI) and subjective cognitive decline, in which patients' network damage is still partially reversible at the neuronal level. A high rate of approximately 10–15% is reported for MCI which annually progresses to AD, and subjective cognitive decline possessing lighter cognitive symptoms is regarded as occurring prior to MCI. Both stages have received much attention in recent years as a possible precursor to this most common dementia state (Cai et al., 2015).

Resting-state functional magnetic resonance imaging (fMRI) has been widely used to investigate the pathogenesis of networks in the course of the disease and has attracted increasing attention. However, little evidence of a self-reference network (SRN) has been found in AD studies. It appears that most research placed the self-reference processing of the SRN under that of default-mode network (DMN) concepts; therefore, there is not much active research being done on their differences (Whitfield-Gabrieli and Ford, 2012; Davey et al., 2016; de Caso et al., 2017; Soch et al., 2017; Kubera et al., 2020). SRN shares some similarities with the DMN in brain regions and the processing function of self-reference (Potvin et al., 2019), whereas the operational type and activated regions (including driving and driven hubs) in the brain have been reported to be different. Wang et al. (2020) has defined the driving hub and driven hub, of which both are composed of brain regions that act similarly in the activation process within a network. The difference between them is that the driving hub takes an active role rather than the passive role taken by the driven hub at the initiation of an activation.

Moreover, neuroimaging has revealed consistent activations in the medial prefrontal cortex (MPFC) and posterior cingulate cortex extending to the precuneus both during explicit self-reference tasks and during rest (Whitfield-Gabrieli et al., 2011). Importantly, the functions between dorsal medial prefrontal cortex (dMPFC) and ventral medial prefrontal cortex (vMPFC) are different (Schwiedrzik et al., 2018; Lieberman et al., 2019). SRN mediates the explicit self-reference in the dMPFC during tasks vs. the DMN actions in the default-mode self-reference in the vMPFC during rest (Whitfield-Gabrieli et al., 2011). The regions mentioned above are major driving hubs within each network. According to the above, the precuneus is involved in all self-reference processing. As mentioned in regard to the driving hubs, the posterior cingulate cortex and precuneus only takes part in the active role within the activation of DMN, while serving a passive role within the activation of SRN (Whitfield-Gabrieli et al., 2011; Wang et al., 2020). Interestingly, dMPFC studies have attracted less attention in AD (Xi et al., 2013; Jedidi et al., 2014; Kurth et al., 2015). Instead, there is more concern with social behavior (Dejean et al., 2016; Goelman et al., 2019; Piva et al., 2019) and psychosis (e.g. depression; Shiota et al., 2017; Schulze et al., 2018) than with neurosis in these studies.

Regarding interactions with other networks, correlations between emotion and attention to cognition scale performance have been clinically discovered, and self-reference processing may be partially involved (Berkovich-Ohana et al., 2012; Amft et al., 2015; Catalino et al., 2020; Tomova et al., 2020; Van der Gucht et al., 2020). The dorsal attention network (DAN) and salience network (SN), which function across both high-level cognitive and attention networks (Arkin et al., 2020; Shi et al., 2020), participate in the regulation of networks between state switching of the brain (Gao and Lin, 2012; He et al., 2014; Chand et al., 2018). Specifically, the right fronto-insular region of the SN plays a critical role in switching between the DMN and the central executive network (He et al., 2014), and the DAN modulates the in-between activity and is damaged in MCI; thus, it is responsible for patients' cognitive impairment (Chand et al., 2018). The actional patterns in AD progression indicate that the mechanisms of healthy cognition and memory are all based on balance. Ultimately, prior stimulation then forms the necessary sensation to attention, and the normal establishment of those functions comes afterwards (Berger et al., 2015; Qin et al., 2016).

Notably, the relationship of the SRN to the other networks in AD remains unclear. In particular, the SRN effect on cognition is associated with AD. The only closer relationship mentioned in the last decade was the overlap between self-reference processing and salience processing and between self-reference processing and executive control processing regions found in amnestic MCI (Bai et al., 2016), in which the patient's cognitive performance corresponded to the decoupled functional connection (FC) within and between modules of a network (Contreras et al., 2019) but not age (Sullivan et al., 2019). Nonetheless, it is difficult to show the directly engaged network based on the interpretation in this research. Given that there are many investigations on the DMN rather than the SRN in AD research, there is a crucial need for SRN research. Furthermore, the impact of SRN interactions that contribute to patient cognition in the disease is nonnegligible.

In this study, we aimed to investigate the interaction of the SRN between the DAN and the SN and the relationship of its patterns combined with behavioral and cognitive development in the course of the disease to promote further research on the SRN in AD.

MATERIALS AND METHODS

Participants

A total of 65 subjects, including 43 with MCI and 22 cognitively normal subjects as healthy controls (HC), participated in the study. HC were free of memory complaints (beyond those of normal aging), verified by a study partner. MCI subjects had a subjective memory concern as reported by the subject, study partner, or clinician. All study subjects met the ADNI inclusion and exclusion criteria. In the ADNI, HC are nondepressed, non-MCI, and presented without dementia and have Mini-Mental

State Examination (MMSE) scores of 24–30 (inclusive) and a Clinical Dementia Rating (CDR) score of 0. Inclusion criteria for ADNI MCI were MMSE scores of 24–30 (inclusive), a subjective memory concern, a CDR of 0.5, an absence of significant levels of impairment in other cognitive domains, and essentially preserved activities of daily living.

Neuropsychological Data

The demographic and clinical measures from the ADNI included in this analysis were age; education; sex; and Clinical Dementia Rating Scale: sum of boxes (CDRSB), Alzheimer's Disease Assessment Scale cognitive subscale (ADAS-Cog11, ADAS-Cog13 and ADAS-Cog Q4), MMSE, Rey Auditory Verbal Learning Test (RAVLT), Logical Memory Test: total number of units recalled (LDELTOTAL), Trail Making Test-B (TRABSCOR), Functional Activities Questionnaire (FAQ), Montreal Cognitive Assessment (MoCA), and Everyday Cognition test: the patient reported version (ECogPT) scores.

Alzheimer's Disease Neuroimaging Initiative (ADNI)

The ADNI was launched in 2003 by the National Institute on Aging (NIA), the National Institute of Biomedical Imaging and Bioengineering (NIBIB), the Food and Drug Administration (FDA), private pharmaceutical companies, and nonprofit organizations as a $60 million, 5-year public-private partnership. The primary goal of the ADNI has been to test whether serial magnetic resonance imaging (MRI), functional MRI, other biological markers, and clinical and neuropsychological assessments can be combined to measure the progression of MCI and early AD. The determination of sensitive and specific markers of very early AD progression is intended to aid researchers and clinicians in developing new treatments and monitoring their effectiveness and to lessen the time and cost of clinical trials. To date, the ADNI has three phases, ADNI-1, ADNI-GO, and ADNI-2, consisting of cognitively normal individuals, individuals with MCI, and individuals with dementia or AD. For more information, see http://www.adni-info.org.

Standard Protocol Approvals, Registrations, and Patient Consent

The ADNI was approved by the institutional review board at each site and was compliant with the Health Insurance Portability and Accountability Act. Written consent was obtained from all participants at each site.

MRI Acquisition

All subjects were scanned on a 3.0-Tesla MRI scanner (GE Healthcare, Philips Medical Systems). Resting-state functional images were obtained by an echo-planar imaging sequence (EPI: a fast MRI technique that allows the acquisition of single images in as little as 20 ms and the performance of multiple-image studies in as little as 20 s (De LaPaz, 1994) with the following parameters: 140 time points; repetition time (TR) = 3,000 ms; echo time (TE) = 30 ms; flip angle = 80°, number of slices = 48; slice thickness = 3.3 mm spatial resolution = 3 × 3 × 3 mm^3 and matrix = 64 × 64. All original image files are available to the general scientific community. Detailed descriptions of the resting-state fMRI and MRI scanner protocols are available online[1]. Scan quality was evaluated by the ADNI MRI quality control center at the Mayo Clinic to exclude "failed" scans because of motion, technical problems, or significant clinical abnormalities (e.g., hemispheric infarction).

Resting-State Functional Image Preprocessing

The fMRI data were processed with the Data Processing Assistant for Resting-State fMRI v2.3 (DPARSFA)[2] and Resting-State fMRI Data Analysis Toolkit[3] based on the Statistical Parametric Mapping 12 (SPM12)[4] and MATLAB (The Math Works, Inc.; Natick, MA, USA) programs (Chao-Gan and Yu-Feng, 2010). The first 10 volumes of the scanning session were abandoned to allow for magnetization equilibration effects. Then, the remaining images were corrected for timing differences in acquisition among slices and head motion effects. No subjects performed a head motion of >3.0 mm of displacement or >3.0° of rotation during the scan. Next, the obtained images were spatially normalized into Montreal Neurological Institute echo-planar imaging templates, resampled to 3 × 3 × 3 mm^3 voxels, and smoothed with a Gaussian kernel of 6 × 6 × 6 mm^3 (full width at half-maximum, FWHM). The nuisance signals, including 24 head motion parameters and global mean, white matter, and cerebrospinal fluid signals, were regressed out as covariates of no interest. Finally, the resulting data were bandpass-filtered within the frequency range of 0.01 and 0.08 Hz to reduce the low-frequency drift and high frequency cardiac and physiological respiration noise.

Resting-State Networks Definition

Seed-based FC analysis was used to construct resting-state networks. The spherical region of interest (ROI) (radius = 8 mm) centered at the dMPFC (Montreal Neurological Institute [MNI] space: −0, 52, 26) (Andrews-Hanna et al., 2010), the medial frontal gyrus (MFG) (MNI space: −8, 57, 12/5, 54, −15) (Jacova et al., 2013), and the bilateral intraparietal sulcus (IPS) (MNI space: −25, −53, 52/25, −57, 52) (Woodward et al., 2011; Ham et al., 2015) served as seed regions for the SRN, bilateral SN, and bilateral DAN, respectively. These seed regions have been widely used to identify the corresponding networks in prior studies. For each subject, an average time series for the ROI was computed as the reference time course. Pearson cross-correlation analysis was then conducted between the average signal change in the dMPFC, MFG, and IPS and the time series of whole-brain voxels. Next, Fisher's z-transform was used to improve the normality of the correlation coefficients (Lowe et al., 1998). Finally, the individual maps of each network were acquired.

[1] http://www.adni.loni.usc.edu/methods/documents/mriprotocols/
[2] http://www.rfmri.org/DPARSFA
[3] http://www.restfmri.net
[4] http://www.fil.ion.ucl.ac.uk/spm

STATISTICAL ANALYSIS

Demographic and Neuropsychological Data

The composite scores were applied to enhance statistical reliability by means of reducing random variability and eliminating floor and ceiling effects (Wilson et al., 2010). The χ^2 test was applied in the comparisons of sex. One-way analysis of variance (ANOVA) was applied in the comparisons of education. The Kruskal–Wallis test was applied in age and other neuropsychological data comparisons, with Monte Carlo significance at $p < 0.05$ due to the nonnormal distributions.

Group-Level Interaction Analysis

Two-way ANOVA with network types (i.e., SRN, left and right DAN, left and right SN) and the two groups (i.e., HC and MCI) was conducted to identify the brain regions showing significant interaction between the two networks in a voxel-wise manner. The thresholds were set at a corrected $p < -0.05$, determined by Monte Carlo simulation for multiple comparisons (AlphaSim-corrected voxel-wise $p < 0.01$, FWHM = 6 mm, cluster size = 756 mm^3). *Post hoc* analysis was conducted to determine the internetwork differences among the groups. To further investigate the associations between cognitive scores and internetwork differences among the two groups, partial correlation analysis was performed, with age, sex, and education included as covariates. All data were analyzed using SPM12 and SPSS Statistics 22 software (SPSS, Inc., Chicago, IL, USA), with statistically significant differences ($p < 0.05$, Monte Carlo simulation) included.

TABLE 1 | Demographic and neuropsychological data.

Items	HC (n = 22)	MCI (n = 43)	p-value[a]
Demographic Data			
Age (years)	73.77 (5.00)	74.22 ± 2.82	0.644
Education (years)	16.27 ± 2.05	15.66 ± 2.53	0.333[b]
Sex (male/female)	7/15	21/22	0.111[c]
Neuropsychological Data			
CDRSB	0.02 (0)	1.66 (2)	<0.001
ADAS11	5.38 (4)	9.88 (7)	<0.001
ADAS13	8.62 (4)	15.93 (11)	<0.001
ADASQ4	2.76 (2)	5.44 (4)	<0.001
MMSE	28.9 (2)	27.8 (3)	0.01
MoCA	25.48 (3)	22.9 (4)	0.001
RAVLT: Immediate recall	47.38 (14)	33.59 (13)	<0.001
RAVLT: Learning	6.29 (4)	3.98 (5)	0.001
RAVLT: Forgetting	3.29 (2)	4.85 (3)	0.024
RAVLT: Percent Forgetting	28.25 (21.47)	63.11 (52.91)	<0.001
LDELTOTAL	14.67 (4)	6.78 (4)	<0.001
TRABSCOR	89.29 (31)	107.85 (74)	0.024
FAQ	0.5 (0)	3.88 (8)	<0.001
ECogPT: Memory	1.6 (0.5)	2.14 (0.94)	0.001
ECogPT: Langue	1.31 (0.44)	1.86 (0.82)	0.002
ECogPT: Visual-spatial	1.17 (0.29)	1.45 (0.79)	0.017
ECogPT: Planning	1.08 (0.2)	1.47 (0.8)	<0.001
ECogPT: Organization	1.17 (0.42)	1.46 (0.67)	0.039
ECogPT: Divided attention	1.52 (0.63)	1.78 (0.75)	0.064
ECogPT: Total score	1.31 (0.29)	1.73 (0.79)	<0.001

Note: values with normal distributions are presented as the mean ± standard deviation (SD); values with nonnormal distributions are presented as the median (interquartile). χ^2 test was applied in the comparisons of sex. One-way Kruskal-Wallis test was applied in age and all neuropsychological data comparisons. [a]Monte Carlo significant. [b]The p-value was obtained by one-way ANOVA. [c]The p-value was obtained by χ^2 test. Abbreviations: HC, healthy control; MCI, mild cognitive impairment; CDRSB, Clinical Dementia Rating Scale: sum of boxes; ADAS, Alzheimer's Disease Assessment Scale cognitive subscales; MMSE, Mini-Mental State Examination; MoCA, Montreal Cognitive Assessment; RAVLT, Rey Auditory Verbal Learning Test; LDELTOTAL, Logical Memory Test: total number of units recalled; TRABSCOR, Trail Making Test-B; FAQ, Functional Activities Questionnaire; ECogPT, Everyday Cognition test: the patient reported version.

RESULTS

Demographic and Neuropsychological Data

As shown in **Table 1**, no significant differences in age, years of education, or sex were detected between the groups. In consideration of the main disease effect, MCI subjects displayed significantly worse performance on general cognition than the HC subjects, excluding ECogPT Divided Attention. Notably, the scores of CDRSB, ADASs, FAQ, TRABSCOR, and ECogPTs and two RAVLTs (i.e., the Forgetting and Percent Forgetting) correlated positively with the disease progression or functional damage degree, with a score of 0 corresponding to normal or no impairment and higher scores representing damage severity. The higher score of MMSE, MoCA, LDELTOTAL, and the other RAVLTs (i.e., Immediate Recall and Learning Score) correlated positively with normal performance (Farias et al., 2008; Battista et al., 2017; Moradi et al., 2017).

Identification of Network Interactions

The spatial maps of each reconstructed network are shown in **Figure 1**. A qualitative visual inspection of networks between the two groups showed similar patterns, in which distributions were demonstrated across the majority of the clusters, including diffuse subcortical and cortical sites, with a corrected threshold at $p < 0.05$ (Monte Carlo simulation), for example, the SRN in medial frontal and other cortical middle regions; the DAN in temporal and parietal regions; and the SN in frontal cortical regions. Nevertheless, MCI patients utilized larger regions in all constructed networks than the HC.

We found four interactions between each pair of networks of the SRN, DAN, and SN, the details of which are shown in **Table 2** and **Figure 2**. The SRN demonstrated interactions with the DAN and SN, respectively, in the left and right hemisphere, whereas the DAN and SN demonstrated interactions in both hemispheres: (1) the SRN and left DAN showed interactions in the main regions of the right precuneus; (2) the left DAN and left SN showed interactions mainly in the left and right cerebellum regions, including the posterior lobe, the inferior lobe, the superior lobe, pyramis, and declive; (3) the SRN and right SN showed interactions in the main region of the right angular gyrus; and (4) the right DAN and right SN showed interactions mainly in the left superior temporal gyrus. The brain regions with the interactions demonstrated above were not limited to the defined ROI coordinates (i.e., the left or right hemisphere) of each constructed network due to the networks' known whole-brain distribution. Surprisingly, modulations of the SRN through its communication with the left DAN (and right

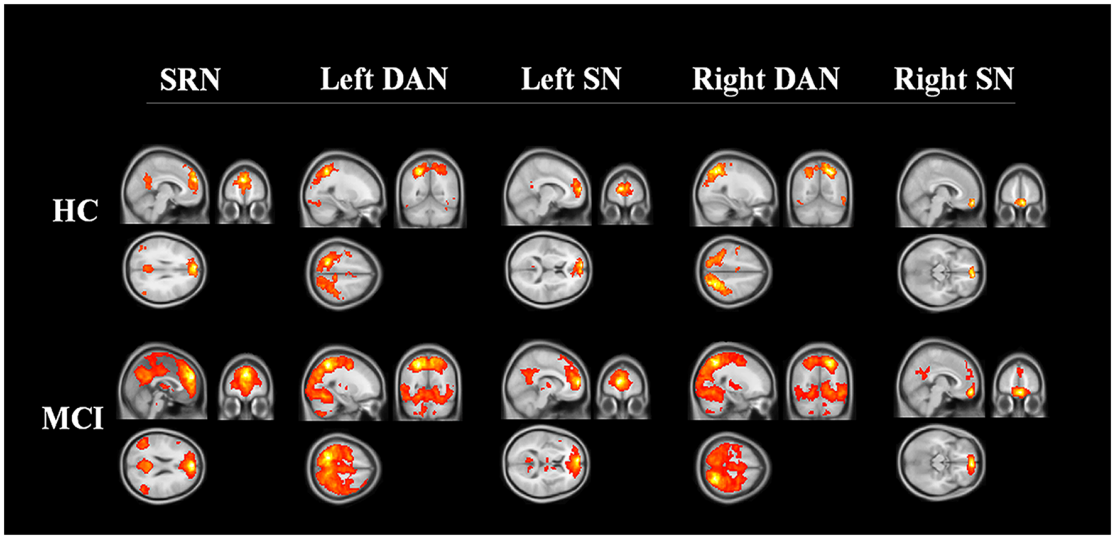

FIGURE 1 | Three networks constructed by region of interest. The networks of HC and MCI showed similar distribution patterns across the majority of the clusters, including the medial frontal, temporal, parietal cortical regions (corrected threshold at $p < 0.05$, Monte Carlo simulation). MCI patients utilized larger regions in all constructed networks than HC. Abbreviations: SRN, self-reference network; DAN, dorsal attention network; SN, salience network; HC, healthy control; MCI, mild cognitive impairment.

SN) to the interactions of the DAN and SN in the left (and right) hemisphere occurred; however, these modulations happened to be damaged in individuals with MCI.

Post hoc tests showed the internetwork differences among the groups. The SRN showed a decrease in all of its related interactions, whereas the corresponding networks within those networks were all increased in MCI patients compared with HC. The FC of each network within the interaction between the DAN and SN demonstrated a decrease in the DAN and an increase in the SN in both the left and right hemispheres. All interactions were significant (corrected $p < 0.05$, Monte Carlo simulation) between HC and individuals with MCI, except the SN within the interactions between the right DAN and right SN ($p = 0.083$).

Behavioral Significance of Network Interactions

The significant results of the behavioral significance of SRN-related interactions that correlated only with MCI (no correlation with HC) are presented in **Figure 3**. The interaction of the SRN with the left DAN correlated positively with MCI patients' visual-spatial performance in the ECogPT test ($r = -0.387$, $p = 0.016$). The interaction of the SRN with the right SN correlated negatively with the MCI patients' clinical test scores on the RAVLTs, including Forgetting ($r = -0.454$, $p = 0.004$) and Percent Forgetting ($r = -0.483$, $p = 0.002$); the FAQ ($r = -0.334$, $p = 0.04$), and the CDRSB ($r = -0.363$, $p = 0.025$), whereas only the RAVLT: Learning Scores ($r = 0.35$, $p = 0.031$) were positively related to the interaction due to its assessment design. According to the above results ("Demographic and Neuropsychological Data" section), the higher the scores were on the RAVLT: Learning test regarding the score design, the better the related performance of patients was; in contrast, higher scores on the other assessments were associated with worse functions. All these data indicated a positive relationship between the functional performances of MCI patients and SRN-related interactions.

DISCUSSION

First Evidence of SRN Modulations and Its Special Distribution Among the Other Networks

We discovered the interactions among the three networks and brain regions. Four interactions (**Table 2** and **Figure 2**) were not limited to the defined ROI coordinate (i.e., the left or right hemisphere) of each constructed network due to the networks' known whole-brain distributions. The network normally interacts between hemispheres; therefore, it might be the crossing recruitment within network in order to adapting to the damage functions (Ptak et al., 2020). Furthermore, SRN anatomical structure is located in the midline of cortex. The ROI coordinate of SRN we selected lies in middle area of brain. Accordingly, these cross-hemisphere results shown in SRN-related interactions is actually reasonable.

To emphasize, the SRN showed a fundamental difference from the DMN in its relationship to the DAN and SN concerning both self-referencing and attentional processes. The DMN tends to be passively regulated by both the DAN and the SN, whereas the SRN plays an active role in the relationship. For the SRN and DMN, a lower FC between these networks has been proven to lead to global decline in episodic memory retrieval or the recognition of amnestic MCI (Bai et al., 2012a). Nonetheless, selective changes within the SRN at least preserved the partial task function of amnestic MCI (Bai et al., 2016).

TABLE 2 | Regions showing self-reference network (SRN) interactions with the dorsal attention network (DAN) and salience network (SN).

Interactions	Brain regions	BA	Peak MNI coordinates			Peak intensity	Number of cluster voxels (mm^3)
			x	*y*	*z*		
SRN × Left DAN	Precuneus. R	7/31	12	−42	42	13.7827	864
Left DAN × Left SN	Cerebellum posterior lobe. L Cerebellum inferior lobe. L Pyramis. L	-	−27	−72	−39	11.0646	1458
	Cerebellum posterior lobe. R Cerebellum superior lobe. R Declive. R	-	15	−66	−21	11.4859	1080
SRN × Right SN	Angular gyrus. R	39	48	−72	33	9.5474	810
Right SN × Right DAN	Superior temporal gyrus. L	13/22/38	−45	9	−9	14.8657	756

Note: BA, Brodmann area; MNI, Montreal Neurological Institute; R, Right; L, Left; $p < 0.01$, AlphaSim corrected.

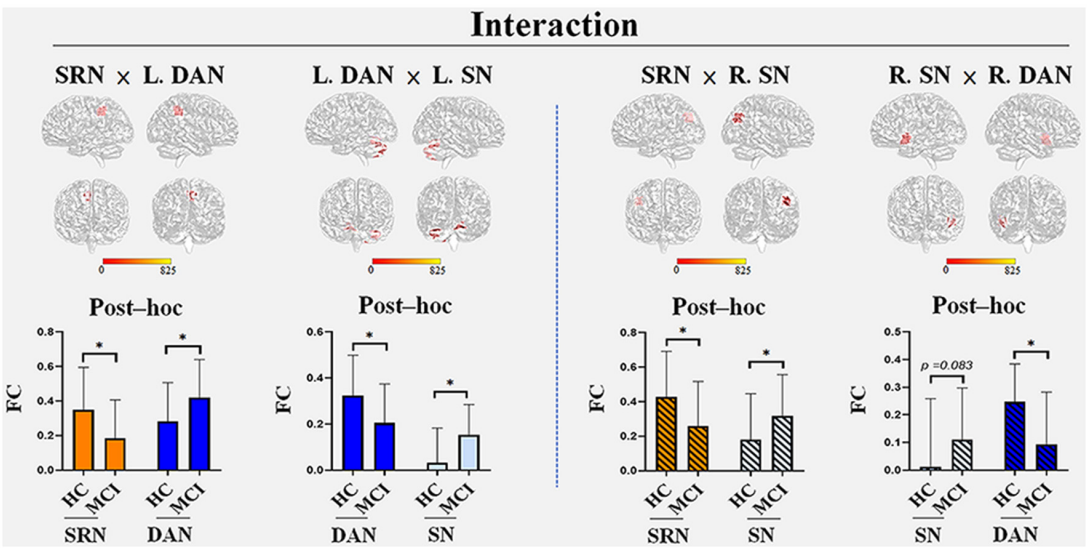

FIGURE 2 | The interactions among the three networks with group differences. Four interactions were found: the SRN demonstrated interactions with the DAN and SN in the left and right hemispheres, respectively, whereas the DAN and SN demonstrated interactions in both hemispheres. (1) The SRN and left DAN demonstrated interactions in the main regions of the right precuneus; (2) the left DAN and left SN demonstrated interactions in both the left and right cerebellum regions, including the posterior lobe, inferior lobe, superior lobe, pyramis, and declive; (3) the SRN and right SN demonstrated interactions in the main region of the right angular gyrus; (4) the right DAN and right SN demonstrated interactions in the left superior temporal gyrus. The brain regions that were demonstrated above were not limited to the defined ROI coordinates (i.e., the left or right hemisphere) of each constructed network due to the networks' known whole-brain distribution. *Post hoc* tests showed the internetwork differences among the groups: (1) the SRN showed a decrease in FC in all its related interactions, whereas increases in FC were found in the corresponding networks (the left DAN and right SN) within the interaction with the SRN; (2) the decreased FC in the DAN and increased FC in the SN were demonstrated within their own interactions of both hemispheres in MCI patients compared with HC. All interactions were significant (corrected $p < 0.05$, Monte Carlo simulation) between HC and MCI patients, except that of the right SN ($p = 0.083$) with the right DAN. Abbreviations: L, left; R, right; SRN, self-reference network; DAN, dorsal attention network; SN, salience network; FC, functional connectivity; HC, healthy control; MCI, mild cognitive impairment; *Monte Carlo significant.

Most importantly, the modulation of the SRN to the interaction between the DAN and the SN (hereafter, DAN-SN) was first evidenced in our study. The SRN regulates the DAN-SN in the left hemisphere through its interactions with the DAN and regulates the DAN-SN in the right hemisphere through the SN.

Furthermore, a different distribution of the SRN interacting with only the left DAN and only the right SN in the left and right hemispheres, respectively, vs. the DAN and the SN interacting in both hemispheres in this study, showed the special characteristic of the SRN in its connection with the two networks. This may be related to the laterality. For instance, the significance of network functional lateralization in AD progression is as follows: (1) in the SN, in which right lateralization has been proven (Zhang et al., 2019), the occurrence of connections with the SRN on the right side rather than the left side significantly reduced FC, especially in the right prefrontal cortex, and has been observed in subjective cognitive decline patients (Hu et al., 2017); (2) however, in the DAN, damage patterns (Zhang et al., 2015) and inhibition in the temporal region of the whole brain have been observed in MCI patients (Chand et al., 2018; Zhang et al., 2019), but evidence for lateralization remains debatable (Corbetta and Shulman, 2002; Vossel et al., 2012; Mayrhofer et al., 2019); and (3) in addition, the DMN also presented left lateralization but functional decline with age and AD (Banks et al., 2018), showing insufficient activation in the right prefrontal region but overactivation in the left prefrontal

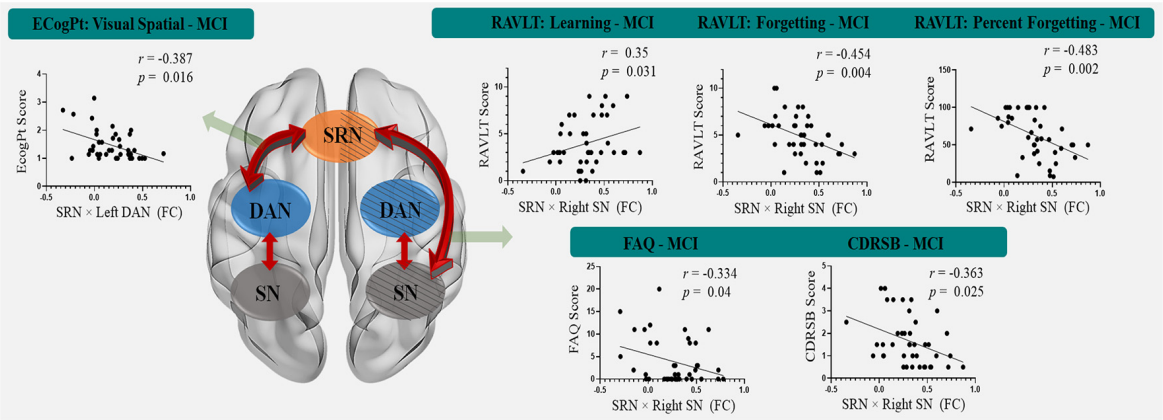

FIGURE 3 | The correlation between SRN-related interactions and cognitive functions in mild cognitive impairment patients. The interaction of the SRN with the left DAN was positively correlated with MCI patients' visual-spatial performance in the ECogPT test. The interaction of the SRN with the right SN was negatively correlated with the MCI patients' clinical test scores on the FAQ, CDRSB, and RAVLTs (the Forgetting and the Percent Forgetting), whereas only the RAVLT: Learning Score was positively correlated with the interaction. Notably, the scores of the CDRSB, FAQ, ECogPTs, and two RAVLTs (i.e., the Forgetting and the Percent Forgetting) were positively correlated with the disease progression or functional damage degree, while a higher RAVLT: Learning Score was positively correlated with normal performance. Therefore, all correlations indicating that these functional performance scores of MCI patients are positively correlated with FC were within SRN-related interactions. Red arrows show the interaction patterns among the SRN, DAN, and SN. Green arrows show the significant correlations of the SRN-related interactions to clinical assessments. The background with the oblique line shows networks in the right hemisphere; the background without the oblique line shows networks in the left hemisphere. Abbreviations: MCI, mild cognitive impairment; SRN, self-reference network; DAN, dorsal attention network; SN, salience network; FC, functional connectivity; ECogPT, Everyday Cognition test: the patient reported version; RAVLT, Rey Auditory Verbal Learning Test; FAQ, Functional Activities Questionnaire; CDRSB, Clinical Dementia Rating Scale: sum of boxes.

region during memory maintenance and reasoning tasks in MCI patients (Melrose et al., 2018). Nevertheless, the hyperactivation in the DAN and SN and the hypoactivation in the DMN were regarded as compensatory due to damage that had been confirmed to be directly related to the AD pathology in the right hemisphere (Wu et al., 2011; Li et al., 2012). Tau protein accumulation is positively related to neurorehabilitation or neural plasticity, regardless of neuron metabolism or nutrition, in AD (Cope et al., 2018), and beta-amyloid appears to be positively correlated with high neuronal activity (Bero et al., 2011; Mormino et al., 2011). Consequently, AD pathology preferentially occurring in the right hemisphere may be related to the fact that the right hemisphere is dominant in most human brains. Therefore, we believe that network lateralization is a natural balance of the brain and affects SRN distributions. Although lateralization does not affect FC performance, in which the rearrangement mechanism follows different pathological stages in AD progression (Bai et al., 2016; Banks et al., 2018), lateralization may participate in the adaptation or compensatory performance of each network.

SRN Exhibits Damage at the Early Stage of the Disease

The larger region of all constructed networks shown in MCI patients compared with HC indicates the impact of the disease on the network modules, in which tropology mainly serves a network function (Contreras et al., 2019). Moreover, group differences in the discovered interaction represent differences not only in damage patterns but also in adaptation to AD. For MCI patients, it was shown that the SRN decreased its participation in all its relating interactions, whereas the corresponding networks all increased their participation within those interactions. For the interaction between the DAN and the SN, the FC of the DAN decreased and that of the SN increased, as shown in both the left and right hemispheres. Accordingly, the degree of impairment among the three networks in MCI patients was most severe in the SRN, least severe in the SN, and intermediate in the DAN. This result is similar to previous studies that have proven functional damage in the DAN and SN (Li et al., 2012; Zhan et al., 2016; Bi et al., 2018; Chand et al., 2018) but observed only several compensatory patterns in the SN (Balthazar et al., 2014; He et al., 2014). Another task state study found that the DMN was capable of better reorganization than the SRN in MCI patients with worse memory performance (Bai et al., 2012b, 2016). Moreover, damage in SRN regions (the left triangular part of inferior frontal gyrus) has been reported to be a problem in maintaining longitudinal memory (Bi et al., 2018). Based on the above, we thought that the SRN also suffered more serious damage than other networks, as in the DMN, in which FC alterations within and to other networks have been suggested to be directly related to AD pathology (Ferreira et al., 2019) at the early stage of the disease (Bai et al., 2016; Melrose et al., 2018). The SRN may have less damage adaptation as it has higher specificity but smaller functionality than the DMN (Whitfield-Gabrieli et al., 2011; Bai et al., 2012a, 2016).

SRN Functional Relationship With Multiple Functions in MCI

The interactional performance of the SRN with the DAN in the left hemisphere was related to only the ECogPT: Visual-

spatial score, whereas that of the SRN with the SN in the right hemisphere was related to FAQ, CDRSB, and RAVLTs (including RAVLT: Learning, Forgetting and Percent Forgetting) scores in MCI patients, showing the functional differences between these SRN interactions.

Visual-spatial organization is reported as a fundamental coding principle to structure the communication between distant brain regions (Knapen, 2021). The connection between the cognitive network and basal ganglia network, which processes the primary integration of information, has been proven to be positively related to visual-spatial performance (Bagarinao et al., 2019; Hucke et al., 2020). Moreover, the attention function is known to be closely connected to the visual system (Sharafeldin et al., 2020; Speed et al., 2020). In addition to engaging in the cognition process, networks composed of frontotemporal regions function to integrate multisensory information, and parietal regions manage attention and visual-spatial functions. Accordingly, we suggest that it might be the possible mechanism underlying the effect of the SRN and left DAN interactions related to the visual-spatial performance of MCI patients.

Researchers have previously identified the influences of other networks on AD and MCI patients' visual-spatial symptoms (Li et al., 2012; Brissenden et al., 2016; Buckley et al., 2017), yet no related study has evaluated the SRN. Our research has provided the first evidence that the visual-spatial performance in MCI patients is affected by the interaction between the SRN and the left DAN.

Next, the SRN also showed an effect on executive and memory function within its interaction with the SN in addition to its own self-referencing. The greater the interaction between the SRN and the right SN is, the more normal the FAQ, CDRSB, and RAVLT performances in MCI patients. Self-reference processing was required more from the SRN than from the DMN when the brain was in a task state and was reflected in the FAQ performance, which is a self-administered functional assessment (Battista et al., 2017) requiring more self-reference processing than other testing scales in this study. These results show that SRN influences are as important as DMN influences on clinical scale scores. Moreover, the CDRSB involves partial executive and memory function assessment, and RAVLTs are tests for episodic memory functions (Battista et al., 2017). The effect we found of a corresponding interaction of the SRN with the SN showed positive enhancement of both the executive and memory functions of MCI patients, especially with no discovery of any two-way impact that occurred in the DMN (showing both positive and negative influences to the cognitions that function different but in the same category (Berger et al., 2015; Gardini et al., 2015; Bi et al., 2018; Melrose et al., 2018) on memory performance (e.g., the RAVLTs used in the study).

Notably, these functions were decreased in MCI patients compared to HC. Although the DAN and SN similarly increased FC within SRN-related interactions, their participation in the regulation of networks between brain-state switching as a feedback loop influenced both themselves and the SRN (Gao and Lin, 2012; He et al., 2014; Chand et al., 2018; Sullivan et al., 2019), indicating a complex explanation of their compensatory effects within SRN-related interactions. In addition, a memory encoding failure is much more likely to occur when the connections of self-reference processing (involved in the SRN and the DMN) are switching between task and rest states of the brain (Bai et al., 2016) while the patient is undergoing clinical assessment. Accordingly, we propose that the relationship between these functions and interactions is highly related to the SRN compensatory ability within the related interaction, which has also been reported to be damaged and therefore does not last long enough to maintain or improve functional performance (Bi et al., 2018).

LIMITATIONS

Since the primary research of this study focuses on the SRN and cognition in AD, less emphasis is placed on neuropsychological assessment considering the self-reference processing function. We should further supplement the related scales and demonstrate a better exploration of SRN development in the course of Alzheimer's disease at follow-up. Regarding reproducibility, another independent sample should be recruited to confirm the present findings. Therefore, these data should be interpreted with caution.

CONCLUSION

We found special regulation of the SRN in cognitive function, with a particular distribution trend between the other networks, the DAN and SN, arranged in both cognitive and attention network systems. The two SRN-related interactions improved some cognitive performance in MCI patients. The fact that no overlap was observed between neuropsychological assessments reflects the different participations of SRN-related interactions. We also demonstrated the damage adaptation among the three networks and pointed out more differences between the SRN and the DMN. On the basis of this primary research on interactions between the SRN and both the DAN and the SN in AD, we strongly suggest that future research should consider the influence of the SRN on cognition. In particular, research conducted in the ultra-early stages may be of more benefit to the field of the disease.

DATA AVAILABILITY STATEMENT

The raw data supporting the conclusions of this article will be made available by the authors, without undue reservation.

ETHICS STATEMENT

The studies involving human participants were approved by the institutional review board at each site and were compliant with the Health Insurance Portability and Accountability Act. ADNI data are disseminated by the Laboratory for Neuro Imaging at the University of Southern

California. The ADNI was performed in accordance with the Good Clinical Practice guidelines, US 21CFR Part 50-Protection of Human Subjects, and Part 56-Institutional Review Boards (IRBs)/Research Good Clinical Practice guidelines Institutional Review Boards (IRBs)/Research Ethics Boards (REBs). More information is available at: http://adni.loni.usc.edu. The patients/participants provided their written informed consent to participate in this study.

AUTHOR CONTRIBUTIONS

P-HW: conceptualization, formal analysis, investigation, writing—original draft, and visualization. HC: methodology and software. QY: methodology. HZ: visualization. YX: visualization. FB: supervision. Alzheimer's Disease Neuroimaging Initiative: resources. All authors contributed to the article and approved the submitted version.

FUNDING

This work was supported partly by grants from the National Natural Science Foundation of China (Nos. 81822013 and 82071186), the Jiangsu Provincial Key Medical Talents (No. ZDRCA2016085), and the Key Research and Development Program of Jiangsu Province of China (No. BE2016610). Grants were also provided by the National Key Research and Development Program of China (No. 2016YFC1300500-504) and the Jiangsu Province Key Medical Discipline (No. ZDXKA2016020). The funding sources had no involvement in the following: study design, collection, analysis, interpretation of data, writing of the report, and the decision to submit the article for publication.

ACKNOWLEDGMENTS

Data collection and sharing for this project was funded in part by the Alzheimer's Disease Neuroimaging Initiative (ADNI; National Institutes of Health Grant U01 AG024904) and DOD ADNI (Department of Defense award number W81XWH-12-2-0012). ADNI is funded by the National Institute on Aging, the National Institute of Biomedical Imaging and Bioengineering, and through generous contributions from the following: AbbVie, Alzheimer's Association; Alzheimer's Drug Discovery Foundation; Araclon Biotech; BioClinica, Inc.; Biogen; BristolMyers Squibb Company; CereSpir, Inc.; Cogstate; Eisai Inc.; Elan Pharmaceuticals, Inc.; Eli Lilly and Company; EuroImmun; F. Hoffmann-La Roche Ltd. and its affiliated company Genentech, Inc.; Fujirebio; GE Healthcare; IXICO Ltd.; Janssen Alzheimer Immunotherapy Research and Development, LLC.; Johnson and Johnson Pharmaceutical Research and Development LLC.; Lumosity; Lundbeck; Merck and Co., Inc.; Meso Scale Diagnostics, LLC.; NeuroRx Research; Neurotrack Technologies; Novartis Pharmaceuticals Corporation; Pfizer Inc.; Piramal Imaging; Servier; Takeda Pharmaceutical Company; and Transition Therapeutics. The Canadian Institutes of Health Research is providing funds to support ADNI clinical sites in Canada. Private sector contributions are facilitated by the Foundation for the National Institutes of Health (www.fnih.org). The grantee organization is the Northern California Institute for Research and Education, and the study is coordinated by the Alzheimer's Therapeutic Research Institute at the University of Southern California. ADNI data are disseminated by the Laboratory for Neuro Imaging at the University of Southern California. The ADNI was performed in accordance with the Good Clinical Practice guidelines, US 21CFR Part 50-Protection of Human Subjects, and Part 56-Institutional Review Boards (IRBs)/Research Good Clinical Practice guidelines Institutional Review Boards (IRBs)/Research Ethics Boards (REBs).

REFERENCES

Amft, M., Bzdok, D., Laird, A. R., Fox, P. T., Schilbach, L., and Eickhoff, S. B. (2015). Definition and characterization of an extended social-affective default network. *Brain Struct. Funct.* 220, 1031–1049. doi: 10.1007/s00429-013-0698-0

Andrews-Hanna, J. R., Reidler, J. S., Sepulcre, J., Poulin, R., and Buckner, R. L. (2010). Functional-anatomic fractionation of the brain's default network. *Neuron* 65, 550–562. doi: 10.1016/j.neuron.2010.02.005

Arkin, S. C., Ruiz-Betancourt, D., Jamerson, E. C., Smith, R. T., Strauss, N. E., Klim, C. C., et al. (2020). Deficits and compensation: attentional control cortical networks in schizophrenia. *Neuroimage Clin.* 27:102348. doi: 10.1016/j.nicl.2020.102348

Bagarinao, E., Watanabe, H., Maesawa, S., Mori, D., Hara, K., Kawabata, K., et al. (2019). Reorganization of brain networks and its association with general cognitive performance over the adult lifespan. *Sci. Rep.* 9:11352. doi: 10.1038/s41598-019-47922-x

Bai, F., Shi, Y., Yuan, Y., Wang, Y., Yue, C., Teng, Y., et al. (2012a). Altered self-referential network in resting-state amnestic type mild cognitive impairment. *Cortex* 48, 604–613. doi: 10.1016/j.cortex.2011.02.011

Bai, F., Watson, D. R., Shi, Y., Yuan, Y., Yu, H., and Zhang, Z. (2012b). Mobilization and redistribution of default mode network from resting state to task state in amnestic mild cognitive impairment. *Curr. Alzheimer Res.* 9, 944–952. doi: 10.2174/156720512803251165

Bai, F., Yuan, Y., Yu, H., and Zhang, Z. (2016). Plastic modulation of episodic memory networks in the aging brain with cognitive decline. *Behav. Brain Res.* 308, 38–45. doi: 10.1016/j.bbr.2016.04.022

Balthazar, M. L. F., Pereira, F. R. S., Lopes, T. M., da Silva, E. L., Coan, A. C., Campos, B. M., et al. (2014). Neuropsychiatric symptoms in Alzheimer's disease are related to functional connectivity alterations in the salience network. *Hum. Brain Mapp.* 35, 1237–1246. doi: 10.1002/hbm.22248

Banks, S. J., Zhuang, X., Bayram, E., Bird, C., Cordes, D., Caldwell, J. Z. K., et al. (2018). Default mode network lateralization and memory in healthy aging and Alzheimer's disease. *J. Alzheimers Dis.* 66, 1223–1234. doi: 10.3233/JAD-180541

Battista, P., Salvatore, C., and Castiglioni, I. (2017). Optimizing neuropsychological assessments for cognitive, behavioral, and functional impairment classification: a machine learning study. *Behav. Neurol.* 2017:1850909. doi: 10.1155/2017/1850909

Berger, C., Erbe, A.-K., Ehlers, I., Marx, I., Hauenstein, K., and Teipel, S. (2015). Effects of task-irrelevant emotional stimuli on working memory processes in mild cognitive impairment. *J. Alzheimers Dis.* 44, 439–453. doi: 10.3233/JAD-141848

Berkovich-Ohana, A., Glicksohn, J., and Goldstein, A. (2012). Mindfulness-induced changes in gamma band activity—implications for the default mode network, self-reference and attention. *Clin. Neurophysiol.* 123, 700–710. doi: 10.1016/j.clinph.2011.07.048

Bero, A. W., Yan, P., Roh, J. H., Cirrito, J. R., Stewart, F. R., Raichle, M. E., et al. (2011). Neuronal activity regulates the regional vulnerability to amyloid-β deposition. *Nat. Neurosci.* 14, 750–756. doi: 10.1038/nn.2801

Bi, X.-A., Sun, Q., Zhao, J., Xu, Q., and Wang, L. (2018). Non-linear ICA analysis of resting-state fMRI in mild cognitive impairment. *Front. Neurosci.* 12:413. doi: 10.3389/fnins.2018.00413

Brissenden, J. A., Levin, E. J., Osher, D. E., Halko, M. A., and Somers, D. C. (2016). Functional evidence for a cerebellar node of the dorsal attention network. *J. Neurosci.* 36, 6083–6096. doi: 10.1523/JNEUROSCI.0344-16.2016

Buckley, R. F., Schultz, A. P., Hedden, T., Papp, K. V., Hanseeuw, B. J., Marshall, G., et al. (2017). Functional network integrity presages cognitive decline in preclinical Alzheimer disease. *Neurology* 89, 29–37. doi: 10.1212/WNL.0000000000004059

Cai, S., Huang, L., Zou, J., Jing, L., Zhai, B., Ji, G., et al. (2015). Changes in thalamic connectivity in the early and late stages of amnestic mild cognitive impairment: a resting-state functional magnetic resonance study from ADNI. *PLoS One* 10:e0115573. doi: 10.1371/journal.pone.0115573

Catalino, M. P., Yao, S., Green, D. L., Laws, E. R., Golby, A. J., and Tie, Y. (2020). Mapping cognitive and emotional networks in neurosurgical patients using resting-state functional magnetic resonance imaging. *Neurosurg. Focus* 48:E9. doi: 10.3171/2019.11.FOCUS19773

Chand, G. B., Hajjar, I., and Qiu, D. (2018). Disrupted interactions among the hippocampal, dorsal attention, and central-executive networks in amnestic mild cognitive impairment. *Hum. Brain Mapp.* 39, 4987–4997. doi: 10.1002/hbm.24339

Chao-Gan, Y., and Yu-Feng, Z. (2010). DPARSF: a MATLAB toolbox for "pipeline" data analysis of resting-state fMRI. *Front. Syst. Neurosci.* 4:13. doi: 10.3389/fnsys.2010.00013

Contreras, J. A., Avena-Koenigsberger, A., Risacher, S. L., West, J. D., Tallman, E., McDonald, B. C., et al. (2019). Resting state network modularity along the prodromal late onset alzheimer's disease continuum. *Neuroimage Clin.* 22:101687. doi: 10.1016/j.nicl.2019.101687

Cope, T. E., Rittman, T., Borchert, R. J., Jones, P. S., Vatansever, D., Allinson, K., et al. (2018). Tau burden and the functional connectome in Alzheimer's disease and progressive supranuclear palsy. *Brain* 141, 550–567. doi: 10.1093/brain/awx347

Corbetta, M., and Shulman, G. L. (2002). Control of goal-directed and stimulus-driven attention in the brain. *Nat. Rev. Neurosci.* 3, 201–215. doi: 10.1038/nrn755

Davey, C. G., Pujol, J., and Harrison, B. J. (2016). Mapping the self in the brain's default mode network. *NeuroImage* 132, 390–397. doi: 10.1016/j.neuroimage.2016.02.022

de Caso, I., Poerio, G., Jefferies, E., and Smallwood, J. (2017). That's me in the spotlight: neural basis of individual differences in self-consciousness. *Soc. Cogn. Affect. Neurosci.* 12, 1384–1393. doi: 10.1093/scan/nsx076

De LaPaz, R. L. (1994). Echo-planar imaging. *Radiographics* 14, 1045–1058. doi: 10.1148/radiographics.14.5.7991813

Dejean, C., Courtin, J., Karalis, N., Chaudun, F., Wurtz, H., Bienvenu, T. C. M., et al. (2016). Prefrontal neuronal assemblies temporally control fear behaviour. *Nature* 535, 420–424. doi: 10.1038/nature18630

Farias, S. T., Mungas, D., Reed, B. R., Cahn-Weiner, D., Jagust, W., Baynes, K., et al. (2008). The measurement of everyday cognition (ECog): scale development and psychometric properties. *Neuropsychology* 22, 531–544. doi: 10.1037/0894-4105.22.4.531

Ferreira, D., Pereira, J. B., Volpe, G., and Westman, E. (2019). Subtypes of Alzheimer's disease display distinct network abnormalities extending beyond their pattern of brain atrophy. *Front. Neurol.* 10:524. doi: 10.3389/fneur.2019.00524

Gao, W., and Lin, W. (2012). Frontal parietal control network regulates the anti-correlated default and dorsal attention networks. *Hum. Brain Mapp.* 33, 192–202. doi: 10.1002/hbm.21204

Gardini, S., Venneri, A., Sambataro, F., Cuetos, F., Fasano, F., Marchi, M., et al. (2015). Increased functional connectivity in the default mode network in mild cognitive impairment: a maladaptive compensatory mechanism associated with poor semantic memory performance. *J. Alzheimers Dis.* 45, 457–470. doi: 10.3233/JAD-142547

Goelman, G., Dan, R., Stößel, G., Tost, H., Meyer-Lindenberg, A., and Bilek, E. (2019). Bidirectional signal exchanges and their mechanisms during joint attention interaction—a hyperscanning fMRI study. *NeuroImage* 198, 242–254. doi: 10.1016/j.neuroimage.2019.05.028

Ham, J. H., Cha, J., Lee, J. J., Baek, G.-M., Sunwoo, M. K., Hong, J. Y., et al. (2015). Nigrostriatal dopamine-independent resting-state functional networks in Parkinson's disease. *NeuroImage* 119, 296–304. doi: 10.1016/j.neuroimage.2015.06.077

He, X., Qin, W., Liu, Y., Zhang, X., Duan, Y., Song, J., et al. (2014). Abnormal salience network in normal aging and in amnestic mild cognitive impairment and Alzheimer's disease. *Hum. Brain Mapp.* 35, 3446–3464. doi: 10.1002/hbm.22414

Hu, X., Uhle, F., Fliessbach, K., Wagner, M., Han, Y., Weber, B., et al. (2017). Reduced future-oriented decision making in individuals with subjective cognitive decline: a functional MRI study. *Alzheimers Dement.* 6, 222–231. doi: 10.1016/j.dadm.2017.02.005

Hucke, C. I., Heinen, R. M., Pacharra, M., Wascher, E., and van Thriel, C. (2020). Spatiotemporal processing of bimodal odor lateralization in the brain using electroencephalography microstates and source localization. *Front. Neurosci.* 14:620723. doi: 10.3389/fnins.2020.620723

Jacova, C., Hsiung, G.-R., Tawankanjanachot, I., Dinelle, K., McCormick, S., Gonzalez, M., et al. (2013). Anterior brain glucose hypometabolism predates dementia in progranulin mutation carriers. *Neurology* 81, 1322–1331. doi: 10.1212/WNL.0b013e3182a8237e

Jedidi, H., Feyers, D., Collette, F., Bahri, M. A., Jaspar, M., d'Argembeau, A., et al. (2014). Dorsomedial prefrontal metabolism and unawareness of current characteristics of personality traits in Alzheimer's disease. *Soc. Cogn. Affect. Neurosci.* 9, 1458–1463. doi: 10.1093/scan/nst132

Knapen, T. (2021). Topographic connectivity reveals task-dependent retinotopic processing throughout the human brain. *Proc. Natl. Acad. Sci. U S A* 118:e2017032118. doi: 10.1073/pnas.2017032118

Kubera, K. M., Wolf, N. D., Rashidi, M., Hirjak, D., Northoff, G., Schmitgen, M. M., et al. (2020). Functional decoupling of language and self-reference networks in patients with persistent auditory verbal hallucinations. *Neuropsychobiology* 79, 345–351. doi: 10.1159/000507630

Kurth, S., Moyse, E., Bahri, M. A., Salmon, E., and Bastin, C. (2015). Recognition of personally familiar faces and functional connectivity in Alzheimer's disease. *Cortex* 67, 59–73. doi: 10.1016/j.cortex.2015.03.013

Li, R., Wu, X., Fleisher, A. S., Reiman, E. M., Chen, K., and Yao, L. (2012). Attention-related networks in Alzheimer's disease: a resting functional MRI study. *Hum. Brain Mapp.* 33, 1076–1088. doi: 10.1002/hbm.21269

Lieberman, M. D., Straccia, M. A., Meyer, M. L., Du, M., and Tan, K. M. (2019). Social, self (situational), and affective processes in medial prefrontal cortex (MPFC): causal, multivariate, and reverse inference evidence. *Neurosci. Biobehav. Rev.* 99, 311–328. doi: 10.1016/j.neubiorev.2018.12.021

Lowe, M. J., Mock, B. J., and Sorenson, J. A. (1998). Functional connectivity in single and multislice echoplanar imaging using resting-state fluctuations. *NeuroImage* 7, 119–132. doi: 10.1006/nimg.1997.0315

Mayrhofer, H. C., Duecker, F., Vincent, V. D. V., Jacobs, H. I. L., and Sack, A. T. (2019). Hemifield-specific correlations between cue-related blood oxygen level dependent activity in bilateral nodes of the dorsal attention network and attentional benefits in a spatial orienting paradigm. *J. Cogn. Neurosci.* 31, 625–638. doi: 10.1162/jocn_a_01338

Melrose, R. J., Jimenez, A. M., Riskin-Jones, H., Weissberger, G., Veliz, J., Hasratian, A. S., et al. (2018). Alterations to task positive and task negative networks during executive functioning in mild cognitive impairment. *Neuroimage Clin.* 19, 970–981. doi: 10.1016/j.nicl.2018.06.014

Moradi, E., Hallikainen, I., Hänninen, T., Tohka, J., and Alzheimer's Disease Neuroimaging Initiative. (2017). Rey's auditory verbal learning test scores can be predicted from whole brain MRI in Alzheimer's disease. *Neuroimage Clin.* 13, 415–427. doi: 10.1016/j.nicl.2016.12.011

Mormino, E. C., Smiljic, A., Hayenga, A. O., Onami, S. H., Greicius, M. D., Rabinovici, G. D., et al. (2011). Relationships between β-amyloid and functional connectivity in different components of the default mode network in aging. *Cereb. Cortex* 21, 2399–2407. doi: 10.1093/cercor/bhr025

Piva, M., Velnoskey, K., Jia, R., Nair, A., Levy, I., and Chang, S. W. (2019). The dorsomedial prefrontal cortex computes task-invariant relative subjective value for self and other. *eLife* 8:e44939. doi: 10.7554/eLife.44939

Potvin, S., Gamache, L., and Lungu, O. (2019). A functional neuroimaging meta-analysis of self-related processing in schizophrenia. *Front. Neurol.* 10:990. doi: 10.3389/fneur.2019.00990

Ptak, R., Bourgeois, A., Cavelti, S., Doganci, N., Schnider, A., and Iannotti, G. R. (2020). Discrete patterns of cross-hemispheric functional connectivity underlie impairments of spatial cognition after stroke. *J. Neurosci.* 40, 6638–6648. doi: 10.1523/JNEUROSCI.0625-20.2020

Qin, P., Grimm, S., Duncan, N. W., Fan, Y., Huang, Z., Lane, T., et al. (2016). Spontaneous activity in default-mode network predicts ascription of self-relatedness to stimuli. *Soc. Cogn. Affect. Neurosci.* 11, 693–702. doi: 10.1093/scan/nsw008

Rafii, M. S., and Aisen, P. S. (2020). The search for Alzheimer disease therapeutics—same targets, better trials? *Nat. Rev. Neurol.* 16, 597–598. doi: 10.1038/s41582-020-00414-3

Schulze, L., Feffer, K., Lozano, C., Giacobbe, P., Daskalakis, Z. J., Blumberger, D. M., et al. (2018). Number of pulses or number of sessions? An open-label study of trajectories of improvement for once-vs. twice-daily dorsomedial prefrontal rTMS in major depression. *Brain Stimul.* 11, 327–336. doi: 10.1016/j.brs.2017.11.002

Schwiedrzik, C. M., Sudmann, S. S., Thesen, T., Wang, X., Groppe, D. M., Mégevand, P., et al. (2018). Medial prefrontal cortex supports perceptual memory. *Curr. Biol.* 28, R1094–R1095. doi: 10.1016/j.cub.2018.07.066

Sharafeldin, A., Mock, V. L., Meisenhelter, S., Hembrook-Short, J. R., and Briggs, F. (2020). Changes in local network activity approximated by reverse spike-triggered local field potentials predict the focus of attention. *Cereb. Cortex Commun.* 1:tgaa014. doi: 10.1093/texcom/tgaa014

Shi, Q., Chen, H., Jia, Q., Yuan, Z., Wang, J., Li, Y., et al. (2020). Altered granger causal connectivity of resting-state neural networks in patients with leukoaraiosis-associated cognitive impairment-a cross-sectional study. *Front. Neurol.* 11:457. doi: 10.3389/fneur.2020.00457

Shiota, S., Okamoto, Y., Okada, G., Takagaki, K., Takamura, M., Mori, A., et al. (2017). Effects of behavioral activation on the neural basis of other perspective self-referential processing in subthreshold depression: a functional magnetic resonance imaging study. *Psychol. Med.* 47, 877–888. doi: 10.1017/S0033291716002956

Soch, J., Deserno, L., Assmann, A., Barman, A., Walter, H., Richardson-Klavehn, A., et al. (2017). Inhibition of information flow to the default mode network during self-reference versus reference to others. *Cereb. Cortex* 27, 3930–3942. doi: 10.1093/cercor/bhw206

Speed, A., Del, R. J., Mikail, N., and Haider, B. (2020). Spatial attention enhances network, cellular and subthreshold responses in mouse visual cortex. *Nat. Commun.* 11:505. doi: 10.1038/s41467-020-14355-4

Sullivan, M. D., Anderson, J. A. E., Turner, G. R., Spreng, R. N., and Alzheimer's Disease Neuroimaging Initiative (2019). Intrinsic neurocognitive network connectivity differences between normal aging and mild cognitive impairment are associated with cognitive status and age. *Neurobiol. Aging* 73, 219–228. doi: 10.1016/j.neurobiolaging.2018.10.001

Tomova, L., Saxe, R., Klöbl, M., Lanzenberger, R., and Lamm, C. (2020). Acute stress alters neural patterns of value representation for others. *NeuroImage* 209:116497. doi: 10.1016/j.neuroimage.2019.116497

Van der Gucht, K., Ahmadoun, S., Melis, M., de Cloe, E., Sleurs, C., and Radwan, A. (2020). Effects of a mindfulness-based intervention on cancer-related cognitive impairment: results of a randomized controlled functional magnetic resonance imaging pilot study. *Cancer* 126, 4246–4255. doi: 10.1002/cncr.33074

Vossel, S., Weidner, R., Driver, J., Friston, K. J., and Fink, G. R. (2012). Deconstructing the architecture of dorsal and ventral attention systems with dynamic causal modeling. *J. Neurosci.* 32, 10637–10648. doi: 10.1523/JNEUROSCI.0414-12.2012

Wang, X., Wang, R., Li, F., Lin, Q., Zhao, X., and Hu, Z. (2020). Large-scale granger causal brain network based on resting-state fMRI data. *Neuroscience* 425, 169–180. doi: 10.1016/j.neuroscience.2019.11.006

Whitfield-Gabrieli, S., and Ford, J. M. (2012). Default mode network activity and connectivity in psychopathology. *Annu. Rev. Clin. Psychol.* 8, 49–76. doi: 10.1146/annurev-clinpsy-032511-143049

Whitfield-Gabrieli, S., Moran, J. M., Nieto-Castañón, A., Triantafyllou, C., Saxe, R., and Gabrieli, J. D. E. (2011). Associations and dissociations between default and self-reference networks in the human brain. *NeuroImage* 55, 225–232. doi: 10.1016/j.neuroimage.2010.11.048

Wilson, R. S., Leurgans, S. E., Foroud, T. M., Sweet, R. A., Graff-Radford, N., Mayeux, R., et al. (2010). Telephone assessment of cognitive function in the late-onset Alzheimer's disease family study. *Arch. Neurol.* 67, 855–861. doi: 10.1001/archneurol.2010.129

Woodward, N. D., Rogers, B., and Heckers, S. (2011). Functional resting-state networks are differentially affected in schizophrenia. *Schizophr. Res.* 130, 86–93. doi: 10.1016/j.schres.2011.03.010

Wu, X., Li, R., Fleisher, A. S., Reiman, E. M., Guan, X., Zhang, Y., et al. (2011). Altered default mode network connectivity in Alzheimer's disease—a resting functional MRI and bayesian network study. *Hum. Brain Mapp.* 32, 1868–1881. doi: 10.1002/hbm.21153

Xi, Q., Zhao, X.-H., Wang, P.-J., Guo, Q.-H., and He, Y. (2013). Abnormal intrinsic brain activity in amnestic mild cognitive impairment revealed by amplitude of low-frequency fluctuation: a resting-state functional magnetic resonance imaging study. *Chin. Med. J.* 126, 2912–2917.

Zhan, Y., Ma, J., Alexander-Bloch, A. F., Xu, K., Cui, Y., Feng, Q., et al. (2016). Longitudinal study of impaired intra- and inter-network brain connectivity in subjects at high risk for Alzheimer's disease. *J. Alzheimers Dis.* 52, 913–927. doi: 10.3233/JAD-160008

Zhang, H., Giannakopoulos, P., Haller, S., Lee, S., Qiu, S., and Shen, D. (2019). Inter-network high-order functional connectivity (IN-HOFC) and its alteration in patients with mild cognitive impairment. *Neuroinformatics* 17, 547–561. doi: 10.1007/s12021-018-9413-x

Zhang, Y., Suo, X., Ding, H., Liang, M., Yu, C., and Qin, W. (2019). Structural connectivity profile supports laterality of the salience network. *Hum. Brain Mapp.* 40, 5242–5255. doi: 10.1002/hbm.24769

Zhang, Z., Zheng, H., Liang, K., Wang, H., Kong, S., Hu, J., et al. (2015). Functional degeneration in dorsal and ventral attention systems in amnestic mild cognitive impairment and Alzheimer's disease: an fMRI study. *Neurosci. Lett.* 585, 160–165. doi: 10.1016/j.neulet.2014.11.050

Conflict of Interest: The authors declare that the research was conducted in the absence of any commercial or financial relationships that could be construed as a potential conflict of interest.

frontiers in Aging Neuroscience

ORIGINAL RESEARCH
published: 25 May 2021
doi: 10.3389/fnagi.2021.682908

Carotid Atherosclerotic Calcification Characteristics Relate to Post-stroke Cognitive Impairment

Yingzhe Wang[1†], Chanchan Li[2†], Mengyuan Ding[1], Luyi Lin[2], Peixi Li[1], Yizhe Wang[3], Qiang Dong[1,4], Yanmei Yang[2‡] and Mei Cui[1,4*‡]*

[1] Department of Neurology, Huashan Hospital, Fudan University, Shanghai, China, [2] Department of Radiology, Huashan Hospital, Fudan University, Shanghai, China, [3] Department of Medicine, Nanchang University, Nanchang, China, [4] The State Key Laboratory of Medical Neurobiology, Fudan University, Shanghai, China

Background: Together with cerebral small vessel disease (CSVD), large vessel atherosclerosis is considered to be an equally important risk factor in the progression of vascular cognitive impairment. This article aims to investigate whether carotid atherosclerotic calcification is associated with the increased risk of post-stroke cognitive impairment (PSCI).

Methods: A total of 128 patients (mean age: 62.1 ± 12.2 years, 37 women) suffering from ischemic stroke underwent brain/neck computer tomography angiography examination. The presence and characteristic of carotid calcification (size, number and location) were analyzed on computer tomography angiography. White matter hyperintensity (WMH) was assessed using Fazekas scales. PSCI was diagnosed based on a battery of neuropsychological assessments implemented 6−12 months after stroke.

Results: Among 128 patients, 26 developed post-stroke dementia and 96 had carotid calcification. Logistic regression found carotid calcification (odds ratio [OR] = 7.15, 95% confidence interval [CI]: 1.07–47.69) and carotid artery stenosis (*OR* = 6.42, 95% CI: 1.03–40.15) both significantly increased the risk for post-stroke dementia. Moreover, multiple, thick/mixed, and surface calcifications exhibited an increasing trend in PSCI (P_{trend} = 0.004, 0.016, 0.045, respectively). The prediction model for post-stroke dementia including carotid calcification (area under curve = 0.67), WMH (area under curve = 0.67) and other covariates yielded an area under curve (AUC) of 0.90 (95% CI: 0.82–0.99).

Conclusion: Our findings demonstrated that the quantity and location of carotid calcifications were independent indicators for PSCI. The significant role of large vessel atherosclerosis in PSCI should be concerned in future study.

Keywords: stroke, cognition, atherosclerosis, calcification, Computed Tomographic Angiography

OPEN ACCESS

Edited by:
Ying Han,
Capital Medical University, China

Reviewed by:
Xihai Zhao,
Tsinghua University, China
Jianliang Fu,
Shanghai Jiao Tong University, China

***Correspondence:**
Yanmei Yang
yym9876@sohu.com
Mei Cui
cuimei@fudan.edu.cn

[†] These authors have contributed equally to this work and share first authorship

[‡] These authors have contributed equally to this work and share last authorship

Received: *19 March 2021*
Accepted: *29 April 2021*
Published: *25 May 2021*

Citation:
Wang Y, Li C, Ding M, Lin L, Li P, Wang Y, Dong Q, Yang Y and Cui M (2021) Carotid Atherosclerotic Calcification Characteristics Relate to Post-stroke Cognitive Impairment. Front. Aging Neurosci. 13:682908. doi: 10.3389/fnagi.2021.682908

Abbreviations: AUC, area under curve; CI, confidence interval; CSVD, cerebral small vessel disease; CTA, computer tomography angiography; ICAS, intracranial artery stenosis; IQR, interquartile range; MMSE, Mini−mental State Examination; MRI, magnetic resonance imaging; NIHSS, National Institute of Health stroke scale; OR, odds ratio; PSCI, post-stroke cognitive impairment; PSCIND, post-stroke cognitive impairment with no dementia; PSD, post-stroke dementia; RI, remodeling index; WMH, white matter hyperintensity.

INTRODUCTION

Stroke is considered to be one of the most widespread and serious cerebrovascular diseases affecting millions of people worldwide. With a high prevalence of 20–80%, post-stroke cognitive impairment (PSCI) is one of the major complications suffered during the chronic stage of ischemic stroke (Sun et al., 2014). As cognitive function can fluctuate due to neurological deficits and subsequent improvement of perfusion in early phases, the diagnosis of PSCI is often postponed by at least 3 months after the onset of stroke (Gottesman and Hillis, 2010). Thus, early identification of patients at high-risk of PSCI, based on patients' baseline characteristics, is essential in the orchestration of appropriate preventataive management.

Several factors, including age, education level, vascular risk factors, extent of stroke, and neuroimaging features, are considered to be important determinants of PSCI (Rasquin et al., 2004; Leys et al., 2005; Lu et al., 2016). Apart from acute stroke, pre-existing cerebral small vessel disease (CSVD) is believed to be closely connected with both the prognosis of stroke and the occurrence of cognitive dysfunction. It has been reported that PSCI was significantly associated with several subtypes of baseline CSVD, including white matter hyperintensity (WMH), cerebral microbleed, enlarged perivascular space and brain atrophy (Wen et al., 2004; Gregoire et al., 2012; Kebets et al., 2015; Molad et al., 2017; Arba et al., 2018). Interestingly, although CSVD is often accompanied by pathological changes in large arteries, the relationship between large vessel diseases (such as stenosis, slow blood flow, malformation, or poor collateral circulation) and PSCI remains ambiguous. While some research has demonstrated that large vessel stenosis was highly predictive of PSCI (Kandiah et al., 2016; Li et al., 2017), not all studies have shown consistent results (Chaudhari et al., 2014). Understanding the relationship between atherosclerotic calcification and PSCI will provide a deeper insight into the pathology of PSCI, which would be beneficial for early diagnosis and prevention.

Therefore, in this study, we aimed to investigate whether the presence of carotid atherosclerotic calcification is an associated risk factor for the development and progression of PSCI, and whether this association depends on the characteristic of calcification.

MATERIALS AND METHODS

Study Population and Design

We utilized a dataset from a prospective study conducted in the Stroke Unit of Huashan Hospital, Shanghai. This longitudinal cohort was designed to investigate the risk factors, clinical features and outcomes of PSCI. The inclusion criteria were as follows: (a) diagnosed with ischemic stroke within 7 days of onset; (b) age $\geq$ 18 years; (c) National Institute of Health stroke scale (NIHSS) score $\leq$ 25; (d) able and willing to accept brain imaging examination and neuropsychological assessment. Subjects with following conditions were excluded: (a) pre-stroke dementia; (b) unable to speak or write due to aphasia or paralysis; (c) renal dysfunction; (d) allergy to iodine; (e) contraindications to magnetic resonance imaging (MRI) examination;(f) patients with abnormal calcium and phosphorus metabolism; (g) known nervous system disease or severe chronic medical disease; (h) mental health conditions, such as anxiety or depression; (i) pregnancy.

The study was approved by the Ethics Committee of Fudan University, Shanghai, China. All participants signed written informed consent before data collection.

Imaging Acquisition

All patients underwent cranio-cervical computer tomography angiography (CTA) within 7 days of stroke onset. CTA was performed on a 256-section scanner (Brilliance i CT, Phillips Medical Systems, Ohio, United States) from the aortic arch to the vertex with parameters as follows: 120 kVp, 150 mAs, slice thickness of 1 mm, pitch of 0.7, field of view of 220 mm, matrix of 512 $\times$ 512, helical scanning mode and intravenous administration of 50 mL non-ionic contrast (Ultravist, Bayer Healthcare, Berlin, Germany) at 5 mL/s via power injector (Stellate Injection System, Indianola, PA, United States) with an 8 s delay. CTA raw data were processed using the Phillips Brilliance Workspace portal software (Vision 5.0.2), including multi-planar reformation, curved planar reformation, maximum intensity projection and volume rendering. All MRI examinations were performed on a 3.0 T scanner (GE Discovery750, Milwaukee, United States, or Siemens MAGNETOM Verio, Erlangen, Germany) using a pre-programmed protocol. The main MRI sequences included: T1-weighted, T2-weighted fluid attenuated inversion recovery, diffusion-weighted imaging, and apparent diffusion coefficient.

Imaging Interpretation

All CTA and MRI images were reviewed and analyzed by two independent neuroradiologists (C.C. Li and L.Y. Lin) with over 3 years' experience in neurovascular imaging. Inconsistent cases were handed to another senior neuroradiologist (Y.M. Yang) and the final decision was made based on their consensus. Raters were blinded to all clinical data.

Carotid arteries were divided into three segments: common carotid arteries, cervical internal carotid arteries, and intracranial internal carotid arteries. The presence, location, number and maximum thickness of calcification on unilateral or bilateral carotid arteries were analyzed and recorded. All arteries with calcified plaques were annotated as single ($<$2) or multiple ($\geq$2), according to the number of plaques. The calcification location was categorized as surface, deep or mixed (with both surface and deep calcification). Surface calcification was defined as a calcified nodule located within or close to the intimal lumen interface. Deep calcification was defined as a calcified nodule located within or close to the media/adventitia border, with fibrous tissue completely covering (Lin et al., 2017). Calcification was also classified as thin ($<$2 mm), thick ($\geq$2 mm) or mixed (with both thin or thick calcification) based on the maximum thickness

(Yang et al., 2018). Rim sign was defined as thin calcification (<2 mm) within the adventitia with thick internal soft plaque (≥2 mm) inside (Eisenmenger et al., 2016). Examples of different radiological characteristic of calcification are illustrated in **Figure 1**.

The degree of carotid artery stenosis, intracranial artery stenosis (ICAS), remodeling index (RI), and soft plaque density was further analyzed. Degree of lumen stenosis was calculated and divided into three groups: mild (0−49.9%), moderate (50−69.9%), and severe (70−99.9%), following the criteria of the North American Symptomatic Carotid Endarterectomy Trial (Committee, 1991). No patients with carotid artery occlusion were enrolled in this study. Intracranial large arteries were categorized into anterior (including anterior cerebral artery, internal carotid artery, and middle cerebral artery) and posterior (including posterior cerebral artery, vertebral artery, and basal artery) circulations. ICAS was defined as moderate–severe stenosis (≥50%) of each artery following the criteria of Warfarin-Aspirin Symptomatic Intracranial Disease (Samuels et al., 2000). RI was defined as the ratio of the cross-sectional vessel area at the maximal stenotic site to the reference vessel area at the nearby disease-free site (Miura et al., 2011). Soft plaque density was analyzed using the mean Hounsfield unit across the whole plaque volume (U-King-Im et al., 2010).

Lacune and WMH were diagnosed according to the Standards for Reporting Vascular Changes on Neuroimaging criteria (Wardlaw et al., 2013). WMH was categorized into three groups based on the sum of Fazekas scales (periventricular and deep): mild(0−2), moderate(3−4), severe(5−6).

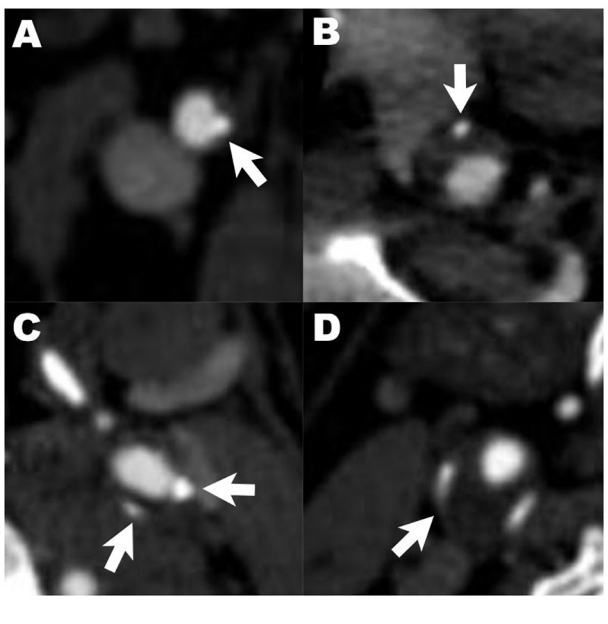

FIGURE 1 | Examples of different radiological characteristics of calcified plaques. Arrows indicate calcification with different characteristics: **(A–C)** describe the relative location of calcified plaques in carotid artery **(A)**, surface calcification; **(B)**, deep calcification; **(C)**, mixed calcification). Panel **(D)** shows calcification with positive rim sign.

Cognitive Function Assessment

Patients' cognitive function was assessed within 7 days of admission and at 6–12 months using the neuropsychological battery, which included global function and separate cognitive domains: (1) Global function: Mini–mental State Examination (MMSE) and Montreal Cognitive Assessment; (2) Memory and execution: memory and executive screening scale; (3) Visuospatial function: visuospatial overlapping diagram from Montreal Cognitive Assessment−Basic; and (4) Language: language screening test. The cut-off was determined by mean − 1.0 standard deviations (SD) or standardized values for all the tests. A patient was considered having PSCI if at least one cognitive domain (memory, execution, visuospatial function and language) was impaired (Jacquin et al., 2014). Among patients with PSCI, post-stroke dementia (PSD) was defined using interviews, neuropsychological battery and clinical dementia rating in accordance with the *Diagnostic and Statistical Manual of Mental Disorders, Fourth Edition*. Those who did not meet the criteria of PSD were classified as post-stroke cognitive impairment with no dementia (PSCIND). Pre-stroke dementia, anxiety and depression was assessed and excluded using informant questionnaire on cognitive decline in the elderly, geriatric depression scale and the 12-item neuropsychiatric inventory questionnaire, separately. All neuropsychological assessments were administered by experienced neurologists (M.Y. Ding, Y.Z. Wang and M. Cui) in our team.

Covariates

Demographic and clinical characteristic data was collected from the database of stroke patients at baseline and follow-up. Obtained information included demographics (age, sex, years of education, body mass index, etc.), vascular risk factors (hypertension, diabetes mellitus, hyperlipidemia, etc.), lifestyle (smoking, alcohol consumption, etc.), stroke severity (NIHSS score), and CSVD (lacune, WMH). Hypertension was defined as systolic pressure ≥140 mmHg and/or diastolic pressure ≥90 mmHg, or the patient having been previously diagnosed and treated. Diabetes mellitus was defined as fasting plasma glucose ≥7.0 mmol/L, or postprandial 2 h glucose ≥11.1 mmol/L, or the patient having been previously diagnosed and treated. Hyperlipidemia was defined as total cholesterol ≥5.2 mmol/L, or low-density lipoprotein cholesterol ≥2.6 mmol/L, or triglycerides ≥1.70 mmol/L, or the patient having been previously diagnosed and treated. Smoking and alcohol consumption were divided into two statuses: current (at least one cigarette per 3 days or at least 50 grams of alcohol per week in the past 6 months) and past (quit smoking or drinking for at least 1 year) (Li et al., 2019).

Statistical Analyses

Variable normality was determined using Kolmogorov−Smirnov test. Continuous variables are presented as mean ± standard deviation (in normality distribution) or median with interquartile range (IQR) (in skewness distribution) and compared using Student's *t*-test or Mann−Whitney *U* test. Categorical variables

are displayed as count with frequency (%) and compared using Pearson's chi–square test or rank sum test (for ordinal categorical variables). Multinomial logistic regression was conducted to estimate the odds ratios (OR), 95% confidence intervals (CI) of PSCIND and PSD based on carotid plaque characteristics. Binary logistic regression with the selected covariates was used to calculate the area under the receiver operator characteristic curve for predicting PSD. Linear regression was performed to investigate the association of carotid atherosclerosis and post-stroke cognitive function in different domains. The scores of each cognitive test were transformed into *Z*-scores [(individual test score – mean score)/SD]. Ordinal logistic regression was performed to obtain *P*-trend value by treating post-stroke cognitive function as an ordinal variable.

Demographics, vascular risk factors and stroke severity were adjusted as covariates in regression models, including age, sex, years of education, NIHSS score at baseline (model 1), as well as hypertension, hyperlipidemia, WMH, and carotid artery stenosis (model 2). All statistical analyses were performed using SPSS v19.0 or R v3.6.2 for Mac OS. $P < 0.05$ was considered to be statistically significant.

RESULTS

One hundred seventy-nine participants who met the criteria from June 2017 to May 2018 were included in this study. Each individual was given a standardized treatment scheme during hospitalization. The median follow-up time was 6.9 months for this study population. Among them, 20 subjects did not undergo brain or neck CTA at baseline. Of the remaining 159 individuals, 29 refused to accept neuropsychological assessment at follow-up; 2 were excluded due to the recurrence of stroke. Therefore, a total of 128 individuals with complete clinical information were included in the final analysis. The flow chart of the enrollment procedures of study individuals is shown in **Supplementary Figure 1**. No significant difference between the baseline profiles of participants involved in this study and those lost in follow-up was found (**Supplementary Table 1**).

Basic Characteristics

The basic characteristics of the study population are demonstrated in **Supplementary Table 1**. The mean age (SD) was 62.1 (12.2) years and 37 (28.9%) of the subjects were women. The population had a median (IQR) 12.0 (9.0, 15.0) years of education. Median (IQR) NIHSS score at baseline was relatively low, at 4.0 (2.0, 6.0). Lacune and severe WMH were found in 53 (41.4%) and 21 (16.4%) patients, respectively. Among all individuals, 96 subjects (75%) had calcification on unilateral or bilateral carotid arteries. 21 subjects (16.4%) had moderate to severe carotid artery stenosis. Cognitive function assessment classified individuals as having normal cognition ($N = 27$), PSCIND ($N = 75$), or PSD ($N = 26$) (**Table 1**). Compared to participants with normal cognition, those who have PSCI (both PSCIND and PSD) were older, less educated, scored higher on NIHSS and grading of WMH at baseline using univariate analyses ($P < 0.05$). The PSCI group also had a higher proportion of calcification and moderate or severe carotid artery stenosis (only in PSD group) ($P < 0.05$). There was no significant association between soft plaque density, RI, ICAS, other vascular risk factors and PSCI.

Carotid Calcification and Post-stroke Cognitive Impairment

Table 2 lists the association between carotid plaque characteristic and PSCI. In logistic regression, the presence of calcification on carotid arteries predicted an increased risk of PSD ($OR = 7.15$; 95% CI: 1.07–47.69). Moreover, we found that the presence of multiple, thick/mixed, surface calcifications were significantly associated with PSD, whereas single, thin, deep/mixed calcifications were not (**Figure 2**). Participants with multiple, thick/mixed, surface calcifications exhibited an increased risk of PSCI compared to those without calcification ($P_{trend} = 0.004, 0.016, 0.045$, respectively). Carotid artery stenosis also significantly increased the risk of PSD ($OR = 6.42$; 95% CI: 1.03–40.15). Rim sign, RI and soft plaque density showed no relationship with PSD in any model. In addition, no association was found between any type of carotid plaque or stenosis and PSCIND.

Figure 3 depicts three logistic regression models predicting PSD. The presence of carotid calcification yielded an area under curve (AUC) of 0.67 (95% CI: 0.55–0.79), similar to the result of WMH (AUC = 0.67, 95% CI: 0.53–0.81). When calcification was combined with WMH and other covariates (including age, years of education and baseline NIHSS), the prediction model reached an AUC of 0.90 with 95% CI 0.82 to 0.99.

Carotid Calcification and Cognitive Impairment in Different Domains

The association between carotid plaque characteristics and cognitive impairment in different domains is displayed in **Table 3**. In liner regression, most types of calcifications correlated with decreased MMSE score. Moreover, multiple and surface calcifications were found to be associated with decreased *Z* scores in memory domain. We also found that soft plaque density and carotid artery stenosis had a negative impact on cognitive function in execution and visuospatial domain, respectively.

DISCUSSION

This study investigated the association between carotid atherosclerotic calcification and PSCI in hospitalized patients with stroke. We found the presence of calcification, especially multiple, thick/mixed, and surface calcification on carotid arteries to be associated with PSCI, after full adjustment (demographics, vascular risk factors, CSVD and stroke severity). In general, our findings suggest that the quantity and location of calcification in carotid atherosclerotic plaques may be independent indicators for PSCI.

Atherosclerosis is a chronic disease affecting the structure and function of blood vessels, leading to neurovascular dysfunction

TABLE 1 | Comparison of clinical and imaging characteristics between groups with different post-stroke cognitive function.

	Normal (*N* = 27)	PSCIND (*N* = 75)	PSD (*N* = 26)	*P*-value (PSCIND vs. Normal)	*P*-value (PSD vs. Normal)
Demographic characteristics					
Age, mean ± SD	52.6 ± 15.6	64.3 ± 10.0	65.3 ± 9.0	0.001	0.001
Female, n (%)	7 (25.9)	19 (25.3)	11 (42.3)	0.952	0.208
Education year, median (IQR)	12.0 (9.8, 15.8)	12.0 (9.0, 12.0)	9.0 (3.0, 11.0)	0.017	0.001
Smoking (ever), n (%)	14 (51.9)	36 (48.0)	15 (57.7)	0.731	0.669
Alcohol consumption (ever), n (%)	7 (25.9)	28 (37.3)	7 (26.9)	0.284	0.934
Hypertension, n (%)	16 (59.3)	57 (76.0)	20 (76.9)	0.098	0.168
Diabetes mellitus, n (%)	5 (18.5)	23 (30.7)	10 (38.5)	0.225	0.107
Hyperlipidemia, n (%)	11 (40.7)	31 (41.3)	9 (34.6)	0.957	0.646
Baseline stroke severity					
NIHSS at baseline, median (IQR)	2.0 (1.0, 4.5)	4.0 (2.0, 6.0)	5.0 (3.0, 8.0)	0.003	0.001
Cerebral small vessel diseases					
Lacune, n (%)	10 (37.0)	30 (40.0)	13 (50.0)	0.576	0.590
WMH					
Mild, n (%)	13 (48.1)	13 (17.3)	1 (3.8)	0.006	0.001
Moderate, n (%)	10 (37.0)	49 (65.3)	21 (80.8)		
Severe, n (%)	4 (14.8)	13 (17.3)	4 (15.4)		
Atherosclerotic characteristics					
Calcification, n (%)	14 (51.9)	59 (78.7)	23 (88.5)	0.008	0.004
Soft plaque density (Hu), mean ± SD	38.8 ± 32.2	36.2 ± 19.7	47.4 ± 27.7	0.854	0.553
Remodeling index, median (IQR)	1.0 (1.0, 1.2)	1.0 (1.0, 1.2)	1.0 (1.0, 1.4)	0.290	0.870
Carotid artery stenosis					
Mild, n (%)	26 (96.3)	63 (84.0)	18 (69.2)	0.222	0.024
Moderate or severe, n (%)	1 (3.7)	12 (16.0)	8 (30.8)		
Intracranial artery stenosis					
Anterior arteries, n (%)	7 (25.9)	25 (33.3)	14 (53.8)	0.601	0.135
Posterior arteries, n (%)	4 (14.8)	15 (20.0)	6 (23.1)	0.505	0.669

IQR, interquartile range; NIHSS, National Institute of Health stroke scale; PSCIND, post-stroke cognitive impairment non-dementia; PSD, post-stroke dementia; WMH, white matter hyperintensity.

which causes cognitive decline (Shabir et al., 2018). The progressive formation of plaque and increased stiffness in carotid arteries accelerates cognitive dysfunction, particularly vascular cognitive impairment, by decreasing cerebral blood flow and promoting a breakdown of neurovascular coupling (Girouard and Iadecola, 2006; Jefferson et al., 2018). Atherosclerotic calcification represents an advanced stage of atherosclerosis pathogenesis. Although few studies have investigated whether atherosclerotic calcification is related with PSCI, the association between calcification and cognitive impairment at the pre-clinical stage has been identified by a range of research. In Rotterdam study, larger calcification volume was found to be associated with a higher risk of dementia and cognitive decline in a population-based cohort (Bos et al., 2012, 2015). In the CARDIA study, subclinical atherosclerotic calcification was related with poorer psychomotor speed and memory in midlife in a community-based sample (Reis et al., 2013). Another hospital-based study proved that common carotid artery calcification increased the risk of cognitive impairment and dementia, and this association appeared independent of arterial stiffness (Di Daniele et al., 2019). All of these findings supported the hypothesis that the presence and amount of calcification is related to cognitive impairment, which is supported by our results.

TABLE 2 | Association between carotid plaque characteristics and post-stroke cognitive impairment.

		Normal (*N* = 27)	PSCIND (*N* = 75)	PSD (*N* = 26)
Calcification	Model 1	1.0 (ref)	2.31 (0.61-8.71)	7.15 (1.07-47.69)*
	Model 2	1.0 (ref)	2.09 (0.45-9.79)	8.72 (1.03-76.99)*
Soft plaque density	Model 1	1.0 (ref)	1.00 (0.96-1.06)	1.03 (0.98-1.09)
	Model 2	1.0 (ref)	1.00 (0.92-1.10)	1.03 (0.93-1.15)
Remodeling index	Model 1	1.0 (ref)	0.35 (0.03-4.06)	1.35 (0.09-19.46)
	Model 2	1.0 (ref)	0.27 (0.02-4.94)	0.83 (0.03-21.48)
Carotid artery stenosis	Model 1	1.0 (ref)	3.34 (0.57-19.46)	6.42 (1.03-40.15)*
	Model 2	1.0 (ref)	5.41 (0.76-38.51)	10.73 (1.34-85.59)*

**P < 0.05.*

All results are presented as OR with 95%CI.

Model 1 was adjusted for age, sex, years of education, and baseline NIHSS; Model 2 was additionally adjusted for hypertension, hyperlipidemia, WMH, and carotid artery stenosis (for calcification, soft plaque density, and remodeling index) based on Model 1.

NIHSS, National Institute of Health stroke scale; PSCIND, post-stroke cognitive impairment non-dementia; PSD, post-stroke dementia; WMH, white matter hyperintensity.

The association between calcified atherosclerosis and PSCI could be explained by several potential pathways. Firstly, chronic hypoperfusion may enhance this association. Carotid artery stiffness caused by calcification may attenuate resting cerebral blood flow in several regions and increase blood-brain barrier permeability, which can lead to disruption of microcirculation and vasculature integrity (Muhire et al., 2019). This may

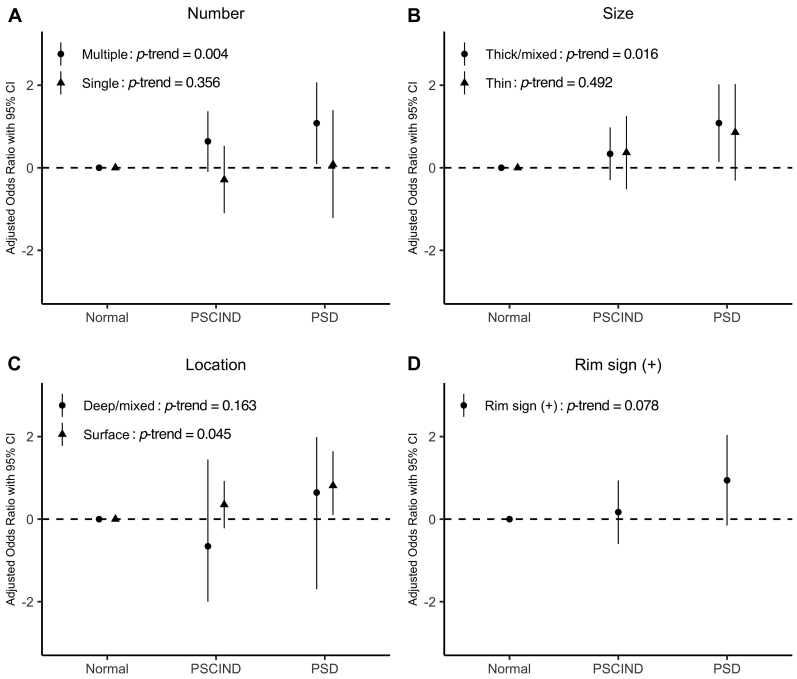

FIGURE 2 | Panel **(A–D)** show the associations between different characteristics of calcified plaques and post-stroke cognitive impairment. Levels of post-stroke cognitive function are shown on the x-axis. Values of odds ratio of specific characteristics of calcified plaques (number, size, location, and rim sign) are transformed using logarithm (log10) and are displayed on the y-axis. Model was adjusted for age, sex, years of education, and baseline NIHSS. *P* for trend is given in each case. NIHSS, National Institute of Health stroke scale; PSCIND, post-stroke cognitive impairment non-dementia; PSD, post-stroke dementia.

contribute to the pathogenesis of vascular dementia, and in turn enhance comorbidity with neurodegenerative diseases (Alzheimer's disease) (Ueno et al., 2016). Secondly, carotid atherosclerotic calcification could increase the risk and severity of stroke, subsequently resulting in a higher likelihood of PSCI. However, our findings showed that the significant association between calcification and PSCI still existed after adjusting baseline NIHSS score. This suggested that stroke played only a limited role in the progression of PSCI, although it cannot be entirely excluded as a contributing factor. Finally, multiple microemboli induced by unstable plaques may accelerate cognitive impairment after stroke. In our study, we found that patients with multiple, thick and surface calcifications were more likely to develop to PSCI. The location, shape, size and gap between calcifications change mechanical stresses and affect cap stability (Cardoso et al., 2014). Compared with deep or mixed calcifications, surface calcifications increase the risk of neovessel rupture and thrombosis by elevating plaque surface stress (Li et al., 2007; Alfonso et al., 2013). Similar mechanisms apply to multiple calcified plaques (Kelly-Arnold et al., 2013). Thus, these calcifications may be representative of vulnerable plaques. This notion is supported by findings, that superficial, multiple and thick (≥2 mm) calcifications were independently related to the presence of intra plaque hemorrhage (Eisenmenger et al., 2016; Lin et al., 2017; Yang et al., 2018). Vulnerable plaques may produce both clinically evident emboli and subclinical multiple microemboli leading to brain atrophy and silent brain infarcts, thus proceeding cognitive impairment (Dempsey et al., 2010).

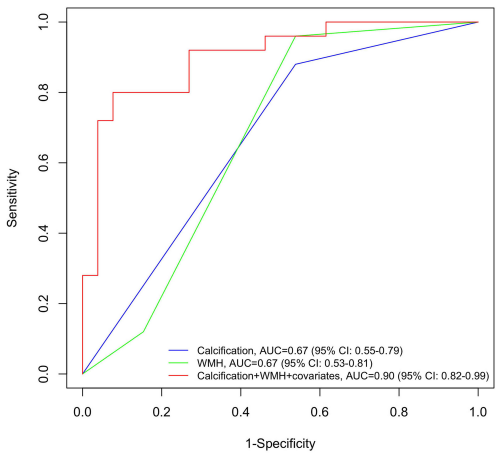

FIGURE 3 | Receiver operating characteristic (ROC) curves for post-stroke dementia by neuroimaging determinants. Blue line: the ROC curve obtained from calcification; green line: the ROC curve obtained from WMH; red line: the ROC curve obtained from the full adjusted model, including calcification, WMH and covariates (age, years of education, and baseline NIHSS). NIHSS, National Institute of Health stroke scale; ROC, receiver operating characteristic; WMH, white matter hyperintensity.

Moreover, we found that carotid calcification, artery stenosis and soft plaque density each had different effects on performance in each cognitive domain. In agreement with others studies,

TABLE 3 | Association between carotid plaque characteristics and post-stroke cognitive impairment in different domains.

		MMSE	Memory	Execution	Language	Visuospatial
Calcification						
Presence	Model 1	−0.66 (0.18)*	−0.34 (0.22)	−0.22 (0.21)	−0.34 (0.23)	−0.41 (0.21)
	Model 2	−0.69 (0.19)*	−0.46 (0.23)*	−0.21 (0.22)	−0.30 (0.24)	−0.38 (0.22)
Number						
Single	Model 1	−0.4 (0.25)	0.03 (0.31)	−0.07 (0.29)	0.06 (0.28)	−0.09 (0.32)
	Model 2	−0.26 (0.3)	0.26 (0.36)	0.20 (0.32)	0.12 (0.32)	0.08 (0.36)
Multiple	Model 1	−0.75 (0.19)*	−0.47 (0.23)*	−0.30 (0.22)	−0.45 (0.25)	−0.43 (0.22)
	Model 2	−0.78 (0.2)*	−0.60 (0.23)*	−0.28 (0.23)	−0.38 (0.26)	−0.39 (0.24)
Size						
Thin	Model 1	−0.76 (0.23)*	−0.19 (0.29)	−0.27 (0.25)	−0.34 (0.26)	−0.34 (0.25)
	Model 2	−0.69 (0.27)*	−0.15 (0.33)	−0.14 (0.29)	−0.38 (0.31)	−0.25 (0.29)
Thick/mixed	Model 1	−0.62 (0.2)*	−0.39 (0.23)	−0.21 (0.23)	−0.29 (0.26)	−0.35 (0.24)
	Model 2	−0.62 (0.21)*	−0.46 (0.24)	−0.17 (0.25)	−0.17 (0.27)	−0.31 (0.26)
Location						
Surface	Model 1	−0.64 (0.18)*	−0.38 (0.23)	−0.22 (0.20)	−0.31 (0.23)	−0.40 (0.21)
	Model 2	−0.67 (0.19)*	−0.48 (0.24)*	−0.22 (0.22)	−0.30 (0.24)	−0.39 (0.22)
Deep/mixed	Model 1	−1.13 (0.39)*	0.27 (0.42)	−0.55 (0.47)	−0.36 (0.37)	0.01 (0.49)
	Model 2	−1.14 (0.43)*	0.45 (0.46)	−0.52 (0.49)	0.11 (0.52)	0.04 (0.54)
Rim sign						
Rim sign (+)	Model 1	−0.61 (0.22)*	−0.28 (0.23)	−0.06 (0.26)	−0.31 (0.25)	−0.19 (0.28)
	Model 2	−0.52 (0.24)*	−0.27 (0.25)	0.06 (0.28)	−0.33 (0.33)	−0.12 (0.31)
Soft plaque density	Model 1	−0.01 (0.01)	0.01 (0.01)	−0.01 (0.01)*	0.01 (0.01)	0.01 (0.01)
	Model 2	−0.01 (0.01)	0.01 (0.01)	−0.02 (0.01)*	0.01 (0.01)	0.01 (0.01)
Remodeling index	Model 1	−0.07 (0.31)	−0.10 (0.36)	0.43 (0.34)	−0.23 (0.36)	0.39 (0.33)
	Model 2	−0.17 (0.33)	−0.33 (0.37)	0.46 (0.37)	0.14 (0.42)	0.48 (0.35)
Carotid artery stenosis	Model 1	−0.05 (0.13)	0.05 (0.15)	−0.16 (0.14)	−0.16 (0.16)	−0.30 (0.14)*
	Model 2	−0.07 (0.13)	0.08 (0.15)	−0.16 (0.14)	−0.16 (0.16)	−0.32 (0.14)*

*$P < 0.05$.

All results are presented as standardized coefficients β with standard error. Values represent differences in Z score for MMSE and cognitive domain.

Complete data of MMSE and each cognitive domain was available in 123 participants.

Model 1 was adjusted for age, sex, years of education, and baseline NIHSS; Model 2 was additionally adjusted for hypertension, hyperlipidemia, WMH, and carotid artery stenosis (for calcification, soft plaque density, and remodeling index) based on Model 1.

MMSE, Mini-mental State Examination; NIHSS, National Institute of Health stroke scale; WMH, white matter hyperintensity.

carotid artery stenosis and soft plaque density were significantly associated with impaired execution and visuospatial function (Bos et al., 2012; Gong et al., 2020). These associations could be explained by the disruption of anterior and posterior watershed areas caused by hypoperfusion. Whereas, multiple and surface calcifications were found to predominantly disrupt function in the memory domain. These unstable carotid atherosclerotic plaques tend to be more likely to induce multiple microemboli, and cause strategic infarcts within the cortex (Hase et al., 2019). Unlike hypoperfusion, emboli may cause more diffuse damage to cortical areas and subsequently impair memory (Fearn et al., 2001). The multiple cognitive domains involved in associations between carotid atherosclerosis and PSCI revealed the sophisticated underlying mechanisms, which need to be further assessed and confirmed through pathological evidence.

The strengths of our study include its longitudinal study design, reliable brain imaging acquisition method and the detailed cognitive function questionnaire including different domains. Several potential limitations should also be illustrated. Firstly, in our study, atherosclerotic calcification and plaque characteristics were recognized by brain/neck CTA. CTA is a sensitive, observer-independent, and reliable tool to evaluate calcification. Compared with high-resolution MRI, CTA is faster, with fewer contraindications, and is generally more feasible. It is therefore widely used in clinical practice, especially for stroke patients. However, CTA has less capacity to identify soft plaque components, such as ulceration and intra plaque hemorrhage. It is also difficult to determine the border of calcification due to blooming artifacts at the vessel wall, which may cause bias in patients with severe calcification. Secondly, the associations which we have found, may be confounded by the lack of quantitative analysis of calcification. Although we categorized calcifications based on their size and numbers, the overall burden of calcification may still influence the result. Thirdly, the limited cases with PSD in this study cause quite broad confidence intervals, especially when calcification was treated as a binary covariate. As shown in **Table 1**, the distribution of calcification showed significant difference between normal, PSCIND, and PSD groups using univariate analysis. A larger sample size is supposed to make our conclusion more accurate and solid.

Finally, selection bias should also be considered when explaining these associations. In our study design, patients who could not complete cognitive function assessment due to hemiplegia or aphasia at baseline were excluded. Thus, the included subjects in our trial had relatively lower NIHSS score (4.0 points) than average. This selection bias may lead to an underestimation of the effect of stroke on PSCI. Additional screening utilizing a cognitive function scale which is more suitable for stroke patients, especially those whom cannot speak or write, is needed in future studies.

CONCLUSION

In this hospital-based study, the presence of carotid calcification was found to be associated with PSCI. This association depended on the size, number, and location of calcifications. In addition to CSVD, large artery atherosclerosis should be considered as an important risk factor for PSD.

DATA AVAILABILITY STATEMENT

The data used in this study are available upon reasonable request from the corresponding author.

ETHICS STATEMENT

The studies involving human participants were reviewed and approved by the Ethics Committee of the Fudan University, Shanghai, China. The patients/participants provided their written informed consent to participate in this study.

AUTHOR CONTRIBUTIONS

YinW, MD, QD, and MC conceived the cohort and take responsibility for its all aspects. YinW and CL wrote the manuscript. YinW completed all the statistical analysis supported by YY and MC. MD led the data collection supported by YizW, PL, and MC. CL, LL, and YY reviewed and commented on the data analysis and drafts. All authors interpreted data, contributed to critical revisions, and approved the final version of the article.

FUNDING

This work was supported by the National Natural Science Foundation of China (Grant Nos: 81870915, 81971013, 81771788, and 82001142), the Shanghai Municipal Science and Technology Major Project (Grant No: 2018SHZDZX03), and the China Postdoctoral Science Foundation (Grant No: 2020M681184). None of these funding sources were involved in the study design, data collection, data analysis, or interpretation, or the writing of the report and the decision to submit the article for publication.

ACKNOWLEDGMENTS

We thank all the patients whom voluntarily participated in this study and appreciate the special contributions of statistical analyses by Yanfeng Jiang.

SUPPLEMENTARY MATERIAL

The Supplementary Material for this article can be found online at: https://www.frontiersin.org/articles/10.3389/fnagi.2021.682908/full#supplementary-material

REFERENCES

Alfonso, F., Gonzalo, N., Nunez-Gil, I., and Banuelos, C. (2013). Coronary thrombosis from large, nonprotruding, superficial calcified coronary plaques. *J. Am. Coll. Cardiol.* 62:2254. doi: 10.1016/j.jacc.2013.04.106

Arba, F., Quinn, T. J., Hankey, G. J., Lees, K. R., Wardlaw, J. M., Ali, M., et al. (2018). Enlarged perivascular spaces and cognitive impairment after stroke and transient ischemic attack. *Int. J. Stroke* 13, 47–56. doi: 10.1177/1747493016666091

Bos, D., Vernooij, M. W., de Bruijn, R. F., Koudstaal, P. J., Hofman, A., Franco, O. H., et al. (2015). Atherosclerotic calcification is related to a higher risk of dementia and cognitive decline. *Alzheimers Dement.* 11, 639–647.e1. doi: 10.1016/j.jalz.2014.05.1758

Bos, D., Vernooij, M. W., Elias-Smale, S. E., Verhaaren, B. F., Vrooman, H. A., Hofman, A., et al. (2012). Atherosclerotic calcification relates to cognitive function and to brain changes on magnetic resonance imaging. *Alzheimers Dement.* 8(5 Suppl), S104–S111. doi: 10.1016/j.jalz.2012.01.008

Cardoso, L., Kelly-Arnold, A., Maldonado, N., Laudier, D., and Weinbaum, S. (2014). Effect of tissue properties, shape and orientation of microcalcifications on vulnerable cap stability using different hyperelastic constitutive models. *J. Biomech.* 47, 870–877. doi: 10.1016/j.jbiomech.2014.01.010

Chaudhari, T. S., Verma, R., Garg, R. K., Singh, M. K., Malhotra, H. S., and Sharma, P. K. (2014). Clinico-radiological predictors of vascular cognitive impairment (VCI) in patients with stroke: a prospective observational study. *J. Neurol. Sci.* 340, 150–158. doi: 10.1016/j.jns.2014.03.018

Committee, (1991). North American symptomatic carotid endarterectomy trial. Methods, patient characteristics, and progress. *Stroke* 22, 711–720. doi: 10.1161/01.str.22.6.711

Dempsey, R. J., Vemuganti, R., Varghese, T., and Hermann, B. P. (2010). A review of carotid atherosclerosis and vascular cognitive decline: a new understanding of the keys to symptomology. *Neurosurgery* 67, 484–494. doi: 10.1227/01.NEU.0000371730.11404.36

Di Daniele, N., Celotto, R., Alunni Fegatelli, D., Gabriele, M., Rovella, V., and Scuteri, A. (2019). Common carotid artery calcification impacts on cognitive function in older patients. *High Blood Press. Cardiovasc. Prev.* 26, 127–134. doi: 10.1007/s40292-019-00301-z

Eisenmenger, L. B., Aldred, B. W., Kim, S. E., Stoddard, G. J., de Havenon, A., Treiman, G. S., et al. (2016). Prediction of carotid intraplaque hemorrhage using adventitial calcification and plaque thickness on CTA. *AJNR Am. J. Neuroradiol.* 37, 1496–1503. doi: 10.3174/ajnr.A4765

Fearn, S. J., Pole, R., Wesnes, K., Faragher, E. B., Hooper, T. L., and McCollum, C. N. (2001). Cerebral injury during cardiopulmonary bypass: emboli impair memory. *J. Thorac. Cardiovasc. Surg.* 121, 1150–1160. doi: 10.1067/mtc.2001.114099

Girouard, H., and Iadecola, C. (2006). Neurovascular coupling in the normal brain and in hypertension, stroke, and Alzheimer disease. *J. Appl. Physiol.* 100, 328–335. doi: 10.1152/japplphysiol.00966.2005

Gong, L., Wang, H., Dong, Q., Zhu, X., Zheng, X., Gu, Y., et al. (2020). Intracranial atherosclerotic stenosis is related to post-stroke cognitive impairment: a cross-sectional study of minor stroke. *Curr. Alzheimer Res.* 17, 177–184. doi: 10.2174/1567205017666200303141920

Gottesman, R. F., and Hillis, A. E. (2010). Predictors and assessment of cognitive dysfunction resulting from ischaemic stroke. *Lancet Neurol.* 9, 895–905. doi: 10.1016/s1474-4422(10)70164-2

Gregoire, S. M., Smith, K., Jager, H. R., Benjamin, M., Kallis, C., Brown, M. M., et al. (2012). Cerebral microbleeds and long-term cognitive outcome: longitudinal cohort study of stroke clinic patients. *Cerebrovasc. Dis.* 33, 430–435. doi: 10.1159/000336237

Hase, Y., Polvikoski, T. M., Ihara, M., Hase, M., Zafar, R., Stevenson, W., et al. (2019). Carotid artery disease in post-stroke survivors and effects of enriched environment on stroke pathology in a mouse model of carotid artery stenosis. *Neuropathol. Appl. Neurobiol.* 45, 681–697. doi: 10.1111/nan.12550

Jacquin, A., Binquet, C., Rouaud, O., Graule-Petot, A., Daubail, B., Osseby, G. V., et al. (2014). Post-stroke cognitive impairment: high prevalence and determining factors in a cohort of mild stroke. *J. Alzheimers Dis.* 40, 1029–1038. doi: 10.3233/JAD-131580

Jefferson, A. L., Cambronero, F. E., Liu, D., Moore, E. E., Neal, J. E., Terry, J. G., et al. (2018). Higher aortic stiffness is related to lower cerebral blood flow and preserved cerebrovascular reactivity in older adults. *Circulation* 138, 1951–1962. doi: 10.1161/CIRCULATIONAHA.118.032410

Kandiah, N., Chander, R. J., Lin, X., Ng, A., Poh, Y. Y., Cheong, C. Y., et al. (2016). Cognitive impairment after mild stroke: development and validation of the SIGNAL2 risk score. *J. Alzheimers Dis.* 49, 1169–1177. doi: 10.3233/JAD-150736

Kebets, V., Gregoire, S. M., Charidimou, A., Barnes, J., Rantell, K., Brown, M. M., et al. (2015). Prevalence and cognitive impact of medial temporal atrophy in a hospital stroke service: retrospective cohort study. *Int. J. Stroke* 10, 861–867. doi: 10.1111/ijs.12544

Kelly-Arnold, A., Maldonado, N., Laudier, D., Aikawa, E., Cardoso, L., and Weinbaum, S. (2013). Revised microcalcification hypothesis for fibrous cap rupture in human coronary arteries. *Proc. Natl. Acad. Sci. U.S.A.* 110, 10741–10746.

Leys, D., Hénon, H., Mackowiak-Cordoliani, M.-A., and Pasquier, F. (2005). Poststroke dementia. *Lancet Neurol.* 4, 752–759. doi: 10.1016/s1474-4422(05)70221-0

Li, S., Fang, F., Cui, M., Jiang, Y., Wang, Y., Kong, X., et al. (2019). Incidental findings on brain MRI among Chinese at the age of 55-65 years: the Taizhou imaging study. *Sci. Rep.* 9:464. doi: 10.1038/s41598-018-36893-0

Li, X., Ma, X., Lin, J., He, X., Tian, F., and Kong, D. (2017). Severe carotid artery stenosis evaluated by ultrasound is associated with post stroke vascular cognitive impairment. *Brain Behav.* 7:e00606. doi: 10.1002/brb3.606

Li, Z. Y., Howarth, S., Tang, T., Graves, M., U-King-Im, J., and Gillard, J. H. (2007). Does calcium deposition play a role in the stability of atheroma? Location may be the key. *Cerebrovasc. Dis.* 24, 452–459. doi: 10.1159/000108436

Lin, R., Chen, S., Liu, G., Xue, Y., and Zhao, X. (2017). Association between carotid atherosclerotic plaque calcification and intraplaque hemorrhage: a magnetic resonance imaging study. *Arterioscler. Thromb. Vasc. Biol.* 37, 1228–1233. doi: 10.1161/ATVBAHA.116.308360

Lu, D., Ren, S., Zhang, J., and Sun, D. (2016). Vascular risk factors aggravate cognitive impairment in first-ever young ischaemic stroke patients. *Eur. J. Neurol.* 23, 940–947. doi: 10.1111/ene.12967

Miura, T., Matsukawa, N., Sakurai, K., Katano, H., Ueki, Y., Okita, K., et al. (2011). Plaque vulnerability in internal carotid arteries with positive remodeling. *Cerebrovasc. Dis. Extra* 1, 54–65. doi: 10.1159/000328645

Molad, J., Kliper, E., Korczyn, A. D., Ben Assayag, E., Ben Bashat, D., Shenhar-Tsarfaty, S., et al. (2017). Only white matter hyperintensities predicts post-stroke cognitive performances among cerebral small vessel disease markers: results from the TABASCO study. *J. Alzheimers Dis.* 56, 1293–1299. doi: 10.3233/JAD-160939

Muhire, G., Iulita, M. F., Vallerand, D., Youwakim, J., Gratuze, M., Petry, F. R., et al. (2019). Arterial stiffness due to carotid calcification disrupts cerebral blood flow regulation and leads to cognitive deficits. *J. Am. Heart Assoc.* 8:e011630. doi: 10.1161/JAHA.118.011630

Rasquin, S. M., Verhey, F. R., van Oostenbrugge, R. J., Lousberg, R., and Lodder, J. (2004). Demographic and CT scan features related to cognitive impairment in the first year after stroke. *J. Neurol. Neurosurg. Psychiatry* 75, 1562–1567. doi: 10.1136/jnnp.2003.024190

Reis, J. P., Launer, L. J., Terry, J. G., Loria, C. M., Zeki Al Hazzouri, A., Sidney, S., et al. (2013). Subclinical atherosclerotic calcification and cognitive functioning in middle-aged adults: the CARDIA study. *Atherosclerosis* 231, 72–77. doi: 10.1016/j.atherosclerosis.2013.08.038

Samuels, O. B., Joseph, G. J., Lynn, M. J., Smith, H. A., and Chimowitz, M. I. (2000). A standardized method for measuring intracranial arterial stenosis. *AJNR Am. J. Neuroradiol.* 21, 643–646.

Shabir, O., Berwick, J., and Francis, S. E. (2018). Neurovascular dysfunction in vascular dementia, Alzheimer's and atherosclerosis. *BMC Neurosci.* 19:62. doi: 10.1186/s12868-018-0465-5

Sun, J. H., Tan, L., and Yu, J. T. (2014). Post-stroke cognitive impairment: epidemiology, mechanisms and management. *Ann. Transl. Med.* 2:80. doi: 10.3978/j.issn.2305-5839.2014.08.05

Ueno, M., Chiba, Y., Matsumoto, K., Murakami, R., Fujihara, R., Kawauchi, M., et al. (2016). Blood-brain barrier damage in vascular dementia. *Neuropathology* 36, 115–124. doi: 10.1111/neup.12262

U-King-Im, J. M., Fox, A. J., Aviv, R. I., Howard, P., Yeung, R., Moody, A. R., et al. (2010). Characterization of carotid plaque hemorrhage: a CT angiography and MR intraplaque hemorrhage study. *Stroke* 41, 1623–1629. doi: 10.1161/STROKEAHA.110.579474

Wardlaw, J. M., Smith, E. E., Biessels, G. J., Cordonnier, C., Fazekas, F., Frayne, R., et al. (2013). Neuroimaging standards for research into small vessel disease and its contribution to ageing and neurodegeneration. *Lancet Neurol.* 12, 822–838. doi: 10.1016/s1474-4422(13)70124-8

Wen, H. M., Mok, V. C. T., Fan, Y. H., Lam, W. W. M., Tang, W. K., Wong, A., et al. (2004). Effect of white matter changes on cognitive impairment in patients with lacunar infarcts. *Stroke* 35, 1826–1830. doi: 10.1161/01.Str.0000133686.29320.58

Yang, J., Pan, X., Zhang, B., Yan, Y., Huang, Y., Woolf, A. K., et al. (2018). Superficial and multiple calcifications and ulceration associate with intraplaque hemorrhage in the carotid atherosclerotic plaque. *Eur. Radiol.* 28, 4968–4977. doi: 10.1007/s00330-018-5535-7

Conflict of Interest: The authors declare that the research was conducted in the absence of any commercial or financial relationships that could be construed as a potential conflict of interest.

frontiers in Aging Neuroscience

ORIGINAL RESEARCH
published: 03 June 2021
doi: 10.3389/fnagi.2021.630677

Disrupted Network Topology Contributed to Spatial Navigation Impairment in Patients With Mild Cognitive Impairment

*Weiping Li[1], Hui Zhao[2], Zhao Qing[1], Zuzana Nedelska[3,4], Sichu Wu[1], Jiaming Lu[1], Wenbo Wu[1], Zhenyu Yin[5], Jakub Hort[3,4], Yun Xu[2] and Bing Zhang[1]**

[1] Department of Radiology, The Affiliated Drum Tower Hospital of Nanjing University Medical School, Nanjing, China, [2] Department of Neurology, The Affiliated Drum Tower Hospital of Nanjing University Medical School, Nanjing, China, [3] Department of Neurology, The Czech Brain Ageing Study, Memory Clinic, Second Faculty of Medicine–Charles University, University Hospital in Motol, Prague, Czechia, [4] International Clinical Research Center, St. Anne's University Hospital Brno, Brno, Czechia, [5] Department of Geriatrics, The Affiliated Drum Tower Hospital of Nanjing University Medical School, Nanjing, China

OPEN ACCESS

Edited by:
Frank Jessen, University of Cologne, Germany

Reviewed by:
Aaron Wilber, Florida State University, United States
Masashi Kameyama, Tokyo Metropolitan Geriatric Hospital and Institute of Gerontology (TMGH-IG), Japan
David Hike, Florida State University, United States, in collaboration with reviewer AW

***Correspondence:**
Bing Zhang
zhangbing_nanjing@nju.edu.cn

Received: *18 November 2020*
Accepted: *08 April 2021*
Published: *03 June 2021*

Citation:
Li W, Zhao H, Qing Z, Nedelska Z, Wu S, Lu J, Wu W, Yin Z, Hort J, Xu Y and Zhang B (2021) Disrupted Network Topology Contributed to Spatial Navigation Impairment in Patients With Mild Cognitive Impairment. Front. Aging Neurosci. 13:630677. doi: 10.3389/fnagi.2021.630677

Impairment in spatial navigation (SN) and structural network topology is not limited to patients with Alzheimer's disease (AD) dementia and can be detected earlier in patients with mild cognitive impairment (MCI). We recruited 32 MCI patients (65.91 ± 11.33 years old) and 28 normal cognition patients (NC; 69.68 ± 10.79 years old), all of whom underwent a computer-based battery of SN tests evaluating egocentric, allocentric, and mixed SN strategies and diffusion-weighted and T_1-weighted Magnetic Resonance Imaging (MRI). To evaluate the topological features of the structural connectivity network, we calculated its measures such as the global efficiency, local efficiency, clustering coefficient, and shortest path length with GRETNA. We determined the correlation between SN accuracy and network topological properties. Compared to NC, MCI subjects demonstrated a lower egocentric navigation accuracy. Compared with NC, MCI subjects showed significantly decreased clustering coefficients in the left middle frontal gyrus, right rectus, right superior parietal gyrus, and right inferior parietal gyrus and decreased shortest path length in the left paracentral lobule. We observed significant positive correlations of the shortest path length in the left paracentral lobule with both the mixed allocentric–egocentric and the allocentric accuracy measured by the average total errors. A decreased clustering coefficient in the right inferior parietal gyrus was associated with a larger allocentric navigation error. White matter hyperintensities (WMH) did not affect the correlation between network properties and SN accuracy. This study demonstrated that structural connectivity network abnormalities, especially in the frontal and parietal gyri, are associated with a lower SN accuracy, independently of WMH, providing a new insight into the brain mechanisms associated with SN impairment in MCI.

Keywords: graph theory, clustering coefficient, spatial navigation, mild cognitive impairment, network topology

INTRODUCTION

There is growing evidence that the human brain is a large-scale complex network (Seeley et al., 2009; Betzel et al., 2012). A network is represented as nodes that are connected by edges in the graph theory. A node is a brain region, and an edge is constructed by anatomical tracts or functional correlations. The structural network topological properties include the network efficiency properties (local efficiency and global efficiency), clustering coefficient (Cp), local shortest path length (Lp), and the node degree and betweenness centrality for the node properties. The global efficiency of a network (Eg) is measured by how information is exchanged over the network, meaning that how efficient the communication is between one brain region to another, and the local efficiency (Eloc) reflects the average efficiency of each local cluster of the network. Cp reflects that regions that are connected to the same region tend to be also connected to each other. Lp describes how many steps is needed for one brain region to be connected to another. The detailed definition of these properties coincided with several previous studies (Watts and Strogatz, 1998; Latora and Marchiori, 2001). The white matter structural networks in the healthy human brain usually exhibit a small-world character, which can optimally balance information segregation and integration, resulting in efficient organization that not only reduces the cost of maintaining many connections but also allows for efficient information movement (Gong et al., 2009). In contrast, patients with Alzheimer's disease (AD) dementia and mild cognitive impairment (MCI) showed abnormal properties of cortical networks and loss of small-world characteristics in previous studies that reported either local or global structural connectivity disruptions in these patients (Shu et al., 2012).

Spatial navigation (SN) is a complex domain that refers to the process of determining and maintaining a trajectory from one place to another (Lithfous et al., 2013). Specifically, there are two basic subtypes of SN: egocentric navigation (body-centered) and allocentric navigation (world-centered) (Nedelska et al., 2012). Impairment in both subtypes of SN is frequently reported in both AD dementia and MCI patients. Previous studies have indicated that these SN impairments are related to the degeneration in several brain regions, such as the hippocampus, caudate nucleus, and medial temporal lobe (Wegman et al., 2014). However, given the complexity of the human brain SN system, the structural connectivity networks that integrate these regions may also play critical roles in the SN process, and it would be beneficial to investigate their possible impairment in AD dementia and MCI. However, to the best of our knowledge, few studies have investigated the influence of structural network topological properties on SN.

In this study, we aimed to identify (1) which structural network topological properties show the greatest differences between MCI patients and normal controls (NCs) and (2) how these network properties of specific brain regions affect egocentric and allocentric SN accuracy in MCIs. We hypothesized that patients with MCI would demonstrate abnormalities in brain network topology and that these topological properties (e.g., global efficiency, clustering coefficient, and shortest path length) derived from the brain structural network could influence SN, which might provide a new insight into the structural basis of SN in the brain.

MATERIALS AND METHODS

Subjects

A total of 60 participants, 32 MCI patients and 28 NCs, were recruited from the Department of Neurology of the Affiliated Drum Tower Hospital of Nanjing University Medical School from May 2015 to June 2017. All subjects gave written informed consent to participate in the study, which was approved by the hospital ethics committee.

Exclusion criteria for NCs were the presence of cognitive complaints and neurological or psychiatric disorders. All participants were right-handed and underwent neuropsychological tests, including the Mini-Mental State Examination (MMSE) and Montreal Cognitive Assessment (MoCA). Patients with MCI met the clinical criteria established by Petersen (2004). The threshold for memory impairment was derived from the same literature and designated as scoring > 1.5 SD below the mean of age- and education-adjusted norms on a memory test.

Spatial Navigation Tests

Spatial navigation accuracy was tested by the PC test AMUNET (NeuroScios GmbH, Austria) that represents a human analog of the Morris water maze (MWM) task screen, which used the hidden goal task similar to previous studies (Weniger et al., 2009; Nedelska et al., 2012; Laczó et al., 2014). It is designed to distinguish two different strategies of navigation, egocentric ("Ego") representations concerning self-centered navigation and encoding spatial information from the viewpoint of the navigator, whereas allocentric ("Allo") strategies are centered on the object rather than on the observer (Lithfous et al., 2013). The AMUNET SN test battery was administered using three SN subtasks. Each subtask involved eight trials, hence 24 trials all together. The tasks were performed in a fixed order with increasing demanded. First, the Allo–Ego mixed subtask was first performed. A large circle representing the overhead view of the task arena was shown on the screen (280 pixels in diameter on a screen with a resolution of 640×480 pixels) (Qing et al., 2017). Participants were required to locate the goal point using its spatial relationship with both the starting position and the two distal orientation cues on the circle. Next, the Ego subtask was performed, which required the participants to use only the starting position to locate the goal when distal orientation cues were not displayed. Finally, in the Allo subtask, the participant was only allowed to use solely two distal orientation cues on the arena wall during SN to the goal, whereas the start position was randomly regenerated in each trial and was therefore unrelated to the correct goal position. The positions of the goal point were stable relative to (1) the positions of the starting location and orientation cues in the mixed Allo–Ego subtask, (2) the positions of the start location in the Ego subtask, and (3) the positions of orientation cues in the Allo task. The accuracy of the task was automatically recorded as

the distance error between the participants' final position and the actual goal location in millimeters. The SN performance from eight attempts per each subtask was averaged into the average total error per task (Chen et al., 2021). The time was unlimited to avoid the effect of individual differences in sensory and physical functioning.

MRI Techniques

Whole-brain MRI scans were obtained using an eight-channel phased array coil (Achieva 3.0T TX, Philips Medical Systems, Best, Netherlands). A three-dimensional high-resolution sagittal T_1W with turbo fast echo (3D-T_1TFE) acquisition was performed with a repetition time (TR), echo time (TE), and inversion time (TI) of 9.8, 4.6, and 900 ms, respectively. The other acquisition parameters were as follows: flip angle, 8°; matrix size, 256 × 256; field of view (FOV), 256 × 256 × 256 mm; isotropic resolution, 1.0 mm; slices in the third dimension, 192; and acquisition time, 6 min 43 s. Diffusion tensor imaging (DTI) was encoded along 32 independent orientations, and the *b*-value was 1,000 s/mm^2. The imaging parameters were as follows: TR/TE, 9,154/55 ms; FOV, 224 × 224 mm; slice thickness 2.5 mm; voxel size 2 × 2 × 2.5 mm^3; and acquisition time, 6 min 27 s.

Network Node and Edge Definition

We used the AAL atlas to parcellate the whole brain into 90 areas (45 regions in each hemisphere), which were defined as the nodes of the brain graph. The AAL atlas was transformed from Montreal Neurological Institute (MNI) space to T1 native space, which was non-linearly registered from the individual T1-weighted images.

The pre-processing of DTI data was carried out by PANDA (a pipeline toolbox for analyzing brain diffusion images) (Cui et al., 2013). The main procedure of PANDA includes (1) converting DICOM files into Neuroimaging Informatics Technology Initiative (NIfTI) imaging, (2) estimating the brain mask by using the bet command of the FMRIB Software Library (FSL), (3) cropping the raw images to cut off non-brain space in the raw images, and (4) correcting for the eddy-current effect by using the flirt and the eddy-correct FSL commands.

Then, we used PANDA to perform deterministic fiber tracking to obtain the fractional anisotropy (FA) matrix in two steps: (1) two nodes (regions) were considered to be structurally connected by an edge when the FA value of fiber tracts located in these two regions were between 0.2 and 1, and then (2) weighted structural networks represented by symmetric 90 × 90 matrices were constructed for each individual.

Network Parameter Analysis

Graph theoretical analysis was performed on the interregional connectivity matrix by using GRETNA[1], a graph theoretical network analysis toolbox for imaging connectomics. The weighted network properties were calculated, with a sparsity range of 0.05–0.4 with a step size of 0.01. Sparsity was defined as the total number of edges divided by the maximum possible number of edges. Because there is no gold standard to select a single threshold, we calculated the parameters with different thresholds. Finally, the networks were constructed at the sparsity of 0.14, which ensured all nodes included in the networks to present the nodal characteristics of the networks and ensured the most characteristic small-world topology. GRETNA was used to calculate the structural network topological properties, including the network efficiency properties (local efficiency and global efficiency), local Cp, global clustering coefficient [M(Cp)], local shortest path length (Lp), global shortest path length [M(Lp)], and the node degree and betweenness centrality for the node properties. For each subject, 1,000 times randomization was applied, and each time a corresponding random network was generated. Then, the random distribution of Cp and Lp was used to transform real Cp and Lp into a Z score by their position in the random distribution as previous studies (Wang et al., 2015). The brain networks were visualized with BrainNet Viewer[2] (Xia et al., 2013).

Measurement of WMH Volume

The total volume of white matter hyperintensity (WMH) on 3D-FLAIR images was automatically detected and quantified using the Wisconsin White Matter Hyperintensities Segmentation Toolbox (W2 MHS), which is an open-source toolbox. The major steps involved in WMH volume detection and measurement are as follows: (1) a pre-processing module in which SPM12b was used to construct the white matter (WM) region of interest and partial volume estimates of the tissues (WM, gray matter, and cerebrospinal fluid); (2) a segmentation module in which the random forest-based regression method was used to detect the WMH; and (3) a quantification module to summarize the WMH segmentations.

Statistical Analysis

Statistical analysis was performed using SPSS version 23.0 for the demographic data. The between-group differences of whole-network and nodal properties and differences in SN accuracy by average total error in each navigational subtask were evaluated by two-sample t-tests using a threshold of $p < 0.05$. For each whole-network topological property showing a significant difference between MCI patients and NCs, a general linear regression analysis was performed using two linear models between each of the network properties with the SN accuracy of each subtask. In model 1, the network property was used as an independent variable, and SN accuracy was used as a dependent variable, with age, sex, and education as covariates. In model 2, WMH volume was additionally included as an independent variable. We used a statistical significance level of $p < 0.05$ for all these analyses. Similarly, for each node showing significantly different nodal topological properties between MCI patients and NCs, the same correlational analyses were performed between the corresponding property and the accuracy of each of the three SN subtasks with the same covariates.

[1]https://www.nitrc.org/projects/gretna

[2]http://www.nitrc.org/projects/bnv/

RESULTS

Demographics and Behavioral Data

In this study, 32 subjects fulfilled the criteria of MCI. No significant differences in age (p = 0.194), sex (p = 0.196), or education level (p = 0.134) were detected between MCI patients and NCs. As expected, pathological alteration led to significant differences in the MMSE and MoCA scores between MCI patients and NCs. The full demographic and clinical characteristics of the subjects are shown in **Table 1**.

Spatial Navigation and Network Topology Properties

Our statistical analyses showed significant decreases in the global clustering coefficient and shortest path length in patients with MCI (**Table 2**). Regarding SN accuracy, MCI subjects showed worse Ego navigation accuracy compared to NCs (**Table 2**) with larger average total error. The specific areas of discrepant network properties of MCI patients and NCs are listed in **Table 3** and **Figure 1**, including the left middle frontal gyrus, right rectus, right superior parietal gyrus, right inferior parietal gyrus, and left paracentral lobule.

The Association Between Nodal Network Topology Properties and Spatial Navigation Accuracy

We observed a significantly positive correlation of the shortest path length in the left paracentral lobule with both the Allo–Ego average total error and the Allo average total error. There are no associations between the network topological properties and Ego average total error. A decreased Cp in the right inferior parietal gyrus was associated with a larger average total error in Allo navigation (**Table 4**).

TABLE 1 | Demographic and clinical characteristics of patients with mild cognitive impairment (MCI) and control participants.

	MCI (n = 32)	NCs (n = 28)	p
Age (years)			
Mean ± SD	65.91 ± 11.33	69.68 ± 10.79	0.194
Sex (%)			
Male	16 (50%)	19 (67.9%)	0.196
Female	16 (50%)	9 (32.1%)	
Edu (years)			
Mean ± SD	13.25 ± 3.46	14.54 ± 3.05	0.134
WMH (volume, mm^3)			
Mean ± SD	35,017 ± 37,275	38,850 ± 39,794	0.702
MMSE (score)			
Mean ± SD	25.97 ± 2.36	28.93 ± 0.97	<0.001*
MoCA (score)			
Mean ± SD	21.81 ± 2.13	27.43 ± 2.36	<0.001*

*Data are presented as the means ± standard deviations. *$p < 0.05$.*
MCI, mild cognitive impairment; NCs, normal controls; Edu, education; WMH, white matter hyperintensity; MMSE, Mini-Mental State Examination; MoCA, Montreal Cognitive Assessment, Beijing Version.

TABLE 2 | Differences in spatial navigation accuracy and the whole-brain network topology properties of patients with MCI and normal controls.

	MCI (n = 32)	NCs (n = 28)	T	p
AEV (mm)				
Mean ± SD	11.28 ± 9.59	8.67 ± 4.30	−1.32	0.190
EV (mm)				
Mean ± SD	15.79 ± 9.86	9.73 ± 5.39	−2.89	0.004*
AV (mm)				
Mean ± SD	12.55 ± 8.05	10.62 ± 5.76	−1.06	0.295
Eg				
Mean ± SD	0.20 ± 0.03	0.20 ± 0.02	0.12	0.901
Eloc				
Mean ± SD	0.27 ± 0.03	0.28 ± 0.02	1.14	0.114
M(Cp)				
Mean ± SD	28.03 ± 5.69	31.58 ± 7.07	2.15	0.035*
M(Lp)				
Mean ± SD	25.02 ± 7.53	28.91 ± 7.37	2.02	0.048*
Node betweenness				
Mean ± SD	67.59 ± 11.33	67.52 ± 9.84	−0.02	0.981
Node degree				
Mean ± SD	4.35 ± 0.95	4.43 ± 0.83	0.341	0.735

Data are presented as the means ± standard deviations. The Eg and Eloc are raw data and the M(Cp) and M(Lp) are z-score data.
MCI, mild cognitive impairment; NCs, normal controls; AEV, "allocentric + egocentric" average total error; EV, egocentric average total error; AV, allocentric average total error; Eg, global efficiency. Eloc, local efficiency; M(Cp), global clustering coefficient; M(Lp), global shortest path length.
$p < 0.05$.

TABLE 3 | Nodal network topology properties in patients with MCI and normal controls.

	MCI (n = 32)	NCs (n = 28)	T	p
Cp				
L-middle frontal gyrus				
Mean ± SD	0.27 ± 0.07	0.32 ± 0.10	2.393	0.020*
R-rectus				
Mean ± SD	0.22 ± 0.08	0.26 ± 0.04	2.335	0.023*
R-superior parietal gyrus				
Mean ± SD	0.28 ± 0.09	0.33 ± 0.09	2.169	0.034*
R-inferior parietal gyrus				
Mean ± SD	0.37 ± 0.09	0.43 ± 0.08	2.687	0.009*
Lp				
L-paracentral lobule				
Mean ± SD	5.55 ± 1.07	5.07 ± 0.86	-2.053	0.045*

Data are presented as the means ± standard deviations.
Cp, local clustering coefficient; Lp, local shortest path length; MCI, mild cognitive impairment; NCs, normal controls.
$p < 0.05$.

Taking the WMH volume into account, we found that the associations of the shortest path length in the left paracentral lobule with both the Allo–Ego average total error and the Allo average total error were the same as the findings for model 1, as was the decreased Cp for the right inferior parietal gyrus and Allo average total error.

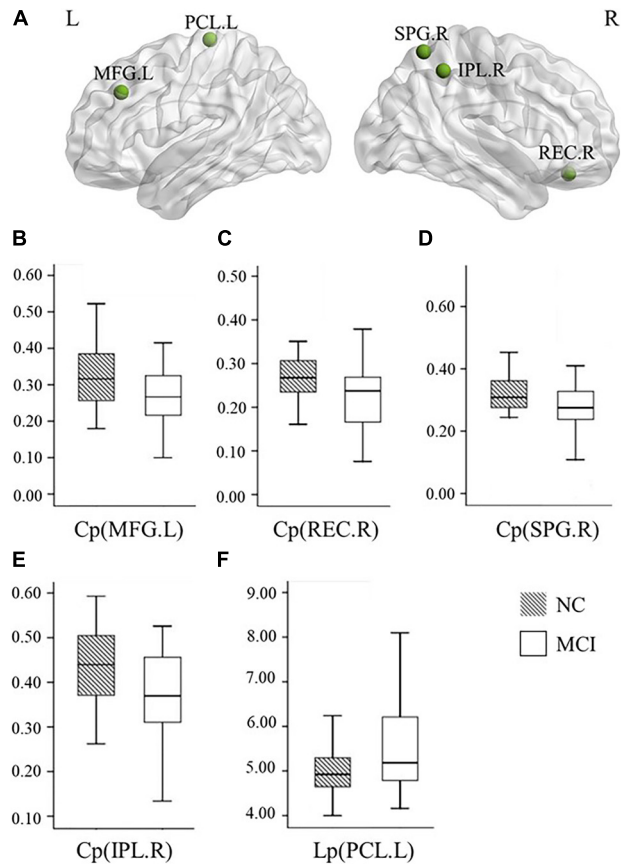

FIGURE 1 | Graphs show differences in the nodal network topological properties between the patients with MCI and normal controls. **(A)** The location of the node with significantly altered nodal network topological properties in MCI patients, compared with normal controls. **(B–E)** The nodal clustering coefficients in the left MFG (p = 0.020), right REC (p = 0.023), right SPG (p = 0.034), and right IPL (p = 0.009) were significantly different between the patients with MCI and normal controls. **(F)** The nodal shortest path length in the left PCL (p = 0.045) was significantly different between the patients with MCI and normal controls. NC, normal controls; MCI, mild cognitive impairment; L, left; R, right; Cp, local clustering coefficient; Lp, local shortest path length; MFG, middle frontal gyrus; REC, rectus; SPG, superior parietal gyrus; IPL, inferior parietal gyrus; PCL, paracentral lobule.

DISCUSSION

This study measured the brain network abnormality, SN, and cognitive impairment in MCI patients. We found a lower egocentric navigation accuracy in MCI patients compared to NCs. We showed an abnormal organization in the structural connectivity networks of MCI patients, reflected by decreased Cp and decreased Lp. The brain areas of abnormal network properties were in the left middle frontal gyrus, right rectus, right superior parietal gyrus, right inferior parietal gyrus, and left paracentral lobule, therefore predominantly in the frontal and parietal gyri. Further, the abnormal network properties were measured in several other brain regions, including the larger shortest path length in the left paracentral lobule and decreased Cp in the right inferior parietal gyrus. These abnormal network properties predicted the SN impairment, irrespective of the white matter hyperintensities.

Egocentric and allocentric navigation strategies involve different neurobiological underpinnings. Generally, allocentric navigation is mainly supported by the hippocampus and parahippocampus (Muller et al., 1996). On the other hand, egocentric navigation is supposed to rely on the parietal lobe and the retrosplenial cortex mostly (Epstein and Ward, 2010; Nemmi et al., 2017). Successful navigation does not rely on one single strategy but requires the ability to switch between and combine the different spatial strategies in a flexible manner (Colombo et al., 2017). In the previous study, the amnestic MCI single-domain patients showed both the allocentric and the egocentric navigation impairment (Hort et al., 2007). Potentially, because we did not classify our MCIs into amnestic versus non-amnestic subtypes, we found egocentric navigation but not allocentric navigation impairment in these MCI patients. It also might be the relatively younger population of MCI patients in our study, which sometimes show hippocampal sparing subtype of AD (Jellinger, 2020).

To date, SN accuracy has not been explored regarding the relationship to whole-brain structural network properties based on the graph theoretical approach. Subjects using an Allo strategy revealed stronger activations in some nearby basal regions (hippocampus and thalamus) (Henke et al., 2003), while Ego navigation has been shown to rely on corticostriatal regions of the brain (Wolbers and Wiener, 2014). A previous study found that the parietal lobe is involved in the dynamic aspects of spatial memory and makes contribution to topographic memory (Berthoz, 1997). We also found a hypoactive brain structural network in the right inferior parietal gyrus is related to worse allocentric navigation skill. Another fMRI study found SN performance-related activation of the inferior parietal cortex, suggesting that this area participates in the encoding of spatial relationships between consecutive landmarks in an egocentric reference frame, defined relative to the observer's direction when facing the first landmark (Wolbers et al., 2004). A study using structural MRI study showed that the atrophy of the right inferior parietal cortex in amnesic MCI patients was related to the deficits in allocentric and egocentric navigation toward a target in a familiar virtual environment (Weniger et al., 2011).

The graph theory measures reflect how well a region is connected to its neighboring areas and within brain modules, providing important information on the network's capability for specialized processing within densely interconnected groups of brain regions (Rubinov and Sporns, 2010). Usually, randomly organized networks are characterized by a low Cp (a measure that depicts the connection of immediate neighbors around individual vertices) and a short path length (an index reflecting the overall integration of the network). The small-world network, characterized by a high degree of clustering and a short path length between individual network nodes, has been an attractive model for the description of complex brain networks (Wu et al., 2012). Researchers have found that both anatomical and functional brain networks are

TABLE 4 | General linear regression analyses between nodal network topology properties and spatial navigation accuracy.

	Allo–Ego				Ego				Allo			
	Model 1		Model 2		Model 1		Model 2		Model 1		Model 2	
	Beta (SE)	*p*	Beta (SE)	*p*	Beta (SE)	*p*	Beta (SE)	*p*	Beta (SE)	*p*	Beta (SE)	*p*
Cp												
	−0.2	0.10	−0.1	−0.2	0.10	0.2	0.15	0.2	−0.2	0.07	−0.2	0.07
L-middle frontal gyrus	14	3	70	13	6	45	3	36	22	8	22	7
R-rectus	−0.601	0.550	−0.075	0.594	−0.043	0.749	−0.084	0.535	0.123	0.343	0.105	0.432
R-superior parietal gyrus	0.005	0.971	0.007	0.965	−0.145	0.270	−0.156	0.233	0.011	0.929	0.005	0.967
R-inferior parietal	−0.235	0.078	−0.235	0.080	−0.127	0.339	−0.126	0.337	−0.278	**0.028***	−0.278	**0.029***
Lp												
L-paracentral lobule	0.361	**0.011***	0.361	**0.011***	0.235	0.099	0.234	0.098	0.348	**0.011***	0.348	**0.011***

The spatial navigation average total errors (AEV, EV, and AV) were set as independent variables. The different network topology properties of specific brain areas in MCI patients were set as dependent variables. In all models, we controlled for age, sex, and education and the volume of WMH was added to model 2.
Cp, local clustering coefficient; Lp, local shortest path length.
*$p < 0.05$.

small-world networks (Achard and Bullmore, 2007; Bassett and Bullmore, 2016). The brain network topology showed the small-world characteristic in both AD dementia and MCI, but it changed significantly compared to NCs (Liu et al., 2012; Zhao et al., 2012). A previous study also indicated increased short path length in AD and decreased Cp in amnestic MCI (Bai et al., 2012). In the current study, we found a decreased Cp in MCI patients, which is similar to a previous study, indicating worse local communication between the left middle frontal gyrus, the right superior and inferior parietal gyrus, and neighboring areas in the brain, respectively.

The brain topology alterations of specific brain node regions were also observed, in addition to global network changes. We found a decreased short path length of the left paracentral lobule, which means a loss of the number of connections between these structures and other regions of the network. This could be related to WM integrity loss or a disruption of WM fibers connecting these brain areas, which has been previously observed in MCI and AD patients in DTI studies (Chua et al., 2008). The decreased connectivity of the left paracentral lobule to neighboring areas was related to worse SN accuracy and, more importantly, the burden of WMH had no effects on this relationship. This may indicate that the network alteration and the SN impairment were due to degeneration, not ischemic lesion, which may need to be confirmed with a larger sample size in the future.

There were some limitations in our study. First, we had a relatively small sample size in this study. Second, the computerized test based on the MWM paradigm may be a useful tool for the evaluation of SN deficits (Laczo et al., 2014). However, it should be noted that the real-space and computerized two-dimensional versions are not fully interchangeable, as the computerized SN tasks lack proprioceptive feedback that is normally available in real-world navigation tasks and that contribute to successful navigation. Third, in humans spatial cognition evaluation is much more difficult, as navigation in complex real-world environments does not allow experimental control of the tasks, making it difficult to determine the mechanisms that sustain performances. Fourth, we did not analyze the specific structural connection between any two brain nodes and this would be of great significance in the future.

In conclusion, patients with MCI demonstrate abnormalities in brain network topology, and the disruption of these topological properties (e.g., Cp and shortest path length) derived from the brain structural network influences the SN process. These results may fuel future research on the brain structure basis of SN, which can provide new insight into brain mechanisms in SN impairments with network topological properties.

DATA AVAILABILITY STATEMENT

The datasets presented in this study can be found in online repositories. The name of the repository can be found at: https://pan.baidu.com/s/14bm0x3tikemnFteKQAJcxw with the following password - r6q8.

ETHICS STATEMENT

The studies involving human participants were reviewed and approved by the Ethics Committee of Gulou Hospital affiliated to Nanjing University Medical College (2016–065–01). The patients/participants provided their written informed consent to participate in this study.

AUTHOR CONTRIBUTIONS

All authors listed have made substantial, direct and intellectual contribution to the work, and approved it for publication.

FUNDING

This work was supported by the National Natural Science Foundation of China (81720108022 to BZ, 81971596 to XZ, and 82071904 to ZQ). This work was also supported by the Fundamental Research Funds for the Central Universities, Nanjing University (2020-021414380462), The Key Project of Jiangsu Commission of Health (K2019025), Key Medical Talents of the Jiangsu Province, the "13th Five-Year" Health Promotion Project of the Jiangsu Province (ZDRCA2016064), Jiangsu Provincial Key Medical Discipline (Laboratory) (ZDXKA2016020), and the Project of the Sixth Peak of Talented People (WSN-138). The funders had no role in the study design, data collection and analysis, decision to publish, or preparation of the manuscript.

REFERENCES

Achard, S., and Bullmore, E. (2007). Efficiency and cost of economical brain functional networks. *PLoS Comput. Biol.* 3:e17. doi: 10.1371/journal.pcbi.0030017

Bai, F., Shu, N., Yuan, Y., Shi, Y., Yu, H., Wu, D., et al. (2012). Topologically convergent and divergent structural connectivity patterns between patients with remitted geriatric depression and amnestic mild cognitive impairment. *J Neurosci.* 32, 4307–4318. doi: 10.1523/JNEUROSCI.5061-11.2012.

Bassett, D. S., and Bullmore, E. T. (2016). Small-world brain networks revisited. *Neuroscientist* 23, 499–516. doi: 10.1177/1073858416667720

Berthoz, A. (1997). Parietal and hippocampal contribution to topokinetic and topographic memory. *Philos. Trans. R Soc. Lond. B Biol. Sci.* 352, 1437–1448. doi: 10.1098/rstb.1997.0130

Betzel, R. F., Erickson, M. A., Abell, M., O'Donnell, B. F., Hetrick, W. P., and Sporns, O. (2012). Synchronization dynamics and evidence for a repertoire of network states in resting EEG. *Front. Comput. Neurosci.* 6:74. doi: 10.3389/fncom.2012.00074

Chen, Q., Wu, S., Li, X., Sun, Y., Chen, W., Lu, J., et al. (2021). Basal forebrain atrophy is associated with allocentric navigation deficits in subjective cognitive decline. *Front. Aging Neurosci.* 13:596025. doi: 10.3389/fnagi.2021.596025

Chua, T. C., Wen, W., Slavin, M. J., and Sachdev, P. S. (2008). Diffusion tensor imaging in mild cognitive impairment and Alzheimer's disease: a review. *Curr. Opin. Neurol.* 21, 83–92. doi: 10.1097/WCO.0b013e3282f4594b

Colombo, D., Serino, S., Tuena, C., Pedroli, E., Dakanalis, A., Cipresso, P., et al. (2017). Egocentric and allocentric spatial reference frames in aging: a systematic review. *Neurosci. Biobehav. Rev.* 80, 605–621. doi: 10.1016/j.neubiorev.2017.07.012

Cui, Z., Zhong, S., Xu, P., He, Y., and Gong, G. (2013). PANDA: a pipeline toolbox for analyzing brain diffusion images. *Front. Hum. Neurosci.* 7:42. doi: 10.3389/fnhum.2013.00042

Epstein, R. A., and Ward, E. J. (2010). How reliable are visual context effects in the parahippocampal place area? *Cereb. Cortex* 20, 294–303. doi: 10.1093/cercor/bhp099

Gong, G., He, Y., Concha, L., Lebel, C., Gross, D. W., Evans, A. C., et al. (2009). Mapping anatomical connectivity patterns of human cerebral cortex using in vivo diffusion tensor imaging tractography. *Cereb. Cortex* 19, 524–536. doi: 10.1093/cercor/bhn102

Henke, K., Treyer, V., Weber, B., Nitsch, R. M., Hock, C., Wieser, H. G., et al. (2003). Functional neuroimaging predicts individual memory outcome after amygdalohippocampectomy. *Neuroreport* 14, 1197–1202. doi: 10.1097/01.wnr.0000081865.45938.64

Hort, J., Laczó, J., Vyhnálek, M., Bojar, M., Bures, J., and Vlcek, K. (2007). Spatial navigation deficit in amnestic mild cognitive impairment. *Proc. Natl. Acad. Sci. U. S. A.* 104, 4042–4047. doi: 10.1073/pnas.0611314104

Jellinger, K. A. (2020). Pathobiological subtypes of Alzheimer disease. *Dement. Geriatr. Cogn. Disord.* 49, 321–333. doi: 10.1159/000508625

Laczó, J., Andel, R., Vyhnalek, M., Vlcek, K., Nedelska, Z., Matoska, V., et al. (2014). APOE and spatial navigation in amnestic MCI: results from a computer-based test. *Neuropsychology* 28:676.

Laczo, J., Andel, R., Vyhnalek, M., Vlcek, K., Nedelska, Z., Matoska, V., et al. (2014). APOE and spatial navigation in amnestic MCI: results from a computer-based test. *Neuropsychology* 28, 676–684. doi: 10.1037/neu0000072

Latora, V., and Marchiori, M. (2001). Efficient behavior of small-world networks. *Phys. Rev. Lett.* 87:198701. doi: 10.1103/PhysRevLett.87.198701

Lithfous, S., Dufour, A., and Despres, O. (2013). Spatial navigation in normal aging and the prodromal stage of Alzheimer's disease: insights from imaging and behavioral studies. *Ageing Res. Rev.* 12, 201–213. doi: 10.1016/j.arr.2012.04.007

Liu, Z., Zhang, Y., Yan, H., Bai, L., Dai, R., Wei, W., et al. (2012). Altered topological patterns of brain networks in mild cognitive impairment and Alzheimer's disease: a resting-state fMRI study. *Psychiatry Res.* 202, 118–125. doi: 10.1016/j.pscychresns.2012.03.002

Muller, R. U., Stead, M., and Pach, J. (1996). The hippocampus as a cognitive graph. *J. Gen. Physiol.* 107, 663–694. doi: 10.1085/jgp.107.6.663

Nedelska, Z., Andel, R., Laczó, J., Vlcek, K., Horinek, D., Lisy, J., et al. (2012). Spatial navigation impairment is proportional to right hippocampal volume. *Proc. Natl. Acad. Sci. U. S. A.* 109, 2590–2594.

Nemmi, F., Boccia, M., and Guariglia, C. (2017). Does aging affect the formation of new topographical memories? Evidence from an extensive spatial training. *Neuropsychol. Dev. Cogn. B Aging Neuropsychol. Cogn.* 24, 29–44. doi: 10.1080/13825585.2016.1167162

Petersen, R. C. (2004). Mild cognitive impairment as a diagnostic entity. *J. Intern. Med.* 256, 183–194. doi: 10.1111/j.1365-2796.2004.01388.x

Qing, Z., Li, W., Nedelska, Z., Wu, W., Wang, F., Liu, R., et al. (2017). Spatial navigation impairment is associated with alterations in subcortical intrinsic activity in mild cognitive impairment: a resting-state fMRI study. *Behav. Neurol.* 2017:6364314. doi: 10.1155/2017/6364314

Rubinov, M., and Sporns, O. (2010). Complex network measures of brain connectivity: uses and interpretations. *Neuroimage* 52, 1059–1069. doi: 10.1016/j.neuroimage.2009.10.003

Seeley, W. W., Crawford, R. K., Zhou, J., Miller, B. L., and Greicius, M. D. (2009). Neurodegenerative diseases target large-scale human brain networks. *Neuron* 62, 42–52. doi: 10.1016/j.neuron.2009.03.024

Shu, N., Liang, Y., Li, H., Zhang, J., Li, X., Wang, L., et al. (2012). Disrupted topological organization in white matter structural networks in amnestic mild cognitive impairment: relationship to subtype. *Radiology* 265, 518–527.

Wang, J., Wang, X., Xia, M., Liao, X., Evans, A., and He, Y. (2015). GRETNA: a graph theoretical network analysis toolbox for imaging connectomics. *Front. Hum. Neurosci.* 9:386. doi: 10.3389/fnhum.2015.00386

Watts, D. J., and Strogatz, S. H. (1998). Collective dynamics of 'small-world' networks. *Nature* 393, 440–442. doi: 10.1038/30918

Wegman, J., Fonteijn, H. M., van Ekert, J., Tyborowska, A., Jansen, C., and Janzen, G. (2014). Gray and white matter correlates of navigational ability in humans. *Hum. Brain Mapp.* 35, 2561–2572. doi: 10.1002/hbm.22349

Weniger, G., Ruhleder, M., Lange, C., Wolf, S., and Irle, E. (2011). Egocentric and allocentric memory as assessed by virtual reality in individuals with amnestic mild cognitive impairment. *Neuropsychologia* 49, 518–527. doi: 10.1016/j.neuropsychologia.2010.12.031

Weniger, G., Ruhleder, M., Wolf, S., Lange, C., and Irle, E. (2009). Egocentric memory impaired and allocentric memory intact as assessed by virtual reality in subjects with unilateral parietal cortex lesions. *Neuropsychologia* 47, 59–69.

Wolbers, T., Weiller, C., and Buchel, C. (2004). Neural foundations of emerging route knowledge in complex spatial environments. *Brain*

Res. Cogn. Brain Res. 21, 401–411. doi: 10.1016/j.cogbrainres.2004.06.013

Wolbers, T., and Wiener, J. M. (2014). Challenges for identifying the neural mechanisms that support spatial navigation: the impact of spatial scale. *Front. Hum. Neurosci.* 8:571. doi: 10.3389/fnhum.2014.00571

Wu, K., Taki, Y., Sato, K., Kinomura, S., Goto, R., Okada, K., et al. (2012). Age-related changes in topological organization of structural brain networks in healthy individuals. *Hum. Brain Mapp.* 33, 552–568. doi: 10.1002/hbm.21232

Xia, M., Wang, J., and He, Y. (2013). BrainNet viewer: a network visualization tool for human brain connectomics. *PLoS One* 8:e68910. doi: 10.1371/journal.pone.0068910

Zhao, X., Liu, Y., Wang, X., Liu, B., Xi, Q., Guo, Q., et al. (2012). Disrupted small-world brain networks in moderate Alzheimer's disease: a resting-state FMRI study. *PLoS One* 7:e33540. doi: 10.1371/journal.pone.0033540

Conflict of Interest: The authors declare that the research was conducted in the absence of any commercial or financial relationships that could be construed as a potential conflict of interest.

frontiers in Aging Neuroscience

ORIGINAL RESEARCH
published: 11 June 2021
doi: 10.3389/fnagi.2021.684918

Local Functional MR Change Pattern and Its Association With Cognitive Function in Objectively-Defined Subtle Cognitive Decline

Liang Cui[1†], *Zhen Zhang*[1†], *Chun-Yi Zac Lo*[2*] *and Qihao Guo*[1*]

[1]*Department of Gerontology, Shanghai Jiao Tong University Affiliated Sixth People's Hospital, Shanghai, China,* [2]*Institute of Science and Technology for Brain Inspired Intelligence, Fudan University, Shanghai, China*

Introduction: To identify individuals with preclinical cognitive impairment, researchers proposed the concept of objectively-defined subtle cognitive decline (Obj-SCD). However, it is not clear whether Obj-SCD has characteristic brain function changes. In this study, we aimed at exploring the changing pattern of brain function activity in Obj-SCD individuals and the similarities and differences with mild cognitive impairments (MCI).

Method: 37 healthy control individuals, 25 Obj-SCD individuals (with the impairment in memory and language domain), and 28 aMCI individuals were included. Resting-state fMRI and neuropsychological tests were performed. fALFF was used to reflect the local functional activity and compared between groups. Finally, we analyzed the correlation between the fALFF values of significantly changed regions and neuropsychological performance.

Results: We found similar functional activity enhancements in some local brain regions in the Obj-SCD and aMCI groups, including the left orbital part of the inferior frontal gyrus and the left median cingulate and paracingulate gyri. However, some changes in local functional activities of the Obj-SCD group showed different patterns from the aMCI group. Compared with healthy control (HC), the Obj-SCD group showed increased local functional activity in the right middle occipital gyrus, decreased local functional activity in the left precuneus and the left inferior temporal gyrus. In the Obj-SCD group, in normal band, the fALFF value of the right middle occipital gyrus was significantly negatively correlated with Mini-Mental State Examination (MMSE) score ($r = -0.450$, $p = 0.024$) and Animal Verbal Fluency Test (AFT) score ($r = -0.402$, $p = 0.046$); the left inferior temporal gyrus was significantly positively correlated with MMSE score ($r = 0.588$, $p = 0.002$). In slow-4 band, the fALFF value of the left precuneus was significantly positively correlated with MMSE score ($r = 0.468$, $p = 0.018$) and AFT score ($r = 0.600$, $p = 0.002$). In the aMCI group, the fALFF value of the left orbital part of the inferior frontal gyrus was significantly positively correlated with Auditory Verbal Learning Test (AVLT) long delay cued recall score ($r = 0.506$, $p = 0.006$).

Conclusion: The Obj-SCD group showed a unique changing pattern; the functional changes of different brain regions have a close but different correlation with cognitive

OPEN ACCESS

Edited by:
Jiehui Jiang,
Shanghai University, China

Reviewed by:
Qianhua Zhao,
Fudan University, China
Bin Zhou,
Foundation for Biomedical Research and Innovation at Kobe, Japan

***Correspondence:**
Chun-Yi Zac Lo
zaclocy@gmail.com
Qihao Guo
qhguo@sjtu.edu.cn

†These authors have contributed equally to this work

Received: *24 March 2021*
Accepted: *10 May 2021*
Published: *11 June 2021*

Citation:
Cui L, Zhang Z, Zac Lo C-Y and Guo Q (2021) Local Functional MR Change Pattern and Its Association With Cognitive Function in Objectively-Defined Subtle Cognitive Decline. Front. Aging Neurosci. 13:684918. doi: 10.3389/fnagi.2021.684918

impairment, indicating that there may be a complex pathological basis inside. This suggests that Obj-SCD may be a separate stage of cognitive decline before aMCI and is helpful to the study of preclinical cognitive decline.

Keywords: objectively-defined subtle cognitive decline, mild cognitive impairment, function activity, resting-state functional MRI, cognitive function

INTRODUCTION

In the study of preclinical Alzheimer's disease (AD), some researchers have proposed that there is another kind of cognitive impairment in addition to SCD (subjective cognitive dysfunction), namely Objectively-defined subtle cognitive decline (Obj-SCD). In individuals with Obj-SCD, only subtle cognitive decline can be objectively detected; they have a roughly normal cognitive function and have no memory decline complaints. Obj-SCD is defined using six neuropsychological test indicators, including two memory function indicators, two language function indicators, and two attention/execution indicators. Memory function indicators include: total score of Auditory Verbal Learning Test (AVLT) 20-min free delayed recall and total score of AVLT recognition language function indicators includes: Animal Fluency (total score) and 30-item Boston Naming Test (BNT; total score) attention/execution indicators includes: Trail Making Test (TMT) A and Trail Making Test B (time to completion). An individual is defined as Obj-SCD if they meet the following conditions: (1) Does not meet the standards of Mild cognitive impairments (MCI); and (2) In two of the three different cognitive domains (memory, language, attention/execution), only one indicator is impaired (>1 SD below demographically adjusted mean; Thomas et al., 2018, 2020).

Currently, the studies on Obj-SCD are mainly focused on preclinical AD. AD is considered a continuous process that can be diagnosed before clinical symptoms appear (Dubois et al., 2016). The National Institute on Aging and Alzheimer's Association (NIA-AA) divided AD's cognitive decline procession into six stages; Obj-SCD locates in the middle state between normal cognitive function and mild cognitive impairment (MCI; Jack et al., 2018). A 10-year longitudinal study based on the AD Neuroimaging Initiative showed that individuals with Obj-SCD progressed to MCI 2.5–3.4 times faster than the normal group (Thomas et al., 2018). An arterial spin labeling MRI study reported that compared with the normal cognitive function group, the cerebral blood flow of the Obj-SCD participants increased in the hippocampus and inferior parietal; compared with the MCI group, the cerebral blood flow increased in the hippocampus, inferior parietal, and inferior temporal (Thomas et al., 2021). A longitudinal study for 4 years found that Obj-SCD amyloid protein accumulated faster and showed faster thinning of the internal olfactory cortex than the normal group (Thomas et al., 2020). However, some researchers have used Obj-SCD to describe the early cognitive decline stage due to other causes, such as Parkinson's dementia (PD). A study of PD patients revealed that participants in the Obj-SCD stage are more likely to progress to MCI due to PD or dementia due to Parkinson's disease within 5 years (Jones et al., 2021).

Amnestic MCI (aMCI) is a subtype of MCI (Petersen, 2011). AMCI can remain stable or progress to AD; it may also develop into other forms of dementia (Petersen et al., 2001; Caminiti et al., 2018; Cerami et al., 2018; Curiel Cid et al., 2020). Individuals with aMCI have objective memory disorders, subjective memory complaints, and slightly impaired daily activities; all of the above can be detected by neuropsychological tests.

AMCI individuals have two impaired indicators in the memory function domain, therefore, there are similarities and differences between memory function impaired Obj-SCD (single memory function indicator and single another cognitive domain indicator) and single-domain aMCI (only two indicators of memory function are impaired). In terms of neuropsychological performance, cognitive impairment of the single-domain aMCI exists only in the memory domain and is severer than that of Obj-SCD.

There are many core biomarkers used in the diagnosis of cognitive impairment. The guidelines on AD proposed by NIA-AA define the biomarkers for early diagnosis of AD as A/T/N regimens, including Aβ42, total Tau, phosphorylated Tau in cerebrospinal fluid, and the detected value of Aβ42 and Tau by PET CT (Scheltens et al., 2016; Jack et al., 2018). The abnormal accumulation of α-synuclein aggregates can be used as a biomarker of some non-AD pathological dementia, such as PD, dementia with Lewy bodies, and multiple system atrophy (Manne et al., 2019). However, some of these biomarkers are too expensive, and some can only be detected through invasive tests; therefore, they are challenging to be popularized and widely adopted.

This calls for the development of a relatively simple and non-invasive method that is needed to detect early cognitive impairment. MRI can be used to screen individuals at risk of cognitive impairment (Dubois et al., 2016). In the various research methods of MRI, Resting-state functional magnetic resonance imaging (rs-fMRI) has been widely applied in the study of cognitive decline (Pan et al., 2017; Bi et al., 2020a,b; Moguilner et al., 2020). A functional connectivity study showed that the normal cognitive individuals with amyloid positive are characterized by decreased functional connectivity between the medial temporal lobe and the anterior temporal lobe system (Berron et al., 2020). Another study on default mode network (DMN) connection found that the change of functional connection mode in AD is mainly in the SLOW-4 and SLOW-5 bands; the change is frequency-dependent (Li et al., 2017). However, functional connections can only reflect the connection between different brain regions and cannot

measure spontaneous activity intensity in a particular brain region (Jia et al., 2020).

Therefore, there is a need for an indicator that reflects the characteristics of local brain activity. The human brain produces numerous oscillatory waves; low-frequency fluctuation amplitude (ALFF) can reflect brain oscillatory activity's local characteristics (Zou et al., 2008). However, ALFF is easily disturbed by physiological noise. Compared with ALFF, fractional ALFF (fALFF) can reflect the relative contribution of low-frequency fluctuations in a specific frequency band to the whole detectable frequency range, and it is not easily affected by noise (Zuo et al., 2010).

However, few studies on Obj-SCD based on fMRI have been conducted so far. We speculate that the reason might be that Obj-SCD is in the very early stage of cognitive decline, and thus detection of minor pathological changes using conventional fMRI methods is difficult. Therefore, we want to study the change of fALFF in multiple frequency bands through frequency division. We also included patients with aMCI in order to understand the similarities and differences between the Obj-SCD and the aMCI group.

This study mainly used fALFF to explore the changing pattern of regional brain function activities of Obj-SCD individuals in different frequency bands and explore the similarities and differences of the patterns between Obj-SCD and aMCI groups. We hypothesized that if Obj-SCD is indeed a unique stage before aMCI, then the local neural activity may have changes similar to aMCI, but some changes may also be different from aMCI. Since Obj-SCD may be in the pathological stage before aMCI, this difference may be related to functional compensation. To prove this hypothesis, we also analyzed the correlation between functional activity and neuropsychological performance.

MATERIALS AND METHODS

Participants

In this study, 90 participants from local communities were recruited, including 37 healthy control individuals, 25 Obj-SCD individuals, and 28 aMCI individuals. Recruitment was carried out through advertising from August 2018 to November 2019.

Participants in this study had to meet the following criteria: (1) Chinese speakers; (2) have no history of disease that seriously affects brain function, such as craniocerebral injury, brain tumor, cerebral hemorrhage, cerebral infarction, and other systemic diseases that affect brain function (such as vitamin B12 deficiency and syphilis); (3) can complete neuropsychological tests, have no severe hearing, and visual impairment; and (4) can complete the examination of craniocerebral MRI.

Inclusion criteria of the healthy control (HC) group: (1) Mini-Mental State Examination (MMSE) score (illiteracy > 19, 1–6 education years >22, more than six education years > 26; Katzman et al., 1988); (2) a Clinical Dementia Rating (CDR) score = 0 (Morris, 1993); (3) Hamilton Depression Rating Scale score of ≤12 (Worboys, 2013); (4) no memory complaints; and (5) no evidence of memory loss provided by the observer.

Inclusion criteria of Obj-SCD group: (1) not meet Jak/Bondi criteria for MCI (Bondi et al., 2014); and (2) have and only have one impaired indicator (>1 SD below demographically adjusted mean) in two different cognitive domains (memory, language, attention/executive; Thomas et al., 2018, 2020). Neuropsychological tests used to diagnose Obj-SCD were as follows. Two measures of language: Animal Fluency (total score) and 30-item BNT (total score), two scores from a measure of attention/executive function: Trail Making Test, Parts A and B (time to completion); two scores from a measure of memory: Auditory Verbal Learning Test (AVLT) 20-min free delayed recall and AVLT recognition. For the consistency of the cohort, we included individuals with cognitive impairment in memory and language domains.

Inclusion criteria of the aMCI group: (1) with evidence of subjective memory complaints in the past year either by themselves or from bystanders; (2) MMSE above cut-off (>24/30); (3) objective memory impairment: two indicators of AVLT (long–delay free recall and recognition of AVLT) lower than the normal average of age correction >1 SD; (4) less than one item in the Activity of Daily Living Scale (ADL) changed; and (5) according to the NIA-AA criteria, there is no evidence of dementia (Bondi et al., 2014).

Neuropsychological Tests

All the individuals participated in the following neuropsychological tests: General cognitive function: MMSE (total score: 30; Folstein et al., 1975).

Memory function: Auditory Verbal Learning Test (AVLT; score: 12 per round, immediate recall score equals the sum of the first, second, and third recall scores, recognition score: 24; Zhao et al., 2015); Brief Visuospatial Memory Test (BVMT; score: 12 per round, immediate recall score equals the sum of the first, second and third recall scores; Pliskin et al., 2020).

Language function: Animal Verbal Fluency Test (AFT; Zhao et al., 2013a), BNT (total score: 30; Mack et al., 1992).

Executive function: Shape Trail Test (STT; Zhao et al., 2013b), Stroop Test (total score: 24; Chen et al., 2019). For cultural fairness, we use STT instead of TMT to evaluate executive function.

Spatial Function: Judgment of Line Orientation (JLO; total score: 30; Qualls et al., 2000).

Attention function: Digit Span Test (DST; forward score: 12; backward score: 10; Johansson and Berg, 1989).

Functional Magnetic Resonance Imaging

MRI Data Acquisition

All Resting-state fMRI images were collected using a 3.0-Tesla scanner (SIEMENS MAGNETOM Prisma 3.0 T, Siemens, Erlangen, Germany). Before the scans, the participants were told to close their eyes, stay relaxed, do not fall asleep, and move as little as possible. The image is obtained through an echo plane imaging sequence with the following parameters: repetition time (TR)/echo time (TE), 800/37 ms, flip angle (FA), 52°, matrix size, 104 × 104, the field of view, 208 mm × 208 mm, slice number, 72 slices, slice thickness, 2 mm, voxel size,

2 mm × 2 mm × 2 mm. It took 404 s to get 488 slices through scanning.

Imaging Data Processing

All functional imaging data were processed by Statistica Parametric Mapping 12 (SPM12)[1] and RESTplus[2] toolkits. The first 30 time points were discarded to stabilize the magnetic field and make the participants adjust to the environment. Then, the following preprocessing steps were performed: realign the head motion (participants whose head movement over 3 mm or more 3° had been excluded), spatially normalized to the Montreal Neurological Institute (MNI) space and resampled to 3 mm isotropic voxels, remove linear and quadratic trends of the time-series signals, regress out the sign (including white matter, cerebrospinal fluid, global mean signal, and Friston-24 motion parameters), the smoothing was done by Full Wave at Half Maximum 6 mm.

The preprocessed data were imported into the RESTplus toolkit and the fALFF in the normal band (0.01–0.08 Hz), slow4 band (0.027–0.073 Hz), and slow5 band (0.01–0.027 Hz) were calculated. For standardization, each voxel's fALFF values were divided by the global average fALFF values of all voxels in the whole brain to obtain each participant's mfALFF map.

Statistical Analysis

Demographic and neuropsychological test scores were analyzed using SPSS (IBM SPSS Statistics, Version 26.0. IBM Corp., Armonk, NY, USA). The normality test of the data was performed using the Shapiro—Wilke normality test. Mean and the standard deviation was used to represent normally distributed data. Median (quartile range) is used to represent non-normally distributed data. Differences in age, education years, sex, hypertension, diabetes, and hyperlipidemia were analyzed using the Pearson chi-square test. ANOVA test was used to analyze neuropsychological test scores that fit the normal distribution between the three groups. Nonparametric tests (the Kruskal-Wallis H test) were used to analyze neuropsychological test scores that did not fit the normal distribution between the three groups. Bonferroni's correction was used for multiple comparisons in posthoc analysis. Spearman rank correlation analysis was used to analyze the correlation between mfALLF and neuropsychological test scores.

RESTplus toolkit was used in the statistical analysis of image data. To accurately display the similarities and differences between the three groups, we conducted ANOVA analysis on the mFalff diagrams of the three groups, the threshold was set to 0.05, and a binary mask was obtained to limit the range of comparison between the groups. Multiple comparison corrections were performed using the false discovery rate (FDR) for the comparison between groups. Since multiple comparisons were involved, the FDR correction threshold was set to 0.017 to reduce the false-positive rate.

[1]http://www.fil.ion.ucl.ac.uk/spm/software/spm12/
[2]http://restfmri.net/forum/restplus

The mfALFF values of the significant clusters were extracted and correlated with neuropsychological tests by Spearman rank analysis.

RESULTS

Demographic Data and Neuropsychological Performances

There were no statistical differences in age, sex, and education years among the three groups. There were no statistical differences in hypertension (24.3% in HC group, 40.0% in SCD group, 32.1% in aMCI group), hypercholesterolemia (8.1% in HC group, 16.0% in SCD group, 10.7% in aMCI group), and diabetes (13.5% in HC group, 20.0% in SCD group, 14.3% in aMCI group) among the three groups (**Table 1**).

All the Obj-SCD individuals included in the study showed impairment of a single neuropsychological test indicator of memory function and language function. Compared with HC group, Obj-SCD group had worse performance in MMSE [27 (26, 29) vs. 29 (28, 30)], AVLT immediate [13 (8, 16) vs. 18 (15.5, 20.5)], AVLT short delay free recall [4 (2, 6) vs. 6 (5, 8)], AVLT long delay free recall [3 (2, 4) vs. 6 (5, 8)], AVLT long delay cued recall [3 (2, 4) vs. 6 (5, 7.5)], BVMT recognition [12 (10, 12) vs. 12 (12, 12)], AFT [15 (13, 17) vs. 19 (18.5, 21)], and BNT [23 (20, 24) vs. 26 (24, 27); **Table 1**].

Compared with HC group, aMCI group had worse performance in MMSE [27 (26, 28) vs. 29 (28, 30)], AVLT immediate [12 (11, 14) vs. 18 (15.5, 20.5)], AVLT short delay free recall [3 (2, 2.75) vs. 6 (5, 8)], AVLT long delay free recall [2 (1, 3) vs. 6 (5, 8)], AVLT long delay cued recall [2 (2, 3) vs. 6 (5, 7.5)], AVLT recognition [18 (14.25, 20.75)], BVMT 6th recall [4 (4, 4) vs. 5 (5, 6)], BVMT recognition [12 (10, 12) vs. 12 (12, 12)], AFT [16 (14, 17.75) vs. 19 (18.5, 21)], BNT [23 (21.25, 26) vs. 26 (24, 27)], STT-A total time [52.5 (39.25, 61.25) vs. 40 (34, 51)], Stroop test B [23 (20, 24) vs. 24 (23, 24)], and DST sequence [7 (5, 8) vs. 8 (7.5, 8.5); **Table 1**].

Compared with the Obj-SCD group, the aMCI group had worse performance in BVMT 6th recall [4 (4, 4) vs. 5 (4, 6); **Table 1**].

Regional Functional Activity

The Obj-SCD Group Compared with the HC Group

In the normal band, compared with the HC group, the Obj-SCD group showed increased fALFF in the left orbital part of inferior frontal gyrus, the right middle occipital gyrus, cerebellar vermis; decreased fALFF in the left inferior temporal gyrus (Two-tailed *t*-test; FDR $p < 0.017$, $k > 10$ voxels; **Table 2**, **Figure 1**).

In the slow-4 band, compared with the HC group, the Obj-SCD group showed increased fALFF in the left median cingulate and paracingulate gyri; decreased fALFF in the left inferior temporal gyrus, and the left precuneus (Two-tailed *t*-test; FDR $p < 0.017$, $k > 10$ voxels; **Table 2**, **Figure 1**).

In the slow-5 band, compared with the HC group, the Obj-SCD group showed increased fALFF in the right middle occipital gyrus, caudate nucleus, and cerebellar vermis (Two-tailed *t*-test; FDR $p < 0.017$, $k > 10$ voxels; **Table 2**, **Figure 1**).

TABLE 1 | Demographic data and neuropsychological tests between groups.

	HC (n = 37)	OBJ-SCD (n = 25)	aMCI (n = 28)	Test statistic
Age (year)[1]	63.86 ± 8.250	64.12 ± 6.978	65.71 ± 6.895	0.531
Sex (Male/Female)[2]	15/22	11/14	13/15	0.231
Edu years (year)[1]	12.11 ± 3.422	10.84 ± 2.511	12.19 ± 3.163	1.575
Hypertension[2]	24.3%	40.0%	32.1%	1.731
Hypercholesterolemia[2]	8.1%	16.0%	10.7%	0.947
Diabetes[2]	13.5%	20.0%	14.3%	0.528
General cognitive function				
MMSE[3]	29 (28, 30)	27 (26, 29)*	27 (26, 28)*	16.268
Memory function				
AVLT immediate recall[3]	18 (15.5, 20.5)	13 (8, 16)**	12 (11, 14)**	34.144
AVLT short delay free recall[3]	6 (5, 8)	4 (2, 6)**	3 (2, 2.75)**	39.854
AVLT long delay free recall[3]	6 (4.5, 7.5)	3 (2, 4)**	2 (1, 3)**	45.121
AVLT long delay cued recall[3]	6 (5, 7.5)	3 (2, 4)**	2 (2, 3)**	47.269
AVLT recognition[3]	22 (21, 23)	21 (19, 23)	18 (16, 18.75)**	52.679
BVMT immediate recall[3]	22 (16.5, 26)	14 (11, 25)	18 (14.25, 20.75)	7.646
BVMT 4th recall[3]	10 (7.5, 11.5)	8 (6, 10)	8 (5.25, 10)	6.806
BVMT 5th recall[3]	10 (8, 11.5)	8 (6, 11)	8 (5.25, 10)	7.100
BVMT 6th recall[3]	5 (5, 6)	5 (4, 6)	4 (4, 4) **,†	17.112
BVMT recognition[3]	12 (12, 12)	12 (10, 12)*	12 (10, 12)**	15.652
Language function				
AFT[3]	19 (18.5, 21.0)	15 (13, 17)**	16 (14, 17.75)**	27.372
BNT[3]	26 (24, 27)	23 (20, 24)**	23 (21.25, 26)*	16.866
Executive function				
STT-A total time (second)[3]	40 (34, 51)	48 (41.5, 53)	52.5 (39.25, 61.25)*	9.335
STT-B total time (second)[3]	113 (89, 137)	124 (107.5, 153)	127.5 (109.25, 171.00)	3.570
Stroop test A[3]	24 (24, 24)	24 (24, 24)	24 (24, 24)	2.107
Stroop test B[3]	24 (23, 24)	24 (23, 24)	23 (20, 24)*	10.893
Spatial Function				
JLO[1]	21.2 ± 5.04	19.79 ± 4.872	21.4 ± 4.32	1.526
Attention function				
DST sequence[3]	8 (7.5, 8.5)	8 (7, 8)	7 (5, 8)*	8.213
DST reverse[3]	5 (4, 6)	5 (4, 6)	4.5 (4, 5)	3.519

*[1]ANOVA test; [2]Chi-square test; [3]Kruskal–Wallis H-test; *compared with HC group, $p < 0.05$; **compared with HC group, $p < 0.001$; †compared with Obj-SCD group, $p < 0.05$. MMSE, mini-mental state examination; AVLT, auditory verbal learning test; BVMT, brief visuospatial memory test; AFT, animal verbal fluency test; BNT, boston naming test; STT, shape trail test; JLO, judgment of line orientation; DST, digit span test. Bonferroni correction for post-hoc analysis.*

The aMCI Group Compared with the HC Group

In the normal band, compared with the HC group, the aMCI group showed increased fALFF in the left orbital part of the inferior frontal gyrus, bilateral median cingulate, and paracingulate gyri (Two-tailed t-test; FDR $p < 0.001$, $k >$ 10 voxels; **Table 2**, **Figure 2**).

In the slow-5 band, compared with the HC group, the aMCI group showed increased fALFF in the right median cingulate and paracingulate gyri (Two-tailed t-test; FDR $p < 0.001$, $k >$ 10 voxels; **Table 2**, **Figure 2**).

The Obj-SCD Group Compared with the aMCI Group

In the normal band, compared with the aMCI group, the Obj-SCD group showed increased fALFF in the right middle occipital gyrus (Two-tailed t-test; FDR $p < 0.017$, $k > 10$ voxels; **Table 2**, **Figure 2**).

Correlation Analysis

In the Obj-SCD group, in normal band, the fALFF value of the right middle occipital gyrus was significantly negatively correlated with MMSE score ($r = -0.450$, $p = 0.024$) and AFT score ($r = -0.402$, $p = 0.046$; **Figure 3**); the left inferior temporal gyrus was significantly positively correlated with MMSE score ($r = 0.588$, $p = 0.002$). In slow-4 band, the fALFF value of the left precuneus was significantly positively correlated with MMSE score ($r = 0.468$, $p = 0.018$) and AFT score ($r = 0.600$, $p = 0.002$; **Figure 3**).

In the aMCI group, the fALFF value of the left orbital part of the inferior frontal gyrus was significantly positively correlated with AVLT long delay cued recall score ($r = 0.506$, $p = 0.006$; **Figure 3**).

DISCUSSION

In the stage of Obj-SCD, the neuropsychological decline includes two cognitive domains but is limited to one indicator of each domain. In the next stage of dementia progression, such as MCI, although cognitive impairment is aggravated, it may only be manifested in a single cognitive domain. Therefore, we speculate that the pathological characteristics of Obj-SCD may lead to a unique changing pattern, which is both similar and different from the next stage. Since the impairment in different cognitive domains will show different brain function activity changes, we made some efforts to select the cohort. For the Obj-SCD group, we chose individuals with impairments only in the memory domain and language domain, which is also the most common Obj-SCD individual. For MCI individuals,

TABLE 2 | Regions with changed functional activity (fALLF) between groups.

	Normal band		Slow-4 band		Slow-5 band	
	CLUSTER (AAL)	**Volume (voxels)**	**CLUSTER (AAL)**	**Volume (voxels)**	**CLUSTER (AAL)**	**Volume (voxels)**
OBJ-SCD vs. HC	**Cluster 1** Peak (MNI): −18 21 −24 Peak t: 4.4407 Frontal_Inf_Orb_L	total: 13 10	**Cluster 1** Peak (MNI): −57 −63 −12 Peak t: −4.1945 Temporal_Inf_L	total: 12 6	**Cluster 1** Peak (MNI): 0 −54 3 Peak t: 4.6911 Vermis_4_5	total: 11 11
	Cluster 2 Peak (MNI): −57 −66 −6 Peak t: −4.4341 Temporal_Inf_L	total: 13 4	**Cluster 2** Peak (MNI): −12 0 42 Peak t: 3.9132 Cingulum_Mid_L	total: 10 6	**Cluster 2** Peak (MNI): 30 −72 15 Peak t: 4.0551 White Matter Occipital_Mid_R	total: 11 11 4
	Cluster 3 Peak (MNI): 0 −57 3 Peak t: 4.5502 Vermis_4_5	total: 10 8	**Cluster 3** Peak (MNI): −9 −51 75 Peak t: −4.6652 Precuneus_L	total: 19 18	**Cluster 3** Peak (MNI): −18 12 21 Peak t: 5.4060 Caudate_L	total: 13 4
	Cluster 4 Peak (MNI): 30 −72 15 Peak t: 3.9545 White Matter Occipital_Mid_R	total: 23 23 10				
	Cluster 5 Peak (MNI): 30 −69 24 Peak t: 4.5089 Occipital_Mid_R	total: 11 8				
aMCI vs. HC	**Cluster 1** Peak (MNI): −18 21 −21 Peak t: 4.1979 Frontal_Inf_Orb_L	total: 10 8			**Cluster 1** Peak (MNI): 6 12 33 Peak t: 4.8347 Cingulum_Mid_R	total: 13 10
	Cluster 2 Peak (MNI): 6 9 33 Peak t: 4.4992 Cingulum_MID_R	total: 14 13				
	Cluster 3 Peak (mni):-12 0 36 Peak t: 4.7156 Cingulum_MID_L	total: 13 7				
OBJ-SCD vs. aMCI	**Cluster 1** Peak (MNI): 30 −78 12 Peak t: 3.5639 Occipital_MID_R	total: 14 8				

AAL, anatomical automatic labeling; MNI, montreal neurological institute; fractional low-frequency fluctuation amplitude (ALFF).

we chose a subgroup with only memory domain impairment, the aMCI group. The common feature of these two groups is the impairment of memory function. The difference lies in the degree of impairment, and the Obj-SCD group also has a slight impairment of language function. By comparing with HC and aMCI groups, we explored the functional activity changing pattern in Obj-SCD individuals. We performed correlation analysis between significant brain regions' functional activities and neuropsychological test scores in order to verify this pattern.

Similar Pattern Between the Obj-SCD and aMCI Groups

Compared with the HC group, we found similar functional activity enhancements in some local brain regions in the Obj-SCD and aMCI groups, including the left orbital part of the inferior frontal gyrus and the left median cingulate and paracingulate gyri.

The frontal lobe may be an essential area of cognitive maintenance associated with AD (Zeng et al., 2019). In terms of cognitive function, it may be involved in episodic memory and working memory (de Chastelaine et al., 2011; Matthews, 2015). Current evidence suggests that the orbitofrontal cortex is associated with memory impairment in AD and frontotemporal dementia (Liu et al., 2021). As an important node of working memory, the orbitofrontal gyrus may play an essential role in integrating and coordinating working memory maintenance, execution, and monitoring (Badre, 2008; Barbey et al., 2011; Costers et al., 2020). The cerebral accumulation of Aβ and the following neurovascular dysfunction were considered the most crucial pathogenesis of cognitive decline and dementia

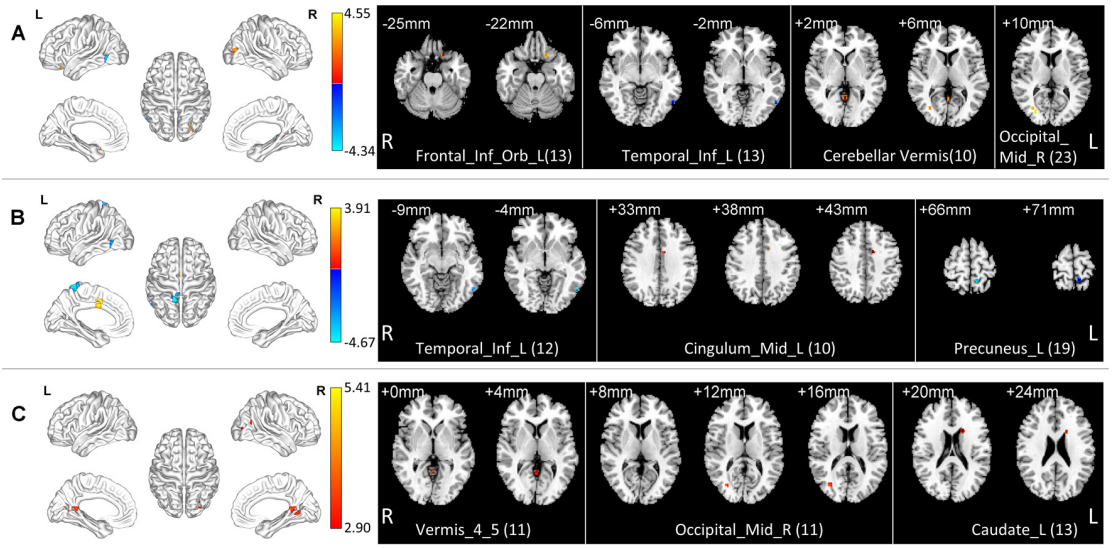

FIGURE 1 | Local functional change pattern of Obj-SCD group. The Obj-SCD group compared with the HC group. **(A)** In the normal band, fALFF increased in the left orbital part of inferior frontal gyrus, the right middle occipital gyrus, cerebellar vermis; decreased fALFF in the left inferior temporal gyrus (Two-tailed *t*-test; FDR $p < 0.017$, $k > 10$ voxels). **(B)** In the slow-4 band, fALFF increased in the left median cingulate and paracingulate gyri; decreased in the left inferior temporal gyrus and the left precuneus (Two-tailed *t*-test; FDR $p < 0.017$, $k > 10$ voxels). **(C)** In the slow-5 band, fALFF increased in the right middle occipital gyrus, caudate nucleus, and cerebellar vermis (Two-tailed *t*-test; FDR $p < 0.017$, $k > 10$ voxels). The numbers in brackets are voxels of significant clusters. Labels of significant clusters are defined with the AAL (Anatomical Automatic Labeling) atlas. Abbreviations: Obj-SCD, objectively-defined subtle cognitive decline; fALFF, low-frequency fluctuation amplitude (ALFF); HC, healthy control; FDR, false discovery rate.

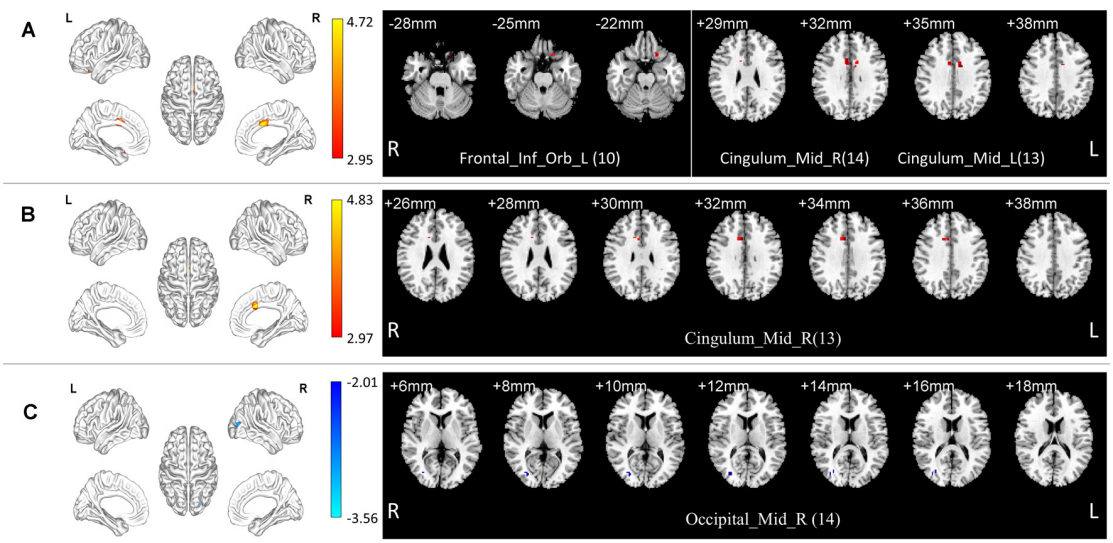

FIGURE 2 | Local functional change pattern of aMCI group. **(A)** In the normal band, compared with the HC group, the aMCI group showed increased fALFF in the left orbital part of the inferior frontal gyrus, bilateral median cingulate, and paracingulate gyri (Two-tailed *t*-test; FDR $p < 0.001$, $k > 10$ voxels). **(B)** In the slow-5 band, compared with the HC group, the aMCI group showed increased fALFF in the right median cingulate and paracingulate gyri (Two-tailed *t*-test; FDR $p < 0.001$, $k > 10$ voxels). **(C)** In the normal band, compared with the Obj-SCD group, the aMCI group showed decreased fALFF in the right middle occipital gyrus (Two-tailed *t*-test; FDR $p < 0.017$, $k > 10$ voxels). The numbers in brackets are voxels of significant clusters. Labels of significant clusters are defined with the AAL (Anatomical Automatic Labeling) atlas. Abbreviation: aMCI, amnestic MCI.

(Scheltens et al., 2016; Lim et al., 2018; Parodi-Rullán et al., 2020). Researchers (Hua et al., 2019) used arteriolar cerebral blood volume to explore the relationship between cerebral blood flow, APOE alleles, and Aβ accumulation in patients with MCI and found an increased blood volume in the orbitofrontal gyrus. Furthermore, they found the arteriolar cerebral blood volume in the orbitofrontal gyrus is closely related to local Aβ burden and APOE4; it also can predict cognitive decline

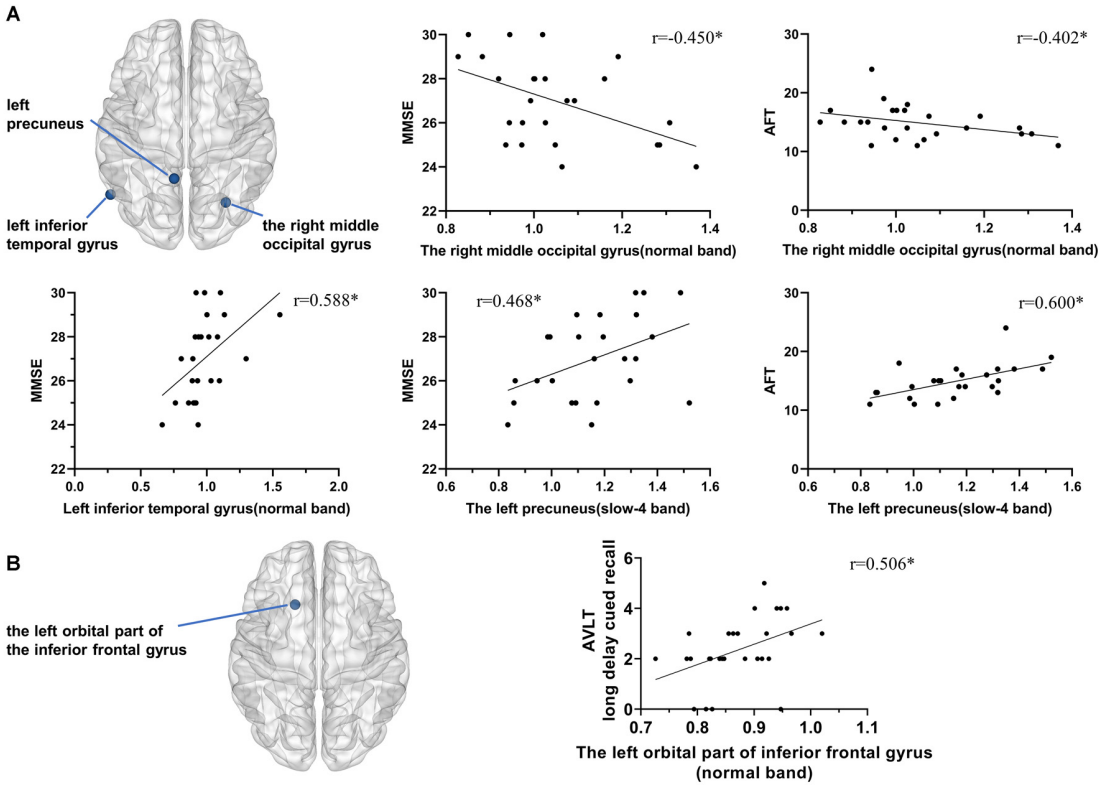

FIGURE 3 | Correlation between local functional activity and neuropsychological performance. **(A)** In the Obj-SCD group, in the normal band, the fALFF value of the right middle occipital gyrus was significantly negatively correlated with the MMSE score and AFT score; the left inferior temporal gyrus was significantly positively correlated with the MMSE score. In the slow-4 band, the fALFF value of the left precuneus was significantly positively correlated with the MMSE and AFT scores. **(B)** In the aMCI group, the fALFF value of the left orbital part of the inferior frontal gyrus was significantly positively correlated with AVLT 6th recall score. $^{*}p < 0.05$. Abbreviations: AFT, Animal Verbal Fluency Test; AVLT, Auditory Verbal Learning Test; MMSE, Mini-Mental State Examination.

within 2 years. Our study also found a similar increased local functional activity in the orbitofrontal gyrus in both Obj-SCD and aMCI groups, consistent with the increase of local blood flow in this area. This enhancement of functional activity may be a compensatory response to early cognitive decline. Considering the role of the orbitofrontal cortex in attention and impulsivity (Bari et al., 2020), it may also be a manifestation of nerve recruitment disorder.

The cingulate cortex is an essential structure in the human brain's medial side, which plays a vital role in cognitive, motor, emotional, and other functional activities. According to the structure and function, the cingulate can be subdivided into several parts, in which the middle cingulate cortex is considered to be related to the function of the Frontoparietal Network (Vincent et al., 2008; Gilmore et al., 2015; Caruana et al., 2018). Specifically, the middle cingulate cortex is associated with emotion, behavior, motor, and somatosensory function; and has a close functional connection with prefrontal, premotor, and primary motor networks (Oane et al., 2020). Compared with the elderly with MCI, the elderly with normal cognition had a better connection between the middle cingulate and the superior frontal gyrus, frontal eye field, orbitofrontal cortex (Cera et al., 2019). Our study found increased functional activity on the middle cingulate cortex in Obj-SCD and aMCI groups, which may be intrinsically associated with the increased functional activity of the orbitofrontal cortex.

Different Pattern Between the Obj-SCD and aMCI Groups

Some changes in local functional activities of the Obj-SCD group showed different patterns from the aMCI group. Compared with HC, the Obj-SCD group showed increased local functional activity in the right middle occipital gyrus, decreased local functional activity in the left precuneus and the left inferior temporal gyrus.

In the elderly with normal cognition, the connection between the occipital lobe and the posterior cingulate and precuneus is related to the tau protein, which may change in preclinical cognitive impairment (Quevenco et al., 2020). In patients with subjective cognitive decline, white matter damage across the frontal and occipital lobes was also found; this track is thought to be related to the gray matter damage such as the medial prefrontal cortex and posterior cingulate cortex in the early stage of AD (Luo et al., 2019). The close connection between the occipital lobe and the frontal lobe is consistent with finding abnormal functional activity in both the orbitofrontal cortex and the occipital cortex in our study. In people with normal cognition with Aβ deposition, it can be observed that the content

of cerebrospinal fluid Progranulin is related to the thickening of the occipital cortex and cognitive decline; this result reflects that the neuroinflammatory reaction in the preclinical stage of Alzheimer's disease may cause the compensatory performance in the occipital lobe (Batzu et al., 2020). Similarly, in individuals with subjective cognitive decline, an increase in the volume of occipital gray matter related to Aβ protein load was also found, and this structural change was associated with the aggravation of cognitive function symptoms (Valech et al., 2019).

Recent studies have shown that the temporal lobe is one of the critical areas of pathological changes in multiple types of dementia (Mak et al., 2020; Sanchez et al., 2021). In preclinical AD, tau protein deposition and Aβ burden in the inferior temporal gyrus is related to cognitive performance, mainly memory function (Schultz et al., 2018; Norton et al., 2020; Scott et al., 2020; Vila-Castelar et al., 2020). Tau accumulation in this area may be associated with hippocampal hyperactivity, which is not associated with Aβ (Huijbers et al., 2019). It is worth noting that in the normal elderly without Aβ deposition and in the elderly with cognitive impairment caused by small vessel disease, the lower functional connection of the inferior temporal gyrus is also related to the accumulation of tau protein (Franzmeier et al., 2019; Rabin et al., 2019). In addition, in normal older adults, the accumulation of tau protein in the inferior temporal gyrus is also associated with progressive thinning of the cortex in many brain regions, especially in the temporal lobe and parietal lobe (LaPoint et al., 2017). Therefore, the inferior temporal gyrus might be a susceptible region of detection of cognitive impaired risks.

In these studies, the changes in brain structure and functional activities are similar to our results of local functional changes observed in our research and may be related to pathological markers. However, considering that no relevant pathological marker detection was performed in our study, our results should still be interpreted with caution and cannot be directly explained by pathological changes.

The Association Between Changing Pattern With Cognitive Function in Obj-SCD Group

In this study, the Obj-SCD group showed a unique changing pattern compared to the aMCI group. We analyzed the correlation between the functional activity of the significant brain regions found in the pattern and neuropsychological tests' performance and found intimate associations.

The fALFF value of the right middle occipital gyrus was increased in the Obj-SCD group and was significantly negatively correlated with MMSE score and AFT score. These results suggested that the increase of local functional activity in this area may be related to the progression of the disease and may be a compensatory manifestation of general cognitive and language dysfunction. The functional activity of the left inferior temporal gyrus was positively correlated with the MMSE score, suggesting that the functional dysfunction was related to general cognitive function. The functional activity of the left precuneus was positively correlated with MMSE and AFT scores, suggesting that its dysfunction was related to the decline of general cognitive function and language function. The correlation between these brain regions and specific cognitive functions is consistent with previous studies. The abnormal brain areas of the Obj-SCD group are distributed in a relatively wide area, and there are differences between their correlations with different cognitive impairments. We speculate that it might because the internal pathological basis of Obj-SCD individuals is complicated. We also speculate that if the progress of different damage areas is inconsistent, Obj-SCD individuals' outcomes may differ, but this speculation needs further follow-up studies to confirm.

Additionally, although the functional activity of the left orbital part of the inferior frontal gyrus changed in both the Obj-SCD and aMCI groups, only in the aMCI group the functional activity was positively correlated with AVLT long delay cued recall score. This can be attributed to the fact that the memory-binding impairment in the aMCI group is more severe than that in the Obj-SCD group.

CONCLUSION

Obj-SCD individuals have a widely distributed pattern of local functional activity changes, and this changing pattern has some similarities with aMCI to a certain extent. However, there were also some differences. In this pattern, the functional changes of different brain regions have a close but different correlation with cognitive impairment, suggesting that there may be a complex pathological basis inside. This suggests that Obj-SCD may be a separate stage of cognitive decline before aMCI and is helpful to the study of preclinical cognitive decline.

LIMITATIONS

The study still had some limitations. First, the sample size is not enough, resulting in insufficient sensitivity of the results. Second, there is no biomarker examination to explore the pathological mechanism. Therefore, the results should be interpreted with caution.

DATA AVAILABILITY STATEMENT

The raw data supporting the conclusions of this article will be made available by the authors, without undue reservation.

ETHICS STATEMENT

The studies involving human participants were reviewed and approved by The Ethics Committee of Shanghai Jiao Tong University Affiliated Sixth People's Hospital. The patients/participants provided their written informed consent to participate in this study.

AUTHOR CONTRIBUTIONS

LC: methodology, data analysis, visualization, and writing—review and editing. ZZ: methodology, data analysis,

investigation, data curation, and writing—original draft. C-YZL: resources, project administration, review, and commentary. QG: resources, supervision, project administration, funding acquisition, review, and revision. All authors contributed to the article and approved the submitted version.

FUNDING

This research was funded by Shanghai Municipal Science and Technology Major Project (No. 2018SHZDZX01), National Key R&D Program of China (2016YFC1306305 and 2018YFE0203600), the National Key Research and Development Program of China (No. 2018YFC0910503), the Young Scientists Fund of the National Natural Science Foundation of China (No. 81801774), and the Natural Science Foundation of Shanghai (No. 18ZR1403700).

ACKNOWLEDGMENTS

We want to thank all the subjects who participated in this study.

REFERENCES

Badre, D. (2008). Cognitive control, hierarchy, and the rostro-caudal organization of the frontal lobes. *Trends Cogn. Sci.* 12, 193–200. doi: 10.1016/j.tics.2008.02.004

Barbey, A. K., Koenigs, M., and Grafman, J. (2011). Orbitofrontal contributions to human working memory. *Cereb. Cortex* 21, 789–795. doi: 10.1093/cercor/bhq153

Bari, A., Xu, S., Pignatelli, M., Takeuchi, D., Feng, J., Li, Y., et al. (2020). Differential attentional control mechanisms by two distinct noradrenergic coeruleo-frontal cortical pathways. *Proc. Natl. Acad. Sci. U S A* 117, 29080–29089. doi: 10.1073/pnas.2015635117

Batzu, L., Westman, E., Pereira, J. B., and Alzheimer's Disease Neuroimaging Initiative (2020). Cerebrospinal fluid progranulin is associated with increased cortical thickness in early stages of Alzheimer's disease. *Neurobiol. Aging* 88, 61–70. doi: 10.1016/j.neurobiolaging.2019.12.012

Berron, D., van Westen, D., Ossenkoppele, R., Strandberg, O., and Hansson, O. (2020). Medial temporal lobe connectivity and its associations with cognition in early Alzheimer's disease. *Brain* 143, 1233–1248. doi: 10.1093/brain/awaa068

Bi, X.-A., Hu, X., Wu, H., and Wang, Y. (2020a). Multimodal data analysis of Alzheimer's disease based on clustering evolutionary random forest. *IEEE J. Biomed. Health Inform.* 24, 2973–2983. doi: 10.1109/JBHI.2020.2973324

Bi, X.-A., Liu, Y., Xie, Y., Hu, X., and Jiang, Q. (2020b). Morbigenous brain region and gene detection with a genetically evolved random neural network cluster approach in late mild cognitive impairment. *Bioinformatics* 36, 2561–2568. doi: 10.1093/bioinformatics/btz967

Bondi, M. W., Edmonds, E. C., Jak, A. J., Clark, L. R., Delano-Wood, L., McDonald, C. R., et al. (2014). Neuropsychological criteria for mild cognitive impairment improves diagnostic precision, biomarker associations, and progression rates. *J. Alzheimers Dis.* 42, 275–289. doi: 10.3233/JAD-140276

Caminiti, S. P., Ballarini, T., Sala, A., Cerami, C., Presotto, L., Santangelo, R., et al. (2018). FDG-PET and CSF biomarker accuracy in prediction of conversion to different dementias in a large multicentre MCI cohort. *Neuroimage Clin.* 18, 167–177. doi: 10.1016/j.nicl.2018.01.019

Caruana, F., Gerbella, M., Avanzini, P., Gozzo, F., Pelliccia, V., Mai, R., et al. (2018). Motor and emotional behaviours elicited by electrical stimulation of the human cingulate cortex. *Brain* 141, 3035–3051. doi: 10.1093/brain/awy219

Cera, N., Esposito, R., Cieri, F., and Tartaro, A. (2019). Altered cingulate cortex functional connectivity in normal aging and mild cognitive impairment. *Front. Neurosci.* 13:857. doi: 10.3389/fnins.2019.00857

Cerami, C., Dodich, A., Iannaccone, S., Magnani, G., Santangelo, R., Presotto, L., et al. (2018). A biomarker study in long-lasting amnestic mild cognitive impairment. *Alzheimers Res. Ther.* 10:42. doi: 10.1186/s13195-018-0369-8

Chen, K., Huang, L., Lin, B., Zhou, Y., Zhao, Q., and Guo, Q. (2019). The number of items on each stroop test card is unrelated to its sensitivity. *Neuropsychobiology* 77, 38–44. doi: 10.1159/000493553

Costers, L., Van Schependom, J., Laton, J., Baijot, J., Sjogard, M., Wens, V., et al. (2020). Spatiotemporal and spectral dynamics of multi-item working memory as revealed by the n-back task using MEG. *Hum. Brain Mapp.* 41, 2431–2446. doi: 10.1002/hbm.24955

Curiel Cid, R. E., Crocco, E. A., Duara, R., Garcia, J. M., Rosselli, M., DeKosky, S. T., et al. (2020). A novel method of evaluating semantic intrusion errors to distinguish between amyloid positive and negative groups on the Alzheimer's disease continuum. *J. Psychiatr. Res.* 124, 131–136. doi: 10.1016/j.jpsychires.2020.02.008

de Chastelaine, M., Wang, T. H., Minton, B., Muftuler, L. T., and Rugg, M. D. (2011). The effects of age, memory performance, and callosal integrity on the neural correlates of successful associative encoding. *Cereb. Cortex* 21, 2166–2176. doi: 10.1093/cercor/bhq294

Dubois, B., Hampel, H., Feldman, H. H., Scheltens, P., Aisen, P., Andrieu, S., et al. (2016). Preclinical Alzheimer's disease: definition, natural history, and diagnostic criteria. *Alzheimers Dement.* 12, 292–323. doi: 10.1016/j.jalz.2016.02.002

Folstein, M. F., Folstein, S. E., and McHugh, P. R. (1975). "Mini-mental state". A practical method for grading the cognitive state of patients for the clinician. *J. Psychiatr. Res.* 12, 189–198. doi: 10.1016/0022-3956(75)90026-6

Franzmeier, N., Rubinski, A., Neitzel, J., Kim, Y., Damm, A., Na, D. L., et al. (2019). Functional connectivity associated with tau levels in ageing, Alzheimer's, and small vessel disease. *Brain* 142, 1093–1107. doi: 10.1093/brain/awz026

Gilmore, A. W., Nelson, S. M., and McDermott, K. B. (2015). A parietal memory network revealed by multiple MRI methods. *Trends Cogn. Sci.* 19, 534–543. doi: 10.1016/j.tics.2015.07.004

Hua, J., Lee, S., Blair, N. I. S., Wyss, M., van Bergen, J. M. G., Schreiner, S. J., et al. (2019). Increased cerebral blood volume in small arterial vessels is a correlate of amyloid-beta-related cognitive decline. *Neurobiol. Aging* 76, 181–193. doi: 10.1016/j.neurobiolaging.2019.01.001

Huijbers, W., Schultz, A. P., Papp, K. V., LaPoint, M. R., Hanseeuw, B., Chhatwal, J. P., et al. (2019). Tau accumulation in clinically normal older adults is associated with hippocampal hyperactivity. *J. Neurosci.* 39, 548–556. doi: 10.1523/JNEUROSCI.1397-18.2018

Jack, C. R. Jr., Bennett, D. A., Blennow, K., Carrillo, M. C., Dunn, B., Haeberlein, S. B., et al. (2018). NIA-AA research framework: toward a biological definition of Alzheimer's disease. *Alzheimers Dement.* 14, 535–562. doi: 10.1016/j.jalz.2018.02.018

Jia, X.-Z., Sun, J.-W., Ji, G.-J., Liao, W., Lv, Y.-T., Wang, J., et al. (2020). Percent amplitude of fluctuation: a simple measure for resting-state fMRI signal at single voxel level. *PLoS One* 15:e0227021. doi: 10.1371/journal.pone.0227021

Johansson, B., and Berg, S. (1989). The robustness of the terminal decline phenomenon: longitudinal data from the Digit-Span Memory Test. *J. Gerontol.* 44, P184–P186. doi: 10.1093/geronj/44.6.p184

Jones, J. D., Uribe, C., Bunch, J., and Thomas, K. R. (2021). Beyond PD-MCI: objectively defined subtle cognitive decline predicts future cognitive and functional changes. *J. Neurol.* 268, 337–345. doi: 10.1007/s00415-020-10163-4

Katzman, R., Zhang, M. Y., Ouang Ya, Q.-Y.-Q., Wang, Z. Y., Liu, W. T., Yu, E., et al. (1988). A chinese version of the mini-mental state examination; impact of illiteracy in a Shanghai dementia survey. *J. Clin. Epidemiol.* 41, 971–978. doi: 10.1016/0895-4356(88)90034-0

LaPoint, M. R., Chhatwal, J. P., Sepulcre, J., Johnson, K. A., Sperling, R. A., and Schultz, A. P. (2017). The association between tau PET and retrospective cortical thinning in clinically normal elderly. *NeuroImage* 157, 612–622. doi: 10.1016/j.neuroimage.2017.05.049

Li, Y., Yao, H., Lin, P., Zheng, L., Li, C., Zhou, B., et al. (2017). Frequency-dependent altered functional connections of default mode network in Alzheimer's disease. *Front. Aging Neurosci.* 9:259. doi: 10.3389/fnagi.2017.00259

Lim, E.-Y., Yang, D.-W., Cho, A.-H., and Shim, Y. S. (2018). Cerebrovascular hemodynamics on transcranial doppler ultrasonography and cognitive decline in mild cognitive impairment. *J. Alzheimers Dis.* 65, 651–657. doi: 10.3233/JAD-180026

Liu, L., Roquet, D., Ahmed, R. M., Hodges, J. R., Piguet, O., and Irish, M. (2021). Examining prefrontal contributions to past- and future-oriented memory disturbances in daily life in dementia. *Cortex* 134, 307–319. doi: 10.1016/j.cortex.2020.11.003

Luo, C., Li, M., Qin, R., Chen, H., Yang, D., Huang, L., et al. (2019). White matter microstructural damage as an early sign of subjective cognitive decline. *Front. Aging Neurosci.* 11:378. doi: 10.3389/fnagi.2019.00378

Mack, W. J., Freed, D. M., Williams, B. W., and Henderson, V. W. (1992). Boston Naming Test: shortened versions for use in Alzheimer's disease. *J. Gerontol.* 47, P154–158. doi: 10.1093/geronj/47.3.p154

Mak, E., Nicastro, N., Malpetti, M., Savulich, G., Surendranathan, A., Holland, N., et al. (2020). Imaging tau burden in dementia with Lewy bodies using [^{18}F]-AV1451 positron emission tomography. *Neurobiol. Aging* 101, 172–180. doi: 10.1016/j.neurobiolaging.2020.11.006

Manne, S., Kondru, N., Hepker, M., Jin, H., Anantharam, V., Lewis, M., et al. (2019). Ultrasensitive detection of aggregated alpha-synuclein in glial cells, human cerebrospinal fluid, and brain tissue using the RT-QuIC assay: new high-throughput neuroimmune biomarker assay for parkinsonian disorders. *J. Neuroimmune Pharmacol.* 14, 423–435. doi: 10.1007/s11481-019-09835-4

Matthews, B. R. (2015). Memory dysfunction. *Continuum* 21, 613–626. doi: 10.1212/01.CON.0000466656.59413.29

Moguilner, S., García, A. M., Perl, Y. S., Tagliazucchi, E., Piguet, O., Kumfor, F., et al. (2020). Dynamic brain fluctuations outperform connectivity measures and mirror pathophysiological profiles across dementia subtypes: a multicenter study. *NeuroImage* 225:117522. doi: 10.1016/j.neuroimage.2020.117522

Morris, J. C. (1993). The Clinical Dementia Rating (CDR): current version and scoring rules. *Neurology* 43, 2412–2414. doi: 10.1212/wnl.43.11.2412-a

Norton, D. J., Parra, M. A., Sperling, R. A., Baena, A., Guzman-Velez, E., Jin, D. S., et al. (2020). Visual short-term memory relates to tau and amyloid burdens in preclinical autosomal dominant Alzheimer's disease. *Alzheimers Res. Ther.* 12:99. doi: 10.1186/s13195-020-00660-z

Oane, I., Barborica, A., Chetan, F., Donos, C., Maliia, M. D., Arbune, A. A., et al. (2020). Cingulate cortex function and multi-modal connectivity mapped using intracranial stimulation. *NeuroImage* 220:117059. doi: 10.1016/j.neuroimage.2020.117059

Pan, P., Zhu, L., Yu, T., Shi, H., Zhang, B., Qin, R., et al. (2017). Aberrant spontaneous low-frequency brain activity in amnestic mild cognitive impairment: a meta-analysis of resting-state fMRI studies. *Ageing Res. Rev.* 35, 12–21. doi: 10.1016/j.arr.2016.12.001

Parodi-Rullán, R., Ghiso, J., Cabrera, E., Rostagno, A., and Fossati, S. (2020). Alzheimer's amyloid beta heterogeneous species differentially affect brain endothelial cell viability, blood-brain barrier integrity, and angiogenesis. *Aging Cell* 19:e13258. doi: 10.1111/acel.13258

Petersen, R. C. (2011). Clinical practice. Mild cognitive impairment. *N. Engl. J. Med.* 364, 2227–2234. doi: 10.1056/NEJMcp0910237

Petersen, R. C., Doody, R., Kurz, A., Mohs, R. C., Morris, J. C., Rabins, P. V., et al. (2001). Current concepts in mild cognitive impairment. *Arch. Neurol.* 58, 1985–1992. doi: 10.1001/archneur.58.12.1985

Pliskin, J. I., DeDios Stern, S., Resch, Z. J., Saladino, K. F., Ovsiew, G. P., Carter, D. A., et al. (2020). Comparing the psychometric properties of eight embedded performance validity tests in the rey auditory verbal learning test, wechsler memory scale logical memory, and brief visuospatial memory test-revised recognition trials for detecting invalid neuropsychological test performance. *Assessment* doi: 10.1177/1073191120929093. [Epub ahead of print].

Qualls, C. E., Bliwise, N. G., and Stringer, A. Y. (2000). Short forms of the Benton Judgment of Line Orientation Test: development and psychometric properties. *Arch. Clin. Neuropsychol.* 15, 159–163. doi: 10.1093/arclin/15.2.159

Quevenco, F. C., van Bergen, J. M., Treyer, V., Studer, S. T., Kagerer, S. M., Meyer, R., et al. (2020). Functional brain network connectivity patterns associated with normal cognition at old-age, local beta-amyloid, tau, and APOE4. *Front. Aging Neurosci.* 12:46. doi: 10.3389/fnagi.2020.00046

Rabin, J. S., Yang, H.-S., Schultz, A. P., Hanseeuw, B. J., Hedden, T., Viswanathan, A., et al. (2019). Vascular risk and beta-amyloid are synergistically associated with cortical tau. *Ann. Neurol.* 85, 272–279. doi: 10.1002/ana.25399

Sanchez, J. S., Becker, J. A., Jacobs, H. I. L., Hanseeuw, B. J., Jiang, S., Schultz, A. P., et al. (2021). The cortical origin and initial spread of medial temporal tauopathy in Alzheimer's disease assessed with positron emission tomography. *Sci. Transl. Med.* 13:eabc0655. doi: 10.1126/scitranslmed.abc0655

Scheltens, P., Blennow, K., Breteler, M. M. B., de Strooper, B., Frisoni, G. B., Salloway, S., et al. (2016). Alzheimer's disease. *Lancet* 388, 505–517. doi: 10.1016/S0140-6736(15)01124-1

Schultz, S. A., Gordon, B. A., Mishra, S., Su, Y., Perrin, R. J., Cairns, N. J., et al. (2018). Widespread distribution of tauopathy in preclinical Alzheimer's disease. *Neurobiol. Aging* 72, 177–185. doi: 10.1016/j.neurobiolaging.2018.08.022

Scott, M. R., Hampton, O. L., Buckley, R. F., Chhatwal, J. P., Hanseeuw, B. J., Jacobs, H. I., et al. (2020). Inferior temporal tau is associated with accelerated prospective cortical thinning in clinically normal older adults. *NeuroImage* 220:116991. doi: 10.1016/j.neuroimage.2020.116991

Thomas, K. R., Bangen, K. J., Weigand, A. J., Edmonds, E. C., Wong, C. G., Cooper, S., et al. (2020). Objective subtle cognitive difficulties predict future amyloid accumulation and neurodegeneration. *Neurology* 94, e397–e406. doi: 10.1212/WNL.0000000000008838

Thomas, K. R., Edmonds, E. C., Eppig, J., Salmon, D. P., Bondi, M. W., and Alzheimer's Disease Neuroimaging Initiative. (2018). Using neuropsychological process scores to identify subtle cognitive decline and predict progression to mild cognitive impairment. *J. Alzheimers Dis.* 64, 195–204. doi: 10.3233/JAD-180229

Thomas, K. R., Osuna, J. R., Weigand, A. J., Edmonds, E. C., Clark, A. L., Holmqvist, S., et al. (2021). Regional hyperperfusion in older adults with objectively-defined subtle cognitive decline. *J. Cereb. Blood Flow Metab.* 41, 1001–1012. doi: 10.1177/0271678X20935171

Valech, N., Sánchez-Benavides, G., Tort-Merino, A., Coll-Padrós, N., Olives, J., Leãn, M., et al. (2019). Associations between the subjective cognitive decline-questionnaire's scores, gray matter volume, and amyloid-beta levels. *J. Alzheimers Dis.* 72, 1287–1302. doi: 10.3233/JAD-190624

Vila-Castelar, C., Muñoz, N., Papp, K. V., Amariglio, R. E., Baena, A., Guzmán-Vález, E., et al. (2020). The Latin American Spanish version of the Face-Name Associative Memory Exam is sensitive to cognitive and pathological changes in preclinical autosomal dominant Alzheimer's disease. *Alzheimers Res. Ther.* 12:104. doi: 10.1186/s13195-020-00671-w

Vincent, J. L., Kahn, I., Snyder, A. Z., Raichle, M. E., and Buckner, R. L. (2008). Evidence for a frontoparietal control system revealed by intrinsic functional connectivity. *J. Neurophysiol.* 100, 3328–3342. doi: 10.1152/jn.90355.2008

Worboys, M. (2013). The Hamilton Rating Scale for Depression: the making of a "gold standard" and the unmaking of a chronic illness, 1960–1980. *Chronic Illn.* 9, 202–219. doi: 10.1177/1742395312467658

Zeng, Q., Luo, X., Li, K., Wang, S., Zhang, R., Hong, H., et al. (2019). Distinct spontaneous brain activity patterns in different biologically-defined Alzheimer's disease cognitive stage: a preliminary study. *Front. Aging Neurosci.* 11:350. doi: 10.3389/fnagi.2019.00350

Zhao, Q., Guo, Q., and Hong, Z. (2013a). Clustering and switching during a semantic verbal fluency test contribute to differential diagnosis of cognitive impairment. *Neurosci. Bull.* 29, 75–82. doi: 10.1007/s12264-013-1301-7

Zhao, Q., Guo, Q., Li, F., Zhou, Y., Wang, B., and Hong, Z. (2013b). The shape trail test: application of a new variant of the trail making test. *PLoS One* 8:e57333. doi: 10.1371/journal.pone.0057333

Zhao, Q., Guo, Q., Liang, X., Chen, M., Zhou, Y., Ding, D., et al. (2015). Auditory verbal learning test is superior to rey-osterrieth complex figure memory for predicting mild cognitive impairment to Alzheimer's disease. *Curr. Alzheimer Res.* 12, 520–526. doi: 10.2174/1567205012666150530202729

Zou, Q.-H., Zhu, C.-Z., Yang, Y., Zuo, X.-N., Long, X.-Y., Cao, Q.-J., et al. (2008). An improved approach to detection of amplitude of low-frequency fluctuation (ALFF) for resting-state fMRI: fractional ALFF. *J. Neurosci. Methods* 172, 137–141. doi: 10.1016/j.jneumeth.2008.04.012

Zuo, X.-N., Di Martino, A., Kelly, C., Shehzad, Z. E., Gee, D. G., Klein, D. F., et al. (2010). The oscillating brain: complex and reliable. *NeuroImage* 49, 1432–1445. doi: 10.1016/j.neuroimage.2009.09.037

Conflict of Interest: The authors declare that the research was conducted in the absence of any commercial or financial relationships that could be construed as a potential conflict of interest.

The reviewer QZ declared a shared affiliation, with no collaboration, with one of the authors LC to the handling editor at the time of the review.

frontiers in Aging Neuroscience

ORIGINAL RESEARCH
published: 25 June 2021
doi: 10.3389/fnagi.2021.701702

Ultrarapid Inflammation of the Olfactory Bulb After Spinal Cord Injury: Protective Effects of the Granulocyte Colony-Stimulating Factor on Early Neurodegeneration in the Brain

Muh-Shi Lin[1,2,3,4†], I-Hsiang Chiu[2] and Chai-Ching Lin[2†]*

[1] Division of Neurosurgery, Department of Surgery, Kuang Tien General Hospital, Taichung, Taiwan, [2] Department of Biotechnology and Animal Science, College of Bioresources, National Ilan University, Yilan, Taiwan, [3] Department of Biotechnology, College of Medical and Health Care, Hung Kuang University, Taichung, Taiwan, [4] Department of Health Business Administration, College of Medical and Health Care, Hung Kuang University, Taichung, Taiwan

OPEN ACCESS

Edited by:
Jiehui Jiang,
Shanghai University, China

Reviewed by:
Cheng-Yu Wei,
Chang Bing Show Chwan Memorial Hospital, Taiwan
Can Sheng,
Capital Medical University, China

***Correspondence:**
Chai-Ching Lin
lincc@niu.edu.tw

†ORCID
Muh-Shi Lin
orcid.org/0000-0002-9798-8160
Chai-Ching Lin
orcid.org/0000-0002-8092-1920

Received: *28 April 2021*
Accepted: *27 May 2021*
Published: *25 June 2021*

Citation:
Lin M-S, Chiu I-H and Lin C-C (2021) Ultrarapid Inflammation of the Olfactory Bulb After Spinal Cord Injury: Protective Effects of the Granulocyte Colony-Stimulating Factor on Early Neurodegeneration in the Brain. Front. Aging Neurosci. 13:701702. doi: 10.3389/fnagi.2021.701702

The correlation among olfactory dysfunction, spinal cord injury (SCI), subjective cognitive decline, and neurodegenerative dementia has been established. Impaired olfaction is considered a marker for neurodegeneration. Hence, there is a need to examine if SCI leads to olfactory dysfunction. In this study, the brain tissue of mice with spinal cord hemisection injury was subjected to microarray analysis. The mRNA expression levels of olfactory receptors in the brain began to decline at 8 h post-SCI. SCI promoted neuroinflammation, downregulated the expression of olfactory receptors, decreased the number of neural stem cells (NSCs), and inhibited the production of neurotrophic factors in the olfactory bulbs at 8 h post-SCI. In particular, the SCI group had upregulated mRNA and protein expression levels of glial fibrillary acidic protein (GFAP; a marker of astrocyte reactivation) and pro-inflammatory mediators [IL-1β, IL-6, and Nestin (marker of NSCs)] in the olfactory bulb compared to levels in the sham control group. The mRNA expression levels of olfactory receptors (*Olfr1494*, *Olfr1324*, *Olfr1241*, and *Olfr979*) and neurotrophic factors [brain-derived neurotrophic factor (BDNF), glial cell-derived neurotrophic factor (GDNF), and nerve growth factor (NGF)] were downregulated in the olfactory bulb of the SCI group mice at 8 h post-SCI. The administration of granulocyte colony-stimulating factor (G-CSF) mitigated these SCI-induced pathological changes in the olfactory bulb at 8 h post-SCI. These results indicate that the olfactory bulb is vulnerable to environmental damage even if the lesion is located at sites distant from the brain, such as the spinal cord. Additionally, SCI initiated pathological processes, including inflammatory response, and impaired neurogenesis, at an early stage. The findings of this study will provide a basis for future studies on pathological mechanisms of early neurodegenerative diseases involving the olfactory bulb and enable early clinical drug intervention.

Keywords: subjective cognitive decline, neurodegenerative disease, olfactory dysfunction, olfactory bulb, spinal cord injury, neuroinflammation, granulocyte colony stimulating factor

INTRODUCTION

The cognitive performance of patients with subjective cognitive decline (SCD) in the objective cognitive examination is within the standard range (Jessen et al., 2014). SCD is considered to be the preclinical stage of Alzheimer's Disease (AD). Approximately 25% of patients with SCD may develop mild cognitive impairment (MCI). The risk of developing dementia within 5 years in patients with SCD was twofold higher than that in patients without SCD (Mitchell et al., 2014) (red arrow numbered 1, **Figure 1**). Therefore, there is a need to further examine the clinical characteristics of patients with SCD. Obscure cognitive symptoms at early stage can be alleviated (Si et al., 2020). Previous studies have reported that SCD is associated with increased glial activation and consequently increased inflammation in the brain (Nordengen et al., 2019; Si et al., 2020).

As shown in **Figure 1** (red arrow numbered 2), the manifestation of olfactory dysfunction is reported in various neurological diseases, such as Parkinson's Disease (PD) (Altinayar et al., 2014), AD (Yoo et al., 2018), stroke (Wehling et al., 2015), and major depression disorder (Negoias et al., 2016; Croy and Hummel, 2017). Additionally, olfactory dysfunction is highly correlated with SCD (Risacher et al., 2017; Jobin et al., 2021; Wang et al., 2021), which may further progress to MCI and neurodegenerative dementia (Devanand et al., 2015; Fullard et al., 2016; Roberts et al., 2016; Dintica et al., 2019; Yahiaoui-Doktor et al., 2019) (red arrow numbered 3 to 1, **Figure 1**). Olfactory deficits increase the risk of developing AD dementia from MCI by four to five times (Devanand et al., 2008). Thus, olfactory impairment is suggested to be a marker for the early detection of cognitive decline and AD dementia (Devanand et al., 2015; Fullard et al., 2016; Roberts et al., 2016).

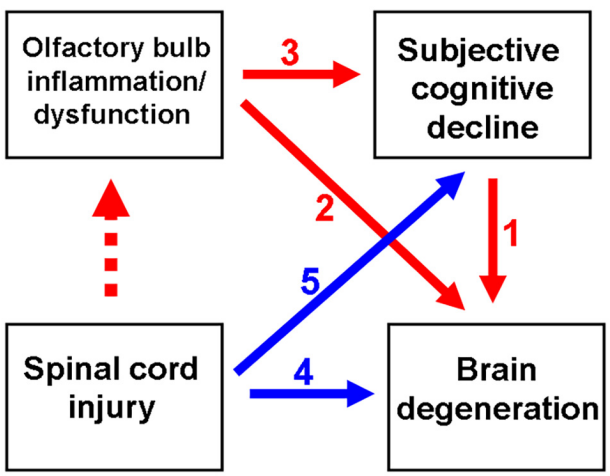

FIGURE 1 | Schematic diagram depicting spinal cord injury (SCI)-mediated olfactory dysfunction and the subsequent subjective cognitive decline (SCD)/neurodegenerative dementia. Olfactory dysfunction is an early indicator of neurological diseases, including SCD and neurodegenerative dementia. Previous studies have reported the correlation between SCD and neurodegenerative disease (ND) (indicated as red arrow no. 1). Generally, olfactory impairment is involved in the progression of ND (indicated as red arrow no. 2) or the progression of SCD to ND (from red arrow no. 3 to 1). Thus, SCI promotes ND (indicated as blue arrow no. 4), as well as the progression from initial SCD to ND (from blue arrow no. 5 to red arrow no. 1). This study demonstrated that SCI promotes neuroinflammation in the olfactory bulb at an ultrarapid stage after SCI. Thus, SCI may mediate the pathological mechanisms of neurodegeneration.

Traumatic spinal cord injury (SCI) leads to neurological deficits or chronic disability. Acute SCIs involve both pathophysiological primary and secondary mechanisms of injuries. Primary injuries involve damages to the neural structures (such as the cell membranes, myelin, axons, and microvessels) and can contribute to the exacerbation of secondary injuries (Kwon et al., 2004). Secondary SCIs include neuroinflammation, production of free radicals, hyperoxidation, and neuronal apoptosis (Tator and Fehlings, 1991; Houle and Tessler, 2003), which lead to irreversible neurological deficits in patients with SCI.

In addition to the spine, SCIs can adversely affect the brain and consequently promote inflammation in the brain (Wu et al., 2014) (blue arrow numbered 4, **Figure 1**). The enhanced production of pro-inflammatory cytokines and neurotoxic molecules post-SCI promotes inflammation in the brain (Tian et al., 2007). In the rat models of SCI, microglial activation promotes chronic inflammation in the thalamus, hippocampus, and cerebral cortex (Wu et al., 2014). Furthermore, suppressed neuroprotective mechanisms may contribute to the exacerbation of cerebral damage post-SCI. The expression of brain-derived neurotrophic factor (BDNF) is downregulated for at least 1 week after SCI, which adversely affects the plasticity of the rat hippocampus (Fumagalli et al., 2009). SCIs are reported to result in cognitive impairment (Craig et al., 2017; Sachdeva et al., 2018; Nightingale et al., 2020) and contribute to the development of neurodegenerative diseases, such as AD (Yeh et al., 2018) and PD (Yeh et al., 2016) (blue arrow numbered 5 to red arrow numbered 1, **Figure 1**). Olfactory dysfunction can predict neurodegeneration. However, the predictive value of olfactory dysfunction for cognitive impairment and subsequent dementia in patients with SCI has not been previously reported.

Granulocyte colony-stimulating factor (G-CSF) or colony-stimulating factor 3 (CSF3) is widely used for the clinical treatment of patients with neutropenia after chemotherapy, radiotherapy, or hematopoietic stem cell transplantation (Welte et al., 1996). The functions of G-CSF are to activate hematopoietic stem cells and stimulate the proliferation, differentiation, and maturation of neutrophils in the bone marrow (Holig, 2013). G-CSF is reported to exert neuroprotective effects in neurodegenerative diseases, including PD and AD (Tsai et al., 2007; Prakash et al., 2013a,b; Safari et al., 2016). The plasma concentrations of G-CSF in patients with early-stage AD are lower than those in healthy individuals (Laske et al., 2009). The administration of G-CSF improves the cognitive functions in patients with early-stage AD (Sanchez-Ramos et al., 2012). Moreover, G-CSF is reported to alleviate depression and motor function in rat PD models and increase the density of neurons in the substantia nigra pars compacta (SNpc) (Prakash et al., 2013a). Additionally, G-CSF can restore the

functions of striatum and SNpc in the 1-methyl-4-phenyl-1,2,3,6-tetrahydropyridine (MPTP)-induced PD mouse model (Song et al., 2011). Furthermore, G-CSF exhibits anti-inflammatory and neuroprotective effects in stroke and SCI (Kadota et al., 2012; Guo et al., 2015; Cui et al., 2016; Weise et al., 2017).

As shown in **Figure 1** (dotted red arrow), the effect of SCI on olfactory function has not been elucidated. This study examined the effect of SCI on neuroinflammation and the levels of olfactory receptors, neurotrophic factors, and neural stem cells (NSCs) in the mouse olfactory bulb. The findings of this study suggested that SCI promotes olfactory dysfunction, which indicated a correlation between SCI and neurodegenerative diseases. This study also used a mouse spinal cord hemisection model to investigate the therapeutic effects of G-CSF on the SCI-induced pathological changes in the olfactory bulb.

MATERIALS AND METHODS

Animals

Adult BLTW: CD1 (ICR) male mice aged 8 weeks and weighing 31–33 g were obtained from the BioLASCO Experimental Animal Center (Taiwan Co., Ltd., BioLASCO, Yilan, Taiwan). The animals were housed in cages (five animals per cage) under a regular circadian cycle with free access to food. This study was performed according to the guidelines outlined by the Experimental Animal Laboratory and approved by the Animal Care and Use Committee at National Ilan University, Yilan, Taiwan (IACUC Approval No.: 106-14).

Experimental Grouping

The animal model of spinal cord hemisection was established as described previously (Lin et al., 2011). Briefly, the mice were divided into the following four groups: sham-operated control (sham control group), animals underwent laminectomy (n = 18); vehicle-treated SCI group (SCI group) (n = 18), animals underwent spinal cord hemisection and administered with physiological saline; SCI + G-CSF i.p. group, SCI mice intraperitoneally administered with G-CSF (n = 18); and SCI + G-CSF oral group, SCI mice orally administered with G-CSF (n = 15). Microarray, mRNA, protein, and immunofluorescence analyses were performed using three, six, six, and three mice from the sham control, SCI, and SCI + G-CSF i.p. groups, respectively. As the SCI + G-CSF oral group comprised three mice less than those in the other groups, microarray analysis was not performed for this group.

Spinal Cord Hemisection

The animals were anesthetized using isoflurane, placed in a stereotactic apparatus (David Kopf Instruments, Tujunga, CA, United States) to secure the spinal cord, and subjected to posterior decompression. Laminectomy was performed at the 9th to 10th thoracic vertebrae with undisturbed intact dura under a dissecting microscope. For spinal cord hemisection, the guide of the wire knife was positioned along the vertical plane close to the lateral surface in the lower thoracic level of the spinal cord. The knife was turned medially and extended 1.5 mm. Next, the guide was lifted 4.0 mm to hemitransect the spinal cord. The sham group only underwent laminectomy but not hemisection. The wound was closed in layers using sutures. The animals were allowed to recover on a heating pad at 36.5°C and fast for 3 h post-surgery. For postoperative care, the animals were subcutaneously injected with saline for rehydration. The mice were returned to their preoperative housing conditions after surgery. The whole brain and the olfactory bulb were excised from mice in all four groups for microarray and gene expression analyses at 8 h post-hemisection.

Administration of G-CSF in SCI Mice

The SCI + G-CSF i.p. and SCI + G-CSF oral groups were intraperitoneally and orally administered with G-CSF (50 μg/kg bodyweight) at 30 min post-SCI. Meanwhile, the SCI group was intraperitoneally administered with physiological saline at 30 min post-SCI. The mice in the sham control group were not administered with physiological saline or G-CSF.

Preparation of Recombinant G-CSF

Recombinant G-CSF (rG-CSF) was synthesized in our laboratory. Briefly, U-87 MG cells (Bioresource Collection and Research Center, Hsinchu, Taiwan) were cultured in Eagle's Minimum Essential Medium (11700-077) (Gibco^{TM}, Thermo Scientific, Waltham, MA, United States) supplemented with 10% fetal bovine serum (A15-101) (PAA Cell Culture Company, BioPath Stores, Cambridge, United Kingdom). Total RNA was extracted from the cells (1×10^6–1×10^7 cells) using TRI Reagent® RNA isolation reagent (15596-018) (Invitrogen, Carlsbad, CA, United States), following the manufacturer's instructions. The RNA was reverse-transcribed to cDNA before PCR. The PCR product was purified from the agarose gel and subcloned into the T&A vector (Yeastern Biotech, Taipei, Taiwan). The recombinant vector was transformed into competent *Escherichia coli* RR1 cells. The final sequences with a size of 525 bp were purified from an agarose gel and subcloned into the pET-24a(+) expression vector (Novagen, Merck KGaA, Darmstadt, Germany) to obtain the pET-24a(+)-rG-CSF construct. Next, the pET-24a(+)-rG-CSF plasmid was transformed into *E. coli* BL21 Codon Plus® (DE3)-RIPL cells. rG-CSF was purified using affinity chromatography using the 6 × His-tagged tail. The levels of proteins, including those after each purification step, were analyzed using sodium dodecyl sulfate-polyacrylamide gel electrophoresis (SDS-PAGE). The yield of recombinant protein was determined using the protein assay kit (500-0006) (Bio-Rad Laboratories GmbH, Vienna, Austria).

Preparation of Water-in-Oil-in-Water Multiple Emulsion of the Oral Form of G-CSF

The water-in-oil-in-water (W/O/W) multiple emulsions were prepared using the two-step emulsified procedure with previously reported modifications (Onuki et al., 2004). Briefly, the droplets were emulsified using an equal volume of the gel solution to obtain the W/O/W emulsified particles. The composition of the three phases (inner aqueous phase:lipid

phase:gel solution in the ratio 1:1:2) was as follows: inner aqueous phase, G-CSF protein solution; lipid phase, glyceryl monostearate (0.05%; v/v), span 80 (0.05%; v/v), soybean lecithin (0.05%; v/v), and soybean oil, 0.85%; v/v); and gel solution, water (1.0%; v/v), Tween 20 (0.4%; v/v), and sodium carboxymethyl cellulose (0.6%; v/v). The W/O/W-emulsified particles were stored at 4°C for further use. The formulation was prepared on ice to avoid degradation of protein at higher temperatures.

Microarray Analysis

Microarray analysis was performed using the Agilent mouse gene expression microarray kit (Welgene Biotech, Taipei, Taiwan), following the manufacturer's instructions. Briefly, 0.2 μg of total RNA extracted from the whole-brain lysates was labeled with Cy3 (CyDye, Agilent Technologies, Santa Clara, CA, United States) using the Low Input Quick-Amp labeling kit (Agilent Technologies, Santa Clara, CA, United States) during the *in vitro* transcription process. Cy3-labeled cRNA (0.6 μg) was fragmented to an average size of approximately 50–100 nt in fragmentation buffer at 60°C for 30 min. The fragmented and labeled cRNA was then pooled and hybridized to Agilent SurePrint Microarray (Agilent Technologies, Santa Clara, CA, United States) at 65°C for 17 h. The microarray was washed, dried using a nitrogen gun, and scanned using an Agilent microarray scanner (Agilent Technologies, Santa Clara, CA, United States) at 535 nm to detect Cy3. The scanned images were analyzed using Feature Extraction 10.7.3.1 Software (Agilent Technologies, Santa Clara, CA, United States), which is an image analysis and normalization software used to quantify signal and background intensity for each feature. The raw signal data were subjected to quantile normalization to identify differentially expressed genes. The differentially expressed genes were subjected to the enrichment test for functional assay. ClusterProfiler was used for gene ontology and Kyoto Encyclopedia of Genes and Genomes pathway analyses.

Histological Analysis

Mice were anesthetized with Zoletil 50 (10 mg/kg i.p.; Virbac, Carros, France) at 8 h post-SCI and perfused with an intracardial infusion of phosphate-buffered saline (PBS; pH 7.4), followed by perfusion with 4% paraformaldehyde in PBS (pH 7.4) at 4°C. The mouse olfactory bulb was immediately excised, postfixed in the same fixative, and transferred to 30% sucrose in PBS until it sank. The fixed tissues were embedded at −25°C and sectioned into 20-μm coronal sections encompassing the entire olfactory bulb.

Immunofluorescence Staining

The tissue sections of the olfactory bulb were washed thrice with PBS for 5 min and blocked with PBS containing 10% goat serum and 0.5% Triton X-100 for 1 h. Next, the sections were incubated overnight at 4°C with mouse anti-glial fibrillary acidic protein (GFAP) (MA5-12023) (1:200; Invitrogen, Carlsbad, CA, United States) in PBS containing 5% goat serum and 0.5% Triton X-100. The sections were then washed thrice with PBS containing 0.5% Triton X-100 for 5 min and incubated with goat anti-mouse IgG (H + L) cross-adsorbed secondary antibody (A11001) (1:1000) (Invitrogen, Carlsbad, CA, United States) for 3 h. After washing thrice with PBS containing 0.5% Triton X-100 for 5 min, the sections were incubated with 4′,6-diamidino-2-phenylindole (1 μg/ml; Sigma-Aldrich, St. Louis, MO, United States) for 5 min. The sections were washed, mounted on coverslips, and observed under a Zeiss AX10-Imager A1 microscope (Carl Zeiss, Thornwood, NY, United States). All images were captured using AxioVision 4.7 microscopy software (Carl Zeiss, Thornwood, NY, United States). The morphological and quantitative analyses of the olfactory bulb were performed (indicated as the region of interest within the dashed box in **Figure 2A**). Cell counting was performed at a magnification of 400 × on every sixth section stained using the antibodies mentioned above. Only cells exhibiting visible indications of staining were counted. All data are presented as mean ± standard error of mean of three consecutive measurements.

Quantitative Real-Rime Polymerase Chain Reaction

Total RNA was extracted from the olfactory bulb tissues using TRIzol reagent (Invitrogen, Carlsbad, CA, United States). The RNA samples were subjected to reverse transcription using oligo-dT and SuperScript II reverse transcriptase (Invitrogen, Carlsbad, CA, United States). The quantitative real-rime polymerase chain reaction (qRT-PCR) analysis was performed using the ABI StepOne sequence detector system (Applied Biosystems, Foster City, CA, United States) with SYBR Green. The expression levels of the target genes were normalized to those of a housekeeping gene (β-actin). The primer sets and product size of each cDNA of interest were as follows: mouse IL-1β (Gene ID: 16176; accession number: NM_008361.4), 5′-AGG CTC CGA GAT GAA CAA-3′ and 5′-AAG GCA TTA GAA ACA GTC C-3′ (product size, 464 bp); IL-6 (Gene ID: 16193; accession number: NM_001314054.1), 5′-CCA CCA AGA ACG ATA GTC AA-3′ and 5′-TTT CCA CGA TTT CCC AGA-3′ (product size, 227 bp); GFAP (Gene ID: 14580; accession number: NM_001131020.1), 5′-CCA ACC CGT TCC ATA-3′ and 5′-TCC GCC TGG TAG ACA TCA-3′ (product size, 405 bp); *Olfr1494* (Gene ID: 258992; accession number: NM_146990.1), 5′-TAT GTA GTG GGC ATC CTG-3′ and 5′-GAT TGA GTA ATG GCG TGA-3′ (product size, 262 bp); *Olfr1324* (Gene ID: 258289; accession number: NM_146292.1), 5′-GCC ATC TGT CAC CCA TTA-3′ and 5′-CAA GCA AGC CTT AAC ACG-3′ (product size, 194 bp); *Olfr1241* (Gene ID: 258447; accession number: NM_146455.1), 5′-TCC ACT GCT ATC TCA CCC AA-3′ and 5′-AGG AAG CAA ACC CGC CTA-3′ (product size, 209 bp); *Olfr979* (Gene ID: 259112; accession number: NM_147108.2), 5′-GCA CCG AGT GTT TCC TGT-3′ and 5′-GAC CAT CTC ATT GGC TGA-3′ (product size, 269 bp); BDNF (Gene ID: 12064; accession number: NM_001048139.1), 5′-GGG TCA CAG CGG CAG ATA AA-3′ and 5′-GCC TTT GGA TAC CGG GAC TT-3′ (product size, 86 bp); glial cell-derived neurotrophic factor (GDNF) (Gene ID: 14573; accession number: NM_001301332.1), 5′-GGA CGC TTG GTG GTT GAT-3′ and 5′-ATG AGA ATG CTG CCG AAA-3′ (product size, 161 bp); nerve growth factor (NGF) (Gene ID: 18049; accession number: NM_001112698.2), 5′-AAG CCC ACT GGA CTA AAC T-3′ and 5′-GTC TTA

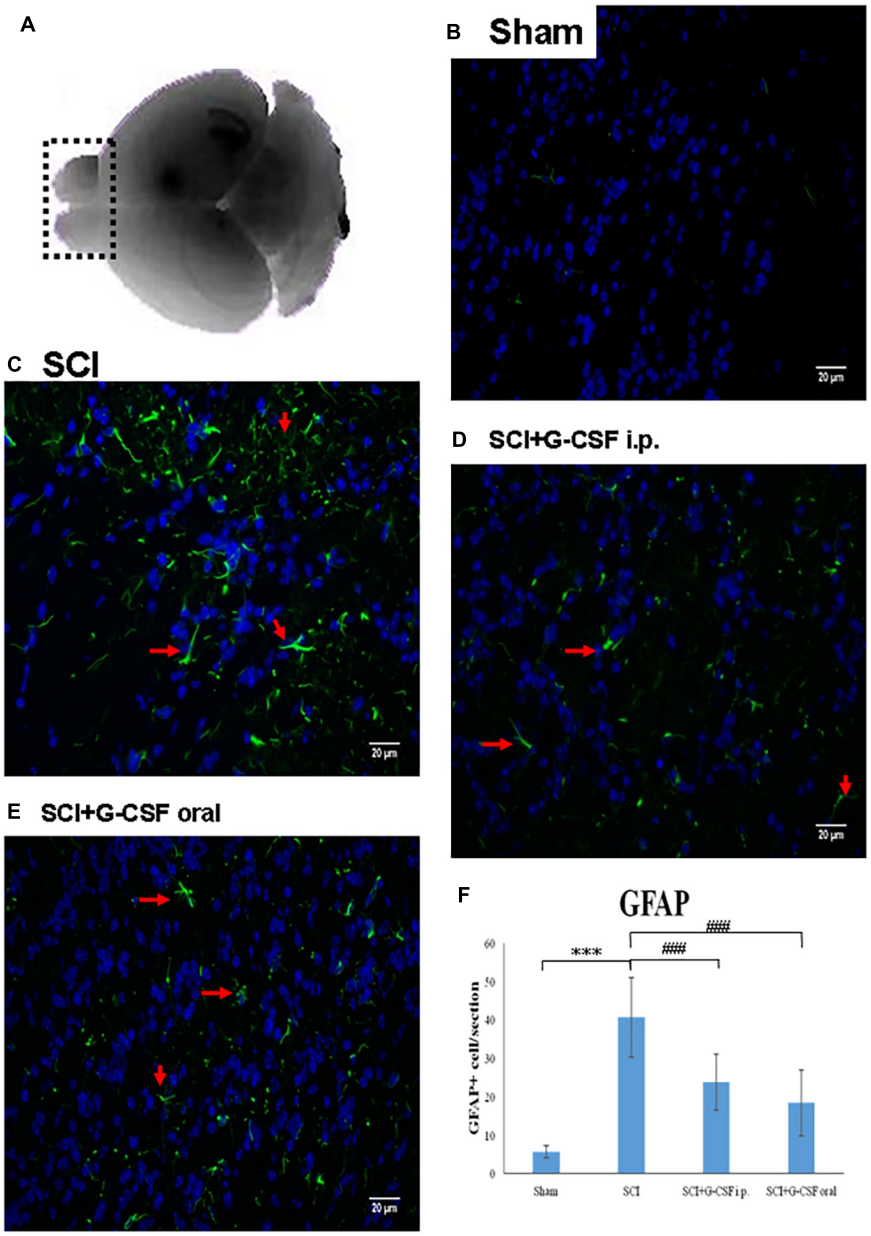

FIGURE 2 | Spinal cord injury (SCI) can activate the astrocytes in the olfactory bulb at 8 h post-spinal cord hemisection injury in mice. Representative images of GFAP-stained sections of the olfactory bulbs of the sham control **(B)**, SCI **(C)**, SCI + granulocyte colony-stimulating factor (G-CSF) i.p., and SCI + G-CSF oral groups. **(A)** Schematic illustration of the olfactory bulb (marked with dashed box) of all groups subjected to mRNA, protein, and immunofluorescence analyses. The SCI group exhibited a higher number of GFAP-positive cells [as indicated by arrow in panel **(C)**] than the sham control group **(B)**. This indicated astrocytic activation and potential astrocyte-mediated inflammatory responses in the olfactory bulb at 8 h post-SCI. The immunofluorescence intensity of GFAP significantly decreased in the SCI + G-CSF i.p. [as indicated by arrow in panel **(D)**] and SCI + G-CSF oral groups [as indicated by arrow in panel **(E)**] [**(B–C)** magnification 400×]. **(E)** Vertical bars indicate the mean ± standard error of mean) number of GFAP-stained cells in each group ($n = 3$). $^{***}P < 0.001$ and $^{###}P < 0.001$.

TCT CCA ACC CAC A-3′ (product size, 340 bp); Nestin (Gene ID: 18008; accession number: NM_016701.3), 5′-CCC TGA AGT CGA GGA GCT G-3′ and 5′-CTG CTG CAC CTC TAA GCG A-3′ (product size 166 bp); and β-actin (Gene ID: 11461; accession number: NM_007393.5), 5′-CTG TCC CTG TAT GCC TCT G-3′ and 5′-ATG TCA CGC ACG ATT TCC-3′ (product size, 218 bp).

Immunoblotting

Total protein was extracted from the mouse olfactory bulb tissues in a lysis buffer containing 0.8% NaCl, 10% glycerol, 0.1% SDS, 1% Triton X-100, 20 mM Tris–HCl, and 1 mM phenylmethylsulfonyl fluoride. The lysates were centrifuged at 13,000 *g* and 4°C for 10 min. The total protein content in the supernatant was determined using a protein assay kit (500-0006)

(Bio-Rad Laboratories GmbH, Vienna, VA, United States). The sample was then boiled for 5 min, and 20 μl (containing 20 μg of protein) aliquot of the sample was subjected to SDS-PAGE using a 12% gel. The resolved proteins were electroblotted to a nitrocellulose membrane. The membrane was blocked with the blocking reagent and incubated with the following primary antibodies for 12 h at 4°C: mouse anti-GFAP (MA5-12023) (1:2500) (Invitrogen, Carlsbad, CA, United States); rabbit anti-Nestin (tcna6785) (1:2500) (Taiclone, Taipei, Taiwan); rabbit anti-IL-6 (tcba214) (1:1000) (Taiclone, Taipei, Taiwan); rabbit anti-IL-1β (tcea9325) (1:1000) (Taiclone, Taipei, Taiwan); rabbit anti-β-actin (ab8227) (1:1000) (Abcam, Cambridge, MA, United States). Next, the membrane was washed thrice with PBS containing 0.05% Tween-20 for 5 min and incubated with goat anti-rabbit IgG (H + L) horseradish peroxidase (HRP)-conjugated secondary antibody (31460) (1:5000) (Invitrogen, Carlsbad, CA, United States), and goat anti-mouse IgG (H + L) HRP-conjugated secondary antibody (31430) (1:5000) (Invitrogen, Carlsbad, CA, United States) for 2 h. Immunoreactive signals were detected using SuperSignal™ West Pico Chemiluminescent Substrate (Catalog: 34080, Thermo Scientific™, Waltham, MA, United States). The protein bands were visualized and quantified using ImageQuant™ LAS 4000 (GE Healthcare Life Sciences, Marlborough, MA, United States).

Statistical Analyses

An independent two-sample *t*-test was used to compare the means of the two groups for microarray analysis. To assess differential mRNA and protein expression, three or more independent groups were compared using one-way analysis of variance. In cases where the differences were apparent, multiple comparisons were made using the Newman–Keuls method. Data are presented as mean ± standard error of mean. All statistical analyses were two-sided tests with the level of significance set at 0.05. All statistical analyses were performed using GraphPad Prism software version 5.0 (GraphPad Software, Inc., La Jolla, CA, United States).

RESULTS

SCI Downregulated the mRNA Levels of Olfactory Receptors in the Brain

Olfactory dysfunction can be an early indicator of neurological disorders, such as SCD or neurodegenerative diseases. SCI can lead to SCD or neurodegenerative diseases. This study examined if impaired olfaction is a risk factor for SCI-mediated neurodegeneration in the brain. An animal model of SCI was established to examine the effect of SCI on olfactory function. The whole-brain lysates of the mice from the sham control, SCI, and SCI + G-CSF i.p. groups ($n = 3$ for each group) were subjected to microarray analysis at 8 h post-SCI.

The microarray analysis revealed that the mRNA expression levels of *Olfr1494*, *Olfr979*, *Olfr424*, *Olfr122*, *Olfr1395*, *Olfr689*, *Olfr1457*, *Olfr384*, *Olfr969*, *Olfr945*, *Olfr788*, and *Olfr1339* (olfactory receptors) in the brain of the SCI group were significantly downregulated when compared to those in the brain of the control group at 8 h post-SCI ($^*P < 0.05$ for all) (**Supplementary Table 1**).

As shown in **Table 1**, the mRNA expression levels of *Olfr1494*, *Olfr979* ($^*P < 0.05$ and $^*P < 0.05$, respectively), *Mc3r* (G-protein-coupled receptor) ($^*P < 0.05$), *Ppp3cb* (regulator of calcium ion-regulated exocytosis), *Drd4* (dopamine neurotransmitter receptor), and *Gabrr3* (GABA-A receptor) in the brain of the SCI group were markedly lower than those in the brain of the sham control group. The mRNA expression levels of *Olfr1494* ($^*P < 0.05$), *Olfr979* ($^*P < 0.05$), *Mc3r*, *Ppp3cb*, *Drd4*, and *Gabrr3* in the SCI + G-CSF i.p. group were higher than those in the SCI group.

Compared with those in the brain of the control group mice, the expression levels of *Mc5r* (G-protein-coupled receptor) and *Ppp2r3a* (regulator of protein binding and bridging) ($^*P < 0.05$) were upregulated in the brain of the SCI group mice at 8 h post-SCI. Additionally, treatment with G-CSF downregulated the expression of *Mc5r* and *Ppp2r3a* ($^*P < 0.05$) in SCI mice.

These findings indicated that acute SCIs elicit inflammatory responses in the spinal cord and the brain. Additionally, SCI can damage the olfactory bulb and consequently decrease the number of olfactory receptors.

SCI Promoted Inflammation in the Brain Through the Activation of Astrocytes

The results of microarray analysis revealed that SCI promoted brain damage as early as 8 h post-SCI, which was characterized by downregulated expression of olfactory receptors. Olfactory defects are highly correlated with neurodegenerative diseases. Hence, this study focused on the pathology of the olfactory bulb in SCI animals (shown in the dashed box in **Figure 2A**). The ability of acute SCIs to induce inflammatory responses in the olfactory bulb and the subsequent neurodegeneration in the brain was examined.

TABLE 1 | Results of mRNA microarray analysis of mouse whole brain 8 h following SCIs.

Gene	SCI/sham (fold change)	Significance	SCI + G-CSF/SCI (fold change)	Significance	Function
Olfr1494	0.323	*	3.607	*	Olfactory reception
Olfr979	0.262	*	3.931	*	Olfactory reception
Mc3r	0.176	*	2.401		G-protein coupled receptor
Mc5r	2.142		0.460		G-protein coupled receptor
Ppp3cb	0.459		2.267		Calcium ion regulated exocytosis
Drd4	0.372		2.636		Dopamine neurotransmitter receptor
Gabrr3	0.400		2.378		GABA-A receptor
Ppp2r3a	5.757	*	0.179	*	Protein binding, bridging

*$^*P < 0.05$.

The mice were divided into the following four groups: sham control, SCI, SCI + G-CSF i.p., and SCI + G-CSF oral (n = 15 for each group). Astrocytes, which are the resident innate immune cells in the central nervous system (CNS), can be reactivated to mediate neuroinflammation. The reactivation is characterized by astrocytic hypertrophy and the release of various pro-inflammatory mediators. The GFAP immunofluorescence (arrow in **Figure 2C**) in the olfactory bulb was higher and denser in the SCI group ($^{***}P < 0.001$; **Figure 2F**) than in the sham control group (**Figure 2B**). This indicated that astrocytes are reactivated in the olfactory bulb at an early phase post-SCI, although the lesion was located at the spinal cord.

The GFAP fluorescence signal in the SCI group ($\#\#\#P < 0.001$ and $\#\#\#P < 0.001$, respectively; **Figure 2F**) was higher and denser than that in the SCI + G-CSF i.p. (**Figure 2D**) and SCI + G-CSF oral groups (**Figure 2E**).

SCI Promoted Neuroinflammation in the Olfactory Bulb *in vivo*

To analyze the effect of SCI on neuroinflammation, the olfactory bulb of the mice in the four groups (n = 6 for each group) was subjected to qRT-PCR analysis. Each experiment was performed three times. SCI promotes the activation of astrocytes and the release of pro-inflammatory cytokines. The mRNA expression levels of IL-1β ($^{*}P < 0.05$; **Figure 3A**), IL-6 ($^{***}P < 0.001$; **Figure 3B**), and GFAP ($^{*}P < 0.05$; **Figure 3C**) in the SCI group were upregulated when compared with those in the sham control group.

Treatment with G-CSF alleviated neuroinflammation in the olfactory bulb in mice with spinal cord hemisection. The mRNA expression levels of IL-1β, IL-6 ($\#\#\#P < 0.001$; **Figure 3B**), and GFAP ($\#\#\#P < 0.001$; **Figure 3C**) were significantly lower in the SCI + G-CSF i.p. group than in the SCI group. Similarly, the mRNA levels of IL-1β ($\#\#P < 0.01$; **Figure 3A**), IL-6 ($\#\#\#P < 0.001$; **Figure 3B**), and GFAP ($\#\#P < 0.01$; **Figure 3C**) in the olfactory bulb were lower in the SCI + G-CSF oral group than in the SCI group.

Western blot analysis was performed to verify neuroinflammation within the olfactory bulb from four groups of mice (n = 6 for each group) at the protein level. Unlike in the sham control group, enhanced astrocyte reactivation (elevated GFAP; $^{*}P < 0.05$; **Figure 3F**) and glial activation-induced pro-inflammatory cytokine production (upregulated expression levels of IL-1β; **Figure 3D** and IL-6; $^{**}P < 0.001$; **Figure 3E**) at 8 h post-SCI was observed in the SCI group. Additionally, the SCI + G-CSF i.p. group exhibited downregulated levels of IL-1β (**Figure 3D**), IL-6 (**Figure 3E**), and GFAP (**Figure 3F**). Similarly, the SCI + G-CSF oral group exhibited downregulated levels of IL-1β (**Figure 3D**), IL-6 (**Figure 3E**), and GFAP ($\#\#\ P < 0.001$; **Figure 3F**).

Previous studies have reported that neurodegeneration in the brain is correlated with olfactory deficits and SCI. The findings of this study indicated that SCI can lead to early neuroinflammation of the olfactory bulb.

G-CSF Mitigates SCI-Induced Downregulated mRNA Expression of Olfactory Receptors

The qRT-PCR analysis revealed that the expression levels of the olfactory receptors *Olfr1494* ($^{***}P < 0.001$; **Figure 4A**), *Olfr1324* ($^{***}P < 0.001$; **Figure 4B**), *Olfr1241* ($^{**}P < 0.01$; **Figure 4C**), and *Olfr979* ($^{***}P < 0.001$; **Figure 4D**) in the SCI group were significantly downregulated at 8 h post-SCI when compared with those in the sham control group.

The mRNA expression levels of *Olfr1494* ($\#\#\#P < 0.001$; **Figure 4A**), *Olfr1324* ($\#\#\#P < 0.001$; **Figure 4A**), *Olfr1241* ($\#\#P < 0.01$; **Figure 4C**), and *Olfr979* ($\#\#\#P < 0.001$; **Figure 4D**) in the olfactory bulb of the SCI + G-CSF i.p. group were significantly upregulated when compared with those in the olfactory bulb of the SCI group. Compared with that in the sham control and SCI groups, the mRNA expression level of *Olfr1241* in the olfactory bulb was significantly upregulated in the SCI + G-CSF oral group ($\#\#\ P < 0.01$; **Figure 4C**).

These results indicate that in the ultrarapid stage of CNS injury (including SCI), the mRNA expression of olfactory receptors is downregulated, which may further contribute to olfactory dysfunction and potential degeneration of the olfactory neural network and consequently neurodegeneration. Previous studies have reported that the olfactory bulb is a sentinel station for neurodegeneration in the brain. G-CSF can mitigate SCI-induced changes in mRNA expression and achieve early preventive effects.

G-CSF Mitigates SCI-Induced Downregulation of mRNA and Protein Levels of Nestin and Neurotrophic Factors in the Olfactory Bulb

The SCI group exhibited significantly downregulated mRNA expression levels of BDNF ($^{**}P < 0.01$; **Figure 5A**), GDNF ($^{**}P < 0.01$; **Figure 5B**), NGF ($^{*}P < 0.05$; **Figure 5C**), and Nestin (marker of NSC) (**Figure 5D**) when compared with the sham control group at 8 h post-SCI.

The mRNA expression levels of BDNF ($\#\#P < 0.01$; **Figure 5A**), GDNF ($\#\#P < 0.01$; **Figure 5B**), NGF ($\#\#P < 0.01$; **Figure 5C**), and Nestin ($\#\#\#P < 0.001$; **Figure 5D**) in the olfactory bulb of the SCI + G-CSF i.p. group were upregulated when compared with those in the olfactory bulb of the SCI group at 8 h post-SCI. Compared with those in the olfactory bulb of the SCI group, the mRNA expression levels of BDNF ($\#\#P < 0.01$; **Figure 5A**), GDNF ($\#P < 0.05$; **Figure 5B**), NGF ($\#P < 0.05$; **Figure 5C**), and Nestin ($\#\#\#P < 0.001$; **Figure 5D**) were significant upregulated in the olfactory bulb of the SCI + G-CSF oral group.

The protein expression of Nestin was quantified using western blotting. Compared with that in sham control, the expression of Nestin was significantly downregulated in the SCI group ($^{***}P < 0.001$; **Figure 5E**). However, the expression levels of Nestin in the SCI + G-CSF i.p. and SCI + oral groups ($\#P < 0.05$; **Figure 5E**) were higher than those in the SCI group.

These findings indicated that neuroinflammation of the olfactory bulb partly affects the neurogenesis-associated

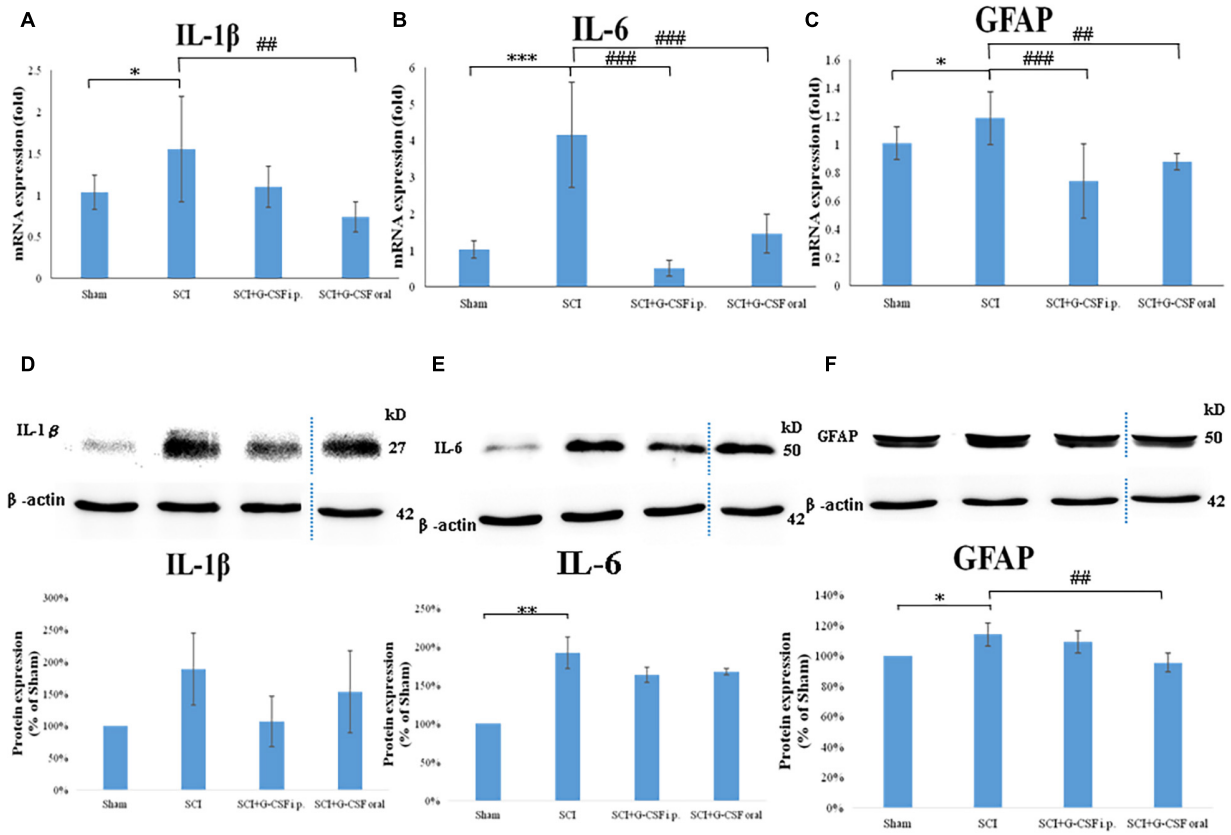

FIGURE 3 | Neuroinflammation in the mouse olfactory bulb at 8 h post-spinal cord injury (SCI). **(A–C)** The mRNA expression levels of IL-1β **(A)**, IL-6 **(B)**, and GFAP **(C)** in the olfactory bulb of the sham control, SCI, SCI + granulocyte colony-stimulating factor (G-CSF) i.p., and SCI + G-CSF oral groups at 8 h post-SCI. Vertical bars indicate the mean ± standard error of the mean (SEM) ($n = 6$ for each group). $^{*}P < 0.05$, $^{***}P < 0.001$, $^{\#\#}P < 0.01$, and $^{\#\#\#}P < 0.001$. **(D–F)** The protein expression levels of IL-1β **(D)**, IL-6 **(E)**, and GFAP **(F)** in the olfactory bulb of the four experimental groups at 8 h post-SCI. Representative immunoblots of IL-1β, IL-6, GFAP, and β-actin (internal control) are shown in the upper panel. The lower panel indicates the ratio of target protein band intensity to β-actin protein band intensity relative to the control group (mean ± SEM). G-CSF mitigates SCI-induced neuroinflammation in the olfactory bulb as evidenced by the decreased expression of IL-1β, IL-6, and GFAP. Vertical bars indicate mean ± SEM ($n = 6$ for each group). $^{*}P < 0.05$, $^{**}P < 0.01$, and $^{\#\#}P < 0.01$.

processes, including the generation of NSCs and the production of associated neurotrophic factors. G-CSF treatment may promote the generation of NSCs and the production of neurotrophic factors and consequently mitigate SCI-induced downregulated olfactory receptors and olfactory dysfunction. Thus, G-CSF may mitigate neurodegeneration in other areas of the brain.

DISCUSSION

Olfactory dysfunction is an indicator of various neurological diseases, such as PD, AD, and depression. Patients with neurodegeneration exhibit significantly impaired odor sensitivity, discrimination, and identification (Altinayar et al., 2014; Negoias et al., 2016; Yoo et al., 2018). Neurological diseases, including PD, AD, and depression, are associated with dysfunctional serotonergic and dopaminergic neurotransmission (Croy and Hummel, 2017). The major transmission routes of the serotonin and dopamine systems include the orbitofrontal cortex, hippocampus, striatum, and amygdala (Drevets, 2007; Hamilton et al., 2008; Gabbay et al., 2013). Additionally, odor molecules are initially sensed by the olfactory receptors in the olfactory bulb. Next, the olfactory signal passes through the prefrontal cortex, hippocampus, striatum, and amygdala (Yang et al., 2011; Negoias et al., 2016; Croy and Hummel, 2017). The transmission route of the olfactory signals overlaps with the dopamine and serotonin pathways. The structural and functional impairments among these brain regions lead to dysfunctional neurotransmission and consequently result in impaired olfactory conduction. This explains the correlation between olfactory dysfunction and neurodegeneration.

Several animal and human experiments have confirmed that the olfactory bulb, which regulates the olfactory receptors, plays an important role in neurodegeneration in the brain. The volume of the olfactory bulb is correlated with depression severity (Negoias et al., 2010). Patients with depression who do not exhibit improvements with psychotherapy are associated with severe olfactory bulb atrophy (Croy and Hummel, 2017).

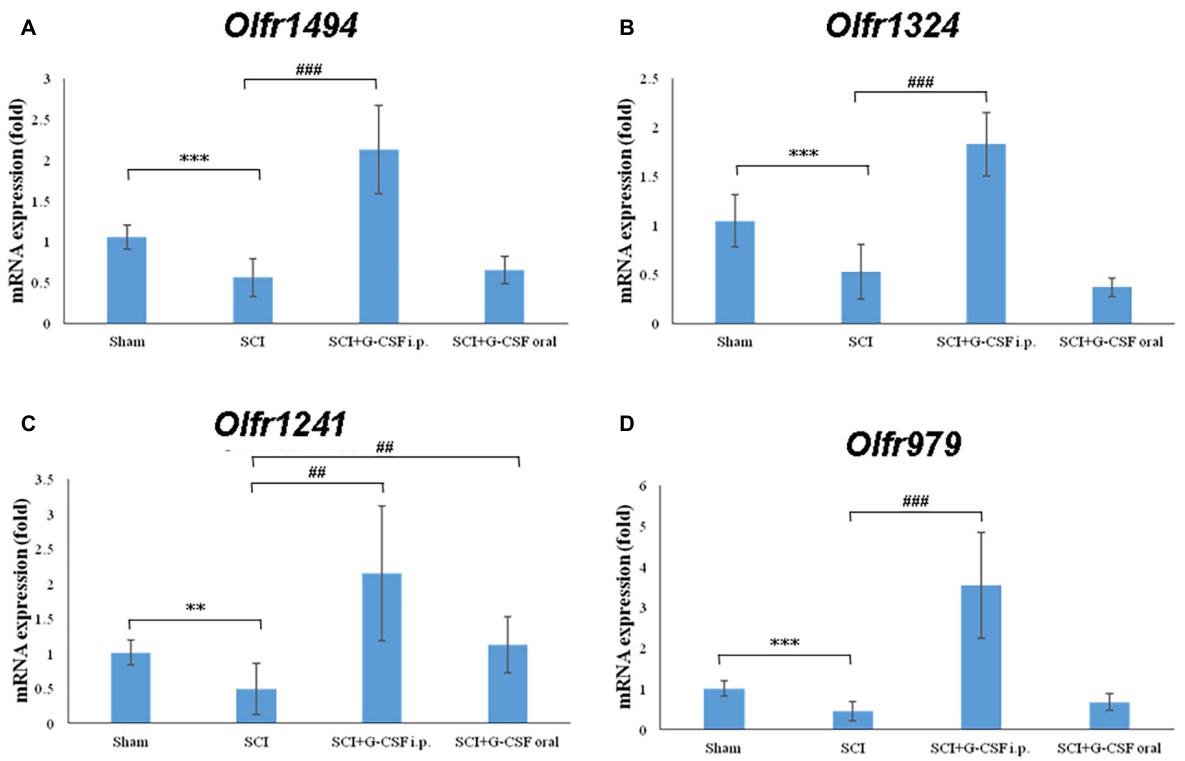

FIGURE 4 | Spinal cord injury (SCI) decreases the expression of olfactory receptors in the olfactory bulb at 8 h post-SCI. The mRNA expression levels of **(A)** *Olfr1494*, **(B)** *Olfr1324*, **(C)** *Olfr1241*, and **(D)** *Olfr979* in the olfactory bulb of the sham control, SCI, SCI + G-CSF i.p., and SCI + G-CSF oral groups. Vertical bars indicate mean ± standard error of mean (n = 6 in each group). $^{**}P < 0.01$, $^{***}P < 0.001$, $^{\#\#}P < 0.01$, and $^{\#\#\#}P < 0.001$.

Various studies have reported that pathogens, including viruses, bacteria, prions, and toxins, can enter the brain directly through the olfactory pathway and damage the neural structure (Doty, 2008). The olfactory epithelium, which is in direct contact with the external environment, is separated from the external environment only by a thin layer of mucus. Thus, the olfactory system is susceptible to various external factors. The olfactory bulb has been considered as the entry point for pathogens, which spread to the brain through the olfactory pathway and consequently cause pathological changes (Rey et al., 2018). Viruses, which are a risk factor for neurodegenerative diseases, can penetrate olfactory receptor neurons. Next, viruses are transported through axons in the space around the nerves, spread through the cribriform plate, and transported to the subarachnoid space and remote brain areas (Dando et al., 2014). Moreover, pathological protein aggregation in the olfactory bulb is detected earlier than that in other regions (Rey et al., 2018). This indicates that the olfactory bulb is vulnerable to environmental insults and that it is involved in early neurodegenerative diseases.

In addition to regulating olfactory function, the olfactory bulb is one of the sites at which NSCs are stored (Pagano et al., 2000). The hippocampus is the other site at which NSCs are stored (Rolando and Taylor, 2014). The characteristics of NSCs include self-renewal and multipotent differentiation into neurons or glial cells. NSCs have been isolated from the olfactory bulb, cortex, hippocampus, or subventricular zone (SVZ) of lateral ventricles of the brain (Marei et al., 2015). Generally, neural progenitors formed during neurogenesis in the SVZ migrate forward along the rostral migratory stream (RMS) (Whitman et al., 2009), and combine neural circuits to develop into interneurons in the olfactory bulb (kay-Sim, 2010). NSCs differentiate into neural cells, including neurons and glial cells, in response to environmental stimuli (Alizadeh et al., 2017). Additionally, NSCs can regenerate olfactory receptor neurons (Godoy et al., 2015). Chronic inflammation may impair the neurogenesis of olfactory NSCs (Rustenhoven and Kipnis, 2019).

Complex mechanisms are involved in neuroblast migration in the RMS. Astrocytes, astrocyte-released growth factors, and neurotrophic factors are the regulatory factors that determine neuroblast migration. The blood vessels are reported to support forward motility during neuroblast migration (Motamed et al., 2019). The generation of blood vessels is mediated by astrocyte-secreted vascular endothelial growth factor (Bozoyan et al., 2012). Astrocytes located at the boundary of RMS undergo hypertrophy and branching and promote the wrapping of neuroblasts along with blood vessels to form glial tubes, which results in the separation of the neuroblasts from the surrounding tissues (Snapyan et al., 2009; Motamed et al., 2019). BDNF, which is secreted from the vasculature, increases the number and motility of neuroblasts (Chiaramello et al., 2007). Astrocytes regulate the activity and migration of neuroblasts through BDNF

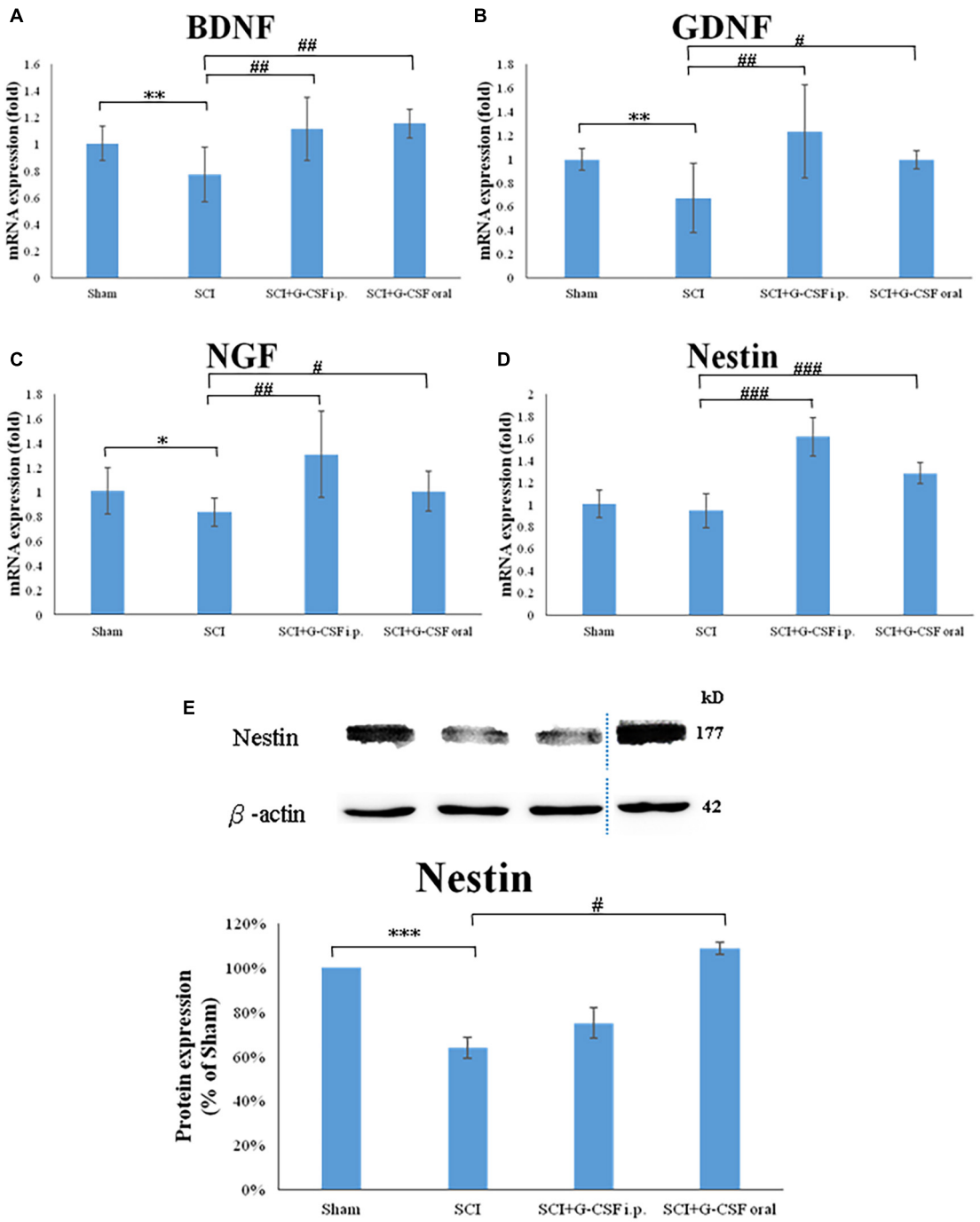

FIGURE 5 | Spinal cord injury (SCI) downregulates the expression of neurotrophic factors and the number of neural stem cells (NSCs) in the olfactory bulb at 8 h post-SCI. **(A–D)** The mRNA expression levels of BDNF **(A)**, GDNF **(B)**, NGF **(C)**, and Nestin (NSC marker) **(D)** in the olfactory bulb of the sham control, SCI, SCI + granulocyte colony-stimulating factor (G-CSF) i.p., and SCI + G-CSF oral groups. **(E)** The protein expression levels of Nestin in the olfactory bulb of the four experimental groups at 8 h post-SCI. The upper panel shows the immunoblot of Nestin (177 kDa). β-Actin (42 kDa) served as an internal control. The lower panel indicates the ratio of Nestin protein band intensity to β-actin protein band intensity relative to the control group. Vertical bars indicate mean ± standard error of mean for mRNA **(A–D)** or protein expression **(E)** [$n = 6$ in each group for panels **(A–E)**]. $^{*}P < 0.05$, $^{**}P < 0.01$, $^{***}P < 0.001$, $\#P < 0.05$, $\#\#P < 0.01$, and $\#\#\#P < 0.001$.

(Snapyan et al., 2009). GDNF serves as a directional cue for the chemotaxis of neuroblasts from SVZ to the olfactory bulb (Paratcha et al., 2006).

Neural stem cells migrate toward lesioned sites upon CNS injury and promote neurogenesis (Imitola et al., 2004; Bai et al., 2018). Similar to the migration mechanism in RMS, neuroblasts

use blood vessels as a physical guide to migrate from SVZ to the lesion site (Kaneko et al., 2017). Newly generated neuroblasts are recruited into blood vessels and redirected to the lesioned site *via* the chemoattractive/trophic factors, such as BDNF, stromal-cell-derived factor-1α (SDF-1α), and metalloproteinase-9 (MMP-9) (Ghashghaei et al., 2007; Grade et al., 2013). However, the intrinsic neuronal repair mechanism is not effective. For example, the endogenous BDNF levels are low and consequently the regeneration process is impaired.

A rat model of systemic lipopolysaccharide (LPS) treatment exhibited inflammatory response and upregulation of cytokines in the olfactory bulb at 6 h post-LPS administration (Doursout et al., 2013). The findings of this study indicated that the olfactory bulb is vulnerable to environmental insults, such as damage from the remote periphery or CNS. This study elucidated the manifestations of neuroinflammatory responses in the olfactory bulb and the potential mechanisms leading to olfactory dysfunction, including the downregulation of olfactory receptors, the production of NSC, and the secretion of neurotrophic factors at 8 h post-SCI. In this study, SCI promoted neuroinflammation in the olfactory bulb, which was characterized by the activation of resident astrocytes and the subsequent release of pro-inflammatory cytokines. Astrocyte reactivation in the olfactory bulb may promote glial stimulation and whole-brain inflammation and impair NSC regeneration. Aberrant activation of innate immune cells and the inflamed brain may lead to neurodegenerative changes in the brain (Kung and Lin, 2021a,b). The decreased number of olfactory receptors may reduce the turnover rate toward the olfactory bulb, which leads to atrophy of the olfactory bulb. The decrease in the olfactory bulb volume eventually leads to a decline in the signal from the olfactory bulb to the amygdala, hippocampus, striatum, and orbitofrontal cortex, which exacerbates neurodegeneration (Croy and Hummel, 2017). Moreover, the olfactory bulb in the SCI group exhibited decreased Nestin expression and downregulated production of neurotrophic factors, including BDNF, NGF, and GDNF. The key factors that promote neurogenesis, including NSCs, supportive neurotrophic/chemotactic factors, and protective astrocytes for constructing glial tubes, are dysregulated, which promotes neurodegeneration in the brain. We hypothesized that the ultrarapid stage after CNS injury [even lesions located at sites distant from the brain (such as SCI)] initiates degenerative changes in the brain, which are characterized by pathological changes in the olfactory bulb, including astrocyte-driven neuroinflammation, olfactory dysfunction, and impaired production of NSCs and neurotrophic factors. G-CSF can mitigate these pathological changes in the olfactory bulb.

The olfactory bulb and the related tracts and projections to specific brain regions, including the hippocampus and amygdala, are responsible for the storage and recovery of memory and emotional regulation (Roberts et al., 2016). Neurodegenerative insults can damage the nuclei that produce acetylcholine, dopamine, and norepinephrine and consequently decrease the production of choline acetyltransferase, which leads to cholinergic, dopaminergic, and noradrenergic deficiencies (Mesholam et al., 1998; Doty, 2012). Thus, olfactory dysfunction is exacerbated with subsequent cognitive decline and dementia. In the amyloid beta-induced AD rat model, G-CSF downregulated the expression of acetylcholinesterase in the brain (Prakash et al., 2013b). G-CSF inhibits the acetylcholinesterase-mediated hydrolysis of acetylcholine into choline and acetic acid, which results in enhanced plasma concentration of acetylcholine. In the MPTP-induced PD mouse model, G-CSF inhibited MPTP-induced cell death of dopaminergic substantia nigra neurons and attenuated the reduction of striatal dopamine (Meuer et al., 2006). G-CSF decreases the reuptake of norepinephrine in the peripheral sympathetic neurons and consequently increases the release of norepinephrine (Lucas et al., 2012). In this study, G-CSF increased the number of NSCs as evidenced by increased expression of Nestin and neurotrophic factors, including BDNF, GDNF, and NGF, in the olfactory bulb. The administration of recombinant BDNF in the brain promotes neurogenesis in the striatum and olfactory bulb (Zigova et al., 1998; Benraiss et al., 2001) in addition to enhancing neuroblast migration to the lesion site in the mouse injury model (Grade et al., 2013). The beneficial effects of epidermal growth factor and fibroblast growth factor-2 on neurogenesis in SVZ and the olfactory bulb have been demonstrated in the PD animal model (Winner et al., 2008). Olfactory deficiency, which is an early marker of neurodegeneration in the brain, is associated with various functional nuclei of olfactory projection that are involved in cognition, memory, and dysfunction of neurotransmission. Therefore, G-CSF can prevent olfactory dysfunction, initial inflammation of the olfactory bulb and brain, and the subsequent neurodegeneration in the brain.

This study is associated with several limitations. In this study, the pathological changes of the olfactory bulb were investigated in the ultrarapid phase after CNS injury to verify the role of the olfactory bulb as an early lesion site of neurodegeneration in the brain. This study demonstrated the local benefits of G-CSF in the early stage of inflammation in the olfactory bulb. Although previous studies have reported the correlation between the olfactory bulb and associated functional nucleus, further studies are needed to examine the effect of the inflammation in the olfactory bulb on the entire brain and the consequent development of neurodegenerative diseases. Additionally, this study examined the markers of NSCs (Nestin) and the production of BDNF. However, neurogenesis and migration of NSCs in the olfactory bulb or SVZ have not been demonstrated. The pathological manifestations of the olfactory bulb were demonstrated in an early stage of CNS injury. Although the mRNA levels varied, the corresponding protein levels did not exhibit a marked change. However, the olfactory bulb exhibited inflammation and impaired neurogenesis at 8 h post-SCI. The novel findings of this study enable the development of clinical interventions for neurodegenerative diseases.

CONCLUSION

Previous studies have reported that the olfactory bulb and olfactory dysfunction are involved in neurodegenerative diseases. This study demonstrated that CNS injury (even SCI located

at a distant site from the brain) promotes inflammatory response in the olfactory bulb at an early stage, which is accompanied by downregulation of olfactory receptors, impaired neurogenesis, and decreased production of NSCs and BDNF. G-CSF administration can mitigate the pathological changes in the olfactory bulb at an early stage of CNS injury in mice with spinal cord hemisection. The findings of this study will contribute to further studies on the pathophysiological mechanisms of early neurodegenerative diseases involving the olfactory bulb and aid in the development of early clinical drug interventions.

DATA AVAILABILITY STATEMENT

The raw data supporting the conclusions of this article will be made available by the authors, without undue reservation.

ETHICS STATEMENT

The animal study was reviewed and approved by Animal Care and Ethics Committee of National Ilan University, Yilan, Taiwan.

AUTHOR CONTRIBUTIONS

M-SL: writing-original draft, writing-review and editing, and formal analysis. I-HC: project administration and methodology. C-CL: resources, funding acquisition, conceptualization, and formal analysis. All authors contributed to the article and approved the submitted version.

ACKNOWLEDGMENTS

Part of the information reported in Results was referenced from the master thesis of I-HC at the National Ilan University, Yilan, Taiwan.

SUPPLEMENTARY MATERIAL

The Supplementary Material for this article can be found online at: https://www.frontiersin.org/articles/10.3389/fnagi.2021.701702/full#supplementary-material

REFERENCES

Alizadeh, R., Hassanzadeh, G., Joghataei, M. T., Soleimani, M., Moradi, F., Mohammadpour, S., et al. (2017). In vitro differentiation of neural stem cells derived from human olfactory bulb into dopaminergic-like neurons. *Eur. J. Neurosci.* 45, 773–784. doi: 10.1111/ejn.13504

Altinayar, S., Oner, S., Can, S., Kizilay, A., Kamisli, S., and Sarac, K. (2014). Olfactory disfunction and its relation olfactory bulb volume in Parkinson's disease. *Eur. Rev. Med. Pharmacol. Sci.* 18, 3659–3664.

Bai, S. M., Wang, Q., Yu, X. L., Chen, T., Yang, J., Shi, J. T., et al. (2018). Grafted neural stem cells show lesion-specific migration in radiation-injured rat brains. *RSC Adv.* 8, 5797–5805. doi: 10.1039/c7ra10151a

Benraiss, A., Chmielnicki, E., Lerner, K., Roh, D., and Goldman, S. A. (2001). Adenoviral brain-derived neurotrophic factor induces both neostriatal and olfactory neuronal recruitment from endogenous progenitor cells in the adult forebrain. *J. Neurosci.* 21, 6718–6731. doi: 10.1523/jneurosci.21-17-06718.2001

Bozoyan, L., Khlghatyan, J., and Saghatelyan, A. (2012). Astrocytes control the development of the migration-promoting vasculature scaffold in the postnatal brain via VEGF signaling. *J. Neurosci.* 32, 1687–1704. doi: 10.1523/jneurosci.5531-11.2012

Chiaramello, S., Dalmasso, G., Bezin, L., Marcel, D., Jourdan, F., Peretto, P., et al. (2007). BDNF/ TrkB interaction regulates migration of SVZ precursor cells via PI3-K and MAP-K signalling pathways. *Eur. J. Neurosci.* 26, 1780–1790. doi: 10.1111/j.1460-9568.2007.05818.x

Craig, A., Guest, R., Tran, Y., and Middleton, J. (2017). Cognitive impairment and mood states after spinal cord injury. *J. Neurotrauma* 34, 1156–1163. doi: 10.1089/neu.2016.4632

Croy, I., and Hummel, T. (2017). Olfaction as a marker for depression. *J. Neurol.* 264, 631–638. doi: 10.1007/s00415-016-8227-8

Cui, L., Wang, D., McGillis, S., Kyle, M., and Zhao, L. R. (2016). Repairing the Brain by SCF+G-CSF treatment at 6 months postexperimental stroke: mechanistic determination of the causal link between neurovascular regeneration and motor functional recovery. *ASN Neuro* 8:175909141665 5010.

Dando, S. J., kay-Sim, A., Norton, R., Currie, B. J., St, John JA, Ekberg, J. A., et al. (2014). Pathogens penetrating the central nervous system: infection pathways and the cellular and molecular mechanisms of invasion. *Clin. Microbiol. Rev.* 27, 691–726. doi: 10.1128/cmr.00118-13

Devanand, D. P., Lee, S., Manly, J., Andrews, H., Schupf, N., Doty, R. L., et al. (2015). Olfactory deficits predict cognitive decline and Alzheimer dementia in an urban community. *Neurology* 84, 182–189. doi: 10.1212/wnl.0000000000001132

Devanand, D. P., Liu, X., Tabert, M. H., Pradhaban, G., Cuasay, K., Bell, K., et al. (2008). Combining early markers strongly predicts conversion from mild cognitive impairment to Alzheimer's disease. *Biol. Psychiatry* 64, 871–879. doi: 10.1016/j.biopsych.2008.06.020

Dintica, C. S., Marseglia, A., Rizzuto, D., Wang, R., Seubert, J., Arfanakis, K., et al. (2019). Impaired olfaction is associated with cognitive decline and neurodegeneration in the brain. *Neurology* 92, e700–e709.

Doty, R. L. (2008). The olfactory vector hypothesis of neurodegenerative disease: is it viable? *Ann. Neurol.* 63, 7–15. doi: 10.1002/ana.21327

Doty, R. L. (2012). Olfaction in Parkinson's disease and related disorders. *Neurobiol. Dis.* 46, 527–552. doi: 10.1016/j.nbd.2011.10.026

Doursout, M. F., Schurdell, M. S., Young, L. M., Osuagwu, U., Hook, D. M., Poindexter, B. J., et al. (2013). Inflammatory cells and cytokines in the olfactory bulb of a rat model of neuroinflammation; insights into neurodegeneration? *J. Interferon. Cytokine Res.* 33, 376–383. doi: 10.1089/jir.2012.0088

Drevets, W. C. (2007). Orbitofrontal cortex function and structure in depression. *Ann. N Y Acad. Sci.* 1121, 499–527. doi: 10.1196/annals.1401.029

Fullard, M. E., Tran, B., Xie, S. X., Toledo, J. B., Scordia, C., Linder, C., et al. (2016). Olfactory impairment predicts cognitive decline in early Parkinson's disease. *Parkinsonism Relat. Disord.* 25, 45–51. doi: 10.1016/j.parkreldis.2016.02.013

Fumagalli, F., Madaschi, L., Caffino, L., Marfia, G., Di Giulio, A. M., Racagni, G., et al. (2009). Acute spinal cord injury reduces brain derived neurotrohic factor expression in rat hippocampus. *Neuroscience* 159, 936–939. doi: 10.1016/j.neuroscience.2009.01.030

Gabbay, V., Ely, B. A., Li, Q., Bangaru, S. D., Panzer, A. M., Alonso, C. M., et al. (2013). Striatum-based circuitry of adolescent depression and anhedonia. *J. Am. Acad. Child Adolesc. Psychiatry* 52, 628–641. doi: 10.1016/j.jaac.2013.04.003

Ghashghaei, H. T., Lai, C., and Anton, E. S. (2007). Neuronal migration in the adult brain: are we there yet? *Nat. Rev. Neurosci.* 8, 141–151. doi: 10.1038/nrn2074

Godoy, M. D., Voegels, R. L., Pinna, F. R., Imamura, R., and Farfel, J. M. (2015). Olfaction in neurologic and neurodegenerative diseases: a literature review. *Int. Arch. Otorhinolaryngol.* 19, 176–179. doi: 10.1055/s-0034-1390136

Grade, S., Weng, Y. C., Snapyan, M., Kriz, J., Malva, J. O., and Saghatelyan, A. (2013). Brain-derived neurotrophic factor promotes vasculature-associated migration of neuronal precursors toward the ischemic striatum. *PLoS One* 8:e55039. doi: 10.1371/journal.pone.0055039

Guo, Y., Liu, S., Zhang, X., Wang, L., Gao, J., Han, A., et al. (2015). G-CSF promotes autophagy and reduces neural tissue damage after spinal cord injury in mice. *Lab Invest.* 95, 1439–1449. doi: 10.1038/labinvest.2015.120

Hamilton, J. P., Siemer, M., and Gotlib, I. H. (2008). Amygdala volume in major depressive disorder: a meta-analysis of magnetic resonance imaging studies. *Mol. Psychiatry* 13, 993–1000. doi: 10.1038/mp.2008.57

Holig, K. (2013). G-CSF in healthy allogeneic stem cell donors. *Transfus. Med. Hemother.* 40, 225–235. doi: 10.1159/000354196

Houle, J. D., and Tessler, A. (2003). Repair of chronic spinal cord injury. *Exp. Neurol.* 182, 247–260.

Imitola, J., Raddassi, K., Park, K. I., Mueller, F. J., Nieto, M., Teng, Y. D., et al. (2004). Directed migration of neural stem cells to sites of CNS injury by the stromal cell-derived factor 1alpha/CXC chemokine receptor 4 pathway. *Proc. Natl. Acad. Sci. U.S.A.* 101, 18117–18122. doi: 10.1073/pnas.0408258102

Jessen, F., Amariglio, R. E., van, B. M., Breteler, M., Ceccaldi, M., Ch蒙telat, G., et al. (2014). A conceptual framework for research on subjective cognitive decline in preclinical Alzheimer's disease. *Alzheimers Dement* 10, 844–852.

Jobin, B., Zahal, R., Bussi?res, E. L., Frasnelli, J., and Boller, B. (2021). Olfactory identification in subjective cognitive decline: a meta-analysis. *J. Alzheimers Dis.* 79, 1497–1507. doi: 10.3233/jad-201022

Kadota, R., Koda, M., Kawabe, J., Hashimoto, M., Nishio, Y., Mannoji, C., et al. (2012). Granulocyte colony-stimulating factor (G-CSF) protects oligodendrocyte and promotes hindlimb functional recovery after spinal cord injury in rats. *PLoS One* 7:e50391. doi: 10.1371/journal.pone.0050391

Kaneko, N., Sawada, M., and Sawamoto, K. (2017). Mechanisms of neuronal migration in the adult brain. *J. Neurochem.* 141, 835–847. doi: 10.1111/jnc.14002

kay-Sim, A. (2010). Stem cells and their niche in the adult olfactory mucosa. *Arch. Ital. Biol.* 148, 47–58.

Kung, W. M., and Lin, M. S. (2021a). Beneficial impacts of alpha-eleostearic acid from wild bitter melon and curcumin on promotion of CDGSH iron-sulfur domain 2: therapeutic roles in CNS injuries and diseases. *Int. J. Mol. Sci.* 22:3289. doi: 10.3390/ijms22073289

Kung, W. M., and Lin, M. S. (2021b). The NF庶B antagonist CDGSH iron-sulfur domain 2 is a promising target for the treatment of neurodegenerative diseases. *Int. J. Mol. Sci.* 22:934. doi: 10.3390/ijms22020934

Kwon, B. K., Tetzlaff, W., Grauer, J. N., Beiner, J., and Vaccaro, A. R. (2004). Pathophysiology and pharmacologic treatment of acute spinal cord injury 7. *Spine J.* 4, 451–464. doi: 10.1016/j.spinee.2003.07.007

Laske, C., Stellos, K., Stransky, E., Leyhe, T., and Gawaz, M. (2009). Decreased plasma levels of granulocyte-colony stimulating factor (G-CSF) in patients with early Alzheimer's disease. *J. Alzheimers Dis.* 17, 115–123. doi: 10.3233/jad-2009-1017

Lin, M. S., Lee, Y. H., Chiu, W. T., and Hung, K. S. (2011). Curcumin provides neuroprotection after spinal cord injury. *J. Surg. Res.* 166, 280–289. doi: 10.1016/j.jss.2009.07.001

Lucas, D., Bruns, I., Battista, M., Mendez-Ferrer, S., Magnon, C., Kunisaki, Y., et al. (2012). Norepinephrine reuptake inhibition promotes mobilization in mice: potential impact to rescue low stem cell yields. *Blood* 119, 3962–3965. doi: 10.1182/blood-2011-07-367102

Marei, H. E., Farag, A., Althani, A., Afifi, N., bd-Elmaksoud, A., Lashen, S., et al. (2015). Human olfactory bulb neural stem cells expressing hNGF restore cognitive deficit in Alzheimer's disease rat model. *J. Cell Physiol.* 230, 116–130. doi: 10.1002/jcp.24688

Mesholam, R. I., Moberg, P. J., Mahr, R. N., and Doty, R. L. (1998). Olfaction in neurodegenerative disease: a meta-analysis of olfactory functioning in Alzheimer's and Parkinson's diseases. *Arch. Neurol.* 55, 84–90. doi: 10.1001/archneur.55.1.84

Meuer, K., Pitzer, C., Teismann, P., Kr奠ger, C., G繹ricke, B., Laage, R., et al. (2006). Granulocyte-colony stimulating factor is neuroprotective in a model of Parkinson's disease. *J. Neurochem.* 97, 675–686.

Mitchell, A. J., Beaumont, H., Ferguson, D., Yadegarfar, M., and Stubbs, B. (2014). Risk of dementia and mild cognitive impairment in older people with subjective memory complaints: meta-analysis. *Acta Psychiatr. Scand.* 130, 439–451. doi: 10.1111/acps.12336

Motamed, S., Del Borgo, M. P., Zhou, K., Kulkarni, K., Crack, P. J., Merson, T. D., et al. (2019). Migration and differentiation of neural stem cells diverted from the subventricular zone by an injectable self-assembling 巻-peptide hydrogel. *Front. Bioeng. Biotechnol.* 7:315. doi: 10.3389/fbioe.2019.00315

Negoias, S., Croy, I., Gerber, J., Puschmann, S., Petrowski, K., Joraschky, P., et al. (2010). Reduced olfactory bulb volume and olfactory sensitivity in patients with acute major depression. *Neuroscience* 169, 415–421. doi: 10.1016/j.neuroscience.2010.05.012

Negoias, S., Hummel, T., Symmank, A., Schellong, J., Joraschky, P., and Croy, I. (2016). Olfactory bulb volume predicts therapeutic outcome in major depression disorder. *Brain Imaging Behav.* 10, 367–372. doi: 10.1007/s11682-015-9400-x

Nightingale, T. E., Zheng, M. M. Z., Sachdeva, R., Phillips, A. A., and Krassioukov, A. V. (2020). Diverse cognitive impairment after spinal cord injury is associated with orthostatic hypotension symptom burden. *Physiol. Behav.* 213, 112742. doi: 10.1016/j.physbeh.2019.112742

Nordengen, K., Kirsebom, B. E., Henjum, K., Selnes, P., G稳slad獰ttir, B., Wettergreen, M., et al. (2019). Glial activation and inflammation along the Alzheimer's disease continuum. *J. Neuroinflamm.* 16:46.

Onuki, Y., Morishita, M., and Takayama, K. (2004). Formulation optimization of water-in-oil-water multiple emulsion for intestinal insulin delivery. *J. Control Release* 97, 91–99. doi: 10.1016/j.jconrel.2004.03.010

Pagano, S. F., Impagnatiello, F., Girelli, M., Cova, L., Grioni, E., Onofri, M., et al. (2000). Isolation and characterization of neural stem cells from the adult human olfactory bulb. *Stem Cells* 18, 295–300. doi: 10.1634/stemcells.18-4-295

Paratcha, G., Ib獺簽ez, C. F., and Ledda, F. (2006). GDNF is a chemoattractant factor for neuronal precursor cells in the rostral migratory stream. *Mol. Cell Neurosci.* 31, 505–514. doi: 10.1016/j.mcn.2005.11.007

Prakash, A., Chopra, K., and Medhi, B. (2013a). Granulocyte-colony stimulating factor improves Parkinson's disease associated with co-morbid depression: an experimental exploratory study. *Indian J. Pharmacol.* 45, 612–615. doi: 10.4103/0253-7613.121374

Prakash, A., Medhi, B., and Chopra, K. (2013b). Granulocyte colony stimulating factor (GCSF) improves memory and neurobehavior in an amyloid-巻 induced experimental model of Alzheimer's disease. *Pharmacol. Biochem. Behav.* 110, 46–57. doi: 10.1016/j.pbb.2013.05.015

Rey, N. L., Wesson, D. W., and Brundin, P. (2018). The olfactory bulb as the entry site for prion-like propagation in neurodegenerative diseases. *Neurobiol. Dis.* 109, 226–248. doi: 10.1016/j.nbd.2016.12.013

Risacher, S. L., Tallman, E. F., West, J. D., Yoder, K. K., Hutchins, G. D., Fletcher, J. W., et al. (2017). Olfactory identification in subjective cognitive decline and mild cognitive impairment: Association with tau but not amyloid positron emission tomography. *Alzheimers Dement (Amst.)* 9, 57–66. doi: 10.1016/j.dadm.2017.09.001

Roberts, R. O., Christianson, T. J., Kremers, W. K., Mielke, M. M., Machulda, M. M., Vassilaki, M., et al. (2016). Association between olfactory dysfunction and amnestic mild cognitive impairment and alzheimer disease dementia. *JAMA Neurol.* 73, 93–101. doi: 10.1001/jamaneurol.2015.2952

Rolando, C., and Taylor, V. (2014). Neural stem cell of the hippocampus: development, physiology regulation, and dysfunction in disease. *Curr. Top Dev. Biol.* 107, 183–206. doi: 10.1016/b978-0-12-416022-4.00007-x

Rustenhoven, J., and Kipnis, J. (2019). Smelling danger: olfactory stem cells control immune defense during chronic inflammation. *Cell Stem Cell* 25, 449–451. doi: 10.1016/j.stem.2019.09.006

Sachdeva, R., Gao, F., Chan, C. C. H., and Krassioukov, A. V. (2018). Cognitive function after spinal cord injury: a systematic review. *Neurology* 91, 611–621. doi: 10.1212/wnl.0000000000006244

Safari, M., Jafari, B., Zarbakhsh, S., Sameni, H., Vafaei, A. A., Mohammadi, N. K., et al. (2016). G-CSF for mobilizing transplanted bone marrow stem cells in rat model of Parkinson's disease. *Iran J. Basic Med. Sci.* 19, 1318–1324.

Sanchez-Ramos, J., Cimino, C., Avila, R., Rowe, A., Chen, R., Whelan, G., et al. (2012). Pilot study of granulocyte-colony stimulating factor for treatment of Alzheimer's disease. *J. Alzheimers Dis.* 31, 843–855.

Si, T., Xing, G., and Han, Y. (2020). Subjective cognitive decline and related cognitive deficits. *Front. Neurol.* 11:247. doi: 10.3389/fneur.2020.00247

Snapyan, M., Lemasson, M., Brill, M. S., Blais, M., Massouh, M., Ninkovic, J., et al. (2009). Vasculature guides migrating neuronal precursors in the adult mammalian forebrain via brain-derived neurotrophic factor signaling. *J. Neurosci.* 29, 4172–4188. doi: 10.1523/jneurosci.4956-08.2009

Song, S., Sava, V., Rowe, A., Li, K., Cao, C., Mori, T., et al. (2011). Granulocyte-colony stimulating factor (G-CSF) enhances recovery in mouse model of Parkinson's disease. *Neurosci. Lett.* 487, 153–157.

Tator, C. H., and Fehlings, M. G. (1991). Review of the secondary injury theory of acute spinal cord trauma with emphasis on vascular mechanisms. *J. Neurosurg.* 75, 15–26. doi: 10.3171/jns.1991.75.1.0015

Tian, D. S., Xie, M. J., Yu, Z. Y., Zhang, Q., Wang, Y. H., Chen, B., et al. (2007). Cell cycle inhibition attenuates microglia induced inflammatory response and alleviates neuronal cell death after spinal cord injury in rats. *Brain Res.* 1135, 177–185. doi: 10.1016/j.brainres.2006.11.085

Tsai, K. J., Tsai, Y. C., and Shen, C. K. (2007). G-CSF rescues the memory impairment of animal models of Alzheimer's disease. *J. Exp. Med.* 204, 1273–1280. doi: 10.1084/jem.20062481

Wang, Q., Chen, B., Zhong, X., Zhou, H., Zhang, M., Mai, N., et al. (2021). Olfactory dysfunction is already present with subjective cognitive decline and deepens with disease severity in the Alzheimer's disease spectrum. *J. Alzheimers Dis.* 79, 585–595. doi: 10.3233/jad-201168

Wehling, E., Naess, H., Wollschlaeger, D., Hofstad, H., Bramerson, A., Bende, M., et al. (2015). Olfactory dysfunction in chronic stroke patients. *BMC Neurol.* 15:199. doi: 10.1186/s12883-015-0463-5

Weise, G., P綷sel, C., M綷ller, K., Kranz, A., Didwischus, N., Boltze, J., et al. (2017). High-dosage granulocyte colony stimulating factor treatment alters monocyte trafficking to the brain after experimental stroke. *Brain Behav. Immun.* 60, 15–26. doi: 10.1016/j.bbi.2016.08.008

Welte, K., Gabrilove, J., Bronchud, M. H., Platzer, E., and Morstyn, G. (1996). Filgrastim (r-metHuG-CSF): the first 10 years. *Blood* 88, 1907–1929. doi: 10.1182/blood.v88.6.1907.bloodjournal8861907

Whitman, M. C., Fan, W., Rela, L., Rodriguez-Gil, D. J., and Greer, C. A. (2009). Blood vessels form a migratory scaffold in the rostral migratory stream. *J. Comp. Neurol.* 516, 94–104. doi: 10.1002/cne.22093

Winner, B., Couillard-Despres, S., Geyer, M., Aigner, R., Bogdahn, U., Aigner, L., et al. (2008). Dopaminergic lesion enhances growth factor-induced striatal neuroblast migration. *J. Neuropathol. Exp. Neurol.* 67, 105–116. doi: 10.1097/nen.0b013e3181630cff

Wu, J., Zhao, Z., Sabirzhanov, B., Stoica, B. A., Kumar, A., Luo, T., et al. (2014). Spinal cord injury causes brain inflammation associated with cognitive and affective changes: role of cell cycle pathways. *J. Neurosci.* 34, 10989–11006. doi: 10.1523/jneurosci.5110-13.2014

Yahiaoui-Doktor, M., Luck, T., Riedel-Heller, S. G., Loeffler, M., Wirkner, K., and Engel, C. (2019). Olfactory function is associated with cognitive performance: results from the population-based LIFE-Adult-Study. *Alzheimers Res. Ther.* 11:43.

Yang, D., Li, Q., Fang, L., Cheng, K., Zhang, R., Zheng, P., et al. (2011). Reduced neurogenesis and pre-synaptic dysfunction in the olfactory bulb of a rat model of depression. *Neuroscience* 192, 609–618. doi: 10.1016/j.neuroscience.2011.06.043

Yeh, T. S., Ho, Y. C., Hsu, C. L., and Pan, S. L. (2018). Spinal cord injury and Alzheimer's disease risk: a population-based, retrospective cohort study. *Spinal Cord* 56, 151–157. doi: 10.1038/s41393-017-0009-3

Yeh, T. S., Huang, Y. P., Wang, H. I., and Pan, S. L. (2016). Spinal cord injury and Parkinson's disease: a population-based, propensity score-matched, longitudinal follow-up study. *Spinal Cord* 54, 1215–1219. doi: 10.1038/sc.2016.74

Yoo, H. S., Jeon, S., Chung, S. J., Yun, M., Lee, P. H., Sohn, Y. H., et al. (2018). Olfactory dysfunction in Alzheimer's disease- and lewy body-related cognitive impairment. *Alzheimers Dement* 14, 1243–1252. doi: 10.1016/j.jalz.2018.05.010

Zigova, T., Pencea, V., Wiegand, S. J., and Luskin, M. B. (1998). Intraventricular administration of BDNF increases the number of newly generated neurons in the adult olfactory bulb. *Mol. Cell Neurosci.* 11, 234–245. doi: 10.1006/mcne.1998.0684

Conflict of Interest: The authors declare that the research was conducted in the absence of any commercial or financial relationships that could be construed as a potential conflict of interest.

frontiers in Aging Neuroscience

ORIGINAL RESEARCH
published: 09 July 2021
doi: 10.3389/fnagi.2021.688113

Morphological, Structural, and Functional Networks Highlight the Role of the Cortical-Subcortical Circuit in Individuals With Subjective Cognitive Decline

Xiaowen Xu[1], Tao Wang[2,3], Weikai Li[4], Hai Li[5,6,7], Boyan Xu[7], Min Zhang[1], Ling Yue[2,3], Peijun Wang[1]* and Shifu Xiao[2,3]**

[1] Department of Medical Imaging, Tongji Hospital, Tongji University School of Medicine, Tongji University, Shanghai, China, [2] Department of Geriatric Psychiatry, Shanghai Mental Health Center, Shanghai Jiao Tong University School of Medicine, Shanghai, China, [3] Alzheimer's Disease and Related Disorders Center, Shanghai Jiao Tong University, Shanghai, China, [4] College of Computer Science and Technology, Nanjing University of Aeronautics and Astronautics, Nanjing, China, [5] Center for MRI Research, Academy for Advanced Interdisciplinary Studies, Peking University, Beijing, China, [6] McGovern Institute for Brain Research, Peking University, Beijing, China, [7] Beijing Intelligent Brain Cloud Inc., Beijing, China

OPEN ACCESS

Edited by:
Jiehui Jiang,
Shanghai University, China

Reviewed by:
Jie Xiang,
Taiyuan University of Technology, China
Christian Sorg,
Technical University of Munich, Germany

***Correspondence:**
Ling Yue
bellinthemoon@hotmail.com
Peijun Wang
tongjipjwang@vip.sina.com
Shifu Xiao
xiaoshifu@msn.com

Received: *30 March 2021*
Accepted: *14 June 2021*
Published: *09 July 2021*

Citation:
Xu X, Wang T, Li W, Li H, Xu B, Zhang M, Yue L, Wang P and Xiao S (2021) Morphological, Structural, and Functional Networks Highlight the Role of the Cortical-Subcortical Circuit in Individuals With Subjective Cognitive Decline. Front. Aging Neurosci. 13:688113. doi: 10.3389/fnagi.2021.688113

Subjective cognitive decline (SCD) is considered the earliest stage of the clinical manifestations of the continuous progression of Alzheimer's Disease (AD). Previous studies have suggested that multimodal brain networks play an important role in the early diagnosis and mechanisms underlying SCD. However, most of the previous studies focused on a single modality, and lacked correlation analysis between different modal biomarkers and brain regions. In order to further explore the specific characteristic of the multimodal brain networks in the stage of SCD, 22 individuals with SCD and 20 matched healthy controls (HCs) were recruited in the present study. We constructed the individual morphological, structural and functional brain networks based on 3D-T1 structural magnetic resonance imaging (sMRI), diffusion tensor imaging (DTI) and resting-state functional magnetic resonance imaging (rs-fMRI), respectively. A *t*-test was used to select the connections with significant difference, and a multi-kernel support vector machine (MK-SVM) was applied to combine the selected multimodal connections to distinguish SCD from HCs. Moreover, we further identified the consensus connections of brain networks as the most discriminative features to explore the pathological mechanisms and potential biomarkers associated with SCD. Our results shown that the combination of three modal connections using MK-SVM achieved the best classification performance, with an accuracy of 92.68%, sensitivity of 95.00%, and specificity of 90.48%. Furthermore, the consensus connections and hub nodes based on the morphological, structural, and functional networks identified in our study exhibited abnormal cortical-subcortical connections in individuals with SCD. In addition, the functional networks presented more discriminative connections and hubs in the

cortical-subcortical regions, and were found to perform better in distinguishing SCD from HCs. Therefore, our findings highlight the role of the cortical-subcortical circuit in individuals with SCD from the perspective of a multimodal brain network, providing potential biomarkers for the diagnosis and prediction of the preclinical stage of AD.

Keywords: subjective cognitive decline, morphological network, structural network, functional network, multiple kernel learning

INTRODUCTION

Alzheimer's Disease (AD) is the most common cause of dementia, characterised by irreversible neurodegeneration and continuous cognitive function decline (Bonte et al., 1986; Scheltens et al., 2016). It is generally believed that the early diagnosis of AD is crucial for early intervention and improving the therapeutic effects of AD treatment. Subjective cognitive decline (SCD) is considered the earliest stage of the clinical manifestations of progressively developing AD (Jessen et al., 2014a, 2020). Thus, SCD is valuable for the early diagnosis and prediction of AD.

Multimodal neuroimaging studies have indicated that individuals with SCD show a greater similarity to AD in their patterns of brain structure and function compared with healthy controls (HCs) (Lin et al., 2019; Wang et al., 2020). In particular, the disconnection hypothesis between different brain regions is considered to mainly contribute to cognitive decline in patients with SCD (Dillen et al., 2016). For instance, for the brain network based on resting-state functional magnetic resonance imaging (rs-fMRI), the identified connectivity disruption of SCD focused on the middle frontal gyrus, precuneus, and cingulate gyrus, which corresponded to the default mode network (DMN) (Greicius et al., 2004; Hafkemeijer et al., 2013; Xu et al., 2020b). Shu et al. analysed the graph theory metrics of structural brain network based on diffusion tensor imaging (DTI) and found that patients with SCD exhibited lower global efficiency and local efficiency of global graph metrics and reduced regional efficiency in the bilateral prefrontal regions and left thalamus (Shu et al., 2018). Moreover, the graph theoretic analysis of the topological properties of the morphological network based on structural magnetic resonance imaging (sMRI) showed that patients with SCD exhibiting lower network parameter values were associated with an increased risk of disease progression (Tijms et al., 2018). Therefore, these results demonstrated that patients with SCD have altered connectivity involving multimodal brain networks. In addition, recent studies have suggested that individuals with SCD exhibited volume atrophy and disconnection of the subcutaneous nuclei, such as basal forebrain, basal ganglia, and thalamus. Some researchers even proposed that the variation of the subcutaneous nuclei might be earlier than the cortex (Hampel et al., 2018; Scheef et al., 2019). However, most previous studies have focused on a single model of the brain network. The relationship between grey matter (GM) morphology, white matter structure and functional connectivity in SCD remains unclear.

Furthermore, to deal with the high-dimensional information yielded from multimodal brain networks, machine learning with multivariate pattern analysis was used to identify potential neuroimaging biomarkers and distinguish patients from HCs at an individual level. At the same time, it can reveal specific spatial distribution information useful exploring the brain network mechanisms underlying the cognitive impairment associated with AD. Previous studies, such as that by Yan et al. (2019) adopted a multimodal support vector machine (SVM) combined with structural and functional connectivity and achieved an accuracy of 98.58% in the AD group, 97.76% in the amnestic mild cognitive impairment (aMCI) group, and 80.24% in the SCD group. Compared with the single modal classification based on functional connectivity by Yu et al. (accuracy of 84.8% in AD), these results suggested that the integration of multimodal features can provide more comprehensive and insightful information than single modal features and achieve a better classification performance. However, to the best of our knowledge, there has been no study directly combining morphological, structural and functional brain networks to explore the relationship of different modalities and identify patients with SCD.

Given that individuals with SCD are often associated with abnormal multimodal brain network connectivity and the involvement of multiple brain regions, alongside the advantages of machine learning, we sought to apply multi-kernel SVM (MK-SVM) for the integration of morphological, structural and functional brain networks based on sMRI, DTI and fMRI. This study aimed to assess (a) whether specific altered patterns of network connectivity discovered by three modal brain networks can discriminate patients with SCD from HCs; (b) whether there is a correlation between different modal biomarkers and brain regions; and (c) whether the combination of multimodal network connectivity analyses may improve the accuracy of identifying patients with SCD from HCs.

MATERIALS AND METHODS

Participants

The samples included in this study were acquired from the longitudinal follow-up data of China Longitudinal Aging Study (CLAS), a community-based study initiated in 2012. All individuals with Han Chinese nationality aged $\geq$60 years in Shanghai. A total of 67 right-handed participants involved in the present study, who underwent a screening process including medical history, epidemiological investigation, baseline and 7-year follow-up assessments of neuropsychological scale, and neuroimaging examinations. At baseline, the neuropsychological assessments included the Mini-Mental State Examination (MMSE) (Tombaugh and McIntyre, 1992), Montreal Cognitive Assessment (MoCA) (Nasreddine et al., 2005), Auditory Verbal

Learning Test (AVLT) (Sheline et al., 1999), and Subjective Cognitive Decline Self-administered Questionnaire (SCD-9) (Shirooka et al., 2018). Meanwhile, T1-weighted MR imaging scan was performed. At 7-year follow-up, in addition to the neuropsychological scale mentioned above, multimodal MRI scans including T1WI, DTI and rs-fMRI were carried out. Therefore, research on the morphological, structural, and functional networks in this study was based on follow-up samples after 7 years. According to the follow-up results, 22 patients with SCD and 20 HCs were enrolled in our study. Due to the limitation of sample size, we considered the study classifies as pilot study.

The inclusion criteria for SCD were based on the conceptual framework proposed by the Subjective Cognitive Decline Initiative (SCD-I) (Jessen et al., 2014b), which included the following: (a) an onset age >60 years; (b) a self-perceived gradual decline in memory compared with a previous normal status within the last 5 years or as confirmed by a close caregiver; (c) MMSE and MoCA scores within the normal range; and (d) a Clinical Dementia Rating (CDR) score of 0. Those who did not experience any signs of cognitive decline and had neuropsychological tests scores in the normal range were included as HCs. The exclusion criteria of participants were as follows: (a) neurology-related or cerebral vascular diseases (e.g., Parkinson's disease, brain tumours, or intracranial aneurysms); (b) systemic diseases that could cause cognitive impairments (e.g., thyroid dysfunctions, syphilis, HIV or severe anaemia); (c) severe schizophrenia according to their medical records; (d) severe problems in vision, hearing, or speaking; and (e) inability to participate actively in the neuropsychological evaluation.

This study was approved by the Institution's Ethical Committee of Shanghai Mental Health Centre of Shanghai Jiao Tong University School of Medicine (NCT03672448). All participants provided written informed consent prior to any experimental procedures in the research. In terms of the statistical analysis of demographics and clinical characteristics between the SCD group and HC group, two-sample *t*-test or a chi-squared ($\chi 2$) test were performed by the Statistical Package for Social Science (SPSS, v20.0)[1]. The significance level was set at $P < 0.05$.

Data Acquisition

T1-weighted structural imaging, DTI, and rs-fMRI scans were performed on each participant simultaneously. All MRI data were acquired on a 3.0 T MR scanner (Magnetom® Verio; Siemens, Munich, Germany) using a 32-channel head coil. All participants were instructed to keep their eyes closed (but no fall asleep), think of nothing, and move as little as possible during the scan.

T1-weighted 3D high-resolution images were acquired using a magnetisation-prepared rapid gradient echo (MPRAGE) with the following parameters: repetition time (TR) = 2,300 ms, echo time (TE) = 2.98 ms, flip angle = 9 degrees, inversion time (TI) = 1,100 ms, matrix size = 240 × 256, field of view (FOV) = 240 × 256 mm^2, slice number = 192, thickness = 1.2 mm and voxel size = 1.0 × 1.0 × 1.2 mm^3. The scan lasted for 5 min and 12 s. DTI data were obtained using an echo planar imaging sequence with the following parameters: 64 non-collinear directions with a *b*-value = 1,000 s/mm^2 and one additional image with no diffusion weighting ($b = 0$), TR = 13,700 ms, TE = 85 ms, FOV = 224 × 224 mm^2, slice number = 75, thickness = 2 mm and voxel size = 2.0 × 2.0 × 2.0 mm^3. In addition, the parameters of the rs-fMRI protocol were collected as follows: axial slices, TR = 2,000 ms, TE = 30 ms, flip angle = 90 degrees, FOV = 224 × 224 mm^2, matrix size = 64 × 64, slice number = 31, thickness = 3.6 mm and voxel size = 3.5 × 3.5 × 3.6 mm^3. Each scan collected 240 volumes with a scan time of 8 min and 6 s.

Image Preprocessing

Brain tissue segmentation was performed using SPM12 (Ashburner and Ridgway, 2012). Individual T1-weighted 3D high-resolution images were segmented into the GM, white matter, and cerebrospinal fluid using a voxel-based morphometric analysis (Ashburner and Friston, 2000). The segmented GM images were realigned to the Montreal Neurologic Institute (MNI) space and normalised by DARTEL (Ashburner, 2007). Jacobian determinants were used to modulate and compensate for spatial normalisation effects (Mueller et al., 2019). A spatial smoothing process with a Gaussian kernel (full width at half maximum, 6 mm) was carried out to render the data more normally distributed and improve the signal-to-noise ratio (Shen and Sterr, 2013).

The PANDA toolbox (Cui et al., 2013) based on FSL (Jenkinson et al., 2012) was used for the pre-processing processes of DTI images, such as the removal of redundant scalp and brain tissues, and head motion and eddy current correction. In addition, the tensor model was fitted using a linear least-squares fitting method, and the fractional anisotropy (FA) value was calculated.

The processing of the fMRI scans was carried out by the Configurable Pipeline for the Analysis of Connectomes (C-PAC), which is a python-based pipeline tool making use of AFNI (Cox, 1996), ANTs (Tustison et al., 2014), FSL, and custom python code. Functional pre-processing included the following steps: (1) The first 10 time points were removed; (2) Slice-time correction was performed; (3) Images were de-obliqued; (4) Images were re-oriented into a right-to-left posterior-to-anterior inferior-to-superior orientation; (5) Motion correction was performed to averaged images to obtain motion parameters; (6) Skull stripping was performed; (7) The global mean intensity was normalised to 10,000; (8) Functional images were registered to anatomical space using a linear transformation, white-matter boundary-based transformation, and the prior white-matter tissue segmentation from FSL; (9) Motion artefacts were removed using ICA-based strategy for Automatic Removal of Motion Artefacts (ICA-AROMA) with partial component regression (Pruim et al., 2015); and (10) A nuisance signal regression was applied, including (a) mean values from the signal in the white matter and cerebrospinal fluid derived from the prior tissue segmentations transformed from anatomical to functional space, (b) motion parameters (six head-motion parameters, six head-motion parameters from one time point before, and the 12 corresponding squared items), (c) linear trends, and (d) global signal only for one set of strategies.

[1] http://www.spss.com/

This entire analysis was accelerated and simplified through a cloud platform ([2]Beijing Intelligent Brain Cloud, Inc.).

Brain Network Construction

In present study, the Human Brainnetome (BN) Atlas (Fan et al., 2016) was used to divide the brain into 246 regions of interest (ROIs) to define the network nodes. Nevertheless, based on different modal brain networks, the definition of network edge was different.

Morphological Networks

Individual morphological brain networks were constructed by evaluating interregional similarity in the distribution of regional GM volume with the Kullback–Leibler divergence measure (Kong et al., 2014). First, the GM volume value of all voxels within the brain node were extracted. Second, the probability density function of these values was calculated with the kernel density estimation (KDE) (Wang et al., 2016). Next, the probability distribution function (PDF) was computed for the obtained probability density function. The variant KL divergence between any pair of ROI was calculated, resulting in a similarity matrix. KL divergence is a measure of the difference between two probability distributions from the perspective of probability theory, or of the information lost when one probability distribution approximates the other from the perspective of information theory. The following formula was used:

$$D_{KL}(P, Q) = \sum_{i=1}^{n} \left(P(i) \log \frac{P(i)}{Q(i)} + Q(i) \log \frac{Q(i)}{P(i)} \right)$$

where P and Q are two PDFs and n is the number of sample points. We selected $n = 2^7$ in this study in reference to the research of Wang et al. (2016). Finally, a KL divergence-based similarity (KLS) measure were calculated to quantify morphological connectivity between two brain regions. The KLS was computed as below:

$$KLS(P, Q) = e^{-D_{KL}(P,Q)}$$

where e is a natural exponent. The KLS ranges from 0 to 1. The higher the value of KLS, the closer GM density distribution of the two brain regions is.

Structural Networks

After the pre-processing of DTI data, probabilistic tractography was used to construct the structural brain network (Behrens et al., 2007). For each seed region, probabilistic tractography was performed by seeding from all voxels of this region. For each voxel, 5,000 fibres were sampled. The connectivity probability from the seed region i to another region j was defined by the number of fibres passing through region j divided by the total number of fibres sampled from region i (5,000 $\times$ n, where n is the voxel number in region i). It is worth noting that the connection probability from i to j was not necessarily equal to that from j to i. These two probabilities were averaged to define the non-directional connection probability Pij between regions i and j.

Functional Networks

For the pre-processed fMRI data, the average time series of 246 ROIs was separately extracted to construct the functional brain network. The Pearson correlation coefficient of ROI pair-wise was defined as the edge of the functional connectivity, which resulted in 30,135 (246 $\times$ 245/2) edges.

The above structural and functional networks were accelerated and simplified through a cloud platform (see text footnote 2, Beijing Intelligent Brain Cloud, Inc.).

Hubs of Each Imaging Modality

For each modal imaging (i.e., sMRI, DTI, and fMRI), the average value of the individual brain network was acquired to generate the group-average network. We identified the hub nodes by ranking the nodal degree. The rank 5% of brain regions were defined as the hubs of the brain network (Zhao et al., 2020).

Feature Selection and Classification

In order to avoid the difficulty in identifying the contribution of kernel combination skills or feature selection to the final accuracy in the classification pipeline, we adopt the simplest method (t-test with $p < 0.01$) for feature selection. Meanwhile, the network-based statistic (NBS) (Zalesky et al., 2010) was used to conduct multiple comparisons correction for multimodal connections. The result of correction for multiple comparisons were listed in the **Supplementary Figure 1**. The LIBSVM toolbox[3] for MATLAB was used to conduct the SVM classification (Xu et al., 2020a). Due to the limited samples, we used a leave one out cross-validation (LOOCV) strategy to evaluate the performance of the classification method. Specifically, inner cross-validation was carried out to determine the optimal parameter (hyper-parameter C for MK-SVM) and outer cross-validation was carried out to determine the classification performance. We compared the classification performance of single modes (i.e., sMRI, DTI and fMRI) and combinations of different modes (i.e., sMRI + DTI, fMRI + sMRI, fMRI + DTI, and fMRI + DTI + sMRI). Multi-kernel learning with a kernel combination trick was applied for multimodal information combination. The details of MK-SVM were listed as follows.

Assuming there are n training samples with connections values and graph metrics. x_i^C and x_i^G $y_i \in \{1, -1\}$ represent the connection value, the graph metrics, and its corresponding class label of the i-th sample, respectively. MK-SVM solves the following primal problem:

$$\min_{W} \frac{1}{2} \sum_{m=1}^{3} \beta_m \| w^m \|^2 + C \sum_{i=1}^{n} \xi_i$$
$$\text{s.t. } y_i \left(\sum_{m=1}^{3} \beta_m (w^m)^T \phi^m (x_i^m) + b \right) \geq 1 - \xi_i$$
$$\xi_i \geq 0, i = 1, 2, \ldots, n$$

where ϕ^m represents mapping from the original space to the Represent Hilbert Kernel Space (RHKS), w^m represents the normal vector of the hyperplane in RHKS, and β_m denotes the

[2]http://www.humanbrain.cn

[3]https://www.csie.ntu.edu.tw/~cjlin/libsvm/

corresponding combining weight on the m-th modality. Next, the dual form of MK-SVM can be represented as:

$$\max_{\alpha} \sum_{i=1}^{n} \alpha_i - \frac{1}{2} \sum_{i,j} \alpha_i \alpha_j y_i y_j \sum_{m=1}^{3} \beta_m k^m (x_i^m, y_i^m)$$
$$\text{s.t.} \sum_{i=1}^{n} \alpha_i y_i = 0$$
$$0 \leq \alpha_i \leq C, i = 1, 2, \ldots, n$$

where $k^m\left(x_i^m, y_i^m\right) = \phi^m(x_i^m)^T \phi^m(x_j^m)$ is the kernel matrix on the m-th modality. After training the model, we tested the new samples $x = \{x_1, x_2, \ldots, x_M\}$. The kernel between the new test sample and the i-th training sample on the m-th modality is defined as $k^m\left(x_i^m, x^m\right) = \phi^m\left(x_i^m\right)^T \phi^m(x^m)$. In the end, the predictive level based on MK-SVM can be formulated as follows:

$$f(x_1, x_2, \ldots, x_M) = \text{sign}\left(\sum_{i=1}^{n} y_i \alpha_i \sum_{m=1}^{3} \beta_m k^m\left(x_i^m, x^m\right) + b\right)$$

The proposed formulation of MK-SVM is similar, but different, to existing multi-kernel learning methods since β_m is selected based on the cross-validation scheme on the grid-searching space with constraints $\sum_m \beta_m = 1$. The range of C was 2^{-5} to 2^5.

Consensus Connections

As mentioned above, we used the most commonly applied nested cross-validation scheme to evaluate the performance of the multi-kernel method proposed in this study. As the selected features by *t*-tests in each validation might be different, we record all the selected connection features during the training process. The consensus connections refer to the features that are consistently selected in all validations (Dosenbach et al., 2010; Zeng et al., 2012). In this study, we concentrate on consensus connections for each modal brain network. All data processing procedures in our study are shown in **Figure 1**.

Robustness of Network Analysis

To demonstrate the robustness of the network analysis, we repeated the same network construction method and analysis process based on the automated anatomical labelling atlas (AAL) with 90 ROIs (Tzourio-Mazoyer et al., 2002).

RESULTS

Demographic and Clinical Characteristics

The demographic and clinical characteristics of all participants are summarised in **Table 1**. The resultant scores of the SCD-9 in the SCD group were significantly higher than those in the HC group ($p < 0.05$). There were no significant differences with respect to age, education, sex, or any other scales.

Multimodal Brain Network Matrix

Figure 2 depicts adjacent matrices of HCs at the group level based on morphological, structural, and functional network. The different colour reflects the weight value of the connectivity edges at group level. As shown in **Figure 2**, both functional and morphological networks, and particularly the functional networks, showed strong homotopic connections. As mentioned above, the network connectivity of different modalities pointed to different physiological mechanisms. The individual morphological brain networks in our study demonstrated that the morphological network showed strong contralateral homotopic connections, indicating that the GM density distributions in the same brain area on the left and right

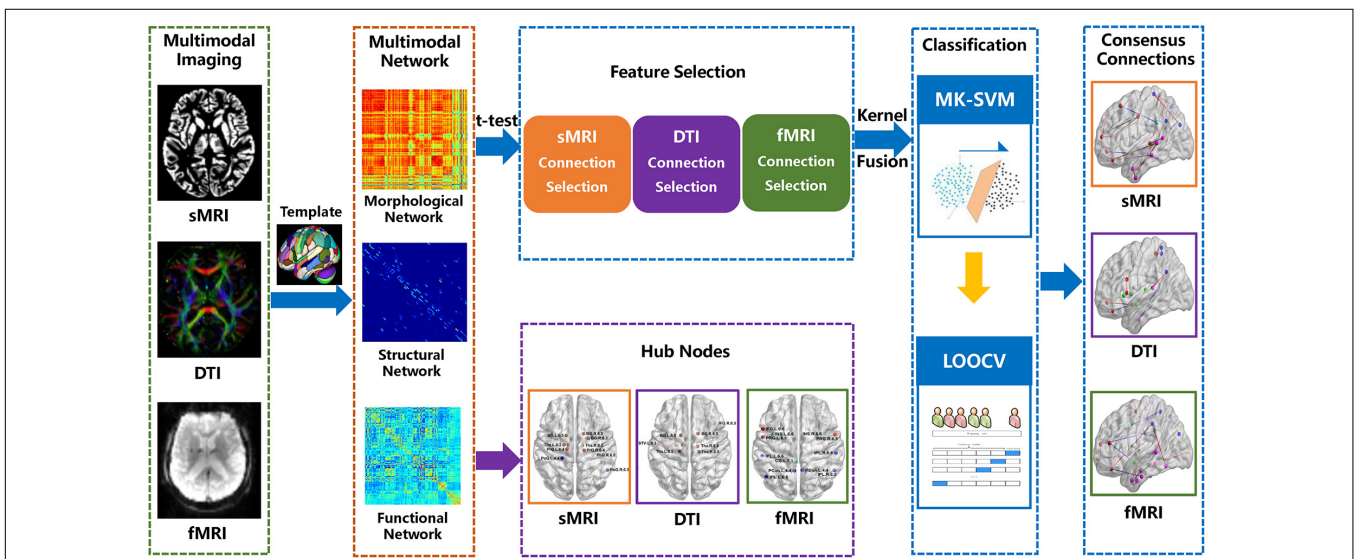

FIGURE 1 | Procedures of data processing in the present study.

TABLE 1 | Demographics and clinical characteristics of patients with SCD and HC.

Characteristic/test	SCD	HC	T/χ^2/Z	P
Age (years)	*74.0 ± 5.6*	71.8 ± 2.9	1.67[a]	0.11
Education	10.1 ± 2.0	10.4 ± 3.0	0.00[c]	1.00
Gender (F/M)	14/8	6/14	5.31 [b]	0.05
MMSE	27.6 ± 1.8	28.2 ± 1.6	−1.13[c]	0.26
MoCA	23.6 ± 3.9	24.1 ± 3.8	−0.48[c]	0.63
AVLT-immediate recall	5.5 ± 1.9	4.8 ± 1.5	−0.98 [c]	0.33
AVLT-short delayed recall	8.1 ± 2.6	8.2 ± 2.1	−0.14 [a]	0.89
AVLT-long delayed recall	30.9 ± 7.7	33.2 ± 7.6	−1.00 [c]	0.32
AVLT-recognition	10.2 ± 3.1	11.2 ± 3.0	−0.95 [c]	0.34
SCD-9	3.8 ± 1.9	2.4 ± 2.0	0.58[a]	0.03*

**p < 0.05 indicates significant differences between the groups.*
[a] T value was obtained by using the two-sample t-test.
[b] χ^2 value was obtained using the chi-square test.
[c] Z value obtained by using the rank-sum test.
MMSE, mini mental state examination; MoCA, Montreal Cognitive Assessment; AVLT, Auditory Verbal Learning Test; SCD-9, Subjective Cognitive Decline Self-administered Questionnaire. Data are presented as the mean ± standard deviation (SD). SCD, subjective cognitive decline; HC, healthy control.

TABLE 2 | Hubs of SCD based on different modal brain network.

sMRI		DTI		fMRI	
Label ID	ROI	Label ID	ROI	Label ID	ROI
156	PoG.R.4.1	107	FuG.L.3.3	64	PrG.R.6.6
226	BG.R.6.4	37	IFG.L.6.5	88	MTG.R.4.4
227	BG.L.6.5	38	IFG.R.6.5	144	IPL.R.6.5
225	BG.L.6.4	245	Tha.L.8.8	13	SFG.L.7.7
211	Amyg.L.2.1	227	BG.L.6.5	146	IPL.R.6.6
245	Tha.L.8.8	239	Tha.L.8.5	176	CG.R.7.1
114	PhG.R.6.3	246	Tha.R.8.8	87	MTG.L.4.4
212	Amyg.R.2.1	237	Tha.L.8.4	14	SFG.R.7.7
221	BG.L.6.2	228	BG.R.6.5	143	IPL.L.6.5
222	BG.R.6.2	215	Hipp.L.2.1	175	CG.L.7.1
234	Tha.R.8.2	103	FuG.L.3.1	154	PCun.R.4.4
233	Tha.L.8.2	104	FuG.R.3.1	153	PCun.L.4.4

sMRI, structural magnetic resonance imaging; DTI, diffusion tensor imaging; fMRI, functional magnetic resonance imaging; SCD, subjective cognitive decline; ROI: region of interest.

cerebral hemispheres were the most similar. Meanwhile, the weak homotopic connections between cortex and subcortex indicated that the GM densities of these two parts were quite different, resulting in lower morphological network connectivity. Thus, the mechanisms underlying the morphological network are basically consistent with the anatomical basis of the brain. Meanwhile, the structural network based on DTI exhibited sparse connections, and its connections were mainly short-distance fibre connections between the neighbouring areas. It corresponds to the pathway of white matter fibres in the structural brain network.

Distribution of Hubs

According to the definition of hub nodes in this study, the hub nodes of the SCD (**Table 2**) and HC groups (**Table 3**) based on three different modal networks were obtained. As shown in **Figure 3**, the distribution of hub nodes in the morphological and structural brain networks was similar, and most of them were located in the subcortical nuclei such as the hippocampus, thalamus, caudate nucleus, and amygdala. In contrast with the morphological and structural brain networks, the hub nodes of functional brain network were widely distributed in the frontal, temporal, and parietal lobes. Furthermore, by comparing the hub nodes between the SCD and HC groups in the same modal network, it was found that most of them overlapped. However, several specific hub nodes corresponded to the different groups. For instance, in the morphological network based on sMRI, the precentral gyrus (PrG) and the inferior parietal lobule (IPL) only appeared in the hub nodes of the HCs. In structural network based on DTI, the superior temporal gyrus (STG) only appeared in the hub node of the HC group, while the inferior frontal gyrus (IFG) only appeared in the SCD group as the hub node. Besides, in the functional brain network based on fMRI scans, the insula (INS) as one of the Hubs only appears in the HC group, while the middle temporal gyrus (MTG) as one of the Hubs only appears in the SCD group.

Classification

After feature selection of the morphological, structural, and functional network connections by *t*-tests, MK-SVM was applied to combine the selected multimodal connections to identify individuals with SCD from HCs. As shown in **Table 4** and **Figure 4**, for the single modality, the classification accuracy of the morphological, structural and functional networks was 73.17,

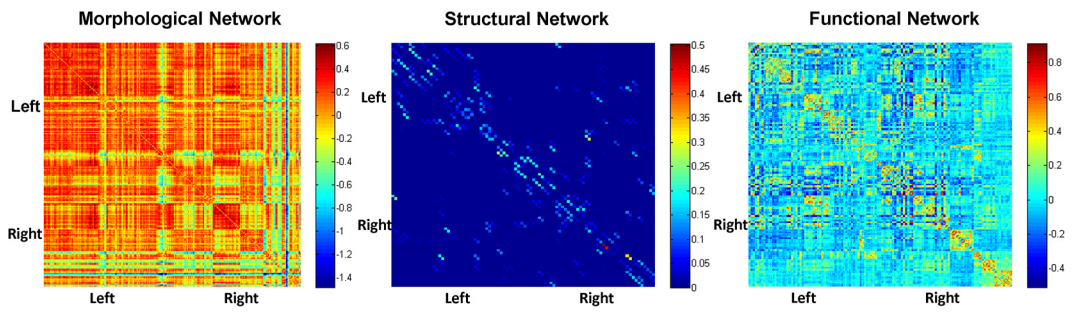

FIGURE 2 | Adjacent matrices of HCs at the group level based on morphological, structural, and functional network.

TABLE 3 | The hubs of HC based on different modal brain network.

sMRI		DTI		fMRI	
Label ID	**ROI**	**Label ID**	**ROI**	**Label ID**	**ROI**
161	PoG.L.4.4	73	STG.L.6.3	174	INS.L.6.6
144	IPL.R.6.5	245	Tha.L.8.8	145	IPL.L.6.6
228	BG.R.6.5	240	Tha.R.8.5	39	IFG.L.6.6
245	Tha.L.8.8	38	IFG.R.6.5	144	IPL.R.6.5
114	PhG.R.6.3	246	Tha.R.8.8	61	PrG.L.6.5
60	PrG.R.6.4	227	BG.L.6.5	146	IPL.R.6.6
227	BG.L.6.5	237	Tha.L.8.4	174	INS.R.6.6
212	Amyg.R.2.1	239	Tha.L.8.5	175	CG.L.7.1
59	PrG.L.6.4	228	BG.R.6.5	143	IPL.L.6.5
222	BG.R.6.2	215	Hipp.L.2.1	62	PrG.R.6.5
234	Tha.R.8.2	103	FuG.L.3.1	154	PCun.R.4.4
233	Tha.L.8.2	104	FuG.R.3.1	153	PCun.L.4.4

sMRI, structural magnetic resonance imaging; DTI, diffusion tensor imaging; fMRI, functional magnetic resonance imaging; HC, healthy control; ROI, region of interest.

80.49, and 85.37%, respectively. That is, the functional network constructed by fMRI exhibited the highest accuracy rate, followed by the structural network constructed by DTI; finally, the morphological network constructed by GM volume showed the lowest accuracy rate. Furthermore, combining the morphological and structural connections (sMRI + DTI), functional and morphological connections (fMRI + sMRI), and functional and structural connections (fMRI + DTI), the accuracy of classification increased to 85.37, 87.80, and 90.24%, respectively. In particular, the best classification performance was obtained by combining the selected connections of three modalities, with an accuracy of 92.68%, sensitivity of 95.00% and specificity of 90.48%. These results suggested that the combination of multimodal network features could significantly improve the classification performance.

Consensus Connections

In this study, we further identified the consensus connections for each modal brain network (**Figure 5**). The morphological brain network based on sMRI yielded a total of 23 consensus connections (**Table 5**), including 7 positive connections and 16 negative connections, which were mainly associated with the frontal lobe (orbital gyrus [OrG], middle frontal gyrus [MFG], superior frontal gyrus [SFG]), temporal lobe (MTG, entorhinal cortex [EC]), parietal lobe (inferior parietal lobule [IPL]), and subcortical nuclei (nucleus accumbens [NAC], occipital thalamus

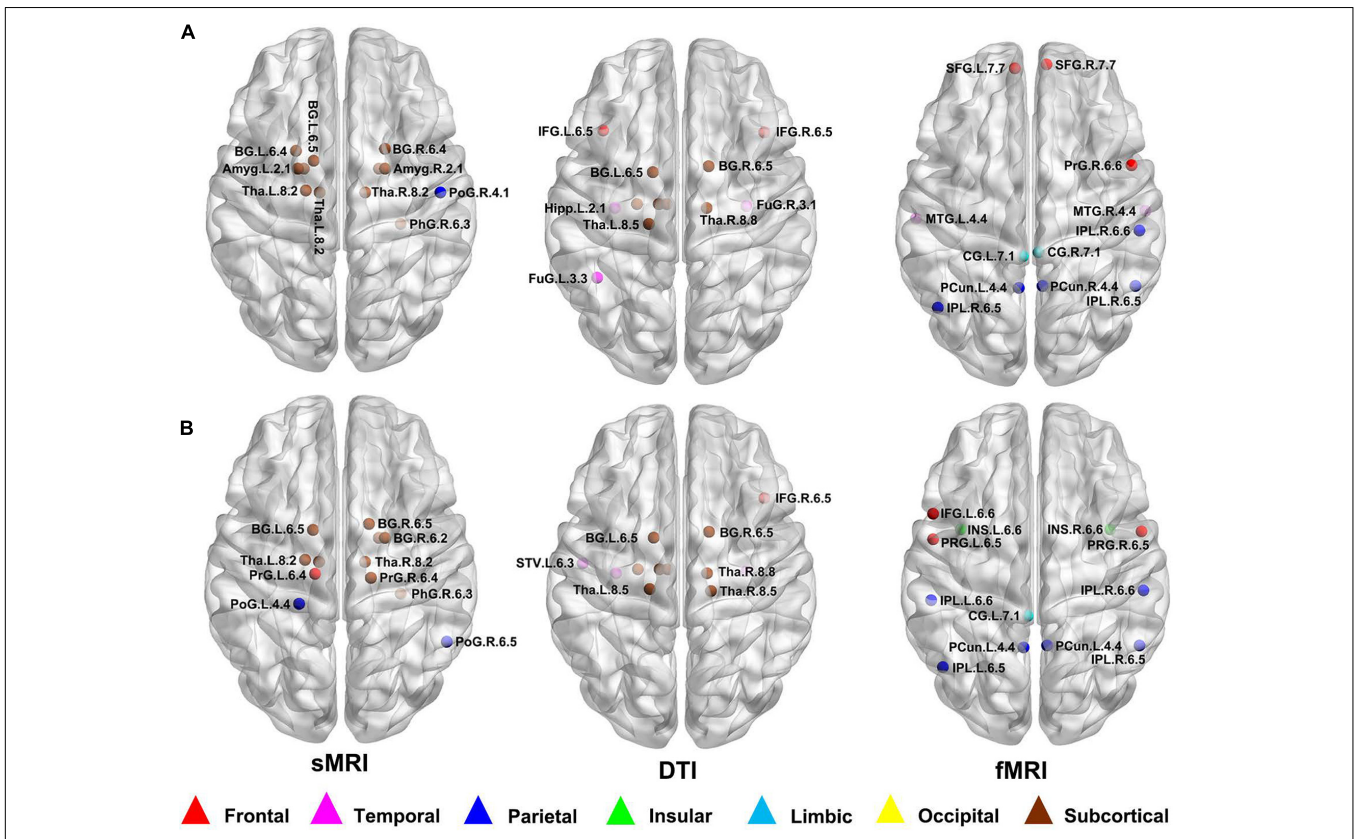

FIGURE 3 | Hub nodes of the SCD and HC groups in different brain networks. **(A)** Hub nodes of SCD in morphological, structural and functional brain network based on sMRI, DTI and fMRI; **(B)** Hub nodes of HC in morphological, structural and functional brain network based on sMRI, DTI and fMRI. The hub nodes were mapped on the ICBM 152 template with the BrainNet Viewer package (http://nitrc.org/projects/bnv/). sMRI, structural magnetic resonance imaging; DTI, diffusion tensor imaging; fMRI, functional magnetic resonance imaging; SCD, subjective cognitive decline; HC, healthy control.

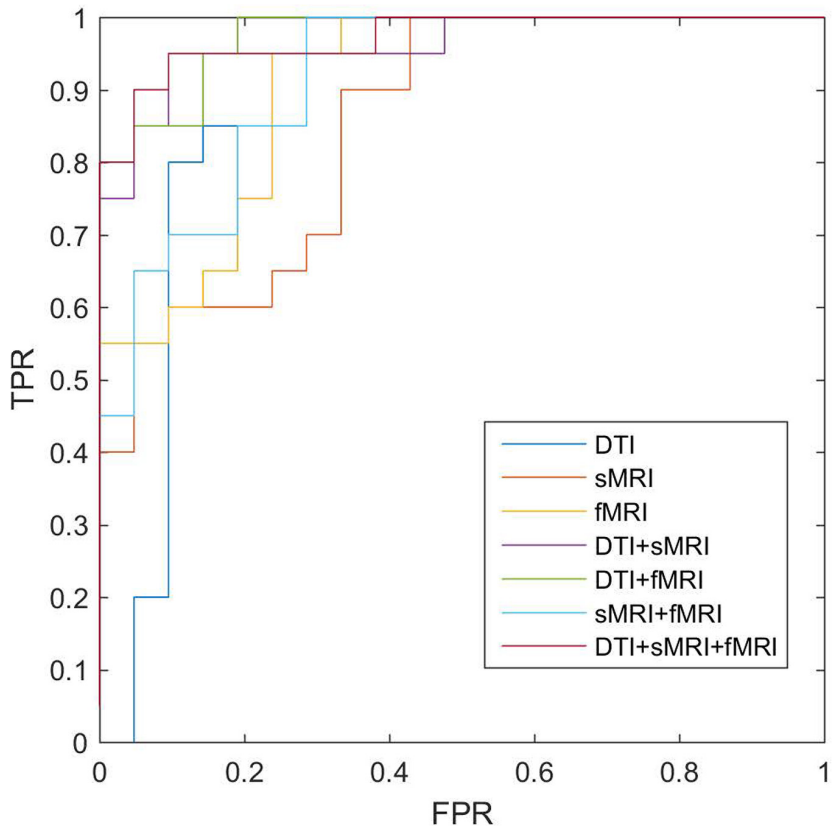

FIGURE 4 | ROC of classifications based on different modalities. sMRI, structural magnetic resonance imaging; DTI, diffusion tensor imaging; fMRI, functional magnetic resonance imaging; ROC, receiver operating characteristic.

TABLE 4 | Classification performance of different modalities.

Modalities	Accuracy (%)	Specificity (%)	Sensitivity (%)	AUC
sMRI	73.17	80.00	66.67	0.8785
DTI	80.49	85.00	76.19	0.8523
fMRI	85.37	90.00	80.95	0.9047
sMRI + DTI	85.37	95.00	76.19	0.9142
fMRI + sMRI	87.80	95.00	80.95	0.9714
fMRI + DTI	90.24	90.00	80.95	0.9619
fMRI + DTI + sMRI	92.68	95.00	90.48	0.9738

AUC, area under the curve; sMRI, structural magnetic resonance imaging; DTI, diffusion tensor imaging; fMRI, functional magnetic resonance imaging.

[Otha]). Meanwhile, the structural brain network based on DTI had a total of 12 consensus connections (**Table 6**), including 7 positive connections and 5 negative connections, which were mainly distributed in the parietal lobe (precuneus [Pcun]), frontal lobe (OrG), insula (INS), temporal lobe (EC), and subcortical nuclei (NAC). In addition, the functional brain network based on fMRI scans had a total of 24 consensus connections (**Table 7**), which were mainly distributed in the parahippocampal gyrus (PhG), INS, SFG, IPL, and subcortical nuclei (medial pre-frontal thalamus [mPFtha], pre-motor thalamus[mPMtha], rostral temporal thalamus [rTtha], dorsolateral putamen [dlPu], lateral amygdala[lAmyg]). Eleven of these connections were positive connections, suggesting that the strength of functional connections of patients with SCD was stronger than that of HCs, and mainly distributed in the cortical-cortical connections between the frontal lobe (MFG, SFG) and the temporal lobe (posterior Superior Temporal Sulcus [pSTS], inferior temporal gyrus [ITG]) and parietal lobe (postcentral gyrus [PoG]). The other 13 negative connections were mainly distributed in the cortical-subcortical connections between the temporal lobe (PhG) and the subcortical nuclei (Tha, amygdala [Amyg]). Therefore, our results indicated that the consensus connections of these three modal networks were involved in a wide range of cortical-subcortical circuits, especially the connection between the cortex and the subcutaneous nucleus including the thalamus, basal ganglia, and amygdala. Furthermore, there existed both positive and negative consensus connections across the three modalities. Positive connections were mainly distributed in the frontal lobe-related connections, and negative connections were mainly distributed in the temporal lobe and subcortical nuclei-related connections.

Robustness of Network Analysis

As mentioned above, we repeated the same network construction method and analysis process based on the AAL, with 90 ROIs,

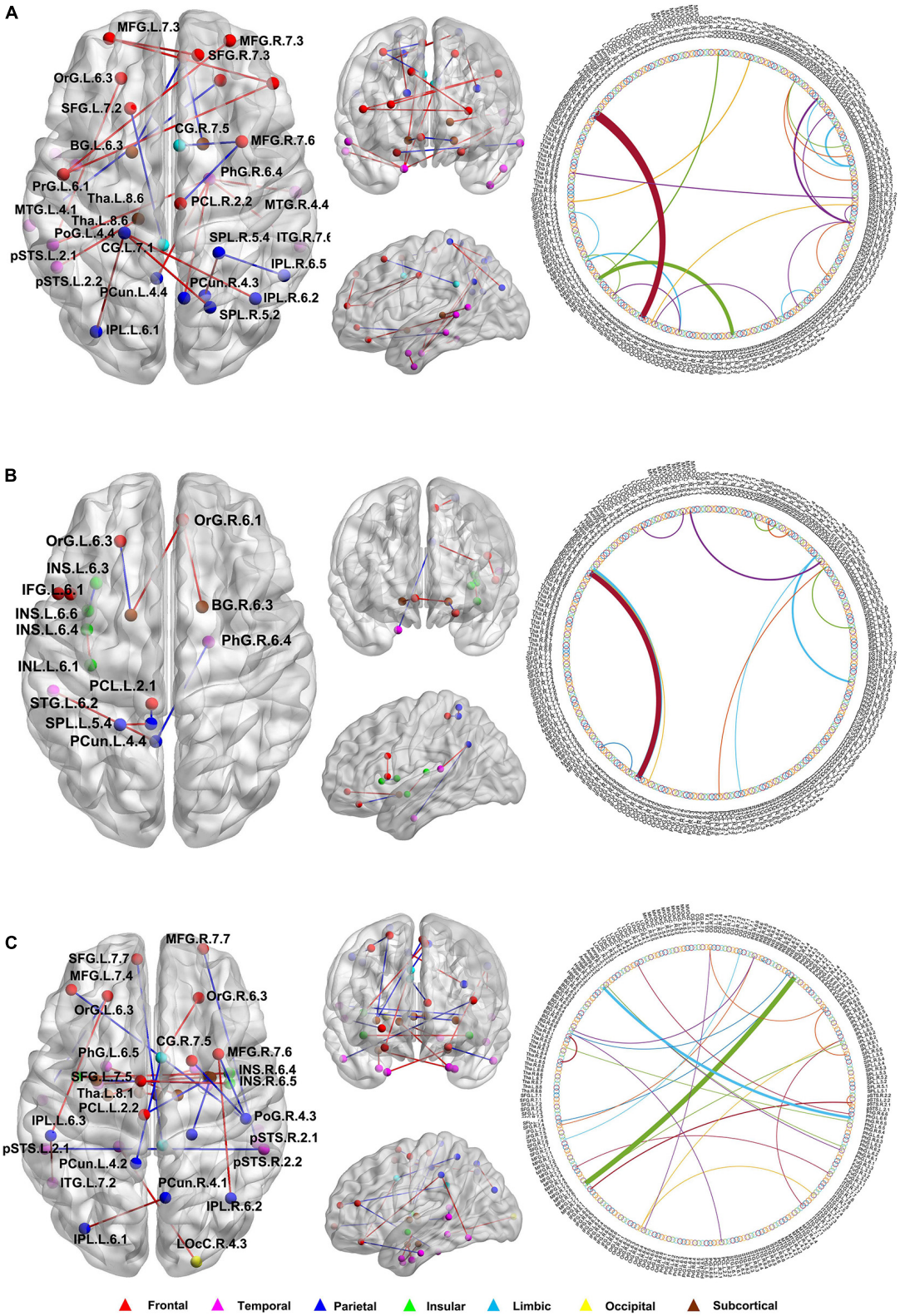

FIGURE 5 | The distribution of consensus connections identified by different modalities. **(A)** Morphological brain network based on sMRI; **(B)** Structural brain network based on DTI; **(C)** Functional brain network based on fMRI. The consensus connections were mapped on the ICBM 152 template with the BrainNet Viewer package (http://nitrc.org/projects/bnv/). Red and blue lines represent the increased and decreased connectivity weight of the SCD group, respectively. sMRI, structural magnetic resonance imaging; DTI, diffusion tensor imaging; fMRI, functional magnetic resonance imaging.

TABLE 5 | Consensus connections identified by the morphological brain network based on sMRI.

ROI	ROI	Mean value		*P*-value
		SCD	HC	
OrG.R.6.1	BG.L.6.3	0.296	0.241	7.34×10^{-5}
OrG.R.6.1	BG.R.6.3	0.480	0.256	8.40×10^{-5}
MFG.R.7.6	PCL.R.2.2	0.767	0.509	1.27×10^{-4}
PhG.R.6.4	PCun.L.4.4	0.094	0.273	2.91×10^{-4}
SPL.R.5.4	IPL.R.6.5	0.387	0.027	3.19×10^{-4}
MFG.R.7.3	PrG.L.6.1	0.461	0.512	4.47×10^{-4}
MFG.R.7.6	CG.R.7.5	0.115	0.002	5.64×10^{-4}
SFG.L.7.2	CG.L.7.1	0.342	0.257	7.98×10^{-4}
pSTS.L.2.2	Tha.L.8.6	0.075	0.297	8.36×10^{-4}
IFG.R.6.2	PrG.L.6.1	0.046	0.452	1.15×10^{-3}
MTG.L.4.2	ITG.L.7.3	0.540	0.634	1.15×10^{-3}
SPL.R.5.4	PCun.R.4.3	0.428	0.446	1.36×10^{-3}
PhG.R.6.4	PCun.R.4.1	0.169	0.225	1.39×10^{-3}
OrG.L.6.3	pSTS.L.2.1	0.118	0.602	1.58×10^{-3}
PhG.R.6.4	pSTS.L.2.1	0.146	0.367	1.67×10^{-3}
SFG.R.7.3	MFG.L.7.3	0.466	0.609	1.72×10^{-3}
SPL.R.5.2	PoG.L.4.4	0.208	0.673	1.76×10^{-3}
OrG.R.6.3	MTG.L.4.1	0.019	0.004	1.92×10^{-3}
IPL.L.6.1	PoG.L.4.4	0.002	0.343	1.95×10^{-3}
MTG.R.4.4	PhG.R.6.4	0.011	0.253	1.99×10^{-3}
MFG.L.7.3	IFG.R.6.2	0.278	0.483	2.25×10^{-3}
IPL.R.6.2	PoG.L.4.4	0.438	0.777	2.29×10^{-3}
ITG.R.7.6	PhG.R.6.4	0.197	0.232	2.57×10^{-3}

sMRI, structural magnetic resonance imaging; SCD, subjective cognitive decline; HC, healthy control; ROI, region of interest.

TABLE 6 | Consensus connections identified by structural brain network based on DTI.

ROI	ROI	Mean value		*P*-value
		SCD	HC	
BG.L.6.3	OrG.R.6.1	0.296	0.241	7.34×10^{-5}
BG.R.6.3	OrG.R.6.1	0.480	0.256	8.40×10^{-5}
PCun.L.4.4	PhG.R.6.4	0.094	0.273	2.91×10^{-4}
PCun.L.4.3	MVOcC .L.5.2	0.002	0.003	3.59×10^{-4}
MVOcC .L.5.3	LOcC.L.4.4	0.021	0.019	8.17×10^{-4}
INS.L.6.1	INS.L.6.4	0.104	0.072	8.47×10^{-4}
INS.L.6.6	INS.L.6.3	0.116	0.180	9.02×10^{-4}
SPL.L.5.4	PCun.L.4.2	0.055	0.052	9.25×10^{-4}
PCL.L.2.1	PCun.L.4.2	0.216	0.242	1.70×10^{-3}
PCun.L.4.4	STG.L.6.2	0.003	0.001	2.22×10^{-3}
IFG.L.6.1	IFG.L.6.6	0.086	0.047	2.32×10^{-3}
OrG.L.6.3	BG.L.6.3	0.002	0.005	2.42×10^{-3}

DTI, diffusion tensor imaging; SCD, subjective cognitive decline; HC, healthy control; ROI, region of interest.

TABLE 7 | Consensus connections identified by functional brain network based on fMRI.

ROI	ROI	Mean value		*P*-value
		SCD	HC	
MFG.R.7.6	PoG.R.4.3	0.221	0.204	4.19×10^{-5}
PhG.R.6.5	Hipp.L.2.1	0.095	0.557	8.91×10^{-5}
Tha.L.8.1	Tha.R.8.4	0.700	0.812	3.22×10^{-4}
MFG.R.7.7	pSTS.R.2.1	0.154	0.027	3.60×10^{-4}
pSTS.L.2.1	pSTS.R.2.2	0.321	0.316	7.94×10^{-4}
INS.R.6.5	BG.L.6.6	0.292	0.075	8.47×10^{-4}
IPL.L.6.1	PCun.R.4.1	0.639	0.660	8.66×10^{-4}
PhG.L.6.1	Amyg.R.2.2	0.143	0.377	1.39×10^{-3}
OrG.L.6.3	ITG.L.7.4	0.443	0.156	1.40×10^{-3}
MFG.R.7.6	IPL.R.6.2	0.540	0.853	1.41×10^{-3}
PCL.L.2.2	BG.R.6.6	0.416	0.097	1.44×10^{-3}
PhG.L.6.6	LOcC .R.4.3	0.109	0.425	1.79×10^{-3}
SFG.R.7.4	PoG.R.4.3	0.282	0.197	1.90×10^{-3}
PCun.L.4.2	CG.R.7.5	0.244	0.059	2.00×10^{-3}
SFG.L.7.5	INS.R.6.5	0.154	0.282	2.10×10^{-3}
PhG.R.6.1	Amyg.R.2.2	0.200	0.577	2.12×10^{-3}
PoG.R.4.4	BG.R.6.6	0.384	0.075	2.14×10^{-3}
PhG.L.6.5	Tha.R.8.2	0.138	0.232	2.27×10^{-3}
ITG.L.7.2	IPL.L.6.3	0.105	0.690	2.35×10^{-3}
INS.L.6.4	INS.R.6.4	0.516	0.587	2.38×10^{-3}
OrG.L.6.3	IPL.L.6.3	0.173	0.192	2.40×10^{-3}
MFG.L.7.4	ITG.R.7.7	0.167	0.140	2.49×10^{-3}
SFG.L.7.7	CG.R.7.1	0.749	0.360	2.51×10^{-3}
OrG.R.6.3	CG.R.7.5	0.170	0.217	2.57×10^{-3}

fMRI, functional magnetic resonance imaging; SCD, subjective cognitive decline; HC, healthy control; ROI, region of interest.

to demonstrate the robustness of our results. **Supplementary Figure 2** describes the multimodal networks at the group level. In terms of the distribution of hub nodes and consensus connections, the AAL90 template and BN template partially overlapped, involving the cortical-subcortical brain regions and their connections (**Supplementary Figures 3, 4**). However, it is worth noting that the number of these features based on the AAL template was significantly reduced compared with the BN template, especially in subcortical nuclei, such as the thalamus. This may be because the AAL template has not yet subdivided the subcortical nuclei into more detailed subregions, resulting in a significant reduction in the number of subcortical nuclei distribution. In addition, the classification results based on the AAL template also demonstrated that compared with the classification accuracy of single modality of the morphological, structural, and functional network (73.17, 58.54, and 78.05%, respectively), the combination of three modalities could significantly improve the classification accuracy of SCD (87.80%) (**Supplementary Table 1** and **Supplementary Figure 5**).

DISCUSSION

In this study, we constructed the morphological, structural, and functional brain networks based on sMRI, DTI and fMRI, respectively, and aimed to explore the biomarkers of brain network in individuals with SCD. Our results indicated that the combination of three modalities using MK-SVM

could significantly improve the classification performance of individuals with SCD. More importantly, the consensus connections based on the morphological, structural, and functional networks identified in our study highlight the role of the cortical-subcortical circuit in the pathological mechanisms associated with individuals with SCD.

Alterations in Morphological Brain Network

In our study, individual morphological brain network was constructed based on the KLS method (Kong et al., 2014). Compared with the previous group-level morphological brain network obtained by estimating the interregional correlations of morphological features (e.g., cortical thickness, cortical surface area or GM volume) (He et al., 2008; Evans, 2013; Matsuda, 2016), the KLS-based morphological brain network could generate an individualised brain network for each participant according to customised brain network nodes defined by specific brain atlases (Kong et al., 2014). Therefore, it is more suitable to construct efficient and stable morphological brain networks and depict complex topological properties of brain network. For the distribution of hubs and consensus connections of morphological brain networks, our results indicated that most of them were involved in cortical-subcortical circuits. Furthermore, the consensus connections among the temporal lobe, parietal lobe, and subcortical nuclei of individuals with SCD were weaker than those of HCs. According to the definition of KLS, the lower value of the KLS, the greater the difference between two brain regions in GM volume distributions (Wang et al., 2016). Our results hinted the heterogeneity of GM volume variation of cortex and subcortical nuclei in SCD patients. Although previous studies have also demonstrated that individuals with SCD exhibited decreased GM volume in hippocampus, entorhinal cortex and amygdala compared to the HCs (Jessen et al., 2006; Stewart et al., 2011; Niemantsverdriet et al., 2018), our results further highlighted the differences in volume changes of brain regions distributed in the cortex and subcortical nuclei.

Alterations in Structural Brain Network

In terms of structural networks based on DTI, most previous structural networks were constructed using deterministic fibre tracking algorithms (Shu et al., 2018; Yan et al., 2018). In comparison, the probabilistic fibre tracking algorithm of this study considered the uncertainty of fibre direction estimation, thereby improving the accuracy of white matter fibre tracking (Ratnarajah et al., 2012). Regarding the distribution of hubs and consensus connections of structural network, our results indicated that the discriminative features of structural network based on DTI and the morphological network based on sMRI involved in overlapped and multiple cortical-subcortical brain regions, such as the frontal lobe, PhG, Tha, and BG. It is consistent with the anatomical basis of brain's GM and white matter distributed. Structural connections reflected the degree of projection connections of white matter fibres between different brain regions (Morris et al., 2008), our findings revealed that SCD patients presented abnormalities of multiple white matter fibre bundles in cortical-subcortical circuit. Previous studies have indicated that most cholinergic fibres originate from the projection of cholinergic neurons in the subcortical nuclei, which connected with hippocampus complex and the cortex through thalamus to constitute the basal forebrain-thalamus-cortex circuit (Hanakawa et al., 2017; Meng et al., 2018; Villagrasa et al., 2018). The input and output of pathway, such as Papez circuit, have been demonstrated to play an important role in memory, learning and attention (Semba, 2000; Aggleton et al., 2016; Agostinelli et al., 2019).

Alterations in Functional Brain Network

Regarding the functional brain networks based on rs-fMRI, functional connections were quantified by calculating the pairwise Pearson's correlation coefficients of blood oxygen level dependent (BOLD) time series obtained for each ROI (Raichle et al., 2001). Based on the distribution of hubs in SCD, we found that most of them, such as the SFG, MTG, cingulate gyrus, and precuneus, were located in the DMN. Similar to previous studies (Greicius et al., 2004; Wang et al., 2013; Chiesa et al., 2019), our study also demonstrated the important role of DMN in the functional brain networks of individuals with SCD. In addition, it is worth noting that compared with the morphological and structural networks, the functional networks exhibited a larger number and wider range of consensus connections between the cortex and subcortical brain regions. Furthermore, we found that the decreased functional connections were mainly distributed in the temporal lobe, thalamus and insula, which might lead to memory impairments (Aggleton et al., 2016). Meanwhile, the increased functional connections related to the frontal lobe might be attributed to the compensatory changes in the functional brain network in the transition stage of SCD.

The Relationship Between the Modalities

Based on the alterations of three different modalities mentioned above, we found that there exists correlation between the morphological, structural, and functional brain networks. Regarding morphological and the structural networks, our results indicated that the hubs and discriminative consensus connections of structural network based on DTI and the morphological network based on sMRI involved in overlapped brain regions, such as the frontal lobe, PhG, Tha, and BG. It is consistent with the anatomical basis of grey matter and white matter distribution in the cortical-subcortical circuit. The related brain regions (e.g., hippocampus, parahippocampal gyrus, cingulate gyrus, amygdala, entorhinal cortex, basal ganglia, and thalamus) were anatomically connected by the white matter fibre bundles such as the fornix, corpus callosum, and external capsule (Schmahmann et al., 2008). Therefore, the alterations between these two modalities were similar. Moreover, compared with the morphological and structural networks, the functional networks exhibited a larger number and wider range of consensus connections between the cortex and subcortical nuclei. As Honey et al. (2009) have demonstrated in previous research, functional connectivity was frequently found between regions without direct structural linkage;

nevertheless, its strength and spatial statistical values remained constrained by the large-scale anatomical structure of the brain and reflected the underlying pathologic alterations. Therefore, different modal brain networks can provide complementary information for detecting abnormalities in SCD individuals.

Abnormalities in the Cortical-Subcortical Circuit

Hub nodes play a critical role in global information transfer and seem to be vulnerable and preferentially affected in patients with AD (Dai and He, 2014). Our results found the disappearance of some hubs in the SCD group, which suggested the brain network integration function of SCD patients may have changed. The reason may be related to the early pathological changes of AD. In additon, for the distribution of the hubs and consensus connections of the morphological, structural, and functional brain networks, our results point to significant abnormalities in the cortical-subcortical brain regions and the connections between them in SCD. In particular, the connections between the subcutaneous nucleus (e.g., BG, amygdala, and thalamus) and the limbic system (e.g., hippocampus, parahippocampal gyrus, cingulate gyrus and entorhinal cortex) and cortex, corresponding to the cortical-subcortical circuit, was significantly aberrant in SCD. Among them, all the subcortical nucleus we identified are highly complex of subnuclei. For instance, thalamus includes more than 10 subnuclei with distinct connections. And the basal nuclei and thalamus participate in many different neuronal pathways, such as cholinergic pathways, with functions related to memory, learning, emotion, attention (Ballinger et al., 2016). Previous studies have found the fewer cholinergic neurons and abnormal amyloid-beta accumulation in cholinergic pathways, are considered important factors leading to the decline of cognitive function in AD (Saxena and Caroni, 2011; Baker-Nigh et al., 2015; Fernandez-Cabello et al., 2020). Therefore, our study provided important clues for the early identification and mechanisms exploration of SCD.

Classification of MK-SVM

In addition, after feature selection of the morphological, structural, and functional network connections by a *t*-test, MK-SVM was applied to combine these features for the classification. For the single modality, we found that the functional network based on fMRI has the highest accuracy rate compared to the morphological and structural networks. This is consistent with the previous study by Yan et al. (2019) that focused on SCD classification based on structural and functional networks. Thus, we speculated that in this stage of SCD, functional changes in the brain were more significant than structural changes in the GM and white matter. In addition, combining two multimodal modalities improved the classification accuracy. Furthermore, the combination of three modalities achieved the best classification performance. The MK-SVM in our study, as an innovative and optimised multimodal information fusion method, can adaptively learn the optimal combined core from a set of base cores and solve the problem of kernel functions selection. Meanwhile, it may address the imbalanced dimension issue across different modalities to some extent and partially alleviate the high-dimensional curve representing multiple features to discriminate individuals with SCD from HCs. Compared with certain previously published research (Yan et al., 2019; Chen et al., 2020), we obtained a better classification performance in response to a multimodal brain network combination. Combined with the model validation based on the AAL template, our findings emphasised that the combination of multimodal brain networks may be considered a potential approach for the early discrimination of individuals with SCD from HCs.

Limitations and Future Directions

Although our study sought to establish a new perspective to explore the brain network mechanisms associated with SCD and early-stage AD identification, several limitations exist with scope for further study. Firstly, a large sample size and multi-centre data are essential to training and validating models. The participant numbers are small for a multi-variate approach. Therefore, the study classifies as pilot study. Although our research has confirmed the stability and repeatability of the methodology based on the AAL template. In future work, we need to use large samples and multi-centre data to further verify the robustness of our proposed method and the repeatability of the results. Secondly, a follow-up study should be carried out for different stages of AD using longitudinal data. In this study, we only detected brain network abnormalities and performed the individual identification in individuals with SCD; longitudinal follow-up studies of the different stages of AD are needed to identify the early and specific imaging markers for diagnosis and prediction. Thirdly, a combination of multimodal diagnostic information should be carried out. We only used different modal brain network connections for the classification of SCD. In the future, we may attempt to identify and explore the pathological mechanisms associated with SCD by combining multimodal diagnostic information such as that stemming from Positron Emission Tomography (PET), Electroencephalography (EEG), and blood biomarker information.

CONCLUSION

We applied the morphological, structural, and functional brain networks based on sMRI, DTI, and fMRI to investigate the pathological mechanisms and potential biomarkers of individuals with SCD. The discriminative connections of three modal brain networks shed light on the abnormality of cortical-subcortical circuit in SCD. Furthermore, the disconnection between different brain regions might lead to the cognitive decline in patients with SCD. In addition, the combination of three modalities with MK-SVM achieved the best classification performance for SCD. Our findings provided novel insights into the pathological mechanisms associated with patients with SCD presenting with early AD pathologies, which will thereby contribute to the

development of more effective diagnostic tools and therapies for preclinical stages of AD.

DATA AVAILABILITY STATEMENT

The original contributions presented in the study are included in the article/**Supplementary Material**, further inquiries can be directed to the corresponding authors.

ETHICS STATEMENT

The studies involving human participants were reviewed and approved by the Institution's Ethical Committee of Shanghai Mental Health Center of Shanghai Jiao Tong University School of Medicine. The patients/participants provided their written informed consent to participate in this study.

AUTHOR CONTRIBUTIONS

XX and WL designed the study and drafted the manuscript. MZ collected the MRI data. LY and TW diagnose the subjects. XX, BX, and HL analyzed and interpreted the results of the data. SX and PW revised the manuscript. All authors approved the final manuscript.

FUNDING

This work was partially supported by the Clinical Research Plan of SHDC (No. SHDC2020CR1038B); National Natural Science Foundation of China (Grant Nos. 81830059, 81771889, and 82001123); The National Pillar Program of China Ministry of Science and Technology (2009BAI77B03); Shanghai Municipal Health and Family Planning Commission Smart Medical Special Research Project (Grant No. 2018ZHYL0105); The Fundamental Research Funds for the Central Universities (Grant No. 22120190219); Shanghai Municipal Commission of Economy and Informatization, Special Fund for Artificial Intelligence Innovation and Development (2019-RGZN-01079); Shanghai Science and Technology Committee (20Y11906800); Shanghai Municipal Commission of Health and Family Planning Science and Research Subjects (201740010); Clinical Research Center Project of Shanghai Mental Health Center (CRC2017ZD02); Shanghai Clinical Research Center for Mental Health (SCRC-MH) (19MC1911100); and Shanghai Mental Health Center (2018-FX-05, 2020zd01).

SUPPLEMENTARY MATERIAL

The Supplementary Material for this article can be found online at: https://www.frontiersin.org/articles/10.3389/fnagi.2021.688113/full#supplementary-material

REFERENCES

Aggleton, J. P., Pralus, A., Nelson, A. J., and Hornberger, M. (2016). Thalamic pathology and memory loss in early Alzheimer's disease: moving the focus from the medial temporal lobe to Papez circuit. *Brain* 139(Pt 7), 1877–1890. doi: 10.1093/brain/aww083

Agostinelli, L. J., Geerling, J. C., and Scammell, T. E. (2019). Basal forebrain subcortical projections. *Brain Struct. Funct.* 224, 1097–1117. doi: 10.1007/s00429-018-01820-6

Ashburner, J. (2007). A fast diffeomorphic image registration algorithm. *Neuroimage* 38, 95–113. doi: 10.1016/j.neuroimage.2007.07.007

Ashburner, J., and Friston, K. J. (2000). Voxel-based morphometry–the methods. *Neuroimage* 11(6 Pt 1), 805–821. doi: 10.1006/nimg.2000.0582

Ashburner, J., and Ridgway, G. R. (2012). Symmetric diffeomorphic modeling of longitudinal structural MRI. *Front. Neurosci.* 6:197. doi: 10.3389/fnins.2012.00197

Baker-Nigh, A., Vahedi, S., Davis, E. G., Weintraub, S., Bigio, E. H., Klein, W. L., et al. (2015). Neuronal amyloid-beta accumulation within cholinergic basal forebrain in ageing and Alzheimer's disease. *Brain* 138(Pt 6), 1722–1737. doi: 10.1093/brain/awv024

Ballinger, E. C., Ananth, M., Talmage, D. A., and Role, L. W. (2016). Basal forebrain cholinergic circuits and signaling in cognition and cognitive decline. *Neuron* 91, 1199–1218. doi: 10.1016/j.neuron.2016.09.006

Behrens, T. E., Berg, H. J., Jbabdi, S., Rushworth, M. F., and Woolrich, M. W. (2007). Probabilistic diffusion tractography with multiple fibre orientations: what can we gain? *Neuroimage* 34, 144–155. doi: 10.1016/j.neuroimage.2006.09.018

Bonte, F. J., Ross, E. D., Chehabi, H. H., and Devous, M. D. Sr. (1986). SPECT study of regional cerebral blood flow in Alzheimer disease. *J. Comput. Assist. Tomogr.* 10, 579–583. doi: 10.1097/00004728-198607000-00005

Chen, H., Sheng, X., Luo, C., Qin, R., Ye, Q., Zhao, H., et al. (2020). The compensatory phenomenon of the functional connectome related to pathological biomarkers in individuals with subjective cognitive decline. *Transl. Neurodegener* 9:21. doi: 10.1186/s40035-020-00201-6

Chiesa, P. A., Cavedo, E., Vergallo, A., Lista, S., Potier, M. C., Habert, M. O., et al. (2019). Differential default mode network trajectories in asymptomatic individuals at risk for Alzheimer's disease. *Alzheimers Dement* 15, 940–950. doi: 10.1016/j.jalz.2019.03.006

Cox, R. W. (1996). AFNI: software for analysis and visualization of functional magnetic resonance neuroimages. *Comput. Biomed. Res.* 29, 162–173. doi: 10.1006/cbmr.1996.0014

Cui, Z., Zhong, S., Xu, P., He, Y., and Gong, G. (2013). PANDA: a pipeline toolbox for analyzing brain diffusion images. *Front. Hum. Neurosci.* 7:42. doi: 10.3389/fnhum.2013.00042

Dai, Z., and He, Y. (2014). Disrupted structural and functional brain connectomes in mild cognitive impairment and Alzheimer's disease. *Neurosci. Bull.* 30, 217–232. doi: 10.1007/s12264-013-1421-0

Dillen, K. N. H., Jacobs, H. I. L., Kukolja, J., von Reutern, B., Richter, N., Onur, O. A., et al. (2016). Aberrant functional connectivity differentiates retrosplenial cortex from posterior cingulate cortex in prodromal Alzheimer's disease. *Neurobiol. Aging* 44, 114–126. doi: 10.1016/j.neurobiolaging.2016.04.010

Dosenbach, N. U., Nardos, B., Cohen, A. L., Fair, D. A., Power, J. D., Church, J. A., et al. (2010). Prediction of individual brain maturity using fMRI. *Science* 329, 1358–1361. doi: 10.1126/science.1194144

Evans, A. C. (2013). Networks of anatomical covariance. *Neuroimage* 80, 489–504. doi: 10.1016/j.neuroimage.2013.05.054

Fan, L., Li, H., Zhuo, J., Zhang, Y., Wang, J., Chen, L., et al. (2016). The human brainnetome atlas: a new brain atlas based on connectional architecture. *Cereb. Cortex* 26, 3508–3526. doi: 10.1093/cercor/bhw157

Fernandez-Cabello, S., Kronbichler, M., Van Dijk, K. R. A., Goodman, J. A., Spreng, R. N., Schmitz, T. W., et al. (2020). Basal forebrain volume reliably predicts the cortical spread of Alzheimer's degeneration. *Brain* 143, 993–1009. doi: 10.1093/brain/awaa012

Greicius, M. D., Srivastava, G., Reiss, A. L., and Menon, V. (2004). Default-mode network activity distinguishes Alzheimer's disease from healthy aging:

evidence from functional MRI. *Proc. Natl. Acad. Sci. U.S.A.* 101, 4637–4642. doi: 10.1073/pnas.0308627101

Hafkemeijer, A., Altmann-Schneider, I., Oleksik, A. M., van de Wiel, L., Middelkoop, H. A., van Buchem, M. A., et al. (2013). Increased functional connectivity and brain atrophy in elderly with subjective memory complaints. *Brain Connect* 3, 353–362. doi: 10.1089/brain.2013.0144

Hampel, H., Mesulam, M. M., Cuello, A. C., Farlow, M. R., Giacobini, E., Grossberg, G. T., et al. (2018). The cholinergic system in the pathophysiology and treatment of Alzheimer's disease. *Brain* 141, 1917–1933. doi: 10.1093/brain/awy132

Hanakawa, T., Goldfine, A. M., and Hallett, M. (2017). A common function of basal ganglia-cortical circuits subserving speed in both motor and cognitive domains. *eNeuro* 4, 1–19. doi: 10.1523/ENEURO.0200-17.2017

He, Y., Chen, Z., and Evans, A. (2008). Structural insights into aberrant topological patterns of large-scale cortical networks in Alzheimer's disease. *J. Neurosci.* 28, 4756–4766. doi: 10.1523/JNEUROSCI.0141-08.2008

Honey, C. J., Sporns, O., Cammoun, L., Gigandet, X., Thiran, J. P., Meuli, R., et al. (2009). Predicting human resting-state functional connectivity from structural connectivity. *Proc. Natl. Acad. Sci. U.S.A.* 106, 2035–2040. doi: 10.1073/pnas.0811168106

Jenkinson, M., Beckmann, C. F., Behrens, T. E., Woolrich, M. W., and Smith, S. M. (2012). FSL. *Neuroimage* 62, 782–790. doi: 10.1016/j.neuroimage.2011.09.015

Jessen, F., Amariglio, R. E., Buckley, R. F., van der Flier, W. M., Han, Y., Molinuevo, J. L., et al. (2020). The characterisation of subjective cognitive decline. *Lancet Neurol.* 19, 271–278. doi: 10.1016/S1474-4422(19)30368-0

Jessen, F., Amariglio, R. E., van Boxtel, M., Breteler, M., Ceccaldi, M., Chételat, G., et al. (2014a). A conceptual framework for research on subjective cognitive decline in preclinical Alzheimer's disease. *Alzheimers Dement* 10, 844–852. doi: 10.1016/j.jalz.2014.01.001

Jessen, F., Amariglio, R. E., van Boxtel, M., Breteler, M., Ceccaldi, M., Chetelat, G., et al. (2014b). A conceptual framework for research on subjective cognitive decline in preclinical Alzheimer's disease. *Alzheimers Dement* 10, 844–852.

Jessen, F., Feyen, L., Freymann, K., Tepest, R., Maier, W., Heun, R., et al. (2006). Volume reduction of the entorhinal cortex in subjective memory impairment. *Neurobiol. Aging* 27, 1751–1756. doi: 10.1016/j.neurobiolaging.2005.10.010

Kong, X. Z., Wang, X., Huang, L., Pu, Y., Yang, Z., Dang, X., et al. (2014). Measuring individual morphological relationship of cortical regions. *J. Neurosci. Methods* 237, 103–107. doi: 10.1016/j.jneumeth.2014.09.003

Lin, Y., Shan, P. Y., Jiang, W. J., Sheng, C., and Ma, L. (2019). Subjective cognitive decline: preclinical manifestation of Alzheimer's disease. *Neurol. Sci.* 40, 41–49. doi: 10.1007/s10072-018-3620-y

Matsuda, H. (2016). MRI morphometry in Alzheimer's disease. *Ageing Res. Rev.* 30, 17–24. doi: 10.1016/j.arr.2016.01.003

Meng, D., Li, X., Bauer, M., Taylor, J. P., Auer, D. P., Alzheimer's Disease, et al. (2018). Altered nucleus basalis connectivity predicts treatment response in mild cognitive impairment. *Radiology* 289, 775–785. doi: 10.1148/radiol.2018180092

Morris, D. M., Embleton, K. V., and Parker, G. J. (2008). Probabilistic fibre tracking: differentiation of connections from chance events. *Neuroimage* 42, 1329–1339. doi: 10.1016/j.neuroimage.2008.06.012

Mueller, S. G., Bateman, L. M., Nei, M., Goldman, A. M., and Laxer, K. D. (2019). Brainstem atrophy in focal epilepsy destabilizes brainstem-brain interactions: preliminary findings. *Neuroimage Clin.* 23:101888. doi: 10.1016/j.nicl.2019.101888

Nasreddine, Z. S., Phillips, N. A., Bédirian, V., Charbonneau, S., Whitehead, V., Collin, I., et al. (2005). The montreal cognitive assessment, MoCA: a brief screening tool for mild cognitive impairment. *J. Am. Geriatr. Soc.* 53, 695–699. doi: 10.1111/j.1532-5415.2005.53221.x

Niemantsverdriet, E., Ribbens, A., Bastin, C., Benoit, F., Bergmans, B., Bier, J. C., et al. (2018). A Retrospective Belgian Multi-Center MRI Biomarker Study in Alzheimer's Disease (REMEMBER). *J. Alzheimers Dis.* 63, 1509–1522. doi: 10.3233/JAD-171140

Pruim, R. H. R., Mennes, M., van Rooij, D., Llera, A., Buitelaar, J. K., and Beckmann, C. F. (2015). ICA-AROMA: a robust ICA-based strategy for removing motion artifacts from fMRI data. *Neuroimage* 112, 267–277. doi: 10.1016/j.neuroimage.2015.02.064

Raichle, M. E., MacLeod, A. M., Snyder, A. Z., Powers, W. J., Gusnard, D. A., and Shulman, G. L. (2001). A default mode of brain function. *Proc. Natl. Acad. Sci. U.S.A.* 98, 676–682. doi: 10.1073/pnas.98.2.676

Ratnarajah, N., Simmons, A., Davydov, O., and Hojjatoleslami, A. (2012). A novel approach for improved tractography and quantitative analysis of probabilistic fibre tracking curves. *Med. Image Anal.* 16, 227–238. doi: 10.1016/j.media.2011.07.005

Saxena, S., and Caroni, P. (2011). Selective neuronal vulnerability in neurodegenerative diseases: from stressor thresholds to degeneration. *Neuron* 71, 35–48. doi: 10.1016/j.neuron.2011.06.031

Scheef, L., Grothe, M. J., Koppara, A., Daamen, M., Boecker, H., Biersack, H., et al. (2019). Subregional volume reduction of the cholinergic forebrain in subjective cognitive decline (SCD). *Neuroimage Clin.* 21:101612. doi: 10.1016/j.nicl.2018.101612

Scheltens, P., Blennow, K., Breteler, M. M., de Strooper, B., Frisoni, G. B., Salloway, S., et al. (2016). Alzheimer's disease. *Lancet* 388, 505–517. doi: 10.1016/S0140-6736(15)01124-1

Schmahmann, J. D., Smith, E. E., Eichler, F. S., and Filley, C. M. (2008). Cerebral white matter: neuroanatomy, clinical neurology, and neurobehavioral correlates. *Ann. N. Y. Acad. Sci.* 1142, 266–309. doi: 10.1196/annals.1444.017

Semba, K. (2000). Multiple output pathways of the basal forebrain: organization, chemical heterogeneity, and roles in vigilance. *Behav. Brain Res.* 115, 117–141. doi: 10.1016/s0166-4328(00)00254-0

Sheline, Y. I., Sanghavi, M., Mintun, M. A., and Gado, M. H. (1999). Depression duration but not age predicts hippocampal volume loss in medically healthy women with recurrent major depression. *J. Neurosci.* 19, 5034–5043. doi: 10.1523/jneurosci.19-12-05034.1999

Shen, S., and Sterr, A. (2013). Is DARTEL-based voxel-based morphometry affected by width of smoothing kernel and group size? A study using simulated atrophy. *J. Magn. Reson. Imaging* 37, 1468–1475. doi: 10.1002/jmri.23927

Shirooka, H., Nishiguchi, S., Fukutani, N., Tashiro, Y., Nozaki, Y., and Aoyama, T. (2018). Subjective cognitive decline and fall risk in community-dwelling older adults with or without objective cognitive decline. *Aging Clin. Exp. Res.* 30, 457–462. doi: 10.1007/s40520-017-0799-3

Shu, N., Wang, X., Bi, Q., Zhao, T., and Han, Y. (2018). Disrupted topologic efficiency of white matter structural connectome in individuals with subjective cognitive decline. *Radiology* 286, 229–238. doi: 10.1148/radiol.2017162696

Stewart, R., Godin, O., Crivello, F., Maillard, P., Mazoyer, B., Tzourio, C., et al. (2011). Longitudinal neuroimaging correlates of subjective memory impairment: 4-year prospective community study. *Br. J. Psychiatry* 198, 199–205. doi: 10.1192/bjp.bp.110.078683

Tijms, B. M., Ten Kate, M., Gouw, A. A., Borta, A., Verfaillie, S., Teunissen, C. E., et al. (2018). Gray matter networks and clinical progression in subjects with predementia Alzheimer's disease. *Neurobiol. Aging* 61, 75–81. doi: 10.1016/j.neurobiolaging.2017.09.011

Tombaugh, T. N., and McIntyre, N. J. (1992). The mini-mental state examination: a comprehensive review. *J. Am. Geriatr. Soc.* 40, 922–935. doi: 10.1111/j.1532-5415.1992.tb01992.x

Tustison, N. J., Cook, P. A., Klein, A., Song, G., Das, S. R., Duda, J. T., et al. (2014). Large-scale evaluation of ANTs and FreeSurfer cortical thickness measurements. *Neuroimage* 99, 166–179. doi: 10.1016/j.neuroimage.2014.05.044

Tzourio-Mazoyer, N., Landeau, B., Papathanassiou, D., Crivello, F., Etard, O., Delcroix, N., et al. (2002). Automated anatomical labeling of activations in SPM using a macroscopic anatomical parcellation of the MNI MRI single-subject brain. *Neuroimage* 15, 273–289. doi: 10.1006/nimg.2001.0978

Villagrasa, F., Baladron, J., Vitay, J., Schroll, H., Antzoulatos, E. G., Miller, E. K., et al. (2018). On the role of cortex-basal ganglia interactions for category learning: a neurocomputational approach. *J. Neurosci.* 38, 9551–9562. doi: 10.1523/JNEUROSCI.0874-18.2018

Wang, H., Jin, X., Zhang, Y., and Wang, J. (2016). Single-subject morphological brain networks: connectivity mapping, topological characterization and test-retest reliability. *Brain Behav.* 6:e00448. doi: 10.1002/brb3.448

Wang, X., Huang, W., Su, L., Xing, Y., Jessen, F., Sun, Y., et al. (2020). Neuroimaging advances regarding subjective cognitive decline in preclinical Alzheimer's disease. *Mol. Neurodegener* 15:55. doi: 10.1186/s13024-020-00395-3

Wang, Y., Risacher, S. L., West, J. D., McDonald, B. C., Magee, T. R., Farlow, M. R., et al. (2013). Altered default mode network connectivity in older adults with cognitive complaints and amnestic mild cognitive impairment. *J. Alzheimers Dis.* 35, 751–760. doi: 10.3233/jad-130080

Xu, X., Li, W., Mei, J., Tao, M., Wang, X., Zhao, Q., et al. (2020a). Feature selection and combination of information in the functional brain connectome for discrimination of mild cognitive impairment and analyses of altered brain patterns. *Front. Aging Neurosci.* 12:28. doi: 10.3389/fnagi.2020.00028

Xu, X., Li, W., Tao, M., Xie, Z., Gao, X., Yue, L., et al. (2020b). Effective and accurate diagnosis of subjective cognitive decline based on functional connection and graph theory view. *Front. Neurosci.* 14:577887. doi: 10.3389/fnins.2020.577887

Yan, T., Wang, W., Yang, L., Chen, K., Chen, R., and Han, Y. (2018). Rich club disturbances of the human connectome from subjective cognitive decline to Alzheimer's disease. *Theranostics* 8, 3237–3255. doi: 10.7150/thno.23772

Yan, T., Wang, Y., Weng, Z., Du, W., Liu, T., Chen, D., et al. (2019). Early-stage identification and pathological development of alzheimer's disease using multimodal MRI. *J. Alzheimers Dis.* 68, 1013–1027. doi: 10.3233/JAD-181049

Zalesky, A., Fornito, A., and Bullmore, E. T. (2010). Network-based statistic: identifying differences in brain networks. *Neuroimage* 53, 1197–1207. doi: 10.1016/j.neuroimage.2010.06.041

Zeng, L. L., Shen, H., Liu, L., Wang, L., Li, B., Fang, P., et al. (2012). Identifying major depression using whole-brain functional connectivity: a multivariate pattern analysis. *Brain* 135(Pt 5), 1498–1507. doi: 10.1093/brain/aws059

Zhao, W., Guo, S., Linli, Z., Yang, A. C., Lin, C. P., and Tsai, S. J. (2020). Functional, anatomical, and morphological networks highlight the role of basal ganglia-thalamus-cortex circuits in schizophrenia. *Schizophr. Bull.* 46, 422–431. doi: 10.1093/schbul/sbz062

Conflict of Interest: HL and BX were employed by the company Beijing Intelligent Brain Cloud Inc., Beijing, China.

The remaining authors declare that the research was conducted in the absence of any commercial or financial relationships that could be construed as a potential conflict of interest.

frontiers in Aging Neuroscience

ORIGINAL RESEARCH
published: 12 July 2021
doi: 10.3389/fnagi.2021.687530

Progressive Brain Degeneration From Subjective Cognitive Decline to Amnestic Mild Cognitive Impairment: Evidence From Large-Scale Anatomical Connection Classification Analysis

Wuhai Tao[1,2], Hehui Li[1], Xin Li[3], Rong Huang[1], Wen Shao[4], Qing Guan[1,2] and Zhanjun Zhang[3]**

[1] Center for Brain Disorders and Cognitive Science, Shenzhen University, Shenzhen, China, [2] Shenzhen-Hong Kong Institute of Brain Science-Shenzhen Fundamental Research Institutions, Shenzhen, China, [3] State Key Laboratory of Cognitive Neuroscience and Learning and IDG/McGovern Institute for Brain Research, Beijing Normal University, Beijing, China, [4] Department of Neurology, China-Japan Friendship Hospital, Beijing, China

OPEN ACCESS

Edited by:
Ying Han,
Capital Medical University, China

Reviewed by:
Zan Wang,
Southeast University, China
Carol D. SanMartín,
University of Chile, Chile

***Correspondence:**
Qing Guan
guanqing@szu.edu.cn
Zhanjun Zhang
zhang_rzs@bnu.edu.cn

Received: 29 March 2021
Accepted: 07 June 2021
Published: 12 July 2021

Citation:
Tao W, Li H, Li X, Huang R, Shao W, Guan Q and Zhang Z (2021) Progressive Brain Degeneration From Subjective Cognitive Decline to Amnestic Mild Cognitive Impairment: Evidence From Large-Scale Anatomical Connection Classification Analysis. Front. Aging Neurosci. 13:687530. doi: 10.3389/fnagi.2021.687530

People with subjective cognitive decline (SCD) and amnestic mild cognitive impairment (aMCI) are both at high risk for Alzheimer's disease (AD). Behaviorally, both SCD and aMCI have subjective reports of cognitive decline, but the latter suffers a more severe objective cognitive impairment than the former. However, it remains unclear how the brain develops from SCD to aMCI. In the current study, we aimed to investigate the topological characteristics of the white matter (WM) network that can successfully identify individuals with SCD or aMCI from healthy control (HC) and to describe the relationship of pathological changes between these two stages. To this end, three groups were recruited, including 22 SCD, 22 aMCI, and 22 healthy control (HC) subjects. We constructed WM network for each subject and compared large-scale topological organization between groups at both network and nodal levels. At the network level, the combined network indexes had the best performance in discriminating aMCI from HC. However, no indexes at the network level can significantly identify SCD from HC. These results suggested that aMCI but not SCD was associated with anatomical impairments at the network level. At the nodal level, we found that the short-path length can best differentiate between aMCI and HC subjects, whereas the global efficiency has the best performance in differentiating between SCD and HC subjects, suggesting that both SCD and aMCI had significant functional integration alteration compared to HC subjects. These results converged on the idea that the neural degeneration from SCD to aMCI follows a gradual process, from abnormalities at the nodal level to those at both nodal and network levels.

Keywords: amnestic mild cognitive impairment, subjective cognitive decline, white matter, network, Alzheimer's disease

INTRODUCTION

The current status of Alzheimer's disease (AD) clinical treatment is not promising, which makes preclinical prediction for AD particularly important (Huang et al., 2020). Many studies have shown that AD manifests significant pathological changes decades before it develops into dementia (Jack et al., 2010; Bateman et al., 2012). Characterized by objective cognitive impairment similar to AD, mild cognitive impairment has been proposed as an important stage in the development of AD. In particular, about one-third of those with amnesiac mild cognitive impairment (aMCI) will develop AD within 5 years (Ward et al., 2013). Similarly, the elderly with subjective cognitive decline (SCD) also has a high risk for developing AD (Jessen et al., 2020). Both at the early stages of AD, the major behavioral difference between SCD and aMCI is that aMCI has severer objective cognitive impairments than SCD. However, knowledge about the relationship between SCD and aMCI neuroimaging characteristics is still insufficient.

Some studies have found that aMCI and SCD have similar structural or functional degeneration with AD (Scheef et al., 2012; Wang et al., 2013, 2016). In general, patients with aMCI had more extensive and severe neurological impairments than the elderly with SCD (Sun et al., 2015). However, regions of differences in structural and functional activities between aMCI and SCD are not the same in different studies. For example, SCD may, in some way, compensate for the negative effects of neurological damage in some distracted areas to ensure that they have normal performance when completing cognitive ability tests (Erk et al., 2011). Recently, studies have shown that neural impairments of aMCI and SCD are not only restricted to individual regions but also extended to the interactions among multiple brain areas (Dai and He, 2014; Tao et al., 2020). Consistent with this, in the last 5 years, extensive research has been conducted on neural substances associated with AD and its development from the perspective of brain networks (Wang et al., 2016; Shu et al., 2018; Lazarou et al., 2019). Graph theoretical analysis offered a new perspective to estimate the changes of multiple properties of brain networks, both at the local and global level, as the disease progresses (Bullmore and Sporns, 2009; He and Evans, 2010). There were also some researchers who suggested that brain connectome research provided a very effective way for SCD studies (Lazarou et al., 2019).

Functional segregation, which can reflect the local information processing, and functional integration, which is a reflection of the global information processing, are two major aspects of the information activity of the brain. In the graph theoretical analysis, the index of clustering coefficient and local efficiency, global efficiency, and path length of brain networks can effectively reflect the two aspects, respectively (Rubinov and Sporns, 2010). One previous study has shown that AD patients had lower brain network integration and higher brain network segregation, and these changes were significantly correlated with cognitive decline (Kabbara et al., 2018). The combination of the features of brain network integration and segregation can distinguish AD patients from healthy elderly with high accuracy (Cai et al., 2020). An earlier review article on the topic of structural and functional networks in the brain reported both functional segregation and functional integration impairments in MCI and AD (Dai and He, 2014). Our previous work also revealed impairments of anterior–posterior brain functional connectivity in SCD in the resting state (Tao et al., 2020). These results may indicate that the brain network of SCD has also been altered. In the meantime, considering that the pathological changes of AD are a gradual process, it is suggested that the problems with the integration and separation of brain networks might occur at both aMCI and SCD stages.

To be considered as a disconnection syndrome (Delbeuck et al., 2003), the white matter (WM) connectivity plays a crucial role in the progress of AD pathology. The microstructural deterioration of WM caused by demyelination and axonal deterioration may result in obstacles of information transfer within the brain network (Bozzali et al., 2002). Both aMCI and SCD have been reported with widespread WM impairment in previous studies (Selnes et al., 2013; Defrancesco et al., 2014; Shao et al., 2019), which further disrupted the topological properties of their brain network (Wang et al., 2016; Shu et al., 2018). Moreover, the degree of WM abnormalities is significantly correlated with the neurofibrillary tangle pathology stage and the severity of the disease (Kantarci et al., 2017). Since aMCI and SCD are in different stages of AD, it is necessary to look further into the phase-specific characteristics of aMCI and SCD WM networks to clarify the structural basis of the specific behavior in each stage.

To address this issue, in the current study, diffusion tensor imaging and deterministic tractography were first used to construct the WM structural network. We then used graph theory approaches to estimate neural indexes, including path length, the global efficiency, the local efficiency, and the clustering coefficient, both the nodal and network levels. Finally, classification models were built to investigate which indexes can significantly identify SCD or aMCI from HC. We hypothesized that neural degeneration follows a gradual change from SCD to aMCI. Specifically, neural differences between SCD and HC were mainly represented by indexes at the node level, whereas that between aMCI and HC were represented by indexes at the network level. We also examined the functional segregation and integration properties between SCD or aMCI and HC, and made further assumption that SCD and aMCI are already impaired in both, but given that they are at distinct stages, there may be subtle differences in the manifestation of the neural impairments between the two.

MATERIALS AND METHODS

Participants

A total of 66 participants (mean age, 64.76 $\pm$ 6.4) were recruited in the current study, including 22 SCD, 24 aMCI, and 23 gender-, age-, and years of education-matched HC. All participants were sourced from the Beijing Aging Brain Rejuvenation Initiative database, which is a project of community-based elderly health study. Participants meeting the following criteria were included: (1) having no less than 6 years of education and being able to complete a series of neuropsychological measurements; (2)

nondementia, the score of Mini-Mental Status Examination (MMSE, Chinese version) $\geq$ 24; (3) no history of coronary disease, psychotic disorders, tumors, motor neuron disease, developmental disability, or diseases that could influence cerebral function; (4) no clinical diagnosis of depression, schizophrenia, and other psychiatric disorders, and no history of taking psychoactive medications; and (5) no physical problems that are not appropriate for MRI scan.

In addition to the above criteria, the SCD participants also had (1) self-reported memory declines in recent years relative to previous states but was not caused by acute events, (2) the normal cognitive function above -1.5 standard deviations (SD) of the Chinese norms, and (3) intact daily living function. For the aMCI participants, they should meet the published inclusion criteria by Petersen et al. (1999): (1) had memory declined complaints, (2) scores of cognitive function below 1.5 SD of the Chinese norm, and (3) no difficulty in daily life.

Neuropsychological Assessment

A series of neuropsychological assessments were used to assess the general mental status and other cognitive functions of all the participants. The general cognitive function was measured by the MMSE, while the memory function was estimated by the Auditory Verbal Learning Test (AVLT) and the Rey-Osterrieth Complex Figure test (ROCF-recall). The Symbol Digit Modalities Test (SDMT) and part A of the Trail Making Test (TMTa) tested the attention ability, while the part B of the TMT (TMTb) and part C of the Stroop Test (Stroop C) tested the executive function.

Image Acquisition

A Siemens 3.0T scanner (Siemens, Munich, Germany) was employed to acquire the MRI imaging data at the Imaging Center for Brain Research, Beijing Normal University. Participants lay flat on their backs with foam pads to minimize head motion. T1-weighted images were acquired using sagittal 3D magnetization prepared rapid gradient echo (MP-RAGE) sequences. The acquisition parameters were as follows: repetition time (TR) = 1,900 ms, echo time (TE) = 3.44 ms, flip angle = 9°, field of view (FOV) = 256 × 256 mm^2, and acquisition matrix = 256 × 256, 1 mm slice thickness, and 176 sagittal slices. Diffusion-weighted images were obtained by an echo-planar imaging sequence with the parameters as follows: TR = 11,000 ms; TE = 94 ms; flip angle = 90°, FOV = 240 × 240 mm^2, acquisition matrix = 128 × 128, 2 mm slice thickness, and 70 sagittal slices. The diffusion sensitizing gradients were applied, 1 image without diffusion-weighted (b = 0 s/mm^2) and 30 diffusion-weighted directions (b = 1,000 s/mm^2).

Image Preprocessing

MATLAB 2018a, SPM12[1], and PANDA (Pipeline for Analysing Brain Diffusion Images)[2] software were used to preprocess the DTI images. Several steps were applied to the data preprocessing: eddy current and motion artifact correction, fractional anisotropy calculation, whole-brain fiber tracking, and diffusion tensor tractography. The fiber tracking was performed by the continuous tracking algorithm, and the fiber tracts were terminated if two consecutive moving directions have a crossing angle above 45°and the fractional anisotropy is out of the threshold 0.2–1 (Cui et al., 2013).

Network Construction

Network nodes and edges are the most basic element of a brain network. We used the standard procedure proposed by Gong et al. (2009) and constructed the WM network as Shu et al. (2018) described in their work. Network nodes were defined using the 90 brain regions subdivided by the automated anatomical labeling (AAL) template. The network nodes were considered structurally connected if the number of fibers between two nodes was $\geq$3 (Shu et al., 2012). We set the thresholds to 1–5 and 10 and observed the effects of diverse thresholds on the differential characteristics between groups, respectively, and no significant changes were observed between the thresholds (see **Figure 1** and **Supplementary Table 1**). Then, the number of valid fibers (FN) between regions was defined as the weights of the network edges. Eventually, each subject was constructed an FN-weighted 90 × 90 matrix WM network.

Network Analysis

For each subject, the GRETNA software[3] was applied to quantify the network metric. The characteristic path length and the global efficiency, which can reflect the structure integration, the local efficiency, and the clustering coefficient, indicating the structure segregation, were calculated for each participant at both network and nodal levels. The smaller the characteristic path length and the higher the local efficiency, the better the structure integration. The higher the local efficiency and the higher the clustering coefficient, the better the structure segregation. The BrainNet Viewer[4] was used to present the network results.

Indexes at the Network Level

The characteristic path length described the mean of the shortest path length between nodes. It can be computed as follows:

$$\mathrm{L}\ (\mathrm{G}) = \frac{1}{\mathrm{N}(\mathrm{N}-1)} \sum_{i \neq j \in G} d_{ij}$$

The global efficiency measures the efficiency of parallel information transfer in the network. It can be computed as follows:

$$\mathrm{E}_{\mathrm{global}}\ (\mathrm{G}) = \frac{1}{N(N-1)} \sum_{i \neq j \in G} \frac{1}{d_{ij}}$$

The local efficiency shows how efficient the communication is among the neighbors of each node. It can be computed as follows:

$$\mathrm{E}_{\mathrm{loc}}\ (G) = \frac{1}{N} \sum_{i \in G} E_{glob}(G_i)$$

[1]http://www.fil.ion.ucl.ac.uk/spm

[2]http://www.nitrc.org/projects/panda/

[3]www.nitrc.org/projects/gretna/

[4]http://www.nitrc.org/projects/bnv/

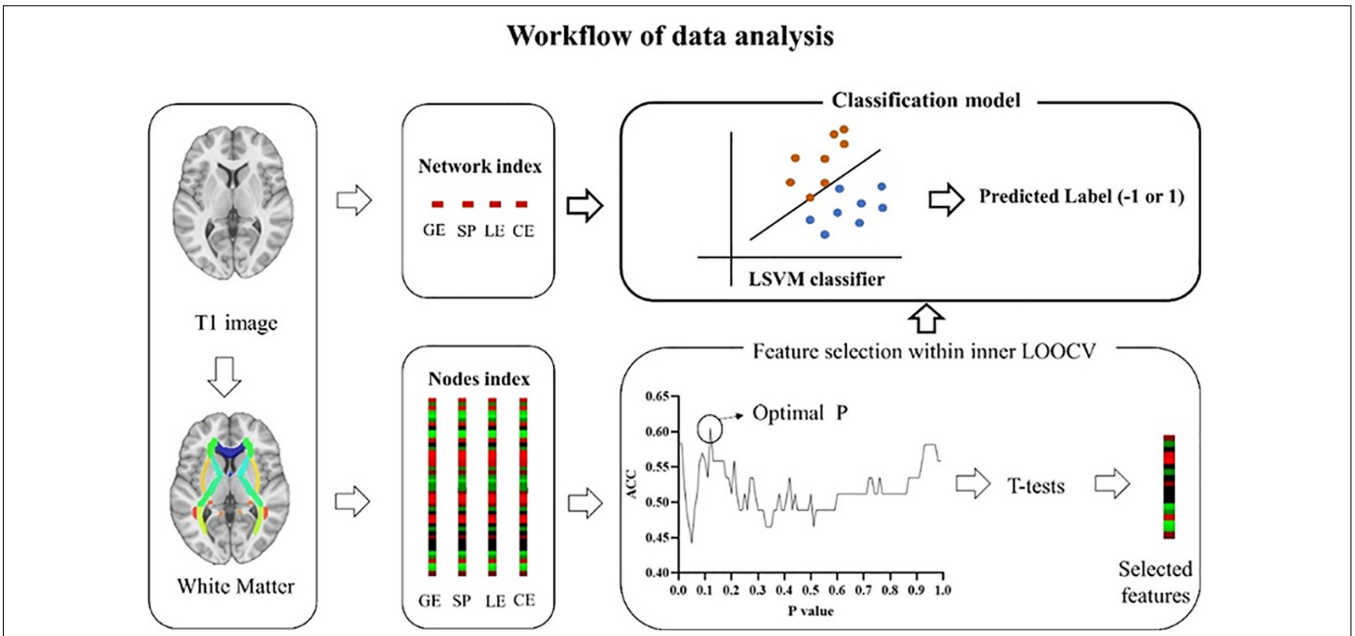

FIGURE 1 | Workflow of data analysis. White matter matrices were constructed based on the AAL template, an automated anatomical parcellation of the spatially normalized single-subject high-resolution T1 volume, during which indexes (GE, SP, LE, and CE) at the network and nodal level were extracted. At the network level, four indexes, including GE, SP, LE, and CE were used separately or combined to build a classifier. GE, global efficiency; SP, short path length; LE, local efficiency; CE, clustering coefficient. At the nodal level, each index includes 90 features. To select the most discriminate features, LSVM (an outer LOOCV) was nested with a feature selection produce (an inner LOOCV). LSVM, linear support vector model; LOOCV, leave-one-out cross-validation. Similar to nodal level, four indexes were used separately or combined to build a classifier.

TABLE 1 | Demographics and neuropsychological characterizations.

	HC (n = 23)	SCD (n = 22)	aMCI (n = 24)	χ^2/F	p
Gender (m/f)	14/9	11/11	11/13	1.13	0.570
Age (years)	65.91 ± 5.86	62.41 ± 5.24	65.71 ± 7.49	2.19	0.120
Education (years)	12.30 ± 2.84	10.50 ± 2.82	10.50 ± 2.96	3.02	0.056
MMSE	29.04 ± 0.93	27.14 ± 1.73	26.04 ± 1.78	21.08[a]	< 0.001
Memory	6.05 ± 0.40	4.94 ± 0.40	4.04 ± 0.37	151.96[b]	< 0.001
Attention	5.58 ± 0.48	5.35 ± 0.57	4.12 ± 0.83	29.79[c]	< 0.001
Executive	5.61 ± 0.27	5.11 ± 0.43	4.31 ± 0.84	30.64[b]	< 0.001

Values are mean ± standard deviation. All covariance analyses used gender, age, and education as covariables. The post hoc tests were corrected by Bonferroni, and $p < 0.05$ was considered significant.
[a]*HC > SCD and HC > aMCI.*
[b]*HC > SCD > aMCI.*
[c]*HC > aMCI and SCD > aMCI.*

The clustering coefficient is defined as the possibility of the neighborhoods that are connected with each other. It can be computed as follows:

$$\mathrm{C\ (G)}\ = \frac{1}{\mathrm{N}} \sum_{i \in G} Ci = \frac{1}{N} \sum_{i \in G} \frac{2\mathrm{t}_i}{k_i(k_i - 1)}$$

Indexes at the Nodal Level

The shortest path length of node i shows the mean distance between node i and other nodes. It can be computed as follows:

$$L\,(i) = \max_j d(1 \rightarrow j)$$

The nodal efficiency for node i shows the efficiency of parallel information transfer of this node in network G. It can be computed as follows:

$$E_{glob}\,(i) = \frac{1}{N-1} \sum_{j \neq i \in G} \frac{1}{d_{ij}}$$

The local efficiency of node i shows the efficiency of the communication among the first neighbors of node i when it is removed. It can be computed as follows:

$$E_{loc}\,(i) = \frac{1}{N_i(N_i - 1)} \sum_{j \neq i \in G_i} \frac{1}{d_{ij}}$$

The clustering coefficient of node i shows the likelihood the neighbors of node i connected to each other. It can be computed as follows:

$$C(i) = \frac{2t_i}{k_i(k_i - 1)}$$

In all the formulas above, N is the total number of nodes in the network, d_{ij} is the shortest path length between node i and node j in network G, and G_i denotes the subgraphs of node i. C_i represents the clustering coefficient of node i, N is the total number of nodes, t is the weighted edges, and k is the number of nodes connecting to node i.

Statistical Analysis

General statistical analyses were performed with SPSS (version 22.0, Chicago, IL, United States). Analysis of covariance (ANCOVA) with age, gender, and years of education as covariates was used to estimate the group difference in neuropsychological tests, global network metrics, and nodal properties. If the main effects of groups were significant, *post hoc t*-tests were performed to further examine the difference between any two groups. A false discovery rate (FDR) correction was performed at a *q*-Value of 0.05 to correct for multiple comparisons. Receiver operating characteristic curve (ROC) analysis was applied to describe the discrimination of network and nodal characteristics on HC, SCD, and aMCI. We also did partial correlation analysis with age, gender, and years of education adjusted to reveal the relationship between cognition and some WM indicators that we selected.

The LSVM-Based Classification

An LSVM method was performed using LIBSVM for Matlab[5] (Chang and Lin, 2011) to differentiate aMCI or SCD from HC with WMV metrics. The leave-one-out cross-validation (LOOCV) was applied for the cross-validation, which has been widely used in previous studies, especially for data with a small sample size (Cui et al., 2016; Pereira et al., 2009). In this dataset, multiple dimensional spaces were represented by all of the features, and each participant was a point in these multiple dimensional spaces. The LSVM used a subset of data (i.e., training set, n - 1 participants) as input to build a modal that can best separate the input data into two categories (Cui et al., 2016). Then, a relatively dependent dataset was used (i.e., testing set, the last participant) to test this classifier. Based on the features that have been used, the last participant can be classified as any of the two classes (e.g., HC or SCD), labeled as 1 or -1. If the predicted label is consistent with the real label, then the classification is correct. After the leave-one-out loop for two groups was finished, a final accuracy represented by the probability to predict accurately can be calculated, which demonstrated the performance of the classification model.

[5]http://www.csie.ntu.edu.tw/~cjlin/libsvm/

Feature Selection at the Nodal Level

Each index (global efficiency, local efficiency, clustering efficiency, and short path) at the node level was represented by a 90 × 1 matrix. To boost classification performance, a nested inner LOOCV loop was conducted, with the outer loop to estimate classification accuracy and the inner loop to select discriminative features and to eliminate the noninformative features (Cui et al., 2016). Detailed steps were as follows. First, N - 1 subjects were used as the training set, the last participant served as the testing set for the outer LOOCV loop. Second, all data were normalized (Cui et al., 2016). Third, an inner LOOCV loop was performed, during which two-sample *t*-tests were applied for each feature within N - 2 participants. Features below a given *p*-Value were selected for inner classification models. The given *p*-Value was set from 0.01 to 0.99 with a step of 0.01. In this way, 99 inter-LOOCV were conducted, and 99 accuracies were obtained. Optimal *p* was determined by the highest classification accuracy. (4) Features thresholded with this optimal *p*-Value were selected for the training set of the outer LOOCV loop. (5) The resultant discriminative weight for each feature was calculated to mark the relative importance of a feature to a classifier (Mourao-Miranda et al., 2005). Notably, this

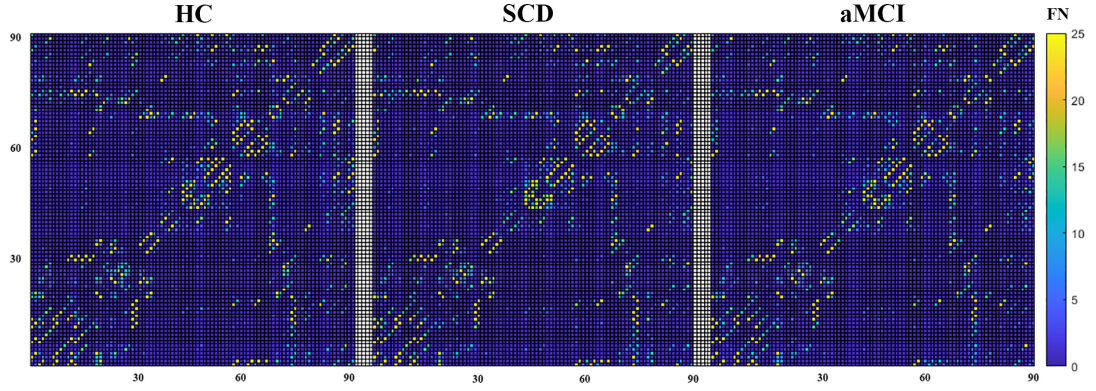

FIGURE 2 | The mean structural network matrix of each group built on the white matter. The horizontal and vertical coordinates represent 90 brain regions in the AAL template. Values in each cell represent the mean FN between two brain areas.

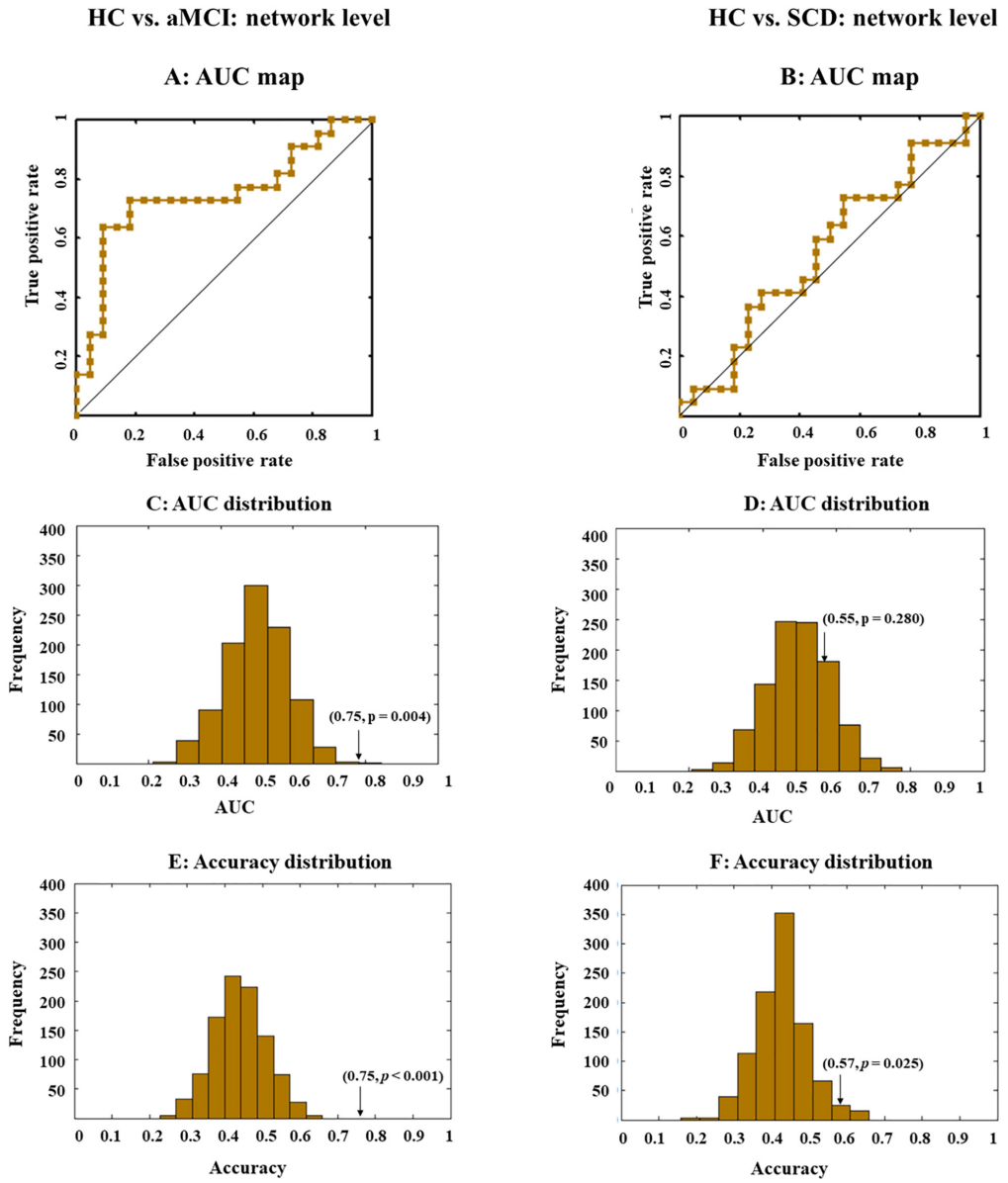

FIGURE 3 | Receiver operating characteristic (ROC) and area under the curve (AUC) or accuracy distribution when all indexes (i.e., global efficiency, local efficiency, cluster efficiency, and short path) at the network level were combined. ROC maps shows the classification performance **(A,B)**, where a greater AUC corresponds to better performance. AUC and accuracy distribution maps **(C–F)** were built by permutation tests, during which group labels were randomly arranged 1,000 times. Arrows in the distribution maps marker AUC or accuracy based on real group labels.

strict feature selection procedure was skipped for indexes at the network level.

Definition of the Discriminate Features

Features selected for each outer loop were slightly different because of the difference in the dataset (n - 1 participants for each time). The absolute weight of features that were used for all outer loops was averaged, which was used to indicate the discriminate weight of each feature (Dai et al., 2012; Cui et al., 2016, Cui and Gong, 2018). The higher the discriminate weight is, the greater the contribution of the corresponding feature to the classifier is. In the current study, the most discriminate features were defined as those with averaged discriminate weight larger than 0.

Evaluation of Classification Performance

Accuracy, specificity, sensitivity, area under the ROC curve (AUC) were estimated to quantify the classification accuracy. As presented earlier, accuracy means the proportion of subjects to be accurately classified. Specificity means the proportion of subjects who can be accurately classified as HC or SCD (or aMCI). Sensitivity means the proportion of subjects who can be accurately classified as SCD (or aMCI). Furthermore, ROC

analysis was used to estimate the effectiveness of each classifier. The AUC indicates the classification performance of a classifier, and a larger AUC represents a better performance (Fawcett, 2006). To estimate the significance of the accuracy and AUC, a 1,000 permutation test was performed to build null distributions, during which labels for each participant were shuffled and the whole classification procedure was reperformed.

RESULTS

Demographic Information

Age, gender, and years of education did not differ significantly among the three groups. MMSE was significantly higher in HC than in SCD and aMCI. Memory and executive functions declined in the order of HC, SCD, and aMCI. The attentional function was significantly stronger in both HC and SCD than in aMCI (**Table 1**). We have reported these behavioral results in another article as well (Tao et al., 2020).

The Mean Structural Network Matrix

The mean structural network matrix for the three groups is presented in **Figure 2**. Notably, the number of fiber tracts between a few brain regions was abundant (nearly 300), but we chose only 25 as the maximum threshold to achieve a better representation of the structural connectivity state between most brain regions. A two-tailed t-test for group comparisons of the structural network ($p < 0.025$) was presented in the **Supplementary Material**. Most group differences were found between HC and aMCI, while relatively few differences were found between HC and SCD (see **Supplementary Figure 2**).

Classification With White Matter Indexes at the Network Level

The LSVM classifier accurately discriminated aMCI from HC when all network indexes (i.e., global efficiency, local efficiency, cluster efficiency, and short path) were combined (brown lines in **Figure 3A**). The result elucidated significant AUC (0.75, $p < 0.001$; **Figure 3E** and **Table 2**) and accuracy (0.75, $p < 0.001$; **Figure 3C** and **Table 2**, bold font), respectively. Then, LSVM was also conducted by using the global efficiency, local efficiency, clustering efficiency, and short path separately. Permutation tests revealed significantly higher accuracy and AUC for all indexes except for the clustering coefficiency (**Table 2**).

However, for SCD and HC, performance accuracies for all classifiers either building on each index or the combined index were all lower than 0.6, with nonsignificant AUCs close to 0.5 (**Figures 3B,D,F**).

Classification With White Matter Indexes at the Nodal Level

Then, the LSVM was conducted at the node level. We first combined all indexes to classify different groups. However, the whole-brain anatomical connection pattern cannot significantly separate aMCI or SCD from HC (**Figures 4A,B**).

Then, we exploited single-type metrics to build classifiers, during which observed a double-dissociation pattern. Specifically, path length can differentiate aMCI and HC but not SCD and HC (**Figure 4A**). Notably, AUC for this classifier was significant (0.66, $p = 0.019$; **Figure 4C** and **Table 2**, bold font), while accuracy was marginally significant (0.66, $p = 0.079$; **Figure 4E** and **Table 2**). Even though the significance was marginal, there was still a trend that path length might be able to identify aMCI from HC. In addition, the most 10 discriminative WM features for this classifier were the left supramarginal gyrus; left amygdala; right inferior frontal gyrus, opercular part; right hippocampus; left temporal pole; middle temporal gyrus; right superior temporal gyrus; left inferior frontal gyrus, triangular part; left lenticular nucleus, pallidum; right inferior parietal, but supramarginal and angular gyri; and right thalamus.

On the other hand, the global efficiency can significantly identify SCD but not aMCI from HC (**Figure 3**). AUC (0.71, $p = 0.014$; **Figure 4D** and **Table 2**, bold font) and accuracy (0.73, $p < 0.001$; **Figure 4F** and **Table 2**) were all significant, with

TABLE 2 | Clustering performance based on each index.

	HC vs. aMCI				HC vs. SCD			
	Network level							
	Accuracy	**AUC**	**Sensitivity**	**Specificity**	**Accuracy**	**AUC**	**Sensitivity**	**Specificity**
Combined	**0.75**	**0.75**	**0.59**	**0.90**	0.57	0.55	0.64	0.50
Global efficiency	0.68	0.77	0.59	0.77	0.45	0.34	0.73	0.18
Local efficiency	0.68	0.71	0.59	0.77	0.55	0.49	0.73	0.36
Clustering co-efficiency	0.16	0.09	0.18	0.14	0.50	0.52	0.59	0.41
Path length	0.70	0.76	0.55	0.84	0.39	0.41	0.36	0.41
Nodal level								
Combined	0.52	0.52	0.50	0.55	0.43	0.39	0.41	0.45
Global efficiency	0.55	0.57	0.50	0.59	**0.73**	**0.71**	**0.68**	**0.77**
Local efficiency	0.61	0.63	0.64	0.59	0.32	0.29	0.41	0.23
Clustering co-efficiency	0.45	0.48	0.41	0.50	0.55	0.61	0.50	0.59
Path length	**0.66**	**0.66**	**0.59**	**0.73**	0.64	0.57	0.50	0.77

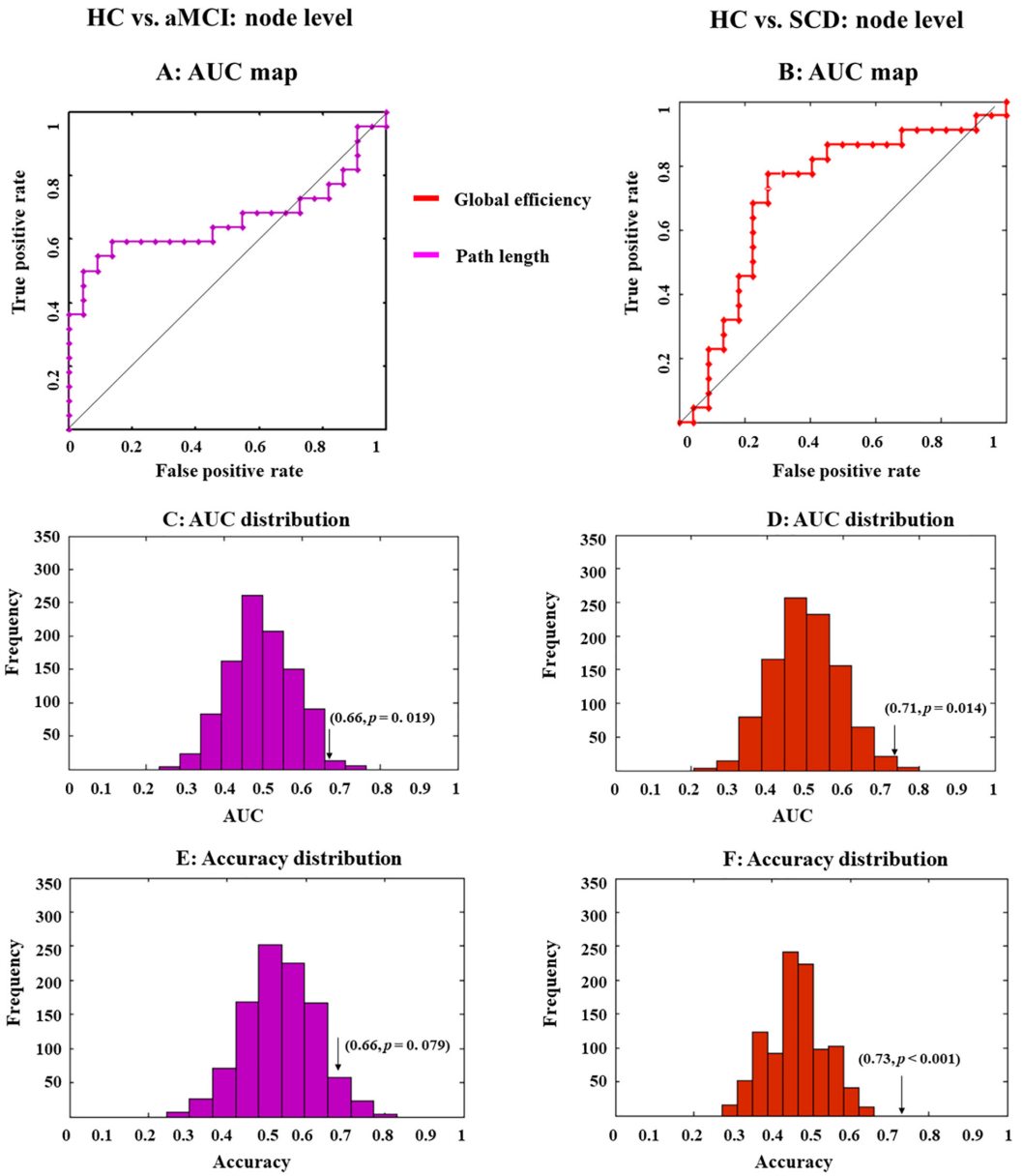

FIGURE 4 | Receiver operating characteristic (ROC) maps and area under the curve (AUC) or accuracy distribution of a classifier built on indexes at the nodal level. ROC maps show the classification performance **(A,B)**, where greater AUC corresponds to better performance. AUC and accuracy distribution maps **(C–F)** were built by permutation tests, during which group labels were randomly arranged 1,000 times. Arrows in the distribution maps marker AUC or accuracy based on real group labels.

most discriminative WM features consisting of the left lenticular nucleus, pallidum; right fusiform gyrus; and right lenticular nucleus, pallidum.

Correlation Between Network Metrics and Cognition

We also calculated the correlation between network properties and cognition with gender, age, and years of education as covariates in each group. In the SCD group, the path length of the left supramarginal was positively correlated with memory ability ($r = 0.723$, $p < 0.001$), but this was not the situation in the group of HC and aMCI (**Figure 5**).

DISCUSSION

We investigated the topological characteristics of the WM network that can successfully identify SCD and aMCI from HC. Compared to the HC group, the combination of multiple indexes at the network level was able to significantly distinguish aMCI, but not SCD. The classifiers built on different indexes at the nodal

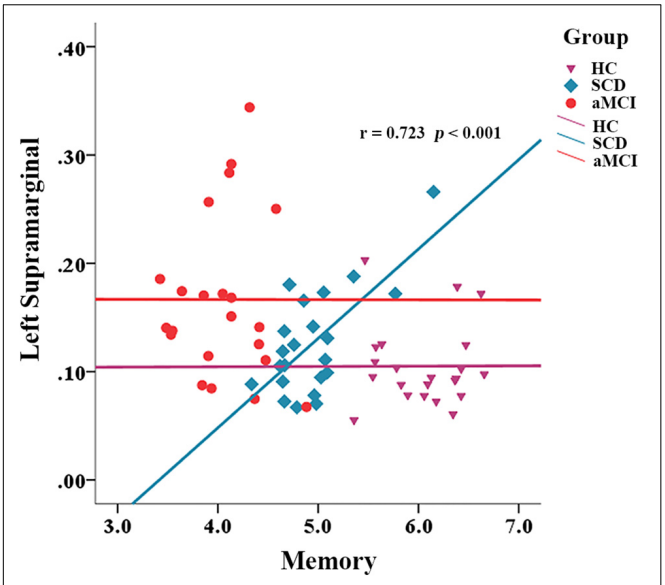

FIGURE 5 | Correlation between network metrics and memory in different groups.

level can identify SCD and aMCI from HC. Specifically, the short-path length at the nodal level was able to significantly distinguish aMCI from HC, whereas the global efficiency at the nodal level was able to identify SCD from HC. The most discriminative short-path length features include the left supramarginal, the left amygdala, the opercularis part of the right inferior frontal, the right hippocampus, and the left temporal pole, whereas the most discriminative global efficiency features contain the left pallidum, the right fusiform, and the right pallidum. Besides, we found that the short-path length of the left supramarginal was significantly correlated with memory performance in the SCD group.

Abnormalities in white matters, which were responsible for transmitting information between brain regions, often cause impairments of higher cognitive functions requiring the collaboration of multiple brain regions. The impairments of WM in AD have been reported in previous studies, which have observed that WM impairments are significantly associated with cognitive decline in AD (Overdorp et al., 2014; Bilello et al., 2015). WM damages are one of the typical features of the pathological development of AD (Lee et al., 2016). This WM degeneration, representing demyelination and microhemorrhages, is also frequently reported in aMCI and SCD (Ohlhauser et al., 2019; Bangen et al., 2020; Li et al., 2020). In the current study, we focused on structural properties (white matter metric) of the brain; therefore, we selected the AAL template that was built on high-resolution T1 volume and has been widely used in previous brain network research (Feng et al., 2015; Qi et al., 2015; Zhuo et al., 2018). Consistent with other studies (Wang et al., 2016; Shu et al., 2018), disconnection symptoms and dynamic network failure in AD were found to be of great significance in the preclinical stages of AD, and this provides the neurostructural basis for the altered behavioral manifestations in these stages.

Compared to aMCI, SCD is at a much earlier stage, where the individual's cognitive abilities are still relatively intact. Our findings also reveal the stage-specific characteristics of WM network disruption in each group. Both aMCI and SCD exhibit impairments in network topological properties at the nodal level, but indexes at the network level can only significantly distinguish aMCI from HC, with no significant classification power in discriminating between SCD and HC. This suggests a progressive degeneration of whiter matter from SCD to aMCI, from WM impairments at the local level to both local and global levels. There is extensive evidence that SCD has similar WM degeneration to aMCI and AD (Selnes et al., 2012; Li et al., 2016), and the degree of degeneration is often intermediate between HC and aMCI (López-Sanz et al., 2017). Our current study further shows that the WM network damage in SCD has not reached the overall level of the whole brain network as in aMCI but is only limited to some local nodes. In this case, SCD may also be able to compensate for the problems caused by local node degeneration through resource allocation at the overall network level or nodes that has been impaired, just like the alternative enhancement of partial regional activation reported by previous authors in functional MRI (Erk et al., 2011). This may be one of the reasons why SCD is still able to maintain good performance in cognitive tasks.

Based on the nodal-level analysis, we found that the attributes that best distinguish SCD and aMCI from HC are the global efficiency and the short-path length. These are two indicators representing the extent of function integration among brain regions (Bullmore and Sporns, 2012). The results suggest that both SCD and aMCI might have pronounced functional integration issues. They may have much more difficulties in accomplishing those higher cognitive functions that require multiple brain regions to collaborate together. Several previous studies have reported altered functional integration and functional segregation in both preclinical stages of AD (Lazarou et al., 2019), and some investigators have suggested that enhanced functional segregation compensates for the problems associated with functional integration impairments (Xu et al., 2020), but the latter was not as evident in our study. In addition, those elderly with amyloidosis are more likely to have functional integration problems (Fischer et al., 2015). This further confirms that SCD and aMCI are two important preclinical risk stages for AD.

We used the fiber number of WM to build the network. The change in the short-path length in aMCI suggests that some of the WM pathways between the nodes have been impaired. The changes in the global efficiency of some nodes in SCD also indicate that the efficiency of information exchange between these nodes and other regions of the brain has been impaired. Some of the nodes with the greatest discriminatory validity were identified in our analysis, and these nodes were mainly distributed in temporal and frontal regions, which is consistent with the sequence of pathological development in early AD (Serrano-Pozo et al., 2011). We found a significant correlation between the left marginal superior gyrus and memory in the SCD group. Some studies suggest that thinner volumes in this region are associated with an increased risk of AD (Verfaillie et al., 2016). As part of the attentional network (Yeo et al., 2011),

the marginal supramarginal gyrus has shown an important role in memory encoding in several studies (Staresina and Davachi, 2006; Rubinstein et al., 2021). In addition, the literature shows that supramarginal gyrus is often functionally involved in action execution, simulation, and observation (Grezes and Decety, 2001), and some researchers have suggested that activation of this component when subjects are memorizing items may reflect the action-oriented approach to memory adopted by the subjects (Russ et al., 2003). However, somewhat curiously, we found that the mean path length of the left marginal superior gyrus, in relation to other nodes of the whole brain, showed a significant positive correlation with memory performance in the SCD group. It appears that better structural segregation of this region from other nodes contributes to better memory performance. In fact, it can be observed from the scatter plot (**Figure 4**) that the HC group did also have a longer mean path length than the aMCI group. We speculate that perhaps the region is undergoing a transition from a cost-effective network to a random network during the SCD stage and that some unnecessary connections to this brain region may cause interference with memory function. This is consistent with the phenomenon of brain dedifferentiation in aging and disease development (Goh, 2011; Caldwell et al., 2020). This is still only our conjecture, and follow-up studies need more experimental evidence to further validate it.

Some limitations of our study should be mentioned. First, our study sample is relatively small, which may affect the generalizability of our current findings, and the seniors who participated in the current study were from the community. While we believe in the importance of focusing on the community elderly, SCD from the clinic did have a higher AD conversion rate (Jessen et al., 2020). Second, the current study is only a cross-sectional study, and the findings need to be confirmed by future longitudinal studies. Third, combining other neuroimaging features such as cerebrospinal fluid markers with the WM network alterations in the current study will help to reveal a more comprehensive picture of the preclinical pathological changes in AD. In conclusion, our study shows that both SCD and aMCI have impairments in the functional integration of WM networks relative to HC and that network impairments in aMCI have undergone a quantitative change from the nodal level to the network level.

DATA AVAILABILITY STATEMENT

The datasets presented in this article are not readily available because raw data will be made public upon completion of subsequent studies. Requests to access the datasets should be directed to twh621@foxmail.com.

ETHICS STATEMENT

The studies involving human participants were reviewed and approved by the Institutional Review Board of the Beijing Normal University Imaging Centre for Brain Research, China, Approval No. ICBIR_A_0041_002_02. The patients/participants provided their written informed consent to participate in this study.

AUTHOR CONTRIBUTIONS

WT contributed to the conceptualization, investigated the data, carried out the formal analysis and funding acquisition, wrote the original draft, and reviewed and edited the manuscript. HL carried out the formal analysis and funding acquisition, wrote, reviewed, and edited the manuscript. XL wrote, reviewed, and edited the manuscript. RH and WS investigated the data and wrote, reviewed, and edited the manuscript. QG and ZZ contributed to the conceptualization, wrote, reviewed, and edited the manuscript, carried out the project administration and funding acquisition, and supervised the data. All authors contributed to the article and approved the submitted version.

FUNDING

This work was supported by the Natural Science Foundation of China (32071100 and 32000793), Science and Technology Planning Project of Guangdong Province, China (2019A050510048), Natural Science Foundation of Guangdong Province, China (2020A1515011394), Shenzhen–Hong Kong Institute of Brain Science–Shenzhen Fundamental Research Institutions (2021SHIBS0003), Natural Science Foundation of Shenzhen, China (JCYJ20190808121415365), Project funded by the China Postdoctoral Science Foundation (2020M682846), and Open Research Fund of the State Key Laboratory of Cognitive Neuroscience and Learning (CNLYB2005).

SUPPLEMENTARY MATERIAL

The Supplementary Material for this article can be found online at: https://www.frontiersin.org/articles/10.3389/fnagi.2021.687530/full#supplementary-material

REFERENCES

Bangen, K. J., Thomas, K. R., Weigand, A. J., Sanchez, D. L., Delano-Wood, L., Edmonds, E. C., et al. (2020). Pattern of regional white matter hyperintensity volume in mild cognitive impairment subtypes and associations with decline in daily functioning. *Neurobiol. Aging* 86, 134–142. doi: 10.1016/j.neurobiolaging.2019.10.016

Bateman, R. J., Xiong, C., Benzinger, T. L., Fagan, A. M., Goate, A., Fox, N. C., et al. (2012). Clinical and biomarker changes in dominantly inherited Alzheimer's disease. *N. Engl. J. Med.* 367, 795–804.

Bilello, M., Doshi, J., Nabavizadeh, S. A., Toledo, J. B., Erus, G., Xie, S. X., et al. (2015). Correlating cognitive decline with white matter lesion and brain atrophy magnetic resonance imaging measurements in Alzheimer's disease. *J. Alzheimers Disease* 48, 987–994. doi: 10.3233/jad-150400

Bozzali, M., Falini, A., Franceschi, M., Cercignani, M., Zuffi, M., Scotti, G., et al. (2002). White matter damage in Alzheimer's disease assessed in vivo using

diffusion tensor magnetic resonance imaging. *J. Neurol. Neurosurg. Psychiatry* 72, 742–746. doi: 10.1136/jnnp.72.6.742

Bullmore, E., and Sporns, O. (2009). Complex brain networks: graph theoretical analysis of structural and functional systems. *Nat. Rev. Neurosci.* 10, 186–198. doi: 10.1038/nrn2575

Bullmore, E., and Sporns, O. (2012). The economy of brain network organization. *Nat. Rev. Neurosci.* 13, 336–349. doi: 10.1038/nrn3214

Cai, L., Wei, X., Liu, J., Zhu, L., Wang, J., Deng, B., et al. (2020). Functional integration and segregation in multiplex brain networks for Alzheimer's disease. *Front. Neurosci.* 14:51.

Caldwell, A. B., Liu, Q., Schroth, G. P., Galasko, D. R., Yuan, S. H., Wagner, S. L., et al. (2020). Dedifferentiation and neuronal repression define familial Alzheimer's disease. *Sci. Adv.* 6:eaba5933. doi: 10.1126/sciadv.aba5933

Chang, C.-C., and Lin, C.-J. (2011). LIBSVM: a library for support vector machines. *ACM Trans. Intell. Syst. Technol. (TIST)* 2, 1–27. doi: 10.1145/1961189.1961199

Cui, Y., Chen, Z., Wei, S., Wang, S., Liu, T., and Hu, G. (2016). Attention-over-attention neural networks for reading comprehension. *arXiv* [Preprint] arXiv:1607.04423,

Cui, Z., and Gong, G. (2018). The effect of machine learning regression algorithms and sample size on individualized behavioral prediction with functional connectivity features. *Neuroimage* 178, 622–637. doi: 10.1016/j.neuroimage.2018.06.001

Cui, Z., Zhong, S., Xu, P., Gong, G., and He, Y. (2013). PANDA: a pipeline toolbox for analyzing brain diffusion images. *Front. Hum. Neurosci.* 7:42.

Dai, Z., and He, Y. (2014). Disrupted structural and functional brain connectomes in mild cognitive impairment and Alzheimer's disease. *Neurosci. Bull.* 30, 217–232. doi: 10.1007/s12264-013-1421-0

Dai, Z., Yan, C., Wang, Z., Wang, J., Xia, M., Li, K., et al. (2012). Discriminative analysis of early Alzheimer's disease using multi-modal imaging and multi-level characterization with multi-classifier (M3). *Neuroimage* 59, 2187–2195. doi: 10.1016/j.neuroimage.2011.10.003

Defrancesco, M., Egger, K., Marksteiner, J., Esterhammer, R., Hinterhuber, H., Deisenhammer, E. A., et al. (2014). Changes in white matter integrity before conversion from mild cognitive impairment to Alzheimer's disease. *PLoS One* 9:e106062. doi: 10.1371/journal.pone.0106062

Delbeuck, X., Van der Linden, M., and Collette, F. (2003). Alzheimer'disease as a disconnection syndrome? *Neuropsychol. Rev.* 13, 79–92.

Erk, S., Spottke, A., Meisen, A., Wagner, M., Walter, H., and Jessen, F. (2011). Evidence of neuronal compensation during episodic memory in subjective memory impairment. *Arch. General Psychiatry* 68, 845–852. doi: 10.1001/archgenpsychiatry.2011.80

Fawcett, T. (2006). An introduction to ROC analysis. *Pattern Recogn. Lett.* 27, 861–874.

Feng, G., Chen, H.-C., Zhu, Z., He, Y., and Wang, S. J. N. (2015). Dynamic brain architectures in local brain activity and functional network efficiency associate with efficient reading in bilinguals. *Neuroimage* 119, 103–118. doi: 10.1016/j.neuroimage.2015.05.100

Fischer, F. U., Wolf, D., Scheurich, A., Fellgiebel, A., and Initiative, A. S. D. N. (2015). Altered whole-brain white matter networks in preclinical Alzheimer's disease. *NeuroImage* 8, 660–666. doi: 10.1016/j.nicl.2015.06.007

Goh, J. O. (2011). Functional dedifferentiation and altered connectivity in older adults: neural accounts of cognitive aging. *Aging Dis.* 2:30.

Gong, G., Rosa-Neto, P., Carbonell, F., Chen, Z. J., He, Y., and Evans, A. C. (2009). Age-and gender-related differences in the cortical anatomical network. *J. Neurosci.* 29, 15684–15693. doi: 10.1523/jneurosci.2308-09.2009

Grezes, J., and Decety, J. (2001). Functional anatomy of execution, mental simulation, observation, and verb generation of actions: a meta−analysis. *Hum. Brain Mapp.* 12, 1–19. doi: 10.1002/1097-0193(200101)12:1<1::aid-hbm10>3.0.co;2-v

He, Y., and Evans, A. (2010). Graph theoretical modeling of brain connectivity. *Curr. Opin. Neurol.* 23, 341–350. doi: 10.1097/wco.0b013e32833aa567

Huang, L.-K., Chao, S.-P., and Hu, C.-J. (2020). Clinical trials of new drugs for Alzheimer disease. *J. Biomed. Sci.* 27:18.

Jack, C. R. Jr., Knopman, D. S., Jagust, W. J., Shaw, L. M., Aisen, P. S., Weiner, M. W., et al. (2010). Hypothetical model of dynamic biomarkers of the Alzheimer's pathological cascade. *Lancet Neurol.* 9, 119–128. doi: 10.1016/s1474-4422(09)70299-6

Jessen, F., Amariglio, R. E., Buckley, R. F., van der Flier, W. M., Han, Y., Molinuevo, J. L., et al. (2020). The characterisation of subjective cognitive decline. *Lancet Neurol.* 19, 271–278.

Kabbara, A., Eid, H., El Falou, W., Khalil, M., Wendling, F., and Hassan, M. (2018). Reduced integration and improved segregation of functional brain networks in Alzheimer's disease. *J. Neural Eng.* 15:026023. doi: 10.1088/1741-2552/aaaa76

Kantarci, K., Murray, M. E., Schwarz, C. G., Reid, R. I., Przybelski, S. A., Lesnick, T., et al. (2017). White-matter integrity on DTI and the pathologic staging of Alzheimer's disease. *Neurobiol. Aging* 56, 172–179. doi: 10.1016/j.neurobiolaging.2017.04.024

Lazarou, I., Nikolopoulos, S., Dimitriadis, S. I., Kompatsiaris, I. Y., Spilioti, M., and Tsolaki, M. (2019). Is brain connectome research the future frontier for subjective cognitive decline? A systematic review. *Clin. Neurophysiol.* 130, 1762–1780. doi: 10.1016/j.clinph.2019.07.004

Lee, S., Viqar, F., Zimmerman, M. E., Narkhede, A., Tosto, G., Benzinger, T. L., et al. (2016). White matter hyperintensities are a core feature of Alzheimer's disease: evidence from the dominantly inherited Alzheimer network. *Ann. Neurol.* 79, 929–939. doi: 10.1002/ana.24647

Li, X., Xia, J., Ma, C., Chen, K., Xu, K., Zhang, J., et al. (2020). Accelerating structural degeneration in temporal regions and their effects on cognition in aging of MCI patients. *Cereb. Cortex* 30, 326–338. doi: 10.1093/cercor/bhz090

Li, X.-Y., Tang, Z.-C., Sun, Y., Tian, J., Liu, Z.-Y., and Han, Y. (2016). White matter degeneration in subjective cognitive decline: a diffusion tensor imaging study. *Oncotarget* 7:54405. doi: 10.18632/oncotarget.10091

López-Sanz, D., Garcés, P., Álvarez, B., Delgado-Losada, M. L., López-Higes, R., and Maestú, F. (2017). Network disruption in the preclinical stages of Alzheimer's disease: from subjective cognitive decline to mild cognitive impairment. *Int. J. Neural Syst.* 27:1750041. doi: 10.1142/s0129065717500411

Mourao-Miranda, J., Bokde, A. L., Born, C., Hampel, H., and Stetter, M. (2005). Classifying brain states and determining the discriminating activation patterns: support vector machine on functional MRI data. *Neuroimage* 28, 980–995. doi: 10.1016/j.neuroimage.2005.06.070

Ohlhauser, L., Parker, A. F., Smart, C. M., Gawryluk, J. R., and Initiative, A. S. D. N. (2019). White matter and its relationship with cognition in subjective cognitive decline. *Alzheimers Dementia* 11, 28–35. doi: 10.1016/j.dadm.2018.10.008

Overdorp, E. J., Kessels, R. P., Claassen, J. A., and Oosterman, J. M. (2014). Cognitive impairments associated with medial temporal atrophy and white matter hyperintensities: an MRI study in memory clinic patients. *Front. Aging Neurosci.* 6:98.

Pereira, F., Gash, J., David, J., David, T., Monteiro, P., and Valente, F. (2009). Modelling interception loss from evergreen oak Mediterranean savannas: application of a tree-based modelling approach. *Agric. Forest Meteorol.* 149, 680–688. doi: 10.1016/j.agrformet.2008.10.014

Petersen, R. C., Smith, G. E., Waring, S. C., Ivnik, R. J., Tangalos, E. G., and Kokmen, E. (1999). Mild cognitive impairment: clinical characterization and outcome. *Arch. Neurol.* 56, 303–308. doi: 10.1001/archneur.56.3.303

Qi, S., Meesters, S., Nicolay, K., Romeny, B. M. T. H., and Ossenblok, P. (2015). The influence of construction methodology on structural brain network measures: a review. *J. Neurosci. Methods* 253, 170–182. doi: 10.1016/j.jneumeth.2015.06.016

Rubinov, M., and Sporns, O. (2010). Complex network measures of brain connectivity: uses and interpretations. *NeuroImage* 52, 1059–1069. doi: 10.1016/j.neuroimage.2009.10.003

Rubinstein, D. Y., Camarillo-Rodriguez, L., Serruya, M. D., Herweg, N. A., Waldman, Z. J., Wanda, P. A., et al. (2021). Contribution of left supramarginal and angular gyri to episodic memory encoding: an intracranial EEG study. *Neuroimage* 225:117514. doi: 10.1016/j.neuroimage.2020.117514

Russ, M. O., Mack, W., Grama, C.-R., Lanfermann, H., and Knopf, M. (2003). Enactment effect in memory: evidence concerning the function of the supramarginal gyrus. *Exp. Brain Res.* 149, 497–504. doi: 10.1007/s00221-003-1398-4

Scheef, L., Spottke, A., Daerr, M., Joe, A., Striepens, N., Kölsch, H., et al. (2012). Glucose metabolism, gray matter structure, and memory decline in subjective memory impairment. *Neurology* 79, 1332–1339. doi: 10.1212/wnl.0b013e31826c1a8d

Selnes, P., Aarsland, D., Bjørnerud, A., Gjerstad, L., Wallin, A., Hessen, E., et al. (2013). Diffusion tensor imaging surpasses cerebrospinal fluid as predictor of cognitive decline and medial temporal lobe atrophy in subjective cognitive

impairment and mild cognitive impairment. *J. Alzheimers Dis.* 33, 723–736. doi: 10.3233/jad-2012-121603

Selnes, P., Fjell, A. M., Gjerstad, L., Bjørnerud, A., Wallin, A., Due-Tønnessen, P., et al. (2012). White matter imaging changes in subjective and mild cognitive impairment. *Alzheimers Dementia* 8, S112–S121.

Serrano-Pozo, A., Frosch, M. P., Masliah, E., and Hyman, B. T. (2011). Neuropathological alterations in Alzheimer disease. *Cold Spring Harb. Perspect. Med.* 1:a006189. doi: 10.1101/cshperspect.a006189

Shao, W., Li, X., Zhang, J., Yang, C., Tao, W., Zhang, S., et al. (2019). White matter integrity disruption in the pre−dementia stages of Alzheimer's disease: from subjective memory impairment to amnestic mild cognitive impairment. *Eur. J. Neurol.* 26, 800–807. doi: 10.1111/ene.13892

Shu, N., Liang, Y., Li, H., Zhang, J., Li, X., Wang, L., et al. (2012). Disrupted topological organization in white matter structural networks in amnestic mild cognitive impairment: relationship to subtype. *Radiology* 265, 518–527. doi: 10.1148/radiol.12112361

Shu, N., Wang, X., Bi, Q., Zhao, T., and Han, Y. (2018). Disrupted topologic efficiency of white matter structural connectome in individuals with subjective cognitive decline. *Radiology* 286, 229–238. doi: 10.1148/radiol.2017162696

Staresina, B. P., and Davachi, L. (2006). Differential encoding mechanisms for subsequent associative recognition and free recall. *J. Neurosci.* 26, 9162–9172. doi: 10.1523/jneurosci.2877-06.2006

Sun, Y., Yang, F. C., Lin, C. P., and Han, Y. (2015). Biochemical and neuroimaging studies in subjective cognitive decline: progress and perspectives. *CNS Neurosci. Therapeut.* 21, 768–775. doi: 10.1111/cns.12395

Tao, W., Sun, J., Li, X., Shao, W., Pei, J., Yang, C., et al. (2020). The anterior-posterior functional connectivity disconnection in the elderly with subjective memory impairment and amnestic mild cognitive impairment. *Curr. Alzheimer Res.* 17, 373–381. doi: 10.2174/1567205017666200525015017

Verfaillie, S. C., Tijms, B., Versteeg, A., Benedictus, M. R., Bouwman, F. H., and Scheltens, P. (2016). Thinner temporal and parietal cortex is related to incident clinical progression to dementia in patients with subjective cognitive decline. *Alzheimers Dementia* 5, 43–52. doi: 10.1016/j.dadm.2016.10.007

Wang, X.-N., Zeng, Y., Chen, G.-Q., Zhang, Y.-H., Li, X.-Y., Hao, X.-Y., et al. (2016). Abnormal organization of white matter networks in patients with subjective cognitive decline and mild cognitive impairment. *Oncotarget* 7:48953. doi: 10.18632/oncotarget.10601

Wang, Y., Risacher, S. L., West, J. D., McDonald, B. C., MaGee, T. R., Farlow, M. R., et al. (2013). Altered default mode network connectivity in older adults with cognitive complaints and amnestic mild cognitive impairment. *J. Alzheimers Dis.* 35, 751–760. doi: 10.3233/jad-130080

Ward, A., Tardiff, S., Dye, C., and Arrighi, H. M. (2013). Rate of conversion from prodromal Alzheimer's disease to alzheimer's dementia: a systematic review of the literature. *Dementia Geriat. Cogn. Disorders Extra* 3, 320–332.

Xu, X., Li, W., Tao, M., Xie, Z., Gao, X., Yue, L., et al. (2020). Effective and accurate diagnosis of subjective cognitive decline based on functional connection and graph theory view. *Front. Neurosci.* 14:577887.

Yeo, B. T., Krienen, F. M., Sepulcre, J., Sabuncu, M. R., Lashkari, D., Hollinshead, M., et al. (2011). The organization of the human cerebral cortex estimated by intrinsic functional connectivity. *J. Neurophysiol.* 106, 1125–1165. doi: 10.1152/jn.00338.2011

Zhuo, Z., Mo, X., Ma, X., Han, Y., and Li, H. J. B. R. (2018). Identifying aMCI with functional connectivity network characteristics based on subtle AAL atlas. *Brain Res.* 1696, 81–90. doi: 10.1016/j.brainres.2018.04.042

Conflict of Interest: The authors declare that the research was conducted in the absence of any commercial or financial relationships that could be construed as a potential conflict of interest.

frontiers in Aging Neuroscience

ORIGINAL RESEARCH
published: 14 July 2021
doi: 10.3389/fnagi.2021.697029

Focused Ultrasound Thalamotomy for the Treatment of Essential Tremor: A 2-Year Outcome Study of Chinese People

Peihan Wu[1†], *Wei Lin*[1†], *Kun Hong Li*[2], *Hui-Chin Lai*[2], *Ming-Tsung Lee*[3,4], *Kevin Wen-Kai Tsai*[5], *Pai-Yi Chiu*[6], *Wei-Chieh Chang*[7*], *Cheng-Yu Wei*[1,8*] and *Takaomi Taira*[9]

[1] Department of Neurology, Chang Bing Show Chwan Memorial Hospital, Changhua County, Taiwan, [2] MR-Guided Focused Ultrasound Center, Chang Bing Show Chwan Memorial Hospital, Changhua County, Taiwan, [3] Research Assistant Center, Show Chwan Memorial Hospital, Changhua, Taiwan, [4] Department of Nursing, Hungkuang University, Taichung, Taiwan, [5] InSightec Ltd., Tirat Carmel, Israel, [6] Department of Neurology, Show Chwan Memorial Hospital, Changhua, Taiwan, [7] Department of Neurosurgery, Chang Bing Show Chwan Memorial Hospital, Changhua County, Taiwan, [8] Department of Exercise and Health Promotion, College of Kinesiology and Health, Chinese Culture University, Taipei, Taiwan, [9] Department of Neurosurgery, Tokyo Women's Medical University, Tokyo, Japan

OPEN ACCESS

Edited by:
Jiehui Jiang,
Shanghai University, China

Reviewed by:
Ling Li,
Huashan Hospital, Fudan University, China
Ben Nephew,
Worcester Polytechnic Institute, United States
Muh-Shi Lin,
Kuang Tien General Hospital, Taiwan

***Correspondence:**
Cheng-Yu Wei
yuyu@seed.net.tw
Wei-Chieh Chang
changweichieh@gmail.com

[†]*These authors have contributed equally to this work*

Received: *18 April 2021*
Accepted: *15 June 2021*
Published: *14 July 2021*

Citation:
Wu P, Lin W, Li KH, Lai H-C, Lee M-T, Tsai KW-K, Chiu P-Y, Chang W-C, Wei C-Y and Taira T (2021) Focused Ultrasound Thalamotomy for the Treatment of Essential Tremor: A 2-Year Outcome Study of Chinese People. Front. Aging Neurosci. 13:697029. doi: 10.3389/fnagi.2021.697029

Background: Essential tremor (ET) is a common movement disorder among elderly individuals worldwide and is occasionally associated with a high risk for mild cognitive impairment and dementia. This retrospective study aimed to determine the clinical outcome of unilateral magnetic resonance-guided focused ultrasound (MRgFUS) thalamotomy in Chinese patients with ET.

Methods: In total, 31 male and 17 female patients with drug-refractory ET were enrolled in this research study from January 2017 to September 2019. The severity of tremor and disability were assessed using the Clinical Rating Scale for Tremor (CRST) within a 2-year follow-up period.

Results: The mean age of the participants was 59.14 ± 13.5 years. The mean skull density ratio (SDR) was 0.5 ± 0.1. The mean highest temperature was 57.0 ± 2.4°C. The mean number of sonications was 10.0 ± 2.6. The average maximum energy was 19,710.5 ± 8,624.9 J. The total CRST scores and sub-scores after MRgFUS thalamotomy significantly reduced during each follow-up ($p < 0.001$). All but four (8.3%) of the patients had reversible adverse events (AEs) after the procedure.

Conclusions: MRgFUS had sustained clinical efficacy 2 years after treatment for intractable ET. Only few patients presented with thalamotomy-related AEs including numbness, weakness, and ataxia for an extended period. Most Chinese patients were treated safely and effectively despite their low SDR.

Keywords: MR-guided focused ultrasound, focused ultrasound, essential tremor, thalamotomy, functional neurosurgery

INTRODUCTION

Essential tremor (ET) is a common movement disorder worldwide, and it affects about 1% of the overall population and 4–5% of elderly individuals (≥65 years old) (Louis and Ferreira, 2010). In a survey conducted in Beijing, the prevalence of ET among people aged ≥55 years is 3.29% (Sun et al., 2020). The condition is characterized by stereotypic tremors at a frequency of 8–12 Hz, and tremors can severely affect daily living. Further, it is occasionally associated with a high risk of mild cognitive impairment and dementia (Louis et al., 2019). Although medical treatment is initially effective, tremors are rarely suppressed with time (Findley et al., 1985; Koller and Vetere-Overfield, 1989; Diaz and Louis, 2010).

Traditionally, the choice of treatment other than drugs includes either thalamotomy, which involves ablation of the ventral intermediate nucleus (VIM) of the thalamus, or thalamic deep brain stimulation (DBS). The latter is an invasive procedure, which includes the insertion of a device inside the brain. Although it has been the standard treatment for medically intractable ET due to its safety and efficacy for long-term tremor control, adverse effects such as hemorrhage, infection, and hardware-related failures are not unusual (Blomstedt and Hariz, 2005; Engel et al., 2018). Further, DBS requires repetitive sittings with increasing expenditures.

For over 50 years, ablative treatment has evolved from invasive radiofrequency to noninvasive gamma knife radiation to magnetic resonance-guided focused ultrasound (MRgFUS). In 2016, the United States Food and Drug Administration (FDA) had approved MRgFUS for the treatment of ET (Ito et al., 2020). Taking into consideration the safety of the noninvasive and radiation-free procedure, it is preferred over other ablative methods for patients with medically refractory ET (Health Quality Ontario, 2018).

However, the efficacy and adverse events (AEs) of MRgFUS among Chinese people have not yet been evaluated extensively. The clinical characteristics of ET might differ between Asians and Caucasians. Therefore, this study aimed to evaluate the outcome of MRgFUS thalamotomy among Taiwanese patients with refractory ET.

METHODS

Patients

This retrospective study included patients with ET treated with focused ultrasound thalamotomy at an MRgFUS Center in Taiwan from 2017 to 2019. The procedure was performed by an experienced team. Patients with a neurodegenerative disorder such as Parkinson's disease (PD), cognitive impairment (Mini-Mental State Examination score of < 24), coagulopathy, and severe depression and those who were not followed up were excluded (Elias et al., 2016). Only patients with ET who underwent unilateral MRgFUS VIM thalamotomy with a follow-up duration of at least 6 months were included in the study. All patients underwent a preoperative brain CT scan, and data on cranial parameters including skull thickness, skull density ratio (SDR), and skull area were obtained. SDR was calculated by obtaining the average ratio of the cancellous to the cortical bone within the skull *via* a CT scan. Patients with an SDR of ≥0.3 were considered for MRgFUS treatment (Wintermark et al., 2014). The study was approved by the institutional review board of Show Chwan Memorial Hospital, Taiwan (IRB approval no.: 1090908).

Magnetic Resonance-Guided Focused Ultrasound

Patients were treated with unilateral VIM thalamotomy with transcranial, noninvasive MRgFUS without general anesthesia. The head of the patient was shaved before treatment, and the scalp was examined for any scars or lesions that might interfere with ultrasound transcranial transmission. The MRI unit General Electric (Chicago, IL) 1.5T Optima MR450W was prepared. The stereotactic frame with a spherical coil and a water-cooling elastic diaphragm was placed over the head of the patient. The setup was connected to the ultrasound transducer (Exablate Neuro, InSightec, Tirat Carmel, Israel) coupled with a software unit.

The treatment targeted the VIM of the thalamus contralateral to the dominant side. VIM was localized from a functional viewpoint, and indirect targeting was performed based on data from stereotactic brain atlases and the previous experience of neurosurgeons (**Figure 1**) (Sharifi et al., 2014). The presumptive site of the VIM was localized at 14 mm from the midline or 11 mm from the lateral wall of the third ventricle and 1/3 from the posterior commissure (PC) on the intercommissural line or 7 mm anterior to the PC on MRI (Elias et al., 2013; Lipsman et al., 2013; Chang et al., 2015).

Patients underwent serial sonications for thalamic lesioning, starting with short and low energy, which produced focal heating of up to 44°C and progressed incrementally, thereby generating increasingly larger concentric lesions. The ultrasound energy was transmitted *via* 1,024 transducer elements, and it focused on the thalamus, creating the ablation at the focus by heating, which is tracked using MRI thermometry (Elias et al., 2013, 2016; Lipsman et al., 2013; Chang et al., 2015). The size and location of the lesion and clinical effects were continuously monitored. In particular, changes in tremors were closely monitored in the treated arm by asking patients for the presence of any AEs during treatment. Lesions progressively enlarged by increasing the temperature or duration of sonication until either tremor suppression is achieved or AEs are encountered. MRI was performed before treatment, immediately after the procedure, 1 day after the procedure, and 6 months after the procedure (**Figure 2**).

Outcome Parameters

The Clinical Rating Scale for Tremor (CRST) is the standard assessment test for tremors in ET, and the CRST score was the primary outcome in this study. CRST has three parts (A, B, and C). Part A rates resting, postural, and action tremors for location and severity of tremors; part B rates hardwiring, drawing, and pouring of specific motor tasks; and part C rates speaking, eating, drinking, hygiene, dressing, writing, working, and social activities for functional disabilities. The score of each item ranges from 0 to 4 (total: 148), and a higher score indicates greater disease severity (Stacy et al., 2007). The dominant tremor score (maximum of 32) was defined as the sum of tremors in parts A and B for the

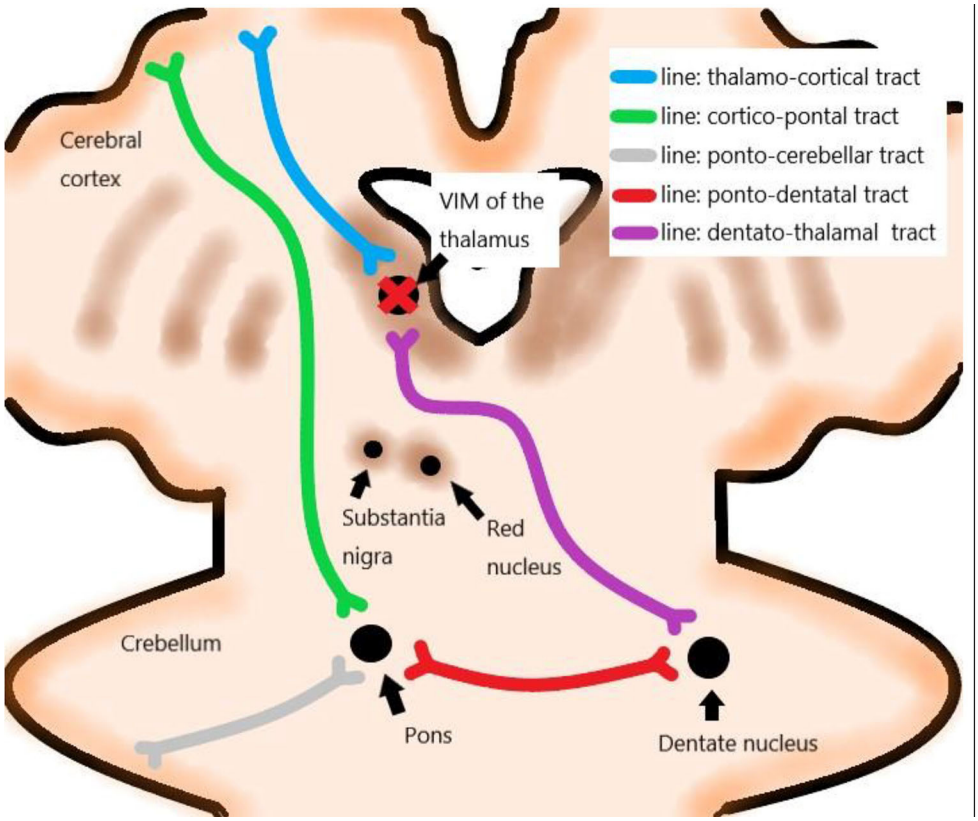

FIGURE 1 | Networks correlated with essential tremor (ET). VIM: ventral intermediate nucleus.

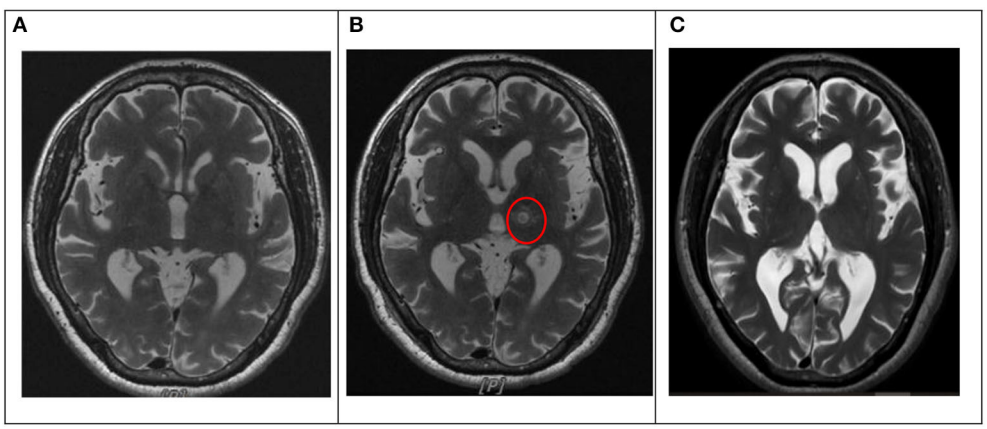

FIGURE 2 | Lesion location on T2-weighted images before and after MRgFUS thalamotomy in one patient. **(A)** Pre-intervention. **(B)** Day 1. The target lesion was in the left VIM of the thalamus (red circle). **(C)** Six months. MRgFUS: magnetic resonance-guided focused ultrasound. VIM: ventral intermediate nucleus.

treated hand. All patients were assessed using CRST by the same neurologists before treatment and were followed up after 1 week; 1, 3, and 6 months; and 1 and 2 years.

The incidence rate of AEs was considered the secondary outcome. AEs were classified as frame-, sonication-, and thalamotomy-related AEs for analysis purposes. Frame-related AEs included ptosis, pin-site bleeding, edema, and pain. Sonication-related AEs included vertigo or dizziness, headache, and nausea. Thalamotomy-related AEs included sensory-related events (numbness or paresthesia of various parts of body and taste disturbance), strength-related events (weakness of extremities), balance-related problems (dysmetria), and ataxia. Dysarthria and dysphagia were thalamotomy-related AEs (Elias et al., 2016). The AEs were recorded and followed up during the

TABLE 1 | Baseline demographic and clinical characteristics.

Variables	Mean ± SD
Age, year	59.2 ± 13.5
Sex (male/female), *N* (%)	31 (64.6)/17 (35.4)
Treated side (left/right), *N* (%)	41 (85.4)/7 (14.6)
Family history (positive/negative/uncertain), *N* (%)	21 (43.8)/20 (41.7)/7 (14.5)
Disease duration, year	19.2 ± 13.6
SDR	0.5 ± 0.1
Average skull thickness, cm	7.1 ± 1.0
Skull area, cm^2	366.2 ± 24.9
Average IA, degree	12.7 ± 1.1
No. of IA, < 20	892.2 ± 62.3
No. of IA, < 25	969.6 ± 34.9
Active elements	985.4 ± 32.0
No. of sonications	10.0 ± 2.6
No. of sonications, ≥ 50°C	4.6 ± 2.2
T max, °C	57.0 ± 2.4
Average total energy, J	97908.6 ± 60052.6
Average maximum energy, J	19710.5 ± 8624.9

SD, Standard Deviation; SDR, Skull Density Ratio; IA, Incident Angle; T max, Maximum Temperature reached after completion of the procedure.

treatment day and after 1 day, 1 week, 3 and 6 months, and 1 and 2 years.

Statistical Analysis

The total CRST scores and sub-scores during each follow-up were compared with the baseline scores using one-way repeated measures ANOVA with the least significant difference *post-hoc* analysis.

The relationships between skull factors and treatment parameters were evaluated *via* Pearson's correlation analysis and using the chi-square test. The skull factors included SDR, average skull thickness, skull volume, and skull area. Meanwhile, the treatment parameters included a total number of active elements (out of 1,024) in the spherical transducer, total energy transmitted, the maximum temperature reached upon completion of the procedure (Tmax), and sonication number and duration.

A p-value of < 0.05 was considered statistically significant, and all analyses were conducted using the Statistical Package for the Social Sciences software version 24.0 (IBM Corp., Armonk, NY, the USA).

RESULTS

Participants

In total, 48 patients, with a mean age of 59.2 ± 13.5 years and a mean duration of disease of 19.2 ± 13.6 years, were included in the analysis. Approximately 64.6% of patients were men, and 43.8% had a family history of ET. The dominant treated side was in the left (85.4%), and the mean SDR was 0.5 ± 0.1 (**Table 1**). The maximum, minimum, and median values of SDR were 0.7, 0.3, and 0.45. Twenty patients (25%) had SDRs of 0.40 or less.

Tremor

The total CRST score at baseline (parts A, B, and C) was 45.6 ± 15.4, and it reduced to 36.4 ± 17.6, 30.6 ± 17.1, 29.4 ± 15.1, 30.3 ± 15.7, 30.5 ± 14.4, and 31.9 ± 15.8 after 1 week, 1 month, 3 months, 6 months, 1 year, and 2 years, respectively ($p < 0.001$). The baseline dominant tremor score was 14.7 ± 4.9, and it reduced to 9.8 ± 7.3, 8.6 ± 6.2, 6.2 ± 5.0, 6.6 ± 5.3, 7.0 ± 5.5, and 7.4 ± 5.8 after 1 week, 1 month, 3 months, 6 months, 1 year, and 2 years, respectively ($p < 0.001$). The total disability score (part C) significantly improved from 13.4 ± 4.6 to 10.2 ± 5.9, 8.0 ± 5.6, 7.6 ± 4.8, 7.8 ± 5.0, 7.6 ± 4.6, and 8.3 ± 5.4 after 1 week, 1 month, 3 months, 6 months, 1 year, and 2 years, respectively ($p < 0.001$). Furthermore, parts A and B were decreased at any posttreatment stage ($p < 0.001$, **Table 2**). The trends in the total CRST scores and sub-scores during follow-up are shown in **Figure 3**.

Adverse Events

Frame-related events were not observed after 1 month. Sonication-related AEs were predominant on the day of treatment. However, they were transient and subsided after 1 week in all patients. Ataxia was the major thalamotomy-related AE. The incidence rates were 83.3, 41.7, 10.4, 6.3, and 4.2% after 1 day, 1 week, 1 month, 3 months, and 6 months, respectively. Complete disappearance was observed after the 6-month follow-up. Approximately 8% of patients complained of sensory-related AEs, including numbness of the tongue and/or fingertip, which persisted during the 2-year follow-up. However, worsening or new AEs were not observed during the 2-year follow-up (**Table 3**).

DISCUSSION

Pharmacological agents such as propranolol and primidone are the primary choice of most physicians as they are recommended by the American Academy of Neurology (AAN) (Zesiewicz et al., 2011). However, even if these agents do not cause AEs, the efficacy rate is only 50–70% (Haubenberger and Hallett, 2018). Recent studies have shown that propranolol may be associated with an increased risk of PD (Mittal et al., 2017; Gronich et al., 2018; Hopfner et al., 2019). Surgical interventions including DBS and MRgFUS are recommended for medically refractory cases; MRgFUS is a novel technique that is less invasive than DBS (Shanker, 2019). Hence, in Taiwan, patients with refractory ET are more likely to be treated with MRgFUS than DBS.

In this retrospective study including 48 patients with drug-refractory ET, MRgFUS thalamotomy significantly reduced hand tremor immediately, and the effect persisted until the 2-year follow-up period. The total CRST scores improved by 35.3, 33.5, and 32.5% after 3 months, 1 year, and 2 years, respectively. The dominant tremor scores improved by 64.0, 60.1, and 58.2% after 3 months, 1 year, and 2 years, respectively. The outcome in this study was not worse than that in previous larger studies ($N, \geq 30$; **Table 4**) (Elias et al., 2016; Chang et al., 2018; Meng et al., 2018). After the achievement of postoperative reduction, the beneficial effect was maintained until the 2-year follow-up period.

The AEs were mostly transient and mild. The incidence rates of sensory deficit and imbalance after the intervention ranged

TABLE 2 | Total CRST scores and sub-scores during each follow-up ($N = 48$).

Evaluation time	Part A	Part B	Part C	Total	Dominant tremor score
Baseline	15.2 ± 6.5	17.0 ± 7.2	13.4 ± 4.6	45.6 ± 15.4	14.7 ± 4.9
1 week	12.9 ± 6.2*	13.3 ± 7.8*	10.2 ± 5.9*	36.4 ± 17.6*	9.8 ± 7.3*
1 month	11.7 ± 6.5*	10.8 ± 6.9*	8.0 ± 5.6*	30.6 ± 17.1*	8.6 ± 6.2*
3 months	11.7 ± 6.4*	10.1 ± 6.0*	7.6 ± 4.8*	29.4 ± 15.1*	6.2 ± 5.0*
6 months	11.9 ± 6.3*	10.7 ± 6.3*	7.8 ± 5.0*	30.3 ± 15.7*	6.6 ± 5.3*
1 year	12.2 ± 5.4*	10.7 ± 6.8*	7.6 ± 4.6*	30.5 ± 14.4*	7.0 ± 5.5*
2 years	12.1 ± 6.0*	11.5 ± 7.2*	8.3 ± 4.8*	31.9 ± 15.8*	7.4 ± 5.8*

*CRST, Clinical Rating Scale for Tremor. *Significant level at $p < 0.001$ compared with the initial score. Data were presented as mean ± SD. Analyses were performed using one-way repeated measures ANOVA with the least significant difference post-hoc analysis.*

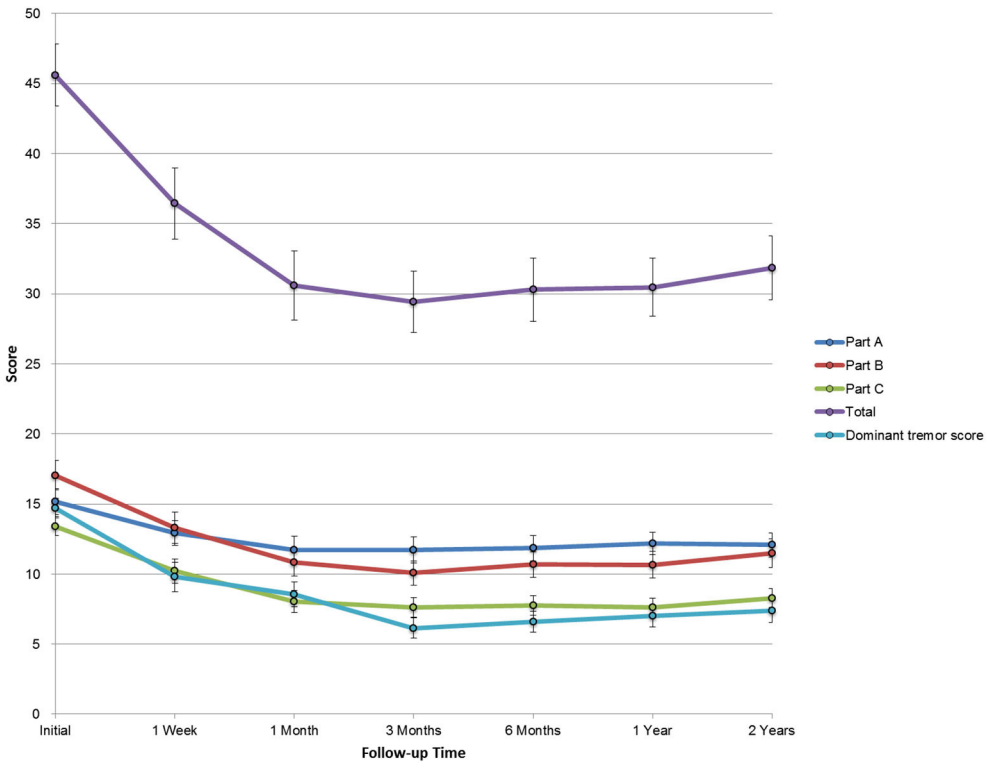

FIGURE 3 | The trend in sub-scores during the 2-year follow-up. CRST: Clinical Rating Scale for Tremor. Error bars were plotted with SE.

from 13% to 19% (Park et al., 2019; Sinai et al., 2019). In this study, the frame- and sonication-related AEs disappeared within 1 week. Vasogenic edema over the outer layer, which was treated with dexamethasone, was correlated with symptom relief. However, 6.3 and 8.3% of patients experienced sensory problems that lasted for 1 and 2 years, respectively. The incidence rates of long-term thalamotomy-related AEs in Chinese individuals were not higher than that in Western individuals according to previous reports (Elias et al., 2016; Chang et al., 2018; Meng et al., 2018). Interestingly, during follow-up, diminished leukoaraiosis was observed on **T2**-weighted-fluid-attenuated inversion recovery (T2 FLAIR), and the accumulation of hemosiderin was observed on susceptibility-weighted imaging (SWI) series (**Figure 2**). We hypothesized that this might be the difference between functional lesioning by focused ultrasound and traditional lesioning by radiofrequency ablation. The accumulation of hemosiderin deposits may influence the connection of the dentatorubrothalamic tract. In addition, the SDR values were proportionally correlated with the incidence of AEs. In addition, while a blood-oxygen-level-dependent (BOLD) signal in resting-state functional MRI (fMRI) analysis reveals a focal lesion in the MRgFUS VIM thalamotomy that results in symptom-related, long-term alterations in the effective connectivity of the dentate nucleus in the motor circuit, a similar experiment also could be

TABLE 3 | Adverse events after MRgFUS thalamotomy ($N = 48$).

Subgroups	Frame-related AEs	Sonication-related AEs	Thalamotomy-related AEs				Others
			Sensory-related	Strength-related	Balance-related	Dysarthria and dysphagia	
0 day	0 (0)	27 (56.3)	2 (4.2)	0 (0)	0 (0)	0 (0)	3 (6.3)
1 day	0 (0)	2 (4.2)	4 (8.3)	2 (4.2)	40 (83.3)	1 (2.1)	3 (6.3)
1 week	1 (2.1)	1 (2.1)	3 (6.3)	3 (6.3)	20 (41.7)	1 (2.1)	10 (20.8)
1 month	0 (0)	0 (0)	5 (10.4)	3 (6.3)	5 (10.4)	2 (4.2)	7 (14.6)
3 months	0 (0)	0 (0)	4 (8.3)	2 (4.2)	3 (6.3)	2 (4.2)	8 (16.7)
6 months	0 (0)	0 (0)	3 (6.3)	2 (4.2)	2 (4.2)	0 (0)	5 (10.4)
1 year	0 (0)	0 (0)	3 (6.3)	2 (4.2)	0 (0)	0 (0)	3 (6.3)
2 years	0 (0)	0 (0)	4 (8.3)	0 (0)	0 (0)	0 (0)	0 (0)

AEs, Adverse Events; MRgFUS, Magnetic Resonance-guided Focused Ultrasound.
Data were presented as numbers (%).

TABLE 4 | Comparison of outcomes between the current and previous studies with a larger sample size ($N \geq 30$).

Author, year	N	Rate of improvement rate in dominant tremor scores		
		6 months	1 year	2 years
The study	48	55.1%	52.4%	49.7%
Meng et al., 2018	37	No data	42.4%	43.4%
Chang et al., 2018	76	56.6%	55.0%	55.6%
Elias et al., 2016	56	44.0%	39.8%	No data

conducted to explore the effective connectivity difference among AEs (Park et al., 2017).

The proportion of men and women affected by ET is equal. However, hand tremor was more severe in men than in women, and head and voice tremors were more severe in women than in men (Shanker, 2019). MRgFUS thalamotomy is more promising in controlling peripheral tremors, and this may be the reason why more male patients received this treatment. Identifying brain targets for resolving head and voice tremors under safety procedures will be an important issue in future studies.

From a technical viewpoint, the energy efficiency is lower in the low SDR group than in the high SDR group (Chang et al., 2016, 2020). Patients can be at risk for long treatment duration due to different kinds of discomforts, including the tightness and pressure from the silicon membrane attached to the head of the patient, the headache caused by cold water between the transducer and the membrane, the pain caused by the pins of the stereotactic frame, and deep vein thrombosis. Based on a balance between clinical benefits and risks, patients with a high SDR (>0.45) must be selected, which is based on the recommendation of the FDA (U.S. Food Drug Administration, 2020a,b). However, this study had shown that there were no significant differences in terms of clinical outcome and safety profile between patients with a low SDR (0.3–0.4) and those with a high SDR (>0.4). Similar reports of Japan and Korea also showed that patients with low SDR can be successfully treated (Chang et al., 2019; Yamamoto et al., 2019). As reported previously, 50% of Chinese and 78.6% of Japanese patients had SDRs of 0.40 or less (Yamamoto et al., 2019; Tsai et al., 2021). Increasing the efficacy of ablation in treating such patients with low SDR is an important issue. During the preparation of the patient, we attempted to enlarge the skull surface, if possible, by placing the membrane as inferior as possible to prevent exceeding the safety limit of 100 J/cm^2. Meanwhile, the membrane fold could be excluded from the region of focused ultrasound penetration. Hence, to achieve better focus, the number of active elements can be increased (Yamamoto et al., 2020).

In this study, we used the conventional stereotactic coordinate to determine the initial target location for the VIM thalamotomy. The tremor control (**Figure 3**) and the reported AE (**Table 3**) indicated that this targeting strategy leads to similar clinical outcomes as the other reports (Elias et al., 2016; Chang et al., 2018; Meng et al., 2018). Recently, the diffusion-weighted MRI was reported and reviewed (Lehman et al., 2020) to facilitate the targeting of the dentatorubrothalamic tract in order to improve symptom control (Chazen et al., 2018) or avoid the potential adverse effects (Krishna et al., 2019). Although there is an existing limitation of diffusion-tensor imaging (DTI) regarding the image distortion and the manual error of this seed-based tractography targeting, this advanced targeting strategy is still promising and could be a valuable reference for this MRgFUS procedure.

Lesion size is associated with the clinical efficacy of MRgFUS thalamotomy in ET (Federau et al., 2018; Harary et al., 2018). At the time of treatment, 3–6 sonications are normally applied to align the center of the hot spot to the selected target; then, the following sonications are used to stimulate the patient, achieve the therapeutic temperature, and consolidate the lesion if there is any. Empirically, the energy efficiency can be lower, and the perifocal edema can be larger if the number of sonications is higher. Hence, instead of moving around the target region to identify a more effective location, a small number of sonications were used, and the treatment was completed to address the aforementioned issues. To date, a high temperature is utilized to create the lesion and control the tremor.

This study was not a randomized controlled trial to ensure efficacy and safety (Elias et al., 2016) but is based on the real-world data like other similar research for safety, effectiveness, and long-term outcomes (Chang et al., 2018; Katkade et al., 2018; Meng et al., 2018; Park et al., 2019; Sinai et al., 2019). It had some limitations. First, retrospective data were collected only for up to 2 years. Hence, a longer follow-up duration is necessary. Second, further analyses of lesions and procedures, which are important in improving the efficacy of treatment and reducing the incidence of AEs, were not performed. Third, the Quality of Life in Essential Tremor Questionnaire (QUEST) was not used. Hence, the quality of life among patients with ET was not evaluated.

In conclusion, the incidence of tremor and disability decreased after MRgFUS thalamotomy among patients with drug-refractory ET. The outcome of this study was similar to that of previous studies, which had <2 years of follow-up. MRgFUS can be performed successfully for patients with normal and low SDR. Therefore, this study suggests the possibility that lowering the cutoff value of SDR ($\geq$0.3) may result in more patients being treated with this nonsurgical and nonionizing intervention.

DATA AVAILABILITY STATEMENT

The original contributions presented in the study are included in the article/supplementary material, further inquiries can be directed to the corresponding authors.

ETHICS STATEMENT

The studies involving human participants were reviewed and approved by Institutional Review Board of Show Chwan Memorial Hospital. The patients/participants provided their written informed consent to participate in this study.

AUTHOR CONTRIBUTIONS

PW and WL performed the literature search and wrote the results. KHL and H-CL collected and edited the clinical data. M-TL participated in data analysis. KW-KT wrote the discussion section. P-YC revised the manuscript. W-CC revised and drafted the manuscript. C-YW contributed to the revisions and final draft of the manuscript. TT provided clinical recommendations. All authors have read and approved the final version of the manuscript.

FUNDING

The study was funded by InSightec (ET002J) and Show Chwan Memorial Hospital (1090908).

ACKNOWLEDGMENTS

The study was greatly supported by Dr. Huang, Min-Ho, the president of Chang Bing Show Chwan Memorial Hospital, and InSightec (Haifa, Israel).

REFERENCES

Blomstedt, P., and Hariz, M.I. (2005). Hardware-related complications of deep brain stimulation: a ten year experience. *Acta Neurochir.* 147, 1061–1064. discussion 1064. doi: 10.1007/s00701-005-0576-5

Chang, J.W., Park, C.K., Lipsman, N., Schwartz, M.L., Ghanouni, P., Henderson, J.M., et al. (2018). A prospective trial of magnetic resonance-guided focused ultrasound thalamotomy for essential tremor: results at the 2-year follow-up. *Ann. Neurol.* 83, 107–114. doi: 10.1002/ana.25126

Chang, K.W., Park, Y.S., and Chang, J.W. (2019). Skull factors affecting outcomes of magnetic resonance-guided focused ultrasound for patients with essential tremor. *Yonsei Med. J.* 60, 768–773. doi: 10.3349/ymj.2019.60.8.768

Chang, K.W., Rachmilevitch, I., Chang, W.S., Jung, H.H., Zadicario, E., Prus, O., et al. (2020). Safety and efficacy of magnetic resonance-guided focused ultrasound surgery with autofocusing echo imaging. *Front. Neurosci.* 14:592763. doi: 10.3389/fnins.2020.592763

Chang, W.S., Jung, H.H., Kweon, E.J., Zadicario, E., Rachmilevitch, I., and Chang, J.W. (2015). Unilateral magnetic resonance guided focused ultrasound thalamotomy for essential tremor: practices and clinicoradiological outcomes. *J. Neurol. Neurosurg. Psychiatry* 86, 257–264. doi: 10.1136/jnnp-2014-307642

Chang, W.S., Jung, H.H., Zadicario, E., Rachmilevitch, I., Tlusty, T., Vitek, S., et al. (2016). Factors associated with successful magnetic resonance-guided focused ultrasound treatment: efficiency of acoustic energy delivery through the skull. *J. Neurosurg.* 124, 411–416. doi: 10.3171/2015.3.JNS142592

Chazen, J.L., Sarva, H., Stieg, P.E., Min, R.J., Ballon, D.J., Pryor, K.O., et al. (2018). Clinical improvement associated with targeted interruption of the cerebellothalamic tract following MR-guided focused ultrasound for essential tremor. *J. Neurosurg.* 129, 315–323. doi: 10.3171/2017.4.JNS162803

Diaz, N.L., and Louis, E.D. (2010). Survey of medication usage patterns among essential tremor patients: movement disorder specialists vs. general neurologists. *Parkinsonism Relat. Disord.* 16, 604–607. doi: 10.1016/j.parkreldis.2010.07.011

Elias, W.J., Huss, D., Voss, T., Loomba, J., Khaled, M., Zadicario, E., et al. (2013). A pilot study of focused ultrasound thalamotomy for essential tremor. *N. Engl. J. Med.* 369, 640–648. doi: 10.1056/NEJMoa1300962

Elias, W.J., Lipsman, N., Ondo, W.G., Ghanouni, P., Kim, Y.G., Lee, W., et al. (2016). A randomized trial of focused ultrasound thalamotomy for essential tremor. *N. Engl. J. Med.* 375, 730–739. doi: 10.1056/NEJMoa1600159

Engel, K., Huckhagel, T., Gulberti, A., Pötter-Nerger, M., Vettorazzi, E., Hidding, U., et al. (2018). Towards unambiguous reporting of complications related to deep brain stimulation surgery: a retrospective single-center analysis and systematic review of the literature. *PLoS ONE* 13:e0198529. doi: 10.1371/journal.pone.0198529

Federau, C., Goubran, M., Rosenberg, J., Henderson, J., Halpern, C.H., Santini, V., et al. (2018). Transcranial MRI-guided high-intensity focused ultrasound for treatment of essential tremor: a pilot study on the correlation between lesion size, lesion location, thermal dose, and clinical outcome. *J. Magn. Reson. Imag.* 48, 58–65. doi: 10.1002/jmri.25878

Findley, L.J., Cleeves, L., and Calzetti, S. (1985). Primidone in essential tremor of the hands and head: a double blind controlled clinical study. *J. Neurol. Neurosurg. Psychiatry* 48, 911–915. doi: 10.1136/jnnp.48.9.911

Gronich, N., Abernethy, D.R., Auriel, E., Lavi, I., Rennert, G., and Saliba, W. (2018). β2-adrenoceptor agonists and antagonists and risk of Parkinson's disease. *Mov. Disord.* 33, 1465–1471. doi: 10.1002/mds.108

Harary, M., Essayed, W.I., Valdes, P.A., McDannold, N., and Cosgrove, G.R. (2018). Volumetric analysis of magnetic resonance-guided focused ultrasound thalamotomy lesions. *Neurosurg. Focus* 44:E6. doi: 10.3171/2017.11.FOCUS17587

Haubenberger, D., and Hallett, M. (2018). Essential Tremor. *N. Engl. J. Med.* 378, 1802–1810. doi: 10.1056/NEJMcp1707928

Health Quality Ontario (2018). Magnetic resonance-guided focused ultrasound neurosurgery for essential tremor: a health technology assessment. *Ont. Health Technol. Assess. Ser.* 18, 1–141.

Hopfner, F., Wod, M., Höglinger, G.U., Blaabjerg, M., Rösler, T.W., Kuhlenbäumer, G., et al. (2019). Use of β2-adrenoreceptor agonist and antagonist drugs and risk of Parkinson disease. *Neurology* 93, e135–e142. doi: 10.1212/WNL.0000000000007694

Ito, H., Yamamoto, K., Fukutake, S., Odo, T., and Kamei, T. (2020). Two-year follow-up results of magnetic resonance imaging-guided focused ultrasound unilateral thalamotomy for medication-refractory essential tremor. *Intern. Med.* 59, 2481–2483. doi: 10.2169/internalmedicine.4360-19

Katkade, V.B., Sanders, K.N., and Zou, K.H. (2018). Real world data: an opportunity to supplement existing evidence for the use of long-established medicines in health care decision making. *J. Multidiscip. Healthcare* 11, 295–304. doi: 10.2147/JMDH.S160029

Koller, W.C., and Vetere-Overfield, B. (1989). Acute and chronic effects of propranolol and primidone in essential tremor. *Neurology* 39, 1587–1588. doi: 10.1212/WNL.39.12.1587

Krishna, V., Sammartino, F., Agrawal, P., Changizi, B.K., Bourekas, E., Knopp, M.V., et al. (2019). Prospective tractography-based targeting for improved safety of focused ultrasound thalamotomy. *Neurosurgery* 84, 160–168. doi: 10.1093/neuros/nyy020

Lehman, V.T., Lee, K.H., Klassen, B.T., Blezek, D.J., Goyal, A., Shah, B.R., et al. (2020). MRI and tractography techniques to localize the ventral intermediate nucleus and dentatorubrothalamic tract for deep brain stimulation and MR-guided focused ultrasound: a narrative review and update. *Neurosurg. Focus* 49, E8. doi: 10.3171/2020.4.FOCUS20170

Lipsman, N., Schwartz, M.L., Huang, Y., Lee, L., Sankar, T., Chapman, M., et al. (2013). MR-guided focused ultrasound thalamotomy for essential tremor: a proof-of-concept study. *Lancet Neurol.* 12, 462–468. doi: 10.1016/S1474-4422(13)70048-6

Louis, E.D., and Ferreira, J.J. (2010). How common is the most common adult movement disorder? Update on the worldwide prevalence of essential tremor. *Mov. Disord.* 25, 534–541. doi: 10.1002/mds.22838

Louis, E.D., Joyce, J.L., and Cosentino, S. (2019). Mind the gaps: what we don't know about cognitive impairment in essential tremor. *Parkinsonism Relat. Disord.* 63, 10–19. doi: 10.1016/j.parkreldis.2019.02.038

Meng, Y., Solomon, B., Boutet, A., Llinas, M., Scantlebury, N., Huang, Y., et al. (2018). Magnetic resonance-guided focused ultrasound thalamotomy for treatment of essential tremor: a 2-year outcome study. *Mov. Disord.* 33, 1647–1650. doi: 10.1002/mds.99

Mittal, S., Bjørnevik, K., Im, D.S., Flierl, A., Dong, X., Locascio, J.J., et al. (2017). β2-Adrenoreceptor is a regulator of the α-synuclein gene driving risk of Parkinson's disease. *Science* 357, 891–898. doi: 10.1126/science.aaf3934

Park, H.J., Pae, C., Friston, K., Jang, C., Razi, A., Zeidman, P., et al. (2017). Hierarchical dynamic causal modeling of resting-state fMRI reveals longitudinal changes in effective connectivity in the motor system after thalamotomy for essential tremor. *Front. Neurol.* 8:346. doi: 10.3389/fneur.2017.00346

Park, Y.S., Jung, N.Y., Na, Y.C., and Chang, J.W. (2019). Four-year follow-up results of magnetic resonance-guided focused ultrasound thalamotomy for essential tremor. *Mov. Disord.* 34, 727–734. doi: 10.1002/mds.27637

Shanker, V. (2019). Essential tremor: diagnosis and management. *BMJ* 366:l4485. doi: 10.1136/bmj.l4485

Sharifi, S., Nederveen, A.J., Booij, J., and van Rootselaar, A.F. (2014). Neuroimaging essentials in essential tremor: a systematic review. *Neuroimage Clin.* 5, 217–231. doi: 10.1016/j.nicl.2014.05.003

Sinai, A., Nassar, M., Eran, A., Constantinescu, M., Zaaroor, M., Sprecher, E., et al. (2019). Magnetic resonance-guided focused ultrasound thalamotomy for essential tremor: a 5-year single-center experience. *J. Neurosurg.* 133, 417–424. doi: 10.3171/2019.3.JNS19466

Stacy, M.A., Elble, R.J., Ondo, W.G., Wu, S.C., and Hulihan, J. (2007). Assessment of interrater and intrarater reliability of the Fahn–Tolosa–Marin Tremor Rating Scale in essential tremor. *Mov. Disord.* 22, 833–838. doi: 10.1002/mds.21412

Sun, H., Sun, F., Zhang, X.Q., Fang, X.H., and Chan, P. (2020). The prevalence and clinical characteristics of essential tremor in elderly chineses: a population-based study. *J. Nutr. Health Aging* 24, 1061–1065. doi: 10.1007/s12603-020-1472-7

Tsai, K.W., Chen, J.C., Lai, H.C., Chang, W.C., Taira, T., Chang, J.W., et al. (2021). The distribution of skull score and skull density ratio in tremor patients for mr-guided focused ultrasound thalamotomy. *Front. Neurosci.* 15:612940. doi: 10.3389/fnins.2021.612940

U.S. Food and Drug Administration (2020a). InSightec ExAb¬late® System information for prescribers [Online]. Available online at: https://www.accessdata.fda.gov/cdrh_docs/pdf15/P150038C.pdf (Accessed Jun 7, 2020).

U.S. Food and Drug Administration (2020b). *Summary of Safety and Effectiveness Data* [Online]. Available online at: https://www.accessdata.fda.gov/cdrh_docs/pdf15/P150038B.pdf (Accessed Jun 7, 2020).

Wintermark, M., Druzgal, J., Huss, D.S., Khaled, M.A., Monteith, S., Raghavan, P., et al. (2014). Imaging findings in MR imaging-guided focused ultrasound treatment for patients with essential tremor. *AJNR Am. J. Neuroradiol.* 35, 891–896. doi: 10.3174/ajnr.A3808

Yamamoto, K., Ito, H., Fukutake, S., Kamei, T., Yamaguchi, T., and Taira, T. (2019). Ventralis intermedius thalamotomy with focused ultrasound for patients with low skull density ratio. *Mov. Disord.* 34, 1239–1240. doi: 10.1002/mds.27726

Yamamoto, K., Ito, H., Fukutake, S., Odo, T., Kamei, T., Yamaguchi, T., et al. (2020). Factors associated with heating efficiency in transcranial focused ultrasound therapy. *Neurol. Med. Chir. (Tokyo)* 60, 594–599. doi: 10.2176/nmc.oa.2020-0225

Zesiewicz, T.A., Elble, R.J., Louis, E.D., Gronseth, G.S., Ondo, W.G., Dewey, R.B. Jr., et al. (2011). Evidence-based guideline update: treatment of essential tremor: report of the Quality Standards subcommittee of the American Academy of Neurology. *Neurology* 77, 1752–1755. doi: 10.1212/WNL.0b013e318236f0fd

Conflict of Interest: KW-KT was employed by company Insightec Ltd. The authors declare that part of this study received funding from Insightec Ltd. under the ET002J protocol. The funder had involvement with the preparation of the manuscript.

frontiers in Aging Neuroscience

ORIGINAL RESEARCH
published: 30 July 2021
doi: 10.3389/fnagi.2021.687927

Combined Support Vector Machine Classifier and Brain Structural Network Features for the Individual Classification of Amnestic Mild Cognitive Impairment and Subjective Cognitive Decline Patients

Weijie Huang[1,2,3†], Xuanyu Li[4,5†], Xin Li[6,7], Guixia Kang[8], Ying Han[4,9,10,11] and Ni Shu[1,2,3]**

[1] State Key Laboratory of Cognitive Neuroscience and Learning, Beijing Normal University, Beijing, China, [2] Center for Collaboration and Innovation in Brain and Learning Sciences, Beijing Normal University, Beijing, China, [3] Beijing Key Laboratory of Brain Imaging and Connectomics, Beijing Normal University, Beijing, China, [4] Department of Neurology, Xuanwu Hospital of Capital Medical University, Beijing, China, [5] Department of Neurology, Beijing Friendship Hospital, Capital Medical University, Beijing, China, [6] School of Electrical Engineering, Yanshan University, Qinhuangdao, China, [7] Measurement Technology and Instrumentation Key Lab of Hebei Province, Qinhuangdao, China, [8] Beijing University of Posts and Telecommunications, Beijing, China, [9] Biomedical Engineering Institute, Hainan University, Haikou, China, [10] Center of Alzheimer's Disease, Beijing Institute for Brain Disorders, Beijing, China, [11] National Clinical Research Center for Geriatric Disorders, Beijing, China

OPEN ACCESS

Edited by:
Fermín Segovia, University of Granada, Spain

Reviewed by:
Yi Su, Banner Alzheimer's Institute, United States
Liyong Wu, Capital Medical University, China

***Correspondence:**
Ying Han
hanying@xwh.ccmu.edu.cn
Ni Shu
nshu@bnu.edu.cn

[†] These authors have contributed equally to this work and share first authorship

Received: *30 March 2021*
Accepted: *30 June 2021*
Published: *30 July 2021*

Citation:
Huang W, Li X, Li X, Kang G, Han Y and Shu N (2021) Combined Support Vector Machine Classifier and Brain Structural Network Features for the Individual Classification of Amnestic Mild Cognitive Impairment and Subjective Cognitive Decline Patients. Front. Aging Neurosci. 13:687927. doi: 10.3389/fnagi.2021.687927

Objective: Individuals with subjective cognitive decline (SCD) or amnestic mild cognitive impairment (aMCI) represent important targets for the early detection and intervention of Alzheimer's disease (AD). In this study, we employed a multi-kernel support vector machine (SVM) to examine whether white matter (WM) structural networks can be used for screening SCD and aMCI.

Methods: A total of 138 right-handed participants [51 normal controls (NC), 36 SCD, 51 aMCI] underwent MRI brain scans. For each participant, three types of WM networks with different edge weights were constructed with diffusion MRI data: fiber number-weighted networks, mean fractional anisotropy-weighted networks, and mean diffusivity (MD)-weighted networks. By employing a multiple-kernel SVM, we seek to integrate information from three weighted networks to improve classification performance. The accuracy of classification between each pair of groups was evaluated via leave-one-out cross-validation.

Results: For the discrimination between SCD and NC, an area under the curve (AUC) value of 0.89 was obtained, with an accuracy of 83.9%. Further analysis revealed that the methods using three types of WM networks outperformed other methods using single WM network. Moreover, we found that most of discriminative features were from MD-weighted networks, which distributed among frontal lobes. Similar classification

performance was also reported in the differentiation between subjects with aMCI and NCs (accuracy = 83.3%). Between SCD and aMCI, an AUC value of 0.72 was obtained, with an accuracy of 72.4%, sensitivity of 74.5% and specificity of 69.4%. The highest accuracy was achieved with features only selected from MD-weighted networks.

Conclusion: White matter structural network features help machine learning algorithms accurately identify individuals with SCD and aMCI from NCs. Our findings have significant implications for the development of potential brain imaging markers for the early detection of AD.

Keywords: subjective cognitive decline, mild cognitive impairment, support vector machine, white matter, diffusion tensor imaging

INTRODUCTION

Subjective cognitive decline (SCD) refers to self-perceived cognitive decline relative to a previously normal status, without impaired performance on standardized neuropsychological tests (Jessen et al., 2014; Molinuevo et al., 2017). There is gathering evidence that SCD may be the first symptomatic manifestation of Alzheimer's disease (AD) occurring prior to amnestic mild cognitive impairment (aMCI) (Jessen et al., 2014; Rabin et al., 2017). Patients with aMCI, even those who temporarily revert to normal cognition, are at higher risk of progressing to dementia than age-matched normal controls (NCs) (Petersen et al., 2018). Effective intervention to delay or prevent pathologic cognitive decline may best be targeted at the SCD or MCI stage, in which cognitive function is still relatively preserved (Smart et al., 2017; Petersen et al., 2018). In consideration of this, it is critical to find sensitive, low-cost methods for the early detection of individuals at risk for further cognitive decline and incident AD dementia.

Recent advances in neuroimaging research suggest that elderly people with SCD have an increased likelihood of AD biomarkers across a range of modalities (Rabin et al., 2017). Diffusion tensor imaging (DTI) is a quantitative MRI technique that has been applied to delineate white matter (WM) microstructure through the characterization of the underlying water molecule diffusion (Amlien and Fjell, 2014). Using DTI measures, previous studies observed WM abnormalities in SCD subjects compared with the normal control (NC) group (Selnes et al., 2012; Li et al., 2016). Such alterations may predict medial temporal lobe atrophy and dementia (Selnes et al., 2013). In addition to the raw features obtained from DTI, characterization of the global architecture or topological property of WM connection patterns has recently drawn a great deal of interest (Sporns et al., 2005; Bullmore and Sporns, 2009). Previous studies suggested that patients with SCD and MCI exhibit global disruption of brain connectivity and topologic alterations of the whole-brain connectome rather than in a single isolated region (Shu et al., 2012, 2018). The topographical metrics of patients with SCD and MCI correlating with impaired cognitive performance suggest their potential use as biomarkers for the early detection of cognitive impairment in elderly individuals.

Over the past decades, neuroimaging measures have been increasingly integrated into imaging signatures of AD by means of classification frameworks, offering promising tools for individualized diagnosis and prognosis (Sajda, 2006; Rathore et al., 2017). Peter et al. (2014) suggested that, even at the SCD stage, structural MRI combined with the SVM method is a sensitive method for identifying subtle brain changes that correspond to future memory decline. Although SVM has been used successfully in several AD and MCI imaging studies involving WM connectivity network measure-based methods (Wee et al., 2012; Prasad et al., 2015; Rathore et al., 2017), it is scarce in SCD populations.

In this study, we wanted to assess the usefulness of multiple-kernel SVM approaches to accurately identify SCD and aMCI patients from normal aging based on different weighted structure networks. The primary aim of this study was to combine multiple weighted networks using multiple-kernel SVM with an SVM machine learning algorithm for each single weighted structure network approach and the direct data fusion method. The study further investigated the effect of feature number and constraint parameter C on classifying NC, SCD, and aMCI. Finally, information on which regions contributed most to the group separation was assessed, allowing for different types of discriminative features to be interpreted with respect to the underlying neurobiology of SCD and aMCI.

MATERIALS AND METHODS

Subjects

This study included 138 right-handed and Mandarin-speaking subjects (51 NC, 36 SCD, and 51 aMCI) who were recruited at the memory clinic of Beijing Xuanwu Hospital of Capital Medical University and the local community in China from May 2011 to June 2016. Written informed consent was obtained from all subjects before inclusion. This study has been registered to ClinicalTrials.gov (NCT02225964[1]).

The patients with aMCI were diagnosed on the basis of Petersen's criteria (Petersen, 2004) and the National Institute on Aging Alzheimer's Association criteria for aMCI due to AD (Albert et al., 2011) as follows: (a) with subjective memory complaint, preferably confirmed by an informant; (b) objective memory impairment confirmed by Mini-Mental State

[1]https://www.clinicaltrials.gov/

Examination (MMSE), Montreal Cognitive Assessment (MoCA), Auditory Verbal Learning Test (AVLT); (c) a Clinical Dementia Rating (CDR) score of 0.5; (d) did not fulfill the criteria for dementia according to the Diagnostic and Statistical Manual of Mental Disorders, fourth edition, revised (DSM-IV); and (e) hippocampal atrophy observed by structural MRI.

The inclusion criteria of SCD, based on the research criteria for SCD (Jessen et al., 2014) and described in our previous study (Sun et al., 2016), included the following: (a) self-reported persistent cognitive decline within the last 5 years, which was confirmed by an informant; (b) performance within the normal range on a Chinese version of the MMSE and the Beijing version of the MoCA (adjusted for age, sex, and education); and (c) a score of 0 on the CDR.

The NC participants were healthy volunteers who met the following conditions: (a) no subjective or objective cognitive decline concerns; (b) normal performance on neuropsychologic test scores; and (c) CDR score of 0.

Subjects were excluded if they had any of the following: (a) structural abnormalities that could impair cognitive function other than cerebrovascular lesions, such as tumor, subdural hematoma, and contusion from a previous head trauma; (b) a history of stroke, addictions, neurologic or psychiatric diseases, or treatments that would affect cognitive function; (c) focal neurologic signs or symptoms (e.g., paralysis, sensory disturbances, dysarthria, gait disorder, and Babinski sign); (d) depression (a score of >7 on the Hamilton depression rating scale); (e) large-vessel disease (e.g., cortical and/or subcortical infarcts and watershed infarcts); (f) and diseases with WM lesions (e.g., normal pressure hydrocephalus and multiple sclerosis). The diagnosis was performed by three neurologists who had between 8 and 28 years of experience. Clinical and demographic data for all 138 participants are shown in **Table 1**.

Data Acquisition

All of the participants were imaged with a 3.0-T MR imager (Magnetom Trio Tim; Siemens, Erlangen, Germany) at the Department of Radiology, Xuanwu Hospital, Capital Medical University. The T1-weighted images were acquired using a magnetization prepared rapid gradient echo sequence with the following parameters: repetition time (TR) = 1,900 ms; echo time (TE) = 2.2 ms; flip angle = 9°; acquisition matrix = 256 × 224; field of view (FOV) = 256 × 224 mm^2; slice thickness = 1 mm; no gap; 176 sagittal slices; and average = 1. The DTI data were acquired using a single-shot EPI sequence with the following parameters: TR = 11,000 ms; TE = 98 ms; flip angle = 90°; acquisition matrix = 128 × 116; FOV = 256 × 232 mm^2; slice thickness = 2 mm; no gap; 60 axial slices; and average = 3. Thirty non-linear diffusion weighting directions with b = 1,000 s/mm^2 and one b0 image were obtained. All images were reviewed, and leukoencephalopathy and vascular comorbidity were evaluated by an experienced neuroradiologist with 18 years of experience in clinical radiology.

Image Preprocessing

All DTI imaging data preprocessing was performed with the FDT toolbox in FSL[2]. Briefly, each diffusion-weighted image was coregistered to the b0 image for eddy current and head motion correction. Accordingly, the b-matrix was reoriented based on the transformation matrix (Leemans and Jones, 2009). For each voxel, the diffusion tensor elements (Basser et al., 1994), fractional anisotropy (FA) value and mean diffusivity (MD) were estimated (Basser and Pierpaoli, 1996).

Network Construction

A network consists of nodes and edges. As shown in **Supplementary Figure 1**, the following procedures were applied to construct WM structural networks.

Network Node Definition

The automated anatomic labeling (AAL) template (Tzourio-Mazoyer et al., 2002) was used to parcel the brain into 90 regions of interest (**Supplementary Table 1**), which represent

[2]https://fsl.fmrib.ox.ac.uk/fsl/fslwiki/

TABLE 1 | Clinical and demographic of amnestic mild cognitive impairment (aMCI), subjective cognitive decline (SCD), and normal controls (NC).

	NC	SCD	aMCI	*P* value			
				NC vs. SCD vs. aMCI	NC vs. SCD	NC vs. aMCI	SCD vs. aMCI
N (M/F)	51 (18/33)	36 (15/21)	51 (22/29)	0.70[a]	0.55[a]	0.42[a]	0.89[a]
Age, years	62.22 ± 9.14	63.47 ± 8.78	64.06 ± 9.54	0.59[b]	0.52[c]	0.32[c]	0.77[c]
Education, years	11.23 ± 4.63	11.44 ± 4.59	9.55 ± 4.14	0.08[b]	0.84[c]	0.06[c]	0.05[c]
AVLT: immediate recall	8.83 ± 1.92	8.14 ± 1.87	5.70 ± 1.53	<0.0001[b]	0.10[c]	<0.0001[c]	<0.0001[c]
AVLT: delayed recall	10.04 ± 3.00	8.56 ± 2.79	3.32 ± 2.87	<0.0001[b]	0.02[c]	<0.0001[c]	<0.0001[c]
AVLT: recognition	11.69 ± 3.23	10.89 ± 2.28	7.38 ± 4.17	<0.0001[b]	0.21[c]	<0.0001[c]	<0.0001[c]
MoCA	28.14 ± 1.99	25.74 ± 2.10	19.34 ± 4.27	<0.0001[b]	0.62[c]	<0.0001[c]	<0.0001[c]
MMSE	28.14 ± 2.01	27.53 ± 1.72	23.78 ± 3.29	<0.0001[b]	0.14[c]	<0.0001[c]	<0.0001[c]

Plus-minus values are means ± S.D.
[a]The P value for gender distribution in the three groups was obtained by Chi-square test.
[b]The P values were obtained by an analysis of covariance.
[c]The P values were obtained by a two-sample t-test.
MMSE, Mini-Mental State Examination; NC, normal control; SCD, subjective cognitive decline; aMCI, amnestic mild cognitive impairment.

nodes in the WM structural network. The procedure was performed using SPM8 software[3] and has been previously described (Zalesky et al., 2010; Bai et al., 2012; Cao et al., 2013). Briefly, we first coregistered individual T1-weighted images to the b0 images in DTI space. Then, we transformed the T1 images in DTI space into the ICBM152 T1 template in Montreal Neurological Institute (MNI) space. Next, the AAL template from the MNI space was warped to the DTI native space by applying the inverse transformation obtained from the previous step. We used a nearest-neighbor interpolation method to preserve discrete labeling values.

WM Tractography

Diffusion tensor tractography was carried out with the "fiber assignment by continuous tracking (FACT)" method (Mori et al., 1999) included in the Diffusion Toolkit software[4]. Briefly, we seeded the voxels with FA greater than 0.2 to compute all the tracts in the diffusion-tensor imaging dataset. For each voxel, eight seeds were evenly distributed. Each streamline was reconstructed starting from each seed following the main diffusion direction from voxel to voxel. The tractography was terminated if it turned at an angle greater than 45° or reached a voxel with an FA less than 0.2.

Network Edge Definition

Each pair of nodes was considered structurally connected if there was at least one streamline whose end points were located in the pair (Zalesky et al., 2011; Bai et al., 2012; Shu et al., 2012). Then, three weighted networks were constructed for each subject: the fiber number (FN)-weighted network, which used the fiber number between two regions as the weight of edges; the FA-weighted network, which used the mean FA of all the voxels on all the fibers between two regions as the weight of edges; and the MD-weighted network, which used the mean MD of all the voxels on all the fibers between two regions as the weight of edges. These three networks had the same topology but conveyed different biophysical properties (Wee et al., 2011). The networks provide the fiber numbers, degree of anisotropy and average diffusivity of fibers connecting a pair of regions.

The 4,005 × 3 = 12,015 edges in the three networks were extracted for each subject as features that were used to classify the NC, SCD, and aMCI.

Feature Selection

Selecting a small subset of features with the greatest discriminative power has been shown to improve the classification performance and avoid overfitting (Dosenbach et al., 2010) because some features are irrelevant or redundant for classification. Several studies have suggested this can also speed up computation (De Martino et al., 2008; Pereira et al., 2009). Therefore, we adopted a univariate feature-filtering step in this study. Given a training dataset $x_k,\ k = 1, \ldots, m$, if n_+ and n_- are the number of positive instances (i.e., SCD) and negative instances (i.e., NC), respectively, then the F-score of the i-th feature can be calculated as:

$$\mathrm{F}(\mathrm{i}) = \frac{(\bar{x}_i^{(+)} - \bar{x}_i)^2 + (\bar{x}_i^{(-)} - \bar{x}_i)^2}{\frac{1}{n_+ - 1}\sum_{k=1}^{n_+}(x_{k,\,i}^{(+)} - \bar{x}_i^{(+)})^2 + \frac{1}{n_- - 1}\sum_{k=1}^{n_-}(x_{k,\,i}^{(-)} - \bar{x}_i^{(-)})^2} \quad (1)$$

Where $\bar{x}_i$, $\bar{x}_i^{(+)}$, $\bar{x}_i^{(-)}$ are the average of the i-th feature of the whole, positive, and negative data sets, respectively; $x_{k,\,i}^{(+)}$ is the i-th feature of the k-th positive instance; and $x_{k,\,i}^{(-)}$ is the i-th feature of the k-th negative instance. The numerator indicates the variance between groups, and the denominator indicates the variance within each of the two groups. The larger the F-score is, the more likely the feature is to be more discriminative. Therefore, we used this score as a feature selection criterion.

Considering that univariate feature selection may overlook the multivariate pattern, we also used a multivariate method, lasso regression, to select features and compared the performance of these two feature selection methods. Because lasso is a penalized least squares method, it performs continuous shrinkage and automatic variable selection simultaneously. There is a hyperparameter to control the degree to norm regularization. We used a nested fivefold cross validation to obtain the optimal hyperparameter.

Multiple-Kernel SVM

Given n training samples with $x_i = \left\{x_i^{(1)}, \ldots, x_i^{(M)}\right\}$ denoting the feature vector of the i-th sample ($M =$ number of white matter networks, $m = 1, \ldots, M$ and $x_i^{(m)} = \left\{edge_i^{(m)}(1), \ldots, edge_i^{(m)}(4005)\right\}$), $y_i \in \{-1,\ 1\}$ denoting the corresponding label, the primal optimization problem of a conventional single kernel SVM is defined as

$$\min_{w,b,\xi_i} \quad \frac{1}{2}||w||^2 + C\sum_{i=1}^{n}\xi_i, \quad (2)$$

$$\text{subject to} \quad y_i \times \left(W^T\phi(x_i) + b\right) \geq 1 - \xi_i$$

$$\text{and} \quad \xi_i \geq 0, \quad \text{for } i = 1, \ldots, n$$

where w, C, ξ_i, $\phi(\cdot)$, and b denote the normal vector to the hyperplane, the model parameter that determines the number of constraint violations, the distance of the i-th misclassified observation from its correct side of the margin, the kernel function and the bias term, respectively.

Normally, Eq. (2) is solved using its dual form with the kernel approach. The dual form is given as

$$\max_\alpha \sum_{i=1}^{n}\alpha_i - \frac{1}{2}\sum_{i,\,j}\alpha_i\alpha_j y_i y_j \times k\left(x_i, x_j\right), \quad (3)$$

$$\text{subject to} \quad \sum_{i=1}^{n}\alpha_i y_i = 0;$$

$$\text{and} \quad 0 \leq \alpha_i \leq C, \quad \text{for } i = 1, \ldots, n$$

[3]https://www.fil.ion.ucl.ac.uk/spm/

[4]http://www.trackvis.org/dtk/

where α is the Lagrange multiplier and $k\left(x_i, x_j\right)$ is the kernel function for training samples, x_i and x_j .

To integrate the three networks, we used a multiple kernel SVM whose primal optimization problem can be defined as

$$\min_{w^{(m)},b,\xi_i} \quad \frac{1}{2}\sum_{m=1}^{M}\beta_m||w^{(m)}||^2 + C\sum_{i=1}^{n}\xi_i, \tag{4}$$

$$\text{subject to} \quad y_i \times \left[\sum_{m=1}^{M}\beta_m\left(\left(w^{(m)}\right)^T\phi^{(m)}\left(x_i^{(m)}\right)+b\right)\right] \geq 1-\xi_i$$

$$\text{and} \quad \xi_i \geq 0, \quad \text{for } i=1,\ldots,n$$

where β_m is the weighting factor on the m-th networks. Similarly, the corresponding dual form is given as

$$\max_{\alpha}\sum_{i=1}^{n}\alpha_i - \frac{1}{2}\sum_{i,j}\alpha_i\alpha_j y_i y_j\sum_{m=1}^{M}\beta_m k^{(m)}\left(x_i^{(m)}, x_j^{(m)}\right), \tag{5}$$

$$\text{subject to} \quad \sum_{i=1}^{n}\alpha_i y_i = 0;$$

$$\text{and} \quad 0 \leq \alpha_i \leq C \text{ for } i=1,\ldots,n$$

where $k^{(m)}\left(x_i^{(m)}, x_j^{(m)}\right)$ is the kernel function for the m-th networks.

Given a new test sample $x = \left\{x^{(1)},\ldots,x^{(M)}\right\}$, the decision function for the predicted label can be determined as

$$F(X) = \text{sign}\left(\sum_{i=1}^{n}\alpha_i y_i\sum_{m=1}^{M}\beta_m k^{(m)}\left(x_i^{(m)}, x^{(m)}\right)+b\right). \tag{6}$$

The multiple kernel SVM can be naturally embedded into the conventional single kernel SVM framework by noting $k\left(x_i, x_j\right) = \sum_{m=1}^{M}\beta_m k^{(m)}\left(x_i^{(m)}, x_j^{(m)}\right)$ as a mixed kernel between the multiple networks training samples x_i and x_j and $k\left(x_i, x\right) = \sum_{m=1}^{M}\beta_m k^{(m)}\left(x_i^{(m)}, x^{(m)}\right)$ as a mixed kernel between the multiple networks training samples between x_i and the test sample x.

Support Vector Machine Training and Classification

The SVM classifier was trained based on the simple MKL (Rakotomamonjy et al., 2008) toolbox, which can train the weighting factors of different kernels. Due to the size limitations of the dataset, leave-one-out cross validation (LOOCV) was used to estimate the performance of the classifier. In LOOCV, each sample was considered the test sample, while the remaining samples were used to train the classifier. Before feature selection performed in training samples, the features of the test samples and training samples were normalized by using the mean value and standard deviation of the training sample. Then, the kernel matrix for each network was calculated. Finally, we trained and tested the classifier with the test sample. To obtain optimal performance, the hyperparameter C and feature number were determined by grid searching. The procedure for multi-kernel SVM training and classification is shown in **Figure 1**. We also applied the same pipeline to train a single-kernel SVM classifier with a single weighted network and a single-kernel SVM with multiple weighted networks. The accuracy, sensitivity and specificity were used to quantify the performance of the classifier.

$$\text{Accuracy} = \frac{TP+TN}{TP+FN+TN+FP} \tag{7}$$

$$\text{Sensitivity} = \frac{TP}{TP+FN} \tag{8}$$

$$\text{Specificity} = \frac{TN}{TN+FP} \tag{9}$$

where *TP*, *FN*, *TN*, and *FP* denote the number of positive instances correctly predicted, the number of positive instances classified as negative instances, the number of negative instances correctly predicted and the number of negative instances classified as positive instances, respectively.

Identification of the Most Discriminative Features

The essence of classification is determining a separating hyperplane. Previous studies have shown that the coefficients of the separating hyperplane quantify the power of discriminative feature information (Mourao-Miranda et al., 2005). The absolute value of the coefficients was multiplied by the weight of the corresponding network as feature weights. The higher the feature weights were, the more discriminative the corresponding features were. In every fold of LOOCV, the selected features differed slightly from fold to fold. Therefore, only the features that appeared in every fold of LOOCV were considered the most discriminative features. Each feature weight was averaged from all folds of LOOCV. To further explore which edge is most discriminative, the weights of each edge were obtained by summing the corresponding edge weights of different networks. We also determined the total weights of each network by computing the sum of feature weights from the corresponding network.

RESULTS

Classification Based on Multi-Weight Networks

A LOOCV was used to estimate the generalizability of the classifier. As shown in **Table 2**, the models using F-score outperformed those using lasso, so the subsequent analyses were based on the results from F-score. The proposed multiple kernel SVM-based multi-weight network approach achieved a

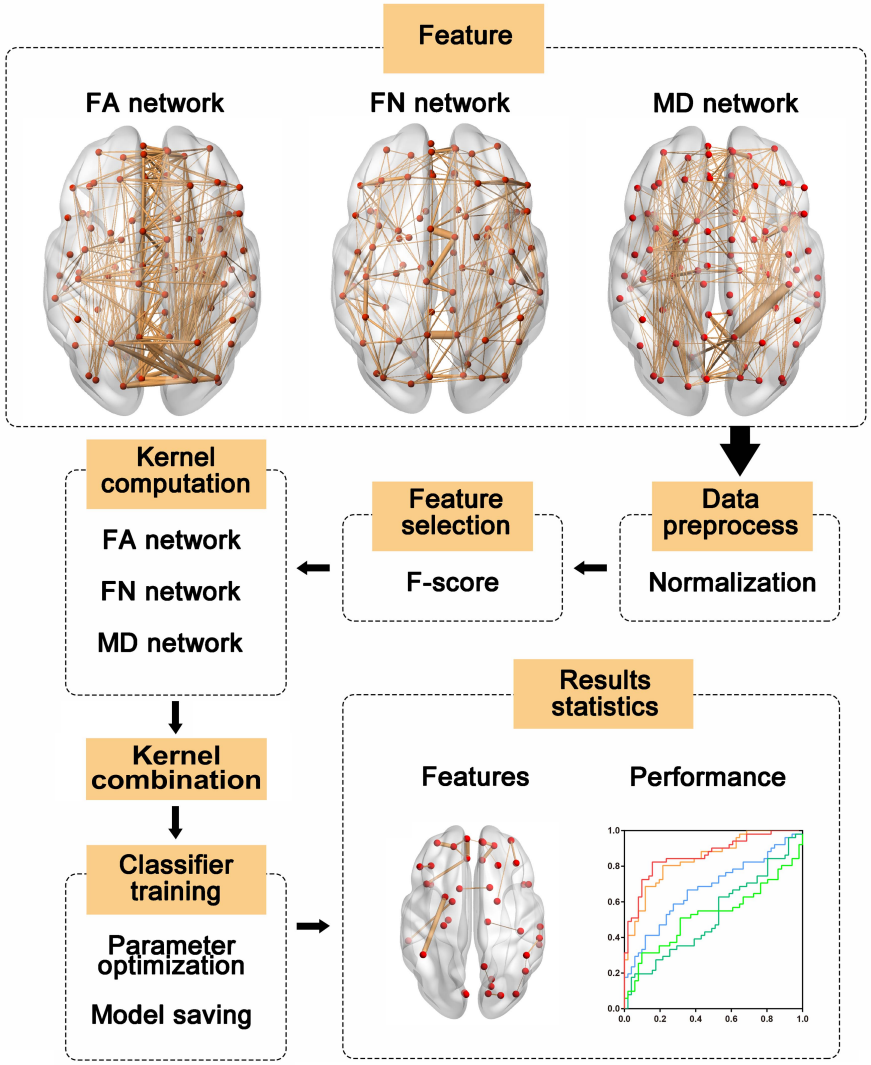

FIGURE 1 | The multi-kernel support vector machine (SVM) procedure. First, features were extracted from three weighted networks and normalized with the mean value and standard deviation of the training sample. Then, features were selected according to F-score and kernel matrices were computed based on the selected features. Next, the kernel matrices were used to train the models, and the label of the test sample was predicted with trained models. Finally, we evaluated the model performances and identified the most discriminative features. FA, fractional anisotropy; FN, fiber number; MD, mean diffusivity.

classification accuracy of 83.9%, with a sensitivity of 77.8% and a specificity of 88.2% in the discrimination between NC subjects and SCD subjects. For the classification between NC subjects and aMCI subjects, the proposed method yielded an accuracy of 83.3%, with a specificity of 84.3% and a sensitivity of 82.4%. The task of discriminating between aMCI subjects and SCD subjects was more difficult than the other classifications, and the proposed method achieved an accuracy of 72.4%, with a specificity of 69.4% and a sensitivity of 74.5%. The three pairs of classification performances using single and multi-weight networks are summarized in **Table 2**. The receiver operating characteristics (ROC) curves for all compared methods in the three pairs of classifications are shown in **Figure 2**. Overall, multiple kernel SVM-based multi-weight networks approach achieved relatively high performance in three pair of classifications, while other methods were not robust across different tasks.

Effect of Constraint Parameter C in Linear Kernel and Nonlinear Kernel Function

To investigate the influence of different constraint parameter C on the classification performance, the feature number was fixed, and the constraint parameter C was varied from 0.5 to 5 in steps of 0.5. The three pairs of classification accuracies with multi-kernel SVMs using different kernel functions and the corresponding C value are shown in **Figure 3**.

For every value of C, the multi-kernel SVM with a linear kernel yielded the highest accuracy compared to the multi-kernel

TABLE 2 | Classification performance of the single network and multi-network methods.

Feature selection	Method	NC and SCD			NC and aMCI			SCD and aMCI		
		Acc (%)	Sen (%)	Spe (%)	Acc (%)	Sen (%)	Spe (%)	Acc (%)	Sen (%)	Spe (%)
F-score	Multi-kernel (FA, FN, and MD)	83.9	**77.8**	88.2	**83.3**	**82.4**	**84.3**	72.4	69.4	74.5
	Single-kernel (FA, FN, and MD)	**85.1**	77.8	**90.2**	77.5	78.4	76.5	71.3	69.4	72.6
	FA	58.6	47.2	66.7	54.9	56.9	52.9	52.9	50.0	54.9
	FN	56.3	44.4	64.7	53.9	60.8	47.1	64.4	52.8	72.6
	MD	56.3	47.2	62.7	75.5	56.9	74.5	**73.6**	69.4	**76.5**
Lasso	Multi-kernel (FA, FN, and MD)	73.6	72.2	74.5	75.5	78.4	72.5	62.1	60.8	63.9
	Single-kernel (FA, FN, and MD)	75.9	77.8	74.5	71.6	72.5	70.6	69.0	**70.6**	66.7
	FA	49.4	63.9	39.2	51.0	45.1	56.9	39.1	49.0	25.0
	FN	56.3	55.6	56.9	52.9	51.0	54.9	54.0	68.6	33.3
	MD	51.7	55.6	49.0	60.8	68.6	52.9	62.1	70.6	50.0

Acc, accuracy; Sen, sensitivity; Spe, specificity; NC, normal control; SCD, subjective cognitive decline; aMCI, amnestic mild cognitive impairment; FA, fractional anisotropy; FN, fiber number; MD, mean diffusivity. The bold values represent the best performance.

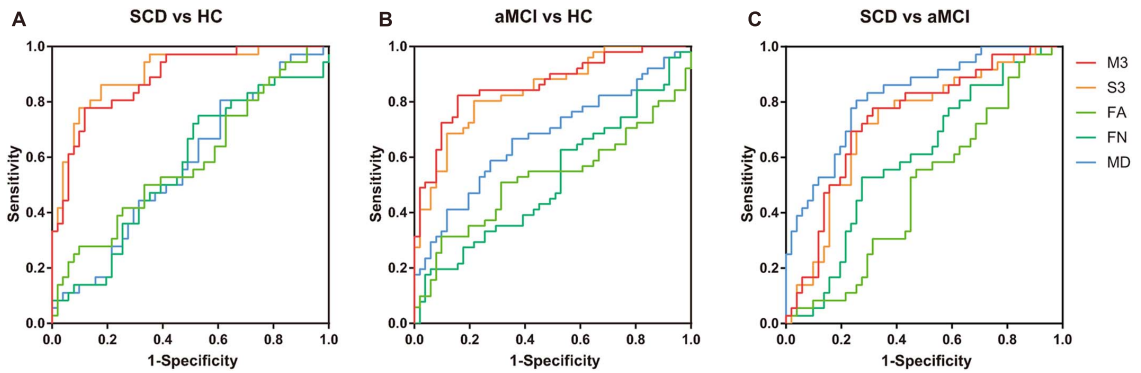

FIGURE 2 | Receiver operating characteristics (ROC) of three pairs of classifications. **(A)** ROC curves of classifying SCD and NC with different models. **(B)** ROC curves of classifying aMCI and NC with different models. **(C)** ROC curves of classifying SCD and aMCI with different models. M3, multi-kernel with FA, FN, and MD weighted network; S3, single-kernel with FA, FN, and MD weighted network. ROC, receiver operating characteristic; NCs, normal controls; SCD, subjective cognitive decline; aMCI, amnestic mild cognitive impairment; FA, fractional anisotropy; FN, fiber number; MD, mean diffusivity.

SVM with a polynomial kernel and radial basis function (RBF) kernel. The multi-kernel SVM with a linear kernel was the most robust to C. The performance of the proposed method was nearly unchanged under the variation of constraint parameter C.

Effect of Number of Features in the Linear Kernel and Nonlinear Kernel Function

In the proposed framework, the F-score was applied to select a subset of features with the most discriminative power. The features with higher F-scores were input to train the model. Therefore, the percentage of features to be selected is determined by the predefined value. In this subsection, to explore the robustness of the multi-kernel SVM, the constraint parameter C was fixed as 1, and the percentage of feature numbers was varied from 0.0014 to 0.0028 in steps of 0.00005. The three pairs of classification accuracies with multi-kernel SVMs using different kernel functions and the corresponding percentage of selected features are summarized in **Figure 4**.

The multi-kernel SVM with a linear kernel yielded the highest accuracy compared to the multi-kernel SVM with polynomial and RBF kernels at the corresponding percentage of feature numbers. For a higher percentage of feature numbers, classification accuracy decreased because the larger amount of features included some redundant and confounding features.

The Most Discriminant Regions

In the classification of SCD and NC, 35 features (14 features from the MD network, 14 features from the FA network, and 7 features from the FN network) appeared in every fold of LOOCV (**Supplementary Table 2**). As shown in **Figure 5A**, the edges with great relative classification power included the connection between the left medial orbital of the superior frontal gyrus (ORBsupmed) and left rectus (REC), the connection between the left putamen (PUT) and left inferior partial lobe (IPL), the connection between the left orbital of the middle frontal gyrus (ORBmid) and left orbital of the superior frontal gyrus (ORBsup), the connection between the right ORBsup and right REC, and the connection between the right ORBsupmed and right ORBsup.

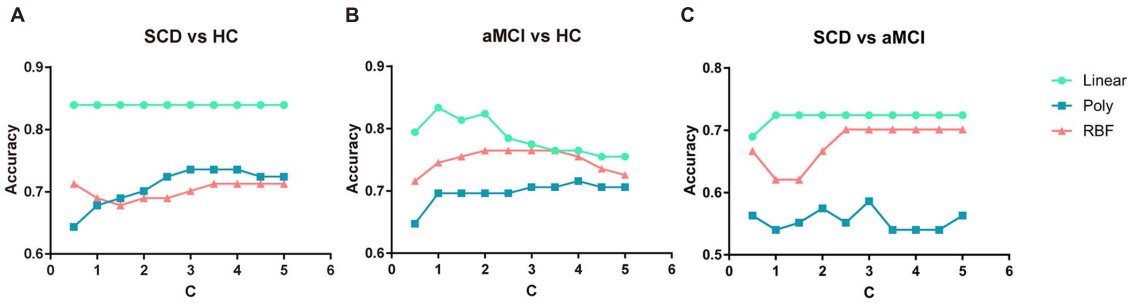

FIGURE 3 | Classification accuracy of three pairs of classifications under different parameter C value and different kernel functions. **(A)** The performance of classifying SCD and NC under different C values. **(B)** The performance of classifying aMCI and NC under different C values. **(C)** The performance of classifying SCD and aMCI under different C values. NC, normal control; SCD, subjective cognitive decline; aMCI, amnestic mild cognitive impairment.

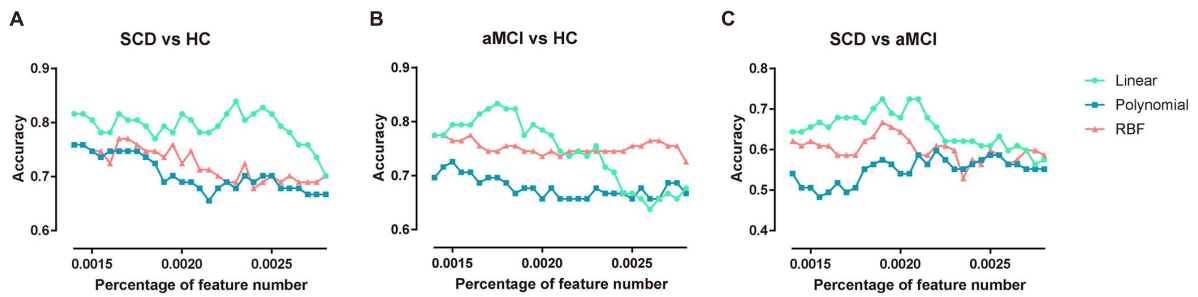

FIGURE 4 | Classification accuracy of three pairs of classifications under different feature numbers and different kernel functions. **(A)** The performance of classifying SCD patients and NC under different selected feature numbers. **(B)** The performance of classifying aMCI and NC under different selected feature numbers. **(C)** The performance of classifying SCD and aMCI under different selected feature numbers. NC, normal control; SCD, subjective cognitive decline; aMCI, amnestic mild cognitive impairment.

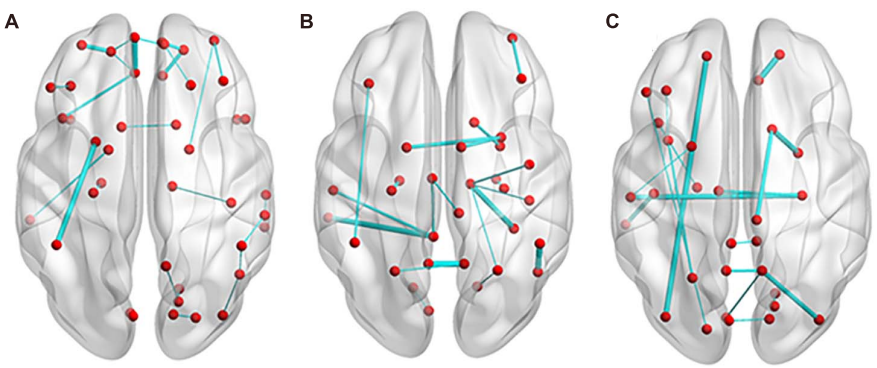

FIGURE 5 | Edges with most discrimination power. **(A)** In the classification of SCD and NC, 27 edges appeared in every fold of leave-one-out cross validation (LOOCV). **(B)** For the discrimination of aMCI and NC, 20 edges appeared in every fold of LOOCV. **(C)** Between SCD and aMCI, 18 edges appeared in every fold of LOOCV. The thickness of the edges represents the weight. NC, normal control; SCD, subjective cognitive decline; aMCI, amnestic mild cognitive impairment.

The total weights of the MD network, FA network, and FN network are 183.75, 145.84, and 47.58, respectively.

For the discrimination of aMCI and NC, 28 features (15 features from the MD network, nine features from the FA network, and 14 features from the FN network) appeared in every fold of LOOCV (**Supplementary Table 3**). As shown in **Figure 5B**, the edges with great relative classification power included the connection between the left precuneus (PCUN) and right PCUN, the connection between the right fusiform gyrus (FFG) and right thalamus (THA), the connection between the left middle temporal gyrus (MTG) and left posterior cingulum gyrus (PCG), and the connection between the right PUT and left PUT. The total weights of the MD network, FA network and FN network are 479.90, 137.37, and 115.09, respectively.

Between SCD and aMCI, 27 features (nine features from the MD network, 10 features from the FA network, and eight

features from the FN network) appeared in every fold of LOOCV (**Supplementary Table 4**). As shown in **Figure 5C**, the edges with great relative classification power included the connection between the right ORBsup and right REC, the connection between the right amygdala (AMYG) and right caudate (CAU), the connection between the left ORBsup and left inferior occipital gyrus (IOG), the connection between the right hippocampus (HIP) and left superior temporal gyrus (STG), and the connection between the right middle occipital gyrus (MOG) and right PCUN. The total weights of the MD network, FA network, and FN network are 183.43, 109.39, and 85.47, respectively.

DISCUSSION

In the current study, we established an efficient classification framework using a multi-kernel SVM based on multi-weight networks, enabling us to distinguish SCD and aMCI patients from NCs with accuracies of 83.9 and 83.3%, respectively. Previous studies have reported accuracy levels ranging from 59.2 to 88.9% for DTI data in the classification of aMCI and NC (Wee et al., 2012; Dyrba et al., 2015; Prasad et al., 2015). In our classification of SCD and NC, an area under the curve (AUC) value of 0.89 was obtained, with an accuracy of 83.9%, sensitivity of 77.8%, and specificity of 88.2%. Considering the relatively subtle alternations in the SCD population, our methods indicate its excellent diagnostic power. Moreover, our proposed classification framework herein relies on a simpler DTI scanning protocol and thus requires less image acquisition effort. This makes the approach more economical and clinically feasible.

In the classification of patients and NCs, the classification accuracy of the multi-kernel approach and direct data fusion method was significantly higher than that of any single weight network approach. The limited information provided by a single WM-weighted network may not be enough for distinguishing SCD and aMCI patients from NCs, as indicated by the much smaller AUC values. Although the multi-kernel approach resulted in slightly inferior accuracy than the direct data fusion method in classification between SCD and NC and the MD-weighted network in discrimination of aMCI and SCD, it was a great overall performer for the three pairs of classifications.

Direct data fusion method suffers from a major pitfall that it may produce models that effectively ignore the modalities that have less features while multi-kernel method does not have this problem because it treats all modalities as equivalent no matter how many features they have (Rathore et al., 2017). In this study, all modalities had the same number of features. So it seems that multi-kernel method did not have clear advantages in the classification between SCD and NC.

In the classification between SCD and aMCI, the results showed MD-weighted network outperformed other models, even the models from multi-weight networks. In addition, MD- and FA-weighted network almost equally contributed to the classification between SCD and NC, while the classification between aMCI and NC was mainly determined by MD-weighted network. It's probably because that MD is more sensitive than FA and FN in revealing early pathological process (Wang et al., 2020). Hence, FA- and FN- weighted network were so redundant for the classification between SCD and aMCI that adding them into the classification lowered the performance.

Comparing the performance between the classification between NCs and SCD patients and the classification between NCs and aMCI patients, we found that the model classifying SCD patients from NCs had slightly higher accuracy as it had comparatively higher specificity. However, the model classifying aMCI patients from NCs had higher sensitivity. These evidences means the classifier between aMCI and NC is more sensitive to patients than the classifier between SCD and NC. It's probably because SCD patients' WM alterations are subtle and intermediate between those in aMCI and NC (Brueggen et al., 2019). So the model classifying SCD patients from NCs tended to label test sample as NC while the model classifying aMCI patients from NCs can better identify patients.

Compared with NC, WM structural network patterns of patients with SCD and aMCI were significantly altered. The most discriminant regions selected for accurate detection of individuals with SCD were from MD- and FA-weighted networks, which include connections among the prefrontal cortex, orbitofrontal cortex, parietal lobe and temporal regions. Some regions like ORBsupmed and hippocampus locate in the default mode network, which are most vulnerable by amyloid (Wang et al., 2020). This indicates that the early deposition of amyloid may impaired the WM connectivities in these regions. From the view of graph theory, we have previously observed less network efficiency and connection strength of the brain structural connectome among these regions in the SCD group (Shu et al., 2018). Moreover, this impaired capacity of information transfer may derive from WM microstructure abnormalities with decreased FA and increased MD patterns observed in SCD subjects, which were demonstrated by previous studies (Selnes et al., 2012; Li et al., 2016). Between aMCI patients and NCs, most discriminative features were from the MD-weighted network and were distributed across parietal, temporal, and frontal lobes, which is largely in line with previous studies (Wee et al., 2011; Selnes et al., 2012; Shu et al., 2012). We can see that there was a difference in the distribution of selected features between the two models. In the classification between SCD and NC, the major features were the connections in frontal lobe while the features mostly located in posterior parietal lobe like precuneus and subcortical nuclei such as hippocampus and thalamus when classifying aMCI and NC. This difference may indicate a pathological development of AD that initial impairment in frontal lobe diffuses to the parietal lobe and subcortical nuclei, which is consistent with a preview study (Yan et al., 2019).

In addition, we investigated the effect of the constraint parameter C and selected feature number for classification performance. The multi-kernel SVM with a linear kernel was found to be most stable and robust to constraint parameter C and feature number compared with the multi-kernel SVM with a polynomial kernel and RBF kernel. These results suggest that the dataset that we acquired and analyzed in this study is more linearly separable than nonlinearly separable. This may be contradictory to reports in a previous study (Wee et al., 2011, 2012). The discrepancy might be due to

methodological differences in parameter selection and image analysis. The performance of the model decreased with an increase in the selected feature number when the feature number exceeded a value, which was nearly consistent among models with different kernel functions. This suggests there were some irrelevant and redundant features that had adverse impact on model performance. Therefore, it is important to perform feature selection before training models.

There are some limitations of our study that should be considered. One limitation of our current study is the relatively limited sample size compared to the dimensionality of the connectivity measurements. Although the LOOCV accuracy obtained may be optimistic, the restricted sample size did not allow us to explore other cross-validation techniques since the nonlinear SVM classifier used might be undertrained. Second, we only identified classification performance in patients with SCD, and longitudinal follow-up studies of the same study population are needed to further confirm our results. Third, the diagnosis of SCD and aMCI were not confirmed by amyloid PET. Forth, the generalizability of the findings is unclear without independent validation dataset. Finally, we only studied WM structural networks. In future studies, whether a combination of multimodal imaging (i.e., structural and/or functional MR imaging) and CSF biomarkers and genetic data provides additional diagnostic accuracy for the SCD population should be further clarified.

In conclusion, a multiple-kernel SVM based on a multi-weight network approach has been proposed to describe the complex WM connectivity patterns for automatically identifying individuals with SCD and aMCI from NCs. The promising results indicate that the proposed classification framework can facilitate and possibly improve individualized clinical diagnosis of alterations in brain structure associated with SCD.

DATA AVAILABILITY STATEMENT

The raw data supporting the conclusions of this article will be made available by the authors, without undue reservation.

ETHICS STATEMENT

The studies involving human participants were reviewed and approved by Beijing Xuanwu Hospital of Capital Medical University. The patients/participants provided their written informed consent to participate in this study.

AUTHOR CONTRIBUTIONS

YH and NS conceived, designed, revised, and finalized the manuscript. WH and XuL contributed equally to perform data analyses and wrote the manuscript. XiL and GK revised and provided critical input to the manuscript. All authors read and approved the final manuscript.

FUNDING

This work was supported by the National Natural Science Foundation of China (Grant Numbers 81671761, 81871425, 61633018, and 82020108031) and Hebei Provincial Natural Science Foundation, China (Grant Number F2019203515). The preliminary results were published in the conference abstract of Alzheimer's Association International Conferences (AAIC) (Li et al., 2018).

ACKNOWLEDGMENTS

The authors thank all the volunteers and patients for their participation in the study and reviewers for their insightful comments and suggestions.

SUPPLEMENTARY MATERIAL

The Supplementary Material for this article can be found online at: https://www.frontiersin.org/articles/10.3389/fnagi.2021.687927/full#supplementary-material

REFERENCES

Albert, M. S., Dekosky, S. T., Dickson, D., Dubois, B., Feldman, H. H., Fox, N. C., et al. (2011). The diagnosis of mild cognitive impairment due to Alzheimer's disease: recommendations from the National Institute on Aging-Alzheimer's Association workgroups on diagnostic guidelines for Alzheimer's disease. *Alzheimers Dement.* 7, 270–279. doi: 10.1016/j.jalz.2011.03.008

Amlien, I. K., and Fjell, A. M. (2014). Diffusion tensor imaging of white matter degeneration in Alzheimer's disease and mild cognitive impairment. *Neuroscience* 276, 206–215. doi: 10.1016/j.neuroscience.2014.02.017

Bai, F., Shu, N., Yuan, Y., Shi, Y., Yu, H., Wu, D., et al. (2012). Topologically convergent and divergent structural connectivity patterns between patients with remitted geriatric depression and amnestic mild cognitive impairment. *J. Neurosci.* 32, 4307–4318. doi: 10.1523/JNEUROSCI.5061-11.2012

Basser, P. J., and Pierpaoli, C. (1996). Microstructural and physiological features of tissues elucidated by quantitative-diffusion-tensor MRI. *J. Magn. Reson.* 111, 209–219.

Basser, P. J., Mattiello, J., and Lebihan, D. (1994). MR diffusion tensor spectroscopy and imaging. *Biophys. J.* 66, 259–267. doi: 10.1016/S0006-3495(94)80775-1

Brueggen, K., Dyrba, M., Cardenas-Blanco, A., Schneider, A., Fliessbach, K., Buerger, K., et al. (2019). Structural integrity in subjective cognitive decline, mild cognitive impairment and Alzheimer's disease based on multicenter diffusion tensor imaging. *J. Neurol.* 266, 2465–2474. doi: 10.1007/s00415-019-09429-3

Bullmore, E., and Sporns, O. (2009). Complex brain networks: graph theoretical analysis of structural and functional systems. *Nat. Rev. Neurosci.* 10, 186–198. doi: 10.1038/nrn2575

Cao, Q., Shu, N., An, L., Wang, P., Sun, L., Xia, M. R., et al. (2013). Probabilistic diffusion tractography and graph theory analysis reveal abnormal white matter structural connectivity networks in drug-naive boys with attention

deficit/hyperactivity disorder. *J. Neurosci.* 33, 10676–10687. doi: 10.1523/JNEUROSCI.4793-12.2013

De Martino, F., Valente, G., Staeren, N., Ashburner, J., Goebel, R., and Formisano, E. (2008). Combining multivariate voxel selection and support vector machines for mapping and classification of fMRI spatial patterns. *Neuroimage* 43, 44–58. doi: 10.1016/j.neuroimage.2008.06.037

Dosenbach, N. U., Nardos, B., Cohen, A. L., Fair, D. A., Power, J. D., Church, J. A., et al. (2010). Prediction of individual brain maturity using fMRI. *Science* 329, 1358–1361. doi: 10.1126/science.1194144

Dyrba, M., Grothe, M., Kirste, T., and Teipel, S. J. (2015). Multimodal analysis of functional and structural disconnection in Alzheimer's disease using multiple kernel SVM. *Hum. Brain Mapp.* 36, 2118–2131. doi: 10.1002/hbm.22759

Jessen, F., Amariglio, R. E., Van Boxtel, M., Breteler, M., Ceccaldi, M., Chetelat, G., et al. (2014). A conceptual framework for research on subjective cognitive decline in preclinical Alzheimer's disease. *Alzheimers Dement.* 10, 844–852. doi: 10.1016/j.jalz.2014.01.001

Leemans, A., and Jones, D. K. (2009). The B-matrix must be rotated when correcting for subject motion in DTI data. *Magn. Reson. Med.* 61, 1336–1349. doi: 10.1002/mrm.21890

Li, X. Y., Tang, Z. C., Sun, Y., Tian, J., Liu, Z. Y., and Han, Y. (2016). White matter degeneration in subjective cognitive decline: a diffusion tensor imaging study. *Oncotarget* 7, 54405–54414. doi: 10.18632/oncotarget.10091

Li, X., Huang, W., Shu, N., and Han, Y. (2018). P1-370: combined Multiplekernel support vector machine classifier and brain structural network features for the individual classification of subjective cognitive decline and amnestic mild cognitive impairment patients. *Alzheimers Dement.* 14, 437–438.

Molinuevo, J. L., Rabin, L. A., Amariglio, R., Buckley, R., Dubois, B., Ellis, K. A., et al. (2017). Implementation of subjective cognitive decline criteria in research studies. *Alzheimers Dement.* 13, 296–311. doi: 10.1016/j.jalz.2016.09.012

Mori, S., Crain, B. J., Chacko, V. P., and Van Zijl, P. C. (1999). Three-dimensional tracking of axonal projections in the brain by magnetic resonance imaging. *Ann. Neurol.* 45, 265–269.

Mourao-Miranda, J., Bokde, A. L., Born, C., Hampel, H., and Stetter, M. (2005). Classifying brain states and determining the discriminating activation patterns: support vector machine on functional MRI data. *Neuroimage* 28, 980–995. doi: 10.1016/j.neuroimage.2005.06.070

Pereira, F., Mitchell, T., and Botvinick, M. (2009). Machine learning classifiers and fMRI: a tutorial overview. *Neuroimage* 45, S199–S209. doi: 10.1016/j.neuroimage.2008.11.007

Peter, J., Scheef, L., Abdulkadir, A., Boecker, H., Heneka, M., Wagner, M., et al. (2014). Gray matter atrophy pattern in elderly with subjective memory impairment. *Alzheimers Dement.* 10, 99–108. doi: 10.1016/j.jalz.2013.05.1764

Petersen, R. C. (2004). Mild cognitive impairment as a diagnostic entity. *J. Intern. Med.* 256, 183–194. doi: 10.1111/j.1365-2796.2004.01388.x

Petersen, R. C., Lopez, O., Armstrong, M. J., Getchius, T. S. D., Ganguli, M., Gloss, D., et al. (2018). Practice guideline update summary: mild cognitive impairment: report of the guideline development, dissemination, and implementation subcommittee of the american academy of neurology. *Neurology* 90, 126–135. doi: 10.1212/WNL.0000000000004826

Prasad, G., Joshi, S. H., Nir, T. M., Toga, A. W., Thompson, P. M., and Alzheimers Disease Neuroimaging Initiative. (2015). Brain connectivity and novel network measures for Alzheimer's disease classification. *Neurobiol. Aging* 36(Suppl. 1), S121–S131. doi: 10.1016/j.neurobiolaging.2014.04.037

Rabin, L. A., Smart, C. M., and Amariglio, R. E. (2017). Subjective cognitive decline in preclinical Alzheimer's disease. *Annu. Rev. Clin. Psychol.* 13, 369–396. doi: 10.1146/annurev-clinpsy-032816-045136

Rakotomamonjy, A., Bach, F. R., Canu, S., and Grandvalet, Y. (2008). SimpleMKL. *J. Mach. Learn. Res.* 9, 2491–2521.

Rathore, S., Habes, M., Iftikhar, M. A., Shacklett, A., and Davatzikos, C. (2017). A review on neuroimaging-based classification studies and associated feature extraction methods for Alzheimer's disease and its prodromal stages. *Neuroimage* 155, 530–548. doi: 10.1016/j.neuroimage.2017.03.057

Sajda, P. (2006). Machine learning for detection and diagnosis of disease. *Annu. Rev. Biomed. Eng.* 8, 537–565. doi: 10.1146/annurev.bioeng.8.061505.095802

Selnes, P., Aarsland, D., Bjornerud, A., Gjerstad, L., Wallin, A., Hessen, E., et al. (2013). Diffusion tensor imaging surpasses cerebrospinal fluid as predictor of cognitive decline and medial temporal lobe atrophy in subjective cognitive impairment and mild cognitive impairment. *J. Alzheimers Dis.* 33, 723–736. doi: 10.3233/JAD-2012-121603

Selnes, P., Fjell, A. M., Gjerstad, L., Bjornerud, A., Wallin, A., Due-Tonnessen, P., et al. (2012). White matter imaging changes in subjective and mild cognitive impairment. *Alzheimers Dement.* 8, S112–S121. doi: 10.1016/j.jalz.2011.07.001

Shu, N., Liang, Y., Li, H., Zhang, J., Li, X., Wang, L., et al. (2012). Disrupted topological organization in white matter structural networks in amnestic mild cognitive impairment: relationship to subtype. *Radiology* 265, 518–527. doi: 10.1148/radiol.12112361

Shu, N., Wang, X., Bi, Q., Zhao, T., and Han, Y. (2018). Disrupted Topologic efficiency of white matter structural connectome in individuals with subjective cognitive decline. *Radiology* 286, 229–238. doi: 10.1148/radiol.2017162696

Smart, C. M., Karr, J. E., Areshenkoff, C. N., Rabin, L. A., Hudon, C., Gates, N., et al. (2017). Non-pharmacologic interventions for older adults with subjective cognitive decline: systematic review, meta-analysis, and preliminary recommendations. *Neuropsychol. Rev.* 27, 245–257. doi: 10.1007/s11065-017-9342-8

Sporns, O., Tononi, G., and Kotter, R. (2005). The human connectome: a structural description of the human brain. *PLoS Comput. Biol.* 1:e42. doi: 10.1371/journal.pcbi.0010042

Sun, Y., Dai, Z., Li, Y., Sheng, C., Li, H., Wang, X., et al. (2016). Subjective cognitive decline: mapping functional and structural brain changes-a combined resting-state functional and structural mr imaging study. *Radiology* 281, 185–192. doi: 10.1148/radiol.2016151771

Tzourio-Mazoyer, N., Landeau, B., Papathanassiou, D., Crivello, F., Etard, O., Delcroix, N., et al. (2002). Automated anatomical labeling of activations in SPM using a macroscopic anatomical parcellation of the MNI MRI single-subject brain. *Neuroimage* 15, 273–289. doi: 10.1006/nimg.2001.0978

Wang, X., Huang, W., Su, L., Xing, Y., Jessen, F., Sun, Y., et al. (2020). Neuroimaging advances regarding subjective cognitive decline in preclinical Alzheimer's disease. *Mol. Neurodegener.* 15:55. doi: 10.1186/s13024-020-00395-3

Wee, C. Y., Yap, P. T., Li, W., Denny, K., Browndyke, J. N., Potter, G. G., et al. (2011). Enriched white matter connectivity networks for accurate identification of MCI patients. *Neuroimage* 54, 1812–1822. doi: 10.1016/j.neuroimage.2010.10.026

Wee, C. Y., Yap, P. T., Zhang, D., Denny, K., Browndyke, J. N., Potter, G. G., et al. (2012). Identification of MCI individuals using structural and functional connectivity networks. *Neuroimage* 59, 2045–2056. doi: 10.1016/j.neuroimage.2011.10.015

Yan, T., Wang, Y., Weng, Z., Du, W., Liu, T., Chen, D., et al. (2019). Early-stage identification and pathological development of Alzheimer's Disease using multimodal MRI. *J. Alzheimers Dis.* 68, 1013–1027. doi: 10.3233/jad-181049

Zalesky, A., Fornito, A., Harding, I. H., Cocchi, L., Yucel, M., Pantelis, C., et al. (2010). Whole-brain anatomical networks: does the choice of nodes matter? *Neuroimage* 50, 970–983. doi: 10.1016/j.neuroimage.2009.12.027

Zalesky, A., Fornito, A., Seal, M. L., Cocchi, L., Westin, C. F., Bullmore, E. T., et al. (2011). Disrupted axonal fiber connectivity in schizophrenia. *Biol. Psychiatry* 69, 80–89. doi: 10.1016/j.biopsych.2010.08.022

Conflict of Interest: The authors declare that the research was conducted in the absence of any commercial or financial relationships that could be construed as a potential conflict of interest.

The reviewer LW declared a shared affiliation, with no collaboration, with several of the authors XuL and YH to the handling editor at the time of the review.

frontiers in Aging Neuroscience

ORIGINAL RESEARCH
published: 02 August 2021
doi: 10.3389/fnagi.2021.681208

The Associations Between White Matter Disruptions and Cognitive Decline at the Early Stage of Subcortical Vascular Cognitive Impairment: A Case–Control Study

*Yanan Qiao[1], Xuwen He[2], Junying Zhang[2], Ying Liang[3], Wen Shao[1], Zhanjun Zhang[2], Sihang Zhang[4] and Dantao Peng[1]**

[1] Department of Neurology, China-Japan Friendship Hospital, Beijing, China, [2] State Key Laboratory of Cognitive Neuroscience and Learning & IDG/McGovern Institute for Brain Research, Beijing Normal University, Beijing, China, [3] School of Biomedical Engineering, Capital Medical University, Beijing, China, [4] Department of Epidemiology and Biostatistics, School of Public Health, Peking University Health Science Center, Beijing, China

Objective: Emerging evidence suggests that white matter (WM) disruption is associated with the incidence of subcortical vascular cognitive impairment (SVCI). However, our knowledge regarding this relationship in the early stage of SVCI is limited. We aimed to investigate the associations between WM disruptions and cognitive declines at the early stage of SVCI.

Method: We performed a case–control study, involving 22 cases and 19 controls. The cases were patients at the early stage of SVCI, which was defined as subcortical ischemic vascular disease with normal global cognitive measures (pre-SVCI). The controls were healthy people matched by age, sex, and education years. We assessed the differences in a battery of neuropsychological tests between the two groups, investigated the diffusion changes in 40 WM tracts among the participants *via* an atlas-based segmentation strategy, and compared the differences between the cases and controls by multiple linear regression analysis. We then evaluated the relationships between diffusion indices and cognitive assessment scores by Pearson's correlation.

Results: The pre-SVCI group exhibited significant differences in the Montreal cognitive assessment (MoCA), Rey–Osterrieth Complex Figure (R-O)-copy, and Trail Making Test (TMT)-B test compared with the controls. Compared with the controls, some long associative and projective bundles, such as the right anterior corona radiata (ACR), the right inferior fronto-occipital fasciculus (IFOF), and the left external capsule (EC), were extensively damaged in cases after Bonferroni correction ($p < 0.05/40$). Damages to specific fibers, such as the right ACR, IFOF, and posterior thalamic radiation (PTR), exhibited significant correlations with declines in MoCA, R-O delay, and the Mini-Mental State Examination (MMSE), respectively, after Bonferroni correction ($p < 0.05/14$).

OPEN ACCESS

Edited by:
Jiehui Jiang,
Shanghai University, China

Reviewed by:
Hao Shu,
Southeast University, China
Janice Hau,
San Diego State University, United States

****Correspondence:***
Dantao Peng
pengdantao2000@163.com

Received: *16 March 2021*
Accepted: *04 June 2021*
Published: *02 August 2021*

Citation:
Qiao Y, He X, Zhang J, Liang Y, Shao W, Zhang Z, Zhang S and Peng D (2021) The Associations Between White Matter Disruptions and Cognitive Decline at the Early Stage of Subcortical Vascular Cognitive Impairment: A Case–Control Study. Front. Aging Neurosci. 13:681208. doi: 10.3389/fnagi.2021.681208

Conclusion: Long WM tracts, especially those in the right hemisphere, were extensively damaged in the pre-SVCI patients and correlated with declines in executive functions and spatial processing. Patients of pre-SVCI are likely at an ultra-early stage of SVCI, and there is a very high risk of this condition becoming SVCI.

Keywords: subcortical vascular cognitive impairment, subcortical ischemic vascular disease, diffusion tensor imaging, white matter hyperintensities, cognitive impairment

INTRODUCTION

Subcortical ischemic vascular disease (SIVD) is widespread among elderly individuals with asymptomatic lacunes and subcortical white matter (WM) hyperintensities (Carey et al., 2008), which is a homogeneous and the most common subtype of cerebral small vessel disease (CSVD) (Román et al., 2002; Rosenberg et al., 2014). Subcortical vascular cognitive impairment (SVCI) has a relatively insidious onset with gradual cognitive deterioration and a severe prognosis. In contrast to Alzheimer's disease (AD), SVCI is widely considered a disease that can be prevented and improved (Sachdev et al., 2014). Therefore, early identification is crucial for preventing SIVD from developing into vascular cognitive impairment (VCI) or dementia.

Most previous studies focused on the moderate and severe stages of SVCI, including subcortical vascular mild cognitive impairment (SvMCI) and subcortical vascular dementia (SVaD). They have revealed significant brain abnormalities in SVCI, such as declines in executive function, attention, processing speed, learning and memory, and lower brain perfusion or abnormal resting-state functional connectivities (FCs) in the thalamus, temporal lobe, inferior frontal lobe, and medial prefrontal cortex (Zhang et al., 2013; Reijmer et al., 2016; Sun et al., 2016; van Leijsen et al., 2019). Among them, WM damage is attracting ever-increasing attention because the pathomechanisms of cognitive injury in SIVD seem to be most closely related to diffuse areas of WM damage with neuronal loss, demyelination, and gliosis (D'Souza et al., 2018).

However, clinicians have also encountered many patients with moderate to serious SIVD with normal global cognition measures, such as the Mini-Mental State Examination (MMSE). The diagnostic criteria for vascular cognitive disorders (VASCOG statement) (Sachdev et al., 2014) suggest that vascular brain damage can exist without any evident cognitive impairment, and such asymptomatic individuals may be at an increased risk of future decline. This stage can be referred to as the pre-stage of SVCI (pre-SVCI). Limited studies focused on these pre-SVCI stage patients. Carey et al. (2008) found that although these patients appear "normal" with normal global cognition measures, they already have poorer executive functions and processing speed based on detailed assessments in different cognitive domains. Moreover, these patients have already exhibited extensive areas of microstructural changes in WM fibers and FC of resting-state networks (Liu et al., 2019a,b). However, these studies mostly used the MMSE as the screening scale. Compared with the Montreal cognitive assessment (MoCA), the MMSE lacks sensitivity in detecting executive function mediated by the frontal lobes where SIVD is often the most prevalent (Tullberg et al., 2004; Carey et al., 2008; Dong et al., 2010, 2016). Using the MMSE alone may lead to a false-negative bias when screening cognitively normal people at the pre-SVCI stage. Therefore, the application of the MMSE and MOCA together as screening scales can more accurately distinguish "normal" patients at the pre-SVCI stage.

Diffusion tensor imaging (DTI) is a sensitive and reliable method used to detect early WM alterations (Nitkunan et al., 2008). Recent DTI studies have demonstrated that patients with cognitive impairment exhibit decreased fractional anisotropy (FA) and increased mean diffusivity (MD), and different combinations of changes in axial diffusivity (DA) and radial diffusivity (DR) of WM tracts especially those located in thalamic- and caudate-prefrontal pathways, such as the corpus callosum (CC), external capsule, and superior and anterior thalamic radiations (ATR) (Chen et al., 2015; Reijmer et al., 2016; D'Souza et al., 2018). These WMs are significantly related to the cognitive domains of executive function, attention, and processing speed. However, limited studies using DTI have been performed in pre-SVCI patients and those that have been performed indicated inconsistent results (Liu et al., 2019a,b; Du et al., 2020). While Liu et al. (2019b) thought the pre-SVCI group exhibited widespread damages in whole-brain WM skeletons, Du et al. (2020) demonstrated well-preserved rich-club organization, less nodal strength loss, and disruption of connections shown in the local connections in the preclinical stage of SVCI. Therefore, to identify pre-SVCI patients at the early stage, we used DTI, which can identify changes in WM microstructure, to perform the current study. The early identification of pre-SVCI should contribute to promoting the further longitudinal studies and the early prevention and treatment of cognitive impairment due to CSVD.

In this explorative case–control study, using a battery of neuropsychological tests and DTI, we aimed to assess changes in 40 WM tracts that can mainly contain the key WMs in the brain (Zhang et al., 2014; Chen et al., 2015) and cognitive domains, including memory, spatial processing, language, attention, and executive function, between pre-SVCI patients and healthy controls. We hypothesized that WM integrity damage and cognitive decline already exist in pre-SVCI patients.

MATERIALS AND METHODS

Study Design and Participants

This case–control study, with prospective recruitment of pre-SVCI cases and a healthy control group, was performed

between January 2016 and January 2018 in the Department of Neurology in the China–Japan Friendship Hospital. Vascular risk factors including hypertension (HT), hypercholesterolemia (HC), coronary atherosclerotic disease (CAD), diabetes mellitus (DM), and smoking and alcohol history were collected from all patients.

The patients with pre-SVCI (case group) were defined as having SIVD on MRI with normal global cognitive measures. Two different radiologists assessed the anatomical MRI scans which contained T1-weighted, T2-weighted, fluid-attenuated inversion recovery (FLAIR) and gave nearly the same reports. The patient will be excluded to whom the two radiologists give the different reports. The SIVD patients met the following brain imaging criteria of SIVD (Román et al., 2002): (1) Binswanger-type WM lesions: hyperintensities extending into the periventricular and deep WM, extending caps (>10 mm as measured parallel to the ventricle) or irregular halos (>10 mm with broad, irregular margins and extending into deep WM), and diffusely confluent hyperintensities (>25 mm, irregular shape) or extensive WM changes (diffuse hyperintensity without focal lesions); (2) lacunar cases: multiple lacunas (>2) in the deep gray matter and at least moderate white-matter lesions; and (3) absence of hemorrhages and cortical and/or territorial infarcts and watershed infarcts, signs of normal-pressure hydrocephalus, and specific causes of white-matter lesions. In addition, the visual Fazekas scale was used on FLAIR images to rate the severity of WM hyperintensities (WMHs) into mild (grade 1), moderate (grade 2), and severe (grade 3) WMHs (Fazekas et al., 1987).

The inclusion criteria for the pre-SVCI included (1) literate Han Chinese, education $\geq$ 6 years, and aged 50–80 years; (2) met with the brain imaging criteria of SIVD above (Román et al., 2002); (3) no cognitive complaints; (4) no impairments of daily life activities with clinical dementia rating (CDR) = 0.5 (Hughes et al., 1982); activities of daily living (ADL) < 23 (Salloway et al., 2004); and (5) normal cognitive screening assessments with MMSE > 26, and MoCA-Beijing version score $\geq$ 26 (Folstein et al., 1975; Petersen, 2004).

The healthy controls were defined as persons with no neurological and psychiatric disorders, no abnormal findings on conventional brain MRI (brain anatomical MRI was reported normal by the same two radiologists who assessed the MRI for the pre-SVCI group) (Carey et al., 2008; Liu et al., 2019a,b), and no cognitive complaints. For each case, one control was matched by age (within 2 years), sex, and years of education. All enrolled subjects underwent a clinical interview, neurologic examinations, comprehensive neuropsychological assessments, and MRI scanning.

Subjects who met the following criteria were excluded: (1) no completion of neuropsychological testing; (2) Hamilton depression scale score > 17, or anxiety; (3) new strokes within 3 months before baseline; (4) signs of large vessel disease, such as cortical and/or cortico-subcortical non-lacunar territorial infarcts and watershed infarcts or hemorrhages; and (5) leukoencephalopathy as a result of other causes, such as normal pressure hydrocephalus, multiple sclerosis, brain irradiation, and metabolic diseases.

Neuropsychological Evaluation

We evaluated the cognition status of the subjects with a modified National Institute of Neurological Disorders and Stroke and Canadian Stroke Network-Canadian Stroke Network protocol (Hachinski et al., 2006; Wong et al., 2013). The following cognitive variables were included in the present analysis: (1) global cognition was measured by the MMSE and MoCA; (2) episodic memory was evaluated by the Auditory Verbal Learning Test (AVLT) and the Rey–Osterrieth Complex Figure Delay Tests (R-O delay); (3) language function was examined by the Boston Naming Test (BNT) and the Category Verbal Fluency Test; (4) visuospatial ability was assessed by the Clock Drawing Test (CDT) and the Rey–Osterrieth Complex Figure Copy Test (R-O copy); (5) executive function was assessed by the Trail Making Tests B (TMT-B) and the Stroop Test C right and time; and (6) attention was evaluated by the Digital Span Test (DST) and the Trail Making Test A (TMT-A). The evaluations of all participants were conducted by the same qualified psychologist, and each evaluation required 90 min.

MRI Acquisition

The MRI data were acquired on a 3.0T Siemens MAGNETOM Prisma MRI scanner. Participants lay supine with the head snugly fixed by a belt. Foam pads were used to restrict head motion, and earplugs were used to minimize the scanner noise. Subjects were told to relax, keep their eyes closed, and remain awake. T1-weighted, sagittal 3D magnetization prepared rapid gradient echo sequences were acquired and covered the entire brain [192 sagittal slices, repetition time (TR) = 2,300 ms, echo time (TE) = 2.32 ms, slice thickness = 0.90 mm, flip angle = 8°, inversion time = 900 ms]. T2-weighted images (TR = 5000 ms, TE = 105 ms, slice thickness = 3 mm, flip angle = 150°, number of slices = 33) and T2-FLAIR images (TR = 9000 ms, TE = 81 ms, slice thickness = 3 mm, flip angle = 150°, number of slices = 25) were acquired. Two sets of DTI data scans were acquired for every subject and then averaged during the data preprocessing. DTI images covering the whole brain were acquired using a single-shot, twice-refocused, diffusion-weighted echo-planar imaging sequence with the following scan parameters: TR = 8,000 ms; TE = 60 ms; 30 diffusion-weighted directions with a b value of 1,000 s/mm^2, and a single image with a b value of 0 s/mm^2; slice thickness = 2 mm; no interslice gap; 75 axial slices; field of view = 282 mm^2; and voxel size = 2 mm^3.

DTI Image Processing

All of the DTI image preprocessing and analyses described below were implemented using a pipeline tool for diffusion MRI, named "Pipeline for analyzing brain diffusion images" (PANDA) (Cui et al., 2013). A similar procedure was shown in our previous studies (Chen et al., 2015; Zhang et al., 2015). First, the DICOM files of all subjects were converted into NIfTI images using the dcm2nii tool embedded in MRI cron. Second, the brain mask was estimated, which was required for the subsequent processing steps. Third, the non-brain spaces in the raw images were removed, leading to a reduced image size, which reduced memory cost and sped up processing in subsequent steps.

Fourth, each diffusion-weighted image (DWI) was coregistered to the b0 image using an affine transformation to correct the eddy-current-induced distortions and slow bulk motion-induced inter-gradient misalignment (Chen et al., 2015). The diffusion gradient directions were adjusted accordingly. Fifth, a voxel-wise calculation of the tensor matrix and the diffusion tensor metrics were yielded for each subject, including FA, MD, DA, and DR.

Mean Diffusion Metrics by an Atlas-Based Segmentation Strategy

White matter atlases (Mori et al., 2008) (e.g., the ICBM-DTI-81 WM labels atlas and the JHU WM tractography atlas) in the standard space allow for parcelation of the WMs into multiple regions of interest (ROIs), each representing a labeled region in the atlas. In our current study, to investigate the diffusion changes in specific tracts, the ICBM-DTI-81 WM label atlas was used to parcel the WMs into 48 ROIs, and only the 40 ROIs in cerebral regions (we focused on the 40 WM tracts within the cerebrum and did not consider the other 8 ROIs within the cerebellum and brain stem) were used for the analysis. Then, the regional mean diffusion metrics including the FA, the MD, the DA, and the DR (Soares et al., 2013; Amlien and Fjell, 2014) were calculated by averaging the values within each region of the WM atlas.

Statistical Analysis

We used IBM SPSS Statistics for Windows version 22.0 (IBM Corp., Armonk, NY, United States) for all statistical analyses. We assessed the normality of the data with Shapiro–Wilk tests and Q–Q plots. Independent two-sample t-tests were used to assess between-group differences for quantitative variables. The Pearson Chi-square test and Fisher exact probability test were used to compare proportions for categorical variables. Multiple linear regression analysis was used to evaluate the group differences in neuropsychological assessments and diffusion metrics including FA, MD, DR, and DA of the atlas-based ROIs. Age, gender, education years, and groups are the variables when the multiple linear regression analysis was performed. Pearson's correlation analysis was used to calculate the correlation between diffusion metrics of atlas-based tracts with significant group effects and behavior performance (age, gender, and education years were included as covariates). For all analyses, a two-tailed p value < 0.05 was considered statistically significant. Bonferroni correction was performed in multiple comparisons of 40 atlas-based ROIs ($p < 0.05/40$) and correlation between diffusion metrics of atlas-based tracts with significant group effects and neuropsychological assessments ($p < 0.05/14$).

RESULTS

Demographics and Neuropsychological Testing

According to the inclusion and exclusion criteria, we ultimately enrolled 22 cases and 19 healthy controls. **Figure 1** shows the participant enrollment process. The demographic and clinical characteristics of the participants are presented in **Table 1**. The distribution of age and education years was normal. There were no significant differences in age, sex, years of education, history of DM, CAD, HC, alcohol intake, and smoking. As expected, there was a significant difference in the history of hypertension between the two groups.

Table 2 presents the cognitive assessment results. The pre-SVCI group exhibited significant differences in the MoCA, Rey–Osterrieth Complex Figure (R-O)-copy, and TMT-B test compared with the H group.

Results of the Atlas-Based Tract ROIs

Table 3 shows the diffusion metrics of WM tracts which are significantly different when comparing the pre-SVCI group to the H group. Compared with the control group, the pre-SVCI group exhibited significantly decreased FA in the right anterior corona radiata (ACR) and inferior fronto-occipital fasciculus (IFOF) ($p < 0.05$). Meanwhile, increased MD in the right side of the posterior thalamic radiation (PTR), the inferior longitudinal fasciculus (ILF), the IFOF, and the left side of the external capsule (EC) were observed ($p < 0.05$). The case group also exhibited increased DA on the bilateral side of the ILF, the EC, and the right side of the PTR and increased DR in the left EC and the right IFOF ($p < 0.05$). Among them, FA values of right ACR, MD values of left EC and right IFOF, DA values of left EC, and DR values of right IFOF are still significantly different after Bonferroni correction ($p < 0.05/40$) for the multiple comparisons (**Figure 2**).

Correlations Between ROI-Wise Diffusion Metrics and Behaviors

We examined the relationship between the mean values of the diffusion metrics of the ROIs extracted from the significant WM regions and neuropsychological scores of the pre-SVCI group and healthy controls. In the pre-SVCI group, the mean FA values of the right ACR were significantly correlated with the MoCA ($r = 0.699$, $p = 0.001$). The R-O delay was positively correlated with the mean FA values ($r = 0.600$, $p = 0.003$) but negatively correlated with the MD values ($r = -0.441$, $p = 0.040$) of the right IFOF. Negative correlations were observed between the mean MD value of the left EC and the Category Verbal Fluency Test (CVFT) (animal) ($r = -0.564$, $p = 0.006$). Negative correlations can be seen between the mean MD value of the right PTR and the Stroop C-right and MMSE scores ($r = -0.458$, $p = 0.032$ and $r = -0.607$, $p = 0.003$, respectively). Notably, the correlations between the FA of right ACR and MoCA, the FA of right IFOF and RO-delay, and the MD of right PTR and MMSE were still significant after Bonferroni correction ($p < 0.05/14$) for multiple comparison (**Figure 3**).

In the control group, there was no negative or positive correlation between the diffusion metrics of the significant WM tracts and neuropsychological scores.

DISCUSSION

In the current study, we evaluated WM alterations and cognitive declines in the early stage of SVCI (pre-SVCI), compared with a

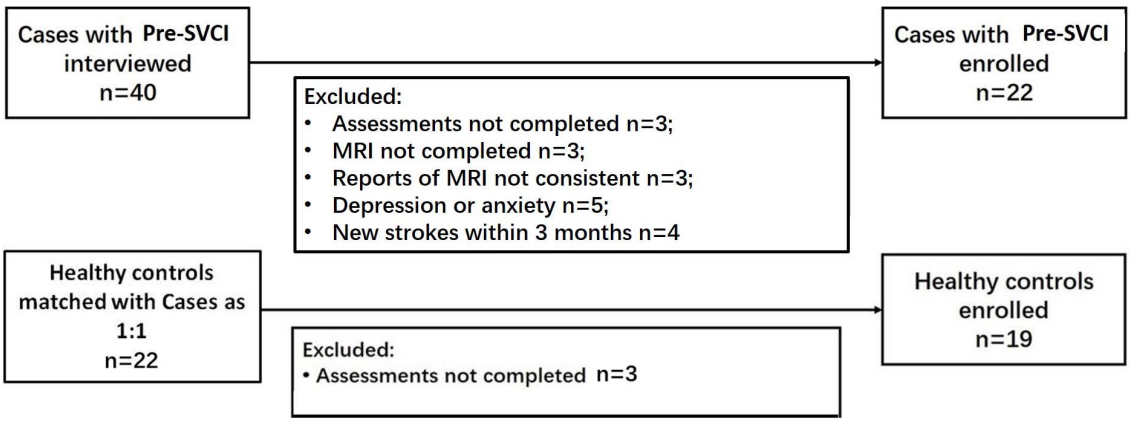

FIGURE 1 | Flowcharts for study enrollment of case participants and control participants. Pre-SVCI is subcortical ischemic vascular disease with normal global cognition measures.

TABLE 1 | Demographics and clinical characteristics of each group.

	Pre-SVCI (*n* = 22)	H (*n* = 19)	t/X^2	Sig
Sex (male/female)	10/12	7/12	0.312	0.577
Age (years)	65.14 ± 1.67	61.58 ± 1.80	−1.543	0.131
Education (years)	12.36 ± 0.76	12.68 ± 0.81	0.304	0.763
Smoking (n)	8 (36.4%)	5 (26.3%)	0.475	0.491
Alcohol (n)	2 (9.1%)	0 (0%)	–	0.490
HT (n)	11 (50.0%)	2 (10.5%)	5.627	0.018*
HC (n)	11 (50.0%)	4 (21.1%)	2.540	0.111
CAD (n)	4 (18.2%)	2 (10.5%)	0.062	0.804
DM (n)	8 (36.4%)	5 (26.3%)	0.475	0.491

*Values are mean ± SD. The comparisons of years of age and education between the two groups were performed using the t-test. The Pearson chi-square was used when expected cell counts are equal to 5 or more. Continuity correction was used when expected cell counts ≥ 1 and < 5. If these conditions are not met, the Fisher exact probability test was be used instead of the chi-square test. P < 0.05 was considered significant. *P < 0.05; HT, hypertension; HC, hypercholesterolemia; CAD, coronary atherosclerotic disease; DM, diabetes mellitus; pre-SVCI, subcortical ischemic vascular disease with normal global cognition measures; H, healthy.*

well-matched healthy group. We made several observations. (1) Executive function and spatial processing were already declined in the pre-SVCI patients. (2) Some long associative and projective bundles were damaged in the pre-SVCI group. In particular, the right IFOF was found to have decreased FA, increased MD, and increased DR. (3) The mean values of the diffusion indices in some specific WM tracts in the pre-SVCI group were significantly correlated with neuropsychological assessments that related to executive functions or spatial processing.

According to the brain connectome theory, disruptions in the global connections between cortical and subcortical networks are partially related to damage in WM fibers (Lo et al., 2010). Thus, SVCI which is characterized by extensive cerebral WM lesions in the periventricular/deep cerebral WM (Román et al., 2002; Rosenberg et al., 2014; Tu et al., 2017), tends to result in cognitive impairment. Previous studies (Biesbroek et al., 2017; Tu et al., 2017; Liu et al., 2019b) have revealed that SVCI patients exhibit nearly global changes with decreased FA and increased MD in WM tracts especially those located in thalamic-prefrontal and caudate-prefrontal pathways. It has been proven that these two pathways are markedly related to neuropsychological assessments of executive function, attention, and processing speed in many task-related functional studies (Block et al., 2007; Müller-Oehring et al., 2015; Liu et al., 2018). Our study showed that the TMT-B assessment was significantly different between the patients and healthy controls. However, the above studies mainly focus on patients at the stages of SvMCI or SVaD and neglect the asymptomatic stage of disease when individuals suffer vascular damage without cognitive impairment.

Our study found that some types of long associative and projective WM such as right ACR, IFOF, and left EC were extensively damaged in the pre-SVCI group even given the strictest Bonferroni correction for multiple comparisons. However, Liu et al. (2019b) found that approximately all cerebral WMs were symmetrically involved in the pre-SVCI group but were less distinct than those in the SVCI group. Our different result from the previous study was mainly due to the discrepant inclusion criteria for including the pre-SVCI group. We used two screening scales, i.e., the MMSE and MoCA, both to include patients with normal global measures. The MoCA is considered more sensitive for screening VCI, which surpasses the well-known limitations of the MMSE (Dong et al., 2010). Because of the lack of sensitivity in detecting

TABLE 2 | Neuropsychological tests result for each group.

	Pre-SVCI (n = 22)	H (n = 19)	t-value	Effect sizes (standardized beta)	p-value
General mental status					
MMSE MoCA	27.95 ± 1.53 26.55 ± 0.67	28.79 ± 1.36 27.97 ± 0.74	−1.302 −3.984	−0.208 −0.544	0.201 <0.001*
Episodic memory					
AVLT-delay	7.73 ± 5.86	6.95 ± 2.46	0.132	0.022	0.895
AVLT-total	32.55 ± 7.42	33.79 ± 6.75	−0.444	−0.076	0.660
R-O delay	18.23 ± 6.89	17.47 ± 7.71	−0.696	−0.115	0.491
Spatial processing					
R-O copy	34.55 ± 2.24	35.37 ± 0.96	−2.151	−0.405	0.045*
CDT	24.00 ± 6.44	24.32 ± 6.77	0.176	0.030	0.861
Executive function					
Stroop C-time	98.57 ± 10.35	78.82 ± 11.40	1.982	0.311	0.055
Stroop C-right	47.80 ± 2.26	45.31 ± 2.49	1.186	0.194	0.243
TMT b	163.57 ± 15.56	113.71 ± 17.16	5.746	0.700	<0.001*
Language ability					
BNT	26.68 ± 1.89	25.79 ± 2.02	1.302	0.213	0.201
CVFT	42.00 ± 12.98	49.58 ± 9.36	−1.946	−0.312	0.059
Attention					
SDMT	34.77 ± 17.08	39.37 ± 7.96	−0.633	−0.099	0.531
TMTa	51.82 ± 31.76	51.84 ± 12.23	−0.087	−0.015	0.931

*The differences in neuropsychological scores between the two groups were tested for significance with multiple linear regression analysis adjusted for age, sex, and education. $P < 0.05$ was considered significant. *$P < 0.05$; MMSE, Mini-Mental State Examination; MoCA, Montreal cognitive assessment; AVLT, Auditory Verbal Learning Test; R-O delay, Rey–Osterrieth Complex Figure delay tests; R-O copy, Rey–Osterrieth Complex Figure copy test; CDT, Clock drawing task; BNT, Boston Naming Test; CVFT, Category Verbal Fluency Test; SDMT, Symbol Digit Modalities Test; TMT, Trail Making Test; Clock Drawing Test; pre-SVCI, subcortical ischemic vascular disease with normal global cognition measures; H, healthy.*

TABLE 3 | Group comparisons of mean DTI diffusion metrics of white matter tracts in two groups.

	Pre-SVCI (n = 22)	H (n = 19)	t-value	Effect sizes (standardized beta)	p-value
ACR.R					
FA	0.3778 ± 0.0213	0.4013 ± 0.0213	−4.150	−0.566	<0.001*
ILF.L					
DA (10^{-3})	1.290 ± 0.495	1.250 ± 0.260	2.549	0.402	0.015
EC.R					
DA (10^{-3})	1.084 ± 0.415	1.046 ± 0.198	3.269	0.471	0.002
PTR.R					
MD (10^{-4})	8.025 ± 4.056	7.749 ± 3.484	2.885	0.436	0.007
DA (10^{-3})	1.329 ± 0.441	1.297 ± 0.443	2.352	0.367	0.024
ILF.R					
MD (10^{-4})	8.129 ± 3.673	7.887 ± 2.014	2.294	0.361	0.028
DA (10^{-3})	1.277 ± 0.438	1.250 ± 0.261	2.307	0.366	0.027
EC.L					
MD (10^{-4})	7.938 ± 3.569	7.537 ± 2.232	4.331	0.586	<0.001*
DA(10^{-3})	1.103 ± 0.457	1.058 ± 0.261	3.893	0.550	<0.001*
DR(10^{-4})	6.391 ± 0.366	6.016 ± 0.247	3.399	0.505	0.002
IFOF.R					
FA	0.43795 ± 0.0219	0.4575 ± 0.0301	−2.337	−0.369	0.025
MD (10^{-4})	7.703 ± 2.302	7.436 ± 1.519	3.841	0.540	<0.001*
DR(10^{-4})	5.690 ± 0.265	5.371 ± 0.226	3.780	0.538	<0.001*

*The differences in diffusion metrics (i.e., FA, MD, DA, and DR) of white matter tracts between the two groups were tested for significance with multiple linear regression analysis adjusted for age, sex, and education. $P < 0.05$ was considered significant. * is significant at $p < 0.05/40$ after Bonferroni correction; FA, fractional anisotropy; MD, mean diffusivity; DA, axial diffusivity; DR, radial diffusivity; pre-SVCI, subcortical ischemic vascular disease with normal global cognition measures; H, healthy. L, left; R, right. For the abbreviations of WM tracts, see* ***Supplementary Table 1****.*

subtle cognitive changes, particularly visuospatial and executive function impairments, using the MMSE alone may lead to a false-negative bias in the recruitment of patients. In our study, the patients had a significant difference compared with the healthy controls in MoCA, but not the MMSE, further confirming the above view.

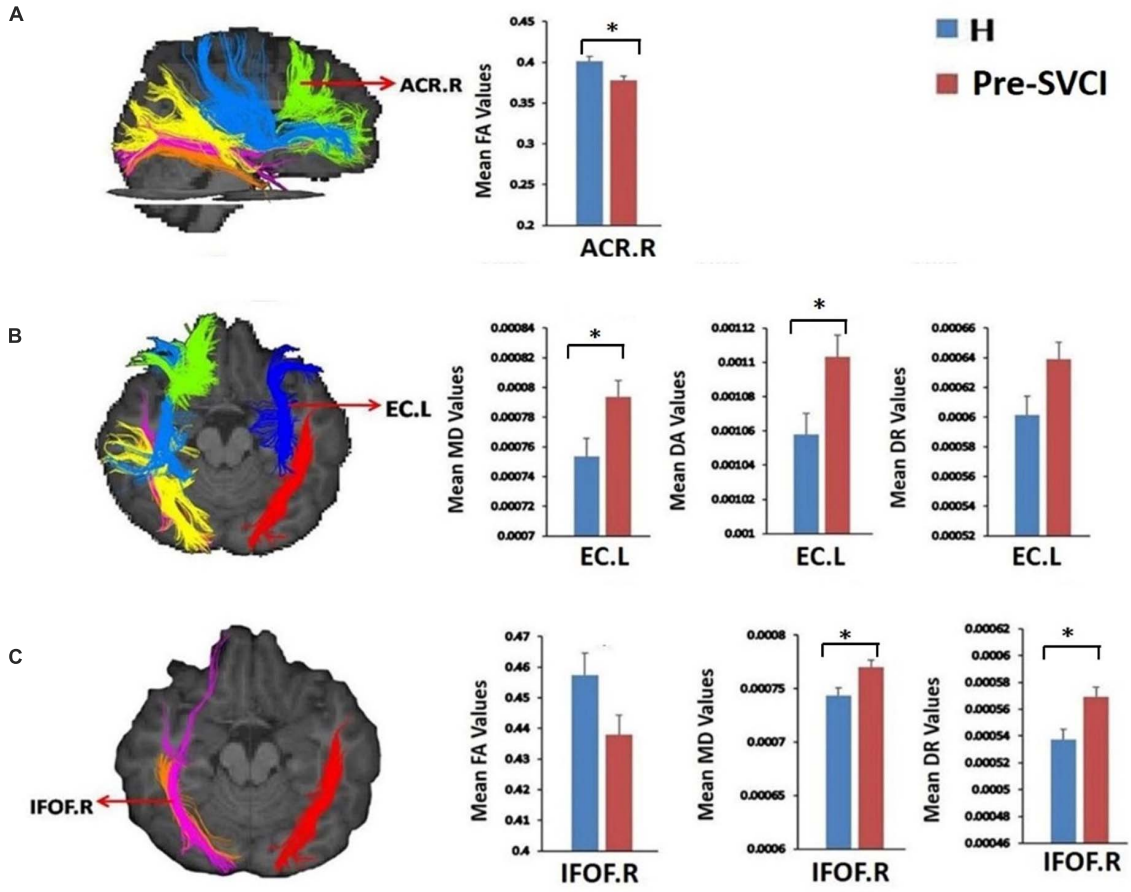

FIGURE 2 | The tracts where diffusion metrics remained significant between the two groups after Bonferroni correction for multiple comparisons. **(A)** Mean FA values of ACR.R; **(B)** Mean MD, DA, and DR values of EC.L; **(C)**, mean FA, MD, and DR values of IFOF.R. *is significant at $p < 0.05/40$ after Bonferroni correction. FA, fractional anisotropy, MD, mean diffusivity; DA, axial diffusivity; DR, radial diffusivity; pre-SVCI, subcortical ischemic vascular disease with normal global cognition measures; H, healthy; L, left; R, right; ACR, anterior corona radiata; EC, external capsule; IFOF, inferior fronto-occipital fasciculus.

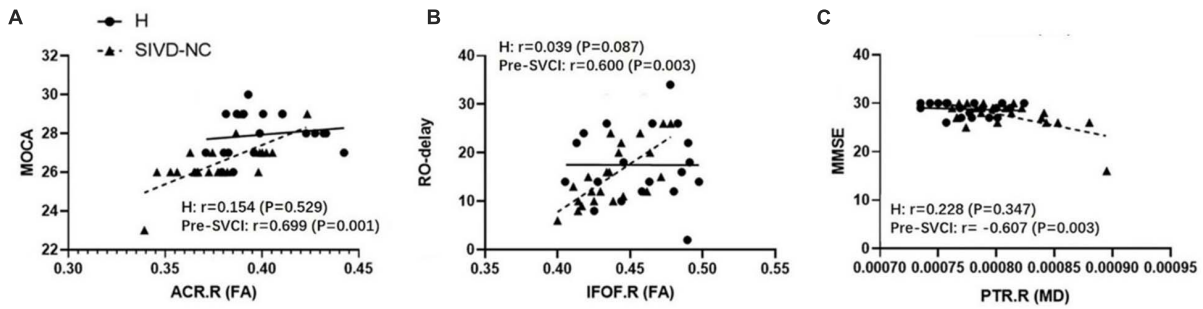

FIGURE 3 | The significant correlations between ROI-wise diffusion metrics and behaviors in the pre-SVCI group and the H group after Bonferroni correction for multiple comparisons. **(A)** MoCA. **(B)** R-O delay. **(C)** MMSE. MoCA, Montreal cognitive assessment; R-O delay, Rey–Osterrieth Complex Figure delay tests; MMSE, Mini-Mental State Examination; FA, fractional anisotropy, MD, mean diffusivity; pre-SVCI, subcortical ischemic vascular disease with normal global cognition measures; H, healthy; L, left; R, right; ACR, anterior corona radiata; IFOF, inferior fronto-occipital fasciculus; PTR, posterior thalamic radiation.

Our results demonstrated that IFOF might be one kind of WM tracts that are much more easily demyelinated in vascular disease. Notably, three of the DTI-derived indices changed with decreased FA, increased MD, and increased DR in the right IFOF. IFOF is one of the longest major associative bundles that was recognized and depicted in 2007 (Schmahmann and Pandya, 2007). It connects the occipital cortex, the superior parietal lobe, and the temporo-basal areas to the frontal cortex (Martino et al., 2010).

Some DTI studies have shown that the IFOF is a probable crucial tract in reading, attention, and visual processing, especially the right IFOF in spatial attention and neglect (Catani and Thiebaut de Schotten, 2008; Urbanski et al., 2008, 2011). Consistently, based on the correlation analysis between WM impairment and cognitive decline, we found that the RO-delay, which represents long-term memory and visuospatial function, was positively correlated with the FA value of the right IFOF after the strictest Bonferroni correction, which further identified that the damage of IFOF is correlated with the decline of visual processing. The right IFOF may be impaired at the early stage because of its long course, which can easily result in myelin injury. According to our findings, the DR of IFOF.R was significantly increased. An increasing DR reflects a decline in myelin sheath integrity (Soares et al., 2013). Thus, we can further infer that long tracts, such as the IFOF, which course from the front regions to the end of the brain, are probably predamaged before the prefrontal thalamus circus. Furthermore, we found that the significantly damaged tracts in the pre-SVCI patients were mainly concentrated in the right hemisphere. The integrity of IFOF, PTR, and ATR in the right hemisphere was extensively damaged which were also correlated with the declines in visuospatial and executive functions. So far, studies (Kleinman et al., 2007; Giussani et al., 2010; Kontaxopoulou et al., 2017; Vilasboas et al., 2017; Bernard et al., 2018) have increasingly found that the non-dominant right hemisphere is responsible for primary cognitive functions such as visuospatial, intentional process, and social cognition. This is consistent with the findings in our study. But why the WMs in right hemisphere are damaged earlier than left hemisphere in SIVD patients is not clear.

There are several limitations in this study. First, although according to previous studies, we supposed that SIVD patients with normal global cognitive measures could be pre-SVCI patients, we could not clearly determine whether these pre-SVCI patients will develop into SVCI, remain unchanged, or improve as a consequence of brain plasticity or reserve capacity. This bias leads our results to underestimate the difference between the cases and the controls. Besides, as previous studies, we did not report measures of head motion for each group and just rely on registration-based correction methods that cannot eliminate the full effects of head motion on the DW images (Yendiki et al., 2014). Therefore, longitudinal follow-up studies with a large-scale and more accurate and comprehensive methods to correct head motion artifacts are needed in the future. Second, our study focused on only WM alterations, but whether cerebral blood perfusion or other elements are correlated with cognitive decline still needs further exploration. Moreover, we did not assess the degree of gray matter atrophy, which can have an impact on cognitive functions. Third, this study involved Chinese individuals, and other ethnic groups need to be further studied.

CONCLUSION

In summary, our study indicated that in SIVD patients, even with normal global cognitive measures, some types of long course tracts, especially the tracts in the right hemisphere, were damaged. Furthermore, damage to these tracts was associated with a decline in some specific cognitive domains, such as executive functions and spatial processing domains. These results indicated that pre-SVCI patients are likely at an ultra-early stage of SVCI, and there was a very high risk of this condition becoming SVCI. To prevent the progression of SVCI, longitudinal studies are needed to explore the dynamic changes from the early stage to the clinical stage of SVCI and to evaluate the value of DTI in predicting the process of SVCI.

DATA AVAILABILITY STATEMENT

The raw data supporting the conclusions of this article will be made available by the authors, without undue reservation.

ETHICS STATEMENT

The studies involving human participants were reviewed and approved by the Institutional Review Board of China-Japan Friendship Hospital. The patients/participants provided their written informed consent to participate in this study. Written informed consent was obtained from the individual(s) for the publication of any potentially identifiable images or data included in this article.

AUTHOR CONTRIBUTIONS

YQ and DP: conceptualization. XH and JZ: methodology. YQ, XH, YL, and WS: formal analysis and investigation. YQ: writing – original draft preparation. SZ: writing, review, and editing. ZZ and DP: supervision. All authors contributed to the article and approved the submitted version.

FUNDING

This study was supported by grants from the Hospital Foundation of China-Japan Friendship Hospital (No. 2016-2-QN-21), the Natural Science Foundation of China (No. 81974220), and the National Key R&D Program of China (No. 2016YFC1306301).

ACKNOWLEDGMENTS

Thanks are given to Xin Li and Yu Sun for the writing assistance.

SUPPLEMENTARY MATERIAL

The Supplementary Material for this article can be found online at: https://www.frontiersin.org/articles/10.3389/fnagi.2021.681208/full#supplementary-material

REFERENCES

Amlien, I. K., and Fjell, A. M. (2014). Diffusion tensor imaging of white matter degeneration in Alzheimer's disease and mild cognitive impairment. *Neuroscience* 276, 206–215. doi: 10.1016/j.neuroscience.2014.02.017

Bernard, F., Lemee, J. M., Ter Minassian, A., and Menei, P. (2018). Right hemisphere cognitive functions: from clinical and anatomic bases to brain mapping during awake craniotomy part I: clinical and functional anatomy. *World Neurosurg.* 118, 348–359. doi: 10.1016/j.wneu.2018.05.024

Biesbroek, J. M., Weaver, N. A., and Biessels, G. J. (2017). Lesion location and cognitive impact of cerebral small vessel disease. *Clin. Sci.* 131, 715–728. doi: 10.1042/cs20160452

Block, A. E., Dhanji, H., Thompson-Tardif, S. F., and Floresco, S. B. (2007). Thalamic-prefrontal cortical-ventral striatal circuitry mediates dissociable components of strategy set shifting. *Cereb. Cortex* 17, 1625–1636. doi: 10.1093/cercor/bhl073

Carey, C. L., Kramer, J. H., Josephson, S. A., Mungas, D., Reed, B. R., Schuff, N., et al. (2008). Subcortical lacunes are associated with executive dysfunction in cognitively normal elderly. *Stroke* 39, 397–402. doi: 10.1161/strokeaha.107.491795

Catani, M., and Thiebaut de Schotten, M. (2008). A diffusion tensor imaging tractography atlas for virtual in vivo dissections. *Cortex* 44, 1105–1132. doi: 10.1016/j.cortex.2008.05.004

Chen, Y., Wang, A., Tang, J., Wei, D., Li, P., Chen, K., et al. (2015). Association of white matter integrity and cognitive functions in patients with subcortical silent lacunar infarcts. *Stroke* 46, 1123–1126. doi: 10.1161/strokeaha.115.008998

Cui, Z., Zhong, S., Xu, P., He, Y., and Gong, G. (2013). PANDA: a pipeline toolbox for analyzing brain diffusion images. *Front. Hum. Neurosci.* 7:42. doi: 10.3389/fnhum.2013.00042

D'Souza, M. M., Gorthi, S. P., Vadwala, K., Trivedi, R., Vijayakumar, C., Kaur, P., et al. (2018). Diffusion tensor tractography in cerebral small vessel disease: correlation with cognitive function. *Neuroradiol. J.* 31, 83–89. doi: 10.1177/1971400916682753

Dong, Y., Sharma, V. K., Chan, B. P., Venketasubramanian, N., Teoh, H. L., Seet, R. C., et al. (2010). The montreal cognitive assessment (MoCA) is superior to the mini-mental state examination (MMSE) for the detection of vascular cognitive impairment after acute stroke. *J. Neurol. Sci.* 299, 15–18. doi: 10.1016/j.jns.2010.08.051

Dong, Y., Xu, J., Chan, B. P., Seet, R. C., Venketasubramanian, N., Teoh, H. L., et al. (2016). The montreal cognitive assessment is superior to National Institute of Neurological Disease and Stroke-Canadian Stroke Network 5-minute protocol in predicting vascular cognitive impairment at 1 year. *BMC Neurol.* 16:46. doi: 10.1186/s12883-016-0570-y

Du, J., Zhu, H., Zhou, J., Lu, P., Qiu, Y., Yu, L., et al. (2020). Structural brain network disruption at preclinical stage of cognitive impairment due to cerebral small vessel disease. *Neuroscience* 449, 99–115. doi: 10.1016/j.neuroscience.2020.08.037

Fazekas, F., Chawluk, J. B., Alavi, A., Hurtig, H. I., and Zimmerman, R. A. (1987). MR signal abnormalities at 1.5 T in Alzheimer's dementia and normal aging. *AJR Am. J. Roentgenol.* 149, 351–356. doi: 10.2214/ajr.149.2.351

Folstein, M. F., Folstein, S. E., and McHugh, P. R. (1975). "Mini-mental state". A practical method for grading the cognitive state of patients for the clinician. *J. Psychiatr. Res.* 12, 189–198.

Giussani, C., Pirillo, D., and Roux, F. E. (2010). Mirror of the soul: a cortical stimulation study on recognition of facial emotions. *J. Neurosurg.* 112, 520–527. doi: 10.3171/2009.5.jns081522

Hachinski, V., Iadecola, C., Petersen, R. C., Breteler, M. M., Nyenhuis, D. L., Black, S. E., et al. (2006). National Institute of Neurological Disorders and Stroke-Canadian Stroke Network vascular cognitive impairment harmonization standards. *Stroke* 37, 2220–2241. doi: 10.1161/01.str.0000237236.88823.47

Hughes, C. P., Berg, L., Danziger, W. L., Coben, L. A., and Martin, R. L. (1982). A new clinical scale for the staging of dementia. *Br. J. Psychiatry* 140, 566–572. doi: 10.1192/bjp.140.6.566

Kleinman, J. T., Sepkuty, J. P., Hillis, A. E., Lenz, F. A., Heidler-Gary, J., Gingis, L., et al. (2007). Spatial neglect during electrocortical stimulation mapping in the right hemisphere. *Epilepsia* 48, 2365–2368.

Kontaxopoulou, D., Beratis, I. N., Fragkiadaki, S., Pavlou, D., Yannis, G., Economou, A., et al. (2017). Incidental and intentional memory: their relation with attention and executive functions. *Arch. Clin. Neuropsychol.* 32, 519–532. doi: 10.1093/arclin/acx027

Liu, J., Wang, C., Diao, Q., Qin, W., Cheng, J., and Yu, C. (2018). Connection disruption underlying attention deficit in subcortical stroke. *Radiology* 288, 186–194. doi: 10.1148/radiol.2018171730

Liu, X., Chen, L., Cheng, R., Luo, T., Lv, F., Fang, W., et al. (2019a). Altered functional connectivity in patients with subcortical ischemic vascular disease: a resting-state fMRI study. *Brain Res.* 1715, 126–133. doi: 10.1016/j.brainres.2019.03.022

Liu, X., Cheng, R., Chen, L., Luo, T., Lv, F., Gong, J., et al. (2019b). Alterations of white matter integrity in subcortical ischemic vascular disease with and without cognitive impairment: a TBSS study. *J. Mol. Neurosci.* 67, 595–603. doi: 10.1007/s12031-019-01266-3

Lo, C. Y., Wang, P. N., Chou, K. H., Wang, J., He, Y., and Lin, C. P. (2010). Diffusion tensor tractography reveals abnormal topological organization in structural cortical networks in Alzheimer's disease. *J. Neurosci.* 30, 16876–16885. doi: 10.1523/jneurosci.4136-10.2010

Martino, J., Brogna, C., Robles, S. G., Vergani, F., and Duffau, H. (2010). Anatomic dissection of the inferior fronto-occipital fasciculus revisited in the lights of brain stimulation data. *Cortex* 46, 691–699. doi: 10.1016/j.cortex.2009.07.015

Mori, S., Oishi, K., Jiang, H., Jiang, L., Li, X., Akhter, K., et al. (2008). Stereotaxic white matter atlas based on diffusion tensor imaging in an ICBM template. *Neuroimage* 40, 570–582. doi: 10.1016/j.neuroimage.2007.12.035

Müller-Oehring, E. M., Sullivan, E. V., Pfefferbaum, A., Huang, N. C., Poston, K. L., Bronte-Stewart, H. M., et al. (2015). Task-rest modulation of basal ganglia connectivity in mild to moderate Parkinson's disease. *Brain Imaging Behav.* 9, 619–638. doi: 10.1007/s11682-014-9317-9

Nitkunan, A., Barrick, T. R., Charlton, R. A., Clark, C. A., and Markus, H. S. (2008). Multimodal MRI in cerebral small vessel disease: its relationship with cognition and sensitivity to change over time. *Stroke* 39, 1999–2005. doi: 10.1161/strokeaha.107.507475

Petersen, R. C. (2004). Mild cognitive impairment as a diagnostic entity. *J. Intern. Med.* 256, 183–194. doi: 10.1111/j.1365-2796.2004.01388.x

Reijmer, Y. D., Fotiadis, P., Piantoni, G., Boulouis, G., Kelly, K. E., Gurol, M. E., et al. (2016). Small vessel disease and cognitive impairment: the relevance of central network connections. *Hum. Brain Mapp.* 37, 2446–2454. doi: 10.1002/hbm.23186

Román, G. C., Erkinjuntti, T., Wallin, A., Pantoni, L., and Chui, H. C. (2002). Subcortical ischaemic vascular dementia. *Lancet Neurol.* 1, 426–436. doi: 10.1016/s1474-4422(02)00190-4

Rosenberg, G. A., Bjerke, M., and Wallin, A. (2014). Multimodal markers of inflammation in the subcortical ischemic vascular disease type of vascular cognitive impairment. *Stroke* 45, 1531–1538. doi: 10.1161/strokeaha.113.004534

Sachdev, P., Kalaria, R., O'Brien, J., Skoog, I., Alladi, S., Black, S. E., et al. (2014). Diagnostic criteria for vascular cognitive disorders: a VASCOG statement. *Alzheimer Dis. Assoc. Disord.* 28, 206–218. doi: 10.1097/wad.0000000000000034

Salloway, S., Ferris, S., Kluger, A., Goldman, R., Griesing, T., Kumar, D., et al. (2004). Efficacy of donepezil in mild cognitive impairment: a randomized placebo-controlled trial. *Neurology* 63, 651–657. doi: 10.1212/01.wnl.0000134664.80320.92

Schmahmann, J. D., and Pandya, D. N. (2007). The complex history of the fronto-occipital fasciculus. *J. Hist. Neurosci.* 16, 362–377. doi: 10.1080/09647040600620468

Soares, J. M., Marques, P., Alves, V., and Sousa, N. (2013). A hitchhiker's guide to diffusion tensor imaging. *Front. Neurosci.* 7:31. doi: 10.3389/fnins.2013.00031

Sun, Y., Cao, W., Ding, W., Wang, Y., Han, X., Zhou, Y., et al. (2016). Cerebral blood flow alterations as assessed by 3D ASL in cognitive impairment in patients with subcortical vascular cognitive impairment: a marker for disease severity. *Front. Aging Neurosci.* 8:211. doi: 10.3389/fnagi.2016.00211

Tu, M. C., Lo, C. P., Huang, C. F., Hsu, Y. H., Huang, W. H., Deng, J. F., et al. (2017). Effectiveness of diffusion tensor imaging in differentiating early-stage subcortical ischemic vascular disease, Alzheimer's disease and normal ageing. *PLoS One* 12:e0175143. doi: 10.1371/journal.pone.0175143

Tullberg, M., Fletcher, E., DeCarli, C., Mungas, D., Reed, B. R., Harvey, D. J., et al. (2004). White matter lesions impair frontal lobe function regardless of their location. *Neurology* 63, 246–253. doi: 10.1212/01.wnl.0000130530.55104.b5

Urbanski, M., Thiebaut de Schotten, M., Rodrigo, S., Catani, M., Oppenheim, C., Touze, E., et al. (2008). Brain networks of spatial awareness: evidence from diffusion tensor imaging tractography. *J. Neurol. Neurosurg. Psychiatry* 79, 598–601. doi: 10.1136/jnnp.2007.126276

Urbanski, M., Thiebaut de Schotten, M., Rodrigo, S., Oppenheim, C., Touze, E., Meder, J. F., et al. (2011). DTI-MR tractography of white matter damage in stroke patients with neglect. *Exp. Brain Res.* 208, 491–505. doi: 10.1007/s00221-010-2496-8

van Leijsen, E. M. C., van Uden, I. W. M., Bergkamp, M. I., van der Holst, H. M., Norris, D. G., Claassen, J., et al. (2019). Longitudinal changes in rich club organization and cognition in cerebral small vessel disease. *Neuroimage Clin.* 24:102048. doi: 10.1016/j.nicl.2019.102048

Vilasboas, T., Herbet, G., and Duffau, H. (2017). Challenging the myth of right nondominant hemisphere: lessons from corticosubcortical stimulation mapping in awake surgery and surgical implications. *World Neurosurg.* 103, 449–456. doi: 10.1016/j.wneu.2017.04.021

Wong, A., Xiong, Y. Y., Wang, D., Lin, S., Chu, W. W., Kwan, P. W., et al. (2013). The NINDS-Canadian stroke network vascular cognitive impairment neuropsychology protocols in Chinese. *J. Neurol. Neurosurg. Psychiatry* 84, 499–504. doi: 10.1136/jnnp-2012-304041

Yendiki, A., Koldewyn, K., Kakunoori, S., Kanwisher, N., and Fischl, B. (2014). Spurious group differences due to head motion in a diffusion MRI study. *Neuroimage* 88, 79–90. doi: 10.1016/j.neuroimage.2013.11.027

Zhang, J., Wang, Y., Wang, J., Zhou, X., Shu, N., Wang, Y., et al. (2014). White matter integrity disruptions associated with cognitive impairments in type 2 diabetic patients. *Diabetes* 63, 3596–3605. doi: 10.2337/db14-0342

Zhang, S., Chen, Y., Liu, Z., Zhang, J., Li, X., Cui, R., et al. (2015). Association of white matter integrity and cognitive functions in Chinese non-demented elderly with the APOE ϵ4 allele. *J. Alzheimers Dis.* 48, 781–791. doi: 10.3233/jad-150357

Zhang, X., Li, G., Guo, L., Nie, K., Jia, Y., Zhao, L., et al. (2013). Age-related alteration in cerebral blood flow and energy failure is correlated with cognitive impairment in the senescence-accelerated prone mouse strain 8 (SAMP8). *Neurol. Sci.* 34, 1917–1924. doi: 10.1007/s10072-013-1407-8

Conflict of Interest: The authors declare that the research was conducted in the absence of any commercial or financial relationships that could be construed as a potential conflict of interest.

Publisher's Note: All claims expressed in this article are solely those of the authors and do not necessarily represent those of their affiliated organizations, or those of the publisher, the editors and the reviewers. Any product that may be evaluated in this article, or claim that may be made by its manufacturer, is not guaranteed or endorsed by the publisher.

frontiers in Aging Neuroscience

ORIGINAL RESEARCH
published: 03 August 2021
doi: 10.3389/fnagi.2021.680706

Electroacupuncture Pretreatment Prevents Cognitive Impairment Induced by Cerebral Ischemia–Reperfusion via Adenosine A1 Receptors in Rats

*Yiyi Shi, Qinxue Dai, Binbin Ji, Luping Huang, Xiuxiu Zhuang, Yunchang Mo and Junlu Wang**

Department of Anesthesiology, The First Affiliated Hospital of Wenzhou Medical University, Wenzhou, China

A previous study has demonstrated that pretreatment with electroacupuncture (EA) induces rapid tolerance to focal cerebral ischemia. In the present study, we investigated whether adenosine receptor 1 (A1 R) is involved in EA pretreatment-induced cognitive impairment after focal cerebral ischemia in rats. Two hours after EA pretreatment, focal cerebral ischemia was induced by middle cerebral artery occlusion for 120 min in male Sprague-Dawley rats. The neurobehavioral score, cognitive function [as determined by the Morris water maze (MWM) test], neuronal number, and the Bax/Bcl-2 ratio was evaluated at 24 h after reperfusion in the presence or absence of CCPA (a selective A1 receptor agonist), DPCPX (a selective A1 receptor antagonist) into left lateral ventricle, or A1 short interfering RNA into the hippocampus area. The expression of the A1 receptor in the hippocampus was also investigated. The result showed that EA pretreatment upregulated the neuronal expression of the A1 receptor in the rat hippocampus at 90 min. And EA pretreatment reversed cognitive impairment, improved neurological outcome, and inhibited apoptosis at 24 h after reperfusion. Pretreatment with CCPA could imitate the beneficial effects of EA pretreatment. But the EA pretreatment effects were abolished by DPCPX. Furthermore, A1 receptor protein was reduced by A1 short interfering RNA which attenuated EA pretreatment-induced cognitive impairment.

Keywords: EA pretreatment, A1 receptors, cognitive impairment, ischemia–reperfusion, cerebral ischemia

OPEN ACCESS

Edited by:
Jiehui Jiang,
Shanghai University, China

Reviewed by:
C. Yan Cheng,
Population Council, United States
Xiaomei Shao,
Zhejiang University, China

***Correspondence:**
Junlu Wang
wangjunlu973@163.com

Received: *15 March 2021*
Accepted: *07 June 2021*
Published: *03 August 2021*

Citation:
Shi Y, Dai Q, Ji B, Huang L, Zhuang X, Mo Y and Wang J (2021) Electroacupuncture Pretreatment Prevents Cognitive Impairment Induced by Cerebral Ischemia–Reperfusion via Adenosine A1 Receptors in Rats. Front. Aging Neurosci. 13:680706. doi: 10.3389/fnagi.2021.680706

INTRODUCTION

Stroke is one of the leading causes of morbidity and mortality worldwide, and is a serious threat to human health (Tsai et al., 2013). And cerebral ischemia is one of the main causes accounting for more than 80% of stroke (Goldstein et al., 2001). These patients with cerebral ischemia may have different degrees of memory problems and learning impairment (Longstreth and Dikmen, 1993), and more than 75% of stroke patients suffer from selective cognitive impairment including memory, orientation, language, and attention (Cumming et al., 2013). The hippocampus is the main area for memory and learning behavior in the brain (Lagali et al., 2010), especially, the CA1 region in the hippocampus is so sensitive to ischemia that neurons are easily damaged (Caraci et al., 2008). Although many studies have explored the mechanism of ischemic stroke, the

study of cognitive function recovery caused by stroke still needs to be further explored to determine effective treatment.

Adenosine is an essential neuromodulator in the brain, and has been shown to play a role in neuroprotection (Bortolotto et al., 2015). And adenosine functions as a signaling molecule through the activation of four distinct adenosine receptors—denoted as A1, A2A, A2B, and A3 (Cunha, 2001). Adenosine receptors are part of the serine/threonine kinase family and widely expressed in the brain (Lopes et al., 2011). High levels of A1 receptors (A1R) are found in the hippocampus, cortex, and cerebellum, while lower levels are found in the striatum (Shen et al., 2008). It has been shown that adenosine A1 receptors tend to play a role in inhibiting presynaptic nerve activity (Gomes et al., 2011). And adenosine may regulate memory and prevent cognitive impairment (Bortolotto et al., 2015). Adenosine A1 receptors mediate dopamine, glutamate, and BNDF signaling via adenosine, regulate synaptic plasticity in the learning and memory area of brain, and act at a molecular and cellular level to regulate cognitive function (Chen, 2014). In addition, studies about humans and animals support the fact that adenosine receptor activity leads to cognitive enhancement, neuroprotection, and reversal of cognitive impairment in animal models of Alzheimer, Parkinson, Huntington, and schizophrenia (Chen et al., 2014). A subsequent study suggests a more central role for A1R in the selective pattern of neuronal loss in the hippocampus, which is associated with global ischemia (Okamura et al., 2004). The results indicate cognitive impairment caused by cerebral ischemia may be mediated through the adenosine neurotransmitter system (Mioranzza et al., 2011). Therefore, the role of adenosine A1 receptors in cognitive impairment caused by cerebral ischemia has not been studied in depth.

Acupuncture is critical to traditional Chinese medicine, while electroacupuncture (EA) combines traditional Chinese acupuncture and modern electrical techniques. In addition, studies have shown that electroacupuncture pretreatment can mediate cognitive impairment of cerebral ischemia reperfusion injury through the CaM-CaMKIV-CREB (Zhang et al., 2016b) and Wnt pathways (He X. et al., 2016; Chen et al., 2020). Meanwhile, electroacupuncture treatment can prevent the impact of cognitive impairment in the brain, heart, and limbs of ischemia reperfusion patients (Chen et al., 2012; Yuan et al., 2014). Furthermore, several recent studies have reported that A1R may confer acute tolerance to cerebral ischemic/reperfusion injury by electroacupuncture, which plays a neuroprotective role via reducing the release of glutamate (Constantino et al., 2015), limiting postsynaptic depolarization and Ca^{2+} influx (Lubitz et al., 1995). However, the link between electroacupuncture pretreatment effect in cognitive function and adenosine A1 receptors is not entirely clear, and more evidence is needed to prove it.

The aim of our study is to investigate the relationship between electroacupuncture pretreatment and adenosine A1 receptors at pharmacological and genetic levels, and to show that electroacupuncture pretreatment prevents cognitive impairment induced by cerebral ischemia–reperfusion via adenosine A1 receptors.

MATERIALS AND METHODS

Animals

Male Sprague Dawley rats (270–310 g) obtained from the Laboratory Animal Center of Sliaike in Shanghai, China were used in the study and were housed at a constant temperature (24 ± 0.5°C) with a humidity of 55 ± 5% on a controlled 12 h light/dark cycle (light on at 7 a.m.) with free access to food and water. The experimental protocol was approved by the Special Committee on Animal Welfare of Wenzhou Medical University, and all animals were treated humanely according to the National Institutes of Health for Care and Use of Laboratory Animals (NIH Publication No. 85-23, 1996, United States). All efforts were made to minimize animal discomfort and the number of animals used.

Electroacupuncture Treatment

EA pretreatment was performed as described previously (He X. et al., 2016). Before intraperitoneal injection of chloral hydrate (3 ml/kg), the rats fasted for 12 h. The stainless acupuncture needles (diameter of 0.3 mm) were inserted into the Baihui (GV 20) acupuncture point at a depth of 2–3 mm, which is located at the intersection of the sagittal midline and the line linking the rat ears. Stimulation was generated by the EA apparatus (Model No. 200110510586; Nanjing Jisheng Medical Technology Co., Ltd., Nanjing, China), and the stimulation parameters were set as follows: Disperse wave, 2/15 Hz; electric current, 1 mA; 30 min of each treatment.

Surgery

Focal cerebral ischemia was induced by middle cerebral artery occlusion (MCAO) using the intraluminal filament technique as previously described (He X. et al., 2016). Two hours after EA pretreatment, the SD rats were deeply anesthetized by chloral hydrate (3 ml/kg). Following exposure of the left common carotid artery (CCA), internal carotid artery (IC), external carotid artery (EC), and proximal branches of the EC, the left MCA was occluded by an insertion of a 0.38 ± 0.02 nylon monofilament suture (Beijing Cinontech Co., Ltd., China) with its tip rounded through the CCA, resulting in the occlusion of the left MCA at its origin. Regional cerebral blood flow was monitored using a transcranial laser Doppler flow meter (PeriFlux5000; Perimed AB, Sweden). MCAO was considered sufficient if the regional cerebral blood flow demonstrated a sharp decrease to 20% of the baseline (pre-ischemic) level; if not, the animal was excluded. Reperfusion was accomplished by withdrawing the suture after 120 min of ischemia. In the group of sham-operated rats, all of the surgical procedures were performed, however, the ICA was not occluded. Following surgery, the rats were transferred to their cage until the animals were completely conscious. Just after reperfusion, the rats were kept in the preoperative state until sampling.

During surgeries for AV-shA1R ($1*10^{11}$ PFU/ml) or AV–shCTRL, 2-chloro-N6-cyclopentyladenosine (0.01 mmol/L, CCPA, Sigma- Aldrich, United States), and 8-cyclopentyl-1, 3-dipropylxanthine (0.01 mmol/L, DPCPX, Sigma-Aldrich, United States) injections were conducted under chloral hydrate

(3 ml/kg, ip). Using aseptic techniques, the rats were injected stereotaxically into the left hippocampus at anterior-posterior = -4.80 mm, medial-lateral = 3.20 mm, and dorsal-ventral = -3.2 mm from the bregma or lateral ventricles at anterior-posterior = -0.05 mm, medial-lateral = 1.80 mm, and dorsal-ventral = -4.8 mm from the bregma of the left hemisphere with recombinant. A 33 g needle was inserted under the epineurium of the nerve, 5 μl of virus, CCPA, or DPCPX solution was injected at 0.25 μl/min, using a 10 μl syringe (Hamilton, Switzerland) mounted onto the stereotaxic apparatus and connected to pump. After the injection was completed, the needle was left for 10 min before being removed to stabilize the injection. Then the skin was sutured together and the wound was closed. Animals were allowed to fully recover from the surgery. At 1 h 30 min after the EA treatment, the rats were injected with CCPA or DPCPX and underwent surgery for MCAO. At 48 h after the AV injection, rats underwent surgery for EA and MCAO which were performed as described above.

Neurobehavioral Evaluation

Twenty-four hours after reperfusion, an observer who was blind to the animal groups assessed the rats using a neurobehavioral test as described previously (Feng et al., 2013). And the scores were determined as follows: Score 0, no neurological deficit; score 1 (failure to fully extend the effect side), mild deficits; scores 2 (circling to the effect side) and 3 (falling to the effect side), moderate deficits; and score 4 (loss of walking), severe deficits.

Morris Water Maze

The Morris water maze (MWM) test was performed as described previously (Wang et al., 2012) with some modifications. This test was used to assess the effects of EA pretreatment on MCAO-induced learning and memory dysfunctions in rats. This consisted of a circular pool of 100 cm in diameter and 60 cm in height, which was divided factitiously into four equal quadrants (SW, NW, NE, and SE). The pool was filled with water (25 ± 1°C) premixed with black non-toxic paint to make it opaque; a platform (10 cm in diameter) was immersed 2 cm under the surface of the water in one of the four identical quadrants. The pool was located in an illuminated room with some external cues, which remained in the same location throughout the training and testing period.

After induction of global cerebral ischemia for 120 min with EA treatment, each animal was subjected to an acquisition trial and a probe trial. In each acquisition trial, the rats were individually placed in the pool facing the wall at one point randomly selected from different starting points. Rats (n = 6) were trained for six blocks on the MWM (three trials per block) 24 h after reperfusion, with a 30-min rest period between trials. During the acquisition trial, the rats were allowed to escape by swimming to the platform and the escape latency was recorded with a cutoff time of 60 s. If the rats failed to locate the platform within 60 s, they were gently guided to the platform and allowed to stay on it for 15 s. Mean escape latency time (MES) to locate the hidden platform in the water maze was recorded as an index of acquisition or learning. Animals that could not swim due to injury following ischemia were eliminated. After the training, the platform was removed from the pool to start the 60 s spatial probe trial test initiated 1 h following the completion of the last trial. Swimming behaviors, including escape latency, swimming speed, and the average time spent in the target quadrant, were monitored using a computer-controlled video-tracking system (CG-400 Image Acquisition System; Institute of Materia Medica, Chinese Academy of Medical Sciences, Shanghai, China). The distance swum, entries and time spent in the target quadrant, and the mean swimming speed were recorded. The mean time taken by the animal searching for the hidden platform in the target quadrant was noted as an index of spatial memory.

Western Blotting and RT-PCR

To investigate alterations in A1 receptor, Bcl-2, and Bax protein expression, the rats were anesthetized with 10% chloral hydrate (3 ml/kg, ip) and decapitated, the hippocampus of the left hemispheres were dissected and stored at −80°C until analysis. In brief, the brain tissues were sonicated by radioimmunoprecipitation assay lysis buffer (Solarbio, Beijing, China) with phenylmethylsulfonyl fluoride on ice. Tissue extracts were centrifuged at 12,000 × g at 4°C for 15 min. Samples (40 μg of protein each) were separated by electrophoresis in 12% polyacrylamide gels and transferred to a polyvinylidene fluoride (PVDF) membrane. Non-specific bindings were blocked with 5% non-fat dry milk in Tris buffer saline (TBS) in 0.1% Tween-20 at room temperature for 120 min. After washing, membranes were subsequently incubated with respective primary antibodies: Anti-A1 receptor antibody (1:1,000, Abcam, Cambridge, United Kingdom), β-actin polyclonal antibody (1:5,000, Biogot Technology, Co., Ltd., United States), Anti-Bcl-2 antibody (1:1,000, Abcam, Cambridge, United Kingdom) and Anti-Bax antibody (1:5,000, Abcam, Cambridge, United Kingdom) in primary antibody dilution buffer (beyotime, China) at 4°C overnight. Subsequently, the samples were incubated for 1 h at room temperature with horseradish peroxidase-conjugated goat anti-rabbit secondary antibodies (1:5,000, Biogot Technology, Co., Ltd., United States). Membranes were developed by an ECL (Electro-Chemi-Luminescence) technique. The signal intensity of the blots was measured through Image Lab analysis software (Bio-Rad, United States).

Total RNA was extracted from the hippocampus of the left hemispheres with TRIzol reagent (Invitrogen, Carlsbad, CA). The reaction mixture was incubated at 50°C for 30 min for reverse transcription. The continuous amplification program (CFX96 Real-Time PCR Detection System) consisted of one cycle at 95°C for 15 min and 40 cycles at 94°C for 20 s, 60°C for 20 s, and 72°C for 35 s. The expression of GAPDH was used as the internal reference gene and relative quantification was performed using the 2-ΔΔCt method.

Nissl Staining

Nissl staining was performed to detect neuronal injury. The brain tissue was collected from the rat after removing its head and then embedded with paraffin. Sections were cut to 3 μM thickness using a sliding microtome. Following washing with phosphate-buffered saline (PBS; pH 7.4), tissue sections were dried at 65°C for 2 h, Nissl stained (Leagene, Beijing, China),

and dehydrated with 70, 80, 90, and 100% ethanol, respectively, for 5 min each. The sections were cleared in xylene for 5 min twice and finally mounted with neutral balsam (Solarbio, Beijing, China). Stained tissue sections were observed in the hippocampus by light microscopy (BX60; Olympus, Tokyo, Japan).

Statistical Analysis

Statistical analysis was performed using SPSS 12.0 for Windows (SPSS Inc., Chicago, IL). Data are expressed as the means ± SEM, with the exception of neurobehavioral scores which are expressed as median. All the data were analyzed using one-way analysis of variance (ANOVA) with Fisher's protected least significance difference test, with the exception of the data of the neurobehavioral scores which were analyzed by the Kruskal-Wallis H test and the data of the water-maze acquisition trials, which were analyzed by multivariate ANOVA with block as a dependent variable, group as a fixed factor, and swimming speed as a covariate followed by Fisher's least significant difference test. Statistical significance was considered when $P < 0.05$.

RESULTS

EA Pretreatment Upregulated A1 Receptor Expression in the Hippocampus

The effects of EA treatment on A1 receptor expression are shown in **Figure 1**. The A1 receptor protein expression level 30 min after EA pretreatment increased significantly in the 90 min group compared to the level in the sham group ($^*P < 0.05$). There was no significant difference in the level of adenosine A1 receptor mRNA in each time period ($P > 0.05$).

CCPA Imitated the Effect of EA Pretreatment on Cognitive Function

To determine whether CCPA and EA treatment reversed cognitive impairment, we examined memory performance in the Morris water-maze test in rats treated with CCPA and EA. Multivariate ANOVA comparisons revealed significant main effects for group ($P < 0.05$), but not for group × swimming speed interaction ($P > 0.05$). Fisher's least significant difference test revealed reduced escape latencies in the EA + MCAO group compared to the MCAO group in all acquisition trials (EA + MCAO vs. MCAO all $P < 0.05$). Escape latency also reduced in the CCPA + MCAO group (CCPA + MCAO vs. MCAO; all $P < 0.05$). During the probe trials, the CCPA + MCAO group and EA + MCAO group had a significantly longer time spent in the target quadrant and faster swimming speed than the DMSO + MCAO group and MCAO group (**Figure 2**).

EA Treatment and CCPA Reduce the Damage in the Hippocampus Following Ischemia–Reperfusion

In order to examine the effects of EA treatment and CCPA on nerve function recovery (as shown in **Figure 3**), we initially

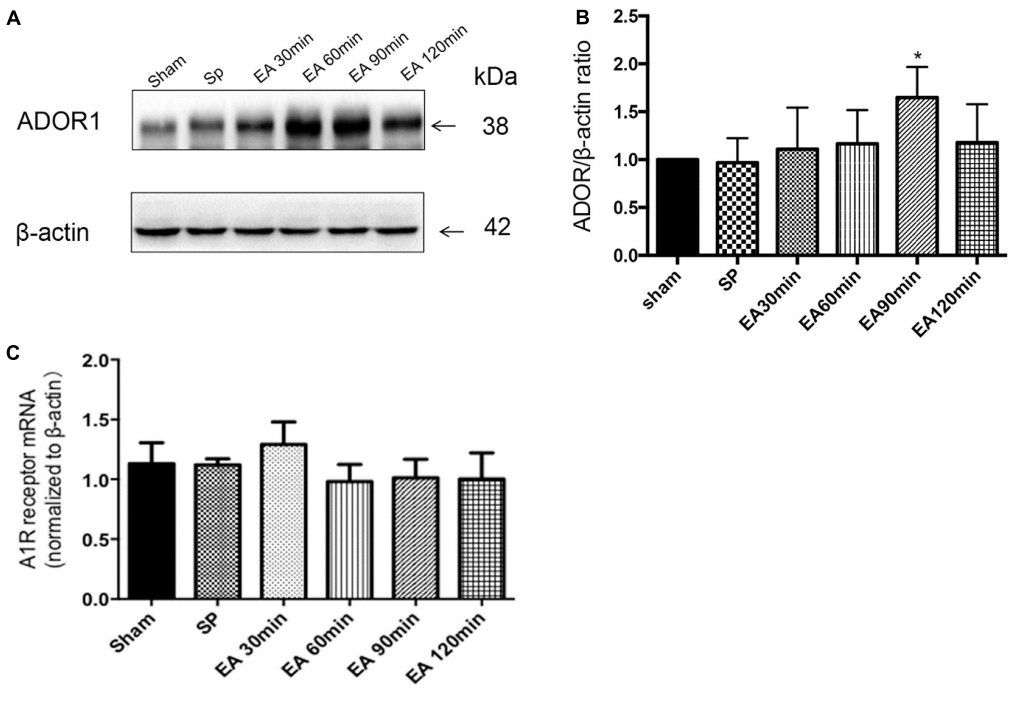

FIGURE 1 | Effects of electroacupuncture (EA) on A1R expression ($n = 4$), as assessed using Western blot and RT-PCR. **(A,B)** Pretreatment with EA significantly increases the expression of A1R protein at 90 min after the completion of EA; **(C)** there is no significant on the expression of A1R mRNA at the times after the completion of EA. $^*P < 0.01$ vs. the sham group.

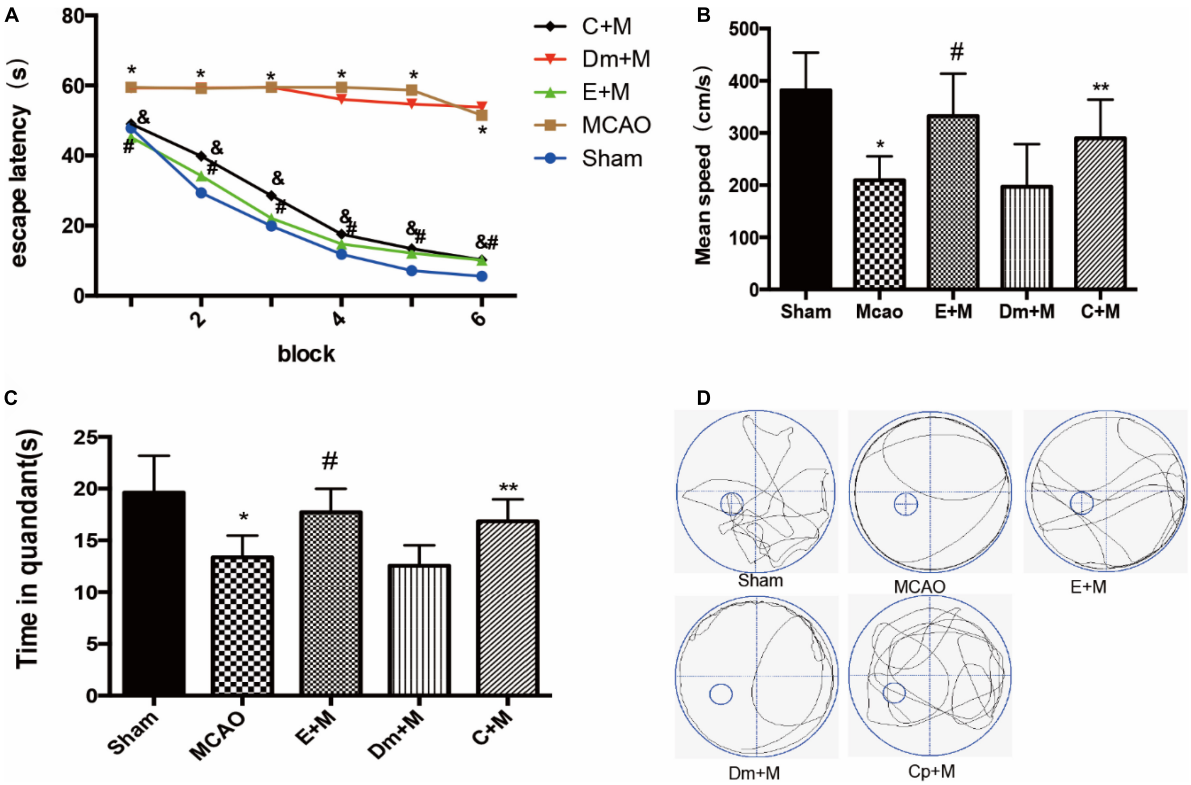

FIGURE 2 | Effects of electroacupuncture (EA) on cognitive function,as assessed using the Morris water maze (MWM) test at 24 h after reperfusion(n = 6). **(A)** Changes in the escape latency (i.e., the time required to locate and climb onto the platform) during six-block acquisition trials. EA pretreatment and administration of CCPA decreases the escape latencies in all trials; **(B,C)** effects of EA pretreatment and administration of CCPA on **(B)** mean speed and **(C)** time in quadrant. **(D)** The swimming tracks of rats in different conditions in the probe trial test. $^{*}P < 0.01$ vs. the sham group, $^{\#}P < 0.05$ vs. the MCAO group, $^{**}P < 0.05$ vs. the MCAO group, $^{\&}P < 0.05$ vs. the MCAO group.

investigated the neurological score and the ratio of Bcl-2/Bax which decreased in the MCAO group (Sham vs. MCAO; all $P < 0.05$). But the neurological score and the Bcl-2/Bax ratio was significantly increased in the CCPA and EA-treated rats (EA + MCAO vs. MCAO; CCPA + MCAO vs. MCAO; all $P < 0.05$), suggesting that there is a neuroprotective effect of CCPA and EA against apoptosis in the rat hippocampus. Whereas DMSO pretreatment had no effect on the EA pretreatment (DMSO + MCAO vs. MCAO; $P > 0.05$). These results suggested that EA treatment and CCPA effectively reduce the neurological dysfunction of cerebral ischemia in the hippocampus, promoting nerve functional recovery.

EA pretreatment and CCPA significantly attenuated neuronal loss in the CA1 region of the hippocampus, a feature that was not observed in the MCAO group (EA + MCAO vs. MCAO, $P < 0.05$). No significant differences in the number of viable neurons were detected between the MCAO and DMSO + MCAO groups (DMSO + MCAO vs. MCAO; $P > 0.05$) (**Figure 3**).

DPCPX Reversed the Effect of EA Pretreatment on Cognitive Function

Whether the cognitive protection of EA pretreatment was reversed by DPCPX pretreatment was examined by the Morris water maze test. The escape latencies in the EA + MCAO group were lower compared to the MCAO group in all acquisition trials (all $P < 0.05$). These findings were reversed by DPCPX (EA + DPCPX + MCAO vs. EA + MCAO, $P < 0.05$; **Figure 4**). The probe test revealed a significant difference between the EA + DPCPX + MCAO and EA + MCAO groups with regard to swimming speed ($P < 0.05$; **Figure 4**). We also found that rats with focal cerebral ischemia spent less time in the target quadrant compared to the sham rats (Sham vs. MCAO; $P < 0.05$). EA pretreatment significantly extended the time spent swimming in the target quadrant following MCAO (EA + MCAO vs. MCAO, $P < 0.05$; **Figure 4**). No significant differences were detected between the MCAO and DPCPX + MCAO groups or between the EA + DMSO + MCAO and EA + MCAO groups (DPCPX + MCAO vs. MCAO; EA + DMSO + MCAO vs. EA + MCAO; all $P > 0.05$).

DPCPX Reversed the Effect of EA Pretreatment Reducing the Damage in the Hippocampus Following Ischemia–Reperfusion

In order to examine the effects of DPCPX on nerve function recovery, the neurological score and the Bcl-2/Bax ratio were

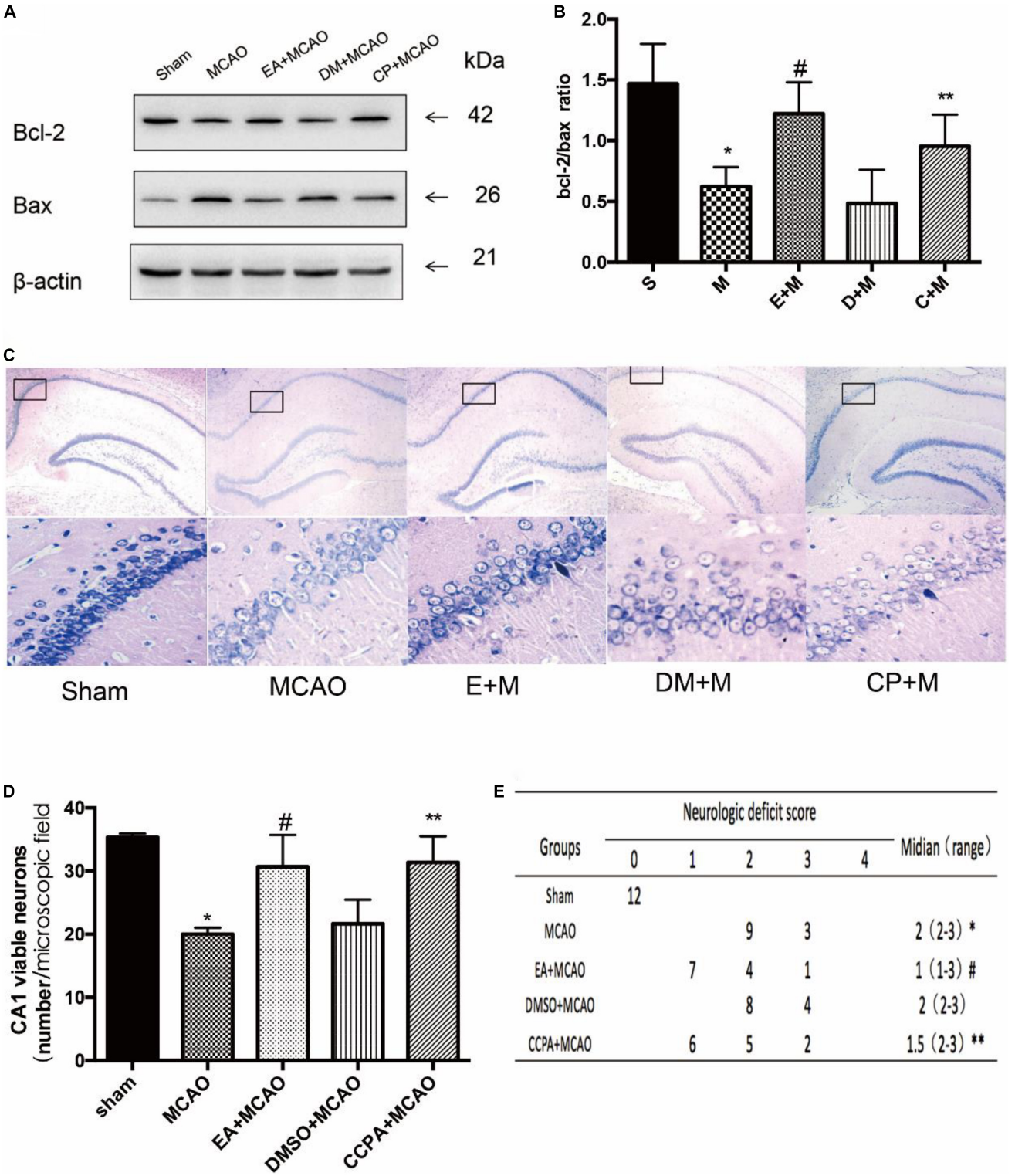

E

Groups	Neurologic deficit score					Midian (range)
	0	1	2	3	4	
Sham	12					
MCAO			9	3		2 (2-3) *
EA+MCAO		7	4	1		1 (1-3) #
DMSO+MCAO			8	4		2 (2-3)
CCPA+MCAO		6	5	2		1.5 (2-3) **

FIGURE 3 | Effect of electroacupuncture (EA) pretreatment and administration of CCPA on the effect of hippocampus damage. **(A,B)** Western blot analysis for Bcl-2 and Bax protein expression in the hippocampus ($n = 3$). **(C,D)** Nissl staining of hippocampus 24 h after reperfusion. Cell counting shows a significant decrease in the number of viable neurons in the hippocampal CA1 region for the middle cerebral artery occlusion (MCAO) group, while the number is significantly increased in the EA + MCAO group and CCPA + MCAO group ($n = 3$). **(E)** Neurologic behavior scores were determined 24 h after reperfusion. $^{*}P < 0.05$ vs. the sham group, $^{\#}P < 0.05$ vs. the MCAO group, $^{**}P < 0.05$ vs. the MCAO group.

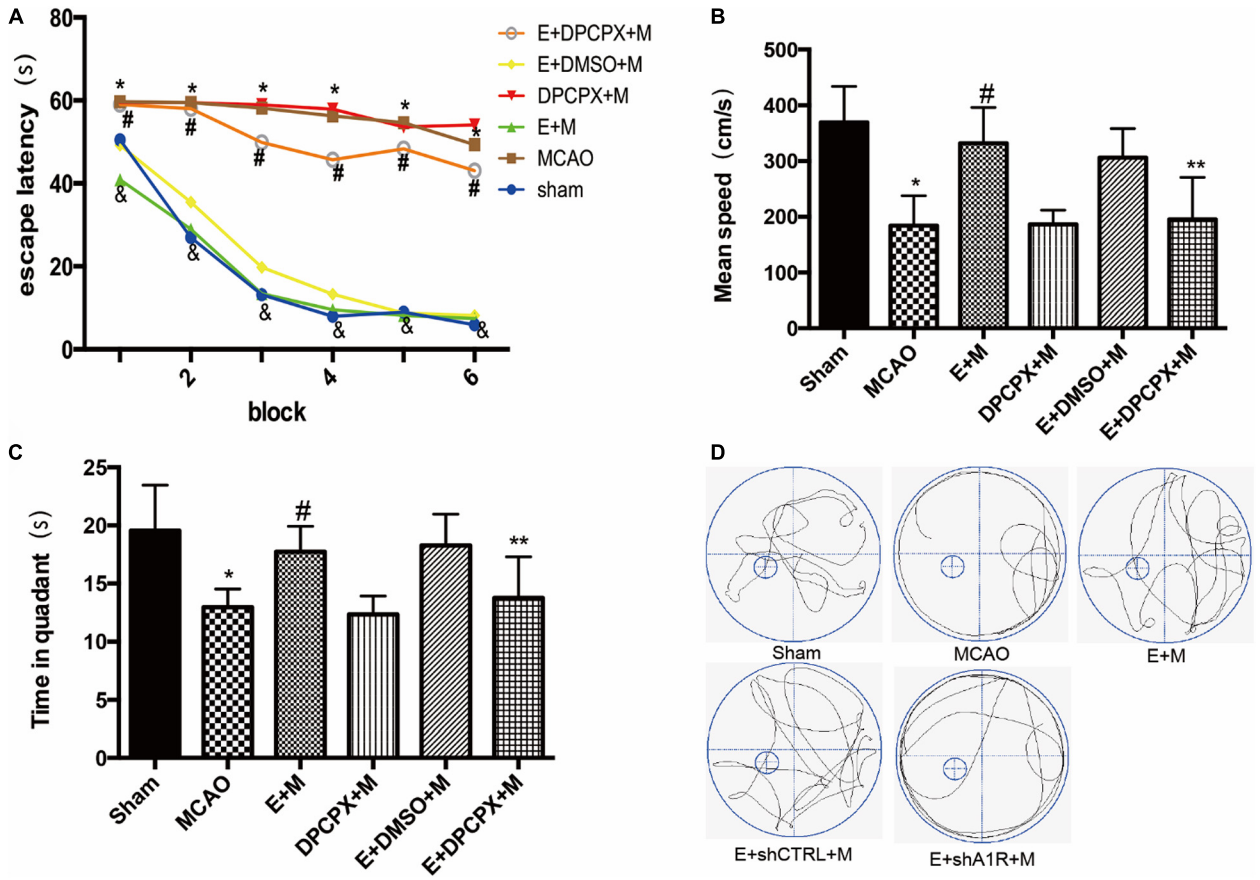

FIGURE 4 | Effects of DPCPX, an adenosine receptor 1 (A1R) antagonist, on cognitive function induced by electroacupuncture (EA) pretreatment ($n = 6$). **(A)** EA pretreatment decreases the escape latencies in all trials; this is reversed by DPCPX; **(B,C)** effects of EA pretreatment with or without DPCPX on **(B)** mean speed and **(C)** time in quadrant. **(D)** The swimming tracks of rats in different conditions in the probe trial test. $^{*}P < 0.01$ vs. the sham group, $^{\#}P < 0.05$ vs. the MCAO group, $^{\&}P < 0.05$ vs. the EA + MCAO group, $^{**}P < 0.05$ vs. the EA + MCAO group.

investigated. The MCAO group demonstrated a significant decreased ratio compared with the ratio of the EA + MCAO group (EA + MCAO vs. MCAO, $P < 0.05$). Furthermore, DPCPX reversed the beneficial effects of EA pretreatment (EA + DPCPX + MCAO vs. EA + MCAO, $P < 0.05$), but did not exert an effect when administered alone (MCAO vs. DPCPX + MCAO, $P > 0.05$).

DPCPX inhibited the beneficial effects of EA pretreatment-attenuated neuronal loss (EA + DPCPX + MCAO vs. EA + MCAO, $P < 0.05$). No significant differences in the number of viable neurons were detected between the MCAO and DPCPX + MCAO groups (MCAO vs. DPCPX + MCAO, $P > 0.05$) (**Figure 5**).

The Effect of AV-shA1R in the Hippocampus

We examined the effects of AV-shA1R in the hippocampus and found that AV-shRNA3 on the nerve cell was effective. And 48 h after administration of AV-shA1R,the expression of the A1R protein was downregulated in the hippocampus of the rats (shA1R vs. sham, $P < 0.05$) (**Figure 6**).

The Effect of AV-shA1R on Cognitive Function

In order to examine the effects of AV-shA1R on cognitive function, we examined memory performance in the Morris water maze test in rats treated with AV-shA1R. And we found there was no significant difference between the two groups ($P > 0.05$) (**Figure 7**).

AV-shA1R Reversed the Effect of EA Pretreatment on Cognitive Function

To determine whether EA pretreatment without the A1 receptor affected cognitive function, we examined memory performance in the Morris water maze test in rats treated with AV-shA1R. As shown in **Figure 8**, escape latency in the EA + MCAO group was reduced compared with the shA1R + EA + MCAO group (EA + MCAO vs. shA1R + EA + MCAO; all $P < 0.05$) or the MCAO group in all acquisition trials (EA + MCAO vs. MCAO; all $P < 0.05$). During the probe trials, the shA1R + EA + MCAO group had a significantly longer time spent in the target quadrant (EA + MCAO vs. shA1R + EA + MCAO; all $P < 0.05$)

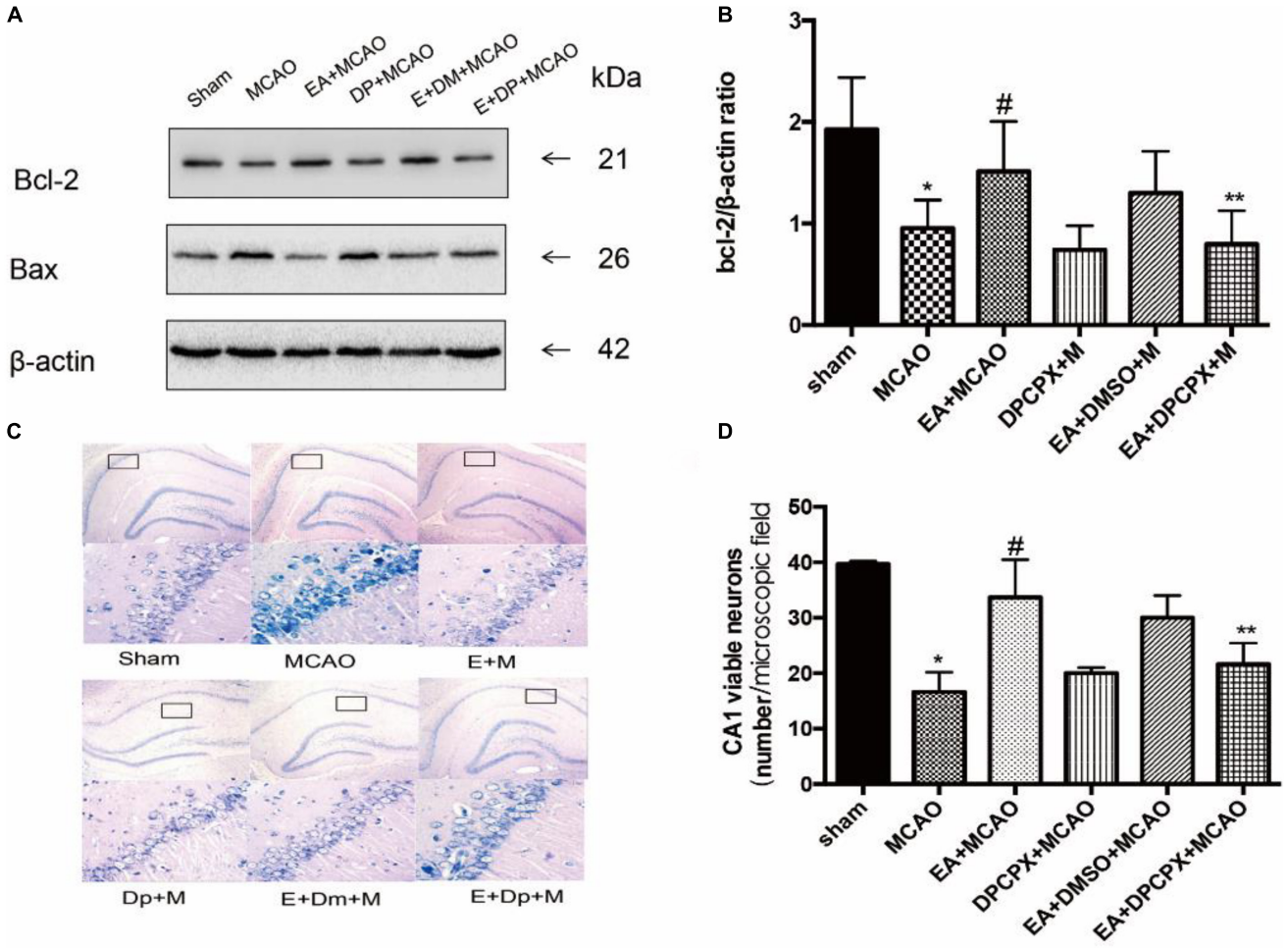

E

Groups	Neurologic deficit score					Midian（range）
	0	1	2	3	4	
Sham	12					
MCAO			8	4		2（2-3）*
EA+MCAO		7	5			1（1-2）#
DPCPX+MCAO			10	2		2（2-3）
EA+DMSO+MCAO		9	3			1（1-2）
EA+DPCPX+MCAO		1	10	1		2（2-3）**

FIGURE 5 | Effect of DPCPX on hippocampus damage induced by electroacupuncture (EA) pretreatment. **(A,B)** Western blot analysis for Bcl-2 and Bax protein expression in the hippocampus (n = 3). **(C,D)** EA pretreatment significantly increases the number of viable pyramidal neurons in the hippocampal CA1 region (n = 3), whereas DPCPX attenuates these beneficial effects. **(E)** Neurologic behavior scores were determined 24 h after reperfusion. *P < 0.05 vs. the sham group, #P < 0.05 vs. the MCAO group, **P < 0.05 vs. the EA + MCAO group.

(**Figure 8**). Consistent with this finding, behavioral tracking showed increased exploration time in the target quadrant for the EA + MCAO and EA + shCTRL + MCAO groups compared with the MCAO group. No significant differences were detected between the EA + shCTRL + MCAO and EA + MCAO groups.

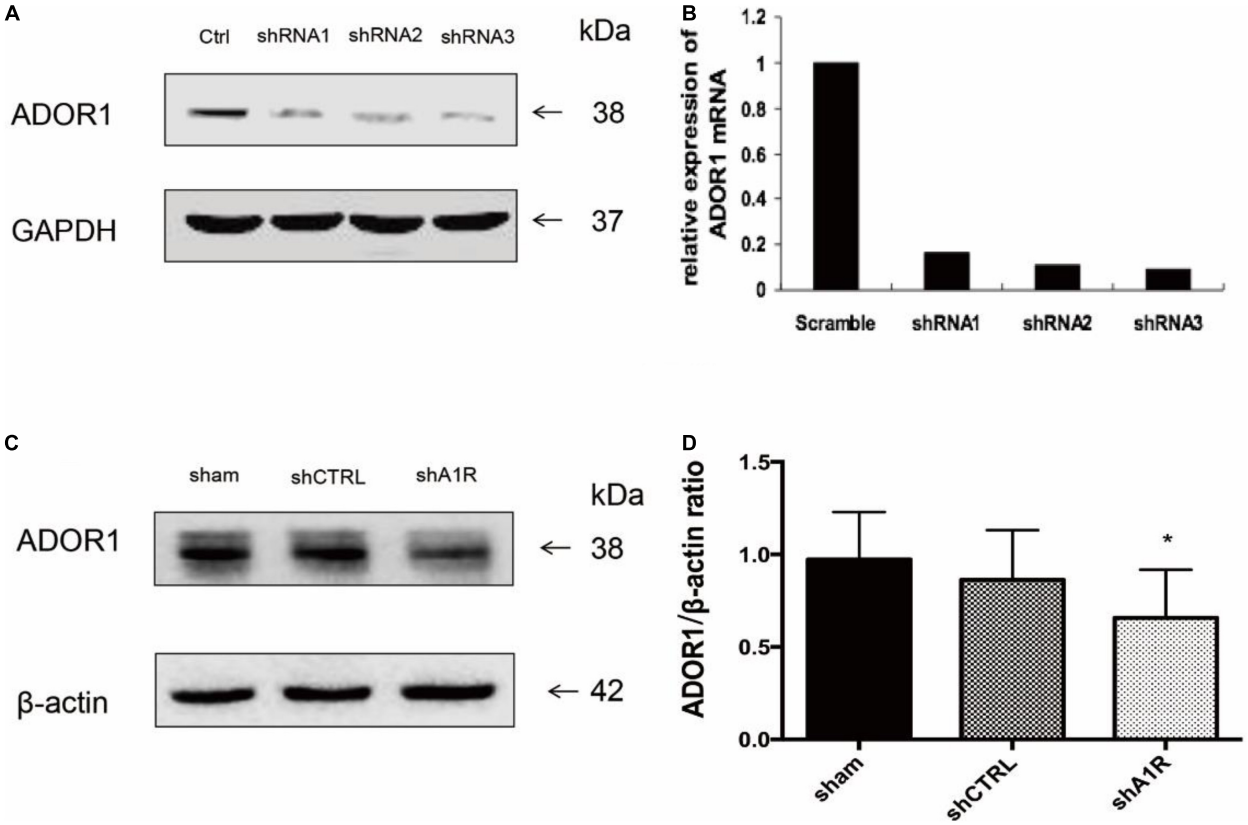

FIGURE 6 | Effect of AV-shRNA on the nerve cells of rats 48 h after administration of AV-shA1R. **(A,B)** Western blot analysis for adenosine receptor 1 (A1R) protein expression and PCR shows A1R mRNA expression ($n = 3$). **(C,D)** A total of 48 h after administration of AV-shA1R and AV–shCTRL on the rats, Western blot analysis for A1R protein expression. *$P < 0.05$ vs. the sham group.

Selective Deletion of A1 Receptor in the Left Hippocampus of Rats Eliminates the Damage in the Hippocampus After EA Pretreatment

Forty-eight hours after administration of AV-shA1R or AV-shCTRL, the western blot result showed that the expression of A1 receptor protein in rats was significantly downregulated in the AV-shA1R administration group (shA1R vs. Sham, shA1R vs. shCTRL; $P < 0.05$), suggesting that the injection sites were on target and AV-shA1R was effective in the rats. The A1R protein deleted by AV-shA1R attenuated the neurological score and the Bcl-2/Bax ratio of EA pretreatment (shA1R + EA + MCAO vs. EA + MCAO, all $P < 0.05$ **Figure 9**), whereas AV-shCTRL had no effect on EA pretreatment (shCTRL + EA + MCAO vs. EA + MCAO, $P < 0.05$) (**Figure 9**).

DISCUSSION

In our study, we found that the A1 receptor protein in the hippocampus was significantly increased at 90 min after electroacupuncture pretreatment of Baihui (GV20). And there was no statistical difference in the levels of adenosine A1 receptor mRNA transcription in each time period. This finding suggests that the adenosine A1 receptor may be involved in the effect of electroacupuncture-preconditioned MCAO model rats. After the subsequent experiments, we explored the hypothesis at the drug level and genetic level. First, we injected the A1 receptor agonist CCPA or A1 receptor antagonist DPCPX into the lateral ventricle of the rats 1 h 30 min after electroacupuncture pretreatment. It was found that A1 receptor activation in MCAO model rats could have the effect of cognitive function recovery. And CCPA imitated the beneficial effects of EA pretreatment. However, DPCPX reversed the protective effect of electroacupuncture. Then we used the transfection technique at the gene level to delete the expression of A1 receptor protein in the hippocampus, which could reverse the protective effect of electroacupuncture. And these results suggest that the A1 receptor is involved in electroacupuncture pretreatment to mediate cognitive impairment after cerebral ischemia, which is a new participatory mechanism.

Previous studies have shown that electroacupuncture pretreatment can be one adjuvant therapy of stroke, and the prospect is considerable (Gosman-Hedstrom et al., 1998). Pretreatment with EA at the Baihui acupoint (GV 20) induces a rapid tolerance 2 h after EA to cerebral ischemic insults (Zhou et al., 2013). And electroacupuncture mediates through

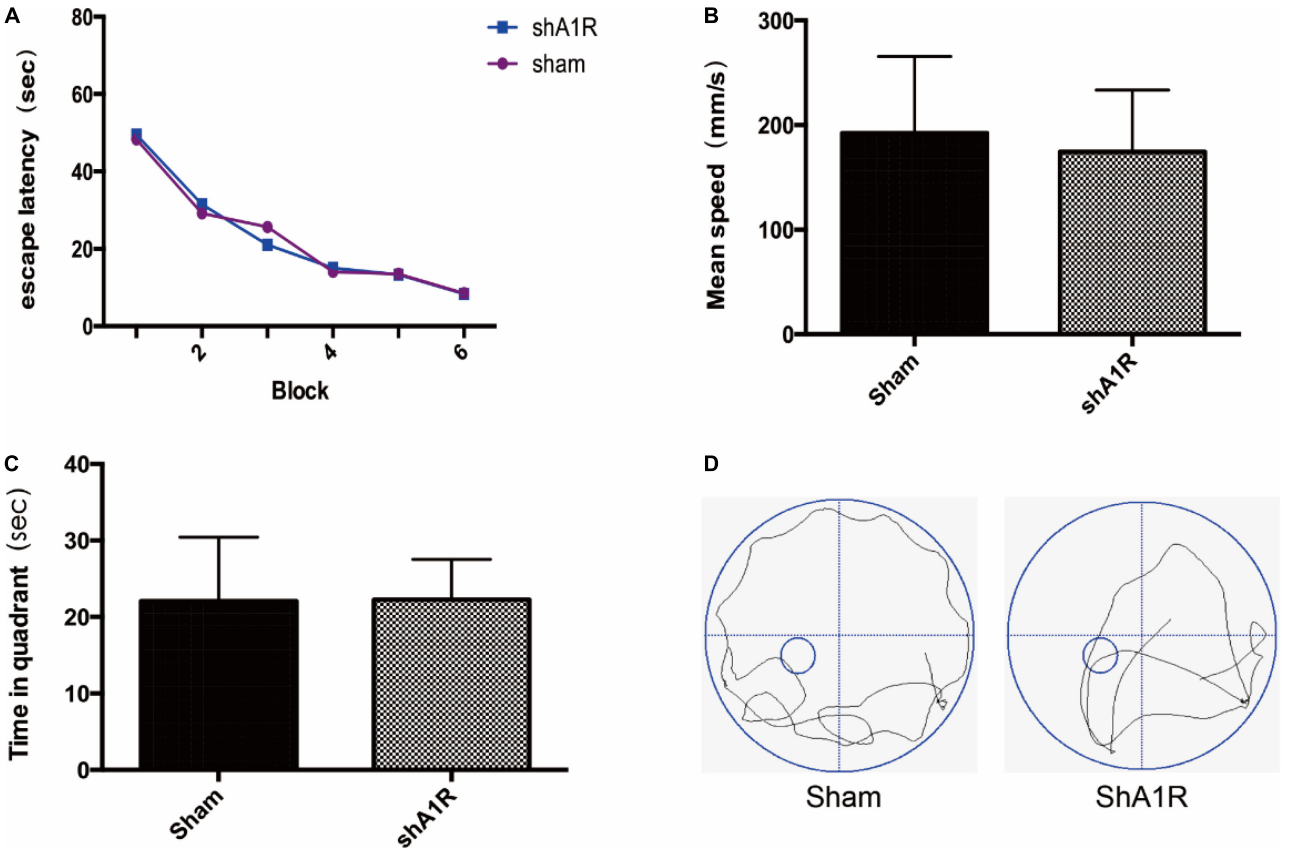

FIGURE 7 | Effects of AV-shA1R on cognitive function (n = 6). **(A)** Changes in the escape latency during six-block acquisition trials; **(B,C)** effects of AV-shA1R on **(B)** mean speed and **(C)** time in quadrant. **(D)** The swimming tracks of rats in different conditions in the probe trial test.

the CB1 receptor (Wang et al., 2009; Du et al., 2010; Ma et al., 2011), Wnt signaling pathway (He X. et al., 2016), and an adenosine A1 receptor-related mechanism against transient cerebral ischemia, by inhibiting apoptosis, producing antioxidant protection, reducing inflammatory mediators, and reducing excitotoxicity to produce brain protection (Shen et al., 2016). In addition, these studies have shown that hippocampus ischemic tolerance is associated with GluR2 elevating after electroacupuncture pretreatment (Liu et al., 2015). And some studies have shown that electroacupuncture pretreatment for hippocampus-related diseases resulted in convalescence (He X. L. et al., 2016; Wang et al., 2016; Liu et al., 2017).

The hippocampus, an important part in the limbic system, is not only very sensitive to cerebral ischemia–reperfusion injury (Lee et al., 1986), where the vertebral neurons of the CA1 region are sensitive and fragile to harmful injury (Caraci et al., 2008), but also plays a major role in the formation and consolidation of learning and memory (Lagali et al., 2010; Bartsch and Wulff, 2015). Simultaneously, the destruction in the hippocampal CA1 area is associated with cognitive impairment (Zhang et al., 2016b). So, the hippocampus is the main tissue to explore in our research. The study has demonstrated that after electroacupuncture pretreatment, the neurobehavioral score was improved, the escape latency was decreased, and target quadrant was increased in the MCAO rats, as in a previous study (He X. et al., 2016). And we also found that after CCPA administration in the MCAO rats, the behavioral score and the results in the water maze test were comparable to electroacupuncture pretreatment, but the effect was reversed after DPCPX administration.

CCPA is an agonist of the adenosine A1 receptor (Cristalli et al., 1986) and is used in A1 receptor-related experiments (Lohse et al., 1988). CCPA administration has protective effects on ischemic neuronal injury (Goda et al., 1998). DPCPX is an adenosine A1 receptor antagonist (Okamura et al., 2004) and is also used in A1 receptor-related experiments. DPCPX administration reduces neuroprotective effects (Yoshida et al., 2004) and attenuates cerebral ischemic tolerance (Nakamura et al., 2002). The adenosine-related drugs are used for the treatment of human cognitive and memory-related pathologies, which is used to treat schizophrenia, panic disorder, and anxiety (Lopes et al., 2011). And other studies show that after cerebral ischemia, A1 receptors attempt to inhibit presynaptic glutamate release and to limit postsynaptic depolarization and Ca^{2+} influx (Lubitz, 1998). In this study, we found that the A1 receptor protein in the hippocampus was significantly increased 90 min after electroacupuncture pretreatment. And under hypoxic conditions, the A1 receptor density in the hippocampus was decreased (Lee et al., 1986). The result suggests

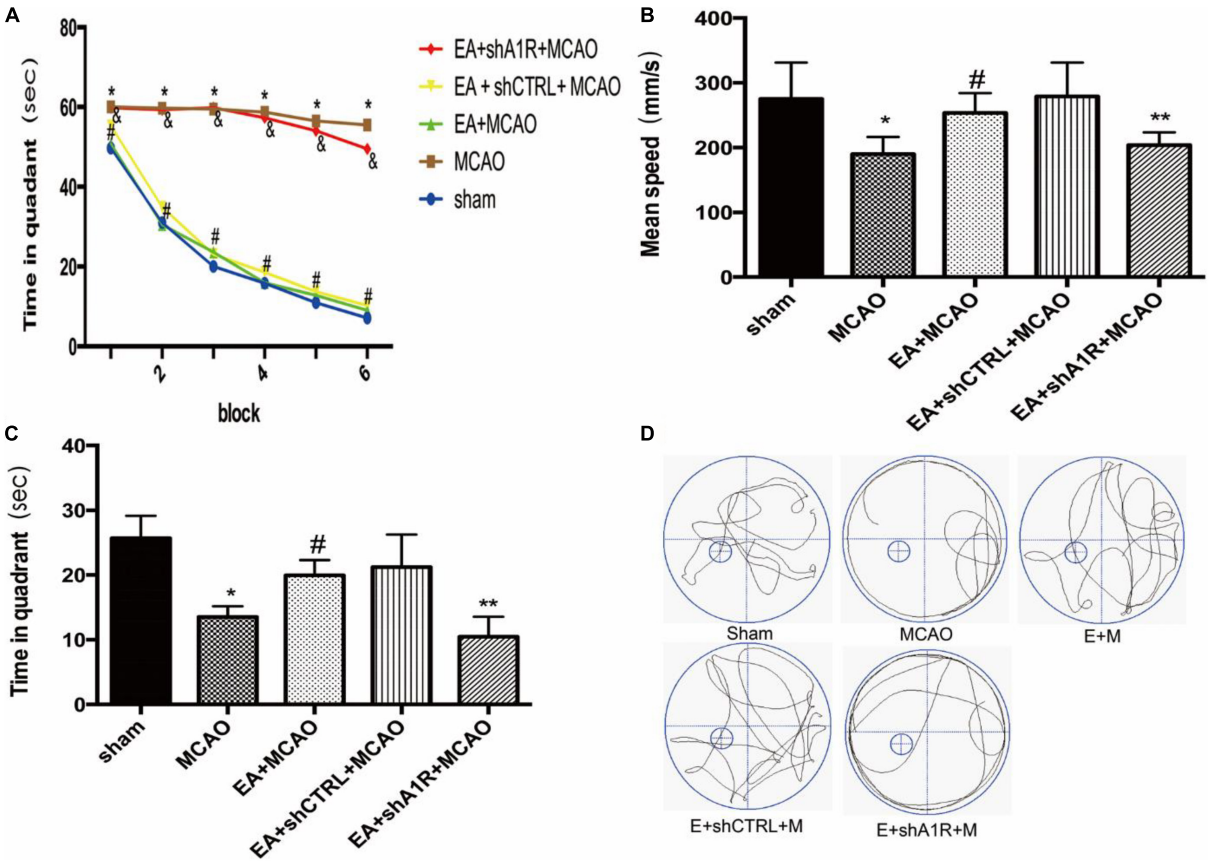

FIGURE 8 | Effects of electroacupuncture (EA) on cognitive function (n = 6). **(A)** EA pretreatment decreases the escape latencies in all trials; this is reversed by AV-shA1R; **(B,C)** effects of EA pretreatment with AV-shA1R on **(B)** mean speed and **(C)** time in quadrant. **(D)** The swimming tracks of rats in different conditions in the probe trial test. $^{*}P < 0.01$ vs. the sham group, $^{\#}P < 0.05$ vs. the MCAO group, $^{**}P < 0.05$ vs. the MCAO group, $^{\&}P < 0.05$ vs. the EA + MCAO group, $^{**}P < 0.05$ vs. the EA + MCAO group.

that A1 receptors may be involved in the electroacupuncture pretreatment mechanism. Meanwhile A1 receptors are associated with neuroprotection (Fedele et al., 2006), and the A1 receptor is necessary to mediate cerebral ischemic tolerance in ischemic conditions (Yoshida et al., 2004). Electroacupuncture has now been used for cerebral ischemic disease (Gao et al., 2006; Wang et al., 2009), and studies have shown that electroacupuncture may stimulate adenosine A1 receptors to mediate rapid cerebral ischemic tolerance and cognitive function (Zhang et al., 2016b). In order to explore the association between A1 receptors and electroacupuncture, CCPA and DPCPX were injected into the lateral ventricle in the rats. We confirmed that CCPA can replicate the effect of electroacupuncture to inhibit neuronal apoptosis in the MCAO rats, whereas DPCPX can reverse this effect, as in a previous study. We also found that electroacupuncture pretreatment stimulates A1 receptors to inhibit neuronal apoptosis and play a protective role in cognitive function after cerebral ischemia, whereas DPCPX can also reverse this protective effect and aggravate cerebral ischemic injury. So, these results suggest that the A1 receptor is involved in electroacupuncture preconditioning-induced cognitive recovery after cerebral ischemia. To further confirm that, we used the transfection technique to silence the A1 receptor. The adenovirus with the shA1R sequence downregulated the expression of A1 receptor protein in the hippocampus. And the cognitive protection effect of electroacupuncture pretreatment was inhibited after the A1 receptor was downregulated. These findings further elucidate that the protective effect on cognitive function induced by electroacupuncture pretreatment is related to the A1 receptor-related signaling pathway.

Cerebral injury is caused by ischemia and hypoxia mainly in the CA1 area of the hippocampus; the hippocampus was the focus in our research. And we found that the memory of animals with hippocampal damage was impaired in the Morris water maze test (Boissardm et al., 1992). So, we chose the Morris water maze to detect the learning and memory function of SD rats. In our study, the memory of AV-shA1R rats and sham-operated rats was no different, indicating that the learning and memory function of rats with downregulated A1 receptors is unchanged. A previous study (Lang et al., 2003) confirmed that the spatial learning ability and exploratory ability of A1 receptor-knockout mice were at normal levels. In our study, the transfection technique reduced the expression of A1 receptor protein in the hippocampus, which reversed the effect of pretreatment electroacupuncture in the

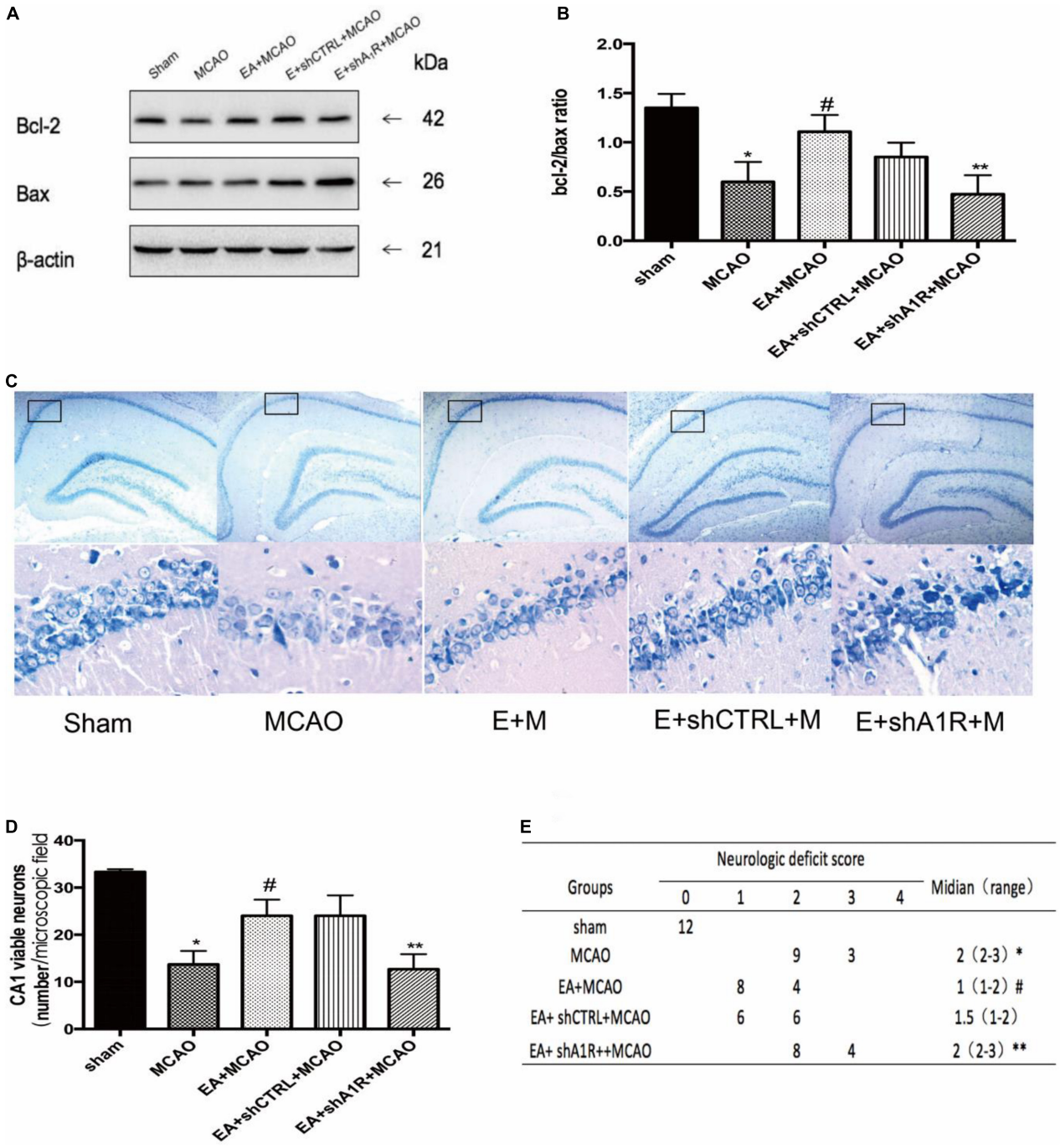

Groups	Neurologic deficit score					Midian (range)
	0	1	2	3	4	
sham	12					
MCAO			9	3		2 (2-3) *
EA+MCAO		8	4			1 (1-2) #
EA+ shCTRL+MCAO		6	6			1.5 (1-2)
EA+ shA1R++MCAO			8	4		2 (2-3) **

FIGURE 9 | Effect of AV-shA1R on neuroprotection. **(A,B)** Western blot analysis for Bcl-2 and Bax protein expression in the hippocampal CA1 region (n = 3). **(C,D)** EA pretreatment significantly increased the number of viable pyramidal neurons in the hippocampal CA1 region (n = 3),whereas AV-shA1R attenuated these beneficial effects. **(E)** Neurologic behavior scores were determined 24 h after reperfusion. *P < 0.01 vs. the sham group, #P < 0.05 vs. the MCAO group, **P < 0.05 vs. the EA + MCAO group.

cognitive impairment induced by cerebral ischemia–reperfusion in the rats. For further study, the expression of A1 receptor protein can be overexpressed by the transfection technique in the hippocampus, and the cognitive impairment induced by cerebral ischemia–reperfusion in rats can be observed. And cognitive impairment caused by hippocampal injury can also be tested by a light and dark shuttle test (Wang et al., 2012; Wang et al., 2020) and other tests. The study needs more cognitive behavioral tests to explore cognitive function. Because Bcl protein and Bax protein activity are critical to the activation

and inhibition of apoptosis and may be associated with the mechanism of brain injury (Goda et al., 1998), we assessed the ischemic injury of the hippocampus by Bcl-2/Bax ratio and the localization of the nucleus and the type and the distribution of neurons by Nissl staining (Zhang et al., 2016a). We used Nissl staining to determine the viable neurons in the CA1 region of the hippocampus. In the end, the results suggest that electroacupuncture pretreatment had an effect on the learning and memory dysfunction of rats, which reduced the degree of hippocampal injury.

Our study demonstrates that electroacupuncture pretreatment can prevent cognitive impairment from cerebral ischemia–reperfusion, in which the effect is mediated through the A1 receptor. The mechanism of electroacupuncture pretreatment reduces cognitive dysfunction by reducing neuronal damage in the hippocampus. The A1 receptor has neuroprotective effects due to adenosine in presynaptic receptors, reducing excitatory neurotransmitters and the activation of postsynaptic receptors that results in K^+ channel hyperpolarization (Ciruela et al., 2012). Previous studies have shown that adenosine of adult animals can inhibit NMDA receptor activation and reduce Ca^{2+} influx to reduce excitotoxicity (Cunha, 2005). And A1 receptor activation has an effect on NMDA receptors to reduce harmful substance release (Constantino et al., 2015). Meanwhile A1 receptors may have an effect on Glu A2 to reduce hippocampal injury after ischemia (Liu et al., 2015; Stockwell et al., 2016). And whether these mechanisms are also involved in A1 receptor-mediated cognitive impairment with cerebral ischemia by electroacupuncture preconditioning requires exploration.

DATA AVAILABILITY STATEMENT

The original contributions presented in the study are included in the article/supplementary material, further inquiries can be directed to the corresponding author/s.

ETHICS STATEMENT

The animal study was reviewed and approved by the Special Committee on Animal Welfare of Wenzhou Medical University. Written informed consent was obtained from the owners for the participation of their animals in this study.

AUTHOR CONTRIBUTIONS

JW and YS designed the study. YS and QD implemented the experimental design and participated in data collection and analysis. BJ, LH, and YM developed the clinical protocols. YS and XZ drafted the manuscript. All authors read and approved the final manuscript.

FUNDING

This research was supported by Zhejiang Province Natural Science Foundation (Grant LY19H290008) and Wenzhou Science and Technology Bureau Foundation (Grants Y20190108 and Y20190202).

REFERENCES

Bartsch, T., and Wulff, P. (2015). The hippocampus in aging and disease: from plasticity to vulnerability. *Neuroscience* 309, 1–16. doi: 10.1016/j.neuroscience.2015.07.084

Boissardm, C. G., Lindner, M. D., and Gribkoff, V. K. (1992). Hypoxia produces cell death in the rat hippocampus in thepresence of an A1 adenosine receptor antagonist an anatomical and behavioral study. *Neuroscience* 48, 807–812. doi: 10.1016/0306-4522(92)90268-7

Bortolotto, J. W., Melo, G. M., Cognato, G. D. P., Vianna, M. R., and Bonan, C. D. (2015). Modulation of adenosine signaling prevents scopolamine-induced cognitive impairment in zebrafish. *Neurobiol. Learn. Mem.* 118, 113–119. doi: 10.1016/j.nlm.2014.11.016

Caraci, F., Busceti, C., Biagioni, F., Aronica, E., Mastroiacovo, F., Cappuccio, I., et al. (2008). The Wnt antagonist, Dickkopf-1, as a target for the treatment of neurodegenerative disorders. *Neurochem. Res.* 33, 2401–2406. doi: 10.1007/s11064-008-9710-0

Chen, C., Yu, Q., Xu, K., Cai, L., Felicia, B. M., Wang, L., et al. (2020). Electroacupuncture pretreatment prevents ischemic stroke and inhibits Wnt signaling-mediated autophagy through the regulation of GSK-3β phosphorylation. *Brain Res. Bull.* 158, 90–98. doi: 10.1016/j.brainresbull.2020.03.002

Chen, J. F. (2014). Adenosine receptor control of cognition in normal and disease. *Int. Rev. Neurobiol.* 119, 257–307. doi: 10.1016/B978-0-12-801022-8.00012-X

Chen, J. F., Lee, C. F., and Chern, Y. (2014). Adenosine receptor neurobiology: overview. *Int. Rev. Neurobiol.* 119, 1–49. doi: 10.1016/B978-0-12-801022-8.00001-5

Chen, Y., Zhou, J., Li, J., Yang, S. B., Mo, L. Q., Hu, J. H., et al. (2012). Electroacupuncture pretreatment prevents cognitive impairment induced by limb ischemia-reperfusion via inhibition of microglial activation and attenuation of oxidative stress in rats. *Brain Res.* 1432, 36–45. doi: 10.1016/j.brainres.2011.11.002

Ciruela, F., Fernandez-Duenas, V., Llorente, J., Borroto-Escuela, D., Cuffi, M. L., Carbonell, L., et al. (2012). G protein-coupled receptor oligomerization and brain integration: focus on adenosinergic transmission. *Brain Res.* 1476, 86–95. doi: 10.1016/j.brainres.2012.04.056

Constantino, L. C., Pamplona, F. A., Matheus, F. C., Ludka, F. K., Gomez-Soler, M., Ciruela, F., et al. (2015). Adenosine A1 receptor activation modulates N-methyl-d-aspartate (n.d.) preconditioning phenotype in the brain. *Behav. Brain Res.* 282, 103–110. doi: 10.1016/j.bbr.2014.12.056

Cristalli, G., Grifantini, M., Vittori, S., Klotz, K.-N., and Lohse, M. J. (1986). Synthesis of 2-azido-(R)-N6-p-hydroxyphenylisopropy-l adenosine (R-AHPIA) as a potential photoaffinity probe for AI adenosine receptors. *Nucleos. Nucleot.* 5, 213–222. doi: 10.1080/07328318608068674

Cumming, T. B., Marshall, R. S., and Lazar, R. M. (2013). Stroke, cognitive deficits, and rehabilitation: still an incomplete picture. *Int. J. Stroke* 8, 38–45. doi: 10.1111/j.1747-4949.2012.00972.x

Cunha, R. A. (2001). Adenosine as a neuromodulator and as a homeostatic regulator in the nervous system: different roles, different sources and different receptors. *Neurochem. Int.* 38, 107–125. doi: 10.1016/s0197-0186(00)00034-6

Cunha, R. A. (2005). Neuroprotection by adenosine in the brain: from A(1) receptor activation to A (2A) receptor blockade. *Purinergic Signal.* 1, 111–134. doi: 10.1007/s11302-005-0649-1

Du, J., Wang, Q., Hu, B., Peng, Z., Zhao, Y., Ma, L., et al. (2010). Involvement of ERK 1/2 activation in electroacupuncture pretreatment via cannabinoid CB1 receptor in rats. *Brain Res.* 1360, 1–7. doi: 10.1016/j.brainres.2010.07.034

Fedele, D. E., Li, T., Lan, J. Q., Fredholm, B. B., and Boison, D. (2006). Adenosine A1 receptors are crucial in keeping an epileptic focus localized. *Exp. Neurol.* 200, 184–190. doi: 10.1016/j.expneurol.2006.02.133

Feng, X., Yang, S., Liu, J., Huang, J., Peng, J., Lin, J., et al. (2013). Electroacupuncture ameliorates cognitive impairment through inhibition of NF-kappaB-mediated neuronal cell apoptosis in cerebral ischemia-reperfusion injured rats. *Mol. Med. Rep.* 7, 1516–1522. doi: 10.3892/mmr.2013.1392

Gao, H., Guo, J., Zhao, P., and Cheng, J. (2006). Influences of electroacupuncfure on the expression of insulin-like growth factor-1 following focal cerebral ischemia in monkeys. *Acupunct. Electro Ther.* 31, 259–272. doi: 10.3727/036012906815844247

Goda, H., Ooboshi, H., Nakane, H., Ibayashi, S., Sadoshima, S., and Fujishima, M. (1998). Modulation of ischemia-evoked release of excitatory andinhibitory amino acids by adenosine A1 receptor agonist. *Eur. J. Pharmocol.* 357, 149–155. doi: 10.1016/s0014-2999(98)00559-7

Goldstein, L. B., Adams, R., Becker, K., Furberg, C. D., Gorelick, P. B., Hademenos, G., et al. (2001). Primary prevention of ischemic stroke: a statement for healthcare professionals from the stroke council of the american heart association. *Circulation* 103, 163–182. doi: 10.1161/01.cir.103.1.163

Gomes, C. V., Kaster, M. P., Tome, A. R., Agostinho, P. M., and Cunha, R. A. (2011). Adenosine receptors and brain diseases: neuroprotection and neurodegeneration. *Biochim. Biophys. Acta* 1808, 1380–1399. doi: 10.1016/j.bbamem.2010.12.001

Gosman-Hedstrom, G., Claesson, L., Klingenstierna, U., Carlsson, J., Olausson, B., Frizell, M., et al. (1998). Effects of acupuncture treatment on daily life activities and quality of life: a controlled, prospective, and randomized study of acute stroke patients. *Stroke* 29, 2100–2108. doi: 10.1161/01.str.29.10.2100

He, X. L., Zhao, S. H., You, W., Cai, Y. Y., Wang, Y. Y., Ye, Y. M., et al. (2016). Neuroprotective effects of electroacupuncture preventive treatment in senescence-accelerated mouse prone 8 mice. *Chin. J. Integr. Med.* 24, 133–139. doi: 10.1007/s11655-016-2265-z

He, X., Mo, Y., Geng, W., Shi, Y., Zhuang, X., Han, K., et al. (2016). Role of Wnt/beta-catenin in the tolerance to focal cerebral ischemia induced by electroacupuncture pretreatment. *Neurochem. Int.* 97, 124–132. doi: 10.1016/j.neuint.2016.03.011

Lagali, P. S., Corcoran, C. P., and Picketts, D. J. (2010). Hippocampus development and function: role of epigenetic factors and implications for cognitive disease. *Clin. Genet.* 78, 321–333. doi: 10.1111/j.1399-0004.2010.01503.x

Lang, U. E., Lang, F., Richter, K., Vallon, V., Lipp, H. P., Schnermann, J., et al. (2003). Emotional instability but intact spatial cognition inadenosine receptor 1 knock out mice. *Behav. Brain Res.* 145, 179–188. doi: 10.1016/S0166-4328(03)00108-6

Lee, K. S., Tetzlaff, W., and Kreutzberg, G. W. (1986). Rapid down regulation of hippocampal adenosine receptors following brief anoxia. *Brain Res.* 380, 155–158. doi: 10.1016/0006-8993(86)91440-x

Liu, W., Wu, J., Huang, J., Zhuo, P., Lin, Y., Wang, L., et al. (2017). Electroacupuncture regulates hippocampal synaptic plasticity via miR-134-mediated LIMK1 function in rats with ischemic stroke. *Neural Plast.* 2017:9545646. doi: 10.1155/2017/9545646

Liu, Z., Chen, X., Gao, Y., Sun, S., Yang, L., Yang, Q., et al. (2015). Involvement of GluR2 up-regulation in neuroprotection by electroacupuncture pretreatment via cannabinoid CB1 receptor in mice. *Sci. Rep.* 5:9490. doi: 10.1038/srep09490

Lohse, M. J., Klotz, K.-N., Schwabe, U., Cristalli, G., Vittoriz, S., and Grifantini, M. (1988). 2-chloro-N6-cyclopentyladenosine a highly selectiveagonist at A1 adenosine receptors. *Naunyn Schmiedeberg's Arch. Pharmacol.* 337, 687–689.

Longstreth, W. T. Jr., and Dikmen, S. S. (1993). Outcomes after cardiac arrest. *Ann. Emerg. Med.* 22, 64–69.

Lopes, L. V., Sebastião, A. M., and Ribeiro, J. A. (2011). Adenosine and related drugs in brain diseases present andfuture in clinical trials. *Curr. Top. Med. Chem.* 11, 1087–1101. doi: 10.2174/156802611795347591

Lubitz, D. K. J. E. V. (1998). Adenosine and cerebral ischemia therapeutic future ordeath of a brave concept. *Eur. J. Pharmacol.* 371, 85–102. doi: 10.1016/s0014-2999(99)00135-1

Lubitz, D. K. V., Lin, R. C., and Jacobson, K. A. (1995). Jacobson, cerebral ischemia in gerbils: effects of acute and chronic treatment with adenosine A2A receptor agonist and antagonist. *Eur. J. Pharmacol.* 287, 295–302. doi: 10.1016/0014-2999(95)00498-x

Ma, L., Zhu, Z., Zhao, Y., Hou, L., Wang, Q., Xiong, L., et al. (2011). Cannabinoid receptor type 2 activation yields delayed tolerance to focal cerebral ischemia. *Curr. Neurovasc. Res.* 8, 145–152. doi: 10.2174/156720211795495394

Mioranzza, S., Costa, M. S., Botton, P. H., Ardais, A. P., Matte, V. L., Espinosa, J., et al. (2011). Blockade of adenosine A(1) receptors prevents methylphenidate-induced impairment of object recognition task in adult mice. *Prog. Neuropsychopharmacol. Biol. Psychiatry* 35, 169–176. doi: 10.1016/j.pnpbp.2010.10.022

Nakamura, M., Nakakimura, K., Matsumoto, M., and Sakabe, T. (2002). Rapid tolerance to focal cerebral ischemia in rats is attenuated by adenosine A1 receptor antagonist. *J. Cereb. Blood Flow Metab.* 22, 161–170. doi: 10.1097/00004647-200202000-00004

Okamura, N., Hashimoto, K., Shimizu, E., Kumakiri, C., Komatsu, N., and Iyo, M. (2004). Adenosine A1 receptor agonists block the neuropathological changes in rat retrosplenial cortex after administration of the NMDA receptor antagonist dizocilpine. *Neuropsychopharmacology* 29, 544–550. doi: 10.1038/sj.npp.1300351

Shen, H. Y., Coelho, J. E., Ohtsuka, N., Canas, P. M., Day, Y. J., Huang, Q. Y., et al. (2008). A critical role of the adenosine A2A receptor in extrastriatal neurons in modulating psychomotor activity as revealed by opposite phenotypes of striatum and forebrain A2A receptor knock-outs. *J. Neurosci.* 28, 2970–2975. doi: 10.1523/JNEUROSCI.5255-07.2008

Shen, M. H., Zhang, C. B., Zhang, J. H., and Li, P. F. (2016). Electroacupuncture attenuates cerebral ischemia and reperfusion injury in middle cerebral artery occlusion of rat via modulation of apoptosis, inflammation, oxidative stress, and excitotoxicity. *Evid. Based Complement. Alternat. Med.* 2016:9438650. doi: 10.1155/2016/9438650

Stockwell, J., Chen, Z., Niazi, M., Nosib, S., and Cayabyab, F. S. (2016). Protein phosphatase role in adenosine A1 receptor-induced AMPA receptor trafficking and rat hippocampal neuronal damage in hypoxia/reperfusion injury. *Neuropharmacology* 102, 254–265. doi: 10.1016/j.neuropharm.2015.11.018

Tsai, C.-F., Thomas, B., and Sudlow, C. L. M. (2013). Epidemiology of stroke and its subtypes in Chinese vs white population. *Neurology* 81, 264–272. doi: 10.1212/wnl.0b013e31829bfde3

Wang, C., Yang, X. M., Zhuo, Y. Y., Zhou, H., Lin, H. B., Cheng, Y. F., et al. (2012). The phosphodiesterase-4 inhibitor rolipram reverses Abeta-induced cognitive impairment and neuroinflammatory and apoptotic responses in rats. *Int. J. Neuropsychopharmacol.* 15, 749–766. doi: 10.1017/S1461145711000836

Wang, J., Li, P., Qin, T., Sun, D., Zhao, X., and Zhang, B. (2020). Protective effect of epigallocatechin-3-gallate against neuroinflammation and anxiety-like behavior in a rat model of myocardial infarction. *Brain Behav.* 10:e01633.

Wang, Q., Peng, Y., Chen, S., Gou, X., Hu, B., Du, J., et al. (2009). Pretreatment with electroacupuncture induces rapid tolerance to focal cerebral ischemia through regulation of endocannabinoid system. *Stroke* 40, 2157–2164. doi: 10.1161/STROKEAHA.108.541490

Wang, X., Huang, Y., Yuan, S., Tamadon, A., Ma, S., and Feng, Y. (2016). The role of hippocampal estradiol receptor-alpha in a perimenopausal affective disorders-like rat model and attenuating of anxiety by electroacupuncture. *Evid. Based Complement. Alternat. Med.* 2016:4958312. doi: 10.1155/2016/4958312

Yoshida, M., Nakakimura, K., Cui, Y. J., Matsumoto, M., and Sakabe, T. (2004). Adenosine A(1) receptor antagonist and mitochondrial ATP-sensitive potassium channel blocker attenuate the tolerance to focal cerebral ischemia in rats. *J. Cereb. Blood Flow Metab.* 24, 771–779. doi: 10.1097/01.WCB.0000122742.72175.1B

Yuan, S., Zhang, X., Bo, Y., Li, W., Zhang, H., and Jiang, Q. (2014). The effects of electroacupuncture treatment on the postoperative cognitive function in aged rats with acute myocardial ischemia-reperfusion. *Brain Res.* 1593, 19–29. doi: 10.1016/j.brainres.2014.10.005

Zhang, Y., Jia, X., Yang, J., Li, Q., Yan, G., Xu, Z., et al. (2016a). Effects of Shaoyao-Gancao decoction on infarcted cerebral cortical neurons: suppression of the inflammatory response following cerebral ischemia-reperfusion in a rat model. *Biomed. Res. Int.* 2016:1859254. doi: 10.1155/2016/1859254

Zhang, Y., Lin, R., Tao, J., Wu, Y., Chen, B., Yu, K., et al. (2016b). Electroacupuncture improves cognitive ability following cerebral ischemia reperfusion injury via CaM-CaMKIV-CREB signaling in the rat hippocampus. *Exp. Ther. Med.* 12, 777–782. doi: 10.3892/etm.2016.3428

Zhou, H., Zhang, Z., Wei, H., Wang, F., Guo, F., Gao, Z., et al. (2013). Activation of STAT3 is involved in neuroprotection by electroacupuncture pretreatment via cannabinoid CB1 receptors in rats. *Brain Res.* 1529, 154–164. doi: 10.1016/j.brainres.2013.07.006

Conflict of Interest: The authors declare that the research was conducted in the absence of any commercial or financial relationships that could be construed as a potential conflict of interest.

Publisher's Note: All claims expressed in this article are solely those of the authors and do not necessarily represent those of their affiliated organizations, or those of the publisher, the editors and the reviewers. Any product that may be evaluated in this article, or claim that may be made by its manufacturer, is not guaranteed or endorsed by the publisher.

frontiers in Aging Neuroscience

ORIGINAL RESEARCH
published: 16 August 2021
doi: 10.3389/fnagi.2021.686598

Divergent Connectivity Changes in Gray Matter Structural Covariance Networks in Subjective Cognitive Decline, Amnestic Mild Cognitive Impairment, and Alzheimer's Disease

Zhenrong Fu[1], Mingyan Zhao[2,3], Yirong He[1], Xuetong Wang[1], Jiadong Lu[1], Shaoxian Li[1], Xin Li[4,5], Guixia Kang[6], Ying Han[3,7,8,9] and Shuyu Li[1]**

[1] School of Biological Science and Medical Engineering, Beijing Advanced Innovation Center for Biomedical Engineering, Beihang University, Beijing, China, [2] Department of Neurology, Tangshan Gongren Hospital, Tangshan, China, [3] Department of Neurology, Xuanwu Hospital of Capital Medical University, Beijing, China, [4] School of Electrical Engineering, Yanshan University, Qinhuangdao, China, [5] Measurement Technology and Instrumentation Key Laboratory of Hebei Province, Qinhuangdao, China, [6] School of Information and Communication Engineering, Beijing University of Posts and Telecommunications, Beijing, China, [7] Biomedical Engineering Institute, Hainan University, Haikou, China, [8] Center of Alzheimer's Disease, Beijing Institute for Brain Disorders, Beijing, China, [9] National Clinical Research Center for Geriatric Disorders, Beijing, China

Alzheimer's disease (AD) has a long preclinical stage that can last for decades prior to progressing toward amnestic mild cognitive impairment (aMCI) and/or dementia. Subjective cognitive decline (SCD) is characterized by self-experienced memory decline without any evidence of objective cognitive decline and is regarded as the later stage of preclinical AD. It has been reported that the changes in structural covariance patterns are affected by AD pathology in the patients with AD and aMCI within the specific large-scale brain networks. However, the changes in structural covariance patterns including normal control (NC), SCD, aMCI, and AD are still poorly understood. In this study, we recruited 42 NCs, 35 individuals with SCD, 43 patients with aMCI, and 41 patients with AD. Gray matter (GM) volumes were extracted from 10 readily identifiable regions of interest involved in high-order cognitive function and AD-related dysfunctional structures. The volume values were used to predict the regional densities in the whole brain by using voxel-based statistical and multiple linear regression models. Decreased structural covariance and weakened connectivity strength were observed in individuals with SCD compared with NCs. Structural covariance networks (SCNs) seeding from the default mode network (DMN), salience network, subfields of the hippocampus, and cholinergic basal forebrain showed increased structural covariance at the early stage of AD (referring to aMCI) and decreased structural covariance at the dementia stage (referring to AD). Moreover, the SCN seeding from the executive control network (ECN) showed a linearly increased extent of the structural covariance during the early and dementia stages. The results suggest that changes in structural covariance patterns as the order of NC-SCD-aMCI-AD are divergent and dynamic, and support the structural disconnection hypothesis in individuals with SCD.

Keywords: structural covariance network, subjective cognitive decline, structural MRI, default mode network, amnestic mild cognitive impairment, Alzheimer's disease

OPEN ACCESS

Edited by:
Dennis Qing Wang,
Southern Medical University, China

Reviewed by:
Tracy Fischer,
Tulane University, United States
Bin Deng,
Southern Medical University, China

****Correspondence:***
Ying Han
hanying@xwh.ccmu.edu.cn
Shuyu Li
shuyuli@buaa.edu.cn

Received: *27 March 2021*
Accepted: *19 July 2021*
Published: *16 August 2021*

Citation:
Fu Z, Zhao M, He Y, Wang X, Lu J, Li S, Li X, Kang G, Han Y and Li S (2021) Divergent Connectivity Changes in Gray Matter Structural Covariance Networks in Subjective Cognitive Decline, Amnestic Mild Cognitive Impairment, and Alzheimer's Disease. Front. Aging Neurosci. 13:686598. doi: 10.3389/fnagi.2021.686598

INTRODUCTION

Alzheimer's disease (AD), beginning with cognitive impairment, is the most common type of dementia, characterized by progressive and irreversible pathology with a long preclinical phase (Masters et al., 2015). Mild cognitive impairment (MCI) is the early symptomatic stage of AD, characterized by objective cognitive impairment, but largely preserves the daily functioning of individuals compared with dementia (Albert et al., 2011; Jack et al., 2018). Subjective cognitive decline (SCD) refers to the self-perceived worsening of cognitive ability, which is defined at the preclinical stage of AD and is independent of the neuropsychological tests (Jessen et al., 2014, 2020). The majority of individuals with SCD will not show sustained cognitive decline or progress to AD (Jessen et al., 2020) because the associations between self-perceived cognitive decline and objective cognitive impairment are complex. However, most of the studies have shown that symptoms of SCD may represent the earliest alert of AD, and individuals with SCD are at higher risk for developing AD or MCI (Rabin et al., 2017; Jessen et al., 2020; Wang et al., 2020b). Early diagnosis and intervention to preserve cognitive function is an important way to combat AD (Livingston et al., 2017); thus, it is critical to investigate the associations among biomarkers of SCD, MCI, and AD to provide a better opportunity for an early therapy (Jessen et al., 2020).

Reliable markers are crucial for diagnosis, intervention, and therapy in neurodegenerative diseases (Gao et al., 2020; Yang et al., 2020). For instance, the Aβ/Tau/neurodegeneration in AD-related disease (Jack et al., 2016), the "Hot cross bun" in multiple system atrophy with cerebellar ataxia (Zhu et al., 2021), and the motor abnormalities and α-synuclein in Parkinson's disease (PD) (Xie et al., 2019) have been proven to be potential biomarkers for an early detection of these diseases. Focusing on AD pathology, both the accumulation of amyloid-β (Aβ) in plaques and aggregation of the protein tau in neurofibrillary tangles are biomarkers that can be used to monitor the progression of AD (Jack et al., 2016). Moreover, the initial locations of Aβ deposition are in the frontal lobes, temporal lobes, hippocampus, and limbic system; and pathologic tau originates in the medial temporal lobes and hippocampus (Braak et al., 2011; Braak and Del Tredici, 2015; Masters et al., 2015). Studies based on neuroimaging have described hippocampal atrophy as an effective biomarker in patients with AD (Zhao et al., 2019; Wang et al., 2020b) and patients with MCI (Jack et al., 2010), and individuals with SCD (Cantero et al., 2016; Zhao et al., 2019). In addition, studies based on the resting-state functional magnetic resonance imaging (rs-fMRI) techniques have revealed that a specific set of brain regions (including the posterior cingulate cortex, anterior medial prefrontal cortex, medial temporal lobe, lateral temporal cortex, and inferior parietal lobule) forms a functional network associated with the resting states (Buckner et al., 2008; Yeo et al., 2011; Montembeault et al., 2016), named as the default mode network (DMN). With regard to the neurodegeneration within the DMN, reduced gray matter (GM) volume in DMN regions in patients with AD (Liu et al., 2011) and patients with MCI (Liu et al., 2011; Tosun et al., 2011), and individuals with SCD (Hafkemeijer et al., 2013) has been found in multiple studies. It is worth noting that pathologic tau and Aβ accumulation in the cholinergic nucleus basalis emerged early in AD (Arendt et al., 1988; Mesulam et al., 2004), and volume reductions in the basal forebrain were observed in patients with AD (Kilimann et al., 2014) and individuals with SCD (Scheef et al., 2019). Collectively, the pathology of Aβ/tau/neurodegeneration in regions of the DMN, hippocampus, and basal forebrain has been investigated but much remains to be learned about the variations in coordination with other regions in normal controls (NCs) and those in SCD, amnestic mild cognitive impairment (aMCI), and AD.

Mapping whole-brain GM correlations with seed regions to construct a GM structural covariance network (SCN) based on structural magnetic resonance imaging (sMRI) has been proposed to investigate the covariance in GM density (Mechelli et al., 2005; Alexander-Bloch et al., 2013; Evans, 2013). Although the biological basis of the SCN is not very clear, there are many hypotheses, such as a result of mutually trophic influences (Mechelli et al., 2005), common experience-related plasticity (Mechelli et al., 2005), common neurodevelopmental blueprints for axonal guidance and neuronal migration (Zielinski et al., 2010), or a combination of these factors (Seeley et al., 2009). However, the SCN technique has been used in many studies, such as those examining development (Zielinski et al., 2010), sex differences in healthy adults (Mechelli et al., 2005), brain plasticity in adults (Guo et al., 2020), and connectivity alterations in patients with MCI (Wang et al., 2018) and patients with AD (Seeley et al., 2009; Montembeault et al., 2016; Li et al., 2019a). In studies of AD, decreased structural associations were observed within the DMN, and increased structural associations were shown within the salience network (SN) and executive control network (ECN) (Montembeault et al., 2016; Li et al., 2019a), which is partially in line with functional network studies (Seeley et al., 2009; Zhou et al., 2010). Moreover, SCNs seeded from subfields of the hippocampus in patients with MCI showed an increased extent of structural association compared with NCs (Wang et al., 2018). It is worth noting that increased functional connectivity in the DMN was observed in individuals with SCD (Hafkemeijer et al., 2013). However, the pattern changes in SCNs as the order of NC-SCD-aMCI-AD are still poorly known. This information may provide a better understanding of the underlying neuropathological mechanisms of SCD and the association between SCD- and AD-related diseases at the network level.

In the present study, we employed the SCN to explore changes in structural connectivity in specific large-scale networks as the order of NC-SCD-aMCI-AD. We defined 10 seed regions at three levels: (1) spheres anchored in the DMN, SN, and ECN; (2) anatomical regions of the bilateral anterior and posterior hippocampus; and (3) two anatomical subregions of the basal forebrain. Our results indicated that the trajectory of change patterns in SCNs along NC-SCD-aMCI-AD potentially provides structural covariance insight into better understanding

of the progressive mechanism of cognitive decline due to AD-related pathology.

MATERIALS AND METHODS

Participants

In the present study, 35 individuals with SCD, 43 patients with aMCI, and 41 patients with AD were recruited from the memory clinic of the Neurology Department of XuanWu Hospital, Capital Medical University, China. Then, 42 NC individuals were enrolled from local communities in Beijing, China. This study was performed in accordance with the rule of ethics of the Medical Research Ethics Committee in Xuanwu Hospital, and every subject gave their written informed consent to participate. The sample size was calculated by the analysis of covariance (ANCOVA) model in G*Power 3.1.9.7 (Faul et al., 2007). The power (1-β) was 80%, α was 0.05, the effect size was 0.35, and the number of groups and covariates was 4. This calculation rendered a total sample size of 142, and 161 is larger than 142. The standard clinical assessments mainly included medical history investigations, neurological examinations, and neuropsychological tests. Cognitive tests included the Montreal Cognitive Assessment (MoCA, Beijing version) (Lu et al., 2011), auditory verbal learning test (AVLT) (namely, three memory tests: the AVLT immediate recall, the AVLT-delayed recall, and the AVLT recognition), the clinical dementia rating (CDR) (Morris, 1993), the Hamilton Depression Rating Scale (HAMD), the Activities of Daily Living (ADL) Scale, the Hachinski Ischemic Scale, and the Center for Epidemiologic Studies Depression Scale (Dozeman et al., 2011). In addition, the volunteers received a neuropsychological evaluation from two neurologists, each with more than 2 years of clinical experience in neurology.

The diagnostic criteria for individuals with SCD were based on the conceptual framework within the context of AD research proposed by the Subjective Cognitive Decline Initiative (Jessen et al., 2014), were described in our previous study (Fu et al., 2021), and included the following: (1) self-perceived memory decline without changes in other cognitive domains (last within 5 years); (2) feeling of worse performance than others of the same age group; (3) MoCA scores in the normal range (threshold was determined based on the different levels of education: primary school or below >19, secondary schooling >22, and university >24); (4) only one of the two memory tests (AVLT-delayed recall and AVLT recognition) was abnormal (one SD below NC performance); and (5) CDR score was 0. The patients with aMCI were identified with the Petersen criteria (Petersen, 2004), which included the following: (1) memory decline confirmed by an informant; (2) objective memory impairment measured by the MoCA and AVLT adjusted for education years (1.5 SD below NC performance); (3) CDR score of 0.5; (4) exclusion of subjects with other types of MCI, such as subcortical vascular MCI; and (5) exclusion of subjects with memory impairment of sufficient severity to affect the activities of daily living of the subject. The patients with AD were diagnosed based on the criteria of the National Institute of Aging-Alzheimer's Association (NIA-AA) (Sperling et al., 2011) for clinically probable AD, which included the following: (1) symptoms consistent with the diagnostic criteria for dementia; (2) brain atrophy in the hippocampus based on sMRI; (3) gradual onset lasting more than 6 months rather than a sudden attack; and (4) CDR scores equal to 1 or higher.

The exclusion criteria for all subjects in the present study were as follows: (1) HAMD scores higher than 24 and a score on the Center for Epidemiologic Studies Depression Scale higher than 21; (2) the Hachinski Ischemic Scale in the abnormal range (higher than 4); (3) left-handedness; (4) impaired executive, visual, or auditory functions; (5) cognitive function decline due to non-AD neurological diseases (e.g., brain tumor, brain injury, PD, encephalitis, and normal pressure hydrocephalus); (6) history of stroke; (7) history of alcohol or drug abuse/addiction within 2 years; (8) large-vessel disease; (9) any other systemic diseases or uncertainty preventing the completion of the project; and (10) frequent head motion that may influence the quality of MRI data. The main demographic and clinical characteristics of the subjects are summarized in **Table 1**.

Image Acquisition

All T1-weighted images were acquired with a 3.0 T Siemens system (Magnetom Trio Tim; Erlangen, Germany) by a 3D sagittal magnetization-prepared rapid gradient echo (MPRAGE) sequence at the Department of Radiology, Xuanwu Hospital, Capital Medical University, Beijing, China. The parameters were as follows: TR = 1,900 ms; TE = 2.2 ms; TI = 900 ms; flip angle = 9°; FOV = 22.4 cm × 25.6 cm; matrix size = 448 × 512; number of slices = 176; and slice thickness = 1 mm (Zhao et al., 2019; Fu et al., 2021).

Image Preprocessing

The non-uniformity intensity (N3) correction was first performed on anatomical T1 images by using FreeSurfer (version 6.0) (Fischl, 2012). After N3 correction, the images were analyzed with the CAT12 toolbox[1]. The pipeline in CAT12 includes removing noise with a spatial-adaptive non-local means denoizing filter (Manjón et al., 2010), segmenting the brain tissues into GM, white matter, and cerebrospinal fluid by local adaptive segmentation, partial volume estimation, and adaptive maximum *a posteriori* techniques, normalizing the images to a standard Montreal Neurological Institute (MNI) space by diffeomorphic anatomic registration through exponentiated Lie algorithm (Ashburner, 2007). Moreover, the GM images were modulated by Jacobian determinants to preserve the regional volume information. Finally, the GM images were smoothed in SPM12[2] with a 6-mm (subregions of hippocampus and basal forebrain) and 12-mm (DMN, SN, and ECN) full-width at half-maximum Gaussian kernel.

Definition of Seed Regions

Anatomical differentiation and functional segregation have been shown along the long axis of the hippocampus, and specializations arise out of differences between the anterior hippocampus and posterior hippocampus in large-scale network

[1]http://dbm.neuro.uni-jena.de/cat/

[2]https://www.fil.ion.ucl.ac.uk/spm/

TABLE 1 | Demographic characteristics and neuropsychological data.

	NC Group (42)	SCD Group (35)	aMCI Group (43)	AD Group (41)
Age (y)	64.24 ± 6.16	64.54 ± 7.29	67.47 ± 10.03	68.88 ± 7.86
Sex (men/women)	15/27	15/20	21/22	17/24
Education (y)	11.17 ± 5.61	11.83 ± 3.67	10.44 ± 4.96	9.68 ± 4.71
eTIV (* 10^6 mm^3)	1.40 ± 0.12	1.44 ± 0.14	1.47 ± 0.16	1.40 ± 0.13
MoCA	26.02 ± 2.95	25.26 ± 2.27	19.67 ± 4.28^{aaabbb}	13.10 ± 5.46^{aaabbbccc}
AVLT immediate recall	9.32 ± 1.94	8.54 ± 1.82	5.84 ± 1.34^{aaabbb}	3.53 ± 1.58^{aaabbbccc}
AVLT delayed recall	10.43 ± 2.31	8.86 ± 2.78^{a}	3.19 ± 2.81^{aaabbb}	0.98 ± 1.60^{aaabbbccc}
AVLT recognition	12.07 ± 2.13	11.37 ± 2.20	6.58 ± 4.28^{aaabbb}	3.51 ± 3.08^{aaabbbccc}

NC, normal control; aMCI, amnestic mild cognitive impairment; SCD, subjective cognitive decline; AD, Alzheimer's disease; MoCA, Montreal Cognitive Assessment (Beijing version); AVLT, auditory verbal learning test; eTIV, estimated total intracranial volume.
The values represent the mean ± standard deviation.
[a]Denotes a significant difference between the NC group and other groups ([a]$p < 0.05$, [aa]$p < 0.01$, and [aaa]$p < 0.001$).
[b]Indicates a significant difference between the SCD group and the other groups ([b]$p < 0.05$, [bb]$p < 0.01$, and [bbb]$p < 0.001$).
[c]Represents a significant difference between the aMCI and other groups ([c]$p < 0.05$, [cc]$p < 0.01$, and [ccc]$p < 0.001$).

connectivity (Poppenk et al., 2013). In this study, the anterior hippocampus and posterior hippocampus were defined based on the previous studies (Poppenk et al., 2013; Li et al., 2018; Nordin et al., 2018), and we adopted the automated anatomical labeling (AAL) (Tzourio-Mazoyer et al., 2002) atlas for the segmentation of the hippocampus. In MNI coordinates, the anterior hippocampus masks from Y: −2 to −18 mm and the posterior hippocampus masks from Y: −24 to −42 mm. The seed regions representing functional large-scale networks were selected within the right entorhinal cortex (R EC) (MNI coordinates: 25, −9, and −28), left posterior cingulate cortex (L PCC) (MNI coordinates: −2, −36, and 35), right frontoinsular cortex (R FIC) (MNI coordinates: 38, 26, and −10), and right dorsolateral prefrontal cortex (R DLPFC) (MNI coordinates: 44, 36, and 20). These regions anchor the DMN (medial temporal lobe subsystem and midline core subsystem), SN, and ECN (Montembeault et al., 2016; Li et al., 2019a). Then, analyses of the contralateral regions of the R EC, L PCC, R FIC, and R DLPFC were performed. Finally, the subregions of the basal forebrain were defined by a basal forebrain atlas in MNI space that has been widely used in the previous studies (Kilimann et al., 2014; Scheef et al., 2019; Chen et al., 2021). The Ch4p (cholinergic system of the posterior nucleus basalis Meynert) and Ch1/2 (cholinergic system of combined clusters of the medial septum and the vertical limb of the diagonal band) with observed volume reductions in SCD (Scheef et al., 2019; Chen et al., 2021) and AD (Kilimann et al., 2014) were selected as seed regions. The volume of the hippocampus and basal forebrain subregions were represented by mean values of the modulated GM voxels within the masks in MNI space. For the functional large-scale network seed regions, 4-mm radius sphere masks were constructed by using the MarsBaR toolbox[3], and the mean GM intensity was calculated.

Structural Covariance Analysis

Multiple regression models combined with voxel-based statistical analysis were performed on the modulated GM images to investigate the structural covariance between seed regions and whole brain voxels in each group. The mean values extracted from the seed regions, age, sex, education years, and estimated total intracranial volume (eTIV) were used as covariates. We performed specific T contrasts to identify voxels expressing a positive correlation within each group (NC, SCD, aMCI, and AD). The resulting maps for each group were thresholded at $p < 0.05$, and the false discovery rate (FDR) was employed for multiple comparison correction. Cluster sizes larger than 100 voxels (337.5 mm^3) were reported.

Furthermore, the between-group differences in structural covariance compared with the NC group were assessed by differences in slopes. We used a linear interaction model combined with dummy coding, and the mean values extracted from the seed regions, group, interaction term (group × mean values of seed regions), age, sex, education years, and eTIV were used as covariates. Specific T contrasts were established to map the significantly different structural covariance voxels in slopes between two groups, including positive and negative correlations. We set the threshold at $p < 0.01$ at the voxel level and $p < 0.05$ at the cluster level with two-tailed Gaussian random field (GRF) correction. Cluster sizes larger than 100 voxels (337.5 mm^3) were reported. The coordinates of the peak intensity of the cluster within the scope of the AAL template were reported, except when there was only one cluster.

To investigate the correlation between the volume of structural covariance peak regions and clinical tests, we performed two-tailed partial correlation analysis within each group, which showed a significant difference in the structural covariance (Li et al., 2019a), and the effects of age, sex, and education years were ruled out ($p < 0.05$). The GM volume of the peak regions was extracted by spheres with a radius of 4 mm around the peak intensity coordinates.

Group differences in age, years of education, eTIV, and neuropsychological test scores (MoCA and AVLT) were evaluated by ANOVA ($p < 0.05$), and Bonferroni *post hoc* analysis was performed. The chi-square test was used to investigate the sex distribution.

[3]http://marsbar.sourceforge.net/

RESULTS

Demographics

There were no significant differences in age, sex, education years, or eTIV for each pair of groups. The AVLT-delayed recall scores were significantly lower in the SCD group compared with the NC group ($p < 0.05$). Moreover, all the neuropsychological test scores (MoCA and AVLT) in the aMCI group were significantly lower than those in the NC and SCD groups ($p < 0.001$). In addition, all the neuropsychological test scores (MoCA and AVLT) in the AD group were lower than those in the other groups ($p < 0.001$). The results are shown in **Table 1** and **Supplementary Figure 1**.

Patterns of Structural Covariance Within Groups

To qualitatively compare the patterns of positive correlations across subjects within all groups, statistical maps are displayed in **Figures 1–3**, and the details are shown in **Supplementary Tables 1–12**. Regarding the DMN medial temporal subsystem, DMN midline core subsystem and SN, the aMCI group showed a greater extent of structural association than the other groups. In the ECN, the AD group exhibited an increased extent of structural association compared with the SCD, aMCI, and NC groups. The SCD group showed a decreased extent of structural covariance in both DMN subsystems, SN and ECN. In the DMN medial temporal subsystem, DMN midline core subsystem and SN, the number of clusters in the SCD group, aMCI and AD groups were decreased compared with the NC group. Regarding the bilateral anterior hippocampus and posterior hippocampus, the aMCI group showed a greater extent of structural covariance than the other groups. In all the subfields of the hippocampus, the subjects in the SCD group presented a decreased extent of structural covariance compared with the NC group. In the SCNs, seeded from subregions of the basal forebrain, both Ch4p and Ch1/2 showed a greater extent of structural covariance in the aMCI group than in the other groups. The results of contralateral seeds for the DMN subsystems, SN, and ECN, obtained by changing the sign on the x coordinate of each seed, are listed in **Supplementary Tables 1–4**. In addition, the

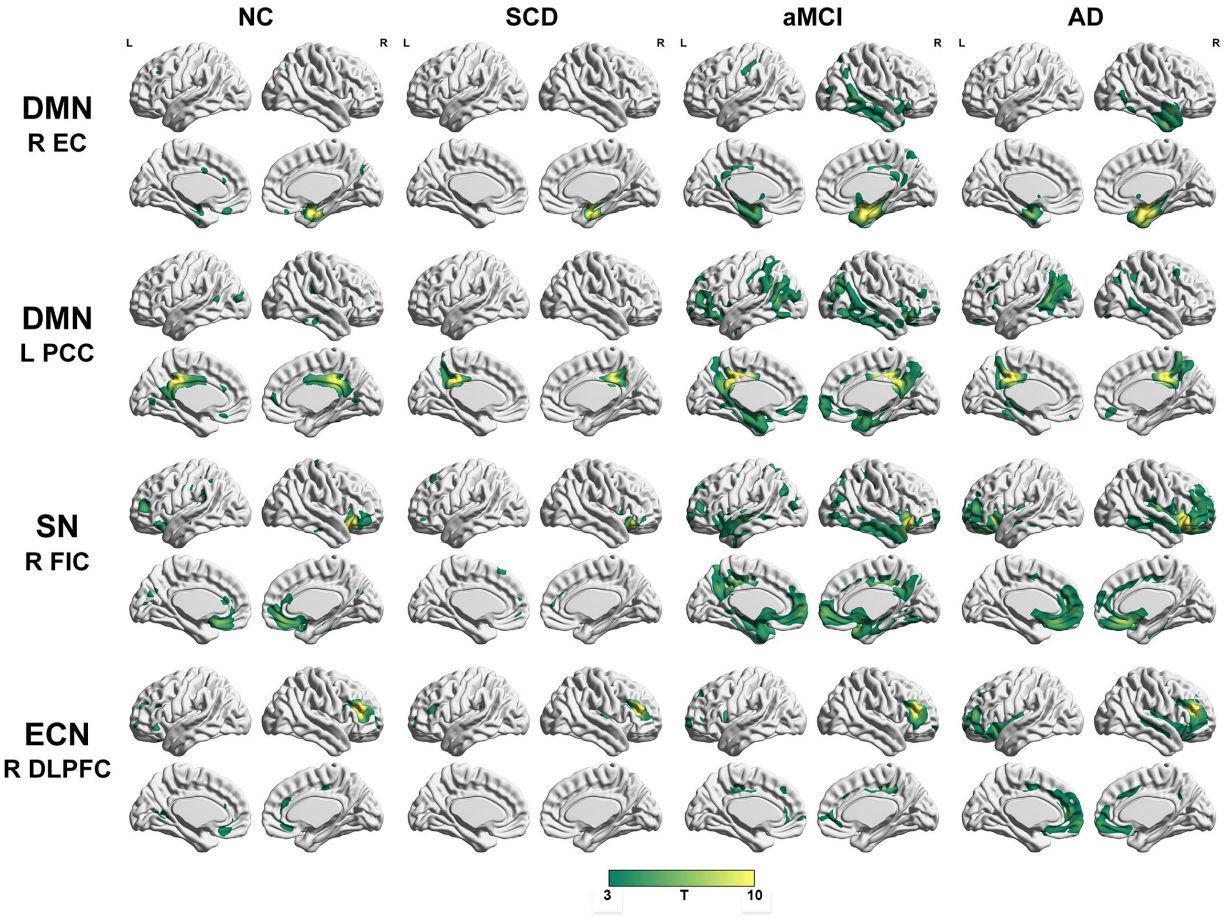

FIGURE 1 | Structural covariance networks seeding from the default mode network, salience network, and executive control network within groups. T-statistic maps, $p < 0.05$, corrected by false discovery rate (FDR) with cluster size larger than 100 voxels. L, left; R, right; EC, entorhinal cortex; PCC, posterior cingulate cortex; DLPFC, dorsolateral prefrontal cortex; FIC, frontoinsular cortex; AD, Alzheimer's disease; NC, normal control; aMCI, amnestic mild cognitive impairment; SCD, subjective cognitive decline.

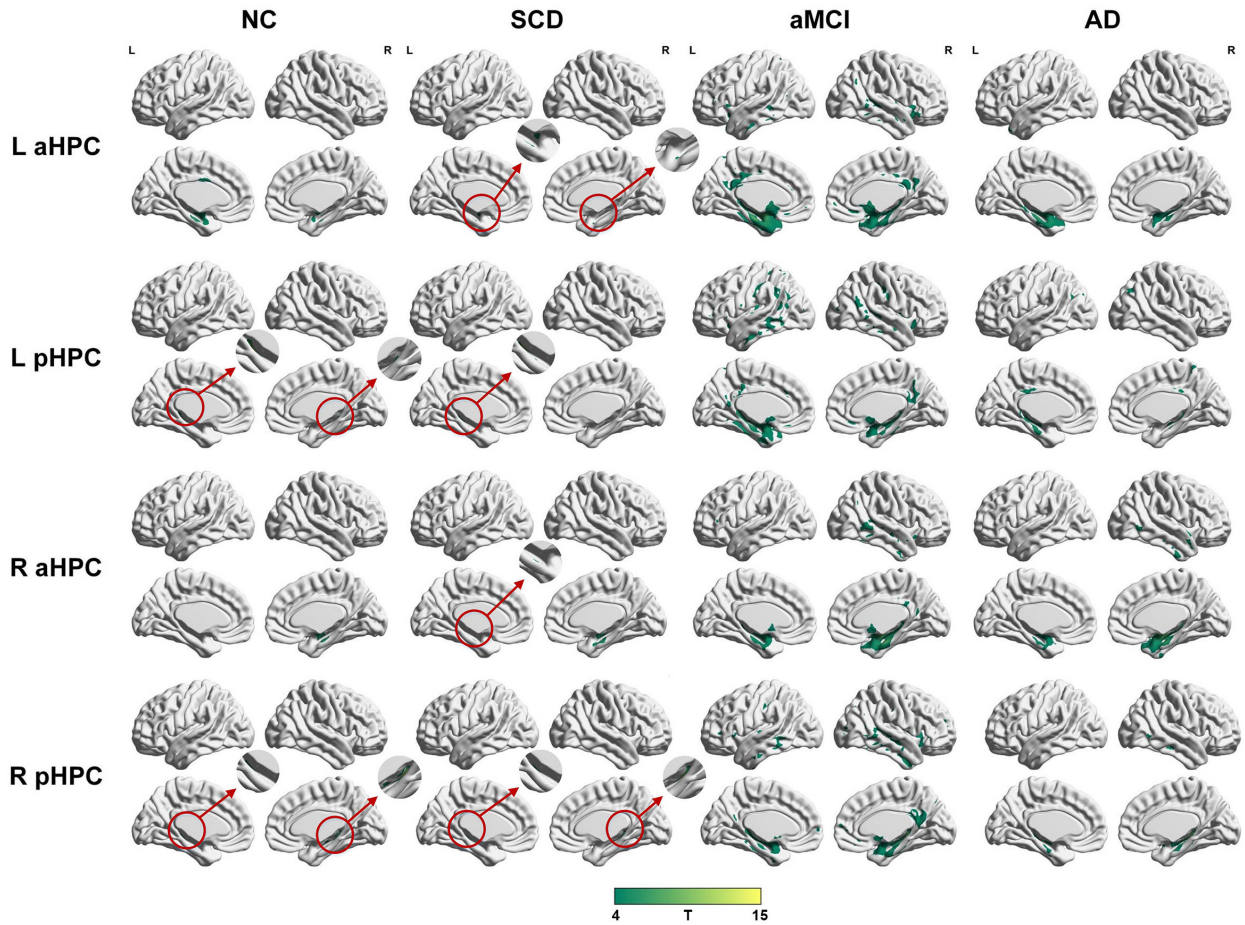

FIGURE 2 | Structural covariance networks seeding from the anterior and posterior hippocampus within groups. T-statistic maps, $p < 0.05$, corrected by false discovery rate (FDR) with cluster size larger than 100 voxels. The small clusters are circled by the red circles, and they are enlarged. L, left; R, right; aHPC, anterior hippocampus; pHPC, posterior hippocampus; AD, Alzheimer's disease; NC, normal control; aMCI, amnestic mild cognitive impairment; SCD, subjective cognitive decline.

results of other subregions of the basal forebrain are listed in **Supplementary Tables 9–12**.

Significant Between-Group Differences in the Structural Covariance GM Network

Regarding the DMN medial temporal subsystem, the subjects in the NC group showed increased strength in structural covariance compared with those in the SCD group in the right supramarginal gyrus (2,280 voxels) and in the left precentral gyrus compared with the aMCI (3,034 voxels) and AD (10,492 voxels) groups. Regarding the DMN midline core subsystem, the subjects in the NC group showed significantly increased strength in the structural covariance compared with those in the SCD group in the right inferior temporal gyrus (5,277 voxels), those in the aMCI group in the left middle frontal gyrus (7,638 voxels), and those in the AD group in the left precentral gyrus (1,743 voxels). Regarding the SN, the subjects in the NC group showed significantly increased strength in structural covariance compared with those in the SCD group in the left inferior parietal gyrus (2,289 voxels) and those in the aMCI group in the right precentral gyrus (1,541 voxels); the subjects in the NC group showed decreased strength in structural covariance in the right middle temporal gyrus compared with subjects in the aMCI group (3,646 voxels). Regarding the ECN, the subjects in the NC group showed significantly increased strength in structural covariance compared with those in the SCD group in the right inferior temporal gyrus (865 voxels); the subjects in the NC group showed decreased strength in structural covariance compared with those in the aMCI group in the right median cingulate (269 voxels) and those in the AD group in the right precuneus (934 voxels). The results are shown in **Table 2** and **Figure 4**.

Within the SCN seeding from the left anterior hippocampus, decreased strength in structural covariance were observed in the SCD (left middle temporal gyrus; 313 voxels), aMCI (right precentral gyrus; 2,119 voxels), and AD (right superior temporal gyrus; 2,665 voxels) groups compared with the NC group. Moreover, within the SCN seeding from the left posterior hippocampus, decreased strength in structural covariance was

TABLE 2 | Significant between-group (NC-SCD, NC-aMCI, and NC-AD) differences in structural covariance seeding from the DMN, SN, and ECN.

Seed	Contrast	Peak region	MNI coordinates			Extent	Peak intensity
			X	Y	Z		
R entorhinal cortex	NC > SCD	SupraMarginal_R	63	−24	43.5	2280	−3.9511
	NC > aMCI	Precentral_L	−7.5	−7.5	39	3034	−3.9178
	NC > AD	Precentral_L	−3.5	−6	43.5	10492	−4.5574
	NC < AD	ParaHippocampal_R	18	−1.5	−2.5	273	3.267
L posterior cingulate cortex	NC > SCD	Temporal_Inf_R	49.5	−36	−6.5	5277	−4.2714
	NC > aMCI	Frontal_Mid_L	−5.5	24	34.5	7638	−5.4367
	NC > AD	Precentral_L	−6.5	−6.5	72	1743	−3.7043
	NC < SCD	Precuneus_R	3	−51	45	357	3.2657
	NC < aMCI	Temporal_Mid_R	51	−58.5	16.5	431	3.3112
	NC < AD	Temporal_Mid_R	42	−52.5	19.5	1034	4.0244
R frontoinsular cortex	NC > SCD	Parietal_Inf_L	−34.5	−45	48	2289	−3.8531
	NC > aMCI	Precentral_R	15	−27	79.5	1541	−4.7806
	NC > AD	Precentral_R	15	−27	75	751	−3.8561
	NC < aMCI	Temporal_Mid_R	49.5	−46.5	6	3646	3.2717
	NC < AD	Supp_Motor_Area_R	12	−18	49.5	489	3.1579
R dorsolateral prefrontal cortex	NC > SCD	Temporal_Inf_R	54	−48	−27	865	−3.3482
	NC > AD	Calcarine_L	−15	−49.5	10.5	106	−3.0684
	NC < SCD	Occipital_Mid_L	−39	−67.5	1.5	313	3.4323
	NC < aMCI	Cingulum_Mid_R	7.5	−39	43.5	269	3.1672
	NC < AD	Precuneus_R	12	−57	40.5	934	3.602

L, left; R, right; AD, Alzheimer's disease; NC, normal control; aMCI, amnestic mild cognitive impairment; SCD, subjective cognitive decline; MNI, Montreal Neurological Institute.

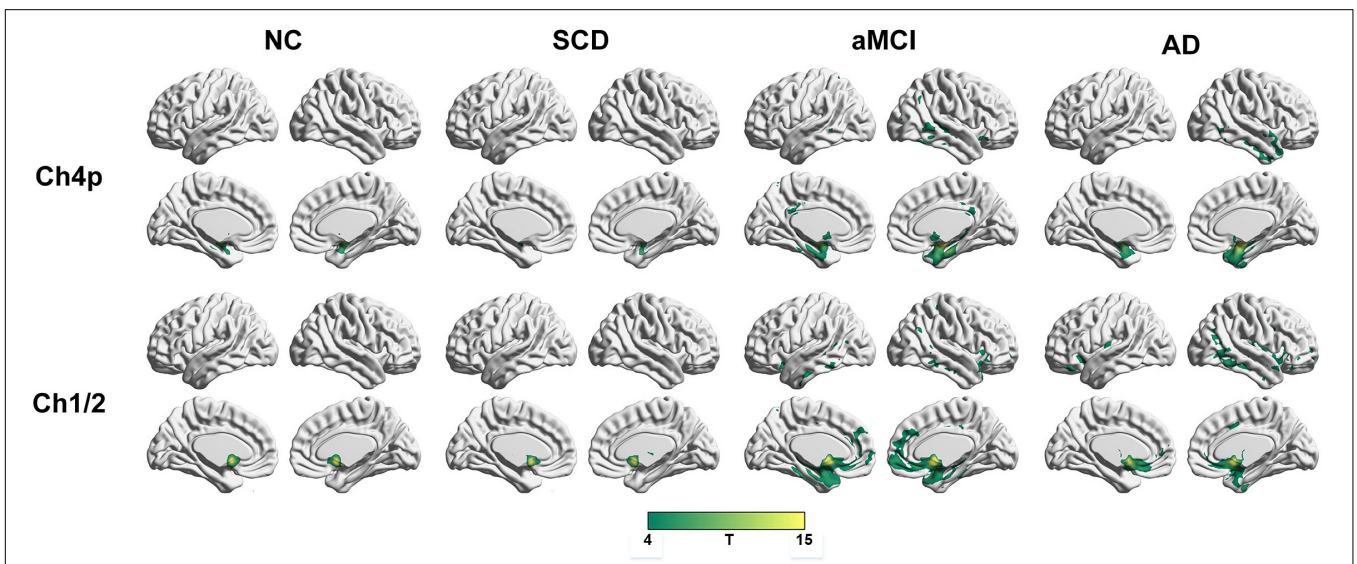

FIGURE 3 | Structural covariance networks seeding from the Ch4p and Ch1/2 within groups. T-statistic maps, $p < 0.05$, corrected by false discovery rate (FDR) with cluster size larger than voxels. L, left; R, right; AD, Alzheimer's disease; NC, normal control; aMCI, amnestic mild cognitive impairment; SCD, subjective cognitive decline.

shown in the SCD group (right middle temporal gyrus; 4,204 voxels) compared with the NC group; subjects in the NC group showed decreased structural covariance compared with those in the aMCI (right middle temporal gyrus; 1,656 voxels) and AD (left angular gyrus; 603 voxels) groups. Then, within the SCN seeding from the right anterior hippocampus, the subjects in the NC group showed increased strength in structural covariance compared with those in the SCD (right supramarginal gyrus; 1,307 voxels) and AD (left middle frontal gyrus; 1,900 voxels) groups. Within the SCN seeding from the right posterior hippocampus, the subjects in the NC group showed increased strength in structural covariance compared with those in the

SCD (left superior frontal gyrus; 2,815 voxels) and AD (right parahippocampal gyrus; 3,511 voxels) groups. In addition, within the SCN seeding from the Ch4p, the subjects in the NC group showed increased strength in structural covariance compared with those in the aMCI (right superior temporal gyrus; 5,533 voxels) and AD (right median cingulate gyrus; 10,790 voxels) groups. In addition, within the SCN seeding from the Ch1/2, the subjects in the NC group showed increased strength in structural covariance compared with those in the SCD (left parahippocampal gyrus; 1,044 voxels) and AD (left superior frontal gyrus; 1,161 voxels) groups. The results are summarized in **Tables 3**, **4** and **Figure 5**. The results with the contralateral seeds for the DMN subsystems, SN and ECN, obtained by changing the sign on the x coordinate of each seed, are listed in **Supplementary Tables 13–15**, and the results of other subregions of the basal forebrain are listed in **Supplementary Tables 19–21**.

Correlation Analysis Between Peak Cluster Volume and Cognitive Test Scores

We then performed partial correlation analysis between the peak cluster volumes with significant interaction effects and cognitive test scores within each group. The correlations were mainly located in the SCN seeding from DMN regions such as the hippocampus and posterior cingulate cortex. In the SCD group, the left anterior hippocampus-anchored ($r = -0.351$, $p = 0.049$)

TABLE 3 | Significant between-group (NC-SCD, NC-aMCI, and NC-AD) differences in structural covariance networks seeding from anterior and posterior hippocampi.

Seed	Contrast	Peak region	MNI coordinates			Extent	Peak intensity
			X	Y	Z		
L anterior hippocampus	NC > SCD	Temporal_Mid_L	–52.5	–49.5	0	313	–3.7864
	NC > aMCI	Precentral_R	43.5	–12	61.5	2119	–4.0192
	NC > AD	Temporal_Sup_R	40.5	–27	10.5	2665	–4.0872
	NC < aMCI	Hippocampus_L	–25.5	–13.5	–13.5	239	5.0774
	NC < AD	Precuneus_R	3	–48	60	411	3.6251
L posterior hippocampus	NC > SCD	Temporal_Mid_R	49.5	–48	15	4204	–5.1987
	NC > aMCI	Precentral_R	16.5	–27	73.5	878	–4.3176
	NC > AD	Frontal_Sup_L	–18	16.5	49.5	1193	–3.9886
	NC < aMCI	Temporal_Mid_R	48	–58.5	13.5	1656	4.5496
	NC < AD	Angular_L	–52.5	–69	30	603	4.1876
R anterior hippocampus	NC > SCD	SupraMarginal_R	58.5	–28.5	42	1307	–4.3683
	NC > aMCI	Temporal_Sup_R	57	–31.5	15	206	–4.1619
	NC > AD	Frontal_Mid_L	–28.5	28.5	36	1900	–4.4319
	NC < SCD	Occipital_Mid_L	–42	–73.5	1.5	123	3.788
	NC < AD	Insula_R	43.5	13.5	–7.5	382	4.2362
R posterior hippocampus	NC > SCD	Frontal_Sup_L	–16.5	22.5	63	2815	–4.5136
	NC > aMCI	Precentral_R	15	–27	75	571	–4.0688
	NC > AD	ParaHippocampal_R	33	–36	–4.5	3511	–4.4366
	NC < aMCI	Temporal_Mid_R	49.5	–60	13.5	570	3.9456

L, left; R, right; AD, Alzheimer's disease; NC, normal control; aMCI, amnestic mild cognitive impairment; SCD, subjective cognitive decline; MNI, Montreal Neurological Institute.

TABLE 4 | Significant between-group (NC-SCD, NC-aMCI, and NC-AD) differences in structural covariance networks seeding from the Ch4p and Ch1/2.

Seed	Contrast	Peak region	MNI coordinates			Extent	Peak intensity
			X	Y	Z		
Ch4p	NC > SCD	Temporal_Mid_L	–52.5	–51	1.5	133	–3.5685
	NC > aMCI	Temporal_Sup_R	55.5	–30	16.5	5533	–5.6571
	NC > AD	Cingulum_Mid_R	1.5	36	31.5	10790	–5.0984
	NC < SCD	Occipital_Mid_L	–40.5	–72	3	126	3.5079
Ch1/2	NC > SCD	ParaHippocampal_L	–30	–18	–22.5	1044	–4.1796
	NC > aMCI	Temporal_Sup_R	57	–30	15	279	–4.4193
	NC > AD	Frontal_Sup_L	–24	6	64.5	1161	–4.2794
	NC < AD	Temporal_Pole_Sup_R	55.5	16.5	–13.5	287	3.8021

Ch4p, cholinergic system of posterior nucleus basalis Meynert; Ch1/2, cholinergic system of combined clusters of the medial septum and the vertical limb of the diagonal band; AD, Alzheimer's disease; NC, normal control; aMCI, amnestic mild cognitive impairment; SCD, subjective cognitive decline; MNI, Montreal Neurological Institute.

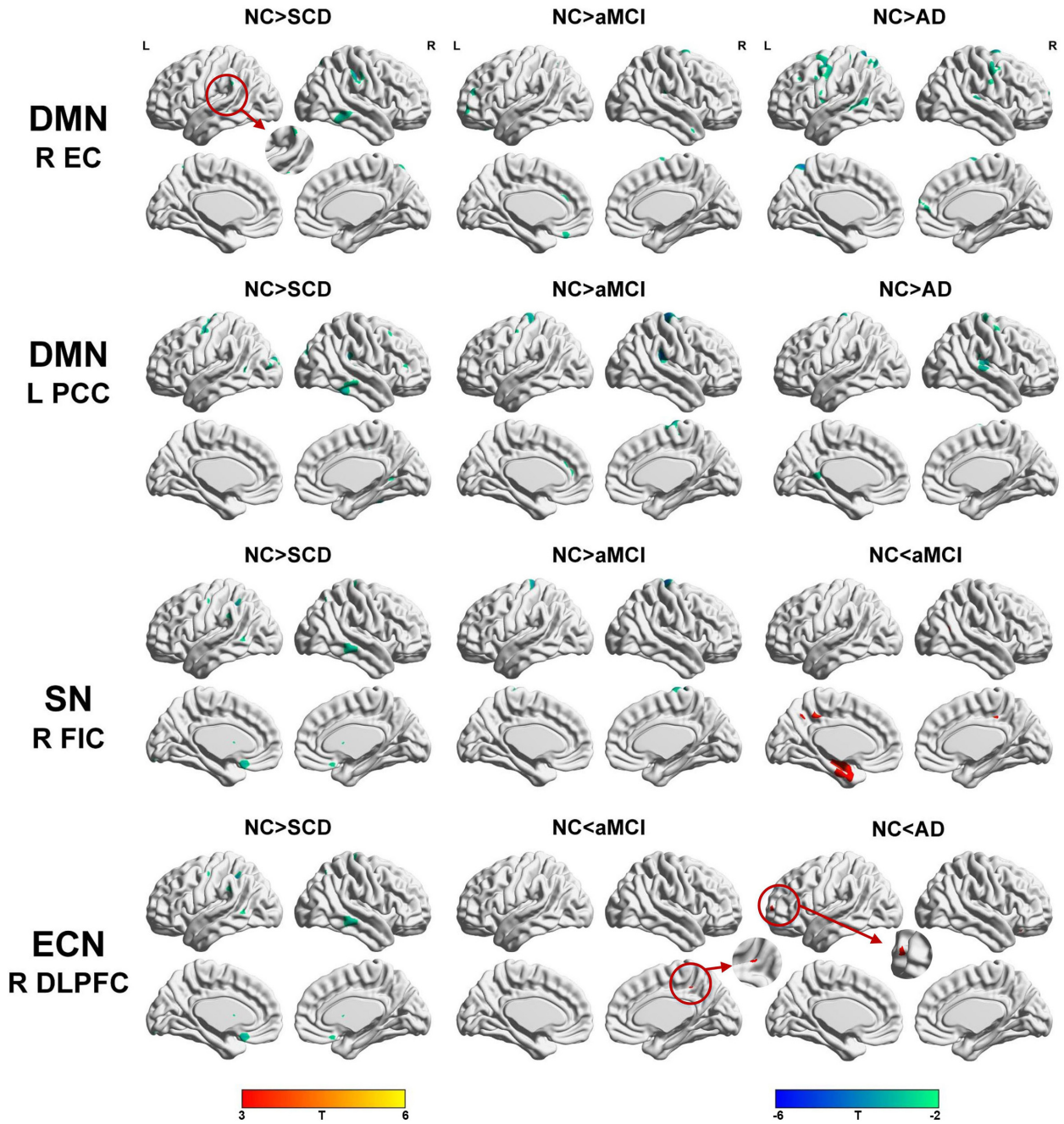

FIGURE 4 | Between-group (NC-SCD; NC-aMCI; and NC-AD) differences in structural covariance networks seeding from the default mode network, salience network, and executive control network. T-statistic maps, $p < 0.01$ at the voxel level and $p < 0.05$ at the cluster level, two-tailed Gaussian random field (GRF) correction with cluster size larger than 100 voxels. The small clusters are circled by the red circles, and they are enlarged. L, left; R, right; EC, entorhinal cortex; PCC, posterior cingulate cortex; DLPFC, dorsolateral prefrontal cortex; FIC, frontoinsular cortex; AD, Alzheimer's disease; NC, normal control; aMCI, amnestic mild cognitive impairment; SCD, subjective cognitive decline.

and posterior hippocampus-anchored ($r = 0.505$, $p = 0.003$) peak volumes (middle temporal gyrus) showed significant correlations with AVLT recognition scores. In the aMCI group, the peak volume in the hippocampus (left anterior hippocampus-anchored) significantly correlated with AVLT-delayed recall ($r = 0.351$, $p = 0.027$) and AVLT recognition ($r = 0.456$, $p = 0.003$) scores; the peak volume in the middle temporal gyrus (left posterior hippocampus-anchored) significantly correlated with AVLT recognition scores ($r = 0.420$; $p = 0.007$); the peak volume in the middle temporal gyrus (right posterior hippocampus-anchored) significantly correlated with AVLT recognition scores ($r = 0.463$; $p = 0.003$); the peak volume in the middle temporal

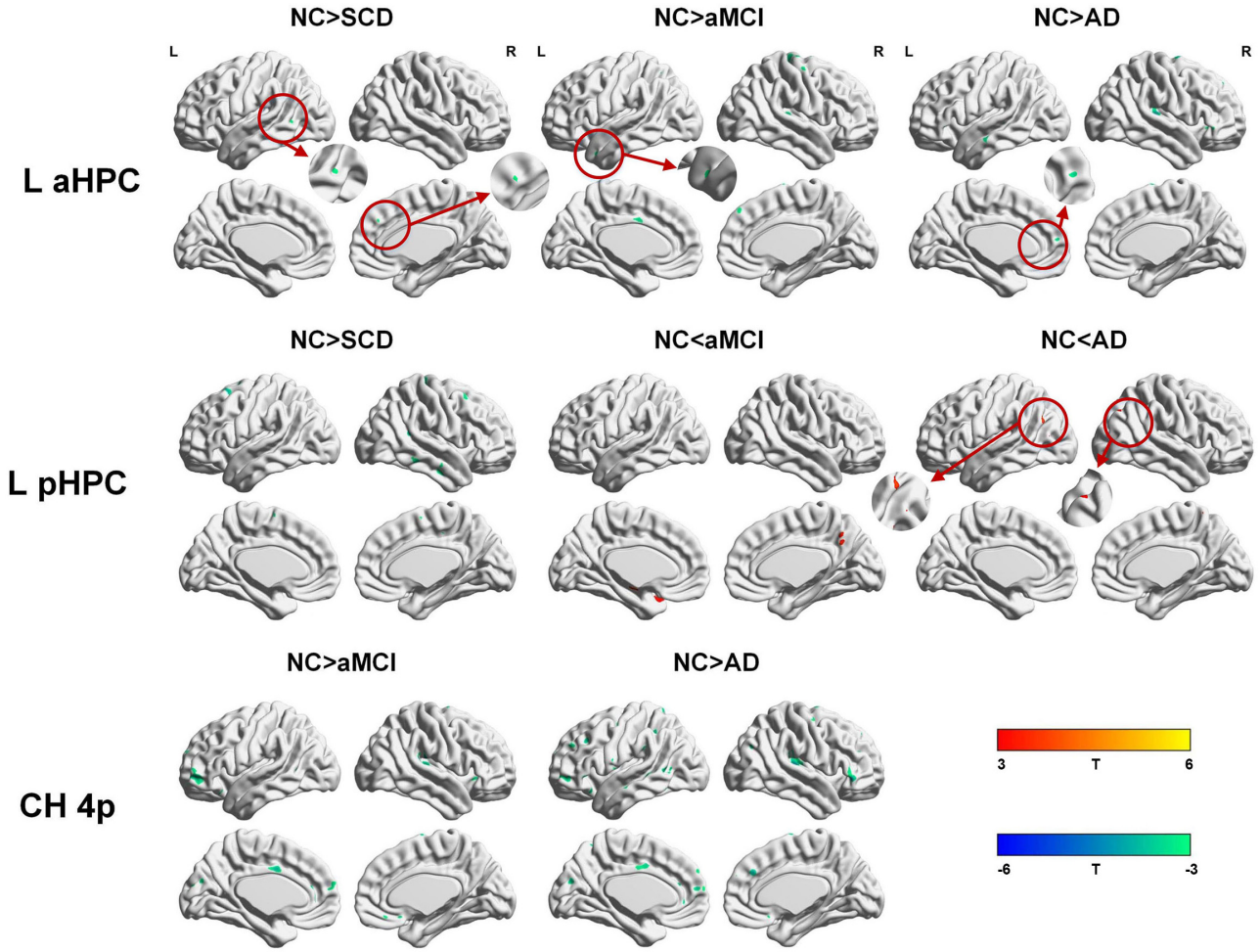

FIGURE 5 | Between-group (NC-SCD; NC-aMCI; and NC-AD) differences in structural covariance networks seeding from the left anterior and posterior hippocampus and Ch4p. T-statistic maps, $p < 0.01$ at the voxel level and $p < 0.05$ at the cluster level, two-tailed GRF correction with cluster size larger than 100 voxels. The small clusters are circled by the red circles, and they are enlarged. L, left; R, right; aHPC, anterior hippocampus; pHPC, posterior hippocampus; AD, Alzheimer's disease; NC, normal control; aMCI, amnestic mild cognitive impairment; SCD, subjective cognitive decline.

gyrus (DMN midline core subsystem-anchored) significantly correlated with AVLT recognition scores ($r = 0.401$; $p = 0.010$); and the peak volume in the middle temporal gyrus (SN-anchored) significantly correlated with AVLT recognition scores ($r = 0.376$; $p = 0.017$). In the AD group, the peak volume in the precuneus showed a significant correlation with AVLT-delayed recall scores ($r = 0.450$, $p = 0.005$). The results of the correlation analyses are summarized in **Supplementary Tables 22–24**.

DISCUSSION

The present study aimed to investigate the AD-related changes in the GM in SCNs in individuals with SCD and the patients with aMCI and AD. Regarding the DMN and SN, the subjects in the aMCI and AD groups showed increased and decreased structural associations, respectively. Regarding the ECN, the subjects in the aMCI and AD groups exhibited linearly increased structural associations. Specifically, the SCNs anchored to the DMN, SN, and ECN decreased in the SCD group compared with the NC group. The pattern changes of SCNs seeding from the anterior hippocampus, posterior hippocampus, Ch4p, and Ch1/2 as the order of NC-SCD-aMCI-AD showed similar trends to the SCNs anchored to the DMN. However, the connectivity strength of the SCNs seeding from the DMN, SN, anterior hippocampus, posterior hippocampus, Ch4p, and Ch1/2 decreased in the individuals with SCD, aMCI, and AD compared with the NCs. In addition, the connectivity strength of the SCNs seeded from the ECN was increased in the patients with aMCI and AD. Our results suggest that the pattern changes in the SCNs as the order of NC-SCD-aMCI-AD are dynamic and divergent, which may provide evidence for disconnection in SCNs in individuals with SCD.

The results are partially consistent with previous studies showing changes in the DMN (Seeley et al., 2009; Zhou et al., 2010; Li et al., 2015; Chang et al., 2018; Xue et al., 2019), SN

(Zhou et al., 2010; Li et al., 2015), and ECN (Weiler et al., 2014; Li et al., 2015) in patients with MCI and AD based on fMRI analysis. Moreover, the results in this study were generally in line with the previous studies based on SCNs, which observed changes in the DMN, SN, and ECN in patients with AD (Montembeault et al., 2016; Chang et al., 2018; Li et al., 2019a) and MCI (Shu et al., 2018). The possible underlying mechanism is that Aβ/tau/neurodegeneration pathological processes originate and concentrate in the DMN regions (Masters et al., 2015), the connectivity strength within the DMN is weakened, and more tissue is needed for the functional compensation. However, functional compensation by a large-scale network was shown in the SN and ECN due to AD pathology in our results. In our opinion, performing functional compensation is a more complex process, indicating that there may be multiple ways to participate in this process, not just compensation by large-scale networks. Although the results from the SCN analysis do not perfectly overlap the results with the functional network, many researchers agree that SCN analysis is an effective tool to investigate the topological organization of the brain and serves as a measure of network integrity in the cross-sectional group studies (Zielinski et al., 2010; Alexander-Bloch et al., 2013; Montembeault et al., 2016; Li et al., 2019a).

SCNs seeded from the anterior hippocampus and posterior hippocampus have been used to investigate the effects of aging (Li et al., 2018; Nordin et al., 2018), memory (Nordin et al., 2018), plasticity (Guo et al., 2020), and sex (Persson et al., 2014). However, the connectivity changes of SCNs induced by AD-related pathology seeding in the anterior hippocampus and posterior hippocampus remain poorly understood. Although the hippocampus belongs to the DMN medial temporal lobe subsystem, the function of the hippocampus is more focused on memory. With specialization along the long axis, the hippocampus was divided into two anatomical structures, the anterior hippocampus and the posterior hippocampus. Moreover, long-range connections between the anterior hippocampus and the perirhinal cortex, amygdala, hypothalamus, temporal lobe, insula, and prefrontal cortex; and long-range connections between the posterior hippocampus and the parahippocampal cortex, cingulate cortex, cuneus, precuneus, prefrontal cortex, and parietal lobe have been confirmed in humans (Poppenk et al., 2013). Our results suggested that the pattern changes in SCNs seeded from the anterior hippocampus and posterior hippocampus were similar to those of SCNs seeded from the DMN. However, a greater extent of structural covariance was shown in the anterior hippocampus than in the posterior hippocampus in all groups, which was consistent with a previous study (Li et al., 2018). The possible mechanism is that the neurodegenerative diseases were similar to the accelerated aging, and the age-related functional connectivity strength in healthy adults between the posterior hippocampus and DMN was stronger than the connectivity between the anterior hippocampus and DMN (Damoiseaux et al., 2016), while the connectivity changes in the DMN induced by AD-related pathology may have a greater impact on the connections between the posterior hippocampus and DMN compared with the connections between the anterior hippocampus and DMN. In addition, a previous study based on SCNs reported that structural connectivity between the hippocampus and DMN regions was limited to the anterior hippocampus, although these discrepancies may have been due to methodological differences (Li et al., 2018).

Atrophy in the cholinergic basal forebrain has been observed in advanced age (Grothe et al., 2012), individuals with SCD (Scheef et al., 2019; Chen et al., 2021), and patients with AD (Grothe et al., 2012; Kilimann et al., 2014). Specifically, a functional network analysis seeding from the anterior basal forebrain observed positive functional connectivity of the anterior basal forebrain mainly located in the DMN; and connectivity of the posterior basal forebrain mainly located in the SN in individuals with SCD (Chiesa et al., 2019). In the present study, the structural connectivity of Ch4p and Ch1/2 was mainly located in the DMN medial temporal subsystem in the individuals with SCD. Thus, the discrepancies may be due to methodological differences and different delineation protocols. However, structural connectivity of the Ch4p and Ch1/2 in the patients with aMCI located in both the medial temporal subsystem and midline core subsystem of the DMN and SN was observed. In addition, the pattern changes of SCN seeding from the Ch4p were similar to the pattern changes of SCN seeding from the R EC, and the pattern changes of SCN seeding from the Ch1/2 were similar to the pattern changes of SCN seeding from the L PCC as the order of NC-SCD-aMCI-AD. In addition, the pattern changes of SCN seeding from the Ch4p were similar to the pattern changes of SCN seeding from the hippocampus as the order of NC-SCD-aMCI-AD. As described in a previous study, a significant association between the volume in the Ch4p and right precuneus hypometabolism was shown in SCD (Scheef et al., 2019). In summary, the atrophy of Ch4p has the potential to be a neurodegeneration biomarker in the early stages of AD.

Regarding the DMN, studies based on the functional network showed that connectivity within the DMN was dysfunctional due to the pathology of AD (Seeley et al., 2009; Zhou et al., 2010), and studies based on the SCN showed that the structural connectivity within the DMN medial temporal subsystem was disrupted due to the pathology of AD (Montembeault et al., 2016; Li et al., 2019a). In the present results, the structural covariance within the DMN medial temporal subsystem in patients with AD was increased compared with that in NCs. Genetic effects may be a reason (Bi et al., 2019; Chang et al., 2019; Huang et al., 2019; Li et al., 2019b; Tao et al., 2019), and studies focusing on the effect of Bcl-2 rs956572 (Chang et al., 2018) and MTHFR C677T (Chang et al., 2017) based on SCN showed that homozygotes and heterozygotes exhibited different SCN patterns, although the subjects were all diagnosed with AD. Moreover, different diagnostic criteria and acquisition parameters may be a reason, and the patients with AD in the Alzheimer's disease Neuroimaging Initiative database[4] are at early stages of AD (CDR > 0.5), but the patients with AD in the present study included those in the early, mid-term, and late stages of AD

[4]http://adni.loni.usc.edu

(CDR $\geq$ 1). However, our results are partially in line with those of an SCN-based study, in which the structural covariance in patients with AD increased compared with NCs within the DMN midline core subsystem (Li et al., 2019a). Specifically, although the scope of structural covariance in the AD-related patients increased compared with the NCs, the connectivity strength weakened in the AD-related patients compared with the NCs. The weakened connections in our results in individuals with SCD, aMCI, and patients with AD were mainly located in the precentral gyrus, temporal lobe, prefrontal cortex, and parietal lobe. Conclusively, we speculate that the structural covariance of the DMN showed structural hyperconnectivity at the aMCI stage, and then hypoconnectivity was observed in the dementia stage.

The large-scale network referred to as the SN due to its consistent activation in response to emotionally significant internal and external stimuli showed altered function in AD-related patients (Zhou et al., 2010; Li et al., 2019a). Our results showed that the structural covariance of the SN increased in the AD-related patients compared with the NCs, which was consistent with a previous study (Montembeault et al., 2016). This result suggested that enhancement of connectivity in the SN may compensate for dysfunction in the DMN due to AD-related pathology (Zhou et al., 2010; Montembeault et al., 2016). Then, a linear increase in structural covariance of the ECN was observed with the progression through the NC-aMCI-AD continuum, which may support the hypothesis that AD is associated with opposing connectivity in the DMN and ECN (Zhou et al., 2010; Montembeault et al., 2016; Li et al., 2019a). In addition, we speculate that the ECN acts as a compensatory large-scale network for disconnections in the DMN due to AD pathology.

The SCNs seeded from the DMN, SN, ECN, anterior hippocampus, posterior hippocampus, Ch4p, and Ch1/2 in the SCD group showed a decreased extent of structural covariance compared with the NC group. However, the interaction model revealed that loss of connectivity strength of SCNs was observed within the DMN, SN, ECN, anterior hippocampus, posterior hippocampus, Ch4p, and Ch1/2 in the individuals with SCD. Regarding the ECN, the subjects with SCD showed enhanced connectivity strength in the middle occipital gyrus with a small cluster (313 voxels). In addition, a previous study based on the functional network revealed that increased functional connectivity in DMN regions was observed in individuals with SCD compared with NCs (Hafkemeijer et al., 2013). However, there are no reported studies based on SCN to explore SCD. Combined with a previous study (Hafkemeijer et al., 2013), the results in the present study suggested that structural associations decreased in individuals with SCD, and functional compensation was observed, but structural compensation was not found. These results are potential to indicate that individuals with SCD are at high risk of cognitive decline further.

Not only AD but also the other neurodegenerative diseases and cerebral small vessel disease (Zhu et al., 2019) may show cognitive decline at the early stage, such as progressive supranuclear palsy (Yang et al., 2021), cerebral autosomal dominant arteriopathy with subcortical infarcts and leukoencephalopathy (CADASIL) (Guo et al., 2021), and subcortical vascular MCI (Wang et al., 2018). Therefore, a specific biomarker is very important for disease diagnosis, intervention, and therapy. This study aimed to explore the imaging markers of SCD, aMCI, and AD based on sMRI at the network level. The results showed that the pattern changes in the SCNs as the order of NC-SCD-aMCI-AD are dynamic and divergent. In addition, the decreased extent of SCNs and the weakened connectivity strength of SCNs compared with NC are potential to be the imaging biomarkers for SCD. It is worth noting that the atrophy of the entorhinal cortex was observed both in patients with AD and PD (Jia et al., 2019). In the future, it will be interesting to investigate whether the SCNs seeding from the entorhinal cortex present distinct patterns in patients with AD and PD for understanding the pathology of two neurodegenerative diseases.

There were some limitations in the present study. First, the study was based on cross-sectional data. Although we examined NCs and those with SCD, aMCI, and AD to investigate the pattern changes of SCN, a further longitudinal study should be conducted. Indeed, a longitudinal study is more appropriate to investigate the pattern changes across time. Second, this study used SCN analysis based only on sMRI to explore the connectivity changes of large-scale networks, and a future study combined with a functional network based on fMRI should be done. The combination of multiple modality images may provide a better understanding of the mechanism of neurodegenerative diseases from both structural and functional sight. Third, there is a very limited neuropsychological battery in this dataset, and more neuropsychological tests should be included in our next dataset. Fourth, previous studies demonstrated that diabetes would affect cognition in patients with PD (Wang et al., 2020a), whether the diabetes would affect cognition in SCD is still poorly known. Moreover, cognitive decline may be induced not only by neurodegenerative diseases but also by mental state or physical frailty (Ma and Chan, 2020), such as depression and anxiety, and more information will be collected in our next cohort study. Finally, the relationship between neurocognitive function and neuropathogenesis is complex, a future study combined with integrated results of neuroimaging and the AD biomarkers such as Aβ and tau should be more persuasive.

CONCLUSION

In the present study, we investigated the connectivity changes of GM SCNs in individuals with SCD, aMCI, and AD. A decreased extent of structural covariance and weakened structural connectivity strength were observed in individuals with SCD compared with NCs. Moreover, the divergent and dynamic connectivity changes of SCNs seeding from the DMN, SN, and ECN as the order of NC-SCD-aMCI-AD were shown in this study. Then, the patterns of SCN seeding from subregions of the hippocampus and basal forebrain were similar to those of SCN seeding from the DMN. In summary, the divergent trajectory of change patterns in SCNs along NC-SCD-aMCI-AD potentially provides structural covariance insight into better understanding the progressive mechanism of cognitive decline due to AD-related pathology at preclinical and early stages.

DATA AVAILABILITY STATEMENT

The raw data supporting the conclusions of this article will be made available by the authors, without undue reservation.

ETHICS STATEMENT

The studies involving human participants were reviewed and approved by Ethics of the Medical Research Ethics Committee in Xuanwu Hospital. The patients/participants provided their written informed consent to participate in this study.

AUTHOR CONTRIBUTIONS

ZF and SyL were responsible for the conception and design of this study and wrote the first manuscript. ZF and XW performed the image preprocessing and experiments. YH and MZ performed the data acquisition. SyL reviewed and critiqued the manuscript. YrH, JL, and SxL assisted in drafting the manuscript. XL and GK reviewed and critiqued the manuscript. All authors contributed to the article and approved the submitted version.

FUNDING

This study was supported by the National Natural Science Foundation of China (Grant Nos. 81972160, 61633018, 82020108013, 82001773, and 81622025) and the Hebei Provincial Natural Science Foundation, China (Grant No. F2019203515).

ACKNOWLEDGMENTS

We would like to thank Ingo Kilimann and Michel Grothe from the German Center for Neurodegenerative Diseases (DZNE) Rostock/Greifswald (Rostock, Germany) for sharing the cholinergic basal forebrain map.

SUPPLEMENTARY MATERIAL

The Supplementary Material for this article can be found online at: https://www.frontiersin.org/articles/10.3389/fnagi.2021.686598/full#supplementary-material

REFERENCES

Albert, M. S., DeKosky, S. T., Dickson, D., Dubois, B., Feldman, H. H., Fox, N. C., et al. (2011). The diagnosis of mild cognitive impairment due to Alzheimer's disease: recommendations from the national institute on aging-Alzheimer's association workgroups on diagnostic guidelines for Alzheimer's disease. *Alzheimers Dement* 7, 270–279. doi: 10.1016/j.jalz.2011.03.008

Alexander-Bloch, A., Giedd, J. N., and Bullmore, E. (2013). Imaging structural co-variance between human brain regions. *Nat. Rev. Neurosci.* 14, 322–336. doi: 10.1038/nrn3465

Arendt, T., Taubert, G., Bigl, V., and Arendt, A. (1988). Amyloid deposition in the nucleus basalis of Meynert complex: a topographic marker for degenerating cell clusters in Alzheimer's disease. *Acta Neuropathol.* 75, 226–232. doi: 10.1007/bf00690530

Ashburner, J. (2007). A fast diffeomorphic image registration algorithm. *Neuroimage* 38, 95–113. doi: 10.1016/j.neuroimage.2007.07.007

Bi, C., Bi, S., and Li, B. (2019). Processing of mutant β-Amyloid precursor protein and the clinicopathological features of familial Alzheimer's disease. *Aging Dis.* 10, 383–403. doi: 10.14336/ad.2018.0425

Braak, H., and Del Tredici, K. (2015). The preclinical phase of the pathological process underlying sporadic Alzheimer's disease. *Brain* 138(Pt 10), 2814–2833. doi: 10.1093/brain/awv236

Braak, H., Thal, D. R., Ghebremedhin, E., and Del Tredici, K. (2011). Stages of the pathologic process in Alzheimer disease: age categories from 1 to 100 years. *J. Neuropathol. Exp. Neurol.* 70, 960–969. doi: 10.1097/NEN.0b013e318232a379

Buckner, R. L., Andrews-Hanna, J. R., and Schacter, D. L. (2008). The brain's default network: anatomy, function, and relevance to disease. *Ann. N. Y. Acad. Sci.* 1124, 1–38. doi: 10.1196/annals.1440.011

Cantero, J. L., Iglesias, J. E., Van Leemput, K., and Atienza, M. (2016). Regional hippocampal atrophy and higher levels of plasma amyloid-beta are associated with subjective memory complaints in nondemented elderly subjects. *J. Gerontol. A Biol. Sci. Med. Sci.* 71, 1210–1215. doi: 10.1093/gerona/glw022

Chang, Y. T., Hsu, S. W., Tsai, S. J., Chang, Y. T., Huang, C. W., Liu, M. E., et al. (2017). Genetic effect of MTHFR C677T polymorphism on the structural covariance network and white-matter integrity in Alzheimer's disease. *Hum. Brain Mapp.* 38, 3039–3051. doi: 10.1002/hbm.23572

Chang, Y. T., Huang, C. W., Chang, W. N., Lee, J. J., and Chang, C. C. (2018). Altered functional network affects amyloid and structural covariance in Alzheimer's disease. *Biomed. Res. Int.* 2018:8565620. doi: 10.1155/2018/8565620

Chang, Y. T., Kazui, H., Ikeda, M., Huang, C. W., Huang, S. H., Hsu, S. W., et al. (2019). Genetic interaction of APOE and FGF1 is associated with memory impairment and hippocampal atrophy in Alzheimer's disease. *Aging Dis.* 10, 510–519. doi: 10.14336/ad.2018.0606

Chen, Q., Wu, S., Li, X., Sun, Y., Chen, W., Lu, J., et al. (2021). Basal forebrain atrophy is associated with allocentric navigation deficits in subjective cognitive decline. *Front. Aging Neurosci.* 13:596025. doi: 10.3389/fnagi.2021.596025

Chiesa, P. A., Cavedo, E., Grothe, M. J., Houot, M., Teipel, S. J., Potier, M. C., et al. (2019). Relationship between basal forebrain resting-state functional connectivity and brain Amyloid-β deposition in cognitively intact older adults with subjective memory complaints. *Radiology* 290, 167–176. doi: 10.1148/radiol.2018180268

Damoiseaux, J. S., Viviano, R. P., Yuan, P., and Raz, N. (2016). Differential effect of age on posterior and anterior hippocampal functional connectivity. *Neuroimage* 133, 468–476. doi: 10.1016/j.neuroimage.2016.03.047

Dozeman, E., van Schaik, D. J., van Marwijk, H. W., Stek, M. L., van der Horst, H. E., and Beekman, A. T. (2011). The center for epidemiological studies depression scale (CES-D) is an adequate screening instrument for depressive and anxiety disorders in a very old population living in residential homes. *Int. J. Geriatr. Psychiatry* 26, 239–246. doi: 10.1002/gps.2519

Evans, A. C. (2013). Networks of anatomical covariance. *Neuroimage* 80, 489–504. doi: 10.1016/j.neuroimage.2013.05.054

Faul, F., Erdfelder, E., Lang, A. G., and Buchner, A. (2007). G*Power 3: a flexible statistical power analysis program for the social, behavioral, and biomedical sciences. *Behav. Res. Methods* 39, 175–191. doi: 10.3758/bf03193146

Fischl, B. (2012). FreeSurfer. *Neuroimage* 62, 774–781. doi: 10.1016/j.neuroimage.2012.01.021

Fu, Z., Zhao, M., Wang, X., He, Y., Tian, Y., Yang, Y., et al. (2021). Altered neuroanatomical asymmetries of subcortical structures in subjective cognitive decline, amnestic mild cognitive impairment, and Alzheimer's disease. *J. Alzheimers Dis.* 79, 1121–1132. doi: 10.3233/jad-201116

Gao, X., Huang, Z., Feng, C., Guan, C., Li, R., Xie, H., et al. (2020). Multimodal analysis of gene expression from postmortem brains and blood identifies synaptic vesicle trafficking genes to be associated with Parkinson's disease. *Brief. Bioinform.* 22:bbaa244. doi: 10.1093/bib/bbaa244

Grothe, M., Heinsen, H., and Teipel, S. J. (2012). Atrophy of the cholinergic Basal forebrain over the adult age range and in early stages of Alzheimer's disease. *Biol. Psychiatry* 71, 805–813. doi: 10.1016/j.biopsych.2011.06.019

Guo, P., Li, Q., Wang, X., Li, X., Wang, S., Xie, Y., et al. (2020). Structural covariance changes of anterior and posterior hippocampus during musical training in young adults. *Front. Neuroanat.* 14:20. doi: 10.3389/fnana.2020.00020

Guo, X., Deng, B., Zhong, L., Xie, F., Qiu, Q., Wei, X., et al. (2021). Fibrinogen is an independent risk factor for white matter hyperintensities in CADASIL but not in sporadic cerebral small vessel disease patients. *Aging Dis.* 12, 801–811. doi: 10.14336/ad.2020.1110

Hafkemeijer, A., Altmann-Schneider, I., Oleksik, A. M., van de Wiel, L., Middelkoop, H. A., van Buchem, M. A., et al. (2013). Increased functional connectivity and brain atrophy in elderly with subjective memory complaints. *Brain Connect.* 3, 353–362. doi: 10.1089/brain.2013.0144

Huang, P., Chen, C. S., Yang, Y. H., Chou, M. C., Chang, Y. H., Lai, C. L., et al. (2019). REST rs3796529 genotype and rate of functional deterioration in Alzheimer's disease. *Aging Dis.* 10, 94–101. doi: 10.14336/ad.2018.0116

Jack, C. R. Jr., Bennett, D. A., Blennow, K., Carrillo, M. C., Dunn, B., et al. (2018). NIA-AA research framework: toward a biological definition of Alzheimer's disease. *Alzheimers Dement* 14, 535–562. doi: 10.1016/j.jalz.2018.02.018

Jack, C. R. Jr., Bennett, D. A., Blennow, K., Carrillo, M. C., Feldman, H. H., et al. (2016). A/T/N: an unbiased descriptive classification scheme for Alzheimer disease biomarkers. *Neurology* 87, 539–547. doi: 10.1212/wnl.0000000000002923

Jack, C. R. Jr., Wiste, H. J., Vemuri, P., Weigand, S. D., Senjem, M. L., et al. (2010). Brain beta-amyloid measures and magnetic resonance imaging atrophy both predict time-to-progression from mild cognitive impairment to Alzheimer's disease. *Brain* 133, 3336–3348. doi: 10.1093/brain/awq277

Jessen, F., Amariglio, R. E., Buckley, R. F., van der Flier, W. M., Han, Y., Molinuevo, J. L., et al. (2020). The characterisation of subjective cognitive decline. *Lancet Neurol.* 19, 271–278.

Jessen, F., Amariglio, R. E., van Boxtel, M., Breteler, M., Ceccaldi, M., Chételat, G., et al. (2014). A conceptual framework for research on subjective cognitive decline in preclinical Alzheimer's disease. *Alzheimers Dement* 10, 844–852. doi: 10.1016/j.jalz.2014.01.001

Jia, X., Wang, Z., Yang, T., Li, Y., Gao, S., Wu, G., et al. (2019). Entorhinal cortex atrophy in early, drug-naive Parkinson's disease with mild cognitive impairment. *Aging Dis.* 10, 1221–1232. doi: 10.14336/ad.2018.1116

Kilimann, I., Grothe, M., Heinsen, H., Alho, E. J., Grinberg, L., Amaro, E., et al. (2014). Subregional basal forebrain atrophy in Alzheimer's disease: a multicenter study. *J. Alzheimers. Dis.* 40, 687–700. doi: 10.3233/jad-132345

Li, H. J., Hou, X. H., Liu, H. H., Yue, C. L., He, Y., and Zuo, X. N. (2015). Toward systems neuroscience in mild cognitive impairment and Alzheimer's disease: a meta-analysis of 75 fMRI studies. *Hum. Brain Mapp.* 36, 1217–1232. doi: 10.1002/hbm.22689

Li, K., Luo, X., Zeng, Q., Huang, P., Shen, Z., Xu, X., et al. (2019a). Gray matter structural covariance networks changes along the Alzheimer's disease continuum. *Neuroimage Clin.* 23:101828. doi: 10.1016/j.nicl.2019.101828

Li, Y. S., Yang, Z. H., Zhang, Y., Yang, J., Shang, D. D., Zhang, S. Y., et al. (2019b). Two novel mutations and a de novo mutation in PSEN1 in early-onset Alzheimer's disease. *Aging Dis.* 10, 908–914. doi: 10.14336/ad.2018.1109

Li, X., Li, Q., Wang, X., Li, D., and Li, S. (2018). Differential age-related changes in structural covariance networks of human anterior and posterior hippocampus. *Front. Physiol.* 9:518. doi: 10.3389/fphys.2018.00518

Liu, Y., Paajanen, T., Zhang, Y., Westman, E., Wahlund, L. O., Simmons, A., et al. (2011). Combination analysis of neuropsychological tests and structural MRI measures in differentiating AD, MCI and control groups–the AddNeuroMed study. *Neurobiol. Aging* 32, 1198–1206. doi: 10.1016/j.neurobiolaging.2009.07.008

Livingston, G., Sommerlad, A., Orgeta, V., Costafreda, S. G., Huntley, J., Ames, D., et al. (2017). Dementia prevention, intervention, and care. *Lancet* 390, 2673–2734. doi: 10.1016/s0140-6736(17)31363-31366

Lu, J., Li, D., Li, F., Zhou, A., Wang, F., Zuo, X., et al. (2011). Montreal cognitive assessment in detecting cognitive impairment in Chinese elderly individuals: a population-based study. *J. Geriatr. Psychiatry Neurol.* 24, 184–190. doi: 10.1177/0891988711422528

Ma, L., and Chan, P. (2020). Understanding the physiological links between physical frailty and cognitive decline. *Aging Dis.* 11, 405–418. doi: 10.14336/ad.2019.0521

Manjón, J. V., Coupé, P., Martí-Bonmatí, L., Collins, D. L., and Robles, M. (2010). Adaptive non-local means denoising of MR images with spatially varying noise levels. *J. Magn. Reson. Imaging* 31, 192–203. doi: 10.1002/jmri.22003

Masters, C. L., Bateman, R., Blennow, K., Rowe, C. C., Sperling, R. A., and Cummings, J. L. (2015). Alzheimer's disease. *Nat. Rev. Dis. Primers* 1:15056. doi: 10.1038/nrdp.2015.56

Mechelli, A., Friston, K. J., Frackowiak, R. S., and Price, C. J. (2005). Structural covariance in the human cortex. *J. Neurosci.* 25, 8303–8310. doi: 10.1523/jneurosci.0357-05.2005

Mesulam, M., Shaw, P., Mash, D., and Weintraub, S. (2004). Cholinergic nucleus basalis tauopathy emerges early in the aging-MCI-AD continuum. *Ann. Neurol.* 55, 815–828. doi: 10.1002/ana.20100

Montembeault, M., Rouleau, I., Provost, J. S., and Brambati, S. M. (2016). Altered gray matter structural covariance networks in early stages of Alzheimer's disease. *Cereb. Cortex* 26, 2650–2662. doi: 10.1093/cercor/bhv105

Morris, J. C. (1993). The Clinical Dementia Rating (CDR): current version and scoring rules. *Neurology* 43, 2412–2414. doi: 10.1212/wnl.43.11.2412-a

Nordin, K., Persson, J., Stening, E., Herlitz, A., Larsson, E. M., and Söderlund, H. (2018). Structural whole-brain covariance of the anterior and posterior hippocampus: associations with age and memory. *Hippocampus* 28, 151–163. doi: 10.1002/hipo.22817

Persson, J., Spreng, R. N., Turner, G., Herlitz, A., Morell, A., Stening, E., et al. (2014). Sex differences in volume and structural covariance of the anterior and posterior hippocampus. *Neuroimage* 99, 215–225. doi: 10.1016/j.neuroimage.2014.05.038

Petersen, R. C. (2004). Mild cognitive impairment as a diagnostic entity. *J. Intern. Med.* 256, 183–194. doi: 10.1111/j.1365-2796.2004.01388.x

Poppenk, J., Evensmoen, H. R., Moscovitch, M., and Nadel, L. (2013). Long-axis specialization of the human hippocampus. *Trends Cogn. Sci.* 17, 230–240. doi: 10.1016/j.tics.2013.03.005

Rabin, L. A., Smart, C. M., and Amariglio, R. E. (2017). Subjective cognitive decline in preclinical Alzheimer's disease. *Annu. Rev. Clin. Psychol.* 13, 369–396. doi: 10.1146/annurev-clinpsy-032816-045136

Scheef, L., Grothe, M. J., Koppara, A., Daamen, M., Boecker, H., Biersack, H., et al. (2019). Subregional volume reduction of the cholinergic forebrain in subjective cognitive decline (SCD). *Neuroimage Clin.* 21:101612. doi: 10.1016/j.nicl.2018.101612

Seeley, W. W., Crawford, R. K., Zhou, J., Miller, B. L., and Greicius, M. D. (2009). Neurodegenerative diseases target large-scale human brain networks. *Neuron* 62, 42–52. doi: 10.1016/j.neuron.2009.03.024

Shu, N., Wang, X., Bi, Q., Zhao, T., and Han, Y. (2018). Disrupted topologic efficiency of white matter structural connectome in individuals with subjective cognitive decline. *Radiology* 286, 229–238. doi: 10.1148/radiol.2017162696

Sperling, R. A., Aisen, P. S., Beckett, L. A., Bennett, D. A., Craft, S., Fagan, A. M., et al. (2011). Toward defining the preclinical stages of Alzheimer's disease: recommendations from the National Institute on Aging-Alzheimer's Association workgroups on diagnostic guidelines for Alzheimer's disease. *Alzheimers Dement* 7, 280–292. doi: 10.1016/j.jalz.2011.03.003

Tao, Q. Q., Chen, Y. C., and Wu, Z. Y. (2019). The role of CD2AP in the pathogenesis of Alzheimer's disease. *Aging Dis.* 10, 901–907. doi: 10.14336/ad.2018.1025

Tosun, D., Schuff, N., Mathis, C. A., Jagust, W., and Weiner, M. W. (2011). Spatial patterns of brain amyloid-beta burden and atrophy rate associations in mild cognitive impairment. *Brain* 134(Pt 4), 1077–1088. doi: 10.1093/brain/awr044

Tzourio-Mazoyer, N., Landeau, B., Papathanassiou, D., Crivello, F., Etard, O., Delcroix, N., et al. (2002). Automated anatomical labeling of activations in SPM using a macroscopic anatomical parcellation of the MNI MRI single-subject brain. *Neuroimage* 15, 273–289. doi: 10.1006/nimg.2001.0978

Wang, T., Yuan, F., Chen, Z., Zhu, S., Chang, Z., Yang, W., et al. (2020a). Vascular, inflammatory and metabolic risk factors in relation to dementia in Parkinson's disease patients with type 2 diabetes mellitus. *Aging (Albany NY)* 12, 15682–15704. doi: 10.18632/aging.103776

Wang, X., Huang, W., Su, L., Xing, Y., Jessen, F., Sun, Y., et al. (2020b). Neuroimaging advances regarding subjective cognitive decline in preclinical Alzheimer's disease. *Mol. Neurodegener.* 15:55. doi: 10.1186/s13024-020-00395-393

Wang, X., Yu, Y., Zhao, W., Li, Q., Li, X., Li, S., et al. (2018). Altered whole-brain structural covariance of the hippocampal subfields in subcortical vascular mild cognitive impairment and amnestic mild cognitive impairment patients. *Front. Neurol.* 9:342. doi: 10.3389/fneur.2018.00342

Weiler, M., Fukuda, A., Massabki, L. H., Lopes, T. M., Franco, A. R., Damasceno, B. P., et al. (2014). Default mode, executive function, and language functional connectivity networks are compromised in mild Alzheimer's disease. *Curr. Alzheimer Res.* 11, 274–282. doi: 10.2174/1567205011666140131114716

Xie, F., Gao, X., Yang, W., Chang, Z., Yang, X., Wei, X., et al. (2019). Advances in the research of risk factors and prodromal biomarkers of Parkinson's disease. *ACS Chem. Neurosci.* 10, 973–990. doi: 10.1021/acschemneuro.8b00520

Xue, C., Yuan, B., Yue, Y., Xu, J., Wang, S., Wu, M., et al. (2019). Distinct disruptive patterns of default mode subnetwork connectivity across the spectrum of preclinical Alzheimer's disease. *Front. Aging Neurosci.* 11:307. doi: 10.3389/fnagi.2019.00307

Yang, W., Chang, Z., Que, R., Weng, G., Deng, B., Wang, T., et al. (2020). Contra-Directional expression of plasma superoxide dismutase with lipoprotein cholesterol and high-sensitivity c-reactive protein as important markers of Parkinson's disease severity. *Front. Aging Neurosci.* 12:53. doi: 10.3389/fnagi.2020.00053

Yang, W., Deng, B., Huang, Y., Liu, J., Huang, Z., Chang, Z., et al. (2021). Two heterozygous progranulin mutations in progressive supranuclear palsy. *Brain* 144:e27. doi: 10.1093/brain/awaa428

Yeo, B. T., Krienen, F. M., Sepulcre, J., Sabuncu, M. R., Lashkari, D., Hollinshead, M., et al. (2011). The organization of the human cerebral cortex estimated by intrinsic functional connectivity. *J. Neurophysiol.* 106, 1125–1165. doi: 10.1152/jn.00338.2011

Zhao, W., Wang, X., Yin, C., He, M., Li, S., and Han, Y. (2019). Trajectories of the hippocampal subfields atrophy in the Alzheimer's disease: a structural imaging study. *Front. Neuroinform.* 13:13. doi: 10.3389/fninf.2019.00013

Zhou, J., Greicius, M. D., Gennatas, E. D., Growdon, M. E., Jang, J. Y., Rabinovici, G. D., et al. (2010). Divergent network connectivity changes in behavioural variant frontotemporal dementia and Alzheimer's disease. *Brain* 133(Pt 5), 1352–1367. doi: 10.1093/brain/awq075

Zhu, S., Deng, B., Huang, Z., Chang, Z., Li, H., Liu, H., et al. (2021). "Hot cross bun" is a potential imaging marker for the severity of cerebellar ataxia in MSA-C. *NPJ Parkinsons Dis.* 7:15. doi: 10.1038/s41531-021-00159-w

Zhu, S., Wei, X., Yang, X., Huang, Z., Chang, Z., Xie, F., et al. (2019). Plasma lipoprotein-associated phospholipase A2 and superoxide dismutase are independent predicators of cognitive impairment in cerebral small vessel disease patients: diagnosis and assessment. *Aging Dis.* 10, 834–846. doi: 10.14336/ad.2019.0304

Zielinski, B. A., Gennatas, E. D., Zhou, J., and Seeley, W. W. (2010). Network-level structural covariance in the developing brain. *Proc. Natl. Acad. Sci. U S A.* 107, 18191–18196. doi: 10.1073/pnas.1003109107

Conflict of Interest: The authors declare that the research was conducted in the absence of any commercial or financial relationships that could be construed as a potential conflict of interest.

Publisher's Note: All claims expressed in this article are solely those of the authors and do not necessarily represent those of their affiliated organizations, or those of the publisher, the editors and the reviewers. Any product that may be evaluated in this article, or claim that may be made by its manufacturer, is not guaranteed or endorsed by the publisher.

Advantages of publishing in Frontiers

OPEN ACCESS
Articles are free to read for greatest visibility and readership

FAST PUBLICATION
Around 90 days from submission to decision

HIGH QUALITY PEER-REVIEW
Rigorous, collaborative, and constructive peer-review

TRANSPARENT PEER-REVIEW
Editors and reviewers acknowledged by name on published articles

Frontiers
Avenue du Tribunal-Fédéral 34
1005 Lausanne | Switzerland

Visit us: www.frontiersin.org
Contact us: frontiersin.org/about/contact

REPRODUCIBILITY OF RESEARCH
Support open data and methods to enhance research reproducibility

DIGITAL PUBLISHING
Articles designed for optimal readership across devices

FOLLOW US
@frontiersin

IMPACT METRICS
Advanced article metrics track visibility across digital media

EXTENSIVE PROMOTION
Marketing and promotion of impactful research

LOOP RESEARCH NETWORK
Our network increases your article's readership